Simulation, Design and Optimization of Membrane Gas Separation, Chemical Absorption and Hybrid Processes for CO_2 Capture

by

Mohammad Hassan Murad Chowdhury

A thesis
presented to the University of Waterloo
in fulfillment of the
thesis requirement for the degree of
Doctor of Philosophy
in
Chemical Engineering

Waterloo, Ontario, Canada, 2011

I hereby declare that I am the sole author of this thesis. This is a true copy of the thesis, including any required final revisions, as accepted by my examiners.

I understand that my thesis may be made electronically available to the public.

Abstract

Coal-fired power plants are the largest anthropogenic point sources of CO_2 emissions worldwide. About 40% of the world's electricity comes from coal. Approximately 49% of the US electricity in 2008 and 23% of the total electricity generation of Canada in 2000 came from coal-fired power plant (World Coal Association, and Statistic Canada). It is likely that in the near future there might be some form of CO_2 regulation. Therefore, it is highly probable that CO_2 capture will need to be implemented at many US and Canadian coal fired power plants at some point.

Several technologies are available for CO_2 capture from coal-fired power plants. One option is to separate CO_2 from the combustion products using conventional approach such as chemical absorption/stripping with amine solvents, which is commercially available. Another potential alternative, membrane gas separation, involves no moving parts, is compact and modular with a small footprint, is gaining more and more attention. Both technologies can be retrofitted to existing power plants, but they demands significant energy requirement to capture, purify and compress the CO_2 for transporting to the sequestration sites.

This thesis is a techno-economical evaluation of the two approaches mentioned above along with another approach known as hybrid. This evaluation is based on the recent advancement in membrane materials and properties, and the adoption of systemic design procedures and optimization approach with the help of a commercial process simulator. Comparison of the process performance is developed in AspenPlus process simulation environment with a detailed multicomponent gas separation membrane model, and several rigorous rate-based absorption/stripping models.

Fifteen various single and multi-stage membrane process configurations with or without recycle streams are examined through simulation and design study for industrial scale post-combustion CO_2 capture. It is found that only two process configurations are capable to satisfy the process specifications i.e., 85% CO_2 recovery and 98% CO_2 purity for EOR. The power and membrane area requirement can be saved by up to 13% and 8% respectively by the optimizing the base design. A post-optimality sensitivity analysis

reveals that any changes in any of the factors such as feed flow rate, feed concentration (CO_2), permeate vacuum and compression condition have great impact on plant performance especially on power consumption and product recovery.

Two different absorption/stripping process configurations (conventional and Fluor concept) with monoethanolamine (30 wt% MEA) solvent were simulated and designed using same design basis as above with tray columns. Both the rate-based and the equilibrium-stage based modeling approaches were adopted. Two kinetic models for modeling reactive absorption/stripping reactions of CO_2 with aqueous MEA solution were evaluated. Depending on the options to account for mass transfer, the chemical reactions in the liquid film/phase, film resistance and film non-ideality, eight different absorber/stripper models were categorized and investigated. From a parametric design study, the optimum CO_2 lean solvent loading was determined with respect to minimum reboiler energy requirement by varying the lean solvent flow rate in a closed-loop simulation environment for each model. It was realized that the success of modeling CO_2 capture with MEA depends upon how the film discretization is carried out. It revealed that most of the CO_2 was reacted in the film not in the bulk liquid. This insight could not be recognized with the traditional equilibrium-stage modeling. It was found that the optimum/or minimum lean solvent loading ranges from 0.29 to 0.40 and the reboiler energy ranges from 3.3 to 5.1 (GJ/ton captured CO_2) depending on the model considered. Between the two process alternatives, the Fluor concept process performs well in terms of plant operating (i.e., 8.5% less energy) and capital cost (i.e., 50% less number of strippers).

The potentiality of hybrid processes which combines membrane permeation and conventional gas absorption/stripping using MEA were also examined for post-combustion CO_2 capture in AspenPlus®. It was found that the hybrid process may not be a promising alternative for post-combustion CO_2 capture in terms of energy requirement for capture and compression. On the other hand, a stand-alone membrane gas separation process showed the lowest energy demand for CO_2 capture and compression, and could save up to 15 to 35% energy compare to the MEA capture process depending on the absorption/stripping model used.

Economics is one of the most important parameters to be investigated for evaluating any process or process alternatives besides the technical evaluation. A detailed techno-economic evaluation for CO_2 capture from coal fired power plant flue gas has been conducted for both the MEA and membrane gas separation processes. It is assumed that the energy requirements to operate the CO_2 capture and compression unit are withdrawn from the main power facility either through electricity or steam which de-rate the plant. A natural gas auxiliary boiler was also considered for supplying steam for the stripper reboiler. It was found that the MEA process results in a lower capture cost of \$103/tonne of CO_2 avoided compared to Membrane process (\$143/tonne of CO_2 avoided). To be competitive with MEA process, slight improvement in membrane properties in terms of selectivity (greater than 80) is expected.

Acknowledgements

The author expresses his profound thanks and praise to **ALLAH**, the Almighty, the most Gracious, the most Merciful and peace be upon His Prophet Mohammad (Sallahu alihi wa sallam).

The author is highly grateful to all thesis supervisors namely Dr. Peter Douglas, Dr. Eric Croiset and Dr. Xianshe Feng for their guidance, encouragement, expert suggestions and generous support throughout this work. The author is especially indebted to Dr. Eric Croiset for reviewing the thesis patiently and providing many constructive comments and stimulating suggestions. Thank you to Dr. Ali Elkamel and Dr. Christine Moresoli for serving as members on my thesis supervising committee.

I would like to thank all graduate students working under the supervision of Prof. P. Douglas and Prof. E. Croiset, especially C. Alie and L. Backham for their valuable suggestions and comments at regular weekly group meeting and help in the past several years during my study. I also express my gratitude to Li Liu, post-doctoral fellow, for her help in Membrane Research Lab of Department of Chemical Engineering during experimental setup of Hollow Fibre Membrane Module.

Special thanks to Kazi Z. Sumon, Ph.D student of University of Regina, for sharing and discussing ideas during my stay in Regina, Saskatchewan. My appreciation also goes to Misbah and Shihab, graduate students of University of Regina for their support. I highly appreciate the support of Dr. Reaz Ahmed of Bangladesh University of Engineering and Technology (BUET) during my Ph.D defence exam.

I am thankful to my beloved family for supporting me during my study period. Special thanks go to my son, Isfar Abdullah Chowdhury, who gave up some of his child-father and recreation time to make this thesis possible. Special thanks also go to my wife, Rejina Kamrul (Rumu), for her continual support, constant prayers and encouragement.

Finally, it should be mentioned that this thesis was made possible through the help of Almighty Allah (God) and the cooperation and financial support received from the supervisors and the Chemical Engineering Department, Faculty of Engineering, University of Waterloo.

Dedicated to My Parents, Wife and Son

Table of Contents

List of Tables

List of Figures

Nomenclature

Abbreviations

BDF	Backward Differentiation Formula
CCS	Carbon Capture and Storage
CMU	Carnegie Mellon University
EOR	Enhanced Oil Recovery
EPRI	Electric Power Research Institute
FGD	Flue gas desulphurisation
GCCSI	Global CCS Institute
GHG	Green house Gas
GHG IA	Greenhouse-Gas Implementing Agreement
GPU	Gas Permeation Unit (1 GPU = 10^{-6} cm^3 (STP)/cm^2.s.cmHg)
IVP	Initial Value Problem
IMSL	International Mathematical and Statistical Library
MEA	Monoethanolamine
MIT	Massachusetts Institute of Technology
MWe	Megawatt electric
MWth	Megawatt thermal
MTR	Membrane Technology and Research Inc.
NETL	National Energy Technology Laboratory
NZEC	Near Zero Emissions Coal Initiative
ODE	Ordinary Differential Equation
OECD	Organization for Economic Co-operation and Development
PRB	Powder River Basin
RITE	Research Institute of Innovative Technology for the Earth
SCPC	Supercritical Pulverized Coal
Sub-PC	Subcritical pulverized Coal
SQP	Sequential Quadratic Programming

USCPC Ultra-Supercritical Pulverized Coal

USLS US low Sulphur

Symbols

c_i	Concentration of component i, mol/m^3
D_{if}	Gas diffusivity coefficient of component i, m^2/s
D_i	Inside diameter of hollow fibre, m
D_o	Outside diameter of hollow fibre, m
J_i	Permeance of component i, mol/m^2.s.Pa
j_i	Flux of component i, mol/m^2.s
K_i	Sorption coefficient of component i, mol/m^3.Pa
L	Effective fibre length, m
l	Membrane thickness, m
M_i	Molecular weight of component i
N	Number of fibres in the module
P_i	Permeability coefficient of component i, mol.m/m^2.s.Pa
P	Feed side pressure, Pa
p	Permeate side pressure, Pa
R	Ideal gas constant, Pa.m^3/mol.K
T	Temperature, K
T_c	Critical temperature, K
T_r	Reduced temperature
T_*	Dimensionless temperature
u	Feed-side flow rate in hollow fibre module, mol/s
u_r	Residue flow rate, mol/s
u_f	Feed flow rate, mol/s
v	Bulk permeate flow rate, mol/s
v_{swp}	Sweep or purge stream flow rate, mol/s
V_c	Critical volume, m^3/mole
$x_{f\,i}$	Feed concentration of component i, mol fraction

$x_{r\,i}$ Residue concentration of component i, mol fraction

x_i Feed-side concentration of component i, mol fraction

y_i Local permeate concentration of component i on membrane surface, mol fraction

y_{swpi} Sweep or purge concentration of component i, mol fraction

$\bar{y}_i$ Bulk permeate concentration of component i in bulk permeate stream, fraction

z Hollow fibre length variable, m

Greek symbols

λ Ratio of permeate pressure to feed pressure

θ Stage cut (ratio of permeate flow to feed flow)

μ_m Viscosity of gas mixture, Pa-s

μ_i Pure component viscosity, Pa-s

ω Acentric factor

γ Dipole moment, debyes

γ_r Dimensionless dipole moment

κ Association factor

Ω_v Viscosity collision integral

α_{ij} Membrane selectivity

α CO_2 loading in the lean solvent stream, (mol CO_2/ mol MEA)

Chapter 1

Introduction

1.1 Background

Gas separation has a long history in the field of chemical engineering as one of the key separation technologies. The chemical absorption based gas separation technology has existed for more than 60 years and was developed primarily for acid gas treating (Kohl and Neilsen, 1997). Over the years, there has been a lot of research that has focused on finding the ultimate solvent for chemical absorption. These solvents include the various classes of amines (primary, secondary, tertiary, and hindered). Some of these amines include monoethanolamine (MEA), diethanolamine (DEA), methyldiethanolamine (MDEA), and isobutanolamine (AMP). Improvements to the current chemical absorption technology will mostly likely occur with the development of better solvents and contactors. Some of the desirable solvent properties include: fast CO_2 absorption rate, high capacity for CO_2, low energy requirements for regeneration, low corrosivity, low degradation rates, low volatility, low solvent costs. The commercially available monoethanolamine (MEA) based process is considered as a viable and the best near-term strategy to retrofit the existing fleet of pulverized coal power plants for capturing CO_2 from combustion process because of its fast reaction rate with CO_2 and low cost of raw materials compared to other amines.

Membrane-based gas separation technology mainly expanded during the last few decades and has led to significant innovation in both processes and products. Possible integration of various membrane operations in the same industrial cycle for high quality of final products, plant compactness, environmental impact, and energetic aspects can be related with the some key developments in industrial membrane technologies (Drioli and Romano, 2001).

Membrane technology first became important during the sixties and seventies in the field of water treatment. Processes like reverse osmosis, ultrafiltration, dialysis and electrodialysis are examples of this development. During the eighties membrane gas

separation technology started to be applied in the field of gas purification on a large scale, mainly because of the introduction of stable and selective polymer membranes (Baker 2002). Membrane gas separation of CO_2 by permeation from light hydrocarbons has met with considerable success in the petroleum, natural gas and chemical industries because of the inherent simplicity resulting from steady state operation, absence of moving parts and modular construction (Kesting and Fritsche, 1993). But gas separation membranes have thus far not been widely explored for CO_2 capture from flue gases due to the comparatively high mixture flows and the need for flue gas pressurization.

Membrane is considered as a permselective barrier or interface between two phases and is the heart of every membrane process (Mulder, 1996). The mechanism behind membrane gas separation is based on the relative permeation rate of different components in a gas mixture through the membrane under the driving force of a pressure differential across the membrane (Feng et al., 1999). The driving force may derive from compression of feed gas to a high pressure; and/or the downstream side evacuation for permeant.

Usually, nonporous polymeric membranes are utilized for gas membrane separation. Porous membranes can also be utilized for the gas separation. The gas mixture is fed in one side (upstream) of a membrane at a high pressure and permeates through the membrane to a low-pressure side (downstream). Faster components more rapidly permeate through the membrane and become enriched on the permeate side, while the slower components are concentrated in the retentate (residue) side.

Permeability and selectivity are the only two criteria that must be met to produce a useful membrane. The industrial success of membrane gas separation is largely attributed to the engineering approach of reducing the membrane effective-thickness, and increasing the packing density of the membrane module. Thin membranes in the form of asymmetric and/or composite membranes are desired to reduce the membrane resistance to permeation. Hollow fiber membranes have the advantages of self-supporting and large membrane area per unit module volume, compared with flat membranes (Liu, 2008).

The economic viability of gas membrane systems can be significantly affected by process design. In most applications, mathematical models are required to predict the performance of gas separation modules for process design and optimization. Process

simulation allows the evaluation of the influence of the variables in the process, and new process configurations. Today, a wide variety of software directed at process engineering is available. Most of the commercial process simulators have built-in process models and optimizer toolbox, thus offering a convenient and time saving means of examining an entire process.

1.2 Motivation

The carbon dioxide content in the atmosphere has risen considerably since the advent of the industrial revolution. It is widely believed that a continuation of this trend will lead to severe climate changes. This is due to the fact that carbon dioxide absorbs infrared radiation, thereby trapping heat in the atmosphere. In spite of the fact that carbon dioxide is just one of the many greenhouse gases, and certainly not the most malignant gas, its huge emissions result in a significant contribution to the greenhouse effect. Therefore, lowering or stabilizing the carbon dioxide content in the atmosphere appears to be of the utmost importance.

Figure 1.1 shows the main greenhouse gases, their relative emissions and their sources. The major long-lived greenhouse gases, coming from utilization of fossil fuels are carbon dioxide, methane, and nitrous oxide. By far the largest potential sources of carbon dioxide today are fossil fueled power plants. Power plants emit more than one-third of the CO_2 emissions worldwide. Power plants are usually built in large centralized units, typically delivering 500-1000 MW of electrical power. A 1000 MW pulverized coal fired power plant emits between 6-8 Mt/y of CO_2, an oil fired single cycle power plant emits about two thirds of that, and a natural gas combined cycle power plant emits about one half of that (Riemer, 1993). In Canada, twenty three coal-fired plants generated 106 TWh of electricity in 2000 (Statistic Canada, 2001).

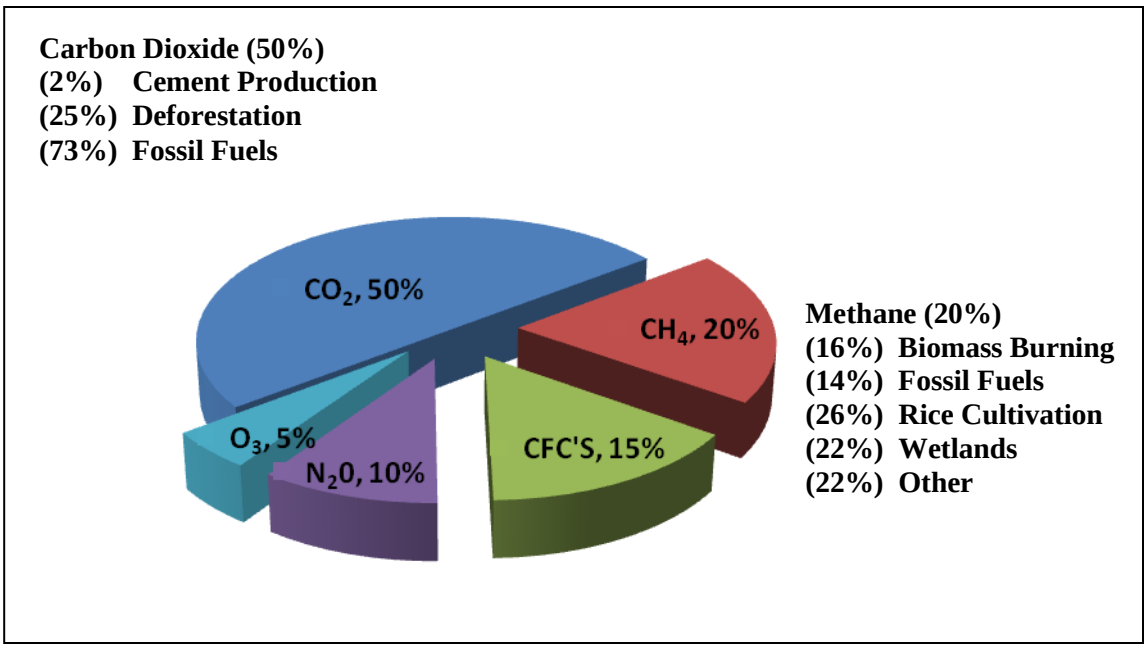

Figure 1.1: Major sources of greenhouse gas emissions (Riemer, 1993).

There are a number of ways to remove CO_2 from the combustion process. Carbon dioxide capture processes can be divided into three categories: precombustion, post-combustion, and oxy-fuel combustion. Within each capture process, a number of separation technologies can be employed as standalone technology or coupled with another separation processes to capture CO_2.

A proven commercial process for capturing CO_2 from flue gas is based on chemical absorption using monoethanolamine (MEA) or diethanolamine (DEA) as solvent. The method is expensive and energy intensive. Alternative technologies may offer improvements, and one of the options could be membrane gas separation technology. In the case of carbon dioxide removal two membrane operations seem to be relevant: 1) gas separation by permeation and 2) gas separation by liquid absorption in membrane contactor. Due to the process simplicity, membrane gas separation by permeation will be considered in the present study.

Based on recent advancement in polymeric membrane materials, and use of systematic design method and optimization approach with the help of commercial process simulator such as AspenPlus®, the present study will explore the potentiality of membrane gas separation technology or hybrid technology (combination of membrane

and MEA) for capturing CO_2 from power station flue gases as an alternative to traditional MEA process technology. This research is a contribution to the exploration of new and existing technologies to mitigate greenhouse gas emission by capturing carbon dioxide from the flue gases in the most realistic and systematic technical way.

1.3 Research Objectives

The overall objective of this research is to develop a rigorous design, simulation and optimization model in one platform to investigate the potential of membrane based gas separation processes and hybrid processes for capturing CO_2 from industrial flue gases as an alternative to traditional amine absorption/stripping system.

The specific objectives of this research have been derived in light of the aforementioned discussions are:

i. Select the best membrane type and module, and a detailed mathematical model of that module for multicomponent gas separation. Develop a robust, reliable and flexible numerical technique for solving the model equations.
ii. Incorporate the membrane model into AspenPlus®. AspenPlus® is a commercial process simulator.
iii. Simulate and design the different membrane process systems for CO_2 Capture from flue gases in AspenPlus®.
iv. Optimise the process design parameters to minimize the overall energy requirements for membrane processes.
v. Design and simulate the MEA process for CO_2 capture.
vi. Investigate and simulate hybrid processes (i.e., combination of membrane and MEA process).
vii. Evaluate the cost of MEA and membrane capture processes.

1.4 Outline of the Thesis

This thesis covers the following aspects to provide information on a systematic development of a design, simulation and optimization model for membrane based gas separation process and hybrid process along with the simulation and design of MEA absorption/stripping process for CO_2 capture from post-combustion exhaust gas streams:

- Chapter 1 presents the background of the study and states the objectives of the study.
- Chapter 2 provides an overview of membrane based gas separation regarding types of membrane, gas transport mechanism in membrane, membrane process design and optimization. It also describes different CO_2 capture technologies, impact of CO_2 on global warming and climate change along with storage and usage of CO_2.The recent information on commercial process simulators is also presented in this chapter.
- A new numerical approach for a detailed multicomponent gas separation membrane model is presented in Chapter 3.
- Chapter 4 describes interfacing of membrane model in AspenPlus® process simulator.
- Design and simulation of different membrane processes in AspenPlus® for CO_2 capture from power plant flue gas is presented in Chapter 5.
- Optimization of membrane process is carried out in Chapter 6.
- Chapter 7 discusses the development of a rigorous model for amine (MEA) process for CO_2 capture.
- Simulation of hybrid processes and comparison of all processes in terms of overall energy requirement is presented in Chapter 8.
- Economic analysis and comparison of the membrane and amine processes including detailed sizing and designs of the equipments are conducted in Chapter 9.
- Finally, the general conclusions drawn from the study along with the contribution to research, and recommendations for future work, are summarized in Chapter 10.

Chapter 2

Literature Review

2.1 Membrane Gas Separation History

Membrane gas separation technology mainly expanded during the last two decades although the study of gas separation has a long history. Thomas Graham first proposed the concept of the solution-diffusion mechanism in 1866. By exploiting this, isotope separation was achieved by a microporous membrane at large scale in 1945. Then, Van Amerongen (1950), Barrer (1951), Mears (1954), Stern (1966) and others laid the foundation of the modern theories of gas permeation by developing solution-diffusion model (Baker, 2000).

In the late 1960s and early 1970s, development of high-flux asymmetric membranes and large-surface-area membrane modules for reverse osmosis applications provided the basis for modern membrane gas separation technology. In 1980, Monsanto launched its hydrogen-separating Prism membrane (Henis and Tripodi, 1980). After Monsanto's success, other companies were encouraged to go ahead with their own membrane technologies. Cynara, Separex, and Grace Membrane Systems started producing membrane plants to remove carbon dioxide from methane in natural gas in the mid-1980s. Dow also launched its first commercial membrane system for nitrogen separation from air around the same time. Application of Gas separation membranes is expanding to a wide variety of other applications ranging from dehydration of air and natural gas to organic vapor removal from air and nitrogen streams (Baker, 2002).

Further growth in membrane gas separation in different areas is expected due to extensive research activities for introducing energy-saving technologies by focusing on: creation of advanced membrane materials, development of high-efficiency modules with large amount of area per unit volume, controlling capability of microscopic transport phenomena inside membrane, and high speed manufacturing method (Koros, 2004).

2.2 Features of Membrane Gas Separation

The basic properties of membrane operations make them ideal for industrial operations. The most attractive features of membrane gas separation compared with other separation methods are the following (Mulder, 1996; Drioli and Mario, 2001; Baker, 2000; Luque et al, 2004):

- Absence of phase and temperature change phenomena, leading to lower energy requirement.
- Low maintenance costs because of the absence of moving parts.
- Easy plant operation due to steady continuous process.
- Due to small foot print and light weight, membranes are ideal for use on offshore platforms, in aboard aircraft, etc. where space and portability are very important factors.
- Easy to scale up based on laboratory or pilot-scale data due to modular design of membrane.
- Can easily be combined with other separation processes in the same facility (hybrid processing).
- Low environmental impacts due to absence of chemical additives etc., and usually high quality of final products.

However, it also has some disadvantages, which constraint its application in different systems. The disadvantages of membrane process include fouling due to contaminated feed, expensive fabrication method, and incapability to handle corrosive substances. In addition, polymer membrane process cannot sustain high temperature condition.

2.3 Types of Gas Separation Membranes

Mainly polymeric materials are used in industrial gas separation processes. Inorganic membranes such as metal and carbon membranes are also getting attention for their high thermal stability. Membranes can be configured as flat or tubular forms. Membrane with high permeability and selectivity is the most wanted one for specific gas separation processes along with other properties such as stable, thin, low-cost and package-able into high-surface-area modules.

Two types of polymeric membranes are widely used commercially for gas separations: Glassy and rubbery polymer. Glassy membranes are rigid and glass-like, and operate below their glass transition temperatures. On the other hand, rubbery membranes are flexible and soft, and operate above their glass transition temperatures. Mostly, rubbery polymers show a high permeability, but a low selectivity, whereas glassy polymers exhibit a low permeability but a high selectivity. Glassy polymeric membranes dominate industrial membrane separations because of their high gas selectivities along with good mechanical properties (Stern, 1994).

Although both porous and dense membranes can be used as selective gas separation barriers, all current commercial gas separation membranes are based on dense polymer. The selective layer of gas separation membranes must be extremely thin to achieve high fluxes. Most of the membranes have effective thickness of less than 0.5 μm. In the 1960s, Loeb and Sourirajan invented extremely thin asymmetric membranes by polymer phase separation process. These membranes consist of a thin, dense, nonporous skin layer that performs the separation, supported on a finely microporous substrate made from the same material that provides mechanical strength (Baker, 2002). Formation of defect free thin skin layer is very difficult. Small membrane defect can dramatically decrease the selectivity. In 1980s, Henis and Tripodi devised a new technique to solve the membrane defect problem. They used thin coating of rubbery materials for plugging the defects of the membranes.

Another type of gas separation membrane is called composite membrane. Composite membranes consist of two or more layers of different materials. The support layer is made by the Loeb-Sourirajan procedure. This layer performs no separation but is mechanically strong and chemically stable and can be made from a number of low-cost polymers. The selective layer can be coated directly onto the microporous support, but better membranes often result when an intermediate gutter layer made from a highly permeable, low-selectivity material is used. This gutter layer provides a smooth surface on which the ultrathin selective layer can be deposited. The gutter layer also serves to conduct the permeating gas to the pores of the microporous support (Baker, 2002).

2.4 Gas Transport Mechanism in Membrane

Gas transport in membranes is a function of membrane properties (physical and chemical structure), the nature of the permeant species (size, shape, and polarity), and the interaction between membrane and permeant species. Membrane properties and the nature of the permeant species, determine the diffusional characteristics of a particular gas through a membrane. Interaction between membrane and permeant refers to the sorptivity or solubility of the gas in the membrane (Stern, 1994, Shekhawat et al., 2003). When an asymmetric or composite membrane is used in gas separation, the gas molecules will tend to diffuse from the high-pressure to the low-pressure side. Various transport mechanisms can be distinguished depending on the structure of the asymmetric membrane (Mulder, 1996). The gas permeation mechanisms in membrane can be described by two well accepted models: pore flow model for porous membrane and solution-diffusion model for dense (nonporous) membrane. Figure 2.1 illustrates the mechanisms of gas permeation in membrane.

The difference between the solution-diffusion and pore flow mechanism lies in the relative size and continuation of the pores. The free-volume elements (pores) in the membrane in which transport are described by solution-diffusion mechanism and Fick's law, are considered as tiny spaces between polymer chains caused by thermal motion of the polymer molecules. These volume elements appear and disappear on about the same time scale as the motions of the permeants traversing the membrane. On the other hand, for a membrane in which transport is best described by a pore flow model and Darcy's law, the free-volume elements (pores) are relatively large and fixed, do not fluctuate in position or volume on the time scale of permeant motion, and are connected to one another (Baker, 2000).

Pore flow model

In the pore flow model, permeants are transported by pressure-driven convective flow through tiny pores. Separation occurs due to filtration of one of the permeants from some of the pores in the membrane through which other permeants move. Three types of porous membranes, differing in pore size, are shown in Figure 2.1. Three mechanisms

were proposed to describe the free gas flow in a pore depending on the size of the pore relative to the mean free path of the permeating gas molecules.

If the membrane pores are relatively large compare to the mean free path of the permeating gas molecules, i.e., from 0.1 to 10 μm, gases permeate through the pores by convective (viscous) flow described by Poiseuille's law, and no separation occurs.

If the membrane pores are smaller than 0.1 μm, then the pore diameter is the same size as or smaller than the mean free path of the gas molecules. Diffusion through such pores is governed by Knudsen diffusion, and the transport rate of any gas is inversely proportional to the square root of its molecular weight. This relationship is called Graham's law of diffusion.

When the membrane pores are extremely small, on the order of 5 to 20 Å, then gases are separated by molecular sieving. Transport through this type of membrane is complex and includes both diffusion in the gas phase and diffusion of adsorbed species on the surface of the pores (surface diffusion). These very small pore membranes have not been used on a large scale, but ceramic and ultramicroporous glassy membranes with extraordinarily high selectivities for similar molecules have been prepared in the laboratory (Baker, 2000). Details mathematical description of transport models related with porous membrane can be found in Matsuura (1994) and Mulder (1996).

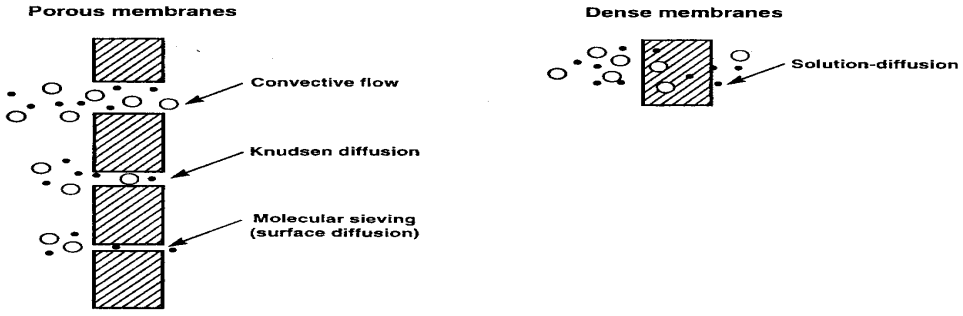

Figure 2.1: Mechanisms for permeation of gases through porous and dense gas separation membranes (Baker, 2000)

Solution-diffusion model

All current commercial gas separation processes are based on the dense polymer membrane. The simplest model used to explain and predict gas permeation through nonporous polymers is the solution-diffusion model as shown in Figure 2.1. In this model it is assumed that the gas at the high-pressure side of the membrane (P_o) dissolves in the polymer and diffuses down a concentration gradient to the low pressure side (p_l). It is further assumed that sorption and desorption at the interfaces is fast compared to the diffusion rate in the polymer. The gas phase on the high- and low-pressure side is in equilibrium with the polymer interface. The permeants are separated because of the differences in the solubility and mobility of the permeants in the membrane material.

Diffusion is the process by which matter is transported from one part of a system to another by a concentration gradient. At steady state, gas diffusion through dense (nonporous) polymeric membrane can be described by Fick's first law. Fick's first law of diffusion states:

$$j_i = -D_{if}\frac{dc_i}{dl} \tag{2.1}$$

where D_{if} is the gas diffusivity coefficient of component *i.* Generally, D_{if} is a function of temperature and the penetrant concentration C_i for a given polymer-penetrant system. For noncondenseable gases, D_{if} is normally regarded as constant, i.e., independent of concentration. For condensable gases, it is generally considered concentration dependent due to the plasticizing effect of the penetrant, swelling of the polymer membrane or interaction leading to morphological changes (Paul and Yampol'skii, 1994). D_{if} reflects the mobility of the individual molecules in the membrane material.

For a membrane thickness of *l*, integration of Eq. 2.1 over the membrane thickness gives

$$j_i = \frac{D_{if}\left(c_{i_{o(m)}} - c_{i_{l(m)}}\right)}{l} \tag{2.2}$$

Solubility gives a measure of the amount of penetrant sorbed by the membrane under equilibrium conditions. The concentration of component *i* at the feed interface of the membrane can be written according to Henry's law as

$$c_{i_{o(m)}} = K_i \; P_{i_o} \tag{2.3}$$

where K_i is the sorption coefficient of component *i.* It reflects the number of molecules dissolved in the material. Sorption coefficient is a function of temperature and may be function of pressure (or concentration). Henry's law is valid when K_i is independent of ambient pressure and penetrant concentration is directly proportional to ambient pressure.

The concentration of component *i* at the membrane-permeate interface can similarly be expressed as

$$c_{i_{l(m)}} = K_i \; p_{il} \tag{2.4}$$

Combining Eqs. 2.3 and 2.4 with Fick's law, Eq. 2.2, gives

$$j_i = \frac{D_{if} \; K_i \left(P_{i_o} - p_{i_l} \right)}{l} \tag{2.5}$$

The product $D_{if}K_i$ can be defined as P_i, which is called the *membrane permeability* and is a measure of the ability of the membrane to *permeate* gas. The measure of the ability of a membrane to *separate* two gases *i* and *j* is the ratio of their permeabilities α_{ij}, called the *membrane selectivity*

$$\alpha_{ij} = \frac{\mathrm{P}_i}{\mathrm{P}_j} \tag{2.6}$$

Eq. 2.5 can be written as

$$j_i = \frac{\mathrm{P}_i \left(P_{i_o} - p_{i_l}\right)}{l} \tag{2.7}$$

Eq. 2.7 is widely used to accurately and predictably rationalize the properties of gas permeation membranes. The solution-diffusion model described above can be utilized to elaborate relationship between polymer structure and membrane permeation. Excellent reviews on relationships between polymer structure and transport properties of gases have been given by Stern (1994), Freeman (1999) and Baker (2000).

2.5 Membrane Module Configurations

Large membrane areas are normally required in industrial scale separation processes. The unit into which membrane area is packed is called a module. The development of the technology to produce low-cost membrane modules was one of the breakthroughs that led to commercial membrane processes in the 1960s and 1970s (Baker, 2000). Based on flat and tubular type of membrane configurations, different module designs are possible. Schematic drawings of all membrane module types are presented in Figure 2.2. Plate-and-frame and spiral-wound modules involve flat membranes whereas tubular, capillary and hollow fibre modules are based on tubular membrane configurations. The differences between tubular, capillary and hollow fibre modules are their tubes' dimensions as shown in Table 2.1.

Table 2.1: Approximate dimensions of tubular membranes (Mulder, 1996)

Configuration	Diameter (mm)
Tubular	> 10.0
Capillary	0.5 – 10.0
Hollow fibre	< 0.5

Plate- and frame modules were one of the earliest types of membrane system. The spiral-wound module is the next logical step from a flat membrane. It is in fact a plate-and-frame system wrapped around a central collection pipe, in similar fashion to a

sandwich roll. Membrane and permeate-side spacer material are then glued along three edges to build a membrane envelope. The feed side spacer separating the top layer of the two flat membranes also acts as a turbulence promoter. Hollow-fibre membrane modules are usually formed in two basic geometries as shown in Figure 2.2. The first is the shell-side feed design and the second is the bore side feed design. In the shell-side feed design, only one active tubesheet is needed for permeate removal from fibre bores. Although the design is simple and module assembling is straightforward, arrangement must be made to pack the fibres properly in order to achieve uniform flow distribution. On the other hand, bore side feed design requires two active tubesheets, one at each end of the fibres. A more even flow distribution of feed on the membrane surface is achieved in the latter case which ultimately favours efficient operation, and also as the pressure at the shell side is substantially low, the mechanical strength requirement to the shell casing of the permeator is minimized. Only the fibre wall and the end capes of the membrane device are pressurized. But when the pressurized gas stream moves to or from the fibre bores, both tubesheets are under significant compressive and shear stresses. Therefore, the bore-side feed permeator design is more complicated than the shell-side feed design because of the problems associated with supporting the tubesheets (Feng et al., 1999).

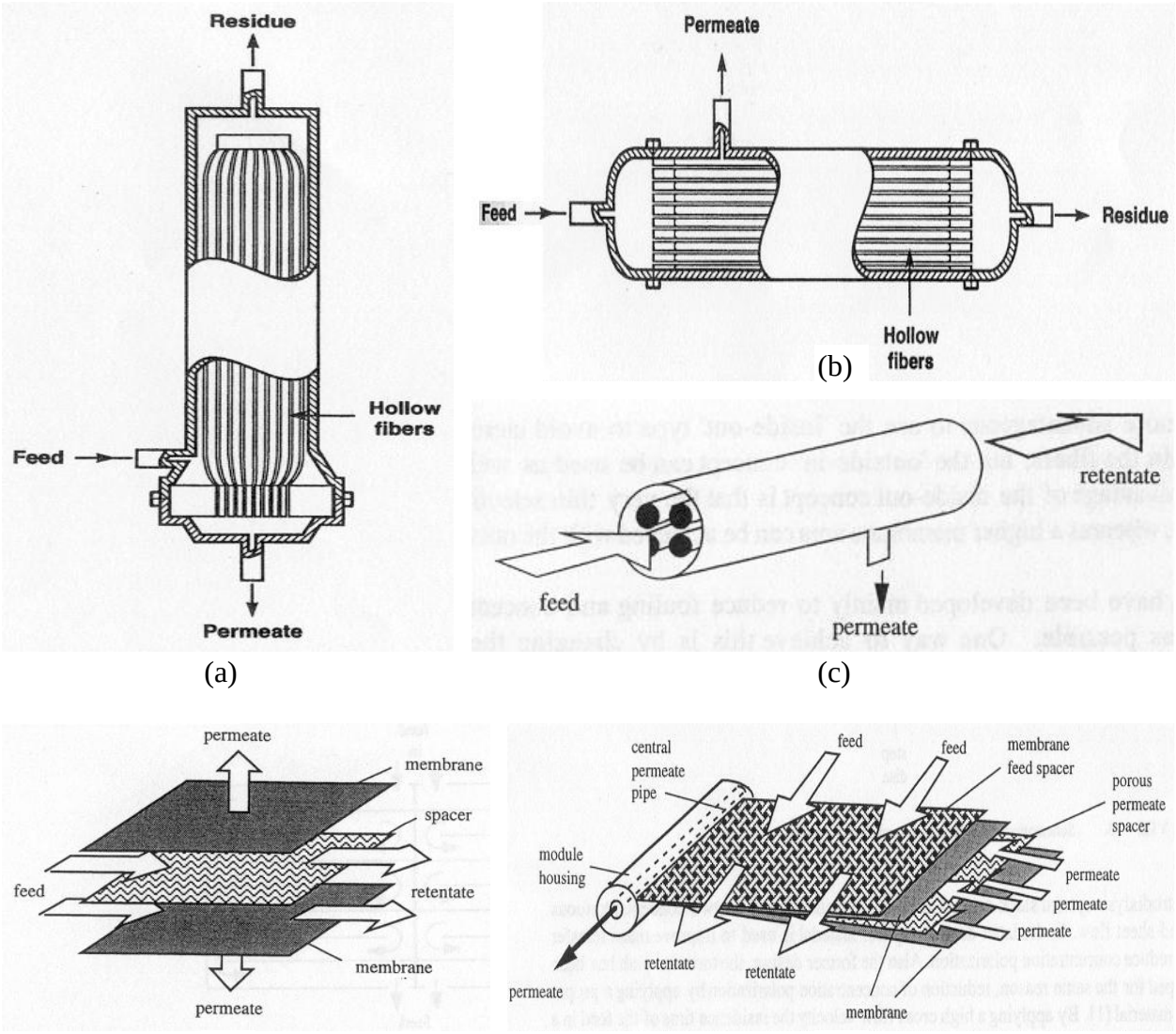

Figure 2.2: Schematic drawing of (a) Hollow fibre module for shell-side feed, (b) Hollow fibre module for bore-side feed, (c) Tubular module, (d) Plate-and-frame module, and (e) Spiral-wound module (Source: Baker, 2000; Mulder, 1996)

A majority of the gas separation membranes are formed into spiral-wound or hollow-fibre modules. The choice of the most suitable membrane module type for a particular membrane separation must balance a number of factors. The principal module design parameters that enter into the decision are summarized in Table 2.2.

Table 2.2: Parameters for membrane Module Design (Baker, 2000)

Parameter	**Hollow fibres**	**Capillary fibres**	**Spiral-wound**	**Plate & frame**	**Tubular**
Manufacturing cost ($/m^2)	2-10	5-50	5-50	50-200	50-200
Concentration polarization/fouling control	Poor	Good	Moderate	Good	Very good
Permeate-side pressure drop	High	Moderate	Moderate	Low	Low
Suitability for high-pressure operation	Yes	No	Yes	Marginal	Marginal
Limitation to specific types of membrane material	Yes	Yes	No	No	No

Membrane fouling is generally more easily controllable in gas separation than in liquid separation. Particulate matter, oil mist, and other potentially fouling materials can be completely and economically removed from gas streams by good-quality coalescing filters. Therefore, the choice of module design is usually decided by cost and the concentration polarization effects in the particular application. The effect of concentration polarization in gas separation processes is assumed to be small because of the high diffusion coefficients of gases. However, the volume flux of gas through the membrane is also high, so concentration polarization effects are still important for several processes (Baker, 2000). High-flux, highly selective membranes are the most susceptible to concentration polarization effects. Because spiral-wound or bore side feed capillary modules offer good control of gas flow across the membrane surface, these module designs are preferred for this type of membrane. If the membrane flux is relatively low and the selectivity is modest, such as in the separation of nitrogen from air, concentration polarization effects are much less significant. In this case hollow-fibre modules are preferred. These modules have relatively poor control over gas flow across the membrane surface and are much more susceptible to concentration polarization effects (Baker,

2000). However, their cost per unit membrane area is significantly lower than that for equivalent spiral-wound modules. Due to its large membrane area per separator volume, along with ease of construction and self-supporting feature, the hollow fibre is a very desirable configuration as far as the overall performance and economical feasibility of membrane process are concerned. Most of today's gas separation membranes are formed into hollow fibre modules, with perhaps fewer than 20% being formed into spiral-wound modules as shown in Table 2.3 (Baker, 2002). But it is also true that, the ease of flat membrane preparation, low pressure build-up of the permeate stream, and low pressure loss of the feed stream promote the popularity of spiral wound membranes in current separator designs (Koros and Chern, 1987; Baker, 2002).

Table 2.3: Principal gas separation markets, producers, and membrane systems (Baker, 2002)

Company	**Principal markets/ estimated annual sales**	**Principal membrane material used**	**Module type**
Permea (Air Products) Medal (Air Liquide) IMS (Praxair) Generon (MG)	Large gas companies Nitrogen/Air ($75 million/year) Hydrogen separation ($25 million/year)	Polysulfone Polyimide/polyaramide Polyimide Tetrabromo polycarbonate	Hollow fibre
GMS (Kvaerner) Separex (UOP) Cynara (Natco)	Mostly natural gas separations Carbon dioxide/methane ($30 million/year)	Cellulose acetate	Spiral-wound Hollow fibre
Aquilo Parker-Hannifin Ube GKSS Licensees MTR	Vapor/gas separation, air dehydration, other ($20 million/year)	Polyphenylene oxide Polyimide Silicone rubber	Hollow fibre Plate-and-frame Spiral-wound

2.6 Hollow Fibre Membrane Module Modeling

For the current study as well as for many modeling studies in the literature, hollow-fibre membrane modules are the focus of the modeling efforts due to much higher packing densities and widespread industrial uses for membrane-based gas separations. Knowledge of changes that occur in process parameters due to permeation is essential in the design of hollow fibre membrane modules. The mode of operation of the membrane module holds practical importance. For understanding the quantitative behavior of such a

system, mathematical analysis and model simulation are important. For instance, the steady state modeling of a gas membrane separator can be utilized:

- to study and investigate the effect of various operating conditions on the process behavior,
- to scale up from pilot plant to large-scale units and to design commercial scale modules,
- to conduct process optimization in order to determine the optimum values of the process operating conditions, and
- to investigate alternative processes using process simulator

The issue of mathematical modeling for membrane gas separators was first addressed by Weller and Steiner (1950). Since then, various models for gas separation permeators have been proposed in the literature and only the important developments are referenced here. Various mathematical models and calculation methods for the symmetric membranes and high-flux asymmetric membranes have been reported in the literature with different flow and module configurations. Most of the models deal with binary systems (Pan, 1983; Chern et al., 1985; Bouclf et al., 1986; Haraya et al., 1988; Sidhoum et al., 1988; Tranchino et al., 1989; Giglia et al., 1991; Lee & Hwang, 1992; Thundyil & Koros, 1997; Kaldis et al., 1998; Feng et al., 1999; Lababidi, 2000; Wang et al., 2002; Lim et al., 2000; Takaba and Nakao 2005; Bouton and Luyben 2008) and few of them deal with ternary or multicomponent gas separation systems with or without consideration of the pressure build-up inside the fibre lumen (Shindo et al., 1985; Pan, 1986; Sengupta & Sirkar, 1987; Li et al., 1990; Kovvali et al., 1994; Peterson & Lien, 1995; Li et al., 1995; Tessendorf et al., 1996; Lie & Teo, 1998; Coker et al., 1998; Tessendorf et al., 1999; Kaldis et al., 2000; Marriott et al., 2001; Marriot and Sørensen 2003a; Katoh et al., 2011). Methods of solution for the model equations differ in each paper depending on specific applications, including trial and error shooting technique, series (linear) approximations, finite difference with iterative approach, finite element, orthogonal collocations, etc. Permeator models for binary gas mixture separation are presented first, and followed by multicomponent separator models.

Pan (1983) reported a mathematical model for predicting the performance of a permeator with asymmetric membrane for a binary gas mixture. The model considered

the permeate pressure drop and was applicable to both hollow-fibre and spiral wound modules. The effect of permeate-feed flow pattern on module performance was analyzed. The mathematical model was verified by large-scale pilot-plant experiments for helium recovery from natural gas using large hollow-fibre module.

Chern et al. (1985) developed a model for simulating the performance of an isothermal hollow-fibre gas separator for binary gas mixtures. The model took into account permeate pressure build-up and concentration dependence of the permeabilities by using the dual-mode sorption and transport models. The effects of possible penetrant competition according to the generalized dual-mode model were examined. They presented the effects on separator performance caused by changes in fibre dimensions, feed pressure, membrane area, feed composition, and feed flow rate. They discussed about a triple-separator arrangement for the separation of a 12%/88% CO_2/CH_4 mixture to illustrate how the results of single-stage studies could be readily extended to multistage design consideration. Direct experimental verification had not been reported.

Pettersen and Lien (1995) studied theoretically the intrinsic behavior of several single-stage and multi-stage permeator systems using an algebraic design model which does not account for permeate side pressure build-up for separating a binary mixture.

Thundyil and Koros (1997) presented and analyzed theoretically a new approach to solve the mass transfer problem posed by the permeation process in a hollow fibre permeator for radial crossflow, countercurrent, and cocurrent flow patterns. They dealt with binary separations. The new approach based on finite element was named as "Succession of States method". Although they claimed that this approach can easily handle incorporation of pressure, composition and temperature dependent permeability, there was no experimental validation.

Feng et al. (1999) investigated integrally asymmetric hollow fibre membranes for air separation to produce nitrogen and oxygen-enriched air. Both bore-side feed and shell-side feed were tested experimentally with cocurrent and countercurrent flow arrangements for a wide range of stage-cuts. They concluded that the bore-side feed countercurrent flow was the most advantageous configuration in the permeator design especially for high stage-cut operations. A mathematical model was developed for this configuration for binary gas mixture separation, and the separation performance was well

predicted by the model. The effects of operating pressure and temperature on the separation performance were also evaluated. A theoretical approach was pursued to formulate the concentration polarisation.

Wang et al. (2002) studied the CO_2/CH_4 mixed gas permeation through hollow fibre membranes permeator. An approach to characterize the true separation performance of hollow fibre membranes for binary gas mixtures was provided based on experiments and simulations. The influences of pressure drop within the hollow fibres, non-ideal gas behavior in the mixture and concentration polarization were taken into consideration in the mathematical model. They obtained calculated CO_2 permeance in a mixed gas permeator close to that obtained in the pure gas tests and they attributed this to the net influence of the non-ideal gas behavior, competitive sorption and plasticization. The CH_4 permeance was higher in the mixed gas tests than that in the pure gas tests, as the plasticization caused by CO_2 dominated the permeation process.

Pan (1986) presented a mathematical model for multicomponent permeation systems with asymmetric hollow-fibre membranes. The model took into account the permeate pressure variation inside the fibre. The driving force for permeation was assumed to be dependent on the local permeate compositions rather than bulk permeate compositions. The solution of the model equations was obtained by iterative method which involves assuming a permeate pressure profile and calculating the area and composition profile. These profiles were used to generate a new pressure profile. This procedure was repeated until all the profiles converge to their respective limits. Multicomponent permeation experiments verified the mathematical model, and demonstrated the technical feasibility of using the high-flux asymmetric cellulose acetate hollow fibre for H_2, CO_2, and H_2S separation.

Li et al. (1990) developed mathematical models for separation of gas mixtures involving three or more permeable components without consideration of pressure drop. The models described the membrane separation process for five different flow patterns of the permeated and unpermeated stream in the permeator theoretically. They discussed the effects of operating variables such as the pressure ratio across the membrane, the stage cut and the flow patterns in the permeator on the extent of separation.

Kovvali et al. (1994) presented a linear approximation model to solve the multicomponent countercurrent gas permeator transport equations considering pressure variation inside the fibre. They assumed a linear relationship between the permeate and feed stream compositions which reduces the computational efforts and also yields analytical expressions for flow rates, permeate pressure, membrane area, and compositions along the length of the permeator. However, their model predictions were not validated by experimental data.

Coker et al. (1998) developed a model for multicomponent gas separation using a hollow-fibre contactor which permits simulation of cocurrent, countercurrent, and cross-flow contacting patterns with permeate purging (or sweep). They followed a stage-wise approach to convert the differential equations to a set of coupled, non-linear differential equations. Although they claimed that their methodology could easily incorporate pressure dependence permeability, they assumed constant permeability in their modeling work. Model validation had not been verified with experimental data.

Tessendorf et al. (1999) developed a model for counter- and crosscurrent membrane modules for multicomponent mixtures and a numerical solution procedure based on orthogonal collocation to solve the differential model equations. They reported that the model considers the effects of pressure drop and energy balance but unfortunately there were no reflection of those considerations in their model equations.

Lim et al. (2000) proposed a new pressure drop equation that had been developed from the continuity equation and the momentum balance equations with the consideration of gas compressibility and fibre permeability. They reported that for the case of negligible permeation flux, the pressure equation reduces to the Hagen-Poiseuille equation. They discussed the effects of design variables such as membrane permeability and fibre radius on the pressure profiles and stage cut obtained from the two pressure models. They concluded theoretically that the use of Hagen-Poiseuille equation will result in either an overestimation or underestimation of the membrane area required at the stipulated stage cut depending on the feed mode operation.

Kaldis et al. (2000) presented a computational method for Pan's (1986) model (modified) based on the orthogonal collocation and validated their model predictions with experimental data for hydrogen recovery from refinery gas. To avoid solution

complexity, they have considered the concentration of the permeate leaving the membrane surface to be identical to that of the bulk permeate stream outside the porous layer, which is considered a major deviation from Pan's (1986) original model. Despite this, their modified model offers a good representation of the operation of a hollow fibre permeator for the case presented.

Marriott et al. (2001) presented another detailed mathematical model of membrane modules for multicomponent gas separation based on rigorous mass, momentum and energy balances, and the orthogonal collocation was the preferred method for solving the partial differential and algebraic equations. The main drawback of this model is that it needs the knowledge of molecular diffusivity and solubility (both are difficult to measure) instead of the permeability or permeance. This is especially the case when asymmetric composite membranes are used. Consequently, the applicability of the model is constrained by the uncertainty in getting such parameters required by the model. Marriot and Sørensen (2003a) extended the work of Marriott et al. (2001) to model also spiral-wound membrane module by following a general approach.

Takaba and Nakao (2005) used computational fluid dynamics (CFD) technique for modeling capillary tube membrane modules without providing detailed descriptions of the models. They used porous ceramic membrane for extracting H_2 from H_2/CO gas mixture in the steam reforming process.

Bouton and Luyben (2008) used a cell model concept to examine the dynamic behavior of a gas permeation membrane process coupled with the hydroalkylation process. Aspen Custom Modeler is used to write and test a dynamic membrane model for use in Aspen Dynamics.

Katoh et al. (2011) developed a simulation model to examine the unsteady-state behaviors of hollow fibre membrane module for multicomponent gas separation. They considered the nonideal mixing flows in permeate and residue sides by using a tanks-in-series model. The relaxation method was applied to solve the governing simultaneous ordinary differential equations.

Table 2.4 presents a list of contributors in the modeling of membrane gas separator systems.

Table 2.4: Contributors in modeling of hollow fibre module for gas separation

Membrane type	Module & flow configuration	Gas mixture	References
Asymmetric	Shell-feed; co- & countercurrent	He/CH_4	Pan, 1983
Asymmetric	Shell-feed	CO_2/CH_4	Chern et al., 1985
Asymmetric & symmetric	Shell-feed; co- & countercurrent	Binary mix.	Bouclf et al., 1986
Asymmetric (Polyimide)	Shell-feed; co- & countercurrent	H_2/CO	Haraya et al., 1988
Asymmetric (Cellulose Acetate)	Shell/Bore side feed; cocurrent & cross flow	CO_2/N_2 & O_2/N_2	Sidhoum et al., 1988
Composite (Aliphatic Copolymer coated polysulfone)	Shell-feed; co- & countercurrent	CO_2/CH_4	Tranchino et al., 1989
Composite	Co- & counter; cross co- & counter	Air & He/N_2	Giglia et al., 1991
Asymmetric (Polyimide)	Shell-feed; co- & countercurrent	C_3H_6/C_3H_8	Lee & Hwang, 1992
General	Shell-feed; radial cross flow, co- & countercurrent	Binary mix.	Thundyil & Koros, 1997
Asymmetric	Shell-feed; countercurrent	Binary mix.	Kaldis et al., 1998
Integrally asymmetric	Shell/Bore-feed; co- & countercurrent	Air	Feng et al., 1999
Asymmetric (Polysulfone)	Bore-feed; co- & countercurrent	Air	Lababidi, 2000
Asymmetric (Polyimide)	Shell-feed; cocurrent	CO_2/CH_4	Wang et al., 2002
Asymmetric (Cellulose Acetate)	Shell-feed; co- & countercurrent	$H_2/N_2/CH_4/Ar$; $CO_2/CH_4/C_2H_6/C_3H_8$; $H_2S/CO_2/CH_4/N_2/C_2H_6$	Pan, 1986
Cellulose Acetate	Shell-feed; cocurrent	$He/CO_2/N_2$	Sengupta & Kirkar, 1987
General	Five flow configurations	Multi Comps.	Li et al., 1990
General	Shell-feed; countercurrent	Multi Comps.	Kovvali et al., 1994
General	Countercurrent	Binary mix.	Peterson & Lien, 1995
Silicone rubber	Bore-feed; co- & countercurrent	$CO_2,/O_2,/N_2$	Li et al., 1995
General	Co- & Countercurrent; Cross	Multi Comps.	Tessendorf et al., 1996
Asymmetric (Polyethersulphone)	Bore-feed; co- & countercurrent	$CO_2,/O_2,/N_2$	Li & Teo, 1998
General	Shell/Bore-feed; co- & countercurrent	Multi Comps.	Coker et al., 1998
General	Co/Counter-& Crosscurrent	Multi Comps	Tessendorf et al., 1999
Polyimide	Shell-feed; co- & countercurrent	$H_2/CH_4/C_2H_6/CO_2$	Kaldis et al., 2000
General	Shell/Bore-feed; countercurrent	Gas/vapor	Lim et al., 2000
General	Shell-feed; Co-/Countercurrent & Cross	Multi Comps.	Marriott et al., 2001
Asymmetric (Cellulose Acetate)	Feed-outside; Countercurrent	CO_2 - Air mix.	Sada et al., 1992
Polyethylene & microporous glass membrane	Co- & countercurrent, cross, perfect & one-side mixing	$NH_3/H_2/N_2$; $H_2/CH_4/CO/N_2/CO_2$	Shindo et al., 1985
Asymmetric (Cellulose Acetate)	Bore-feed; parallel	$H_2/N_2/CH_4/Ar$	Marriot &Sørensen, 2003a
Porous ceramic (capillary tube)	Co-current	H_2/CO	Takaba & Nakao, 2005
General	Cross and counter-current flow	N_2/O_2 H_2/CH_4	Bouton & Luyben, 2008
General	Shell-feed, parallel flow Bore-feed, counter-current	$H_2/N_2/CH_4/Ar$; $N_2/O_2/CO2/H2O$	Katoh et al., 2011

2.7 Membrane Process Design

The economic viability of gas membrane systems can be significantly affected by process design. The process design of a membrane system involves the determination of the system size and the configuration necessary to meet the project scope and specifications. The design of membrane processes can differ significantly due to the application specificity, and module configurations. The module is the heart of any membrane process, often referred as the separation unit. When a number of modules are connected together in series or parallel, it is called a stage. A combination of stages is called a cascade. In membrane process design, the major concern is to find the right module configuration, membrane material, and to determine the required membrane area in each of the membrane modules, as well as the compression/vacuum work needed to operate the system.

The role of membrane module configurations, and the flow patterns of the feed and the permeate streams in the performance of the final separator system has been discussed elsewhere (Pan, 1974; Koros & Chern, 1987; Mulder, 1996; Feng & Ivory, 2000). Besides module configurations, and flow patterns of the feed and the permeate streams, other factors that determine the performance of a membrane gas separation system are: membrane selectivity, pressure ratio, and stage cut. Selectivity is the ratio of the permeabilities of two gases in the mixture, pressure ratio is the ratio of feed pressure to the permeate side pressure across the membrane, and stage cut is the fraction of the feed gas that permeates the membrane. Selectivity directly impacts the recovery of the process and indirectly impacts membrane area and feed gas flow requirements. The relationship between pressure ratio and membrane selectivity is important because of the practical limit of the pressure ratio achievable in gas separation systems. Compressing the feed stream to very high pressure and drawing a very hard vacuum on the permeate side of the membrane to achieve large pressure ratios both require large amounts of energy and expensive pumps. More discussion on pressure ratio and membrane selectivity can be found elsewhere (Baker, 2000). The degree of separation required is the other factor that also affects the membrane system design. Production of a residue stream essentially stripped of the permeable component and a concentrated permeate stream are the usual

target of any gas separation system. It is difficult to achieve these two requirements simultaneously; a trade-off must be made between removal from the feed gas and enrichment in the permeate. This trade-off is generally characterized by stage-cut which is the fraction of the feed gas that permeates the membrane. Because membrane selectivity and pressure ratio achievable in a commercial membrane system are limited, mutistep or multistage or recycle membrane systems must be used depending on the system requirements i.e., high purity or high product recovery etc.

As the number of possible system designs is large, systematic design methods or guidelines are indispensable tools for deriving a close-to-optimal design. Unfortunately, few general design guidelines are currently available for design of membrane permeation processes. In the development of a suitable membrane-based gas separation system, the following phases of the design process are typically observed, which are similar to those for other traditional separation process (Koros & Chern, 1987).

- *Preparation of Flow Diagrams*. First a preliminary schematic is prepared for the proposed process-option being considered. Possible variables are specified on the diagram (temperatures, pressures, flows, etc.). Material balance constraints are fixed by using required outlet purities and key component recoveries.
- *Acquirement of Basic Data*. A scarcity of important design data for a membrane system is often encountered because of the novelty of membrane-based gas separation system. Some tabulated data do exist but not sufficient. Otherwise, membrane manufactures can be of great help for common systems. Some experimental determination of permeabilities is likely to be necessary for unusual systems or novel membranes. Procedures and equipment for determining permeabilities are described elsewhere (Koros & Chern, 1987).
- *Detailed Design Calculations*. Several authors have considered this issue with varying degrees of complexity. Weller and Steiner in 1950 treated this problem first. They considered a simple case assuming that both the feed and permeate streams are well mixed and a negligible recovery of feed occurs. Although this assumption is not valid for practical modern modules, nevertheless, one can use the convenient results for this case even in real separators under conditions of low permeant recovery, since compositional changes are small in these cases. The assumption of perfect mixing

can lead to substantial errors for higher product recoveries, which are typically of practical interest. More detailed treatments of module operation require consideration of a variety of feed-permeate flow patterns, pressure drop etc. Figure 2.3 shows some idealized flow patterns in a membrane gas separator. In general, it has been concluded that countercurrent flow is the most efficient flow pattern, requiring the lowest membrane area and producing the highest degree of separation, at the same operating conditions. The order of separation efficiency for the four flow patterns is countercurrent flow > cross flow > cocurrent flow > perfect mixing (Pan, 1974; Koros & Chern, 1987; Feng & Ivory, 2000).

- *Modification of Preliminary Flow Diagrams*. Most of the time, target product compositions and recoveries cannot be achieved by a single-module process. So, multi-stage or recycle strategies are needed. A considerable literature exist dealing with the potential benefits and energy requirements associated with these approaches. These techniques typically are applied in cases where high recoveries are desired.
- *Economic Evaluation of Chosen Design*. This is very important for judging if the proposed process design is economically viable or not. This part of the project is the same as for any other separation operation. After all flows, compositions, and equipment ratings are known; capital, energy, and other operating costs can be assessed by some formulas.

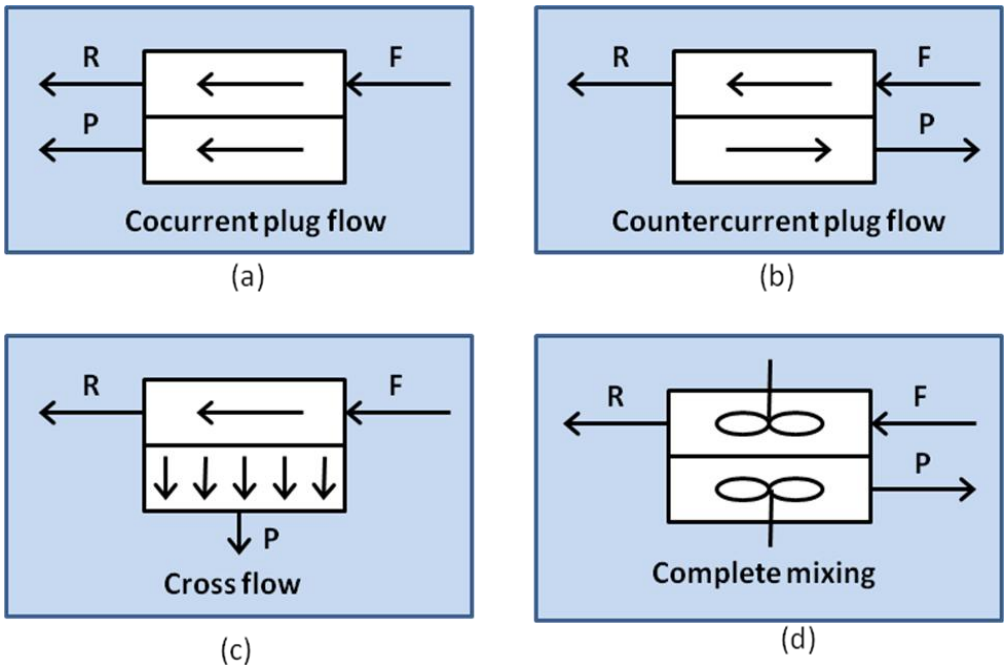

Figure 2.3: Idealized flow patterns in a membrane gas separator

2.8 Membrane Process Optimization

Optimization is the process of improving any existing situation, device, or system such as a chemical process (Turton et al., 2003). The process optimization means "design & operate processes in the best possible way" (Douglas, 2002). Every optimization problem contains three essential categories:

1. At least one objective function (performance criteria) to be optimised (profit or cost function, energy consumption, etc.).
2. Equality constraints (equations)
3. Inequality constraints (inequalities)

Category 1 is sometimes called the economic model which should be minimized or maximized. Categories 2 and 3 constitute the mathematical model of the process or equipment. The mathematical models can be classified as equalities, inequalities and logical conditions. The model equalities are usually composed of mass balances, energy balances, equilibrium relations and engineering relations which describe the physical phenomena of the system. The model inequalities often consist of allowable operating limits, specification on purities, performance requirement and bounds on availability's and demand. The logical conditions provide the connection between the continuous and integer variables. Variables that can be adjusted or be chosen to minimise or maximise the objective function are called decision variables or independent or optimization variables. Variables can be real (e.g., flow rates), integers (e.g., number of fibres) or binary (e.g., yes or no). Mathematically the above mentioned three categories can be represented as:

$\min_{\mathbf{x}} f(\mathbf{x}, \mathbf{p})$	(objective function)
such that,	
$h(\mathbf{x}, \mathbf{p}) = 0$	(equality constraints)
$g(\mathbf{x}, \mathbf{p}) \geq 0$	(inequality constraints)
Where	
$\mathbf{x} \in X \leq R^n$	**x** is a vector of continuous variables
p	**p** is a vector of parameters

Optimization problems can be classified as following types:

i. Linear programming (LP) problems: Objective function and constraints are linear.
ii. Mixed Integer linear Programming (MILP) problems: Objective functions and constraints are linear, involve integer variables in addition to the continuous variables in optimization problem.
iii. Nonlinear programming (NLP) problems: Nonlinear terms in the objective function and constrains exist.
iv. Mixed Integer Nonlinear Programming (MINLP) problems: Nonlinear terms in the objective function and constraints exist, involve integer variables in addition to the continuous variables in optimization problem.

Detailed descriptions of different optimization theory and methods are available elsewhere (Floudas, 1995; Edgar et al., 2001).

Different approaches and methods have been employed to optimise membrane gas separation processes by various investigators with different objective functions consideration (Babcock et al., 1988; Bhide & Stern, 1991a; 1991b; 1993a; 1993b; Bhide et al., 1998; Qi & Henson, 1998a; 1998b; 2000; Agrawal, 1997; Xu & Agrawal, 1996; Agrawal & Xu, 1996a; 1996b). The optimization methods used in most of these studies are: NLP (Non-linear Programming) and MINLP (Mixed-integer Non-linear Programming); and commercial softwares used are: GAMS (General Algebraic Modeling Systems) and OPTISIM (from Linde AG).

Babcock et al. (1988) evaluated the economics of single- and three-stage membrane systems for natural gas treatment by providing comparisons with amine treatment process. Bhide and Stern (1991a; 1991b; 1993a & 1993b) presented detailed case studies of membrane separation systems for natural gas treatment and oxygen enrichment of air by utilizing new optimization variables rather than the usual operating variables; a grid search method was used to optimize the operating conditions for several different configurations. A stepwise procedure for design of membrane cascades using a limited number of recycle compressors is described elsewhere (Agrawal, 1997; Xu & Agrawal, 1996; Agrawal & Xu, 1996a; 1996b). The superstructure optimization approach using MINLP technique is also employed to process design for different membrane

systems by various investigators (Qi & Henson, 1998a; 2000; Kookos, 2002; 2003). This approach provides a systematic framework for simultaneous optimization of the process and operating conditions (Floudas, 1995). A brief overview of the considerable work that has been performed for the systematic synthesis of process flowsheets and corresponding subsystems is available elsewhere (Grossmann & Daichendt, 1996). Sequential procedure is also used for designing membrane system, in which the permeator configurations are chosen a priori, and then best configuration and the operating conditions are determined using some type of optimization procedure (Hao et al., 2002; Spillman, 1989; Lababidi et al., 1996; Hinchlife & Porter, 1997; Qiu et al., 1989).

2.9 CO_2 and Climate Change

Rising of global temperature due to emissions of greenhouse gases resulting from human activity are causing global climate to change. If the global temperatures do rise significantly due to greenhouse effects, there are likely to be a range of repercussions on the planet's natural systems and balance. Ecosystems, agriculture and forestry, and human health are all sensitive to the planet's climate. The main greenhouse gases with climate change potential identified by IPCC (Intergovernmental Panel for Climate Change) are: carbon dioxide (CO_2), methane (CH_4), nitrous oxide (N_2O) and a group of chlorine and fluorine containing gases such as halo carbons (HFC's) perfluorocarbons (PFC's) and sulphur hexafluoride (SF_6). Greenhouse effect refers to the natural phenomenon by which gases in the atmosphere absorb a portion of the earth-radiated heat.

The comparison of the ability of each GHG to trap heat in atmosphere relative to another gas is expressed as Global Warming Potential. Among the greenhouse gases, although CO_2 has the lowest Global Warming Potential, but due to its much higher total emissions than any other greenhouse gases, it has the largest climate change impact on our planet. Since the industrial revolution the concentration of CO_2 has increased globally by 30%. Figure 1 shows a breakdown of global greenhouse gas emissions by each gas in 2000 (EPA website, 2009). As CO_2 accounts for the largest proportion of the greenhouse gases, most current efforts for preventing climate change focus on the strategies for the reduction of CO_2 emissions.

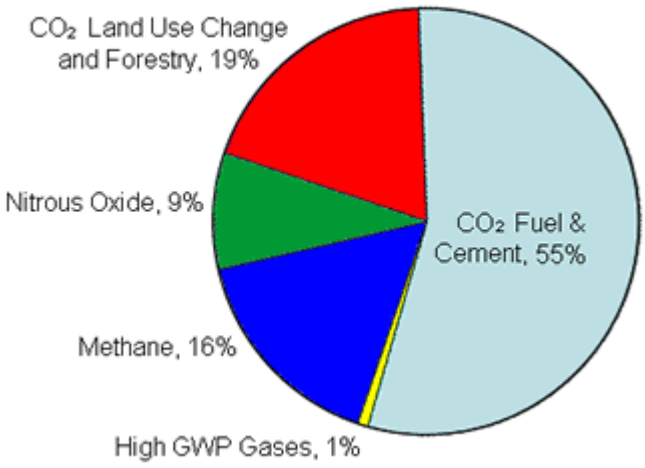

Figure 2.4: Global greenhouse gas emissions by each gas in 2000 (EPA, 2009)

2.10 CO_2 Capture Technologies

As discussed above, the role of carbon dioxide (CO_2) in global warming is one of the most important contemporary environmental issues and it is therefore necessary to have available technologies that minimize the discharge of CO_2 into the atmosphere. Amongst the anthropogenic sources of CO_2, electric power stations utilizing fossil fuels (especially coal and heavy hydrocarbons), petroleum refineries, natural gas plants and certain chemical plants are the largest single-point sources of CO_2 and, therefore, deserve particular attention. In the aforementioned cases, the CO_2 is discharged into the atmosphere in the form of mixtures with other constituents, principally N_2, H_2O vapor, O_2, CO, SO_x, NO_x and/or particulates (Meisen and Shuai, 1997).

Several strategies have been proposed to reduce CO_2 emissions from fossil fuel combustion which include: fuel switching (from higher carbon content to lower carbon content fuels), switching from CO_2 emitting to non-CO_2 emitting sources, improving plant efficiencies, and CO_2 capture and sequestration. There are three process options for CO_2 capture from fossil fuel-fired power stations: pre-combustion, post-combustion, and oxyfuel combustion. Depending on the process, various technologies for CO_2 capture can be used, including absorption, adsorption, membranes, cryogenic, and hybrid applications

of these. The judging criteria are capture effectiveness, process economy, energy consumption, and other technical and operational issues (Plasynski & Chen, 2000).

Chemical Absorption

This method was originally used for removing CO_2 from other gases such as methane, hydrogen, etc. Chemical absorption uses the different reactivities of various gases with sorbents to separate them. The reactions need be reversible so that the spent sorbent can be regenerated. For separating CO_2 from flue gas, chemical absorption appears appropriate because CO_2 is acidic and the majority of the rest of flue gas, N_2, is not. CO_2 can be absorbed by many basic sorbents including alkali carbonate, aqueous ammonia, and alkanolamines. Attention needs to be paid to the regeneration of the sorbents. The binding between sorbent molecules and CO_2 generally is strong and this offers a fast and effective removal of most of CO_2 in one stage of absorption. However, the strong binding between CO_2 and the sorbent molecules is also one of the causes for high regeneration energy requirements. A second concern is the control of impurities and minor components in the flue gas including SO_2, O_2, etc. that may degrade the sorbents. These components have to be removed before the gas enters the absorber, or treated with appropriate measures. Lastly, because many sorbents are corrosive, only diluted solutions (around 30% for MEA) are used. In addition to the regenerator, a reclaiming operation is conducted periodically to recover sorbent by decomposing heat stable salts and to dispose of degradation products. The two chemical absorption processes most commonly applied to remove CO_2 from flue gases are the monoethanol amine (MEA) process and the activated potassium carbonate process (Plasynski & Chen, 2000).

Physical Absorption

In physical absorption, the gas CO_2 molecules are dissolved in a liquid solvent, and no chemical reaction takes place. The binding between the CO_2 molecules and solvent molecules, being either Van der Waals type or electrostatic, is weaker than that of chemical bonds in chemical absorption. The amount of gas absorbed is linearly proportional to its partial pressure (Henry's law). Thus the physical absorption is more effective when the partial pressure of the gas to be absorbed is high. The amount of gas absorbed also depends on temperature. The lower the temperature the more the gas is

absorbed. The desorption can be achieved either by lowering pressure as in the pressure swing absorption (PSA), or raising the temperature as in the temperature swing absorption (TSA). Physical absorption has been used in gas production processes to separate CO_2 from hydrogen and CO. These processes include: Rectisol® that uses cool methanol as solvent, Selexol® that uses dimethyl ether of polyethylene glycol (DMPEG), Sepasolv that uses n-oligoethylene glycol methyl isopropyl ethers (MPE), Purisol that uses N-methyl-2-pyrrolidone (NMP), and Gaselan that uses N-methylcaprolactam (NMC) (Plasynski & Chen, 2000). The application of Physical absorption method looks promising for capturing CO_2 from IGCC power plant flue gas (O'Keefe, 2001).

Physical Adsorption

In physical adsorption, gas is adsorbed on the solid surface by a Van der Waals force. Most important adsorbents are activated carbon, zeolite, silica gel, and aluminium oxide. The separation is based on the difference in gas molecule sizes (Steric Effect), or different binding forces between gas species and the adsorbent (Equilibrium Effect or Kinetic Effect). Like physical absorption, two types of processes: Pressure Swing Adsorption and Temperature Swing Adsorption are used. Because the gas molecules are attached on the solid surface and form mono or multi-layers in physical adsorption, the gas loading capacity could be lower than in physical absorption, even though many adsorbents have large surface area per unit volume. Because of the large volume of CO_2 in the flue gas, it appears physical adsorption might not be an effective and economical solution for separating CO_2 from flue gas. The other limit in using physical adsorption for this purpose is the low gas selectivity of available sorbents. However, in combining with other capture methods, physical adsorption may become attractive. Such applications include membrane technologies.

Membrane Separation

Two types of promising membrane technologies can be used for separating CO_2 from flue gas:

***Gas Separation Membranes*:**

As already discussed in the previous sections, the separation of species in case of gas separation membranes relies on a difference in physical or chemical interaction

between components present in a gas mixture with the membrane material, causing one component to permeate faster through the membrane than another. Usually the separation can be explained by a solution-diffusion mechanism, i.e., the gas component dissolves into the membrane material and diffuses through it to the other side. Both solution and diffusion determine the separation of species. The driving force for the permeation through the membrane is a difference in partial pressure between the feed side and the permeate side. Membrane separation of CO_2 from light hydrocarbons has met with considerable success in the petroleum, natural gas and chemical industries because of the inherent simplicity resulting from steady state operation, absence of moving parts and modular construction (Meisen and Shuai, 1997). Gas separation membranes have thus far not been widely explored for CO_2 capture from flue gases due to the comparatively high mixture flows and the need for flue gas pressurization.

***Gas Absorption Membranes*:**

Gas absorption membranes consist of microporous solid membranes in contact with a liquid absorbent. Liquid sorbent is used to carry away CO_2 molecules that diffuse through the membranes. In this technology, the membrane serve as an interface between the feed gas and liquid sorbent. Some investigators (Feron & Jenson, 1995; Feron et al., 1992; Nishikawa et al., 1995; deMontigny et al., 2006a; 2006b; Franco et al., 2008; Khaisri et al., 2010; 2011) considered gas absorption membranes for CO_2 capture from flue gases and found them to be promising but still requiring considerably more research.

Cryogenic Separation

Cryogenic separation of gas mixture uses the difference in boiling points of various gas species to separate them. Cryogenic separation of gas mixtures involves compressing and cooling the gas mixtures in several stages to induce phase changes in CO_2 and, in the case of flue gases, invariably other mixture components. Cryogenic processes are inherently energy intensive although high recovery of CO_2 is achievable through this process (Plasynski & Chen, 2000). The most promising applications for cryogenics are expected to be for separation of CO_2 from high-pressure gases, such as in pre-combustion capture processes, or oxyfuel combustion in which the input gas contains a high concentration of CO_2.

2.11 MEA Process for CO_2 Capture

Most commercial CO_2 capture plants use processes based on chemical absorption with a monoethanolamine (MEA) solvent until to date. MEA is an organic chemical belonging to the family of compounds known as amines. It was developed 70 years ago as a general non-selective solvent to remove acid gases, such as CO_2 and H_2S from natural gas stream. The process was then modified to treat flue gas streams. Separation and capture of CO_2 from flue gas stream of power plants started in the 1970s as a potential economic source of CO_2 for different applications such as enhanced oil recovery (EOR) but did not start with concern about the greenhouse effect. Fluor Daniel Inc., Dow Chemical Co., ABB lummus Crest Inc., and Kerr-McGee Chemical Corp. were few of the initial developer of MEA-based technology for CO_2 capture (Herzog, 1999; Rao and Rubin, 2002). MEA-based technology can capture more than 95% of the CO_2 from flue gases to yield a fairly pure (>99%) CO_2 product stream.

Flue gas from power plant is first treated to reduce the levels of particulates and other impurities present, pressurized to overcome the pressure losses in the downstream processing section, and cooled before sending to absorption tower (absorber). Cooled flue gases flow vertically upwards through the absorber countercurrent to the absorbent (MEA solution, with some additives). The MEA reacts chemically with the CO_2 in the flue gases to form a weakly bonded compound (carbamate). The scrubbed gases are then washed and vented to the atmosphere. The CO_2-rich solution leaves the absorber and passes through a heat exchanger, then further heated in a reboiler using steam. The weakly bonded compound formed during absorption is broken down by the application of heat, regenerating the sorbent, and producing a concentrated CO_2 stream. The hot CO_2-lean sorbent is then returned to the heat exchanger, where it is cooled, then sent back to the absorber. Some fresh MEA is added to make up for losses incurred in the process. The CO_2 product is separated from the sorbent in a flash separator, and then taken to the drying and compression unit. It is compressed to very high pressures so that it is liquefied and transported to long distances to the designated storage or disposal facility or it may be utilized for different applications. A schematic of amine (MEA) process for CO_2 capture from power plant flue gas is presented in Figure 2.5.

Aqueous solutions of MEA absorb CO_2 by chemical reactions. The chemistry is quite complex, but the main reactions taking place in the absorber and stripper can be represented as follows (Sander and Mariz, 1992):

CO2 Absorption: $2\ R\text{-}NH_2 + CO_2 \rightarrow R\text{-}NH_3^+ + R\text{-}NH\text{-}COO^-$ (2.1)

MEA Regeneration: $R\text{-}NH\text{-}COO^- + R\text{-}NH_3^+ + (Heat) \rightarrow CO_2 + 2\ R\text{-}NH_2$ (2.2)

Pure MEA (with R = $HO\text{-}CH_2CH_2$) forms a weakly bonded intermediate called "carbamate" which is fairly stable. Only half a mole of CO_2 is absorbed per mole of amine, as shown in the CO_2 absorption equation above. On application of heat, this carbamate dissociates to give back CO_2 and amine sorbent, as shown in the second equation above. Since the carbamate formed during absorption is quite stable, it takes lot of heat energy to break the bonds and to regenerate the sorbent.

Although MEA-based absorption process is the most suitable technology available for captureing CO_2 from power plant flue gases commercially, it has its own limitations. As mentioned above, one of the major drawbacks is excessive energy penalty due to regeneration of the solvent. The other two factors are corrosion and loss of solvent. Corrosion control is very important in amine systems due to processing of oxygen-containing flue gases. In order to reduce corrosion rates, corrosion inhibitors, lower concentrations of MEA, appropriate materials of construction and mild operating conditions are required (Barchas and Davis, 1992). Some of the sorbent is lost during the process because of a variety of reasons including mechanical, entrainment, vaporization and degradation. All the sorbent entering the stripper does not get regenerated. Flue gas impurities, especially oxygen, sulfur oxides and nitrogen dioxide react with MEA to form heat-stable salts, thus reducing the CO_2-absorption capacity of the sorbent. The heat-stable salts that are formed may be treated in a side stream MEA-reclaimer, which can regenerate some of the MEA (Rao and Rubin, 2002)

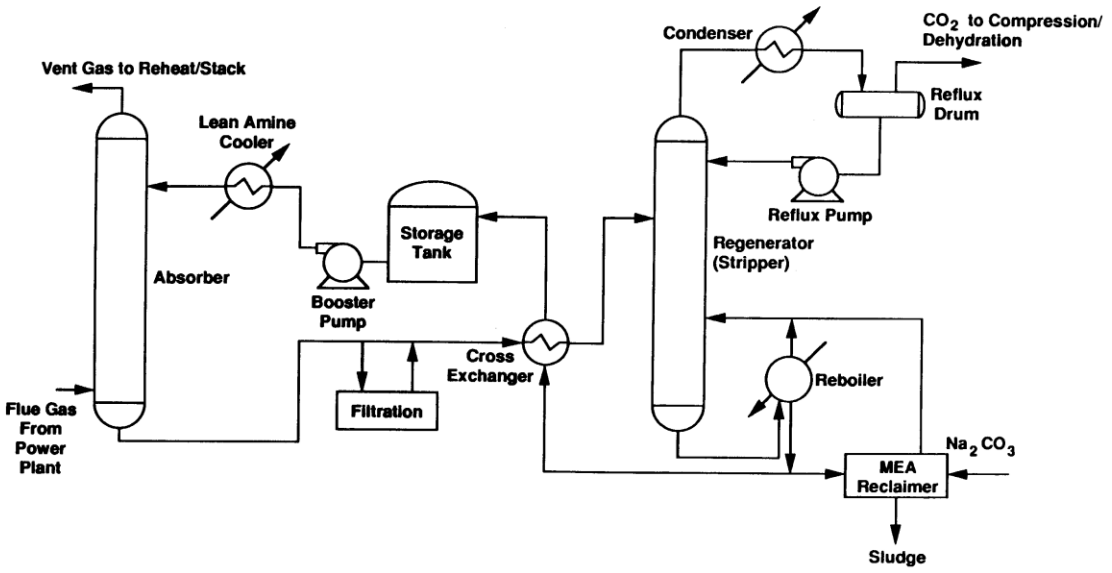

Figure 2.5: Schematic of Amine Capture Process (Herzog & Golomb, 2003)

2.12 CO_2 Storage and Usage

After capturing CO_2 from industrial processes in order for it to be an effective climate change mitigation solution, it must be stored safely and securely away from the atmosphere or it should be utilized. Various forms have been conceived for permanent storage of CO_2. These forms include gaseous storage in various deep geological formations (including saline formations and exhausted gas fields), liquid storage in the ocean, and solid storage by reaction of CO_2 with metal oxides to produce stable carbonates. Geological storage involves injecting carbon dioxide, generally in supercritical form, directly into underground geological formations. Oil fields, gas fields, saline formations, unminable coal seams, and saline-filled basalt formations have been suggested as storage sites. Liquid storage in the ocean can be implemented in two ways. In one way CO_2 is injected into the water column to a depth of 1000 m or more where it might be dispersed or induced to form a sinking plume. Another way of storing in deep ocean is by injecting CO_2 as a liquid denser than water at a 3000 m or more depth, where it is deposited on a sea floor (Freund, 1999). Carbon sequestration by reacting naturally occurring Mg and Ca containing minerals with CO_2 to form stable carbonates is also considered as another option of CO_2 storage.

Captured CO_2 in different forms (i.e., gas, solid and liqiud) can be utilized in different applications. Large quantities of CO_2 are used as a raw material in the chemical process industry, especially for methanol and urea production. It is also used to carbonate soft drinks, and to prevent fungal and bacterial growth. Liquid carbon dioxide is a good solvent for many organic compounds. It is used to de-caffeinate coffee. The cooling and freezing of food, especially ice cream, meat products, and frozen foods, is the main user for both solid and liquid CO_2. Carbon dioxide is used on a large scale as a shield gas in welding, where the gas protects the weld puddle against oxidation by the surrounding air. Carbon dioxide is used in metals industry in the manufacture of casting moulds to enhance their hardness. Carbon dioxide can also be utilized to produce micro algae biomass production.

CO_2 captured from industrial flue gases, such as power plants, can be utilised to enhance oil recovery (EOR) and to enhance coal bed methane recovery (ECBM). Using EOR, 30-60 %, or more, of the reservoir's original oil can be extracted compared with 20-40% using primary and secondary recovery (DOE, 2008; Stevens et al., 1999).

2.13 Commercial Process Simulators

The simulation of a process allows the engineer to evaluate the influence of the variables in the process, to evaluate new configurations and make the optimization. Process simulation is not just for experts anymore. Although its use has been broadening for some time, current developments in simulators are making them more amenable to general application in chemical engineering. Today, a wide variety of software directed at process engineering is available. Among the more commonly used process modeling and simulation software in the chemical industry are systems from Aspen Technology Inc. (AspenTech), Simulation Sciences Inc. (SimSci), Hyprotech; and Chemstations Inc. Steady state simulator, such as AspenPlus^{TM} from AspenTech, has applications in a wide range of areas. Among them are investigating alternative process flow sheets in R&D, optimizing plant and process schemes in design work, improving yield and throughput of existing plants, and training operators.

Most of the commercial process simulators have built-in process models and optimizer toolbox, thus offering a convenient and time saving means of examining an

entire process. Two types of process simulator software are available. In one type, the process model comprises a set of equations so that the process model equations form the constraints for optimization. This type is known as an *equation-oriented* process simulator. The equations can be solved simultaneously by Newton's method or by employing sparse matrix techniques to reduce the extent of matrix manipulations (Edgar et al., 2001). Three of the better known equation-based codes are Aspen Custom Modeler (Aspen Technology), ASCEND (Wester-berg) and OPTISIM (Linde AG). Equation-based codes such as DMCC and RT-OPT Modeler (Aspen Technology) and ROMEO (Simulation Sciences) dominate closed-loop, real-time optimization applications. On the other hand, the process can be represented on a flowsheet by a collection of modules (a modular-based process simulator) in which the equations (and other information) representing each subsystem or piece of equipment are coded so that a module may be used in isolation from the rest of the flowsheet and hence portable from one flowsheet to another. Examples of modular-based simulator are ASPEN PLUS (Aspen Technology), HYSYS (Hyprotech, acquired now by AspenTech Inc.), ChemCAD (Chemstations), PRO/II (Simulation Sciences), and Batch Pro and Enviro Pro Designer (Intelligen). Combination of equations and modules can also be used (Edgar et al., 2001).

2.14 Economic Analysis

The term economics refers to the evaluation of capital costs and operating costs associated with the construction and operation of a chemical process/plant. The economic assessment of a given separation process depends on the method of analysis used and on the values assigned to the selected economic parameters. Therefore, economic assessments made by different evaluators may differ considerably from each other. Nevertheless, such differences can be informative if the methodology used in economic assessments is clearly described. The details of engineering economic analysis of chemical processes are available elsewhere (Peter et al., 2003; Turton et al., 2003; Biegler et al., 1997)

2.14.1 Capital Costs

This represents all of the expenses made at the beginning of the plant life. Various methods can be employed for estimating capital investment. The choice of any one

method depends upon the amount of detailed information available and the accuracy desired. Several methods are outlined elsewhere (Peter et al., 2003). This study estimates the total capital investment based on the percentage of delivered/purchased equipment cost. Capital investment can be divided into two categories namely fixed capital investment (the capital needed to supply the necessary manufacturing and plant facilities) and the working capital (for the operation of the plant). Fixed capital investment may be further subdivided into direct (manufacturing) and indirect (nonmanufacturing) costs. Direct costs include the costs for following items: purchased equipment, purchased-equipment installation, instrumentation and controls, piping, electrical installations, building (including services), yard improvements, service facilities and land. Indirect costs include the costs for engineering and supervision, construction expenses, contractor's fee and contingency. After plant construction, there are quite frequent changes that have to be made before the plant can operate at maximum design conditions. Capital for these startup changes should also be the part of any capital investment.

2.14.2 Operating Costs

The capital investment is only one part of a complete cost estimate. Another equally important part is the estimation of costs for operating the plant which is generally divided into the categories of manufacturing costs and general expenses. All expenses directly connected with the manufacturing operation or the physical equipment of the process plant are included in the manufacturing costs. These expenses can be divided into the following three classifications: direct production costs, fixed charges and plant-overhead costs. Direct production costs include expenses directly associated with the manufacturing operation such as expenditures for raw materials, supervisory and operating labor, plant maintenance and repairs, operating supplies, royalties, etc. Fixed charges include depreciation, property taxes, insurance and rent which remain practically constant and do not very widely with changes in production rate. Plant-overhead costs include hospital and medical services, safety services, payroll overhead, restaurant and recreation facilities, etc. In addition to the manufacturing costs, other general expenses involved are administrative expenses, R&D expenses, etc.

Chapter 3

A New Numerical Approach for a Detailed Multicomponent Gas Separation Membrane Model

3.1 Introduction

The application of mathematical modeling to the design of membrane processes is an important issue to be considered, and hollow fiber membrane modules have been the focus of the modeling efforts due to their high packing densities and widespread industrial uses for membrane-based gas separations. A detailed model of hollow fibre membrane module and a robust, reliable and flexible method for solving the model can provide useful guidelines to achieve desirable separations of multicomponent gas mixtures. Combination of these two can also be utilized for detailed design and optimization studies of membrane-based gas separation systems. Chapter 2 has reported in details various mathematical models and calculation methods for hollow fibre module with different flow configurations for symmetric and high-flux asymmetric membranes available in the literature.

Among the multicomponent gas separation models available so far in the literature, Pan's (1986) model is widely accepted as the most practical representation of multicomponent gas separation in hollow fiber asymmetric membranes. However, the solution technique is complicated and requires initial estimates of the pressure and concentration profiles along the fiber. To overcome this mathematical complexity, different modifications and different approaches to solve the model equations have been proposed [Kovvali et al., 1994; Coker et al., 1998; Kaldis et al., 2000; Marriott et al., 2001; Marriott and Sørensen, 2003a, Katoh et al., 2011). Kovvali et al. (1994) adopted a linear approximation method to represent the feed and permeate compositions at certain intervals along the fiber length. Coker et al. (1998) presented a model for multicomponent gas separation using hollow fiber contactor, and proposed a stage-wise approach using the first order finite difference method to develop a set of equations from the differential mass balances. This method requires an initial guess of the component flow rates at each stage. Experimental validation of the method and the sensitivity of the technique to initial estimates are not presented. Kaldis et al. (2000) developed a model based on Pan's (1986) initial

theoretical formulation and a computational method was presented on the basis of the orthogonal collocation. The model predictions were validated with experimental data for hydrogen recovery from refinery gas. To avoid the solution complexity, they considered the concentration of the permeate leaving the membrane surface to be identical to that of the bulk permeate stream outside the porous layer, which is a major deviation from Pan's (1986) original model. Despite this, their modified model offers a good representation of the operation of a hollow fiber permeator for the case presented. Marriott et al. (2001) presented a detailed mathematical model for hollow fibre module for multicomponent gas separation based on rigorous mass, momentum and energy balances, and the orthogonal collocation method was preferred for solving the partial differential and algebraic equations. A challenge of this model is that in addition to membrane permeance or permeability, it also requires the knowledge of diffusion and dispersion coefficients in the fluid phase. It is difficult to describe accurately the mass transfer in the porous substrate because the membrane structure in asymmetric membranes can hardly be defined precisely. Consequently, the applicability of the model is constrained by the uncertainty in getting such type of parameters required by the model. They validated their model predictions by the experimental data of Pan (1986), and a good agreement was reported. However, it was not clear from their work what values of other parameters were used in the model validation as only membrane permeability data are available from Pan's (1986) work. Marriot and Sørensen (2003a) extended the work of Marriott et al. (2001) to model also spiral-wound membrane module by following a general approach.

Takaba and Nakao (2005) used computational fluid dynamics (CFD) technique for modeling capillary tube membrane modules without providing detailed descriptions of the models. They used porous ceramic membrane for extracting H_2 from H_2/CO gas mixture in the steam reforming process.

Bouton and Luyben (2008) studied the optimum economic design and control of a gas permeation membrane coupled with the hydroalkylation process using a cell model. Aspen Custom Modeler is used to write and test a dynamic membrane model for use in Aspen Dynamics without considering pressure drop in the permeate side for cross-flow membrane flow configuration.

Katoh et al. (2011) recently proposed a simulation model to examine the unsteady-state behaviors of hollow fibre membrane module for multicomponent gas separation. They

considered the nonideal mixing flows in permeate and residue sides by using a tanks-in-series model. The relaxation method was applied to solve the governing simultaneous ordinary differential equations. It was found that effects of mixing degree in the feed side is more significant as compared with that in the permeate side.

This chapter presents a new numerical solution approach for a widely accepted model developed earlier by Pan (1986) for multicomponent gas separation by high-flux asymmetric membranes. The advantage of the new technique is that it can be incorporated into commercial process simulators such as AspenPlus^{TM} easily as a user-model for overall membrane process study and for the design and simulation of hybrid processes (i.e., membrane plus chemical absorption or membrane plus physical absorption). The proposed technique does not require initial estimates of the pressure, flow and concentration profiles inside the fibre as does in Pan's original approach, thus allowing faster execution of the model equations. The model predictions will be validated with experimental data reported in the literature for different types of membrane gas separation systems with or without purge streams, and the robustness of the new numerical technique will also be tested by simulating stiff types of problems such as air dehydration.

3.2 Mathematical Modelling

The basic model is based on Pan's (1986) theoretical formulation. The basic model has been simplified in a way different from Pan's original simplification. The temperature and concentration dependence of the gas mixture viscosity has been taken into account in the present study. The viscosity of the gas mixtures is calculated using the Wilke method, and the method of Chung et al. has been employed to calculate the component viscosity as a function of temperature (Reid et al., 1987). The present solution technique has been applied to different flow and module configurations (i.e., co- and counter-current flow, and bore- and shell-side feed). Figure 3.1 illustrates the permeation of a gas mixture through an asymmetric hollow fiber membrane for different module and flow configurations. The concentration of the local permeate stream leaving the membrane surface, y_i, is generally different from that of the bulk permeate stream, $\bar{y}_i$. The assumptions involved in the mathematical model formulation are as follows:

- The effect of back-diffusion from bulk permeate ($\bar{y}_i$) to local permeate (y_i) is negligible;

- Steady state and isothermal operation;
- The deformation of the hollow fibre under existing pressure is negligible;
- The pressure change in the shell side is negligible;
- The pressure change in the bore side is given by the Hagen-Poiseuille equation;
- The membrane permeability is independent of pressure and concentration.

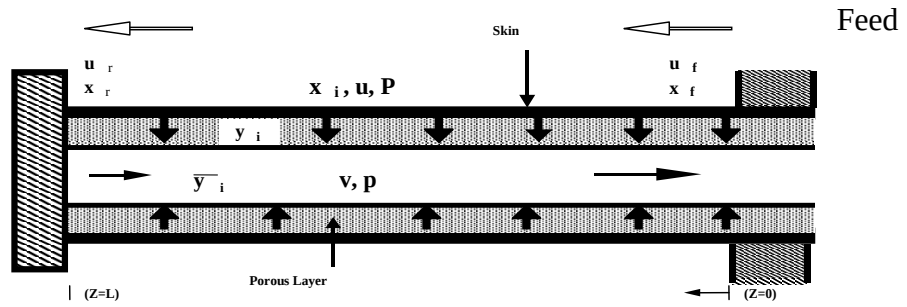

(a) Shell side feed/countercurrent flow

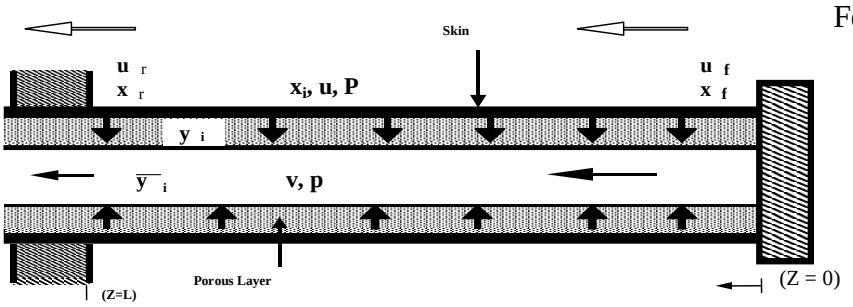

(b) Shell side feed/cocurrent flow

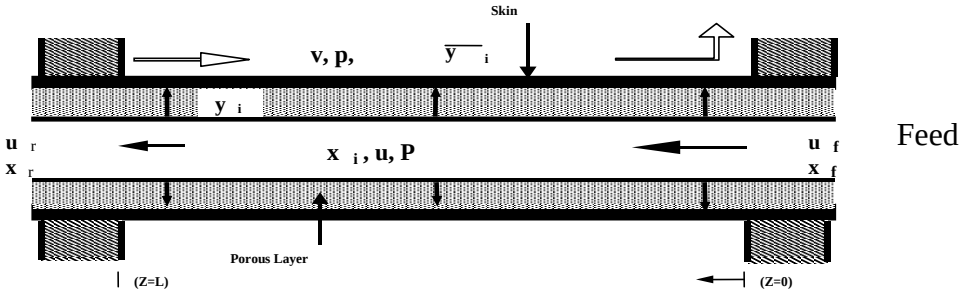

(c) Bore side feed/countercurrent flow

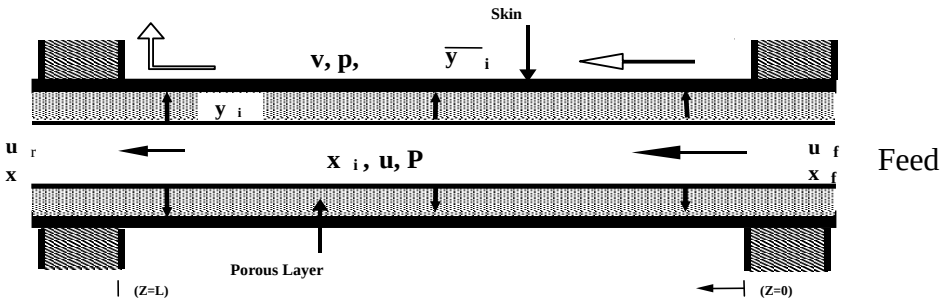

(d) Bore side feed/cocurrent flow

Figure 3.1: Gas permeation through asymmetric hollow fibre

3.2.1 Shell side feed

The permeation of a multicomponent gas mixture through an asymmetric hollow fiber module can be described by the following set of equations. Referring to Figure 3.1(a), the basic model equations for shell side feed with counter-current flow pattern are:

Permeation

$$\frac{d(u\,x_i)}{d\,z} = -\pi D_0\, N\, J_i\, (P\,x_i - p\,y_i) \qquad i = 1, n \tag{3.1}$$

$$\frac{d(u\,x_i)}{d\,u} = y_i \tag{3.2}$$

Where $J_i = P_i / l$

Permeate side pressure drop

$$\frac{d\,p^2}{d\,z} = \frac{256\,RT\,\mu_m}{\pi D_i^4 N}\,\mathrm{v} \tag{3.3}$$

Material balance

$$u + \mathrm{v} = u_f \tag{3.4}$$

$$u\,x_i + \mathrm{v}\,\bar{y}_i = u_f\,x_{f\,i} \tag{3.5}$$

With a permeate sweep or purge stream, Eqs. 3.4 and 3.5 become Eqs. 3.4a & 3.5a, respectively.

$$u + \mathrm{v} = u_f + \mathrm{v}_{\mathrm{swp}} \tag{3.4a}$$

$$u\,x_i + \mathrm{v}\,\bar{y}_i = u_f\,x_{f\,i} + \mathrm{v}_{\mathrm{swp}}\,y_{\mathrm{swp\,i}} \tag{3.5a}$$

Equations 3.1–3.5 are also applicable to the co-current flow pattern. In either case, the feed flow is considered to be in the direction of positive values of z. According to Figure 3.1(b), for co-current flow, the negative sign will be assigned to the right hand side of Equation 3.3 and the other equations will remain the same.

3.2.2 Bore side feed

Referring to Figure 3.1(c), the basic model equations for bore side feed with counter-current flow pattern can be written as:

Permeation

Equations 3.1-3.2 will be the same as before.

Feed side pressure drop

$$\frac{dP^2}{dz} = -\frac{256\,RT\mu_m}{\pi D_i^4 N}u \tag{3.6}$$

Material balance

Eqs. 3.4-3.5 are applicable to bore side feed configuration for both flow patterns. The equations for counter-current flow bore side feed also apply to co-current flow bore side feed, and only the direction of the permeate flow will be opposite.

3.2.3 Simplification of model equations

The simplification of the model equations for all the module and flow configurations has been made in similar fashion, but to be concise, the detailed treatment of the model equations is described here only for the first case, Figure 3.1(a) (i.e., counter-current flow shell side feed).

Feed side flow rate

Taking the sum of the Eq. 3.1 for each component yields:

$$\frac{du}{dz} = -\pi D_0 N \sum_{i=1}^{n} J_i \left(P x_i - p y_i\right) \quad i = 1, n \tag{3.7}$$

Residue side concentration

After application of the product rule in the left hand side and rearrangement, Eq. 3.1 becomes:

$$\frac{dx_i}{dz} = -\frac{1}{u}\left[x_i \frac{du}{dz} + \pi D_0 N J_i \left(P x_i - p y_i\right)\right] \tag{3.8}$$

Local permeate concentration

Dividing both sides of Eq. 3.1 by J_i and taking the sum for each component, and then substituting Eq. 3.2, one obtains

$$\frac{d\,u}{d\,z} = -\frac{\pi D_o N P(1-\lambda)}{y_o} \tag{3.9}$$

$$\text{where } \lambda = \frac{p}{P}, \quad y_o = \sum_{i=1}^{n} y_i / J_i$$

Eqs. 3.1 and 3.2 also lead to the following equation after rearrangement:

$$\frac{du}{dz} = -\frac{\pi D_o N J_i P(x_i - \lambda y_i)}{y_i} \tag{3.10}$$

From Eqs. 3.9 and 3.10, one obtains the following equation that relates the local permeate concentration to the feed side concentration.

$$y_i = \frac{J_i x_i y_o}{1-\lambda+\lambda J_i y_o} \tag{3.11}$$

Eq. 3.11 must satisfy the following condition,

$$\sum_{i=1}^{n} y_i = 1 \tag{3.12}$$

Permeate side pressure drop

After differentiation and replacement of *v* with the help of Eq. 3.4, Eq. 3.3 becomes:

$$\frac{d\,p}{d\,z} = \frac{128\,RT\,\mu_m}{\pi D_i^4 N}\frac{(u_f - u)}{p} \tag{3.13}$$

Bulk permeate concentration

Substituting Eq. 3.4 into Eq. 3.5 yields:

$$\bar{y}_i = \frac{u_f\,x_{f\,i} - u\,x_i}{u_f - u} \qquad ;\ u \neq u_f \tag{3.14}$$

$$\bar{y}_i = u\,\frac{\left(dx_i/dz\right)\Big|_{z=0}}{\left(du/dz\right)\Big|_{z=0}} + x_i \quad ;\ u = u_f \tag{3.15}$$

Eq. 3.15 is obtained by applying the l'Hôspital's rule (Li et al., 1990) as $u \rightarrow u_f$ which implies that $z \rightarrow 0$, and the differentiation is carried out with respect to z.

3.3 Numerical Technique

After simplification, the model equations can be solved numerically as an initial value problem (IVP) despite the boundary value nature of the problem for both shell side feed and bore side feed with either a co-current or counter-current flow pattern. FORTRAN program was developed for this purpose. Compaq Visual Fortran (Professional Edition 6.1, Digital Equipment Corporation, 1999) was used as the FORTRAN compiler, and a simple and direct approach has been adopted to obtain the solution. This technique does not require initial estimates of the pressure, flow or concentrations profiles inside the hollow fiber as does in the original Pan's approach.

The set of coupled first order non-linear ordinary differential equations (Eqs. 3.7, 3.8 and 3.13) were solved using the IMSL routine DIVPAG (Visual Numeric Inc., 1997), which uses either Adams-Moulton's or Gear's BDF method. The first is an implicit Adams-Moulton method (up to order twelve accuracy); the second uses the backward differentiation formulas BDF (up to order five accuracy). The BDF method is often called Gear's stiff method. The IMSL routines included with the Fortran compiler are widely used by programmers to avoid writing their own codes.

The system of nonlinear equations for local permeate concentration (Eq. 3.11) was solved by using another IMSL routine DNEQNF (Visual Numeric Inc., 1997), which uses a modified Powell hybrid algorithm and a finite-difference approximation of the Jacobian. The requirement that the sum of all mole fractions of the components must be equal to unity (i.e., Eq. 3.12) has to be satisfied every time after the local permeate concentrations (y_i) along the membrane length are calculated for each integration step. An iterative approach has been employed to satisfy convergence criterion.

The stand alone FORTRAN program takes only 2-3 CPUs for membrane systems involving four component gas mixtures when the simulation is performed on a personal computer with Pentium 4 processor of 1.6GHz speed running under Widows XP operating environment. The robustness of the numerical technique has been tested with various types of

membrane gas separations systems, which include stiff and non-stiff problems. There are no significant differences between the calculation procedures for the shell and bore side feed modes, and thus the detailed calculation procedure is illustrated here only for the shell side feed mode.

Shell side feed:

The membrane permeator performance problem can be classified as either a rating problem or a design problem. For rating problems, the membrane areas are known and the residue and permeate stream conditions are to be determined. For design problems, one of the product stream conditions (i.e., residue or permeate concentration) will be specified with the membrane area to be determined. The results for both types of problems are shown in Section 3.4 for different membrane systems to verify the model prediction and robustness of the present numerical approach.

The solution algorithm for the rating type of problems with counter-current flow is:

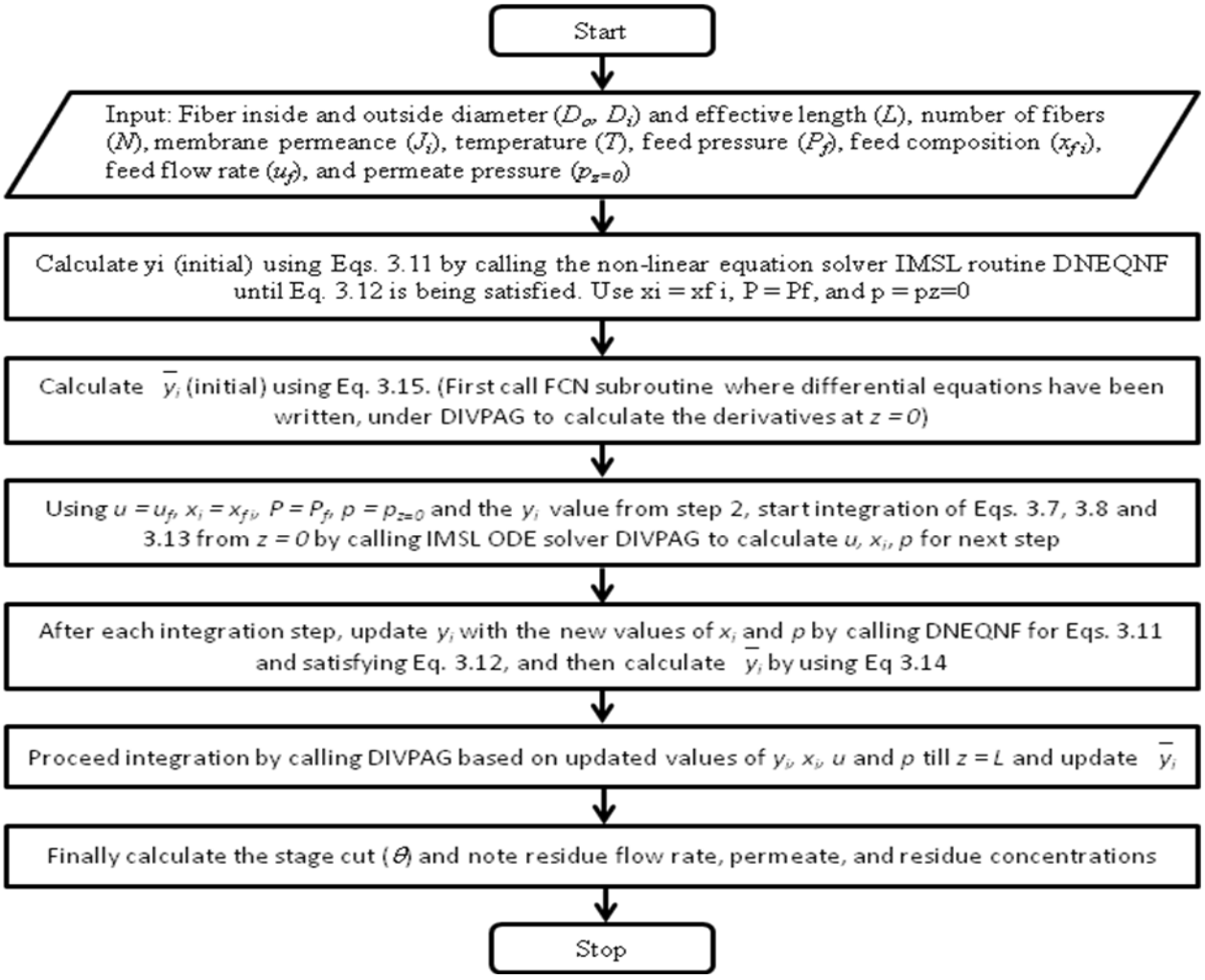

The permeator performance study is based on the input feed conditions (i.e., feed pressure, temperature, flow rate and composition), the permeate pressure exiting the module, the membrane permselectivity (i.e., permeance and permeance ratio) and the membrane module information (i.e., fiber diameter, length and number of fibers). The variables to be examined are: the stage cut (i.e., the permeate to feed flow rate ratio), the concentrations of the permeate and residue streams.

For co-current flow, the same procedure can be used by taking care of the negative sign in Eq. 3.13, but one has to guess a starting value for the permeate side pressure, p at $z = 0$ i.e., at the closed end of the fiber. Logically, the guess value must be higher than the specified exit permeate pressure ($p_{z=L}$). In this study, $p = 1.5 \times p_{z=L}$ was used as a starting value for the permeate side pressure at $z = 0$. We used the Secant Method to automate the calculation for the next value of p at $z = 0$ after a comparison of the calculated value of p at $z = L$ with the specified value to satisfy some specified tolerance. This approach has been found to be very effective; it converges very quickly without the need for manual trial and error manipulation.

The design type of problems follows the similar procedure as the rating type of problems but needs an extra Secant loop like an optimization block to vary the membrane area to meet the product specification in both flow patterns (co- and counter-current flows).

Bore side feed:

The calculation procedure for both bore side feed co-current flow and bore side feed counter-current flow for the rating type of problems is the same and it follows a similar approach as the shell side feed/counter-current flow with appropriate equations, as mentioned before. The model predictions for the bore side feed have also been verified with experimental data, which will be presented in Section 3.4. For solving the design type of problems, we only need to apply the Secant method as an extra calculation loop, as described before.

3.4 Results and Discussion

The present solution technique has been applied to simulate and compare the original simulation and experimental data reported by Pan (1986) for hydrogen recovery from simulated purge gas of ammonia plant. The module design and operating parameters are given in Table 3.1. It has been found that, as expected, the present simulation technique gives identical results as those from Pan's simulation. Figure 3.2(a) and Figure 3.2(b) show the permeate purity

(hydrogen) and impurity concentrations (nitrogen, methane and argon) in the permeate stream as a function of stage cut, respectively. The agreement between the experimental data and the calculated values is good over a wide range of stage cuts. Pan (1986) reported that the discrepancy at stage cuts greater than 0.55 was larger than the estimated experimental error of ± 3.5%, and it might be due to the fact that the mathematical assumption of negligible back-diffusion in the porous supporting layer of the membrane is not totally satisfied under extreme operating conditions. The simulation results for co-current and counter-current flow modes with same operating conditions have been found almost identical.

Once the present solution was validated with Pan's (1986) original solution and with his experimental data, we applied the present solution technique for Pan's (1986) model to other membrane systems reported in the literature to demonstrate the potential of the new solution technique in handling different membrane systems. The module and operating parameters for the membrane systems studied here are summarized in Table 3.1.

Sidhoum et al. (1988) investigated the separation performance of asymmetric cellulose acetate hollow fibers with and without sweep gas on the permeate side. Two systems were studied: CO_2/N_2 and O_2/N_2 (air) separations. They used two different models (homogeneous model and asymmetric model) to explore the gas separation behaviour. Their experimental and simulation results for the two different systems without permeate sweeping are compared with our simulation, as shown in Figures 3.3(a)-3.3(b). The overall agreement is good although the present model slightly over predicts the permeate concentration at low stage cuts (<0.25) in Figure 3.3(a).

Haraya et al. (1988) studied the performance of high-flux polyimide hollow fiber membranes for the separation of binary H_2/CO mixtures with two different modules: one was at a miniature scale and another at pilot scale. They also used two mathematical models to describe their experimental results. The model used for the miniature permeator was based on the conventional symmetric membrane and the model used for the pilot plant took into account the longitudinal mixing in the shell side. Their experimental results from the two membrane modules are compared with our model simulation in Figure 3.4(a) and Figure 3.4(b). A fairly good agreement is obtained between their experimental data and our model calculations for both cases.

Table 3.1: Different multicomponent gas separation systems

	Pan, 1986	Sidhoum, 1988	Sidhoum, 1988	Haraya, 1988 (Mini Sep.)	Haraya, 1988 (Pilot Sep.)	Tranchino, 1989	Sada et al., 1992)
Membrane	Asymmetric cellulose acetate hollow fiber	Asymmetric cellulose Acetate hollow fiber	Asymmetric cellulose Acetate hollow fiber	Asymmetric polyimide hollow fiber	Asymmetric polyimide hollow fiber	Composite hollow fiber	Asymmetric cellulose triacetate hollow fiber
Flow configuration	Co-& counter-current, Shell side feed	Counter-current, Shell side feed	Counter-current, Bore side feed	Counter-current, Shell side feed	Counter-current, Shell side feed	Co-current, Shell side feed	Counter current, Shell side feed
No. of fibers	20	70	70	6	8700	6	270
Inner diameter (μm)	80	84	84	212	220	389	63
Outer diameter (μm)	200	230	230	389	390	735	156
Active length (cm)	15	63.8	64	143	150	15	26
Feed composition	51.78% H_2, 24.69% N_2, 19.57% CH_4, 3.96% Ar	40% CO_2 60% N_2	Air (20.5% O_2, 79.5% N_2)	50.5% H_2 49.5% CO	46.5% H_2 53.5% CO	60.0% CO_2 40.0% CH_4	50.0% CO_2 10.5% O_2 39.5% N_2
Temperature (K)	298	298	298	373	373	301	303
Feed pressure (kPa)	6964	404	708	592	3040	405.3	1570
Permeate pressure (kPa)	1123	101	101.2	101	690	101.3	101.3
Permeance, (10^{-10} mol/s.m^2.Pa)	H_2 : 284 N_2 : 2.95 CH_4 : 2.84 Ar : 7.70	CO_2: 63.6 N_2 : 3.05	O_2 : 8.67 N_2 : 2.89	H_2 : 670 CO : 12.9	H_2 : 603 CO : 9.7	CO_2 : 31.6 CH_4 : 8.81	CO_2 : 204.2 O_2 : 60.2 N_2 : 13.1

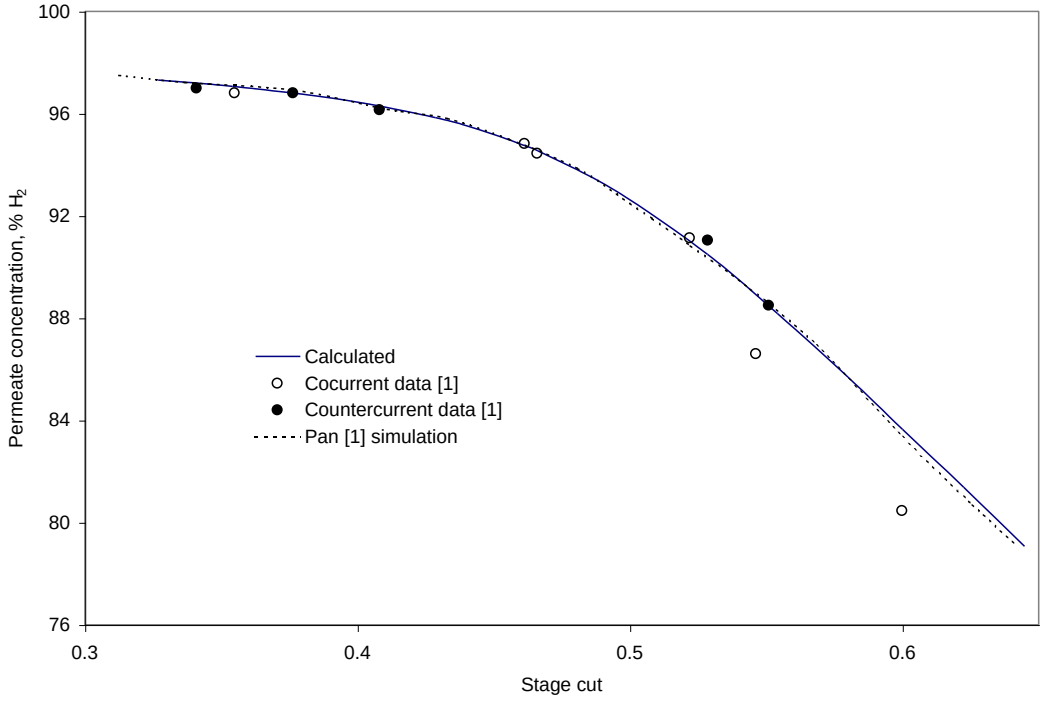

(a)

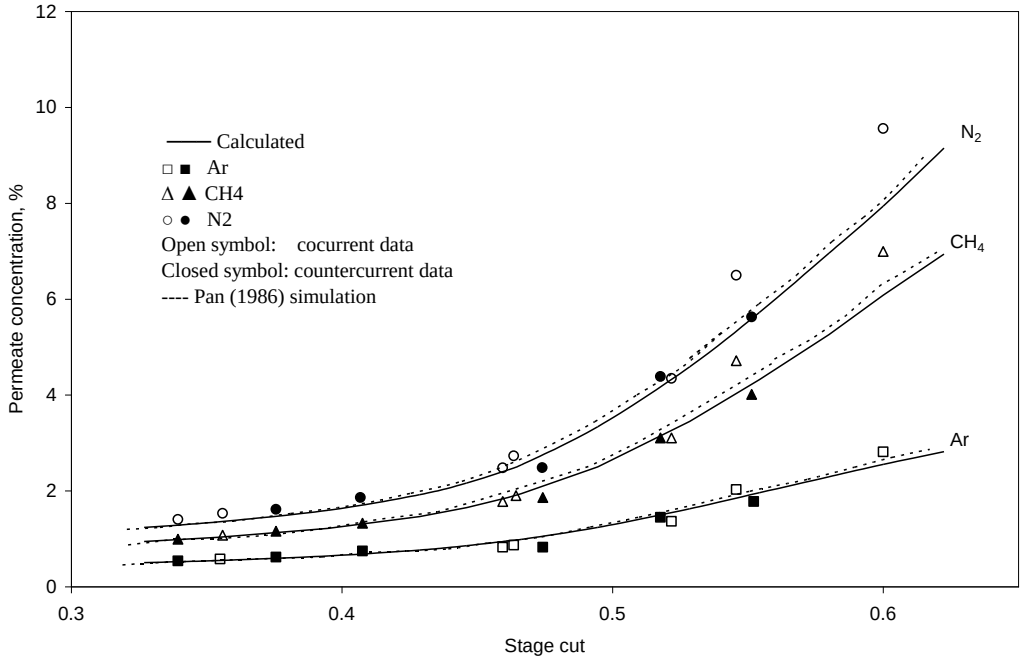

(b)

Figure 3.2: Comparison of model prediction with experimental data of Pan (1986) for hydrogen recovery from simulated purge gas of ammonia plant system- effect of stage cut on (a) hydrogen purity; (b) on impurity concentration

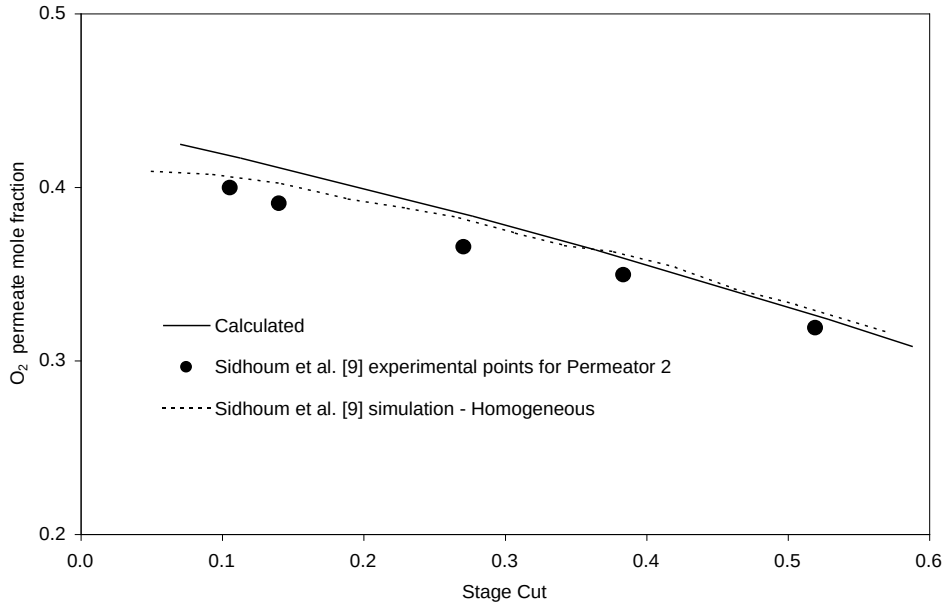

(a)

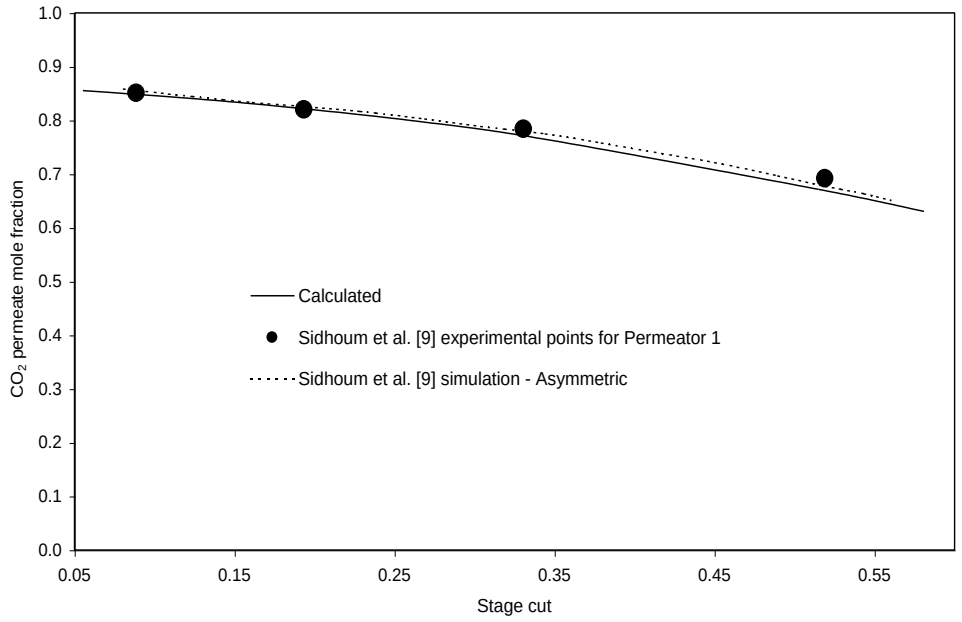

(b)

Figure 3.3: Comparison of model prediction with experimental data of Sidhoum et al. (1988) for permeate purity as a function of stage cut – (a) for no sweep mode in Permeator 1 for CO_2 / N_2 system; (b) for Air separation in Permeator 2

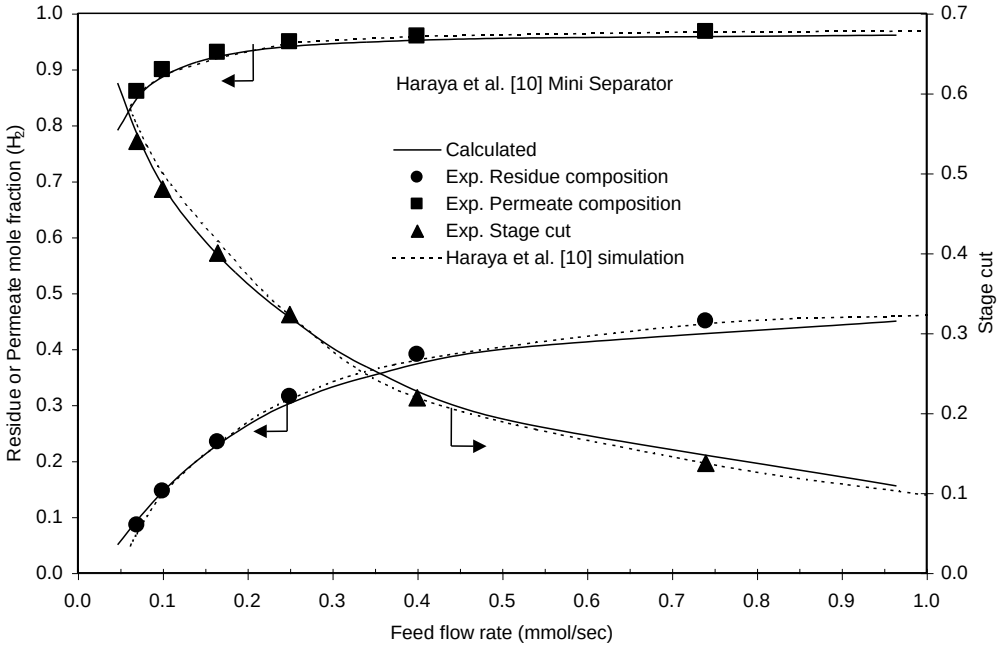

(a)

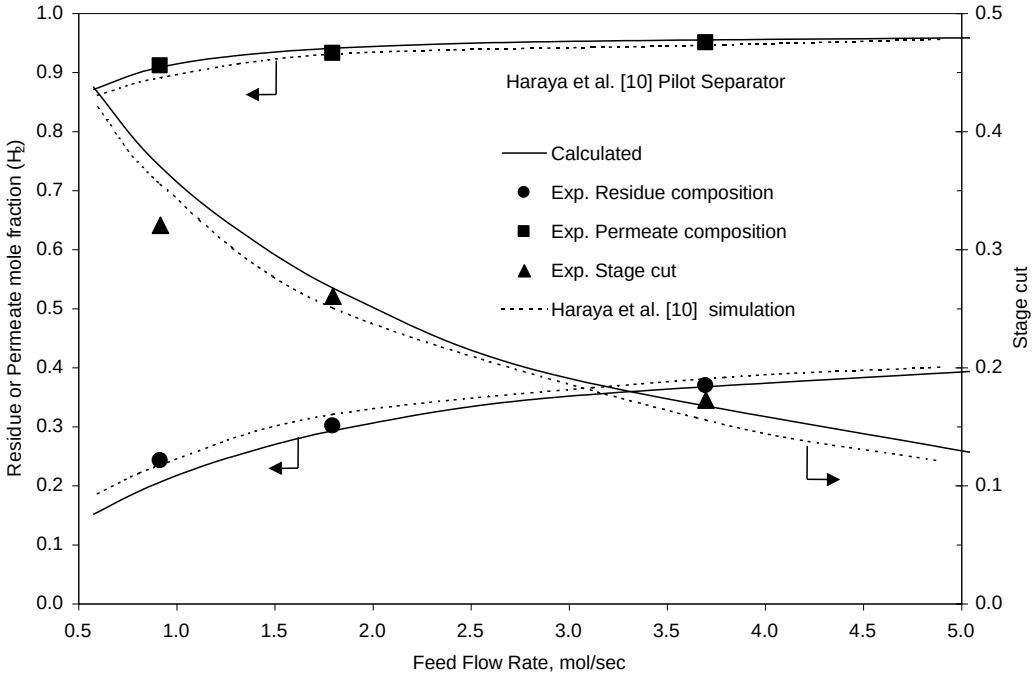

(b)

Figure 3.4: Comparison of model prediction with experimental data of Haraya et al. (1988) for H_2 / CO separation in – (a) mini separator; (b) pilot separator

Tranchino et al. (1989) tested a laboratory membrane unit using composite hollow fibers comprising of an aliphatic copolymer coated on a polysulfone support for CH_4/CO_2 separation. They reported the module performance as functions of temperature, pressure, stage cut, feed gas composition, and flow regime. Their experimental results for permeate composition as a function of stage cut are compared with our simulation, as shown in Figure 3.5. A very good agreement is obtained between their experimental results and our model calculations. They also reported three simple mathematical models for perfect mixing, co-current and counter-current plug flow conditions without consideration of the bore side pressure drop. Their simulation results based on the co-current model are also presented in Figure 3.5.

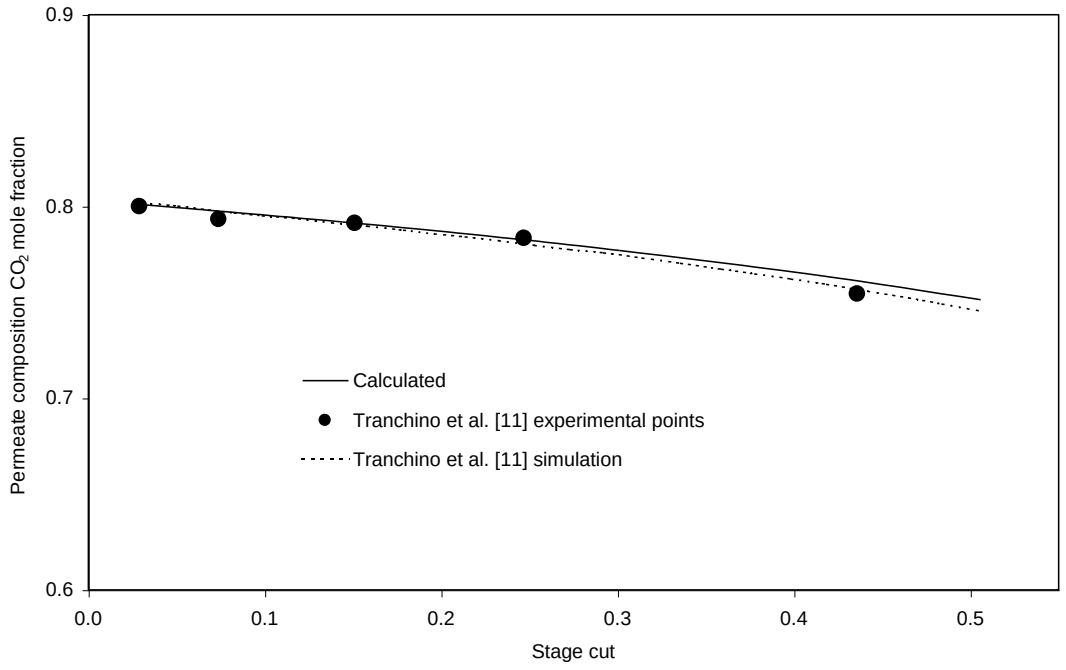

Figure 3.5: Comparison of model prediction with experimental data of Tranchino et al. (1989) for CO_2 / CH_4 separation

Sada et al. (1992) reported the separation of carbon dioxide from air by asymmetric hollow fiber cellulose triacetate membranes. The experimental data for permeate composition as a function of stage cut are compared with our simulation results in Figure 3.6, which showed a good agreement between the experimental data and our model calculations. They also reported a simple counter-current plug flow model to validate their experimental data. Their model prediction has also been shown in Figure 3.6.

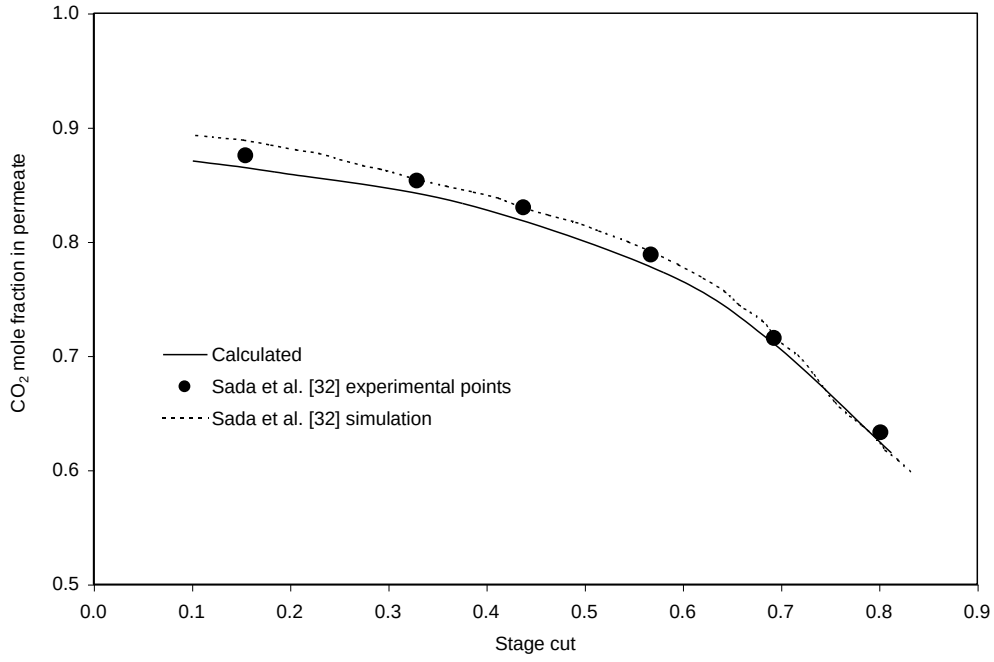

Figure 3.6: Comparison of model prediction with experimental data of Sada et al. (1992) for CO_2 - O_2 - N_2 mixture separation

Rigorous testing of the new technique for Pan's (1986) model from a numerical point of view was done by considering a stiff type of problem such as air dehydration. In air dehydration system, water has a permeability coefficient of 2-3 orders of magnitudes higher than other components. The concentration of water vapour in the air feed stream is also very low. Coker et al. (1998) simulated this type of system using their model but no experimental validation was provided. We used their parameters (as presented in Table 3.2) to simulate the same system by using Pan's model and our new numerical technique, and the simulation results of both approaches are presented in Figure 3.7b.

Table 3.2: Air dehydration system (Coker et al., 1998)

	Module
Membrane type	Polysulfone
Flow configuration	Counter-current, bore side feed, with permeate purge
No. of fibers	300,000
Inner diameter (μm)	150
Outer diameter (μm)	300
Active length (cm)	80
Feed mole fraction	N_2: 0.7841 O_2: 0.2084 CO_2: 0.0003 H_2O: 0.0072
Temperature (K)	313
Feed pressure (kPa)	1010
Permeate pressure (kPa)	101.3
Permeance (10^{-10} mol/s.m^2.Pa)	H_2O : 3346 CO_2 : 200.76 N_2 : 11.95 O_2 : 66.92

The overall product (residue) recovery represents the amount of residue gas available for downstream uses after removing the purge stream. It is the fraction of the feed stream (R'/F) that exits the module in the residue stream as shown in Figure 3.7a. The fairly good agreement between both simulation results clearly shows that Pan's model is valid for stiff type of problem as well.

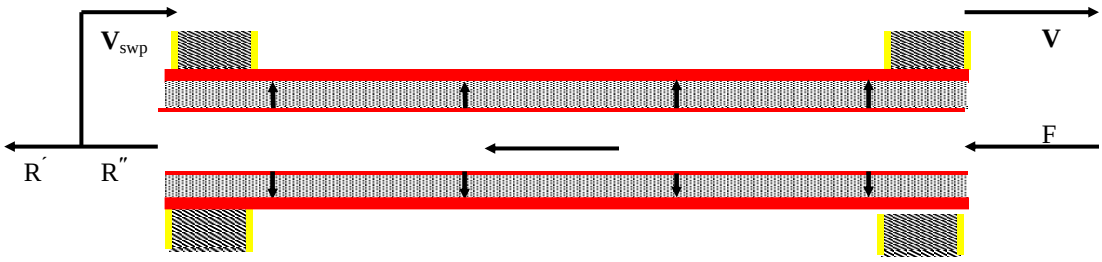

Figure 3.7a: Flow configuration with permeate purge in which a portion of the residue stream, V_{swp}, is sent to the permeate side of the membrane as a sweep or purge stream to increase the driving force for removal of water (Coker et al., 1998)

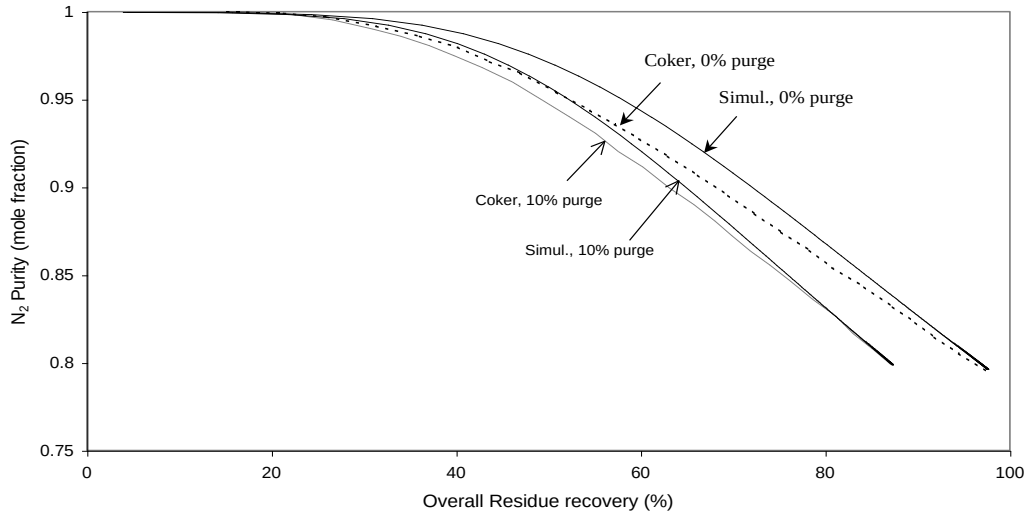

Figure 3.7b: Simulation results of new numerical approach for Pan's (1986) model and Coker et al. (1998)

3.5 Summary

A new solution approach has been developed to solve Pan's model for multicomponent gas separation by asymmetric hollow fiber membranes. This new approach eliminates the complex trial-and-error procedure required to solve the boundary value problem in the original approach adopted by Pan (1986). The initial estimates of the pressure, flow and concentration profiles inside the hollow fiber are no longer required, allowing faster execution of the model equations. The numerical solution is formulated as an initial value problem (IVP) and coded in FORTRAN language. Either Adams-Moulton's or Gear's backward differentiation formulas (BDF) method is used for solving the non-linear differential equations, and a modified Powell hybrid algorithm with a finite-difference approximation of the Jacobian is used to solve the non-linear algebraic equations. The new solution algorithm can easily handle both rating and design types of problems. The model predictions and the robustness of the new numerical technique have been validated with literature data for several membrane systems with different flow and module configurations with or without purge stream and are found very satisfactory.

Chapter 4

Interfacing of Multicomponent Gas Separation Membrane Model with a Commercial Process Simulator

4.1 Introduction

The simulation of a process allows evaluation of the operating variables, process configurations, and optimization. Most commercial process simulators have built-in process models and optimization toolboxes, thus offering a convenient and time saving means of examining the entire process. Usually all steady-state simulation packages are used as a tool to simulate and design chemical processes. With process simulators users can interactively change specifications such as process flow diagram configuration, operating conditions and feed compositions, to run new cases and analyze process alternatives. In addition to process simulation, process simulators allow user to perform a wide range of other tasks such as estimating and regressing physical properties, generating custom graphical and tabular output results, fitting plant data to simulation models, optimizing process, and interfacing results to spreadsheets. Process simulators offer the possibility of simulation of any combination of various unit operations (reactors, distillation towers, condenser, compressor, etc.) using built-in process models. They also offer the option of using custom or proprietary models. The advantages of implementing user defined custom module for membrane gas separation unit into a commercial process simulator can be summarized as follows (Rautenbach et al., 1996):

- Development of different membrane processes is possible by the combination of custom membrane unit with all other built-in units of the process simulator including internal recycle streams.
- Utilization of different thermodynamic models, and property data bases available in the simulator is possible.
- Costing, sizing and sensitivity analysis can be performed.

- Multiple design cases at a fraction of the cost can be studied.
- Process optimization can be performed.

Detailed membrane model for multicomponent gas separation processes are not available as a built-in process model in any of the leading commercial process simulation packages, and consequently process combinations including a membrane unit are not covered by the standard process simulators. Custom-built membrane models need thus to be interfaced with the commercial process simulator.

An example of a simple hollow fiber ultrafiltration model for protein separation in Excel as well as in FORTRAN as a user model is available in AspenPlus User Guide (Aspen Engineering Suite, 2001). Although a built-in stand-alone model for membrane gas separation processes is not available in the standard version of AspenPlus® (Aspen Engineering Suite, 2001), a detailed membrane model and a solution procedure can be implemented in AspenPlus® as a user–supplied FORTRAN routine. Rautenbach et al. (1996) implemented a user-model in AspenPlus for gas separation by membranes using a simple cross-flow model without consideration of pressure drop and used it for design and simulation of vapour recovery unit for the treatment of tank farm off-gas, for reverse osmosis plant for organic/-organic separation and for the separation of dimethylcarbonate/methanol mixture. Tessendorf et al. (1999) presented a user-supplied membrane model without consideration of the bore side pressure drop in OPTISIM (Linde AG) to simulate and optimize the CO pre-treatment of steam reformer gas. Davis (2002) also presented a model for gas permeation through hollow fibers by assuming a negligible pressure drop along the membrane, and implemented it in HYSYS (Hyprotech Ltd.) without the need of external custom programming. The model was used to simulate an air separation process. To avoid the solution of non-linear differential equations, he considered the logarithmic-mean average of species trans-membrane partial pressure as the driving force. It should be mentioned that the membrane models (Rautenbach et al. 1996; Tessendorf et al., 1999; Davis 2002) used in the above mentioned commercial process simulators have not been validated over a wide range of applications. It was shown that the performance of narrow hollow fibers could be significantly affected by the permeate pressure build-up inside the fiber lumen (Pan and Habgood, 1978b), and the accuracy of the design and simulation of membrane processes based on these models can thus be greatly affected. Hagg and Lindbrathen (2005) interfaced an in-house program of

hollow fiber membrane to HYSYS program to capture CO_2 from exhaust stream of natural gas fired power plants. Model details were not presented. Zhao et al. (2008) used built-in model for hollow fiber membrane gas separation in Pro/II (Version 8.2) of Simulation Science Inc., to simulate a single stage membrane process for capturing CO_2 from power plant flue gas. Although this built-in membrane model considered bore side pressure drop, but can handle only binary gas mixture.

In the previous chapter, a new solution technique for the widely accepted model developed by Pan (1986) for multicomponent gas separation using high-flux asymmetric membranes was presented and it was shown to be applicable to a wide range of gas separation membrane systems. This chapter highlights the efficient implementation of the new solution technique of a detailed membrane model into a commercial process simulator to develop a custom unit operation model for hollow fiber membrane module for simulating overall membrane and hybrid processes.

4.2 Selection of a Commercial Process Simulator

A discussion on current available steady-state commercial chemical process simulator packages was presented in Chapter 2. The main two factors that usually determine the selection of any simulation package for a particular application are: cost, and satisfying capability of application specific requirements. Several base requirements which usually are the part of any process simulator, can be noted as:

- reliable thermodynamic models that account also non-ideal behaviour,
- reliable thermodynamic properties database,
- ability for a stream to contain solid, liquid, and/or gas phases with multiple chemical species able to exist in all phases present,
- perform optimization of individual unit operations and also for the whole process,
- capability to perform a multiple case study (automated consecutive running of pre-specified scenarios),
- rigorous modules for different unit operations such as reactors, heat exchangers, distillation columns, and pumps/compressors etc.,
- economic and sensitivity analysis of the process, and

- allowing easy user intervention for overriding of default values in the database, additions to the database, and creation of custom models using mainstream computer programming languages

As the overall objective of the present research is to develop a design, simulation and optimization tool to investigate the potential of membrane based gas separation processes along with hybrid processes with application to CO_2 capture from flue gases, most of the simulators such as Aspen Plus, HYSYS (now Aspen HYSYS), PRO/II and ChemCAD can satisfy the application needs. During the start of this thesis work, the Chemical Engineering Department of University of Waterloo had licenses for Aspen Plus, HYSYS, and ChemCAD. ChemCAD has been discarded because of the lack of electrolyte models which are needed for MEA process simulation. Both Aspen Plus and Aspen HYSYS have extension capability for user supplied models. HYSYS needs Visual basic and C++ programming languages capability for extensibility, and Aspen Plus prefers Fortran language. In Hysys, Fortran coded routine can be interfaced with the help of Visual basic and C++, so extensive knowledge of Visual basic and some knowledge of C++ are required. On the other hand, Fortran coded routine can be much easily integrated with Aspen Plus without the help of Visual basic and C++. As our membrane model with new numerical technique presented in the previous chapter was coded in Fortran language, Aspen Plus was chosen as the process simulator for our research.

4.3 Integration Procedures in AspenPlus®

Aspen Plus offers powerful features that facilitate the use of simulations containing proprietary models. The following can be created in Aspen Plus (Aspen Engineering Suite, 2001):

- Custom Model Libraries,
- user-defined variables that become part of the Aspen Plus data structure as an alternative to Real and Integer arrays,
- custom icons to better represent the equipment that your models describe, and
- standard and default model input templates.

Aspen Plus provides several methods to create custom models:

- Fortran

- Excel
- Component Object Models (COM) based on CAPE-OPEN standard using Visual basic, C++ and J++ languages
- Aspen Custom Modeler

This section will focus only on the Fortran method to describes how to create custom or proprietary models for unit operation, and how to specify the location of the Fortran user models to use during Aspen Plus runs. An Aspen Plus Fortran user model may consists of one or more subroutines that users can write to extend the capabilities of Aspen Plus. Six kinds of Fortran user models can be written for use in Aspen Plus:

- User unit operation models: units not represented by Aspen Plus built-in unit operation models
- User physical property models for calculating the various physical properties
- User models for sizing and costing
- User models for special stream properties
- User stream reports
- User models for performing various types of calculations within Aspen Plus unit operation models e.g., reaction rates, heat transfer rates/coefficients, pressure drop, and liquid-liquid distribution coefficients.

Fortran user models can call available Aspen Plus utility routines to perform flash and physical property calculations, and the Aspen Plus handler to report calculations.

Aspen Plus dynamically loads and executes Fortran user models during the run (Aspen Engineering Suite, 2001). Before beginning a simulation run that refers Fortran user models, users must:

- Write the user models.
- Compile the user models using the **aspcomp** procedure.
- Link the user models into a Fortran shared library using the **asplink** procedure (optional).
- Supply the object files or shared library to the Aspen Plus system.

During a run, Aspen Plus determines the symbol names of all Fortran user models needed for the run. It then resolves symbols from any shared libraries specified via the DLOPT

file. If any symbols remain unresolved, it terminates with an error message. All messages generated during dynamic linking process are written to the file named *runid.ld*. After resolving all symbols, Aspen Plus invokes the Fortran user models at the appropriate points in the run via a special interface routine named DMS_DOCALL. The detailed information regarding writing, compiling, linking and customizing Fortran user models is available in Aspen Plus User Manuals (Aspen Engineering Suite, 2001). The following subsections highlight those important steps in a systematic way.

4.3.1 Writing Fortran User Model

Aspen Plus allows two models such as "User" and "User2" to write own unit operation models as Fortran subroutines. The proper argument list needed to interface user unit operation model (User2) to Aspen Plus is described in Appendix [A]. The Argument List Descriptions describe the input and/or output variables to the subroutines. The Fortran program developed in the previous chapter is modified according to the requirement of Aspen Plus user model subroutine i.e., User2 and is attached in Appendix [B]. Following are rules to follow during conversion from the main Fortran program to the User2 subroutine:

- The *filename* which contains the Fortran user model may be given any name with ".f" extension at the end. As for example, the name of Fortran file which contain user model subroutine (SFCRGE) is SFCR_PF_Gen.f.
- *Subroutine* names should not exceed six characters limit.
- All *real* variables must be declared as double precision (REAL*8).
- To refer any Aspen Plus *common block* variables in the user model, the appropriate files using C pre-processor syntax should be included. Extreme care should be taken not to modify the value of any Aspen Plus common block variables by the user routine.
- All variables in the argument list are in *SI* units.

4.3.2 Compiling Fortran User Model

User Model has to compile first before any Aspen Plus run. In order to insure consistent compiler options, **aspcomp** procedure for compiling is used. Steps followed are:

- Lunch the Aspen Plus Simulation Engine window.
- Set the default directory to the location of Fortran user model file **SFCR_PF_Gen.f**, using DOS **cd** command.
- Type **aspcomp SFCR_PF_Gen.f** and pressing enter to compile the subroutine in the file. If there are no errors, an object file (**SFCR_PF_Gen.obj**) with the same name is created in the same directory of **SFCR_PF_Gen.f**.
- Keep the DOS window open for linking step.

4.3.3 Linking/Supplying Fortran User Model

The simplest method of supplying Fortran user models to Aspen Plus is by putting the user model's object module file (**SFCR_PF_Gen.obj**) in the run directory. Alternatively, users can write a Dynamic Linking Options (DLOPT) file that specifies the objects to use when creating the run-specific Fortran shared library. The DLOPT file can also specify shared libraries created by the **asplink** procedure for use when resolving user model symbols instead of, or in addition to, linking a run-specific shared library. (Aspen Engineering Suite, 2001). The later option has been adopted in this study. Two DLOPT (dynamic linking option) files control the linking process: one creates a DLL from specified .OBJ files and another tells Aspen Plus where to find the DLL being used for a particular run.

The following steps were used to create a shared library:

- Create a DLOPT file (**SFCR_PF_List_objs_gen.opt**) by using a text editor such as Notepad. DLOPT files can contain: **dlopt** commands, and file specifications referring to object module files, object module libraries (archives), or Fortran shared libraries.
- Write the full path to **SFCR_PF_Gen.obj** in the top line of the text file. For example: N:\Documents\Aspen\ . . .\ **SFCR_PF_Gen.obj**
- Save the file and exited the text editor.
- Type the following command in the DOS window of the Aspen Plus Simulation Engine: **asplink** [**dlopt SFCR_PF_List_objs_gen.opt**] **SFCR_PF_Gen**

  A DLL file called **SFCR_PF_Gen.dll** is created based on **SFCR_PF_Gen.obj** file. This Fortran shared library avoids the need for a linking step when Aspen

Plus runs. Once the shared library is created, it can be used with Aspen Plus even without Fortran compiler.

- Create another DLOPT file (**SFCR_PF_loc_dll_gen.opt**) by using the same text editor. In the top line of this file typed the full path to **SFCR_PF_Gen.dll**.
- Save the text file and exited the text editor.
- Put a copy of the **SFCR_PF_Gen.dll** in your Aspen Plus working directory. When running Aspen Plus from the Windows user interface, specify the DLOPT file in the Run Settings dialog box. From the Run menu, select Settings. On the Engine sheet of the dialog box, specify the DLOPT file (**SFCR_PF_loc_dll_gen.opt**) in the Linker Options field.

4.3.4 Customizing Fortran User Model

A customized Fortran model can have its own unit operation model stored in an Aspen Plus Library file (.apm extension) and displayed in the Model Library palette. Real and integer parameters needed for calculation in the model can be entered using the Aspen Plus User Arrays data sheet. But with a customized unit operation model, user need to enter these parameters once and they will be automatically included whenever the customized block is placed on the process flowsheet. In addition, the name of the user Fortran subroutine can be associated with the customized model. The icon itself can be custom drawn. A Configured Variables sheet is available in which the set of real and integer parameters are associated with character strings and identified as input or output. This data can be accessed in the user Fortran subroutine by referring to the variable names, thereby simplifying the code.

4.3.4.1 Creating a Model Library

Creating an empty Custom Model Library

A model library consists of three levels: the **library** itself consists of a set of **categories** each identified by a tab in the Model Library palette. Each category consists of a set of **models**. Each model is represented by an icon and has default parameters associated with it. Steps to create an empty model library are as follows:

- A sub-folder named, **lib** is created in Aspen Plus Working Folder to contain library files.

- By opening an Aspen Plus blank simulation, **Library | New** is selected. The **Create Aspen Plus User Model Library** dialog box appeared
- Enter the library name as "**General HFiber Memb. Gas Sep."** in the **Enter Display Name** field.
- Click **Save**. The previous dialog box reappears.
- Click **Create**. An empty library is created without categories and models.

Creating a Custom Model from a Template

The next step is to create a template first, and then create the customized model that contains the default parameters and subroutine name.

- From the Model Library, place a **User Models|User 2|FILTER** block on the process flowsheet. It has the default ID **B1**.
- Open the Data Browser to go to the **Blocks|B1|Setup|Subroutines** sheet.
- In the **Model** field, type the name of the Fortran subroutine, **SFCRGE**.
- Click the **User Arrays** tab for entering the real and integer parameters by selecting size of the arrays first.
- Select Block **B1** by going back to the Process Flowsheet, right click, and select **Add to Model Library**. The Add Custom Model Type to User Model Library Wizard dialog box appears.
- Select **Add: Create a new**, and click **Next**.
- In the **Choose Custom Model Category** dialog box, click **Create New Category.**
- Type **Gen HF Memb Mod** and click **OK**. The **Choose Custom Model Category** dialog box reappears.
- Select **Gen HF Memb Mod** and click **Next.** The **Choose Single Block or Multi Record Custom Model Type** dialog box appears.
- Select **Single Block Custom Model Type** and click **Next**. The **Choose Custom Model Type Creation Options** dialog box appears with the block ID (**B1**) entered automatically.
- Replace **B1** with **HFMGe**. Chose any icon option.

- Select the **Copy/create model template** checkbox. Aspen Plus copies the data entered on the **Subroutines** sheet and on the **User Arrays** sheet into the new model.
- Select the **Copy/create user model configuration** checkbox. Aspen Plus will make the **Configured Variables** sheet available to the new model so that variable names with real and integer parameters can be associated.
- Click **Finish**. Aspen Plus automatically saved the new library. Select **Library | General HFiber Memb. Gas Sep**; the **Save** option should be shaded. A tab for the **Gen HF Memb Mod** category of the **General HFiber Memb. Gas Sep** library appeared alongside the tabs of the **Built-in** library.
- In the Model Library click the **Gen HF Memb Mod** tab. The model created is visible.
- Delete the block on the Process Flowsheet that was used as a template.
- From the Model Library, dragg a **HFMGe** unit operation model onto the Process Flowsheet.
- Open the Data Browser and the **Blocks B1 Setup** form, and check that the default data appears correctly on the **Subroutines** sheet and on the **User Arrays** sheet.
- Exit Aspen Plus.

Now, whenever the user starts Aspen Plus, select **Library | References** and click the **General HFiber Memb. Gas Sep** checkbox to have access to the **HFMGe** unit operation model with default user subroutine name, real and integer parameters values.

4.3.4.2 Editing the Custom Model

Creating References to the Real and Integer Parameters

- Select **Library | General HFiber Memb. Gas Sep | Edit**, and then **Edit User Configuration**. The **User Model Configuration Editor** appears.
- Create names for the 1 integer and 16 real parameters in the order that they appear on the **Blocks Gen HF Memb Mod Setup User Arrays** sheet.
- Real is the default type. For **NF**, click in the **Type** field and selected **Integer** from the drop-down menu.

- Parameters are designated as **Input** by default. For the last two real parameters, Stage cut and recovery, clicked in the **Input/Output** field and select **Output only**. The completed table is then shown.
- Exit the **Configuration Editor** by closing the window.
- Select **Library | General HFiber Memb. Gas Sep | Save**.
- Exit the Model Library Editor by closing the window. The variable names will now appear whenever the **HFMGe** model is used.

4.3.4.3 Running the Simulation

Before running the simulation, the named references on the **Configured Variables** sheet must be supported by a short Fortran subroutine that must be created, compiled, and linked along with the user model subroutine file **SFCR_PF_Gen.f**. The **Model Library Editor** will write this new subroutine to handle variables of the **Configured Variables** sheet.

Inserting the New Model

- Open an Aspen Plus blank simulation.
- Select **Library | References.** and then **General HFiber Memb. Gas Sep** (**General HFiber Memb. Gas Sep** library has one category called **Gen HF Memb Mod** and its tab appears in the Model Library).
- Place a **HFMGe** block on the Process Flowsheet. Default block name changes to **HF1**.
- FEED, RETENTAT and PERMEATE streams are connected with **HF1** block in that particular order. The order matters because the first stream connected comes first in the output stream data array (SOUT).
- Components and Property method are specified. The feed stream is also specified.
- A Temperature and Pressure Flash for each product stream is specified from the Stream Flash sheet.
- The process Flowsheet is now completed.

Creating a Fortran Subroutine for Configured Variables

- Select **Library | General HFiber Memb. Gas Sep | Writable** and then **Library |General HFiber Memb. Gas Sep | Edit** to open the **Model Library Editor**.

- Select the **HFMGe** model, right-click, and select the **Edit User Configuration** to open the **User Model Configuration Editor**.
- Select **Fortran | Export** and save the Fortran file as **sfcrgevr.f** to the folder that contains **SFCR_PF_Gen.f**.
- Exit the Configuration Editor by closing the window.
- Save the library (**Library** | **General HFiber Memb. Gas Sep** | **Save**) and exit the Model Library Editor.
- Save the run as **Test-HF**.apw and exit Aspen Plus.

Creating a Shared Library from the both Subroutines

- Open DLOPT file, **SFCR_PF_List_objs_gen.opt** and add a line indicating the path of **sfcrgevr.obj** file.
- Save the DLOPT file and exit the text editor.
- Start the Aspen Plus Simulation Engine to get the DOS window and set the default directory to the location of Fortran files using DOS **cd** command.
- Type **aspcomp sfcrgevr.f** and press Enter to compile the new Fortran subroutine, named **sfcrgevr** to generate **sfcrgevr.obj** file. The **SFCRGE** subroutine of **SFCR_PF_Gen.f** was compiled before; so the obj file **SFCR_PF_Gen.obj** already exist.
- Type **asplink** [**dlopt SFCR_PF_List_objs_gen.opt**] **SFCR_PF_Gen** and pressed enter to generate an updated shared library **SFCR_PF_Gen.dll** from both object files i.e., **sfcrgevr.obj** and **SFCR_PF_Gen.obj**.
- Aspen Plus Simulation Engine Window is closed.
- Check that the other DLOPT file, **SFCR_PF_loc_dll_gen.opt** is still in the Aspen Plus Working Folder and contains the location of **SFCR_PF_Gen.dll**.

Running the Simulation

- Start Aspen Plus, and open **Test-HF**.apw.
- Select **Run | Settings**. Type the path of **SFCR_PF_loc_dll_gen.opt** in the **Linker Options** field to tell Aspen Plus where to find the shared library.
- Click OK.
- Reinitialize and Run the simulation.

- Go to the **Blocks | HF1 | Results | Summary** sheet to see the entire real and integer parameter lists including the two real parameters that were specified as output only.
- Go to the **Configured Variables** sheet to see just the two output parameters.
- Save the simulation.

4.4 Validation of Integration

To confirm the integration of the user Fortran subroutine of hollow fiber membrane module in Aspen Plus has been done properly, the same set of input data as shown in Table 4.1 is used in Aspen Plus simulation run and in stand-alone Fortran main program run. In stand-alone program, components' critical and other properties are provided to calculate mixture properties such as viscosity etc. In AspenPlus run, the user Fortran routine uses Aspen Plus data banks for pure component properties. Stage cut, recovery and concentration of permeate components calculated by both runs are compared, and presented in Table 4.2. A table of membrane block parameters specified in Configured Variables sheet as input and output variables, and a process flowsheet built in AspenPlus® with customized model are presented in Figure 4.1(a) and 4.1(b). Results for two output parameters specified in Configured Variables sheet of Aspen Plus user membrane model, are also presented in Figure 4.1(c). The simulation results from both platforms should be identical to the results presented in Table 4.2.

Table 4.1: The module and operating parameters for the validation run

Hollow Fiber Module (Sada et al., 1992)	
Membrane	Asymmetric cellulose triacetate hollow fiber (Sample 31)
Flow configuration	Counter current, Shell side feed
No. of fibers	270
Inner diameter (μm)	63
Outer diameter (μm)	156
Active length (cm)	26
Feed Flow rate, Mol/Sec	0.0002518
Feed composition	50.0% CO_2 10.5% O_2 39.5% N_2
Temperature (K)	303
Feed pressure (KPa)	1570
Permeate pressure (KPa)	101.3
Permeance, (10^{-10} mol/s.m^2.Pa)	CO_2 : 204.2 O_2 : 60.2 N_2 : 13.1

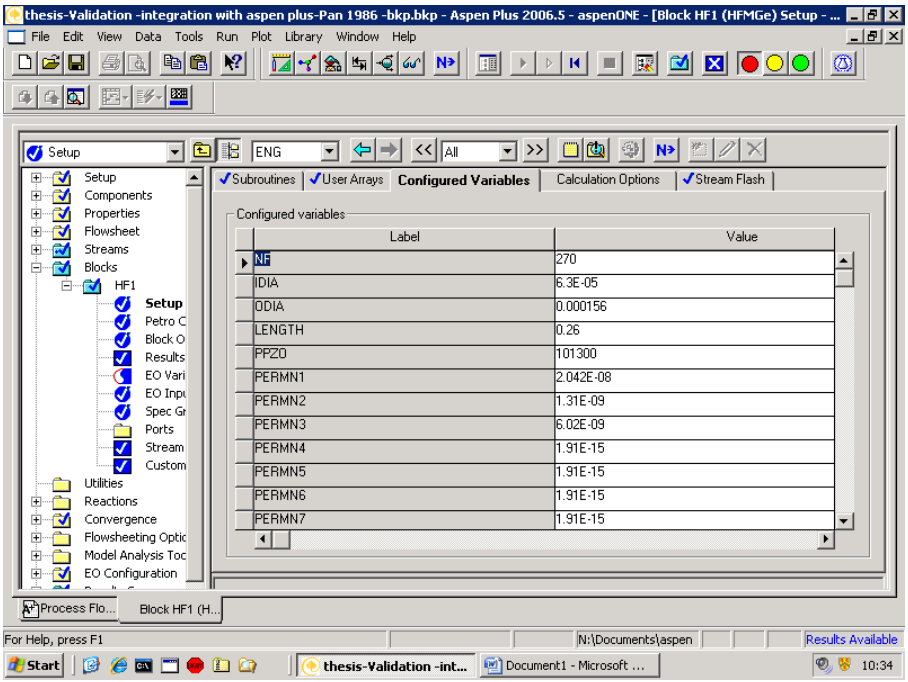

Figure 4.1(a): Hollow fibre membrane module parameters incorporated in Aspen Plus as configured variables

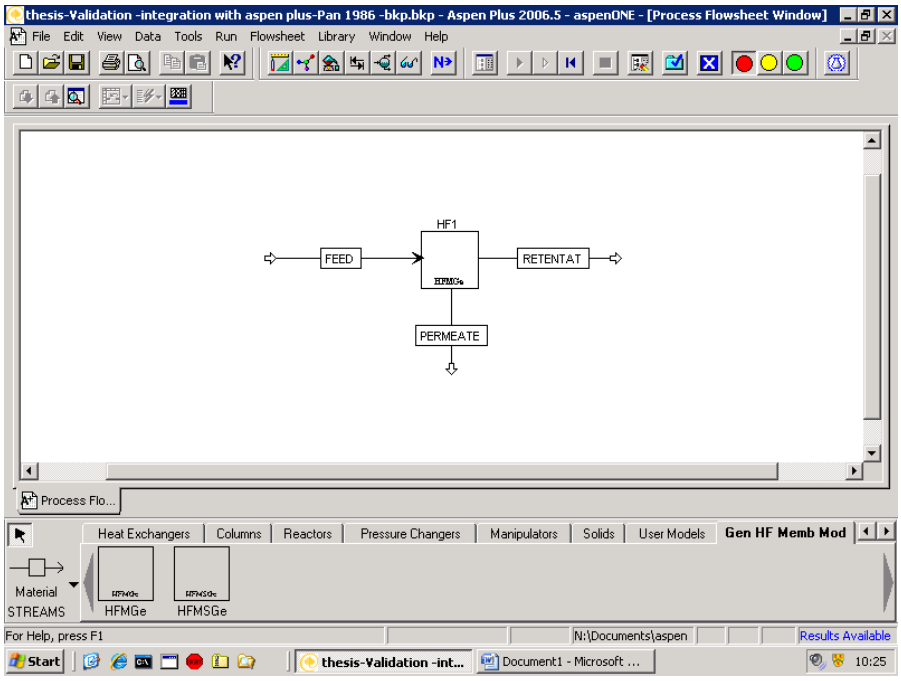

Figure 4.1(b): Simulated AspenPlus® flowsheet for multicomponent gas separation by asymmetric hollow fibre membrane

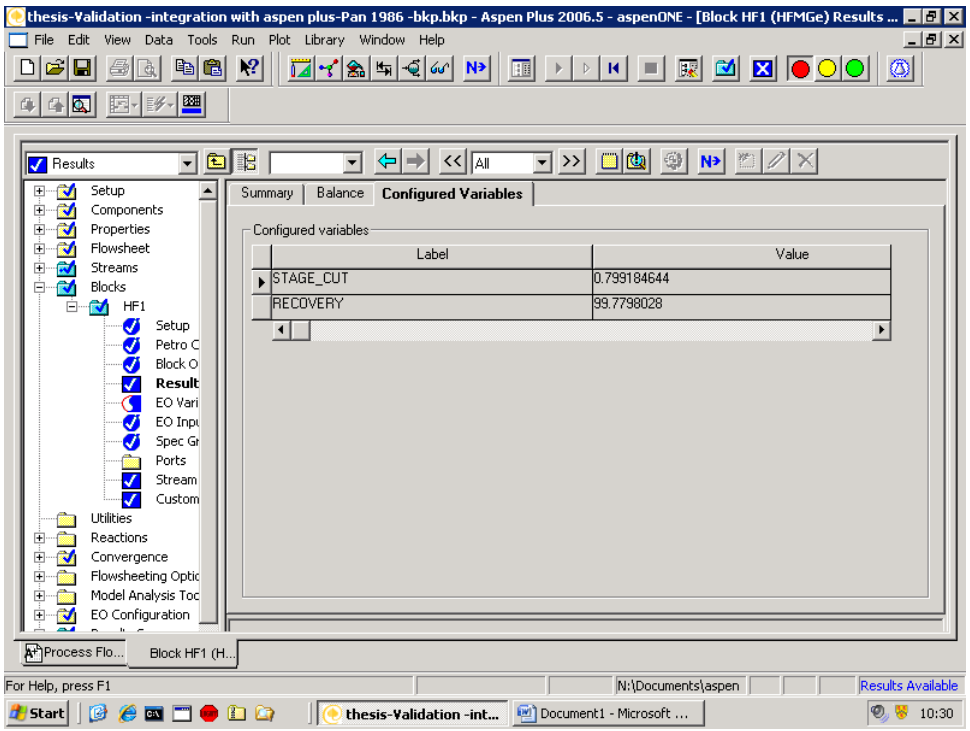

Figure 4.1(c): Simulation result for configured (output) variables for multicomponent gas separation by asymmetric hollow fibre membrane in AspenPlus®

Table 4.2: Aspen Plus and Stand-alone Fortran program results

	AspenPlus	Stand-alone Program
	Permeate Stream	
Component Mole Fraction		
CO_2	0.62	0.62
N_2	0.25	0.25
O_2	0.12	0.12
Total Mole Flow, mol/Sec	0.0002	0.0002
Stage cut	0.80	0.80
Recovery (%)	99.8	99.8

4.5 Summary

The incorporation of the detailed membrane model (shell side feed/ counter-current flows) for multicomponent gas separation by hollow fiber module into Aspen Plus for design and optimization of hybrid separation processes that involve membranes and other separation units, has been completed successfully. The model is portable to any other PC which has only Aspen Plus software because of the creation of *.dll file as done for Tarun et al. (2007) for studying CO_2 capture from natural gas based hydrogen plants. It does not need the external FORTRAN compiler and IMSL routines for that PC. This provides a convenient tool for process simulation and optimization study of any membrane-based processes.

Chapter 5

Simulation and Design of Membrane Gas Separation Processes in AspenPlus® for CO_2 Capture

5.1 Introduction

Based on a newly developed solution technique presented in Chapter 3 for Pan's (1986) model of hollow fibre membrane module for multicomponent gas separation, a custom user unit operation model has been implemented in Aspen Plus as a membrane unit, as described in Chapter 4. The model predictions and the robustness of the new numerical technique have been validated with literature data for several membrane gas separation systems with different flow and module configurations (i.e., shell side feed/co- and counter-current flows, and bore side feed/co- and counter-current flows) with or without purge stream. Counter-current shell side feed flow and pressure drop inside the fibre bore have been considered for the user membrane unit interfaced with Aspen Plus. With the help of this user membrane model and the other Aspen Plus built-in process models, different membrane gas separation processes can be simulated and designed for different specific systems. This chapter will focus on the design and simulation of CO_2 capture processes using interfaced gas separation membrane model from industrial flue gases especially from post-combustion power plant flue gases, to contribute to CO_2 mitigation efforts by utilizing captured CO_2 in Enhanced Oil Recovery (EOR) application.

Worldwide global climate change concerns have prompted interest in reduction of CO_2 emissions, a greenhouse gas (GHG) produced in the most significant quantities. The primary source of man-made CO_2 is combustion of fossil fuels. It is estimated roughly that one-third of CO_2 emissions come from fossil fuels used for generating electricity. Other industrial processes such as oil refineries, cement plants and fertilizer also emit large amount of CO_2. The existing coal-based power plants have the highest CO_2 emissions of any power generating systems, and have among the lowest cost of electricity generation relative to other generation types. Stabilizing the concentration of atmospheric CO_2 in a safe level will likely require a variety of actions such as switching from CO_2 emitting to non- CO_2 emitting energy sources, improving energy efficiency of energy conversion processes, usage of lower carbon intensity fuels, carbon

capture and storage (CCS), etc. CCS would permit the continuing use of coal and other fossil fuels in power generation while significantly reducing GHG emissions. It is easier to capture CO_2 from a large stationary point source (i.e., power plant) rather than from a mobile source (i.e., the transportation sector). However, the energy required to operate CO_2 capture systems reduces the overall efficiency of the power plant. Minimization of energy requirements for capture, together with improvements in the efficiency of energy conversion processes will continue to be high priorities for future technology development in order to minimize overall environmental impacts and costs (Davidson and Metz, 2005).

Approaches to CO_2 capture from coal-fired power plants can be divided into three categories: post-combustion capture, oxygen-fired combustion, and pre-combustion capture (Gottlicher, 2004). In post-combustion, carbon dioxide recovery is performed at the end of pipe i.e. from the fume exhaust. Post-combustion CO_2 capture involves treating the boiler exhaust gases immediately before entering the stack. The advantage of this approach is that it would allow retrofit at existing facilities that can accommodate the necessary capturing hardware and ancillary equipment. Post-combustion capture offers a significant design challenge due to the relatively low partial pressure of the carbon dioxide in the flue gas. Nevertheless, it shows the essential advantage to be compatible to a retrofit strategy. There are several technologies that can be employed within this category. Out of the four traditional methods of CO_2 capture (absorption by liquid MEA, adsorption by activated carbon, membrane separation and cryogenic fractionation), absorption is usually considered to be the best available technology for post-combustion application (Simmonds et al., 2003; Davison and Thambimuthu, 2004; Metz et al., 2005). Due to the significant energy consumption associated with the regeneration step, solvent losses, and secondary CO_2 production associated with solvent regeneration by steam, extensive research efforts are continuing focusing on the improvement of the absorption processes and finding other efficient capture alternatives at the same time (Aron and Tsouris, 2005; Oexmann et al., 2008).

Membrane gas separation of CO_2 from light hydrocarbons has met with considerable success in the petroleum, natural gas and chemical industries, because of the introduction of stable and selective polymer membranes, plant compactness, environmental impact, energetic aspects, and possibility of integrating various membrane operations in the same industrial cycle (Kesting and Fritsche, 1993). But membrane gas separation faces strong challenges in the post-

combustion CO_2 capture at power plants due to the low CO_2 concentration in the flue gas and the pressure of the flue gas, which is in the range of ambient pressure rather than being pressurized (Koros and. Fleming, 1993).

Van der Sluijs et al. (1992) examined the feasibility of polymer membranes for the separation of carbon dioxide from post-combustion flue gas of a conventional coal-fired power plant (600 MW_e) by using binary gas separation model. They studied single membrane stage and two stage cascade with recycle by using compression energy for driving force and three available commercial polymer membranes with maximum CO_2/N_2 selectivity of 43. The authors concluded that available polymer membranes are not economically competitive with other separation methods for CO_2 separation from flue gas due to excessive energy consumption, and suggested that a polymer membrane would require a CO_2/N_2 selectivity greater than 200. A techno-economic evaluation of different CO_2 capture processes for capturing CO_2 from different power plants flue gases including membrane gas separation process (using CO_2/N_2 selectivity of 20 and CO_2 permeance of 570) was investigated by The IEA Greenhouse gas Program (Riemer, 1993). In this report, an analysis of the performance of gas separation polymeric membrane technology compare to gas absorption membrane (with MEA) and conventional MEA scrubbing was presented based on overall plant efficiency and cost of CO_2 avoided. It was concluded that for CO_2 separation from flue gas mixture of pulverized coal fired plant, the performance of gas separation membrane was not satisfactory. The study considered single stage membrane plant based on cross-flow model without recycle stream. Göttlicher (2004) and Metz et al. (2005) both considered gas separation by polymeric membrane as inappropriate technology for post-combustion CO_2 capture based on the above mentioned studies in their process selection projects.

Many membrane researchers were unsatisfied with this conclusion. Further systematic critical engineering analysis of membrane processes for post-combustion application emphasised to reassess the above conclusion with the help of recent advancement in polymeric membrane material as reported elsewhere (Kazama et al., 2005; Powell and Qiao, 2006; Du et al., 2006; Lin et al, 2007; Kai et al., 2008, Yave et al., 2010, Merkel et al., 2010). Kazama et al. (2005) carried out an economic analysis for CO_2 capture using hollow fiber membrane followed by a liquefaction process. They considered properties of a newly developed Cardo polyimide asymmetric membrane (CO_2/N_2 selectivity: 40; CO_2 permeance: 1000 GPU) for a flue gas from a

coal fired power station (CO_2 concentration 13.2%) and from a steel plant (CO_2 concentration 26.8%). Based on 189 ton/hr CO_2 recovery and 99.9% purity (liquid CO_2), they concluded that the total cost of CO_2 separation and liquefaction strongly depends on the CO_2 concentration of source gases. In the CO_2 concentration around 25% or more, membrane has an advantage over amine absorption. The authors also concluded that electricity consumption of the vacuum pump contributed to 50% or more of the total cost. It was not clear in this analysis what type of membrane process system was employed, and what was the separation target (i.e., % CO_2 recovery) specified for CO_2 capture.

Bounaceur et al. (2006) evaluated a single stage gas permeation module with a binary carbon dioxide/nitrogen feed mixture for post-combustion CO_2 capture by considering different feed composition (0.1, 0.2, 0.3 CO_2 mole fraction) and membrane selectivity (50, 100, 150, 200). Their target specifications for CO_2 recovery and purity were within the ranges of 80 to 90%. Feed compression (multistage) in the upstream side and vacuum operation in the downstream side were employed. A compression strategy for combined capture and injection processes to minimize the overall compression energy was investigated. They concluded that when the recovery ratio and permeate composition do not exceed 0.8 and the carbon dioxide composition in the flue gas exceeds 0.2, existing materials can purify the flue gas with only about 0.5–1 GJ/tonne CO_2 recovered compare to 4 to 6 GJ/tonne CO_2 recovered of amine absorption. Membranes that are currently available are not sufficiently selective to produce the recovery ratios and permeate compositions to meet proposed government regulations when coal-fired power plants has the flue gas stream of 10% CO_2 concentration. They concluded that a membrane with selectivity above 100 is required for less concentrated flue gas stream. Favre (2007) also provided a critical comparison of dense polymeric membrane capture processes with amine absorption in a post-combustion flue gas treatment. He discussed the technological and scientific challenges of gas separation polymeric membrane process faced in this area. His conclusions were almost the same as the previous article (Bounaceur et al., 2006). The author also concluded that increasing membrane selectivity does not change significantly energy requirements in the range of variables which was covered, and stressed that selectivity is not necessarily the only issue in this field.

Lin et al. (2007) simulated and designed different membrane gas separation processes based on MTR (Membrane Research and Technology) Polaris^{TM} membrane (CO_2/N_2 selectivity:

50; CO_2 permeance: 1000 GPU) for capturing CO_2 from coal combustion flue gas (600 MW) and compared the process energy (including sequestration) and membrane area requirement for all proposed process configurations. MTR process solution with recycle gas (with air sweeping) to combustor showed the best performance in terms of minimum energy and membrane area for the specified target of 90% CO_2 recovery and 88% purity. Spiral wound membrane module was considered in the design and simulation work. This process configuration may not be a suitable option for retrofit strategy because of the need of design change for existing combustor to accommodate extra flow of recycle stream, and also the efficiency of the conventional pulverized coal boiler might be decreased due to the increased CO_2 content in the air.

Kai et al. (2008) developed a commercial-sized modules of the poly(amidoamine) (PAMAM) dendrimer hollow fiber composite membrane with high CO_2/N_2 selectivity (150) and CO_2 permeance (29 GPU) for CO_2 removal from flue gas. They conducted a long-term stability test (running for 1000 h) using a real exhaust gas at a steel manufacturing plant and found that the membrane module was stable for at least 1000 hour of exposure to real exhaust gas.

Ho et al. (2008) investigated ways to reduce CO_2 capture cost from coal-fired power-plant (500 MW) flue gas using a hollow fiber membrane model (Shindo et al., 1985) by operating under vacuum conditions. Three process layouts were chosen to evaluate the cost and performance of CO_2 capture. These include a single stage membrane system and a two-stage cascade membrane system with and without retentate recycle. For the baseline economic evaluation of the vacuum permeate system, the feed gas was set at 1.5 bar and the permeate pressure was set at 0.08 bar. For the high-pressure feed operation, the feed-gas pressure was set 15 bar and the permeate pressure was set at atmospheric condition. Using membrane of CO_2 permeability of 70 barrer and CO_2/N_2 selectivity of 20, the maximum purity of CO_2 achieved was 77% in the permeate side for the specified recovery of 85%. The separated enriched CO_2 stream is compressed to 100 bar for transport along with cooling for further enrichment (at least 90% purity) of the product stream. The authors concluded that operating membrane processes under vacuum conditions could reduce the capture cost by 35% compared with a pressurized feed operation. Their results also indicated that the capture cost can be reduced to less than U.S. \$25/tonne CO_2 avoided when the CO_2 permeability is 300 barrer (assuming membrane thickness of 125 μm, CO_2/N_2 selectivity is 250, and a membrane cost of USD10/m^2.

Zhao et al. (2008) conducted a series of parametric studies of membrane gas separation processes for post-combustion CO_2 capture from 1000 MW coal-fired power plant. A single stage membrane process with permeate side vacuum operation was simulated in Pro/II process simulator (Simulation Sciences Inc.) using a built-in binary gas separation membrane model, and Cardo polyimide membrane properties developed by RITE (Kazama et al., 2005). The influence of membrane quality and operating conditions on the membrane performance was investigated comprehensively. They concluded that one stage membrane process alone cannot fulfill the high degree of separation and the high CO_2 purity at the current level of development of the membrane technology. The authors stressed that a multi-stage gas separation membrane system should be considered to reach the specified target which combines the advantages of membranes with high permeability and membranes with high selectivity. They suggested that in order to obtain the required CO_2 purity for the future transport and injection requirements, multi-stage membrane arrangements coupled with a CO_2 liquefaction process should be adopted for the system design with current levels of membrane selectivity.

He et al. (2009) conducted a simulation study of CO_2 capture by hollow fibre carbon membrane using an in-house program integrated with Aspen Hysys® as a user operation module. Three different membrane configurations such as co-current, perfect-mixed, and counter-current were simulated using a single stage membrane unit to obtain optimum configuration. The counter-current configuration showed the best performance compared to the other two configurations based on the required membrane area and total energy demands. A three-stage membrane process was optimized based on economic evaluation by adjusting operation conditions. The process design was based on the flue gas stream of a typical coal fired power plant (400 MW). It was emphasized that the performance of hollow fibre carbon membranes should be further improved in order to reduce the capital cost for CO_2 capture at an industrial scale.

Merkel et al. (2010) extended the work of Lin et al. (2007) with slight modification in the previous process design that uses the incoming combustion air as a sweep gas to generate driving force by incorporating a compression-condensation-membrane loop with the third membrane stage. They concluded based on process sensitivity studies using Polaris^{TM} membrane (CO_2/N_2 selectivity: 50; CO_2 permeance: 1000 GPU) that improving the membrane permeance is more important than increasing the selectivity to further reduce the cost of CO_2 capture from flue gas.

It was found that increasing membrane CO_2/N_2 selectivity above ~ 30 had little cost benefit. They used ChemCad (ChemStations, Houston, TX) simulation software with differential element subroutines written at MTR for the membrane separation steps.

System analysis and design help us to understand and arrange the membrane process effectively. It is generally agreed that membrane area and energy consumption are the key factors determining the cost of membrane separation processes. Designing a membrane gas separation process for capturing CO_2 from coal-fired power plant flue gas, and utilizing it in EOR application, needs to satisfy capture requirements of CO_2 purity $\geq$ 98% (Alie et al., 2005; Zhao et al., 2008) and recovery > 80% (Davison and Thambimuthu, 2004) along with compression requirement for injection with specified pressure such as 110 bar or higher. So far, no process configuration as discussed above has been able to meet both high purity and high recovery requirements for captured CO_2. The other major issue in the design of membrane process is the minimization of capture and compression energy for injection since it will drive to a large extent the corresponding operating costs. Keeping in mind the above mentioned points i.e., high purity, high recovery and lower energy consumption, the author will simulate and design various membrane process configurations based on the advancements in the membrane gas separation technologies and commercial process simulation software for CO_2 capture from coal-fired power plant flue gas for applying to EOR. The process configuration with minimum energy requirement (capture and injection) will be selected as a base case for process optimization studies in the next chapter for further improvement.

5.2 Design Basis

Coal-fired power plants are the largest anthropogenic point sources of atmospheric CO_2 in Canada (Alie, 2004). Post-combustion capture of CO_2 seems most promising as a near-term strategy for mitigating CO_2 emissions from these facilities. The study basis considered by Alie (2004) has been adopted here. The Nanticoke Generating Station is the largest coal-fired power plant in North America, delivering up to 4096 MW of power (eight 500 MW boilers) into the southern Ontario power grid from its base in Nanticoke, Ontario, Canada. Nanticoke is owned by Ontario Power Generation. Flue gas from a 500 MW coal-based unit of Nanticoke Generating Station will be considered for this study. All of the membrane capture processes will be designed based on the flue gas leaving from this (500 MW) coal-fired power plant to capture 85% of CO_2 with a purity of 98%. The captured CO_2 will be compressed to 110 bar at 25^oC for transporting via pipeline. This pressure specification may vary depending on the pipeline length and design, and the location of booster compressors. It is assumed that the capture plant imports required electric power either from the existing power plant or from an auxiliary NGCC plant, and in that case, the CO_2 generated by the combustion of natural gas will not be captured in this study because of lower concentration of the flue gas. It is also assumed that the capture plant uses locally available 12^oC lake water for cooling requirements.

5.3 Flue Gas Analysis and Pre-conditioning

Alie (2004) developed a model in Aspen Plus to predict the flow rate and composition of flue gas based on the information provided for fuel used, boiler operating conditions, and plant power output. Based on a 50/50 blend of PRB (Powder River Basin) and USLS (US low Sulphur) coals, the estimated flue gas mass and volumetric flow rates are moderately higher and lower respectively than that of observed at plant. The flue gas flow rate, composition and conditions are presented in Table 5.1. The characteristics of the PRB and USLS coals are given in Appendix C.

As membrane replacement is a critical operating cost, pre-treatment of feed stream (i.e. flue gas) is necessary to increase the membrane life. Scholes et al. (2009) reviewed the effect of minor components (i.e., SO_x, NO_x, CO, Ar, H_2O etc.) on polymeric membrane gas separation for application in pre- and post-combustion CO_2 capture. Generally, SO_x, NO_x, and H_2O have

greater permeability through glassy polymeric membranes than CO_2 and therefore will enrich the permeate stream. This permeability increase can be related to the higher critical point of these species. CO and Ar have lower permeability compared with CO_2 and therefore remain in the retentate stream. In this study, we assumed that NO_x are removed by selective reduction with ammonia in a Denox unit, that particulate removal systems (bag filter, coalescing filter, E-filter etc.) are already in place, that water vapor is removed by molecular sieves, and that SO_x is removed by limestone in a desulphurisation (FGD) unit from flue gas before CO_2 recovery.

Table 5.1: Flue gas characteristics based on a 50/50 blend of PRB and USLS coals from a 500 MWe power plant with thermal efficiency of 36% (Alie, 2004)

Mass flow rate (kg/hr)	2424400
Mole flow rate (kmol/hr)	82157.6
Volumetric flow rate (m^3/hr)	4182700
Temperature (°C)	134.0
Pressure (kPa)	101.0
Composition (mol %)	
N_2	72.86
CO_2	13.58
H_2O	8.18
O_2	3.54
Ar	0.87
NO_x	0.5
CO	0.37
SO_2	0.05
H_2	0.04

5.4 Design Strategy and Selection of Process Alternatives

Process design plays a vital role in the economic viability of any chemical processes. The design of membrane gas separation processes involves the determination of an appropriate membrane modules/permeators' arrangement/configuration as well as specification of process unit (i.e., module) sizes and operating conditions. The design of membrane processes can differ significantly due to the application specificity. Two approaches can be employed to design a membrane system: sequential and superstructure. In the sequential design approach, the membrane configurations are chosen a priori and the operating conditions are determined using

an optimization procedure. This approach is well suited for detailed evaluation of a small number of alternative flowsheets. Superstructure design approach provides a systematic framework for simultaneous optimization of the membrane process configurations and operating conditions (Floudas, 1995). As a detailed multicomponent membrane model is comprised of differential-algebraic equations with mixed boundary conditions, superstructure design approach is particularly difficult to use with a detailed multicomponent gas separation membrane model due to computational complexity. To avoid this complexity, approximate modeling technique for membrane module was used elsewhere (Qi and Henson, 2000). In this study, the sequential design approach will be adopted.

A single stage arrangement with feed compression/or permeate vacuum or both, and without any recycle stream is the most common and simplest design consideration. It should be noted that this individual stage may actually consist of several permeators arranged in parallel. The demand for higher product purity and recovery of the desired species necessitates the use of recycle streams as well as multi-stage configurations (Koros and Chern, 1987). The multi-stage configurations are designed usually using two, three or four stages. Several investigators considered the design of multi-stage configurations for CO_2/CH_4 separation (Spillman, 1989; Chern et al., 1985; Babcock et al., 1988; Bhide and Stern, 1993a, 1993b; Petterson and Lien, 1995; Qi and Henson, 1998a) and for the oxygen-enrichment of air (Bhide and Stern, 1991a). Besides single and multi-stage systems, configurations similar to distillation column such as two strippers in series permeator, and continuous membrane column were also investigated by some authors for CO_2/CH_4 separation (Hwang and Ghalchi, 1982; Qui et al., 1989; Lababidi et al., 1996). Two distinct options can be considered at the downstream side of a gas membrane separation process in order to induce a driving force from that side during design consideration. Vallieres and Favre (2004) explored the pros and cons of vacuum versus gas sweeping operation for dense membrane for pervaporation application in terms of overall energy consumption. They concluded that gas sweep generally offers the lowest raw energy consumption (pump work) unless a low vacuum level such as 20 mbar is practically achievable, and for pure compounds recovery, vacuum operation is preferable.

Extensive design, simulation and optimization works on membrane gas separation processes for CO_2 recovery from high pressure feed stream e.g., natural gas were conducted by different researchers as cited earlier. Very few design studies are found related to membrane CO_2

separation from low pressure feed stream such as flue gas from power plant post-combustion processes (Van der Sluijs et al., 1992; Lin et al., 2007; Ho et al., 2008). Few design studies related to low pressure feed stream for O_2 enrichment from air (Bhide and Stern, 1991) and H_2 purification from CO and CO_2 mixture are available (Xu, 1994). By following the sequential design methodology, fifteen process layouts were pre-chosen for design and simulation to evaluate the performance of CO_2 capture processes for power plant flue gas using polymeric membrane and are presented in Figures 5.1 to 5.15. These include single and multistage systems with and without recycle stream, feed compression, permeate compression, permeate vacuuming or permeate sweeping. Description of each process layout (i.e. configuration) is given in the next section. The process layout presented in Fig. 5.15 is a new configuration solely presented in this study. Symbols used in the process layout are presented in Fig. 5.16.

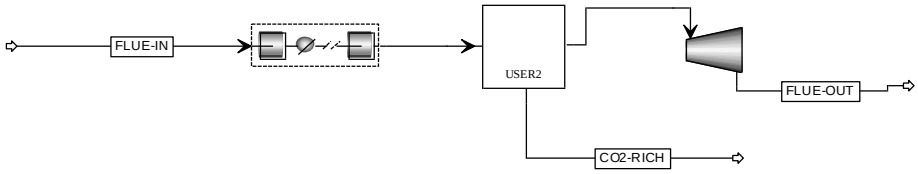

Figure 5.1: Configuration 1

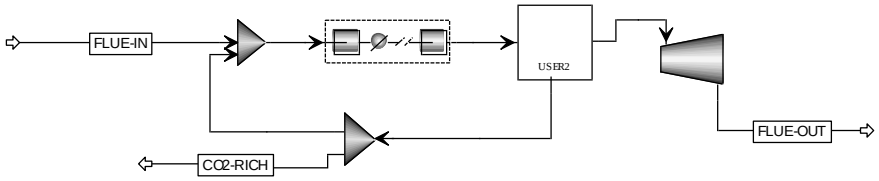

Figure 5.2: Configuration 2

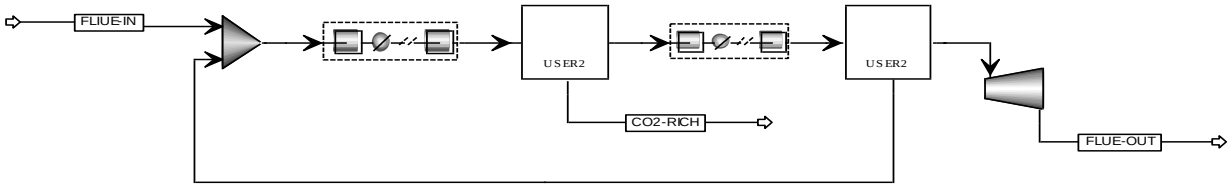

Figure 5.3: Configuration 3

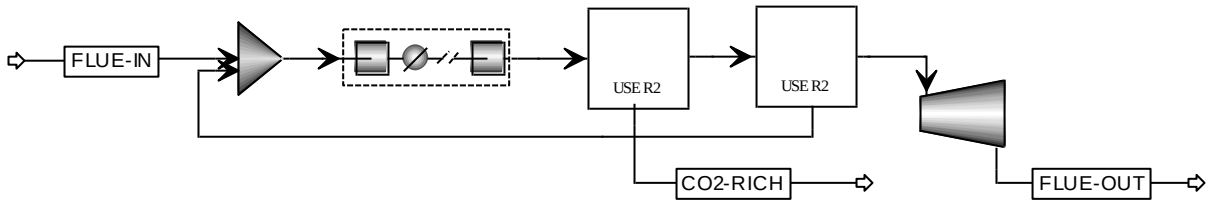

Figure 5.4: Configuration 4

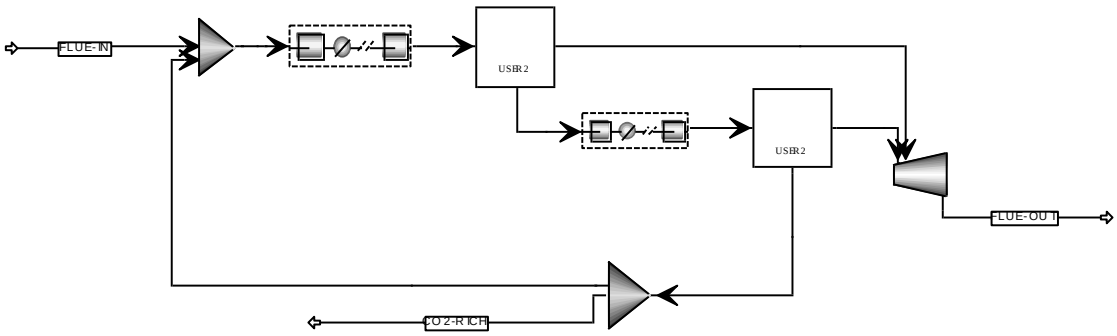

Figure 5.5: Configuration 5

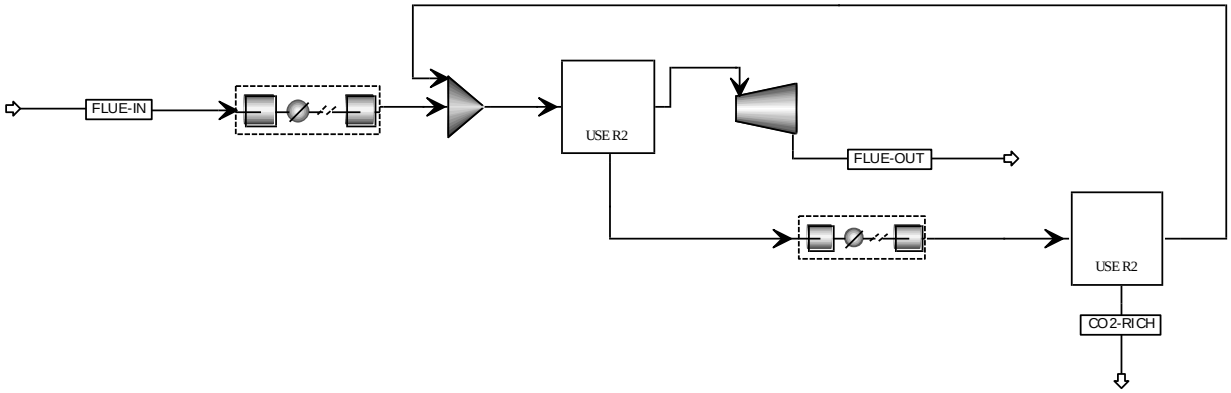

Figure 5.6: Configuration 6

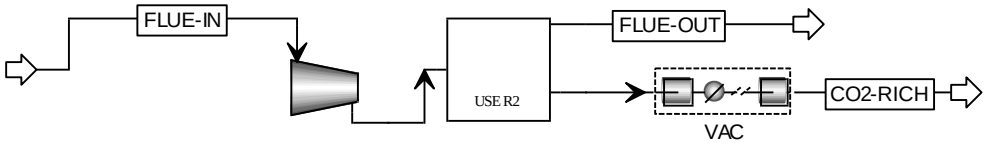

Figure 5.7: Configuration 7

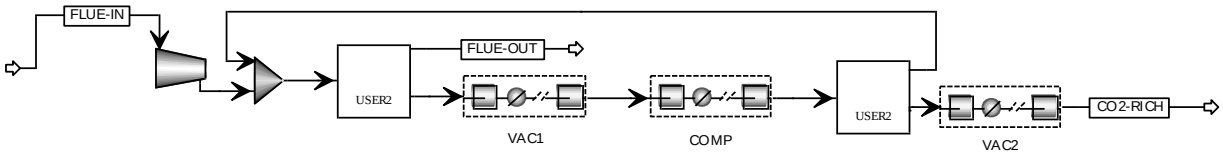

Figure 5.8: Configuration 8

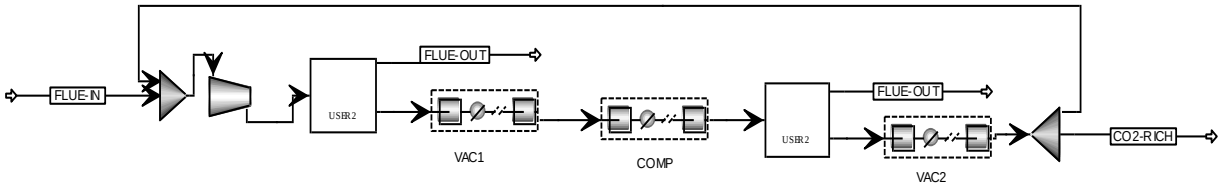

Figure 5.9: Configuration 9

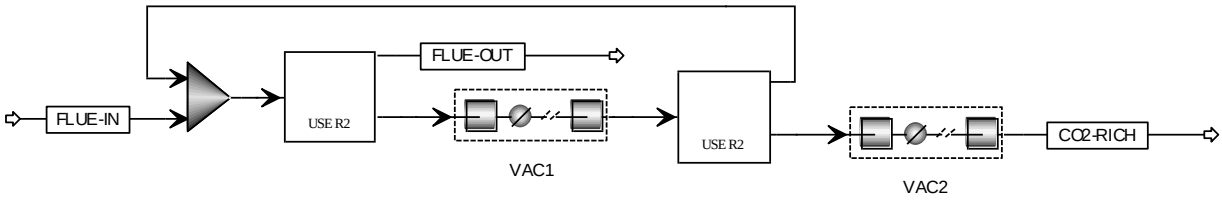

Figure 5.10: Configuration 10

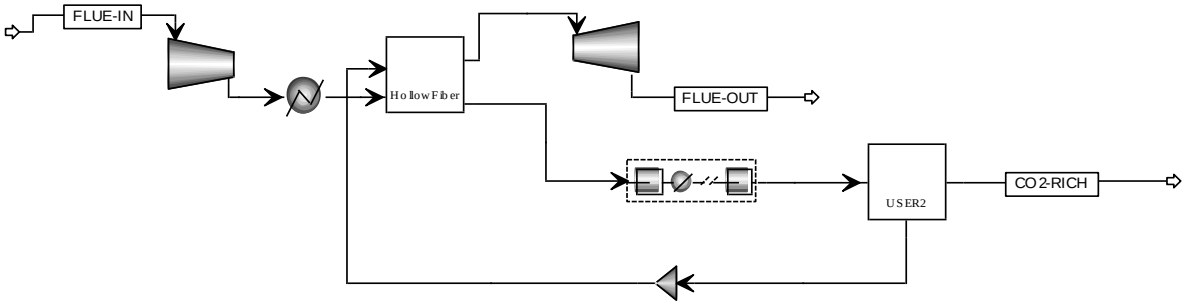

Figure 5.11: Configuration 11

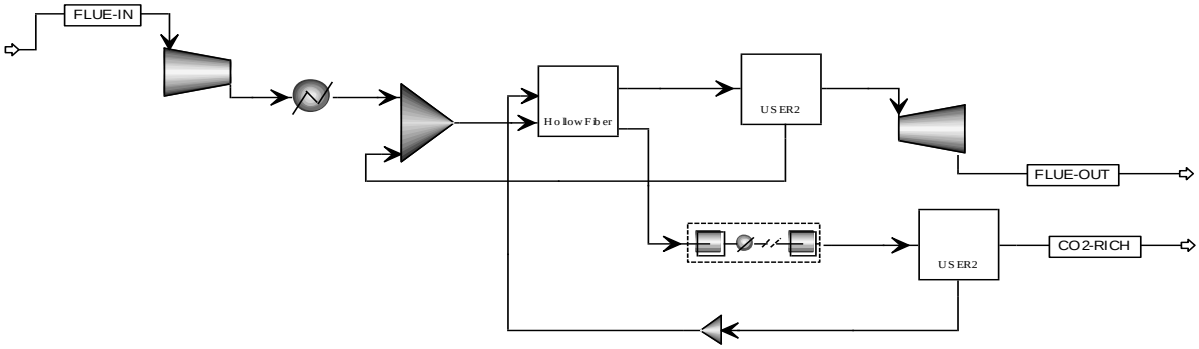

Figure 5.12: Configuration 12

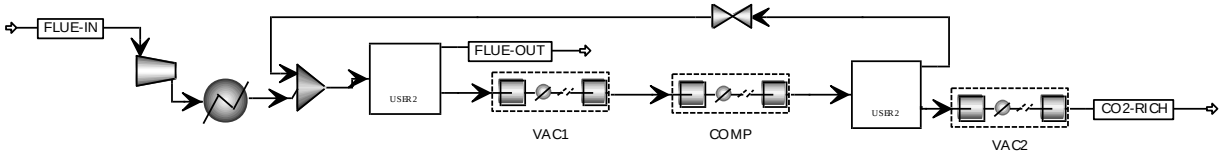

Figure 5.13: Configuration 13

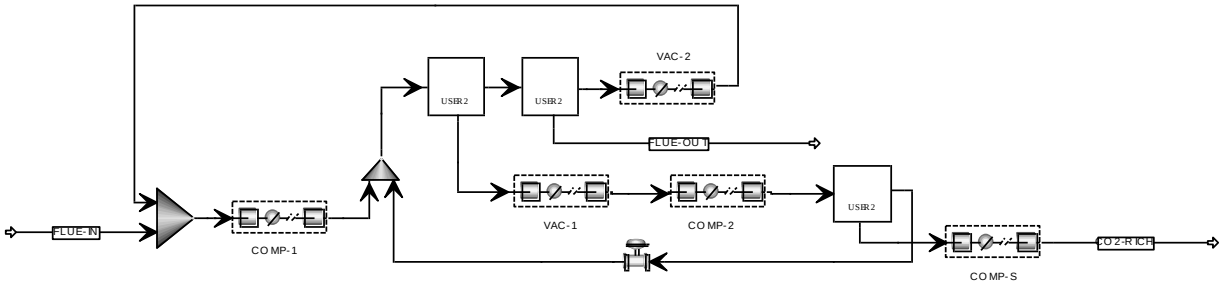

Figure 5.14: Configuration 14

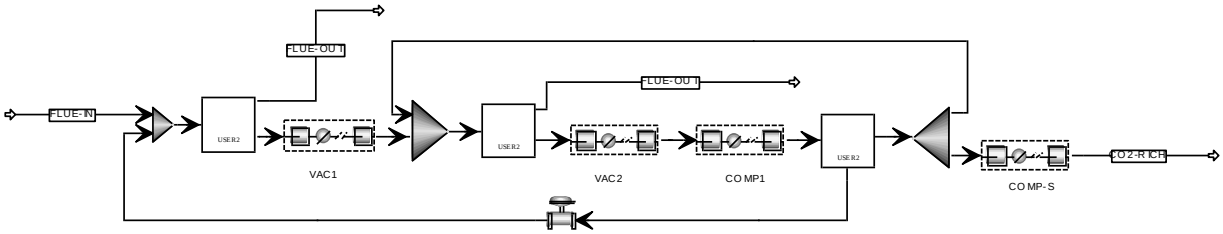

Figure 5.15: Configuration 15

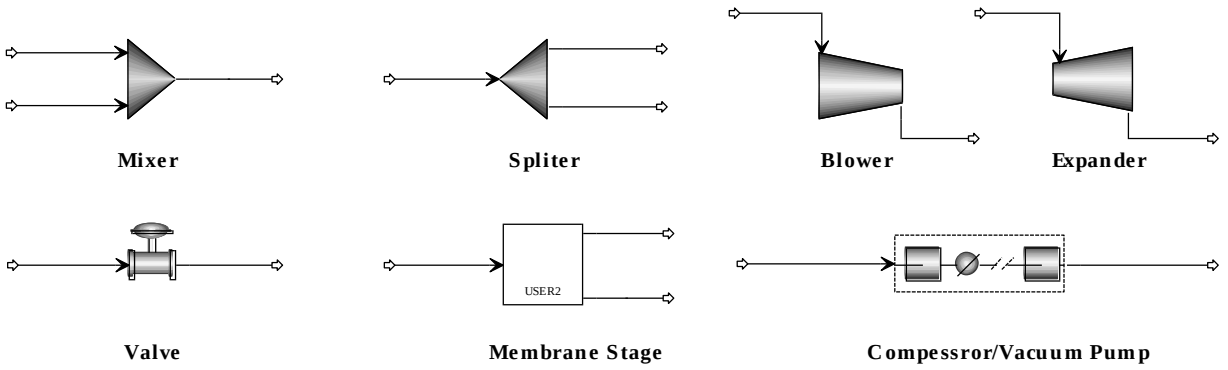

Figure 5.16: Symbols used in process configurations

5.5 Description of the Processes

Process layouts illustrated in Figs. 5.1 to 5.6 employ feed compression strategies.

- Fig. 5.1 represents a single-stage membrane process where the flue gas stream (FLUE-IN) is compressed and feed to the membrane unit. The membrane unit separates the flue gas in a CO_2 rich permeate stream (CO2-RICH) and a CO_2 lean retentate stream (FLUE-OUT). As the retentate stream remains on high pressure, the energy contained in the retentate stream can be recovered by using an Expander before emitting into the atmosphere.
- In the process of Fig. 5.2, a fraction of the CO_2 rich permeate stream is recycled back to increase the concentration of CO_2 in the permeate stream.
- Fig. 5.3 is a two-stage compression process with permeate recycle from 2^{nd} stage.
- A two-step permeation process in series arrangement with permeate recycle from 2^{nd} stage, is shown in Fig. 5.4.
- Two-stage cascade configurations with fraction of permeate recycle from 2^{nd} stage in one configuration and with retentate recycle in another configuration are shown in Fig. 5.5 and Fig. 5.6 respectively.

The processes represented in Figs. 5.7 to 5.10, mainly employ permeate vacuuming in the down stream side of the membrane unit for generating the driving force, and some also uses blower for slight feed compression. Vacuum operation utilizes less power energy but requires much more membrane area than the compression strategy.

- The single-stage membrane process configuration in Fig. 5.7 uses a blower for slight feed compression and vacuum pump for permeate vacuuming to maximise the transmembrane pressure difference.
- Figs. 5.8 and 5.9 show the simplified schematics of the two-stage cascade membrane configurations with vacuum permeate condition, and feed compression with retentate and permeate (fraction) recycle from the 2^{nd} stage.
- A two-stage cascade arrangement with permeate vacuum condition and retentate recycle, and without feed compression is shown in Fig. 5.10.
- Process configurations represented by Figs. 5.11 and 5.12 employ permeate sweeping operation along with feed compression. In Fig. 5.11, the flue gas is introduced to the low-pressure i.e., permeate side of the 1^{st} membrane stage as a sweep gas. Then, the permeate

stream from the 1st stage is compressed and introduced to the high-pressure (feed) side of the 2nd stage. The retentate stream from the 2nd stage is recycled to the high-pressure side of the first stage.

- Fig. 5.12 uses another membrane stage (3rd) for further processing of retentate stream of 2nd stage. Permeate stream from the 3rd stage is combined with the flue gas before entering to the low-pressure side of the membrane stage. An expander is used to recover energy from retentate stream in both configurations.
- Process configuration in Fig. 5.13 is almost the same as the configuration in Fig. 5.9 with little modification. Here, high pressure is used to compress the permeate stream from the first stage. This process is used here to compare permeate sweep vs. permeate vacuum operation.
- Fig. 5.14 is a two-step, two stage process with feed compression and permeate vacuum. A control valve is used to reduce the stream pressure. Flue gas is compressed and feed to the 1st membrane unit which is attached to a permeate vacuum pump. The retentate stream is again processed with another membrane stage with vacuum operation. The CO_2 rich stream from this unit is recycled and mixed with the flue gas stream before being compressed. The permeate stream from the 1st stage is compressed and fed to the third membrane stage to get the desired purity in the final permeate stream. The retentate stream is recycled and mixed with compressed flue gas stream after pressure reduction by a control valve. The permeate stream is compressed to a specified pressure for transportation to an injection site.
- The main difference between the two process configurations presented in Fig. 5.14 and Fig. 5.15 is: one (i.e., Fig. 5.14) considers feed compression with permeate vacuum approach for the 1st stage while the other (Fig. 5.15) considers only permeate vacuum operation for the 1st stage. The opposite is considered for the 3rd stage, i.e., vacuum in Fig. 5.14 and compression in Fig. 5.15. Overall, the Fig. 5.15 process eliminates a compressor.

5.6 Development of Aspen Process Flowsheets

All the process layouts presented above has been implemented in Aspen Plus to design and simulate post-combustion CO_2 capture processes for a coal-fired power plant exhaust gases. Flue gas from the Nanticoke power plant is emitted through the stack into the atmosphere usually at a temperature of 134^{o}C. It is assumed that flue gas is free from all impurities (such as fly ash, SO_x, $NO_{x,}$) after conditioning, being dried, and cooled down to 40^{o}C before entering the

membrane unit. The flue gas flow rate, composition, temperature and pressure after treatment are presented in Table 5.2. Shell side feed and countercurrent flow configurations of hollow fibre membrane modules are considered for designing the membrane processes. Three polymeric membrane properties were considered during the different development stages of the study and are presented in Table 5.3. The following design criteria were set for the membrane capture processes: 85% capture rate with 98% (mol%) CO_2 purity in the permeate stream.

Table 5.2: Flue gas characteristics (after treatment, and before entering the membrane unit)

Flow rate (kmol/s)	20.95
Temperature (°C)	40
Pressure (kPa)	101.0
Composition (mol %)	
CO_2	14.95
N_2	80.2
O_2	3.9
Ar	0.95

Table 5.3: Membrane properties considered in simulation at different stages

References	Polymer	Permeance (10^{-10} mol/m^2.s.Pa)		Selectivity (CO_2/N_2)
Reimer, 1993	Polyphenyleneoxide & polydimethylsiloxane	CO_2	1910	20
		N_2	95.7	
		O_2	478	
		Ar	191	
Kazama et al., 2005	Cardo Polyimides	CO_2	3347	40
		N_2	84	
Lin et al., 2007	Polaris^{TM} (unknown)	CO_2	3350	50
		N_2	67	
		O_2	168	
		Ar	168	

5.6.1 Specifying Property Methods

PENG_ROB property method has been used as the base property method. It uses standard Peng-Robinson equation of state for all thermodynamics properties except liquid molar

volume. This property method is particularly suitable for high pressure and high temperature region.

5.6.2 Specifying Streams

Only one input stream has to be specified i.e., flue gas feed stream, **Flue-in**. Its conditions and flow rate are given in Table 5.2. Although the present membrane model can handle any number of components, due to lack of membrane property data and long execution time of the membrane model, only CO_2, N_2, O_2 and Ar components have been considered.

5.6.3 Specifying Blocks

The flowsheets consist of the following blocks:

Blower

A blower is used to compress the flue gas slightly above the atmospheric pressure. It was implemented using a polytropic single stage centrifugal compressor unit operation model (UOM), **COMPR.** A polytropic efficiency of 80% and mechanical efficiency of 90% wee assumed. Operating pressure e.g., 1.5 bar was specified as outlet pressure in one process.

Expander

An expander is used to recover energy from the high pressure retentate stream. **COMPR** was also used for expander modeling but used an isentropic turbine model. The isentropic and motor's mechanical efficiency were assumed 80% and 90%, respectively. The expander also needs outlet pressure specification. In our study, 2.0 bar was used to avoid liquid formation.

Compressor/Vacuum Pump

In feed compression membrane processes, compressors are used to compress the feed stream or compress the permeate stream. A vacuum pump is used for permeate vacuuming to increase the driving force in the downstream side of the membrane module. A compressor is also required to compress the captured CO_2 for transportation to the injection site. Compressor and Vacuum pump were implemented in Aspen Plus using the **MCOMPR** UOM. **MCOMPR** is used for modelling a multistage compressor with inter-cooling. Five inter-stages with outlet cooling temperature of 40^oC from each stage were considered. Same polytropic and mechanical efficiency for centrifugal compressor were specified as above. For the vacuum pump, three vacuum conditions (0.3, 0.25 and 0.1 bar) were considered depending on the case studies. The

outlet pressure of the compressor considered here were: 3, 10, 20 and 27 bar. For captured CO_2 compression for transportation via pipeline, the pressure was specified at 110 bar at 25^{o}C.

Membrane Stage

A membrane unit based on **USER2** subroutine described in the previous chapter was used for design calculation. In a membrane stage several membrane modules are arranged in parallel or series combination. This unit requires some input parameters value such as fiber inner and outer diameter, numbers, components' permeance data and permeate pressure.

Valve

A valve is used to reduce the inlet stream pressure to a desired level. The **VALVE** model was used for specifying the outlet stream pressure.

Mixer

A mixer is used to combine several streams into a single stream flow and was implemented with the **MIXER** unit operation model.

Splitter

Splitter is used to split a single stream to multiple streams. **FSPLIT** UOM was used to implement a splitter operation.

5.6.4 Design Specifications

Using **Design Spec** form of the Flowsheeting Options sheet of Aspen Plus data browser, design specifications for this study (i.e. 85% CO_2 recovery and 98% CO_2 concentration in the permeate stream) were specified. Design specifications are similar to feedback controllers. With a feedback control, users can set the value for a flowsheet variable or some function of flowsheet variables, and manipulate other variables (block input variable or process feed stream variable) until the desired value for the set variable is achieved. In this study, the membrane area i.e., hollow fibre numbers was used as the manipulated variable.

5.6.5 Simulation Parameters

For simulation, some input parameters values such as inner and outer diameters of hollow fibre, fibre length, permeate side pressure, component permeance, and fibre numbers (i.e., membrane area) are required for membrane unit. The values used in the present study are presented in Table 5.4. The permeate side pressure specification for the membrane unit depends on the type of operation: permeate vacuum operation or feed compression operation. For the feed compression operation, it is specified as atmospheric pressure and for permeate vacuum operation it depends on what vacuum condition is desired. The outlet pressure of the vacuum pump is 1 bar. Feed flow rate, composition and conditions are presented in Table 5.2. The operating pressure for the blower, compressor and vacuum pump need to be specified as well and values considered were mentioned earlier.

Table 5.4: Module and process simulation parameters for Membrane Unit

Module		
Membrane type	Asymmetric Hollow fibre	
Flow configuration	Counter-current, shell side feed	
Fibre inner diameter (μm)	300	
Fibre outer diameter (μm)	500	
Fibre active length (m)	0.5	
Permeance, (10^{-10} mol/s.m^2.Pa)	CO_2	3350
	N_2	67
	Ar	168
	O_2	168

5.7 Results and Discussions

Membrane process design involves the determination of the membrane unit size i.e., membrane area requirement, and the configuration necessary to meet the simulation scope and specifications. The scope of the simulation is limited to the post-combustion CO_2 capture from a 500 MW coal-fired power plant flue gas, and compression of the captured CO_2. The capture process needs to meet the following specifications: 85% CO_2 recovery -and 98% CO_2 purity in the CO_2 rich stream with minimum power consumption. Compression pressure for captured CO_2 is specified to 110 bar at a temperature of 25^oC for transportation through pipeline.

Detailed parametric studies of CO_2/N_2 gas separation membrane processes for post-combustion capture are available elsewhere (Bounaceur et al., 2006; Favre, 2007; Zhao et al., 2008). Their studies included the investigation of the influence of membrane quality and operating conditions on the membrane performance using a single stage membrane process by varying the following parameters: (i) CO_2 permeability and CO_2/N_2 selectivity, (ii) membrane area, (iii) process selectivity i.e., separation coefficient, (iv) pressure ratio, and (v) CO_2 concentration in the feed gas. The present study focuses mainly on process design with minimum energy and membrane area requirements to meet the above mentioned specifications as no comprehensive previous design study was found in the literature for this type of specifications requirement. The membrane area and the compressor/vacuum pump duty are the most important factors which determine the operating and investment costs associated with a membrane gas separation system. Compressor or vacuum pump duty is mainly determined by the flow rate through the unit and the pressure ratios across the unit.

The purity of recovered CO_2 depends mainly on the selectivity of membrane, the pressure ratio, the CO_2 concentration in the feed gas, and the degree of separation i.e., CO_2 recovery rate. As membrane selectivity, feed composition, and CO_2 recovery rate are considered constant in all these membrane processes design studies, the pressure ratio plays an important role on the product purity. Usually for a given CO_2 recovery, high pressure ratio operation means high power consumption but lower membrane area requirement and high product purity. On the other hand, operating the system at low pressure ratio means less power consumption, less product purity and large membrane module installation. This behaviour is easily understood from a simple single stage membrane gas separation process study but for more complex processes i.e.,

multi-stage processes with permeate and retentate recycle streams as shown in Fig. 5.14 and 5.15, explanation of the overall behaviour is much less straightforward. The optimal trade-off between the pressure ratio (i.e., power consumption) and membrane area is the key point for judging the best design configuration.

The feed compression related processes (Configurations 1 to 6) are widely used for purifying high pressure natural gas stream from CO_2. They are thus investigated first. The simulation and design results with operating conditions for those processes are presented in Table 5.5. It is clear that, among Configurations 1 to 6, none is capable of meeting the CO_2 purity requirement of 98%. A maximum purity of 96.7% is achieved with Configuration No. 6 (Fig. 5.6). It is also observed that the energy requirement to run the best capture process (i.e. Configuration No. 6) is almost equivalent to 50% of the net power output of the power plant before CO_2.

Table 5.5: Aspen Plus results with operation conditions for feed compression processes (Configurations No. 1 to 6)

Process Configurations			**Fig. 5.1**	**Fig. 5.2**	**Fig. 5.3**	**Fig. 5.4**	**Fig. 5.5**	**Fig. 5.6**
Streams name		FLUE-IN	CO2-RICH	CO2-RICH	CO2-RICH	CO2-RICH	CO2-RICH	CO2-RICH
Mole fraction	**CO_2**	0.1495	0.653	0.690	0.848	0.850	0.943	**0.967**
	N_2	0.8020	0.3047	0.2714	0.1307	0.1293	0.0435	0.0239
	O_2	0.0390	0.0340	0.0310	0.0169	0.0167	0.0109	0.0070
	Ar	0.0096	0.0084	0.0076	0.0041	0.0041	0.0027	0.0017
Total flow, kmol/sec		20.95	4.08	3.86	3.14	3.13	2.82	2.75
Temperature, K		313.0	313.0	313.0	313.0	313.0	313.0	313.0
Pressure [10^5 Pa]		1.01	1.01	1.01	1.01	1.01	1.01	1.01
CO_2 capture rate			85%	85%	85%	85%	85%	85%
Pressure ratio (feed/perm.out)			20	20	10 & 10	20	20	20
Split fraction				0.25			0.1	
Stage-cut in each mem. unit			0.19	0.23	0.12, 0.20	0.13, 0.15	0.27, 0.55	0.21, 0.57
Membrane Area, [10^6 m^2]			0.107	0.107	0.197	0.076	0.201	**0.135**
Blower power, MW_e			-	-	-	-	-	-
Compressor power, MW_e			251.6	266.8	283.7	288.5	323.2	308.5
Expander power, MW_e			-53.4	-54.1	-56.4	-56.4	-59.8	-60.0
Net (Capture) Power, MWe			198.2	212.7	227.3	232.1	263.4	**248.5**

The next step is the investigation of the vacuum pumping operation for generating transmembrane driving force for separation with or without slight feed compression by a blower. The simulation and design results of the permeate vacuum operation processes (Configurations No. 7 to 10) are presented in Table 5.6. It is found that two-stage vacuum processes with a feed permeate pressure ratio of 15 (feed side pressure 1.5 bar and permeate side pressure 0.1 bar) can not satisfy the permeate purity requirement. Although some researchers (Ho et al., 2008) considered permeate vacuuming condition at 0.08 bar, still it will be difficult to meet the process specification by applying hard vacuum with these processes. Comparison of Configurations 3 and 4 with Configuration 8 and 9 indicates that vacuum operation needs less energy and more membrane area compare to the feed compression operation for same target specifications.

Table 5.6: Aspen Plus results for permeate vacuuming processes (Configurations No. 7 to 10)

Process Configurations			**Fig. 5.7**	**Fig. 5.8**	**Fig. 5.9**	**Fig. 5.10**
Streams name		FLUE-IN	CO2-RICH	CO2-RICH	CO2-RICH	CO2-RICH
Mole fraction	CO_2	0.1495	0.5503	**0.868**	**0.869**	0.777
	N_2	0.8020	0.3981	0.1014	0.1041	0.1762
	O_2	0.0390	0.0415	0.0242	0.0220	0.0373
	Ar	0.0096	0.0102	0.0060	0.0054	0.0092
Total flow, kmol/sec		20.95	4.8	3.1	3.1	3.4
Temperature, K		313.0	313.0	313.0	313.0	313.0
Pressure [10^5 Pa]		1.01	1.01	1.01	1.01	1.01
Feed Blower pressure [10^5 Pa]			1.5	1.5	1.5	-
Vacuum pump condition [10^5 Pa]			0.1	0.1	0.1	0.1
Compressor pressure [10^5 Pa]			-	1.5	1.5	-
CO_2 capture rate			85%	85%	85%	85%
Split fraction					0.25	
Stage-cut in each mem. unit			0.23	0.23, 0.57	0.31, 58	0.27, 0.53
Membrane Area, [10^6 m^2]			2.27	**3.07**	**4.10**	7.03
Blower power, MW_e			32.6	32.6	34.2	-
Compressor power, MW_e			-	7.9	10.4	-
Vacuum pump power, MWe			44.7	76.7	97.0	84.5
Net (Capture) Power, MWe			77.3	**117.2**	**141.6**	84.5

Permeate sweeping operation was also investigated to make a comparison with vacuum operation, and results are presented in Table 5.7. The objective of this comparison was to decide which type of operation (permeate sweeping vs. vacuum operation) to be investigated in the next development stages. First, the two permeate sweeping process Configurations (i.e. Configuration 11 and 12) were simulated and designed. Between these two permeate sweeping process Configurations, Configuration 12 exhibits better performance in terms of both membrane area and energy consumption for the same target specifications. Then, Configuration 12 was compared to a permeate vacuum operation with slight feed compression (Configuration 13). It is found that vacuum operation requires 35% and 28% less membrane area and power consumption respectively, compared to permeate sweeping. Based on these findings, the vacuum operation was selected for further investigation. It should be noted that the flue gas is pressurised to 2.2 bar and cooled to 40^{o}C before using it as sweep gas. It is also important to note that vacuum operation needs an extra smaller compressor which may affect overall project investment cost.

Table 5.7: Aspen Plus results for permeate sweeping (Configurations No. 11 to 13)

Process Configuration			**Fig. 5.11**	**Fig. 5.12**	**Fig 5.13**
Streams name		FLUE-IN	CO2-RICH	CO2-RICH	CO2-RICH
Mole fraction	CO_2	0.1420	**0.650**	**0.650**	**0.659**
	N_2	0.8000	0.2498	0.2571	0.2160
	O_2	0.0490	0.0939	0.0868	0.1181
	Ar	0.0090	0.0063	0.0061	0.0074
Total flow, kmol/sec		18.46	3.2261	3.2263	3.19
Temperature, K		313.0	313.0	313.0	313.0
Pressure [10^5 Pa]		1.01	1.01	1.01	1.01
Blower Pressure [10^5 Pa]			2.2	2.2	2.2
Vac. Pump condition [10^5 Pa]			-	-	0.1
Compressor Pressure [10^5 Pa]			20	20	13
CO_2 removal rate			80%	80%	80%
Stage-cut in each mem. unit			0.17	0.17	0.32, 0.45
Membrane Area, [$10^6 m^2$]			**0.33**	**0.19**	**0.14**
Blower duty, MWe			59.5	59.5	59.5
Vacuum pump duty, MWe			-	-	91.2
Compressor duty, MW_e			306.5	274.0	70.8
Expander duty, MW_e			-50.2	-50.2	
Net (Capture) Power, MW_e			**315.8**	**283.2**	**221.5**

The only two process Configurations among all the configurations considered that satisfy both design specifications are Configurations 14 and 15. Configuration 14 was developed by Lin et al. (2007) for post-combustion CO_2 capture using spiral-wound membrane modules, and it is a two-step, two-stage process with feed compression and permeate vacuum. With this process three case studies were conducted with the variation of permeate side vacuum condition such as 0.33, 0.25 and 0.1 bar. The results are presented in Table 5.8. Low vacuum condition means hard vacuuming, and it is more challenging for industrial vacuum pump manufacturers to deliver such vacuum condition. It is found that variation of permeate side condition from 0.33 bar to 0.25 bar does not improve any power saving but contribute to membrane area savings up to 24%. If further vacuum is applied i.e., 0.1 bar, significant improvement in power consumption for both capture and compression is achieved which is nearly 15.5% and but the membrane area savings is lowered, from 24% to 11%.

Table 5.8: Aspen Plus results for a two-step, two-stage process (Configuration 14)

Process Configuration			**Fig. 5.14**		
			Case-1	**Case-2**	**Case-3**
Streams name		FLUE-IN	CO2-RICH	CO2-RICH	CO2-RICH
Mole fraction	CO_2	0.1495	**0.980**	**0.985**	**0.985**
	N_2	0.8020	0.0142	0.0104	0.0105
	O_2	0.0390	0.0047	0.0034	0.0033
	Ar	0.0096	0.0011	0.0008	0.0008
Total flow, kmol/sec		20.95	2.73	2.70	2.70
Temperature, K		313.0	313.0	313.0	313.0
Pressure [10^5 Pa]		1.01	1.01	1.01	1.01
Feed Blow/Comp pressure [10^5 Pa]			3	3	2
Permeate Vacuum condition, [10^5 Pa]			**0.33**	**0.25**	**0.1**
Permeate Compressor pressure [10^5 Pa]			20	20	8
Injection (EOR) pressure [10^5 Pa]			110	110	110
CO_2 capture rate			85%	85%	85%
Stage-cut in each membrane Stage			0.25, 0.39, 0.12	0.24, 0.41, 0.11	0.24, 0.44, 0.09
Membrane Area, [10^6 m^2]			**2.25**	**1.70**	**2.01**
Feed Blow/Comp power, MW_e			96.1	94.5	57.4
Permeate Compressor power, MW_e			81.5	76.2	48.7
Permeate Vacuum pump power, MWe			39.9	45.8	70.2
Net (Capture) Power Consumption, MW_e			**217.5**	**216.4**	**176.2**
Compression (Injection) power, MWe			51.2	50.7	50.7
Net (Capture + Compression) Consumption, MW_e			**268.6**	**267.1**	**227.0**

The new process Configuration considered in this study is Configuration 15, which is different from Configuration 14 in several aspects. First, the new process has replaced the feed compression step by a permeate vacuuming step for the first membrane stage. Secondly, it has completely removed the vacuum operation from the third stage. Overall, the process has eliminated a compressor which can contribute to reduce the total plant cost. The simulation and design results with operating conditions for the Configuration 15 are presented in Table 5.9. It is found that with milder vacuum condition such as 0.25 bar, this configuration is short of meeting the target CO_2 purity of 98%. But for 0.1 bar vacuum condition, the new process shows better performance than Configuration 14 in term of power consumption by saving 12.7% of it. However, the performance of this process in term of membrane area utilization is not satisfactory. It utilizes nearly 278% more membrane area than for Configuration 14.

Table 5.9: Aspen Plus results for a two step, two-stage process without feed compression (Configuration 15)

Process Configuration		**Fig. 5.15**		
			Case-1	**Case-2**
Streams name:		FLUE-IN	CO2-RICH	CO2-RICH
Mole fraction,	CO_2	0.1495	0.948	**0.98**
	N_2	0.8020	0.0344	0.0123
	O_2	0.0390	0.0141	0.0062
	Ar	0.0096	0.0035	0.0015
Total flow, kmol/sec		20.95	2.81	2.72
Temperature, K		313.0	313.0	313.0
Pressure [10^5 Pa]		1.01	1.01	1.01
Permeate Vacuum condition, [10^5 Pa]			**0.25, 0.25**	**0.1, 0.1**
Permeate Compresor pressure [10^5 Pa]			27	27
Injection (EOR) pressure [10^5 Pa]			110	110
CO_2 capture rate			85%	85%
Stage-cut in each membrane Stage			0.58, 0.59, 0.38	0.32, 0.53, 0.77
Membrane Area, [10^6 m^2]			**30.5**	**7.6**
Permeate Compressor power, MW_e			129.3	50.7
Permeate Vacuum pump power, MWe			135.0	98.4
Net (Capture) Power Consumption, MW_e			**264.3**	**149.1**
Compression (Injection) power, MWe			54.1	52.3
Net (Capture + Compression) Consumption, MW_e			**318.4**	**201.4**

The lowest net power consumption for the capture plant alone, and for the capture and compression plant together is 30% and 40% of the total plant output respectively. 10% extra energy is required for compression to transport the captured CO_2. In the last two processes, a let down valve is used in the simulation to reduce the pressure of a high pressure process stream (recycle) instead of turbo expander. It is possible to recover some energy from the high pressure stream but need installation of a heating system to maintain the desired process stream temperature.

It is possible to attain the same purity and recovery ratio by introduction of more membrane stages by use of less membrane area and less power consumption. But concerns remain for the total cost as the number of compressors or vacuum pumps increases. It is difficult to conclude at this stage which process configuration among these last two processes is better without conducting an optimization study for the operating and design variables, and also without complete cost analysis. In the next chapter an optimization study is presented to find out the optimal-design configuration in terms of the minimization of power consumption.

5.8 Summary

Various single and multi-stage process configurations with or without recycle streams have been proposed for post-combustion CO_2 capture from a 500 MW coal-fired power plant flue gas stream. Based on a detailed multicomponent gas separation membrane model, proposed process configurations have been designed and simulated in Aspen Plus process simulator with fixed membrane properties and feed composition for meeting target specifications set for CO_2 capture. The performance of all process configurations is compared on the basis of membrane area and power consumption requirements. The compression pressure for transport and injection of captured CO_2 was set at 110 bar. It was found that only two process configurations can satisfy the process specifications (85% CO_2 recovery rate, and 98% CO_2 purity) as represented by Fig. 5.14 and 5.15 among fifteen configurations. The lowest energy penalty found for the new proposed capture process as illustrated in Fig. 5.15 is 30% of the total plant output. There is still enough room for further improvement in the present process design study by conducting an optimization study to determine the optimal process design conditions and membrane process configuration.

Chapter 6

Optimization and Sensitivity Analysis of Membrane Gas Separation Processes in AspenPlus®

6.1 Introduction

Optimization is the process of improving any existing situation, device, or system (Turton et al., 2003). Biegler et al. (1997) defined the optimization term as "Given a system or process, find the best solution to this process within constraints". The process optimization problem can be stated in words as: select the variable(s) in a process which yield the best value of a performance criterion without violating any restrictions on the process models or in another word "design & operate processes in the best possible way" (Douglas, 2002). Choosing the optimal system for a particular separation from all the available and possible process configurations is a difficult task, and needs a systematic design approach. For a given separation, it appears that although a configuration may be most favourable in terms of product purity and recovery, capital and operating costs may outweigh these advantages when compared to other configurations (Bhide and Stern, 1991b). Although complex membrane systems may be necessary to meet the desired separation demands, currently few design guidelines can be drawn for the selection of optimal membrane configurations. The problem-specific nature of membrane selection, and the wide choice of membranes and membrane unit configurations, then necessitates a model-based optimization approach for membrane process design (Purnomo & Alpay, 2000). Model-based optimization of membrane design was found effective in the economic evaluation of different gas membrane process configurations (Bhide and Stern, 1991a). Energy consumption, product recovery & purity, and equipment size (e.g., membrane module, compressor or vacuum pump) are some criteria generally considered in the performance optimization for gas membrane separation systems. It is also considered that complex relationships exist between the performance of the membrane system and many factors such as product purity and recovery, design and operation variables, and component permselectivity (Chang & Hou, 2006). Different approaches and methods have been employed to optimise different membrane gas separation processes by various investigators with different types of objective functions consideration

(Babcock et al., 1988; Bhide & Stern, 1991a; 1993a; Qi & Henson, 1998a; 1998b; 2000; Purnomo & Alpay, 2000; Kookos, 2002; 2003; Marriott and Sørensen, 2003b; Chang & Hou, 2006; Datta and Sen, 2006; Hao et al., 2002; 2008; Safari et al., 2009; Ahmad et al., 2010; Merkel et al., 2010). The optimization methods used mainly in most of these studies are: Grid search, Genetic algorithm, NLP (Non-linear Programming) and MINLP (Mixed-integer Non-linear Programming). The commercial softwares used in those studies are: GAMS (General Algebraic Modeling Systems), gOPT (Process Systems Enterprises (PSE) Ltd.), HYSYS (Aspentech) and OPTISIM (Linde AG).

Babcock et al. (1988) evaluated the economics of single- and three-stage membrane systems for natural gas treatment by providing comparisons with an amine treatment process. Bhide and Stern (1991a; 1993a) presented detailed case studies of membrane separation systems for natural gas treatment and oxygen enrichment of air by utilizing the so-called new optimization variables rather than the usual operating variables; a grid search method was used to optimize the operating conditions for different configurations. Qi and Henson (1998b) conducted a systematic design strategy for spiral-wound membrane systems for CO_2/CH_4 separations in natural gas treatment and enhanced oil recovery applications based on an algebraic approximate binary model. The nonlinear programming (NLP) problem was solved with GAMS/CONOPT software for six proposed configurations to determine the optimum operating conditions which satisfy the separation requirements with minimization of annual processing cost. Parameter sensitivities were studied by changing the operating conditions, membrane properties, and economic parameters. Qi and Henson (1998a; 2000) adopted a superstructure strategy for designing membrane systems separating binary (1998a) and multicomponent gas mixtures (2000) respectively based on an approximate permeator model. A MINLP (mixed-integer nonlinear programming) design model was developed for simultaneous optimization of the permeator (spiral-wound) configuration and operating conditions to minimize the total annual processing cost. The case studies considered for the binary system were CO_2/CH_4 separations in natural gas treatment and enhanced oil recovery (1998a). Separation of acid gases (CO_2 and H_2S) from crude natural gas mixtures was considered for multicomponent case studies. The MINLP problem was solved via DICOPT^{++} solver in the GAMS environment. Tessendorf et al. (1999) used cost optimization features of on equation –oriented simulator, OPTISIM from Linde AG for investigating hybrid schemes, combinations of a cryogenic system with a membrane module, and

for CO pre-treatment of steam reformer gas. A SQP (sequential quadratic programming) algorithm was used for minimizing the total annual cost.

Purnomo and Alpay (2000) designed two membrane configurations with recycle streams for the bulk separation of air. Model equations for membrane systems (without consideration of pressure drop) were solved using the orthogonal collocation on finite element technique within the gPROMS modelling environment (Process Systems Enterprises (PSE) Ltd.). Optimization was performed with gOPT software (PSE Ltd.) which uses Successive Reduced Quadratic Programming technique. The optimization strategy employed in this work was to maximise the Rony separation index for specified product (O_2) purity.

Kookos (2002) proposed a targeting approach for the design of the membrane-based gas separation network as a non-linear programming problem where the membrane material is optimized together with the structure and the parameters of the membrane network. Two case studies for the production of nitrogen and oxygen enriched air were presented to demonstrate the usefulness of the proposed methodology based on a membrane model without fibre bore side pressure drop consideration.

Kookos (2003) also presented a mathematical methodology for the structural and parametric optimization of hybrid systems consisting of membranes and distillation columns. The proposed morphological representation was used to optimize a hybrid system for the propylene/ propane separation. This mathematical formulation was a mixed integer nonlinear programming (MINLP) problem and used the same membrane model as mentioned elsewhere (Kookos, 2002). DICOPT solver of GAMS was used for solving this MINLP problem.

Marriott and Sørensen (2003b) implemented an optimization technique based on genetic algorithm for designing membrane gas separation systems in gPROMS. A pervaporation case study for ethanol dehydration was investigated using this optimal design strategy and a significant improvement in the design was achieved. The optimal solution of genetic algorithm was also compared with MINLP solution technique based on a manual branch and bound method. Although the computational requirement of the genetic algorithm was found relatively large compared to conventional MINLP method, it was mentioned that finding a global optimum was guaranteed.

Datta and Sen (2006) used BFGS (Broyden–Fletcher–Goldfarb–Shanno) algorithm to find out the optimum configuration and design variables for the asymmetric spiral-wound

membrane separation system for carbon dioxide removal from natural gas. They optimized gas processing cost of the membrane system having up to three stages based on a fundamental model. They concluded that no unique configuration is always optimum irrespective of the values of carbon dioxide concentration and natural gas price. But within certain ranges of carbon dioxide concentration and natural gas price, the optimum configuration may be unique and the minimum gas processing cost can be achieved by adjusting stage-module numbers and compressor power. They also reported that in most cases there are no significant cost differences between two- and three-stage optimum configurations.

Chang and Hou (2006) applied multi-objective optimization (single and triple objective functions) using genetic algorithm to optimize membrane gas separation system for enriched oxygen production from air. The objective functions considered were the Rony separation index, power consumption per unit equivalent pure oxygen, and membrane surface area or length. The material balance models of the systems were solved by the orthogonal collocation method. The optimization process involved the selection of the optimal system configuration among three alternatives, as well as the optimal operating conditions. Negligible permeate side pressure drop was considered in the binary membrane model.

Lie et al. (2007) simulated and optimized four cases of single and two stage membrane processes for the treatment of blast furnace gas in a steel making plant with an FSC (Fixed site carrier) membrane and with respect to required membrane area, energy demands for compression/cooling and recovery and purity of CO_2. A rough cost function, which incorporated electrical power consumption, the membrane, compressor and turbine capital and a penalty for CO_2 release based on Norwegian CO_2 tax, was minimised to find the best membrane configuration. Operating conditions were optimised using a rough operating cost relationship, based only on the membrane area and compression duties. Simulations were done with HYSYS, utilising membrane user modules written for HYSYS. Information on optimization method and membrane model details was not reported.

Optimal design of a multiple stage (four stages) membrane process for carbon dioxide separation from LNG flue gas was performed based on numerical analysis of five cases studies with a binary membrane gas separation model without consideration of pressure drop (Song et al. 2008). The authors found that the pressure ratio of the permeate side to the feed side was an

important factor since it affects both the CO_2 concentration in the final permeate and the membrane area required for CO_2 recovery.

Hao et al. (2008) examined five two and three stage membrane process configurations with recycle streams using two different types of hollow fibre polymer membranes for upgrading low-quality natural gas by removing CO_2 and H_2S to meet pipeline specifications. Their optimization goal was to determine the most economical configurations. They employed a simulation and optimization technique known as "Infeasible Path Method" (IPM) by coding a computer program consisting of 10,000 lines. A sensitivity analysis was done to determine the effects of variation in feed flow rate, feed pressure, membrane module cost, and wellhead price of natural gas on the process economics. They found that three-stage membrane process configuration was not economically competitive under the conditions considered in their study.

Corriou et al. (2008) investigated a pulsed cyclic membrane process for CO_2/H_2 separation through a simulation and optimization study. Both Multi-objective optimization by means of genetic algorithm and nonlinear programming optimization based on sequential quadratic programming (SQP) were employed for the optimization study.

Safari et al. (2009) modeled and simulated a two-stage membrane process for CO_2-removal from natural gas in MATLAB using pressure and temperature dependence permeability and selectivity models for CO_2/CH_4 system in 6FDA- 2,6-DAT membrane. It seems that they optimised the process based on sensitivity analysis to achieve high extents of hydrocarbon recovery (methane losses $\leq$2%) as no information regarding the optimization method and procedures are reported. They considered two main design parameters: total membrane area and recycle flow rate. They reported that there exist minima for the total required area, and as CO_2 load increases in the feed, the position of the minima shifts to the higher value of methane loss.

Ahmad et al. (2010) investigated different membrane configurations for the optimized design of CO_2/CH_4 separation system based on a cross-flow model without consideration of bore side pressure drop. It was concluded that methane recovery could be improved by recycling permeate stream as well as by using double stage membrane system.

Merkel et al. (2010) highlighted the potential of membrane processes for cost-effective CO_2 capture from power plant flue gas. They focused on the challenges of minimizing energy use through process designs, and optimizing membrane properties and operating conditions (i.e.

feed compression, membrane area, and sweep flow rate) through sensitivity studies to reduce cost.

Although a large number of research articles are present in the open literature aiming at optimizing the membrane-based gas separation processes with emphasis on the production of oxygen or nitrogen enriched air and the CO_2/CH_4 separation as mentioned above, no single optimization study is available for CO_2/N_2 separation from post-combustion power plant flue gas. AspenPlus® has a built-in optimization and sensitivity analysis toolbox. It offers a convenient and time saving means for examining and improving an entire process without need of any code writings. In the previous chapter, different process configurations were simulated and designed for post-combustion CO_2 capture from power plant exhaust gas. Among those configurations only two configurations (configuration 14 & 15) have been able to meet both design specifications for EOR application i.e., 85% CO_2 recovery and 98% CO_2 purity in the product stream. This chapter will conduct an optimization study to find out the most efficient membrane process configuration from these two process alternatives as well as optimal design & operating conditions in terms of minimum process power requirements with subject to given feed stream conditions, and required CO_2 recovery and purity. After selection of an optimum process configuration, a parametric sensitivity analysis will be studied. The sensitivity analysis will be performed to provide the important information about the effect of each parameter whether it needs to be considered further for the accurate evaluation or can be neglected. Results of the sensitivity analysis identify the adequacy of process models and the key areas that affect the process performance.

6.2 Membrane Model and Process Configurations

The basic multicomponent hollow fibre membrane model used in this study is based on Pan's (1986) theoretical formulation. The basic model has been simplified in a way different from Pan's original simplification. Details about model simplification and new solution algorithm have been presented in Chapter 3 and elsewhere (Chowdhury et al., 2005). The detailed model with the new solution algorithm has been incorporated into AspenPlus as a User-Model, as described in Chapter 4. This model was established to study the design and optimization of membrane processes and hybrid processes involving membranes and other separation units. Each membrane unit is considered as a shell and tube type module with feed stream in shell side and permeate stream in tube side, and consists of thousands of hollow fibres. Tube side pressure drop has been considered in the model equations. A separation stage consists of a number of identical membrane modules connected in parallel. The main model assumptions are presented in the Chapter 3. The membrane module parameters and feed conditions of the flue gas (after removal of SO_X, NO_X, water, and other impurities) from a 500 MW coal-fired plant are summarized in Table 6.1.

In the Chapter 5, fifteen membrane process configurations were simulated and designed. It was found that only two process configurations, as illustrated in Figs. 5.14 and 5.15 were able to satisfy the design specifications. In this chapter, these process configurations are considered for further improvement via an optimization study. The process configuration presented in the Fig. 5.14 is a two-step, two-stage process with feed compression and permeate vacuum. The flue gas is compressed and fed to the 1st membrane stage, which is connected to a permeate vacuum pump. The retentate stream is again processed with another membrane stage with vacuum operation. The CO_2 rich stream from this unit is recycled and mixed with the flue gas stream before being compressed. The permeate stream from the 1st stage is compressed and fed to the 3rd membrane stage to get the desired purity in the final permeate stream and the retentate stream is recycled and mixed with compressed flue gas stream after pressure reduction by a control valve. The permeate stream is compressed to a specified pressure for transportation to an injection site. The main difference between the two process configurations presented in Fig. 5.14 and Fig. 5.15 is: one (i.e., Fig. 5.14) considers feed compression with permeate vacuum approach for 1st stage

and the other (Fig. 5.15) considers only permeate vacuum operation for 1st stage. The opposite is considered for the 3rd stage, i.e., vacuum in Fig. 5.14 and compression in Fig. 5.15. The other advantage of the Fig. 5.15 process configuration is that it eliminates one compressor which in turn may reduce the overall capital and operating expenses. Both process configurations are presented below.

Table 6.1: Feed conditions and membrane module parameters

Feed Conditions	
Flow rate (kmol/s)	20.95
Temperature (^{0}C)	40
Pressure (kPa)	101.0
Composition (dry basis), mol	
CO_2	14.95
N_2	80.2
O_2	3.9
Ar	0.95
Membrane Module Parameters	
Module Type	Shell-and-Tube
Membrane type	Asymmetric Hollow fibre
Flow configuration	Counter-current, shell side
Fibre inner diameter (μm)	300
Fibre outer diameter (μm)	500
Fibre active length (m)	0.5
Permeance, (10^{-10} mol/s.m^2.Pa) (Lin et al., 2007)	CO_2 : 3350 N_2 : 67 O_2 : 168 Ar : 168

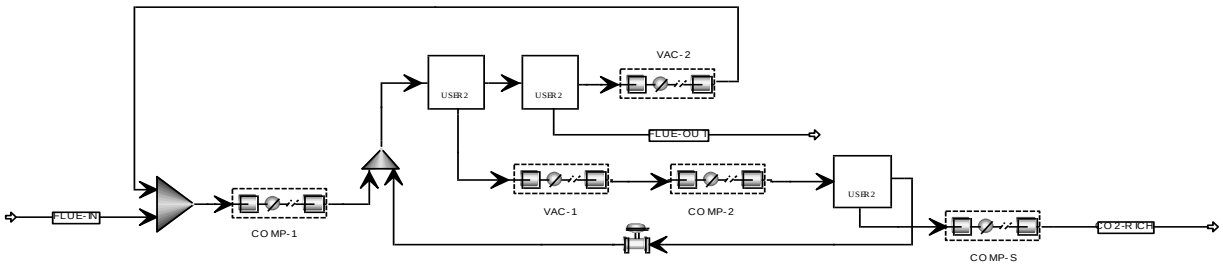

Figure 5.14: Two-step, two-stage process with feed compression and permeate vacuum (Lin et al., 2007)

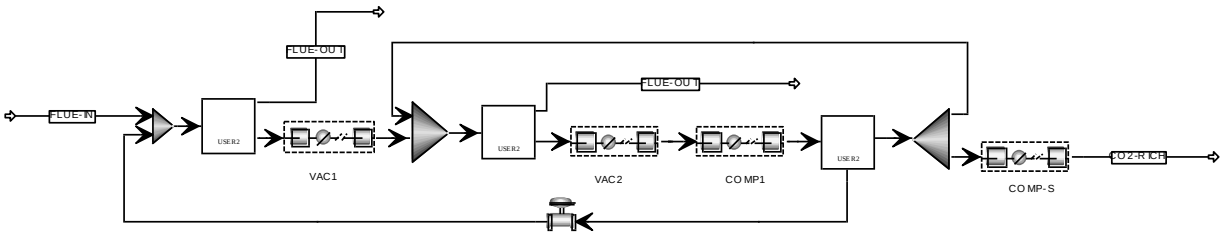

Figure 5.15: Three-stage process with permeate vacuum

6.3 Optimization procedures and methods in AspenPLus®

AspenPlus is a sequential modular simulator. It is generally recommended to develop a base-case simulation before defining the optimization problem in AspenPlus as the optimization problems can be difficult to formulate and converge. First, the decision variables are identified, they are then adjusted in order to achieve the optimum. Only inlet stream properties and process unit (block) variables can act as manipulated variables in the sequential modular simulator. Once the adjusted variables are determined, the objective function is formulated next. The objective function can be formulated in a Fortran block using process variables that were defined in the "Define" sheet under Optimization block of Model Analysis Tool. Virtually all process variables can be accessed and defined. After defining the appropriate process variables and constraints (i.e., product purity etc.), and completing coding for the objective function, the user must indicate to the program whether it has to minimise or maximise the objective function. The optimization routine also allows the user to adjust certain optimization parameters such as convergence tolerances, manipulated variable ranges, maximum number of iterations, etc. The tolerance of the objective function is the tolerance of the convergence block associated with the optimization problem. AspenPlus has the option for imposing equality and inequality constraints on optimization. Equality constraints of optimization problem are similar to design specifications in non-optimization problem. The constraints can be any function of flowsheet variables computed using any Fortran expressions or in-line Fortran statements and the tolerance for each constraints need to be specified. Tear streams and the optimization problem can be converged simultaneously or separately. If both are converged simultaneously, the tear stream is treated as an additional constraint.

AspenPlus solves optimization problems iteratively. By default AspenPlus generates and sequences a convergence block for the optimization problem. The user can override the convergence defaults, by entering convergence specifications on convergence forms. The values of the manipulated variables that are provided in the Stream or Block inputs are used as the initial estimates. Providing a good estimate for the manipulated variables helps the optimization problem to converge in fewer iterations.

Two optimization algorithms are available in AspenPlus: The COMPLEX method and The SQP (Sequential Quadratic Programming) method. The COMPLEX method uses the well-

known Complex algorithm, a feasible path direct search method. The method can handle inequality constraints and bounds on decision variables. Equality constraints are handled as design specifications. Separate convergence blocks are used to converge any tear streams or design specifications. The COMPLEX method frequently takes many iterations to converge, but does not require numerical derivatives. The SQP method is a state-of-the-art, quasi-Newton nonlinear programming algorithm. It can converge tear streams, equality constraints, and inequality constraints simultaneously with the optimization problem. The SQP method usually converges in only a few iterations but requires numerical derivatives for all decision and tear variables at each iteration. SQP method is used as the default optimization convergence method in AspenPlus where tear streams and optimization problem are converged simultaneously (Aspen Engineering Suite, 2001). Due to the non-linear nature of the membrane process, SQP was used as the preferred optimization method in this study.

6.4 Optimization Problem Formulation

The objective of the current optimization problem is to search for the optimal membrane process configuration and design and operating conditions subject to given feed conditions & membrane properties, and required product recovery & purity specifications. The two process configurations illustrated in Fig.5.14 and Fig. 5.15 were considered for optimization studies. Both processes configurations were simulated and designed in the previous chapter for post-combustion CO_2 capture from a 500 MW power plant flue gas. The base-case design parameters for both configurations are presented in Table 6.2 and Table 6.3 respectively.

Every optimization problem contains three essential categories:

1. At least one objective function (performance criteria) to be optimised (profit or cost function, etc.)
2. Equality constraints (equations)
3. Inequality constraints (inequalities)

Category 1 is sometimes called the economic model which should be minimized or maximized. Categories 2 and 3 constitute the mathematical model of the process or equipment. The mathematical models can be classified as equalities, inequalities and logical conditions. The model equalities are usually composed of mass balances, energy balances, equilibrium relations and engineering relations which describe the physical phenomena of the system. The model

inequalities often consist of allowable operating limits, specification on purities, performance requirement and bounds on availability's and demand. The logical conditions provide the connection between the continuous and integer variables. Variables that can be adjusted or be chosen to minimise or maximise the objective function are called decision variables or independent or optimization variables. Variables can be real (e.g., flow rates), integers (e.g., number of fibres) or binary (e.g., yes or no).

It is found that different objective functions are considered by different researchers for different gas membrane separation processes optimization in the literature. Some objective functions are directly related with process economic (e.g., gas processing cost, annualized cost, annual operating cost, etc.) and some are indirectly related (e.g., Rony separation index which reflects product recovery, product loss, power consumption, membrane area, etc.). The economic assessment of a specific membrane separation process depends on the method of analysis used and on the values assigned to the selected economic parameters. Therefore, economic assessments made by different evaluators may differ considerably from each other as market conditions vary with time and site. The investment i.e., capital cost of a membrane gas separation plant mainly depends on the compressor, vacuum pump and membrane module (including membrane) cost, and the operating cost mainly depends on the compression and/or vacuuming duties, membrane replacement, labour and maintenance cost. The fixed capital cost for the gas compressor or vacuum pump depends on the flow rate of the stream handled, and the operating cost is influenced by the compressor efficiency, inlet and outlet pressure, stream temperature, and gas properties.

Energy/power consumption is the major concern of the any post-combustion CO_2 capture process. The conventional chemical absorption process produces relatively pure carbon dioxide stream. The technology is well-developed and commercially available. The disadvantage of the process is that it consumes a significant amount of the energy produced by the power plant. A typical "energy penalty", which is defined as the percentage of the net power output consumed for the chemical absorption process installed on a conventional coal-fired power plant is between 25% and 37% (Herzog, 1999). The energy penalty introduces a significant operating cost for the chemical absorption process. As one of the objectives of this thesis is to compare both the CO_2 capture processes i.e., chemical absorption by MEA and gas separation by polymer membrane, the energy consumption of the whole capture process could be a reasonable basis for

comparison. Therefore, the objective function or performance criteria in this research is the total power consumption for capture and compression for transport and injection, which should be minimised to determine the optimum process conditions for particular membrane process configuration while satisfying the product purity and recovery constraints. The compressors and vacuum pumps are the main components for power consumption in any gas separation membrane process. The compressors and vacuum pumps are modeled by using multistage polytropic compressors with intermediate heat exchange, and operating with 80% polytropic and 90% mechanical efficiency. The inter-stage cooling temperature is specified at 40^{o}C. The compression pressure for transport and injection of captured CO_2 is considered at 110 bar application although it may vary depending on the injection site location from the capture plant.

The objective function, defined as total power consumption, can be represented as follows:

Minimize Total Power Consumption (MWe)

Where,

Total power consumption = Capture power + Compression Power

Capture power = Net-work (duty) of all compressors (MWe) + Net-work (duty) of all vacuum pumps (MWe)

Compression Power = Net-work (duty) of the compressor at 110 bar (MWe)

Optimization or decision variables are the number of fibres for each membrane stage, permeate recycle fraction, feed and permeate compressor's outlet pressure. Both membrane processes consist of three membrane stages, and variation in the number of fibres means variation in the total membrane area of each stage. The base-case design conditions obtained from the previous chapter was used as initial estimate for the optimization runs and are presented in Tables 6.2 and 6.3 along with limits on decision variables. Two vacuum conditions i.e., 0.33 and 0.1 bar are specified for the vacuum pump. The constraints specified in the optimization study for CO_2 recovery and purity are as follows:

CO_2 recovery rate in the permeate stream $\geq$ 85%, and

CO_2 purity in the permeate stream (mol%) $\geq$ 98%.

The CO_2 recovery rate means the percentage of CO_2 that has to be captured from the feed flue gas stream. The above objective function and constraints are implicit and difficult to express explicitly in terms of all decision variables. It should be also mentioned here that in this

optimization-based design study, the membrane properties, membrane module configuration and flue gas feed conditions are fixed and presented in Table 6.1. Finally, it has been found that the formulation of the NLP type optimization problem is very easy to construct in the AspenPlus environment after the base case simulation is developed. The software requires the objective function, the selected constraints, and the upper and lower limits of each decision variable without need of extensive code writing.

6.5 Optimization Results

The SQP convergence method in AspenPlus used in this nonlinear (because of nonlinear membrane model equations) optimization problem was found very effective and fast. Selection of decision variables/ranges was found very crucial for process convergence stability. Both the inequality constraints are found active after the each converged optimization cases. It should be noted that the SQP method usually guarantees for only local optima over the domain of decision variables. Although the objective of the present optimization-based design problem is to select the optimum process flowsheet by minimizing the total power consumption, membrane area requirement is also a very important design criterion which will affect the overall CO_2 capture plant cost. Therefore, the optimal design of the gas membrane separation system for CO_2 capture, demands a trade-off between the total membrane area requirement and total power i.e., energy consumption. The optimization results with decision variables ranges for both process configurations (configurations 14 and 15) as illustrated in Fig. 5.14 and in Fig. 5.15 are presented in the Table 6.2 and Table 6.3.

For the process configuration 14, two optimization case studies at different permeate vacuum conditions (0.33 bar and 0.1 bar) were conducted. For Case-1 i.e., 0.33 bar vacuum condition, significant improvement in power consumption (9% reduction) is observed through the optimization study compared to the base case design, although the membrane area requirement remain the same. The opposite is true (i.e., 8.5% reduction in membrane area, and no significant improvement in power consumption) for the Case-2 optimization study at 0.1 bar permeate vacuum condition. For Case-1, four optimum variables are found at their upper bound values, and for Case-2 one variable is in the upper bound, and another in the lower bound. For the process configuration (configuration 15) presented in Fig. 5.15, it is found that 13% power consumption and almost 8% membrane area can be saved using the optimal design compared to

the base case design. Only one decision variable is found on the lower bound for this optimized process.

Fig. 6.1 presents the total power consumption for capture, and capture plus compression before and after optimization for both process configurations and Fig. 6.2 shows the total membrane area requirements. Considering Case-1 (0.33 bar) and Case-2 (0.1 bar) for the process configuration 14, it is noticed that low vacuum operation favours lower power consumption and lower membrane area requirements. To compare both process configurations on an equal basis, optimization results at permeate vacuum operation at 0.1 bar was considered. It was found that in terms of energy consumption the optimized process configuration (configuration 15) represented by Fig. 5.15 can save 25% more power compared to the optimized process configuration (configuration 14) illustrated by Fig. 5.14. This is attributed to the absence of a compressor in the previous process i.e., configuration 15. Another important point is that this optimized process does not need permeate recycle stream which simplify the process flowsheet and ease plant construction. The final optimized process configuration 15 looks now like in Fig. 6.3. But the performance of this optimized process in terms of membrane area requirements is not satisfactory. It utilizes 3.8 times more membrane area which eventually will increase the plant foot-print, and also fixed capital investment. Therefore, membrane unit price will also be a decisive factor for the final judgement of the optimum process configuration selection.

Table 6.2: Optimization and base case results for the process Configuration 14

Process configuration	**Configuration 14**			
	Case-1		Case-2	
	Base-case design	Optimal-design	Base-case design	Optimal-design
Permeate side Vacuum condition, [10^5 Pa]	**0.33**	**0.33**	**0.1**	**0.1**
Constraints				
CO_2 capture rate $\geq$ 85%	**85%**	**85%**	**85%**	**85%**
Purity of captured $CO_2 \geq$ 98%	98%	98%	98.54%	98%
Decision Variables				
Feed Compressor pressure, [10^5 Pa] (lower bound - upper bound)	3	3 (2-3)	2	2.2 (2-3)
Permeate Compressor pressure, [10^5 Pa] (lower bound - upper bound)	20	10 (5-10)	8	5.8 (2-8)
Number of fibres, Stage-I [10^6] (lower bound - upper bound)	1616	1467 (210-1467)	1556	1886 (210-1886)
Number of fibres, Stage-II [10^6] (lower bound - upper bound)	1238	1370 (210-4191)	976	419 (419-1886)
Number of fibres, Stage-III [10^6] (lower bound - upper bound)	10	21 (2-42)	24	40 (2-42)
Objective Function (*minimization of*)				
Feed Blower/Compressor power, MWe	96.1	97.5	57.4	60.5
Permeate Vacuum pumps (both) power, MWe	39.9	40.3	70.2	67.7
Permeate Compressor power, MWe	81.5	59.4	48.7	45.5
Capture Power (total), MWe	217.5	197.2	176.2	173.6
Compression (Injection) power, MWe	51.2	51.0	50.7	51.0
*Total (**Capture + Compression**) power, MWe*	**268.6**	**248.2**	**227.0**	**224.6**
Membrane **Area** (total) requirement, [10^6 m^2]	**2.2**	**2.2**	**2.0**	**1.8**

Table 6.3: optimization and base case results for Configuration15

Process configuration	**Configuration 15**	
	Base-case design	Optimal-design
Permeate side Vacuum condition, [10^5 Pa]	**0.1**	**0.1**
Constraints:		
CO_2 capture rate ≥ 85%	85%	85%
Purity of captured CO_2 ≥ 98%	98%	98%
Decision Variables:		
Permeate recycle fraction (lower bound - upper bound)	0.09	0 (0-0.25)
Permeate Compressor pressure, [10^5 Pa] (lower bound - upper bound)	27	9.3 (5-50)
Number of fibres, Stage-I [10^6] (lower bound - upper bound)	8085	7179 (1-10477)
Number of fibres, Stage-II [10^6] (lower bound - upper bound)	1603	1742 (1-10477)
Number of fibres, Stage-III [10^6] (lower bound - upper bound)	8	22 (1-30)
Objective Function (*minimization of*):		
Permeate Vacuum pump-stage I power, MWe	63.7	60.9
Permeate Vacuum pump-stage II power, MWe	34.7	35.1
Permeate Compressor power, MWe	50.7	33.6
Capture (total) Power, MWe	149.1	129.6
Compression (Injection) power, MWe	52.3	52.1
*Total (**Capture + Compression**) power, MWe*	**201.4**	**181.7**
Total Membrane **Area** requirement, [10^6 m^2]	**7.6**	**7.0**

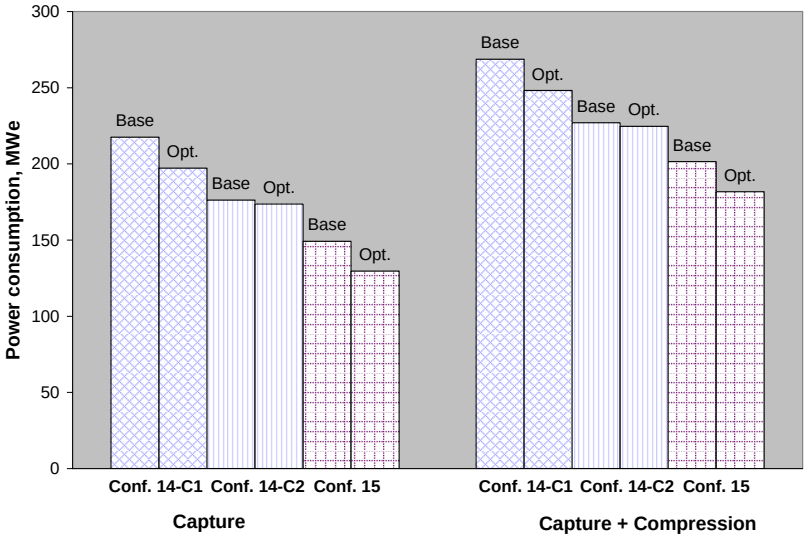

Figure 6.1: Comparison of power consumption

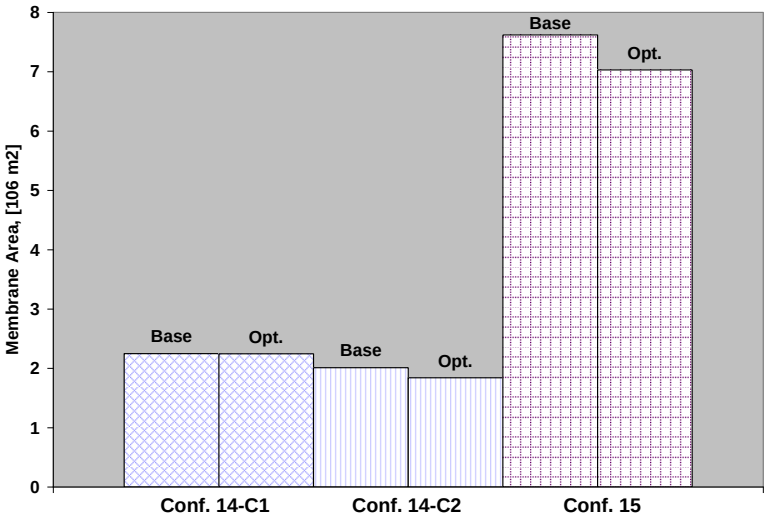

Figure 6.2: Comparison of membrane area requirements

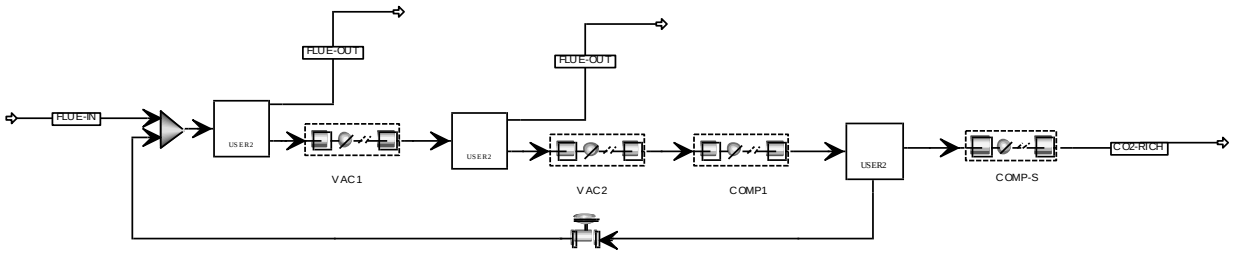

Figure 6.3: Simplified form of process configuration illustrated in Fig. 5.15 after optimization

6.6 Sensitivity Analysis

The sensitivity analysis is an investigation of the effects exerted by changes in input variables on the output variables characterizing the behaviour of the system. Post-optimality analysis using sensitivity analysis helps to evaluate the influence of uncertain parameters in the optimal design. It also examines the applicability of the determined optimal set of manipulated variables and checks for violations of the feasible operating window of the process. Parametric sensitivity analysis provides useful information about the variation of the optimal solution for a given change in the parameter values. The AspenPlus built-in sensitivity analysis tool also allows multiple variables (input) variation simultaneously. The optimal process configuration presented in Fig. 6.3 is re-simulated using the determined optimal set of decision variables to ensure the feasibility of the optimum condition and it is considered as base case for sensitivity analysis.

The power consumption of the post combustion CO_2 capture plant depends on a number of operating factors. Some of the most important of these factors are the feed flow rate, CO_2 concentration in the feed, permeate vacuum and compression condition. Variations in these factors can have a strong impact upon the operating expenses of the capture plant. Therefore, a sensitivity analysis was made in order to evaluate the effects of these factors on the plant power consumption and also on the product purity and recovery. The results of the sensitivity analysis for single parameter variations are presented in Fig. 6.4 through Fig. 6.8 and for simultaneous multiple (two) parameter variations in Fig. 6.9 to Fig. 6.11. The vertical line on the X-axis indicates the optimal point.

Fig. 6.4 shows that power consumption is increasing and CO_2 recovery rate is decreasing almost linearly as the feed flow rate increases. However, the purity is not very sensitive with respect to feed flow rate variations. This indicates that membrane selectivity is good enough to handle feed flow disturbances without sacrificing product purity much. This product purity is very important for storage site. Fig. 6.5 shows the variations in the power consumption, product recovery and purity as a function of CO_2 concentration in the flue gas. To show the effect of CO_2 mole fraction, the feed flow rate is changed simultaneously in order to keep the incoming flow rate of CO_2 constant. As the CO_2 fraction in the feed stream increases, it is observed that the power consumption is increasing. The power requirement for CO_2 capture is found highly sensitive to lower CO_2 feed concentration i.e. below < 14% and the sensitivity gradually diminishes as the concentration increases above 14%. The product recovery is showing very high

sensitivity at low to moderate CO_2 feed concentration. It is also showing a polynomial response with a maxima which indicates occurrence of opposite effects, and after the optimal point, the recovery rate is decreasing slowly with increase of CO_2 concentration. Purity is found sensitive at lower CO_2 concentration (< 7%).

Effect of compression of permeate stream of 2nd membrane stage (before entering as feed stream for 3rd stage) on power consumption is shown in Fig. 6.6. The power consumption and purity are always found highly sensitive, and the product recovery is only sensitive at lower compression (<10 bar). At lower compression i.e., < 10 bar, the power consumption is decreased stiffly, and then increases steadily. On the other hand, purity is decreasing in a linear fashion and recovery is insensitive to permeate compression after certain pressure i.e. 11 bar. Fig. 6.7 and 6.8 show respectively the effect of permeate vacuuming from 1st and 2nd membrane stages on power consumption, product recovery and purity. Both power consumption and recovery is decreasing steadily with ease of vacuum condition, and purity remains in both cases insensitive. Note that the rate of decreasing of power consumption and recovery for 1st stage when increasing the vacuum pressure is higher than that of 2nd stage.

The effects of variation of both permeates vacuum condition simultaneously on power consumption, product recovery and purity was investigated and are presented in Fig. 6.9 to 6.11, respectively. Both power consumption and product recovery rate are found sensitive to permeate vacuum conditions as before and product purity is found least sensitive.

It can be concluded that any changes in any of factors such as feed flow rate, feed concentration (CO_2), permeate vacuum and compression condition has great impact on plant performance especially on power consumption and product recovery. It is also concluded from this sensitivity analysis that the optimal process configuration based on the optimal design and operating conditions is capable of handling a wide range of different upsets efficiently.

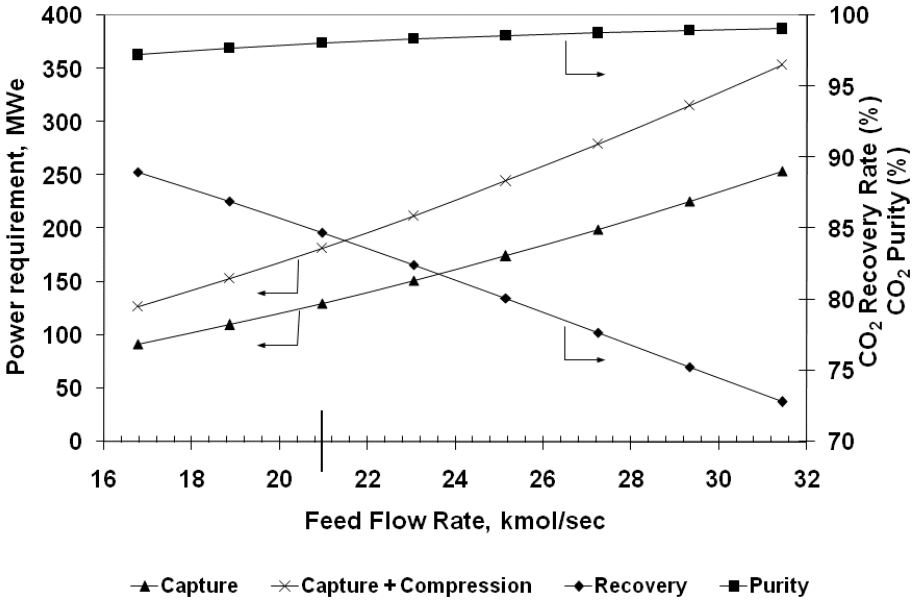

Figure 6.4: Effect of feed flow rate variation on optimal design

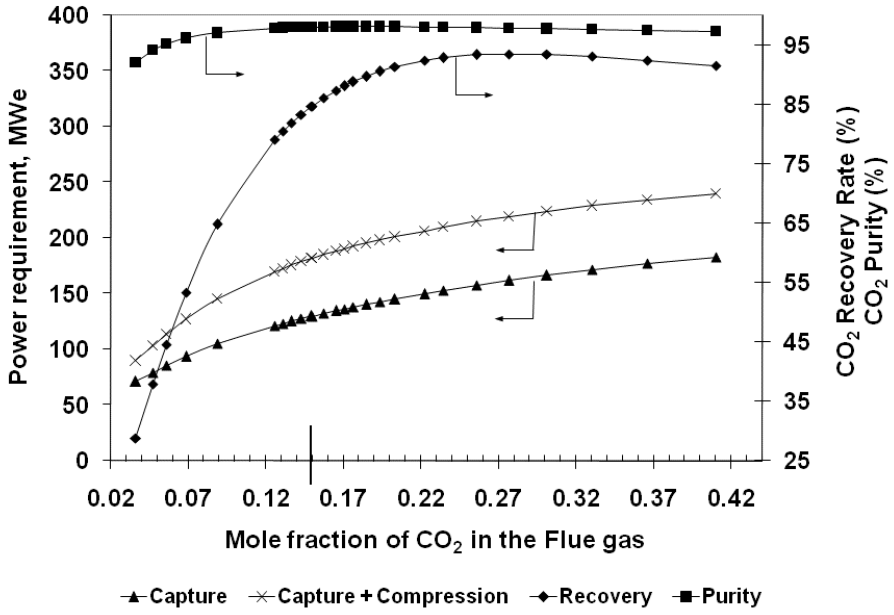

Figure 6.5: Effect of change of CO_2 concentration in the flue gas on optimal design

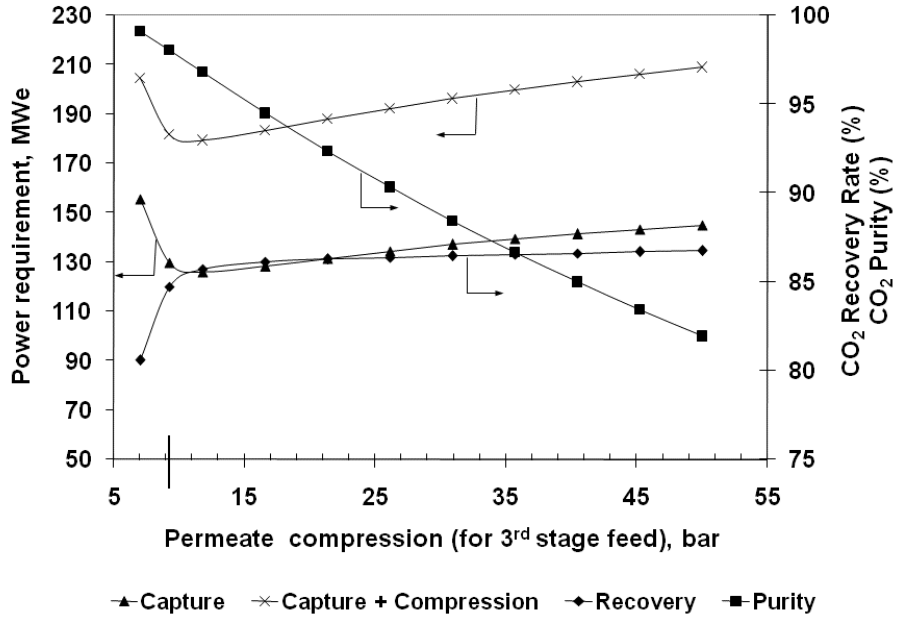

Figure 6.6: Effect of permeate compression on optimal design

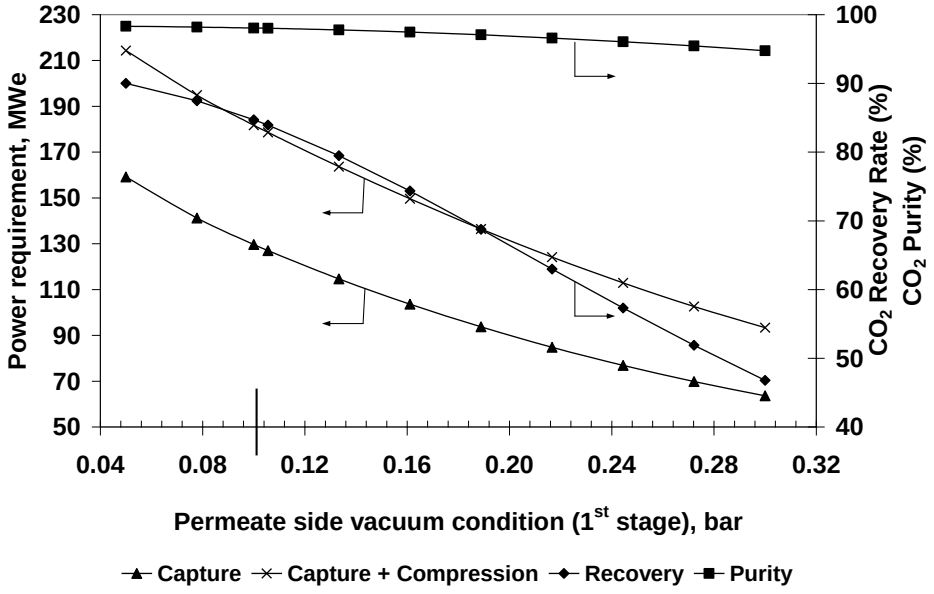

Figure 6.7: Effect of permeate vacuuming (for 1st membrane stage) on optimal design

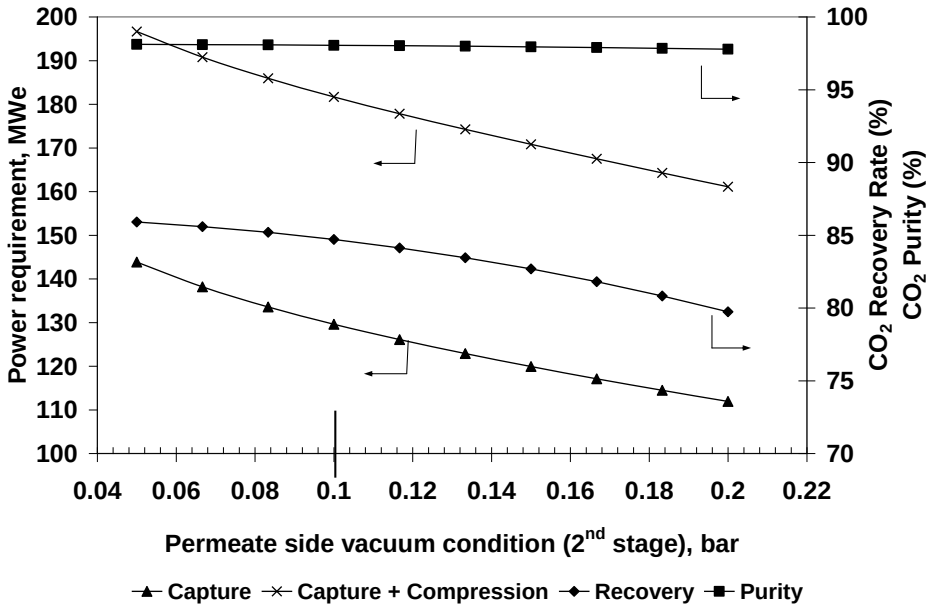

Figure 6.8: Effect of permeate vacuuming (for 2nd membrane stage) on optimal design

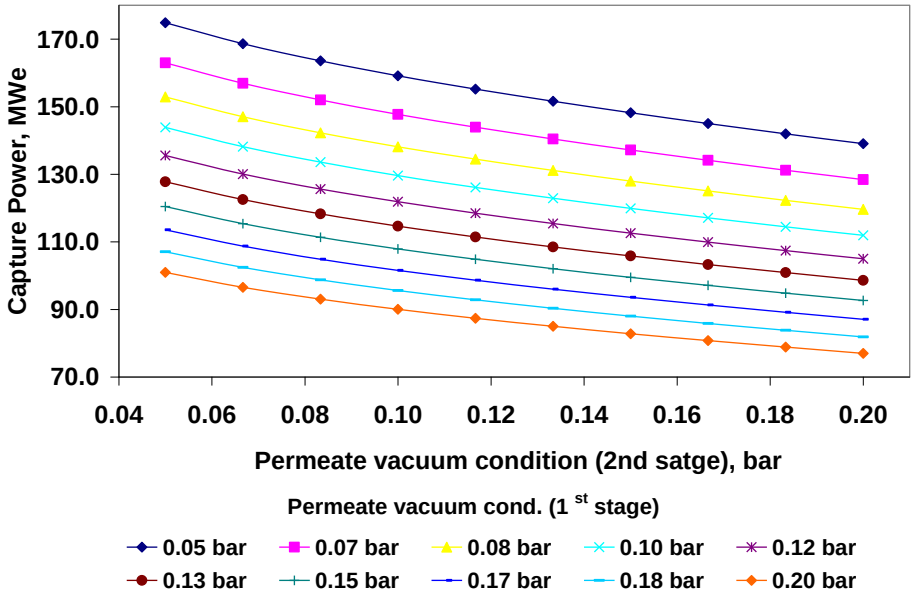

Figure 6.9: Effect of varying both permeate vacuuming conditions simultaneously on power consumption

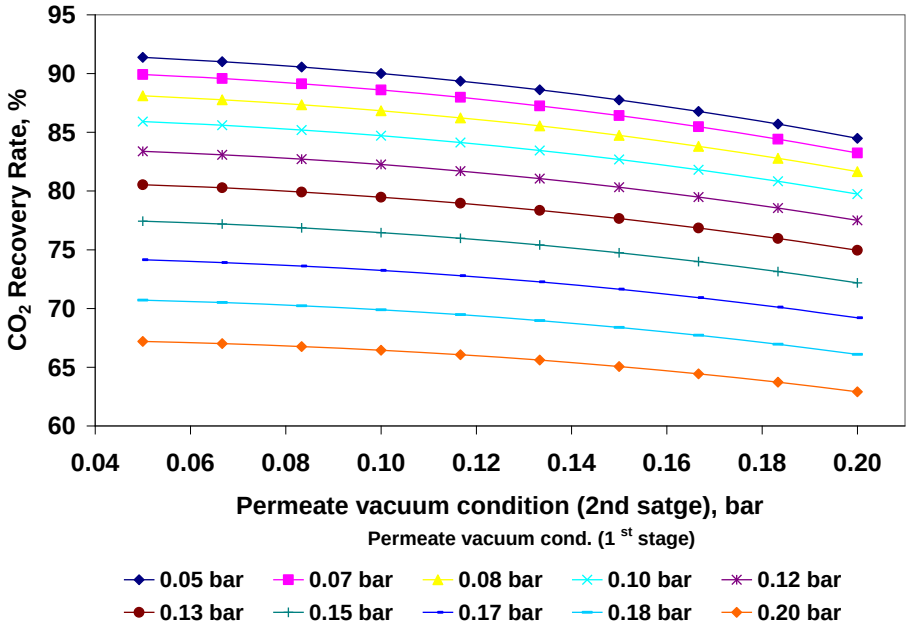

Figure 6.10: Effect of varying both permeate vacuuming conditions simultaneously on CO_2 recovery rate

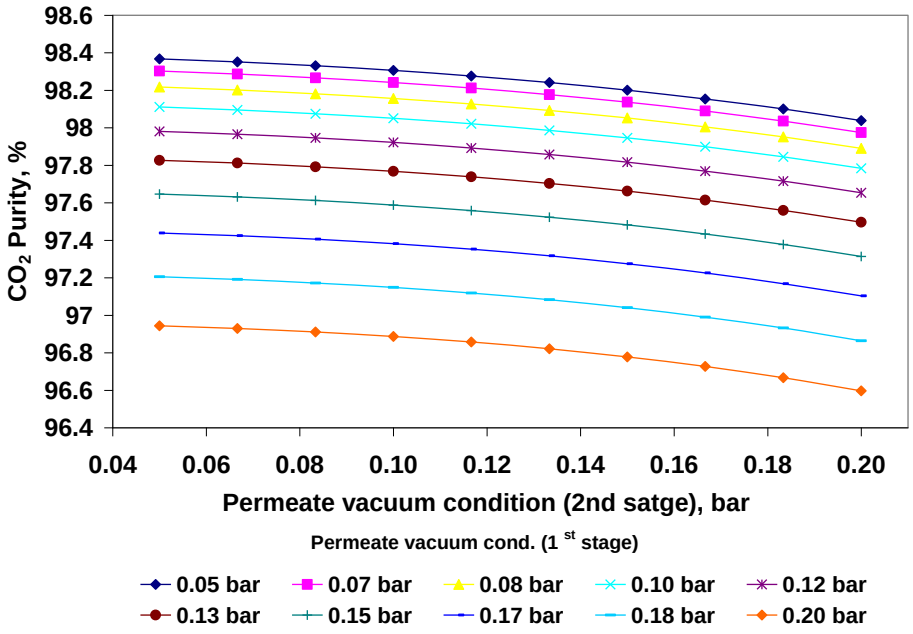

Figure 6.11: Effect of varying both permeate vacuuming conditions simultaneously on CO_2 purity

6.7 Summary

This chapter has highlighted the importance of an optimization study in the process design. Optimization-based design methodology has been employed for selecting optimal process configuration from the two process alternatives selected from the previous chapter and associated optimum operating and design conditions for CO_2 capture from post-combustion power plant exhaust gas. AspenPlus optimization tool utilizing a nonlinear Sequential Quadratic Programming (SQP) method was used for the optimization study for the entire process as a time saving means by avoiding programming code writing (may be thousands lines or more). It is found that power consumption and membrane area requirement can be reduced by up to 13% and 8% respectively when optimizing the based design. To evaluate the influence of uncertain parameters in the optimal design a post-optimality sensitivity analysis was conducted using AspenPlus® built-in sensitivity analysis tool. It is concluded that any changes in any of these factors such as feed flow rate, feed concentration (CO_2), permeate vacuum and compression condition has great impact on plant performance especially on power consumption and product recovery. An economic analysis based on the technical findings of this chapter will help to identify the best membrane gas separation configuration finally.

Chapter 7

Simulation and Design of Chemical Absorption/Stripping Process for Post-combustion CO_2 Capture in AspenPlus®

7.1 Introduction

Chemical absorption has been regarded as one of the most promising methods to capture CO_2 from flue gas due to the advantage of dealing with low concentration, low pressure and large flux exhaust gas. Amine-based (with aqueous Monoethanaolamine) chemical absorption/stripping technology which is currently commercially available, is recognized as the leading technology for post-combustion CO_2 capture from coal-fired power plant flue gas stream (Rao and Rubin, 2002). While other less expensive and better performance CO_2 capture technologies with new solvents, combined with advanced industrial process designs, may be developed in the future, some of them may be years away from commercial availability. The advantage of post-combustion process is the possibility of retrofitting a state-of the-art power plant with a capture plant under reasonable effort. Fluor Daniel Inc., Dow Chemical Co., ABB Lummus Crest Inc., and Kerr-McGee Chemical Corp. were few of the initial developers of Monoethanaolamine (MEA)-based technology for CO_2 capture. MEA-based technology can capture more than 95% of the CO_2 from diluted (i.e., CO_2 concentration 10-15% by volume) and low pressure flue gases to yield a product stream with CO_2 purity > 99%. There are major R&D efforts going on worldwide to improve this technology – mainly to reduce the high energy penalty. A substantial part of the energy requirement consists of heat or steam requirement for solvent regeneration (Herzog, 1999; Rao and Rubin, 2002). The conventional MEA flowsheet for CO_2 capture is shown in Fig. 7.1.

While CO_2 capture by absorption/stripping with MEA is being considered for large scale application such as processing flue gas streams from 500 MW power plant, it is essential to investigate the overall process performance by detailed design-optimization study of the individual process unit. This needs rigorous modeling and simulation of the

process along with fundamental understanding of the underlying complex phenomena taking place in the process e.g., electrolyte thermodynamics, chemical reactions, heat and mass transfer across the gas-liquid interface, etc.

Several approaches have been adopted to model steady-state post-combustion chemical (or reactive) absorption/stripping processes with different levels of complexity depending on the consideration of mass transfer characteristics and chemical reactions between CO_2 and the chemical solvent (Kenig et al., 2001). Traditional equilibrium-stage modeling approach assumes that each theoretical stage is composed of a well mixed vapour phase and liquid phase which are in phase equilibrium with each other. Models based on this approach may assume the reactions are at equilibrium or may consider reaction kinetics which does not have any physical basis. Real absorption/stripping processes, however, normally do not operate at equilibrium because phase equilibrium is hardly attained in practice. The departure from equilibrium is accounted for by introducing efficiencies (tray columns) or the height equivalent of a theoretical plate (HETP, packed columns) in equilibrium-stage modeling (Taylor et al., 2003). The mass transfer rate-based or nonequilibrium modeling approach is rigorous and offers higher model reliability over the traditional equilibrium-stage modeling approach (Zhang et al., 2009). At its lowest level of complexity, the chemical reactions are considered to be at equilibrium for the rate-based model. In a more rigorous approach for rate-based model, the reaction kinetics is accounted for in the bulk solution and enhancement factors are used to account for the reactions in the film. In the most rigorous rate-based modeling approach, reaction kinetics is modelled directly. Mass transfer resistances, electrolyte thermodynamics and the reaction system as well as the column configurations are considered in this final stage of rate-based modeling. Models also provide a direct estimation of concentration and temperature profiles by implementing reaction rates directly into the transport and balance equations in the film and the bulk of the fluid (Lawal et al., 2009).

Industrial MEA-based CO_2 capture processes basically rely on a pair of columns, one absorber and one stripper. The absorber is used to capture the carbon dioxide, and the stripper is used to regenerate the MEA solvent, so that it is ready to be recycled to the absorber. Two design variables such as the column type (e.g., valve or sieve tray,

structured or random packing) and the size of the mass transfer region (i.e., height of packing, number of trays) play significant roles in any absorption/stripping process design and economics. Mass transfer mechanisms of tray and packing differ due to different ways of generating large amounts of interfacial area. In tray column this interfacial area results from the passage of vapour through the perforations of trays, and in packed column, from the spreading of liquid on the surface of packing materials. Lower cost and more economical handling of high liquid rate are some advantages of tray column. Low pressure drop, greater stable operating range, and capability of handling various fluid characteristics such as acids and many other corrosive materials, favour packed type column selection (Perry and Green, 1997; Bennett and Kovak, 2000).

Besides those two important design variables, there are other few points that should be taken into consideration for a realistic and more accurate process simulation and design in spite of the difficulty of simulating/converging the process flowsheet. Several factors contribute to the convergence difficulties such as recycle structure of the flowsheet, rigorous nonlinear models of absorber and stripper, and initial estimate to initialize the columns. To obtain an initial estimate to initialize the absorber and stripper, a method to decompose the process flowsheet into a stand alone absorber and a stand alone stripper is proposed (Alie et al., 2005). To predict accurately the amount of make-up MEA and water needed due to losses from evaporation in the absorber and stripper, the recycled loop in the flowsheet should be closed during the simulation run. Without closed recycle loop, water make-up cannot be varied properly to retain a constant wt% of MEA solution (e.g., 30%) in the system to avoid build-up of high concentration of MEA which usually favour corrosion. As the pressure drop across a column is apparently dependent upon process operating conditions, column type, and column internal configurations, calculated column pressure profile need to be updated after each iteration in the Absorber and Stripper models. The column hydrodynamic performance criteria such as downcomer flooding for tray column should be checked explicitly during process design for stable and feasible operation (Alie, 2004). Especially in the stripper model, care should be taken so that the reboiler temperature does not exceed the MEA solvent degradation limit, i.e., 122ºC as recommended by selected property method.

Extensive research works have been reported elsewhere in almost all related fundamental aspects of amine-based chemical absorption process, including chemical kinetics, thermodynamics and transport properties as well as mathematical model developments (Augustin, 1989; Versteeg et al., 1990; Versteeg and Swaaij, 1998; Pacheco and Rochelle, 1998; Freguia and Rochelle, 2003; Aboudheir et al., 2003; deMontigny et al., 2006; Chen et al., 2008; Zhang et al., 2009; Plaza et al., 2010). Although most of the works emphasised the absorption process, the theoretical fundamentals are well applicable to both absorption and desorption. Steady state models for simulating chemical absorption/desorption process for post-combustion capture of CO_2 using amines have been developed at different level of complexity such as open/or close recycled loop, equilibrium-stage/or rate-based modeling, reaction kinetics considered/or not, column pressure profile updated/or not from hydraulic calculations, different absorber/stripper configurations or process alternatives considered or not (Pintola, 1993; Alatiqi et al., 1994; Desideri and Paolucci, 1999; Singh, 2001; Al-Baghli et al., 2001; Freguia and Rochelle, 2003; Alie, 2004; Chang and Shih, 2005; Alie et al., 2005; Oyenekan and Rochelle, 2006; Tobiesen et al., 2007; Zhang et al., 2009; Sanpasertparnich et al., 2010; Plaza et al., 2010; Pellegrini et al., 2010; Schach et al., 2010). The authors used either commercial software (e.g., AspenPlus®, Aspen Custom Modeler, HYSYS, TSWEET, gPROMS, ProMax or ProTreat) or language code (e.g., Fortran or Visual Basic). Previously, the RateFrac model in AspenPlus® and recently the new RateSep model, a second generation rate-based process modeling, are mostly used for process simulation and design study, and also for simulating pilot plants (Zhang et al., 2009) for CO_2 capture with amine solution. Alie (2004) developed a model in AspenPlus® that simulates the removal of CO_2 from a 500 MW power plant flue gas using MEA solution. The author used the Aspen RateFrac model with equilibrium reactions consideration for both absorber and stripper, and interfaced a user subroutine for sizing and hydrodynamic evaluation of the tray columns. But very high tray spacing, i.e., 4.9 m for absorber (10 trays) and 5.5 m for stripper (7 trays) at lean loading of 0.25 was reported for a single train process to keep downcomer flooding less than or close to 50%.

The objective of this chapter is to simulate and design an industrial-scale post-combustion CO_2 capture process for a 500 MW coal-fired power plant using 30 wt% MEA solvent in AspenPlus® platform by considering all levels of modeling complexities, i.e. maintaining of MEA design concentration with proper balancing of make-up water and MEA by closed loop simulation, controlling of downcomer flooding level for stable operation and reboiler maximum temperature to avoid solvent degradation, updating of column pressure profile and same time sizing the column using design mode option with consideration solvent foaming condition. This will provide a clear picture of work and heat duties requirements to achieve a particular recovery of CO_2 based on a set of nominal equipment specifications and operating conditions. Various absorber-stripper models capable of taking into consideration column mass transfer resistances and reaction kinetics will be considered in this study for two process alternatives. Emphasis will be given on realistic absorption/desorption industrial process simulation and design for stable and/or feasible operation of the columns by assessing detailed hydrodynamic performance of the individual column.

7.2 Process Simulation Design Basis

Flue gas from a 500 MW coal-based unit of a Nanticoke Generating Station, Ontario, with thermal efficiency of 36% is considered in this study. Alie (2004) developed a model in Aspen Plus to predict the flow rate and composition of flue gas based on a 50/50 blend of PRB (Powder River Basin) and USLS (US low Sulphur) coals for that plant. The flue gas flow rate, composition and conditions are presented in Table 5.1 of Chapter 5. The two MEA-based (30% wt) capture processes considered in this work are shown in Fig. 7.1 and Fig. 7.2 and will be described in details in the next section. These two processes were simulated and designed based on a flue gas leaving from a 500 MW coal-fired power plant to capture 85% of CO_2 with a purity greater than 98%. As acid gases such as SOx and NOx react with MEA to form heat-stable salts which in turn reduce the CO_2 absorption capacity of the solvent and also raise the MEA make-up to cover additional losses, low concentrations of these gases (typically 10 ppm or less) are desirable to avoid excessive loss of solvent. It is assumed that a wet flue gas desulfurization (FGD) scrubber is applied to the flue gas from the coal-fired power plant

to achieve both SO_2 removal (to prevent interference with the MEA) and cooling of the inlet gas stream to the CO_2 capture system. It is also assumed no interferences from NOx or other pollutants such as fly ash are expected. The inlet flue gas conditions are presented in Table 7.1. The captured CO_2 will be compressed and pumped to 110 bar at 25ºC for transport via pipeline. This pressure specification may vary depending on the pipeline length and design, and the location of booster compressors. It is assumed that heat required to regenerate the solvent is provided to the kettle reboiler by steam extracted from the existing power plant connected to the CO_2 removal plant. It is also assumed that the capture plant uses locally available 12ºC lake water for cooling requirements.

Table 7.1: Flue gas conditions and solvent characteristics

Flue gas	
Flow rate (kg/hr)	2424400.0
Temperature (ºC)	40
Pressure (kPa)	101.0
Composition (mol %)	
CO_2	13.6
H_2O	8.2
N_2	74.7
O_2	3.5
Solvent	
Composition, unloaded (mol %)	
MEA (30% wt)	11.2
H_2O	88.8
Lean solvent temperature, (ºC)	40

7.3 Process Alternatives and Description

Two different system configurations are examined in this study. Figs. 7.1 and 7.2 present the process flow diagrams for the conventional i.e., base case, and Fluor's concept (Simmonds et al., 2003), respectively. Since the flue gas flow rate is very high, it is decided to divide the CO_2 capture operation into multiple amine trains. This allows the use of absorbers and strippers with diameters which are found in present commercial units. The entire CO_2 capture system consists of a single inlet gas train (gas blower and direct contact cooler), multiple parallel amine units, and a single, common CO_2 compression train. Four and two parallel amine trains have been considered, respectively, for base case and Fluor's case. In the base case, each train consists of mainly one absorber, one stripper for solvent regeneration, one lean/rich heat exchanger, one lean cooler, one lean pump and one rich pump. In the Fluor's case, each train has two absorbers and one stripper along with the above mentioned heat exchangers and pumps.

Pre-treated flue gas is pressurized by a blower to overcome the pressure losses in the downstream processing section, and cooled in a direct contact cooler with circulating water before being sent to an absorption tower. Cooled flue gas flows vertically upwards through the absorber counter currently to the lean MEA solution. The MEA reacts chemically with the CO_2 in the flue gas to form a weakly bonded compound (carbamate). The scrubbed gases are then washed and vented to the atmosphere. The CO_2-rich solution is pumped to the top of a stripper via a lean/rich cross heat exchanger in which the rich solution is heated to a temperature close to the stripper operating temperature by the hot lean solution returning from the stripper on its way back to the absorber. The rich solution flows down the stripper counter-currently to the steam and solvent vapour which are generated at the bottom of the stripper. The weakly bonded compound formed during absorption is broken down by the thermal energy of steam, regenerating the sorbent, and producing a concentrated CO_2 stream. When the amine solution reaches the bottom of the stripper, part of the liquid flow is sent to the reboiler where it is boiled to create the steam that travels up the column, the other part of the amine flow then travels back to the absorber. Uncondensed steam and carbon dioxide leave the top of the regenerator at high temperature and are sent to a condenser from where condensate is returned to the stripper

as reflux and where the concentrated CO_2 is sent to the compression unit. The hot CO_2-lean solvent solution is then pumped through the lean/rich heat exchanger, where it is cooled, then sent back to the absorber after further cooling in a cooler. Some fresh MEA and water are added to make up the losses incurred in the process.

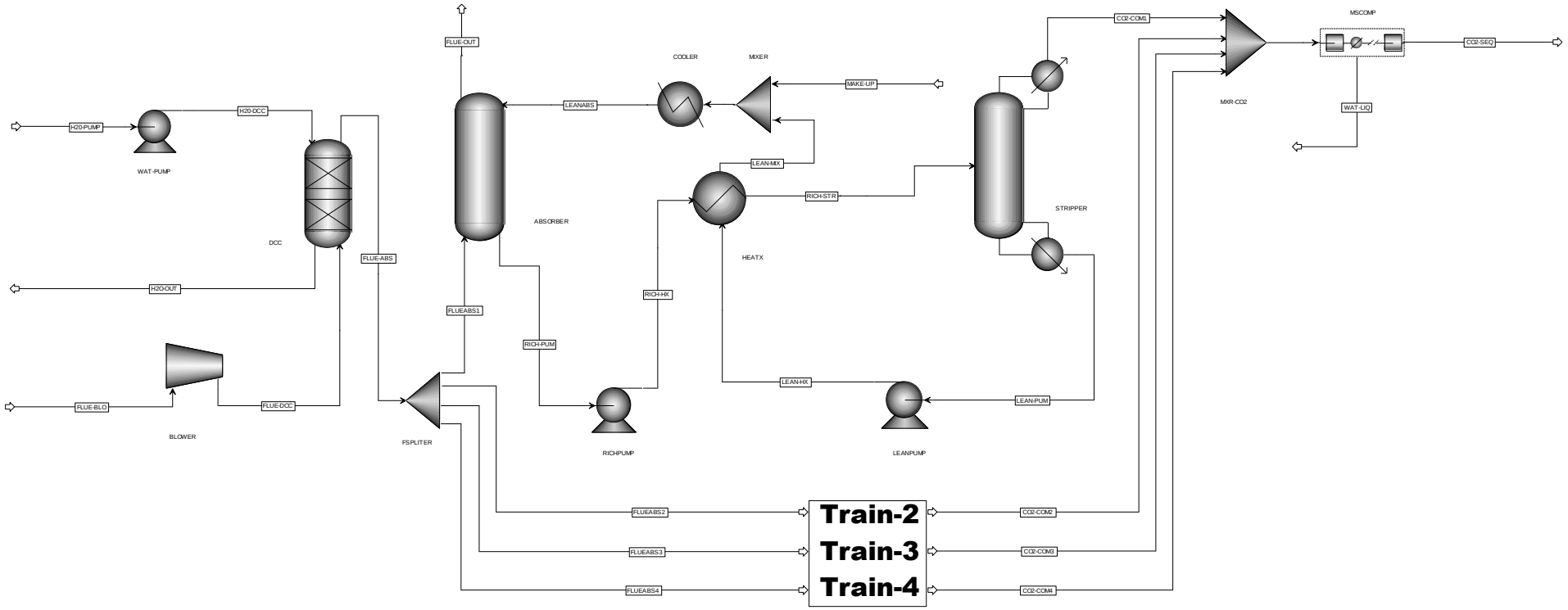

Figure 7.1: Base case flowsheet in AspenPlus®

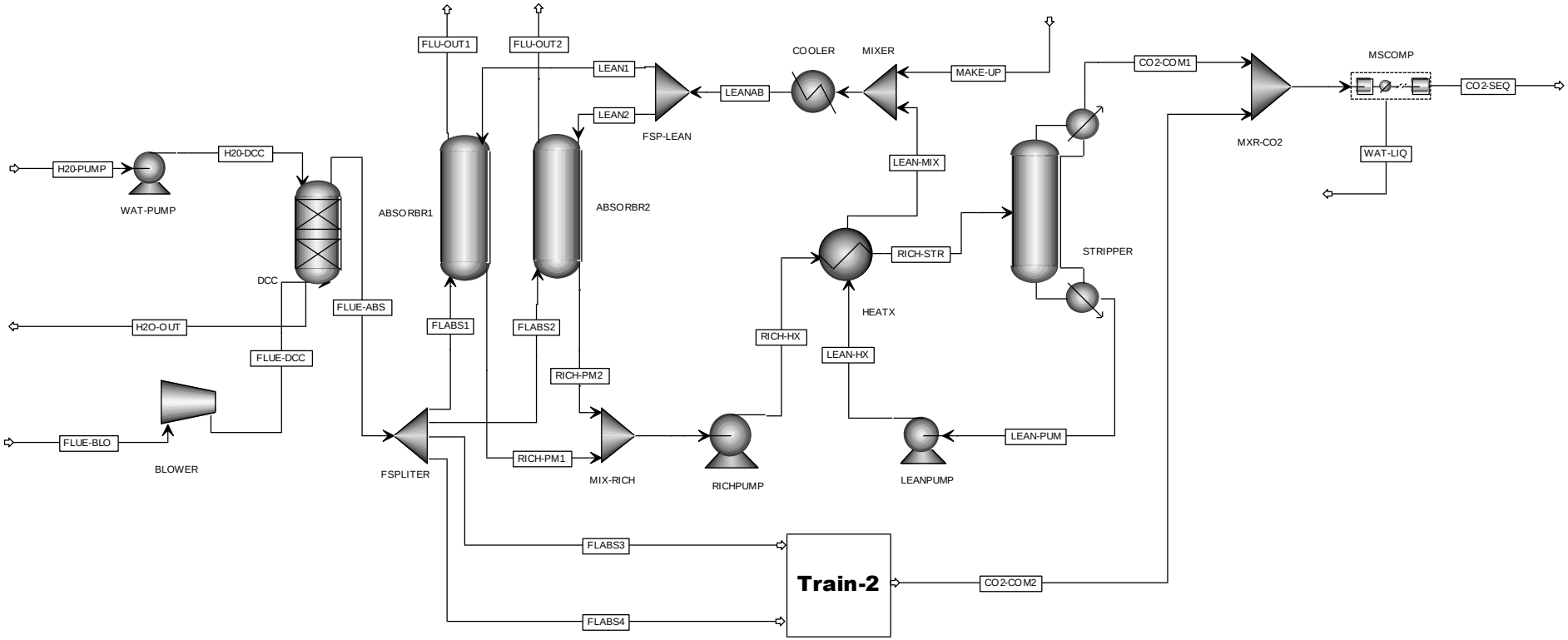

Figure 7.2: Fluor's (Simmonds et al., 2003) concept type flowsheet in AspenPlus®

7.4 RadFrac Model in AspenPlus® under aspenONE®

To study the coupled mass and heat transfer effects, an adequate model capable of taking into consideration column mass transfer resistances, reaction kinetics, thermodynamics, and hydrodynamics is essential. RadFrac unit operation model in AspenPlus® version 2006.5 under aspenONE® engineering suite of AspenTech was used to model absorber and stripper columns. RadFrac is a rigorous model for simulating all types of multistage two- or three-phase fractionation operations. RadFrac has the capability to model the columns either in equilibrium mode or in rate-based mode with chemical reactions. RadFrac can handle solids and pumparound works. It can be used to size and rate the columns consisting of trays and/or packings.

In equilibrium mode, RadFrac assumes equilibrium stages in which vapour and liquid phases attain equilibrium and perfect mixing occurs, with option for specifying Murphree and vaporization efficiencies or height equivalent to a theoretical plate (HETP) to match plant performance.

For rate-based modeling, RadFrac uses RateSep model which extends the functionality of RadFrac. RateSep is designed to model reactive multistage separation problems rigorously and accurately. RateSep model considers separation is caused by mass transfer between the contacting phases. Equilibrium is achieved only at the vapour-liquid interface, and RateSep uses the Maxwell-Stefan theory to calculate mass transfer rates (Chen et al., 2008). RateSep uses mass- and heat transfer correlations to predict column performance, without the need of efficiency factors. RateSep takes into account mass and heat transfer limitations, liquid and vapor film diffusion, equipment hydrodynamics and chemical reaction mechanisms.

RateSep balances gas and liquid phase separately and considers mass and heat transfer resistances according to the film theory by explicit calculation of interfacial fluxes and film discretization. The film model equations are combined with relevant diffusion and reaction kinetics and include the specific features of electrolyte solution chemistry, electrolyte thermodynamics, and electroneutrality where appropriate. The hydrodynamics of the column is accounted for via correlations for interfacial area, hold-up, pressure drop, mass and heat transfer coefficients.

RateSep allows the user to discretize the gas and liquid film and incorporate kinetic reactions within the segments of each film. Figure 7.3 illustrates the discritized film concept for CO_2 transfer across the vapor and liquid films (Chen et al., 2008). Film discretization facilitates precise modeling of the chemical reactions taking place in the liquid film. Without film discretization, the liquid film reaction rates are computed based on an average liquid phase composition. With film discretization, the liquid film reaction rates are computed by multiple sets of liquid phase compositions with each set representing the average liquid phase composition for the particular film segment. The various schemes for film discretization are considered and presented in Table 7.2. The "Nofilm" method assumes no liquid film and considers neither the film diffusion resistance nor film reactions. The "Film" method considers diffusion resistance but no reactions in the film. The "Filmrxn" method considers the film resistance and reactions without film discretization. The "Discrxn" considers the film resistance and reactions with film discretization.

RateSep provides four flow models which determine how the bulk properties are calculated relative to the inlet and outlet properties for each phase on each stage to evaluate mass and energy fluxes and reaction rates. The four flow models are Mixed, Countercurrent, VPlug, and VPlug-Pavg. In the Mixed flow model, the bulk properties for each phase are assumed to be the same as the outlet conditions for that phase leaving that stage. In the Countercurrent flow model, the bulk properties for each phase are an average of the inlet and outlet properties. In the VPlug flow model, outlet conditions are used for the liquid and average conditions are used for the vapor. The outlet pressure is used. In the VPlug-Pavg flow model, outlet conditions are used for the liquid and average conditions are used for the vapor. The average pressure is used.

RateSep allows the user to divide the column into segments, perform material and energy balances at each segment and integrate across the entire column. The calculation methods for the mass and heat transfer coefficients, interfacial area, liquid hold-up, and pressure drop can be specified using Aspen supplied correlations. The reaction kinetics can be specified using a power-law form. User can also supply custom FORTRAN subroutines if the Aspen supplied correlations are not adequate.

There are also a number of parameters that can be adjusted such as Chilton-Colburn averaging parameter, reaction and transfer condition factors, film discretization

ratio, interfacial area factor, average flow path factor, film non-ideality correction etc. The "Chilton-Colburn averaging parameter", a weighting parameter used in average diffusivity and average mass transfer coefficient calculations for calculating heat transfer coefficient by the Chilton-Colburn analogy. This parameter provides stability when compositions change, especially in reactive systems when some compositions may go to zero at the boundary. The "reaction condition" factor, the weighting factor for conditions (temperature and liquid composition) used to calculate reaction rates for the film. The condition used is the "factor × bulk condition + (1 - factor) × interface" condition. A factor of 0 indicates the interface, and a factor of 1 represents the edge of the film next to the bulk. A higher weighting factor means liquid conditions closer to the bulk liquid will carry higher weight. The "transfer condition" factor, the weighting factor for conditions (temperature and liquid composition) is used to calculate mass transfer coefficient. The "top/bottom stage condition" weighing factor is used to calculate flux and reaction extents for top and bottom segments. The "film discretization ratio" is the ratio of the thickness of the adjacent discretization regions. A value of film discretization ratio greater than 1 means thinner film regions near the vapor-liquid interface. The "interfacial area factor" is a scaling factor for interfacial area. The area predicted by the correlation is multiplied by this factor. For highly non-ideal phases, film non-ideality correction is selected for fugacity calculation.

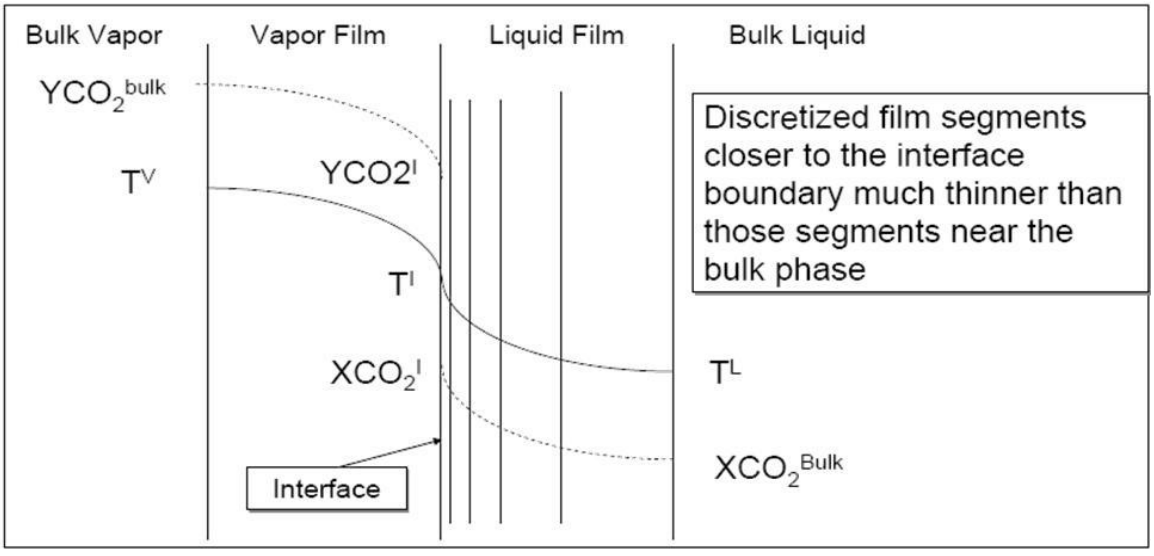

Figure 7.3: Discretized film concept in RateSep for CO_2 Transfer (Chen et al., 2008)

RateSep uses Newton-method to solve the system of equations. The solution obtained from the equilibrium-based mode is used as the initial guess. RateSep also provides simple continuation/homotopy method that allows the user to choose option for easy switching from equilibrium to rate-based solution. The binary diffusivity and mass transfer coefficients are not considered as independent variables because of too many variables. The computational time increases with the square of the number of components.

Some important features of Aspen RateSep model are highlighted below (Aspen RateSep Brochure available at www.aspentech.com):

- Provides a rigorous, consistent framework for the modeling of rate-based separations
- Seamless switch from equilibrium to rate-based calculations
- Different column configurations including multiple feeds and side-draws, pumparounds, multi-diameter columns etc.
- Homogeneous kinetic reactions, equilibrium reactions, true and apparent component electrolyte reactions
- Hydraulics for trays and packing, option to update pressure profile from hydraulic calculations
- Mass and heat transfer correlations for a wide range of trays and packings type
- Interface for user models of binary mass transfer coefficients, heat transfer coefficients, interfacial area, pressure drop across trays and packing, reaction kinetics
- Design mode for calculating column diameter based on approach to flooding
- Continuation/homotopy method for easy transition from equilibrium initialization to rate-based calculations
- No need to guess efficiencies

7.5 Process Simulation in AspenPlus®

The process flowsheets presented in Section 7.3 were simulated in Aspen Plus® based on the design basis described in Section 7.2 using RadFrac model for absorber and

stripper. The inlet flue gas entering the blower is considered free from all contaminants and consists primarily of CO_2, H_2O, N_2 and O_2. Flue gas and solvent characteristics are presented in Table 7.1. The design objective is set for 85% CO_2 capture with 98% (mol %) or more CO_2 purity. Different absorber and stripper models in Aspen RadFrac framework using RateSep model, as shown in Table 7.2, are investigated based on mass transfer methods and options to account for chemical reactions in the liquid phase. In the first option, the reaction kinetics for CO_2 absorption by MEA-H_2O solution are modeled explicitly and the remaining liquid phase reactions are in chemical equilibrium. Chemical equilibrium conditions are assumed for all liquid phase reaction in the second option. The goals of the investigation are many folds e.g., performance characteristic analysis with different reaction kinetics, finding optimum operating and design conditions with minimum work and heat duties requirement, and selection of alternate process configuration with different process design considerations. The simulation models must properly account for thermodynamics of the CO_2-water-MEA system, reaction kinetics of CO_2 with MEA solution, and the various transport properties affecting the mass and heat transfer. True component approach is chosen to represent the compositions of the electrolyte systems (including ionic species) in the calculation. In this approach, the chemical equilibrium equations that describe the solution chemistry are solved simultaneously with the material balance, energy balance and phase equilibrium equations that describe the unit operation model.

The capture process is simulated using a complete closed flowsheet to keep the overall water and MEA balance to zero. This makes the flow sheet more difficult to converge due to the recycle structure in the flow sheet. However, it is important for the CO_2 capture unit to maintain the design MEA concentration, since any reductions in MEA (exiting with the Flue Gas from the Absorber) can degrade the unit performance. It is common for water to be lost by evaporation in the Absorber, and not having sufficient water can cause drying up of the Absorber or Stripper. The choice and the initial estimation of the tear streams are important factors in the flow sheet convergence.

The following assumptions are considered in developing the process simulation models:

- Corrosion and degradation due to the presence of O_2 in the flue gas is negligible
- Liquid phase reaction only
- Negligible heat loss to the surroundings

- Negligible solvent degradation due to heat-stable salt formation

The CO_2 loading (α) in the lean and rich MEA stream is defined as the molar ratio of CO_2 to MEA (i.e., mol CO_2/mol MEA) including ionic components. The rich stream which exits the absorber at the bottom of the column is preheated in a heat exchanger by the lean stream leaving the stripper. The development of AspenPlus® flowsheet needs input file specifications i.e., specifying properties calculation methods, streams, all unit operations blocks etc.

Table 7.2: Details of Rate-based and Equilibrium-stage modeling approaches using RadFrac unit operation model in AspenPlus®

Absorber-Stripper integrated Models	**Model Identification**	**Mass transfer method**	**Method for liquid phase chemical reactions**		**Film Resistance with/without Reaction**				**Film Non-ideality correction**			
			Absorber	Stripper	Absorber		Stripper		Absorber		Stripper	
					Liquid	Vapor	Liquid	Vapor	Liquid	Vapor	Liquid	Vapor
Rate, Kinetics (discrxn-film, yes-yes), Equilibrium (nofilm-nofilm, no-no)	Model-I	Rate-based	Kinetics	Chemical Equilibrium	Discrxn	Film	Nofilm	Nofilm	Yes	Yes	No	No
Rate, Kinetics (discrxn-film, yes-yes), Kinetics (nofilm-nofilm, no-no)	Model-II	Rate-based	Kinetics	Kinetics	Discrxn	Film	Nofilm	Nofilm	Yes	Yes	No	No
Rate, Equilibrium (nofilm-nofilm, no-no), Equilibrium (nofilm-nofilm, no-no)	Model-III	Rate-based	Chemical Equilibrium	Chemical Equilibrium	Nofilm	Nofilm	Nofilm	Nofilm	No	No	No	No
Equilibrium, Kinetics, Kinetics	Model-IV	Equilibrium-Stage	Kinetics	Kinetics	n/a	n/a	n/a	n/a	n/a	n/a	n/a	n/a
Equilibrium, Equilibrium, Equilibrium	Model-V	Equilibrium-Stage	Chemical Equilibrium	Chemical Equilibrium	n/a	n/a	n/a	n/a	n/a	n/a	n/a	n/a
Rate, Kinetics (discrxn-film, yes-yes), Kinetics (discrxn-film, yes-yes)	Model-VI	Rate-based	Kinetics	kinetics	Discrxn	Film	Discrxn	Film	Yes	Yes	Yes	Yes
Rate, Kinetics (nofilm-nofilm, no-no), Kinetics (nofilm-nofilm, no-no)	Model-VII	Rate-based	Kinetics	kinetics	Nofilm	Nofilm	Nofilm	Nofilm	No	No	No	No
Rate, Equilibrium (discrxn-film, yes-yes), Equilibrium (nofilm-nofilm, no-no)	Model-VIII	Rate-based	Chemical Equilibrium	Chemical Equilibrium	Discrxn	Film	Nofilm	Nofilm	Yes	Yes	No	No

Nofilm: No film reactions and resistance in specified phase
Film: Diffusion resistance but no reactions in film in specified phase
Filmrxn: Diffusion resistance with reactions in film in specified phase
Discrxn: Diffusion resistance with reactions in film in specified phase. Film is discretized.

Description of Model-I:
Rate, Kinetics (discrxn-film, yes-yes), Equilibrium (nofilm-nofilm, no-no):

Rate – This term describes modeling approach selection for both absorber and stripper. Rate-based modeling approach adopted for both absorber and stripper by using RateSep model under RadFrac unit operation model.

Kinetics (discrxn-film, yes-yes) – First term describes the type of chemical reactions specified in the absorber for bulk liquid phase and film. Here Absorber model uses combination of kinetic and equilibrium reactions as presented in Table 7.4 & 7.5. Terms inside brackets describe film details i.e., as film resistance with or without reaction & non-ideality correction considered or not for both liquid and vapour film.

Equilibrium (nofilm-nofilm, no-no) – First term describes type of chemical reactions specified in the stripper for bulk liquid phase and film. Here Stripper model uses only equilibrium reactions as presented in Table 7.3. Terms inside brackets describe film details i.e., as film resistance with or without reaction & non-ideality correction considered or not for both liquid and vapour film.

7.5.1 Specifying properties and Reactions

To calculate fluid thermodynamic and transport properties, AspenPlus input file specifies the property method and solution chemistry of MEA-water-CO_2 system which is an aqueous electrolyte solution of ionic and molecular species. AspenPlus® 2006.5 documentation (help) indicates two electrolyte property methods or three inserts (as *.bkp files) for use in modelling processes containing CO_2, MEA, and H_2O. Electrolyte solutions are extremely nonideal because of the presence of charged species. Property methods based on correlations can handle specific components under well-described conditions but rigorous models-based methods are generally applicable. AMINES is a correlation-based property method which uses Kent-Eisenberg correlation. It is recommended with systems where temperatures between 32-138ºC, a maximum CO_2 loading of 0.5, and 15-30 wt% MEA in solution. ELECNRTL is an activity coefficient model-based property method uses electrolyte NRTL model for liquid phase and Redlich-Kwong EOS for vapour phase. The ELECNRTL property method is the most versatile electrolyte property method and can handle very low and very high concentrations (AspenPlus documentation). It can handle aqueous and mixed solvent systems. ELECNRTL uses the databank for binary molecular interaction parameters for the NRTL-RK property method. Many binary and pair parameters and chemical equilibrium constants from regression of experimental data are included in Aspen Physical Property System databanks. The solubility of supercritical gases is modeled using Henry's law. The three property inserts are “mea”, “emea” and “kemea”. The last insert, i.e., “kemea” considers ELECNRTL property method with reaction kinetics for systems containing CO_2, H_2S, MEA and H_2O with temperatures up to 120ºC and MEA concentration up to 50 wt%. The property insert “kemea” is used in this simulation work and which is accessible through AspenTech\AspenPlus® 2006.5\GUI\Elecins\kemea.bkp. CO_2 and H_2S are selected as Henry’s components in the “kemea” insert. O_2 and N_2 are not available as components in the “kemea” property insert. These two are added as components and specified to obey Henry’s law.

The electrolyte-NRTL model uses the following default models to predict the physical and transport properties of the system. Viscosities are based on the DIPPR (Design Institute for Physical Properties) model for non-electrolytes and on the Andrade

correlation with the Jones-Dole correction for electrolyte species. The diffusivity of each species is determined using the Chapman–Enskog–Wilke–Lee model for non-ion components and the Nernst–Hartley model for ions. The liquid molar volume of the liquid is calculated using the Clarke model. Vapor thermal conductivity is calculated using DIPPR model. Thermal conductivity of the liquid is calculated using the Sato–Riedel and DIPPR models and a correction due to the presence of electrolytes is applied using the Reidel model. The surface tension of the liquid mixture is calculated by the Onsager–Samaras model. Details of these models are available in AspenPlus® documentation.

Electrolyte solution chemistry is used in connection with the electrolyte property method, ELECNRTL to predict equilibrium mass fractions in the liquid and vapour phases for equilibrium-stage modeling approach and at the vapour-liquid interface for rate-based modeling approach. Chemistry Form under Reactions folder of Data menu is used to define the solution chemistry. The electrolyte solution chemistry considered in the property insert ("kemea") is represented by the equilibrium reactions as listed in the Table 7.3 under Chemistry ID named KEMEA. Equilibrium constant can be computed from Gibbs energies or from a built in polynomial expression by providing the coefficients. If the reaction does not actually reach equilibrium, Temperature Approach to Equilibrium option can be used to compute equilibrium constant.

To account reaction for kinetics, Reactions Form under Reactions folder can be used to specify kinetic data for rate-controlled reactions by specifying stoichiometry and rate parameters. Nonelectrolyte equilibrium reactions can also be specified in the Reactions Form. RadFrac model uses "Reactive Distillation" Reaction Form. For rate-controlled reactions, AspenPlus provides a built-in power law expression for calculating the rate of reaction. User own kinetics subroutines can be supplied if the expression is inadequate to represent the kinetics for the current Reaction ID. For rate controlled reactions, the amount of hold-up or residence time within the distillation block must be specified to calculate the rate of reaction. The kinetic and equilibrium reactions considered in kemea insert are presented in Table 7.4 under Reaction ID named MEA-CO_2. AspenPlus® 2006.5 also provides a backup file as an application example for MEA process modeling with ELECNRTL property method. It includes a different kinetic model with two extra kinetic reactions (as shown in Table 7.5 with Reaction ID named

MEA-REA) and is used to simulate pilot plant data of University of Texas, Austin (AspenTech\AspenPlus® 2006.5 \GUI \App \Amines \Rate_based_MEA_Model.bkp). The electrolyte solution chemistry has been modeled with a chemistry model and the Chemistry ID is MEA. Chemical equilibrium is assumed with all the ionic reactions in the Chemistry MEA. In addition, a kinetic model is created with a Reaction ID MEA-REA (Table 7.5). In MEA-REA, all reactions are assumed to be in chemical equilibrium except the reactions of CO_2 with OH^- and the reactions of CO_2 with MEA.

The Chemistry ID KEMEA and MEA are exactly the same (Table 7.3) and uses same number of reactions. The relevant data for equilibrium and kinetic reactions such as K-values, rate constants, activation energies etc. are available in their respective Chemistry and Reaction forms in AspenPlus®.

Table 7.3: Reactions in the Chemistry Form (ID: KEMEA or MEA)

Rxn no.	Reaction Type	Stoichiometry
1	Equilibrium	$MEA^+ + H_2O \leftrightarrow MEA + H_3O^+$
2	Equilibrium	$CO_2 + 2.0\, H_2O \leftrightarrow H_3O^+ + HCO_3^-$
3	Equilibrium	$HCO_3^- + H_2O \leftrightarrow H_3O^+ + CO_3^{--}$
4	Equilibrium	$MEACOO^- + H_2O \leftrightarrow MEA + HCO_3^-$
5	Equilibrium	$2.0\, H_2O \leftrightarrow H_3O^+ + OH^-$
6	Equilibrium	$H_2O + H_2S \leftrightarrow HS^- + H_3O^+$
7	Equilibrium	$H_2O + HS^- \leftrightarrow S^{-2} + H_3O^+$

Table 7.4: Reactions in the Reactions Form (ID: MEA-CO_2)

Rxn no.	Reaction Type	Stoichiometry
1	Equilibrium	$MEA^+ + H_2O \leftrightarrow MEA + H_3O^+$
2	Equilibrium	$2.0\ H_2O \leftrightarrow H_3O^+ + OH^-$
3	Equilibrium	$HCO_3^- + H_2O \leftrightarrow H_3O^+ + CO_3^{--}$
4	Equilibrium	$MEACOO^- + H_2O \leftrightarrow MEA + HCO_3^-$
5	Kinetic	$CO_2 + OH^- \rightarrow HCO_3^-$
6	Kinetic	$HCO_3^- \rightarrow CO_2 + OH^-$
7	Equilibrium	$H_2O + H_2S \leftrightarrow HS^- + H_3O^+$
8	Equilibrium	$H_2O + HS^- \leftrightarrow S^{-2} + H_3O^+$

Table 7.5: Reactions in the Reactions Form (ID: MEA-REA)

Rxn no.	Reaction Type	Stoichiometry
1	Equilibrium	$MEA^+ + H_2O \leftrightarrow MEA + H_3O^+$
2	Equilibrium	$2.0\ H_2O \leftrightarrow H_3O^+ + OH^-$
3	Equilibrium	$HCO_3^- + H_2O \leftrightarrow H_3O^+ + CO_3^{--}$
4	Kinetic	$CO_2 + OH^- \rightarrow HCO_3^-$
5	Kinetic	$HCO_3^- \rightarrow CO_2 + OH^-$
6	Kinetic	$MEA + CO_2 + H_2O \rightarrow MEACOO^- + H_3O^+$
7	Kinetic	$MEACOO^- + H_3O^+ \rightarrow MEA + H_2O + CO_2$
8	Equilibrium	$H_2O + H_2S \leftrightarrow HS^- + H_3O^+$
9	Equilibrium	$H_2O + HS^- \leftrightarrow S^{-2} + H_3O^+$

7.5.2 Specifying Streams

The conditions and flow rates of all input streams must be specified i.e., **FLUE-BLO**, **H2O-PUMP** and **MAKE-UP** as shown in Fig. 7.1 and 7.2 must be defined to run the simulation.

- **FLUE-BLO** is the flue gas stream entering to the capture process after modification of original flue gas synthesis results presented in Chapter 5. Its flow rate and composition are presented in Table 7.1. The sole purpose of excluding other components is to reduce the flowsheet convergence time. The time required for convergence of RadFrac models, specified for absorber and stripper, is strongly depended upon the number of components present in the feed. CO_2, H_2S, N_2 and O_2 are selected as Henry-components to which Henry's law is applied.
- **H2O-PUMP** is a complete water stream. It is assumed that water is available at atmospheric pressure at an average temperature of 12ºC from Lake Erie for Nanticoke plant for whole year. The flow rate of this stream is adjusted such that the flue gas is cooled to the desired Absorber inlet temperature.
- **MAKE-UP** stream provides fresh MEA and H_2O to the process to exactly balance the loss from the top of the absorber and stripper. It is assumed that this make-up solvent is available at atmospheric pressure and a temperature of 25ºC. The molar flow rates of MEA and water in this stream are calculated immediately prior to Mixer execution by a Calculator block under Flowsheeting options. Initial specification is needed for this stream.

Additionally, two tear streams, **LEANABS** and **LEAN-HX** also need initial specification for easy closed-loop flowsheet convergence.

7.5.3 Specifying Blocks

The flowsheets mainly consist of the following AspenPlus® unit operation blocks:

Blower

AspenPlus® **Compr** unit operation model is specified to model *Blower* to increase the flue gas pressure to overcome the pressure drop in the *Direct Contact Cooler* and the *Absorber* units. COMPR represents a single stage compressor. A polytrophic efficiency

of 80% and mechanical efficiency of 90% is assumed. The outlet pressure of the Blower depends on the calculated column pressure drop in the *Absorber* and specified pressure drop for *Direct Contact Cooler*.

Direct Contact Cooler

It is used to cool down the hot outlet flue gas stream of *Blower* using lake water at 12ºC to a specified temperature i.e., 40ºC to maximize CO_2 absorption in the *Absorber.* The unit is modeled as two equilibrium-stage tower using AspenPlus® RadFrac unit operation model with consideration of 0.1 bar pressure drop.

Pump (Water, Lean and Rich)

All pumps are modeled with the AspenPlus® **Pump** unit operation model. Outlet pressure or pressure rise which are determined by upstream units, need to be specified to calculate pump's power requirement. For *Water Pump* the pressure rise is required to overcome the pressure drop of the *Direct Contact Cooler*. For *Rich Pump* the pressure rise is necessary to avoid acid gas breakout in the *Lean/Rich Heat Exchanger (Heatx)* and to overcome the operating pressure and height requirements in the *Stripper*. Lean amine solution from the bottom of the stripper is pumped by *Lean Pump* to an elevated pressure to overcome the pressure drops in the rich/lean amine exchanger and lean amine cooler, and the elevation at the top of the absorber. For all pumps default efficiency is considered i.e., 90%.

Lean/Rich Heat Exchanger (Heatx)

In the ***Lean/Rich Heat Exchanger,*** the rich amine is preheated prior to regeneration by hot lean amine coming from the bottom of the regenerator. It is modeled in AspenPlus® using two-stream heat-exchanger unit operation model, **HeatX**. A heat transfer coefficient of 1134 W/m^2-C for hot water-watery solution (liquid-liquid) system is considered here for counter current type heat exchanger (Alie, 2004). For most of the cases 5ºC hot outlet temperature approach (i.e., hot outlet-cold inlet temperature difference are specified for the ***Lean/Rich Heat Exchanger***) is chosen. However, for few cases 10°C and 15ºC have also been used for converging flowsheet when it was found difficult using 5ºC temperature approach. 5ºC temperature approach helps to reduce the reboiler steam requirements but for this aggressive temperature approach the penalty is the larger size of heat exchanger requirement.

Cooler

The lean amine must be further cooled in a *Cooler* before it is pumped back into the absorber column. The cooler lowers the lean amine temperature to the desired *Absorber* inlet temperature such as 40ºC. The Cooler is modeled with AspenPlus® **Heater** unit operation model which is mainly used as thermal and state phase changer.

Mixer

Mixer is used to combine several streams into a single stream flow and is implemented with the **Mixer** unit operation model.

Splitter

Splitter is used to split a single stream to multiple streams. **FSplit** UOM is used to implement a splitter operation.

Absorber and Stripper

Both the *Absorber* and *Stripper* are modeled with the AspenPlus® **RadFrac** unit operation model for equilibrium–stage and rate-based modeling as described in Table 7.2. RadFrac directly includes mass and heat transfer rate processes in the system of equations representing the operation of separation process units. The types of equations required by the two kinds of modeling approaches are summarized in Table 7.6, and the details of these equations are available in AspenPlus documentation.

Sieve trays are used for both the *Absorber and Stripper.* Other types of trays such as bubble-cap and valve trays can also be specified along with options for different kind of packings for packed column as RadFrac has built-in routines for them. Sieve trays are selected because they are the cheapest and easiest to construct. They are commonly used and AspenPlus has strong data bases for correlations that characterize their hydrodynamic performance. This could be a good starting point to compare more advanced and sophisticated column types.

Absorber does not have any condenser and reboiler. The inlets and outlets are connected to the top and bottom of the column for *Absorber*. The pressure at the top of the *Absorber* and *Stripper* is fixed at 101.3 kPa. For *Stripper*, a partial condenser at the top and a kettle type reboiler at the bottom are considered. Reboiler and condenser are always modeled as equilibrium stage. Increasing the Stripper pressure raises the column

temperature which in turn helps to lower energy requirements for solvent regeneration. But to avoid excessive degradation of MEA (30 % wt) solution due to temperature rise in the reboiler beyond 122ºC (395 K), the pressure of the *Stripper* reboiler is closely monitored for each simulation.

Some design parameters such as tray geometry (i.e., tray spacing, weir height, number of passes, downcomer clearance etc.), approach to flooding (80% and 70%), an initial estimate of column diameter and number of trays need to be specified. RadFrac has options to choose design mode to calculate column diameter based on base stage and base flooding, and pressure profile update based on calculated pressure drop on each tray. Both options are used for both columns. Key specifications for both columns are presented in the Table 7.7 to 7.12 and for remaining specifications AspenPlus® default values are used.

Aspen Plus® RadFrac model using RateSep features provides several built-in correlations for mass transfer coefficient, heat transfer coefficient, interfacial area, liquid hold-up and pressure drop calculation for tray column and also the option for the user to provide their own correlation or subroutine. The Zuiderweg (1982) correlation is used to calculate the gas and liquid mass transfer coefficient and the interfacial area in both columns. The parameters for the correlations are supplied from the Aspen Plus® database. RateSep uses a rigorous multicomponent mass transfer theory (Krishna and Standard, 1976) with the binary mass transfer coefficients to evaluate multicomponent mass transfer coefficients and components mass transfer rates between vapour and liquid phases. For interfacial area, a scaling factor can be specified on the Tray **Rating|RateSep|Rate Based** sheet. This factor can be used to adjust the correlation results to match the observed behaviour for the plant. The interfacial area used by AspenPlus is the area from correlation equation multiplied by this factor. The default value i.e., 1 is used here for this scale factor.

The Chilton–Colburn method is used to calculate the heat transfer coefficients from the binary mass transfer coefficients in both columns. For the heat transfer calculation, RateSep™ uses the calculated interfacial area as the area for heat transfer. The Chilton–Colburn averaging parameter under **RateSep Setup|Specifications**, can be adjusted to weigh the average diffusivity and average binary mass transfer coefficients for the calculation of the heat transfer coefficient in Chilton–Colburn analogy. AspenPlus

default value, i.e., 0.0001 is used here. An accurate representation of the heat transfer coefficients depends not only on an adequate estimate of the mass transfer coefficients, but also on the physical and transport properties as well.

Liquid hold-up is used for the calculation of the kinetic reaction rates in the bulk liquid and in the liquid film. For sieve tray, RateSep has several built-in correlations for hold-up that the user can select from **Rating|RateSep|Holdups**. As the mass transfer coefficient, interfacial area and hold-up correlations are related; the same correlation i.e., the Zuiderweg (1982) is used to calculate the liquid hold-up as AspenPlus recommendation. The hold-up that is specified under **Reactions|Holdups** is only used for the initialization of the calculation, but not for the actual calculations of the kinetic reactions. Also, the liquid hold-up that is specified in the **Rating|RateSep|Holdups** is used only to calculate the kinetic reaction rates. It is not used for the calculation of mass or heat transfer coefficients.

For sieve trays, AspenPlus provides two procedures for calculating the approach to flooding. The first procedure is based on the Fair method. The second uses the Glitsch procedure for ballast trays. This procedure de-rates the calculated flooding approach by 5% for sieve trays. The first procedure based on Fair method is chosen here for calculating the approach to flooding in both columns.

For pressure drop calculation, RadFrac uses a built-in correlation for sieve tray based on the method described elsewhere (Smith, 1963; Perry's handbook, 1973). The calculation method approximated the pressure drop across the tray as the sum of two terms, the pressure drop across a dry hole, coupled with the pressure drop through the aerated mass of liquid and around the hole.

Table 7.6: Equations used in solving the equilibrium-stage and rate-based modeling problem in Absorber and Stripper[¥]

Rate-based	Equilibrium-stage
Material Balances for all phases[*]	Material Balances
Energy Balances for all phases[*]	Energy Balances
Phase Equilibrium Eqs. at gas-liquid interface	Equilibrium Eqs.
Summation Eqs. for mole fractions	Summation Eqs for mole fractions
Mass transfer Eqs in bulk gas phase	
Mass transfer Eqs for bulk liquid phase	
Heat transfer Eqs for bulk gas phase	
Heat transfer Eqs in bulk liquid phase	
Electrolyte neutrality Eqs	

*- all phases mean bulk gas, bulk liquid, gas film and liquid film

¥- Stripper needs extra equations for condenser and reboiler

CO_2 Compressor

The CO_2 from the amine unit is compressed in a single train to 110 bar to form supercritical CO_2 (a dense liquid-like phase) for transportation and injection to an off-site location. The *CO_2 Compressor* is implemented in Aspen Plus using the **MCompr** UOM. **MCompr** is used for modelling a multistage compressor with inter-cooling. This block requires that the number of stages, fixed discharge pressure from last stage or compression ratio, efficiency and interstage cooler outlet temperature to be specified. Five interstages with outlet cooling temperature of 40ºC, and a polytrophic efficiency of 80% and mechanical efficiency of 90% are specified. The outlet pressure for CO_2 compression is considered 110 bar.

7.5.4 Design Specifications

Using **Design Specs** and **Vary** sheets inside the *Stripper* block, the molar reflux ratio is varied to achieve a specified condenser temperature (i.e., 70ºC) and the bottom-to-feed ratio is adjusted to achieve the desired molar flow rate of CO_2 in the distillate (i.e., 85% CO_2 recovery of the flue gas). The condenser temperature selection is a trade-off between the reduction of the water flow rate exiting with CO_2 towards the compression units and the temperature of the fluid returning to the column which should be high enough for good regeneration efficiency. The desired CO_2 purity (≥98%) is achieved during the compression process of the vapor stream leaving the condenser by removing liquid water. Other two design specs are also specified using **Flowsheeting Options**: one for maintaining a specified absorber inlet flue gas temperature (i.e., 40ºC) by varying cooling water flow rate in the *Direct Contact Cooler* and another for maintaining a specified CO_2 loading in the lean MEA solution entering at the top of absorber by manipulating the flow rate of the inlet MEA solution.

7.5.5 Key Process Simulation Parameters Specification

Summary of process simulation inputs are presented in Table 7.6 through Table 7.12 for different models along with the flue gas conditions and solvent characteristics presented in the Table 7.1. Some parameters need initial estimates although these are the output of the model.

Table 7.7: Process simulation input specifications - single train basis- Model I

	Input specifications for Model-I									
Lean loading (mol CO_2/mol MEA)	**0.2**		**0.25**		**0.3**		**0.35**		**0.4**	
Flue gas flow rate, kmol/sec	5.5		5.5		5.5		5.5		5.5	
Flue gas Absorber-inlet temperature, ºC	40		40		40		40		40	
Lean solvent temperature, ºC	40		40		40		40		40	
Lean solvent flow rate (initial), kmol/sec	21		25		30		32		38	
Water make-up rate (initial), kmol/sec	0.25		0.25		0.25		0.25		0.25	
MEA make-up rate (initial), kmol/sec	0.25		0.25		0.25		0.25		0.25	
Lean-rich heat-exchanger temp. appro., ºC	5		5		5		5		5	
	Absorber	**Stripper**	**Absorber**	**Stripper**	**Absorber**	**Stripper**	**Absorber**	**Stripper**	**Absorber**	**Stripper**
Simulation approach	Rate-based	Rate-based	Rate-based	Rate-based	Rate-based	Rate-based	Rate-based	Rate-based	Rate-based	Rate-based
Reaction ID	MEA-REA (1-7)		MEA-REA (1-7)		MEA-REA (1-7)		MEA-REA (1-7)		MEA-REA (1-7)	
Chemistry ID		MEA (1-9)		MEA (1-9)		MEA (1-9)		MEA (1-9)		MEA (1-9)
System foaming factor	0.85	0.85	0.85	0.85	0.85	0.85	0.85	0.85	0.85	0.85
Flow model	mixed	mixed	mixed	mixed	mixed	mixed	mixed	mixed	mixed	mixed
Pressure profile update	Yes	Yes	Yes	Yes	Yes	Yes	Yes	Yes	Yes	Yes
Design mode	Yes	Yes	Yes	Yes	Yes	Yes	Yes	Yes	Yes	Yes
Trays/stages (no. of downcomer pass)	7 (2)	9 (2)	7 (2)	9 (2)	7 (2)	9 (2)	7 (2)	9 (2)	7 (2)	9 (2)
Base stage	3	8	3	8	4	8	4	8	5	8
Approach to Flooding (fractional)	0.7	0.7	0.7	0.7	0.7	0.7	0.7	0.7	0.7	0.7
Tray spacing, m	1.4	1.7	1.4	1.7	1.4	1.6	1.4	1.6	1.4	1.6
Weir height, m	0.14	0.15	0.14	0.15	0.14	0.15	0.14	0.15	0.14	0.15
Downcomer clearance, m	0.115	0.125	0.115	0.125	0.115	0.125	0.115	0.125	0.115	0.125
Column diameter (initial), m	7	4.4	6	4.3	7	4.4	8	4.6	9	6.8
Top stage pressure, N/m^2	101300	101300	101300	101300	101300	101300	101300	101300	101300	101300
Bottom stage pressure (initial), N/m^2	177000	128000	177000	128000	177000	128000	177000	128000	177000	128000
Reflux ratio (initial)		0.45		0.35		0.4		0.4		0.65
Bottom to feed ratio (initial)		0.95		0.95		0.95		0.95		0.95

Table 7.8: Process simulation input specifications - single train basis - Model II

	Input specifications for Model-II									
Lean loading (mol CO_2/mol MEA)	**0.2**		**0.25**		**0.3**		**0.35**		**0.4**	
Flue gas flow rate, kmol/sec	5.5		5.5		5.5		5.5		5.5	
Flue gas Absorber-inlet temperature, ºC	40		40		40		40		40	
Lean solvent temperature, ºC	40		40		40		40		40	
Lean solvent flow rate (initial), kmol/sec	22		27		32		32		42	
Water make-up rate (initial), kmol/sec	0.25		0.25		0.25		0.25		0.25	
MEA make-up rate (initial), kmol/sec	0.25		0.25		0.25		0.25		0.25	
Lean-rich heat-exchanger temp. appro., ºC	5		5		5		5		5	
	Absorber	**Stripper**	**Absorber**	**Stripper**	**Absorber**	**Stripper**	**Absorber**	**Stripper**	**Absorber**	**Stripper**
Simulation approach	Rate-based	Rate-based	Rate-based	Rate-based	Rate-based	Rate-based	Rate-based	Rate-based	Rate-based	Rate-based
Reaction ID	MEA-REA (1-7)	MEA-REA (2-8)	MEA-REA (1-7)	MEA-REA (2-8)	MEA-REA (1-7)	MEA-REA (2-8)	MEA-REA (1-7)	MEA-REA (2-8)	MEA-REA (1-7)	MEA-REA (2-8)
Chemistry ID		MEA (1,9)		MEA (1,9)		MEA (1,9)		MEA (1,9)		MEA (1,9)
System foaming factor	0.85	0.85	0.85	0.85	0.85	0.85	0.85	0.85	0.85	0.85
Flow model	mixed	mixed	mixed	mixed	mixed	mixed	mixed	mixed	mixed	mixed
Pressure profile update	Yes	Yes	Yes	Yes	Yes	Yes	Yes	Yes	Yes	Yes
Design mode	Yes	no	Yes	no	Yes	no	Yes	no	Yes	no
Trays/stages (no. of downcomer pass)	7 (2)	9 (2)	7 (2)	9 (2)	7 (2)	9 (2)	7 (2)	9 (2)	7 (2)	9 (2)
Base stage	3		3		4		4		5	
Approach to Flooding (fractional)	0.7		0.7		0.7		0.7		0.7	
Tray spacing, m	1.4	1.9	1.4	1.8	1.4	1.8	1.4	1.8	1.4	1.8
Weir height, m	0.14	0.15	0.14	0.15	0.14	0.15	0.14	0.15	0.14	0.15
Downcomer clearance, m	0.115	0.125	0.115	0.125	0.115	0.125	0.115	0.125	0.115	0.125
Column diameter (initial), m	7	4.5	7	4.4	7.5	4.3	7.8	4.9	8	5.2
Top stage pressure, N/m^2	101300	101300	101300	101300	101300	101300	101300	101300	101300	101300
Bottom stage pressure (initial), N/m^2	177000	128000	177000	128000	177000	128000	177000	128000	177000	128000
Reflux ratio (initial)		0.65		1		0.45		0.35		3.2
Bottom to feed ratio (initial)		0.95		0.95		0.95		0.95		0.95

Table 7.9: Process simulation input specifications - single train basis - Model III

	Input specifications for Model-III									
Lean loading (mol CO_2/mol MEA)	**0.2**		**0.25**		**0.3**		**0.35**		**0.4**	
Flue gas flow rate, kmol/sec	5.5		5.5		5.5		5.5		5.5	
Flue gas Absorber-inlet temperature, ºC	40		40		40		40		40	
Lean solvent temperature, ºC	40		40		40		40		40	
Lean solvent flow rate (initial), kmol/sec	18		24		28		37.5		54	
Water make-up rate (initial), kmol/sec	0.25		0.25		0.25		0.25		0.25	
MEA make-up rate (initial), kmol/sec	0.25		0.25		0.25		0.25		0.25	
Lean-rich heat-exchanger temp. appro., ºC	5		5		5		5		10	
	Absorber	**Stripper**	**Absorber**	**Stripper**	**Absorber**	**Stripper**	**Absorber**	**Stripper**	**Absorber**	**Stripper**
Simulation approach	Rate-based	Rate-based	Rate-based	Rate-based	Rate-based	Rate-based	Rate-based	Rate-based	Rate-based	Rate-based
Reaction ID										
Chemistry ID	MEA (1-9)	MEA (1-9)	MEA (1-9)	MEA (1-9)	MEA (1-9)	MEA (1-9)	MEA (1-9)	MEA (1-9)	MEA (1-9)	MEA (1-9)
System foaming factor	0.85	0.85	0.85	0.85	0.85	0.85	0.85	0.85	0.85	0.85
Flow model	mixed	mixed	mixed	mixed	mixed	mixed	mixed	mixed	mixed	mixed
Pressure profile update	Yes	yes	Yes	yes	Yes	yes	Yes	yes	Yes	yes
Design mode	Yes	yes	Yes	yes	Yes	yes	Yes	yes	Yes	yes
Trays/stages (no. of downcomer pass)	9 (2)	9 (2)	9 (2)	9 (2)	9 (2)	9 (2)	9 (2)	9 (2)	9 (2)	9 (2)
Base stage	2	8		8		8		8		7
Approach to Flooding (fractional)	0.7	0.7	0.7	0.7	0.7	0.7	0.7	0.7	0.7	0.7
Tray spacing, m	1.7	1.7	1.7	1.6	1.7	1.7	1.7	1.7	1.7	1.8
Weir height, m	0.15	0.15	0.15	0.15	0.15	0.15	0.15	0.15	0.15	0.15
Downcomer clearance, m	0.125	0.125	0.125	0.125	0.125	0.125	0.125	0.125	0.125	0.125
Column diameter (initial), m	5.5	4.1	5.6	4.3	5.7	4.0	5.9	4.4	6.3	5.8
Top stage pressure, N/m^2	101300	101300	101300	101300	101300	101300	101300	101300	101300	101300
Bottom stage pressure (initial), N/m^2	177000	128000	177000	128000	177000	128000	177000	128000	177000	128000
Reflux ratio (initial)		0.3		0.45		0.4		0.45		0.1
Bottom to feed ratio (initial)		0.95		0.95		0.95		0.95		0.95

Table 7.10: Process simulation input specifications - single train basis - Model IV

	Input specifications for Model-IV									
Lean loading (mol CO_2/mol MEA)	**0.2**		**0.25**		**0.3**		**0.35**		**0.4**	
Flue gas flow rate, kmol/sec	5.5		5.5		5.5		5.5		5.5	
Flue gas Absorber-inlet temperature, ºC	40		40		40		40		40	
Lean solvent temperature, ºC	40		40		40		40		40	
Lean solvent flow rate (initial), kmol/sec	21		24		31		42		65	
Water make-up rate (initial), kmol/sec	0.25		0.25		0.25		0.25		0.5	
MEA make-up rate (initial), kmol/sec	0.25		0.25		0.25		0.25		0.5	
Lean-rich heat-exchanger temp. app., ºC	10		10		5		10		10	
	Absorber	**Stripper**	**Absorber**	**Stripper**	**Absorber**	**Stripper**	**Absorber**	**Stripper**	**Absorber**	**Stripper**
Simulation approach	Equilibrm.	Equilibrm.	Equilibrm.	Equilibrm.	Equilibrm.	Equilibrm.	Equilibrm.	Equilibrm.	Equilibrm.	Equilibrm.
Reaction ID	MEA-REA (1-9)	MEA-REA (2-8)	MEA-REA (1-9)	MEA-REA (2-8)	MEA-REA (1-9)	MEA-REA (2-8)	MEA-REA (1-9)	MEA-REA (2-8)	MEA-REA (1-9)	MEA-REA (2-8)
Chemistry ID		MEA (1,9)		MEA (1,9)		MEA (1,9)		MEA (1,9)		MEA (1,9)
System foaming factor	0.85	0.85	0.85	0.85	0.85	0.85	0.85	0.85	0.85	0.85
Flow model	mixed		mixed		mixed		mixed		mixed	
Pressure profile update	yes	Yes	yes	Yes	yes	Yes	yes	Yes	yes	Yes
Design mode										
Trays/stages (no. of downcomer pass)	9 (2)	9 (2)	9 (2)	9 (2)	9 (2)	9 (2)	9 (2)	9 (2)	9 (2)	9 (2)
Base stage										
Approach to Flooding (fractional)										
Tray spacing, m	1.8	1.8	1.7	1.7	1.7	1.7	1.7	1.7	1.7	1.7
Weir height, m	0.15	0.15	0.15	0.15	0.15	0.15	0.15	0.15	0.15	0.15
Downcomer clearance, m	0.125	0.125	0.125	0.125	0.125	0.125	0.125	0.125	0.125	0.125
Column diameter (initial), m	5.1	4.9	5.5	4.6	5.8	4.5	6	4.8	6.8	6
Top stage pressure, N/m^2	101300	101300	101300	101300	101300	101300	101300	101300	101300	101300
Bottom stage pressure (initial), N/m^2	177000	128000	177000	128000	177000	128000	177000	128000	177000	128000
Reflux ratio (initial)		4		0.75		0.65		0.5		0.45
Bottom to feed ratio (initial)		0.95		0.95		0.95		0.95		0.95

Table 7.11: Process simulation input specifications - single train basis - Model V

	Input specifications for Model-V									
Lean loading (mol CO_2/mol MEA)	**0.2**		**0.25**		**0.3**		**0.35**		**0.4**	
Flue gas flow rate, kmol/sec	5.5		5.5		5.5		5.5		5.5	
Flue gas Absorber-inlet temperature, ºC	40		40		40		40		40	
Lean solvent temperature, ºC	40		40		40		40		40	
Lean solvent flow rate (initial), kmol/sec	19		22		28		37		55	
Water make-up rate (initial), kmol/sec	0.25		0.25		0.25		0.1		1	
MEA make-up rate (initial), kmol/sec	0.25		0.25		0.25		0.1		1	
Lean-rich heat-exchanger temp. appr., ºC	5		5		5		10		15	
	Absorber	**Stripper**	**Absorber**	**Stripper**	**Absorber**	**Stripper**	**Absorber**	**Stripper**	**Absorber**	**Stripper**
Simulation approach	Equilibrm.	Equilibrm.	Equilibrm.	Equilibrm.	Equilibrm.	Equilibrm.	Equilibrm.	Equilibrm.	Equilibrm.	Equilibrm.
Reaction ID										
Chemistry ID	MEA (1-9)	MEA (1-9)	MEA (1-9)	MEA (1-9)	MEA (1-9)	MEA (1-9)	MEA (1-9)	MEA (1-9)	MEA (1-9)	MEA (1-9)
System foaming factor	0.85	0.85	0.85	0.85	0.85	0.85	0.85	0.85	0.85	0.85
Flow model	mixed		mixed		mixed		mixed		mixed	
Pressure profile update	Yes	Yes	Yes	Yes	Yes	Yes	Yes	Yes	Yes	Yes
Design mode										
Trays/stages (no. of downcomer pass)	9 (2)	9 (2)	9 (2)	9 (2)	9 (2)	9 (2)	9 (2)	9 (2)	9 (2)	9 (2)
Base stage										
Approach to Flooding (fractional)										
Tray spacing, m	1.7	1.7	1.7	1.7	1.7	1.7	1.7	1.7	1.8	1.8
Weir height, m	0.15	0.15	0.15	0.15	0.15	0.15	0.15	0.15	0.15	0.15
Downcomer clearance, m	0.125	0.125	0.125	0.125	0.125	0.125	0.125	0.125	0.125	0.125
Column diameter (initial), m	5.5	4.2	5.6	4.0	5.7	4.1	5.9	4.5	5.9	5.5
Top stage pressure, N/m^2	101300	101300	101300	101300	101300	101300	101300	101300	101300	101300
Bottom stage pressure (initial), N/m^2	177000	128000	177000	128000	177000	128000	177000	128000	177000	128000
Reflux ratio (initial)		1		0.95		0.4		0.45		0.2
Bottom to feed ratio (initial)		0.95		0.95		0.95		0.95		0.95

Table 7.12: Process simulation input specifications - single train basis - Model VI

	Input specifications for Model-VI									
Lean loading (mol CO_2/mol MEA)	**0.2**		**0.25**		**0.3**		**0.35**		**0.4**	
Flue gas flow rate, kmol/sec	5.5		5.5		5.5		5.5		5.5	
Flue gas Absorber-inlet temperature, ºC	40		40		40		40		40	
Lean solvent temperature, ºC	40		40		40		40		40	
Lean solvent flow rate (initial), kmol/sec	20.5		26		35		35		68	
Water make-up rate (initial), kmol/sec	0.25		0.25		0.25		0.25		0.5	
MEA make-up rate (initial), kmol/sec	0.25		0.25		0.25		0.25		0.5	
Lean-rich heat-exchanger temp. appro., ºC	5		5		5		5		5	
	Absorber	**Stripper**	**Absorber**	**Stripper**	**Absorber**	**Stripper**	**Absorber**	**Stripper**	**Absorber**	**Stripper**
Simulation approach	Rate-based	Rate-based	Rate-based	Rate-based	Rate-based	Rate-based	rate-based	Rate-based	Rate-based	Rate-based
Reaction ID	MEA-REA (1-7)	MEA-REA (2-8)	MEA-REA (1-7)	MEA-REA (2-8)	MEA-REA (1-7)	MEA-REA (2-8)	MEA-REA (1-7)	MEA-REA (2-8)	MEA-REA (1-7)	MEA-REA (2-8)
Chemistry ID		MEA (1,9)		MEA (1,9)		MEA (1,9)		MEA (1,9)		MEA (1,9)
System foaming factor	0.85	0.85	0.85	0.85	0.85	0.85	0.85	0.85	0.85	0.85
Flow model	mixed	mixed	mixed	mixed	mixed	mixed	mixed	mixed	mixed	mixed
Pressure profile update	Yes	Yes	Yes	Yes	Yes	Yes	Yes	Yes	Yes	Yes
Design mode	Yes	no	Yes	no	Yes	no	Yes	no	Yes	no
No. of trays (& no. of downcomer pass)	7 (2)	9 (2)	7 (2)	9 (2)	7 (2)	9 (2)	7 (2)	9 (2)	7 (2)	9 (2)
Base stage	3		4		4		5		5	
Approach to Flooding (fractional)	0.7		0.7		0.7		0.7		0.7	
Tray spacing, m	1.4	1.9	1.4	1.7	1.4	1.7	1.4	1.7	1.4	1.7
Weir height, m	0.14	0.15	0.14	0.15	0.14	0.15	0.14	0.15	0.14	0.15
Downcomer clearance, m	0.115	0.125	0.115	0.125	0.115	0.125	0.115	0.125	0.115	0.125
Column diameter (initial value), m	7	4.68	7	4.815	7	4.75	7	4.73	8	4.62
Top stage pressure, N/m^2	101300	101300	101300	101300	101300	101300	101300	101300	101300	101300
Bottom stage pressure, N/m^2	177000	128000	177000	128000	177000	128000	177000	128000	177000	128000
Reflux ratio (initial value)		0.3		0.55		0.7		0.7		0.7
Bottom to feed ratio (initial value)		0.95		0.95		0.95		0.95		0.95

7.6 Results and Discussions

This section describes the results of the process simulation and design tasks.

7.6.1 Kinetic Models

The kinetics of the reaction of CO_2 with aqueous solution of Monoethanolamine (MEA) is of considerable importance for accurately designing or simulating absorption/stripping column. The overall CO_2-MEA reaction which consists of a number of steps is heterogeneous because of the involvement of more than one phase. Several process variables affect the rate of this heterogeneous chemical reaction. These are temperature, pressure, composition, mass transfer and heat transfer. The rate of mass transfer becomes important as CO_2 diffusion occurs from a gas phase to a liquid phase. On the other hand, the rate of heat transfer becomes important as the reaction between CO_2 and MEA is an exothermic reaction. These heat and mass transfer effects become increasingly important when there is a fast reaction. As mentioned earlier in the previous section, two kinetic models are available in AspenPlus® 2006.5 version for modeling reactive absorption/stripping process for CO_2 capture by aqueous MEA solution., one consists of two kinetic reactions (Reaction ID: MEA-CO_2, Table 7.4) and another has four kinetic reactions (Reaction ID: MEA-REA, Table 7.5) along with other equilibrium reactions. We named these two kinetic models as "MEA-CO_2" and "MEA-REA" respectively using their Reaction ID. A thorough simulation and design study is conducted using three absorber-stripper integrated models (Model-I, II & VI) based on the process design basis described in Section 7.2 and the process flowsheet illustrated in Figure 7.1, to find out the effects of these kinetic models on absorber and stripper performance for capturing 85% CO_2 from a power plant flue gas at a lean solvent loading of 0.25. Both absorber and stripper are sized based on 70% entrainment flooding approach. The simulation results are summarised in Table 7.13 and all column profiles are presented in Figure 7.4 – 12 for Model-VI as this rate-based model considers kinetics for both the absorber and stripper with diffusion resistance and reactions in film for liquid phase and diffusion resistance for gas phase film. It is found that the calculated reboiler duties based on "MEA-REA" kinetics are found always less than that of "MEA-CO_2" kinetics in all models (Table 7.13). The differences in reboiler duties between two kinetic

schemes are 4%, 31% and 24% in Model-I, II and VI, respectively. It is also observed that computed downcomer floodings for all models are higher in "MEA-CO_2" kinetics. 1000 times greater scaling factor for interfacial area is needed for "MEA-CO_2" kinetics to maintain the same capture target (Table 7.13). Higher temperature bulge in Absorber is observed with "MEA-CO_2" kinetic due to higher heat of reaction (Figure 7.4). This temperature bulge can significantly affect the absorption rates in the column since the kinetics of the absorption reaction, the phase composition of the system, and the fluid transport properties depend on temperature. The transfer of water between two phases increases as a result of high heat of absorption (Figure 7.9). Higher reboiler temperature with "MEA-CO_2" kinetic needs higher thermal energy requirement (Figure 7.5). The patterns of pressure drop profile (per tray) show similar trends for the absorber but different trends for the stripper (Figure 7.6). The differences in components reaction rates are not significant in absorber (Figure 7.7) but significant differences are observed in striper top and bottom stage (Figure 7.8) due to the modeling of them i.e., partial condenser and reboiler as equilibrium-stages using equilibrium reactions. The effects of different kinetic models on interfacial mass transfer rates of various components from vapour phase in both absorber and striper are found less significant compare to the transfer rates from liquid phase (Figure 7.9-7.12). As the "MEA-REA" kinetic model is validated with pilot plant data (AspenPlus 2006.5 documentation) and does not need big interfacial area factor, this model will be used in the next simulation and design studies.

Table 7.13: Comparison of kinetic models (lean loading: 0.25; CO_2 recovery: 85%; Operational flooding approach: 70%)

Absorber-Stripper Model	Model-I		Model-II		Model-VI	
Kinetic model	MEA-CO_2	MEA-REA	MEA-CO_2	MEA-REA	MEA-CO_2	MEA-REA
Absorber						
No of Trays (single pass)	7	7	7	7	7	7
Tray spacing, m	1.6	1.4	1.6	1.4	1.6	1.4
Column diameter, m	7.5	6.9	7.4	6.9	7.5	6.9
Downcomer flooding, %	0.6	0.6	0.6	0.6	0.6	0.6
Lean stream flow rate, kmol/sec	26.2	25.2	24.9	24.9	24.2	25.3
Bottom Stage pressure, N/m^2	120542	123843	120574	123877	120363	123827
Bottom stage temp. (liquid), K	324.9	326.9	324.9	326.9	325.0	326.9
Interfacial area factor	**1000**	***1***	**1000**	***1***	**1000**	***1***
Stripper						
No of Trays (single pass)	9	9	9	9	9	9
Tray spacing, m	1.6	1.7	2.2	1.8	2.3	2
Column diameter, m	4.8	4.3	4	4.4	3.6	3.9
Downcomer flooding, %	79.4	75.0	124	79.4	135	95.8
Bottom Stage pressure, N/m^2	127041	131374	190043	146627	204795	164444
Bottom stage temp. (liquid), K	382.4	383.3	394.5	386.5	396.9	389.7
Reboiler duty, MWth	130.6	125.4	275.6	189.2	258.7	197.0
Reboiler duty (4 trains), MWth	**522.5**	***501.7***	**1102.2**	***756.9***	**1034.7**	***787.8***

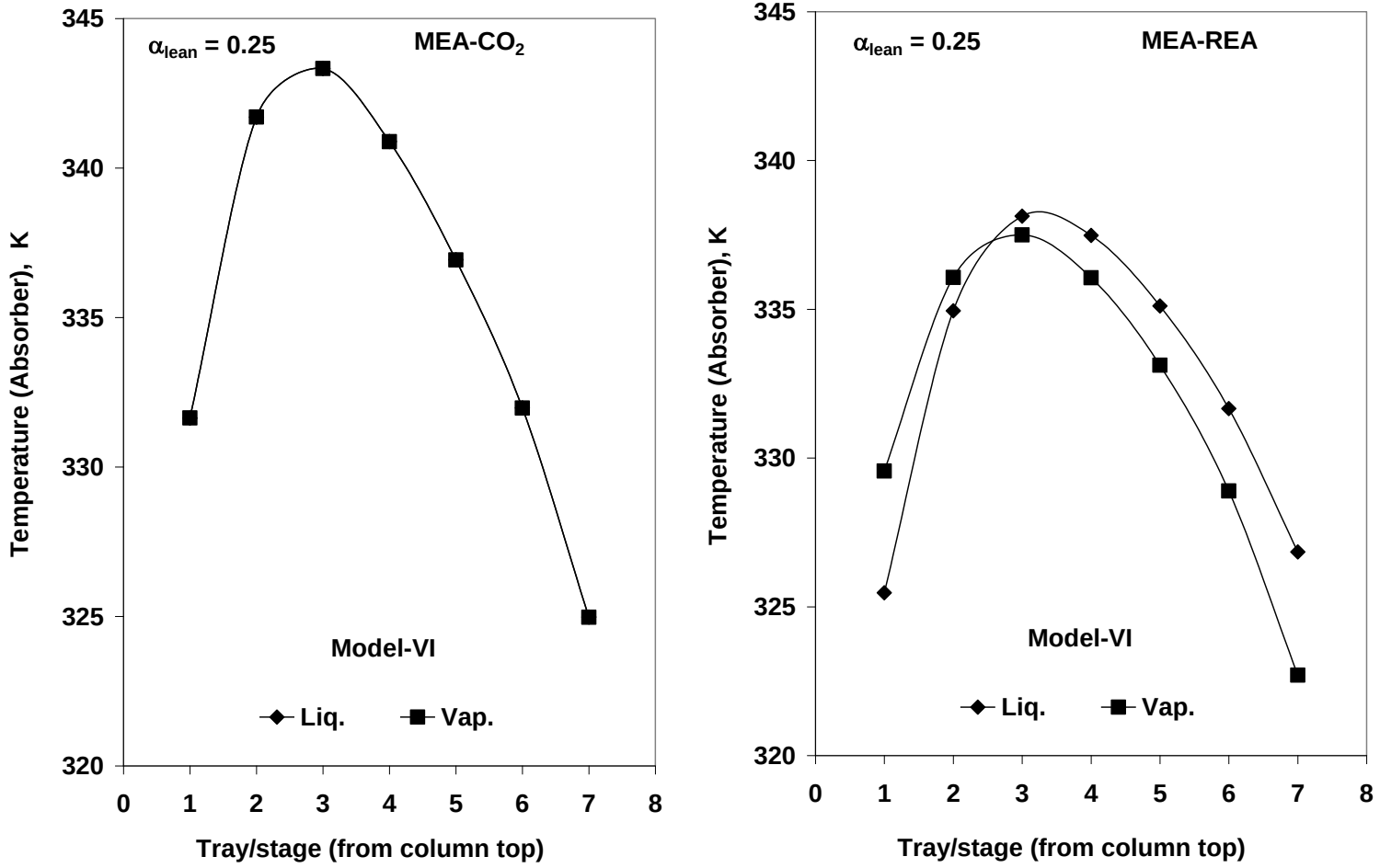

Figure 7.4: Effect of kinetics on Absorber temperature profile at lean loading of 0.25 for Model-VI (CO_2 recovery: 85%; Operational flooding approach: 70%)

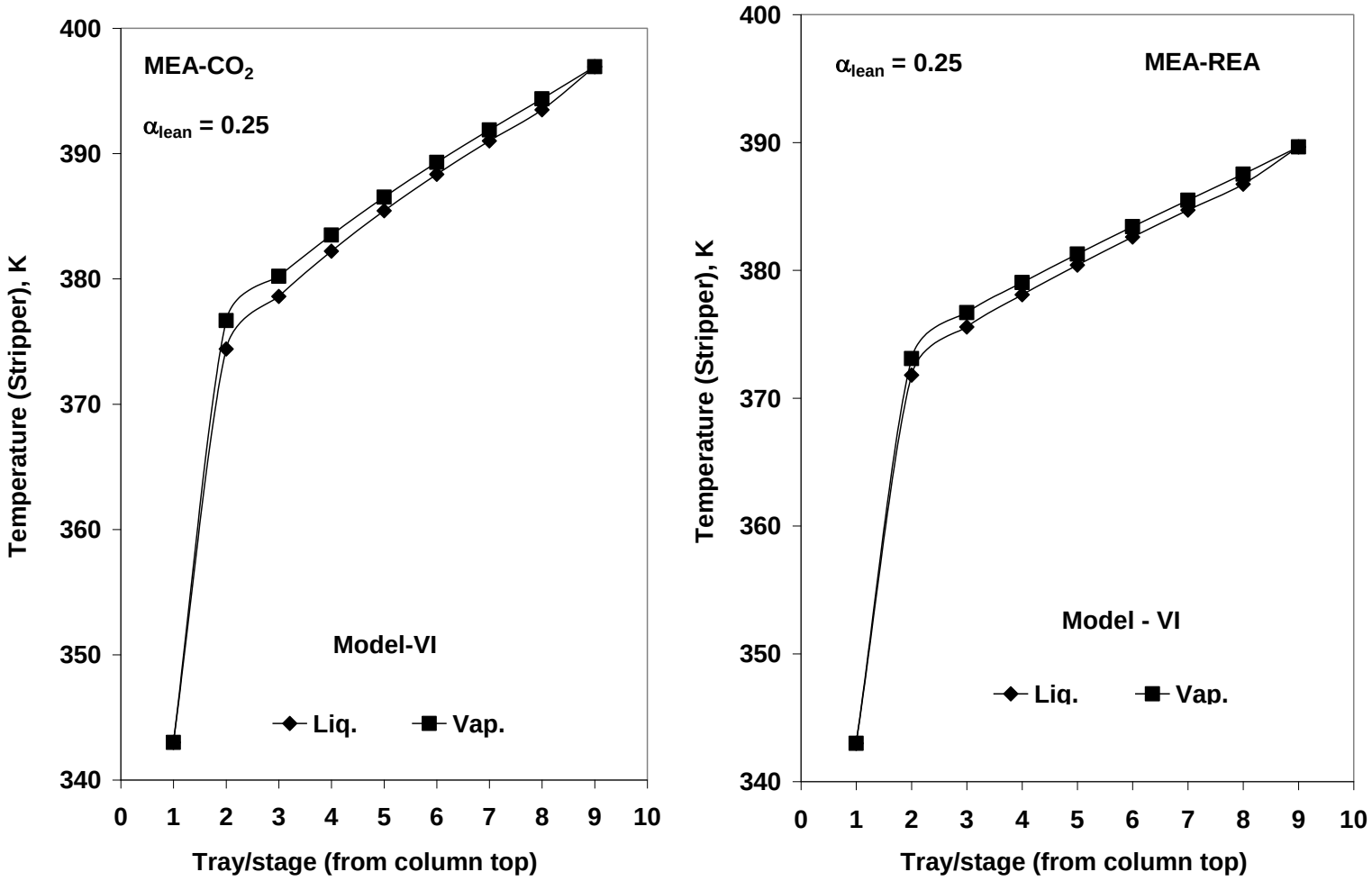

Figure7.5: Effect of kinetics on Stripper temperature profile at lean loading of 0.25 for Model-VI (CO_2 recovery: 85%; Operational flooding approach: 70%)

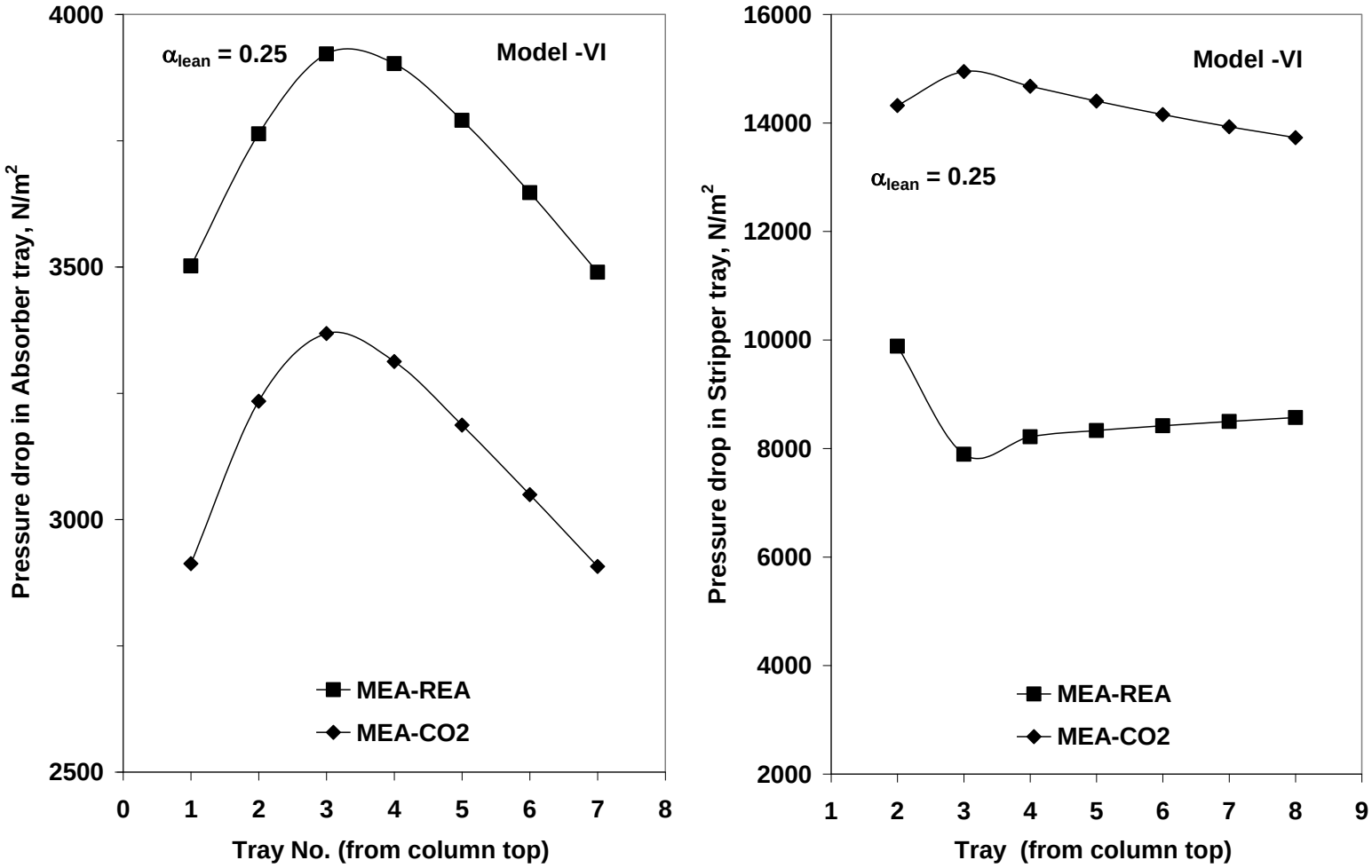

Figure 7.6: Effect of kinetics on column's (Absorber and Stripper) tray/stage pressure drop at lean loading of 0.25 for Model-VI (CO_2 recovery: 85%; Operational flooding approach: 70%)

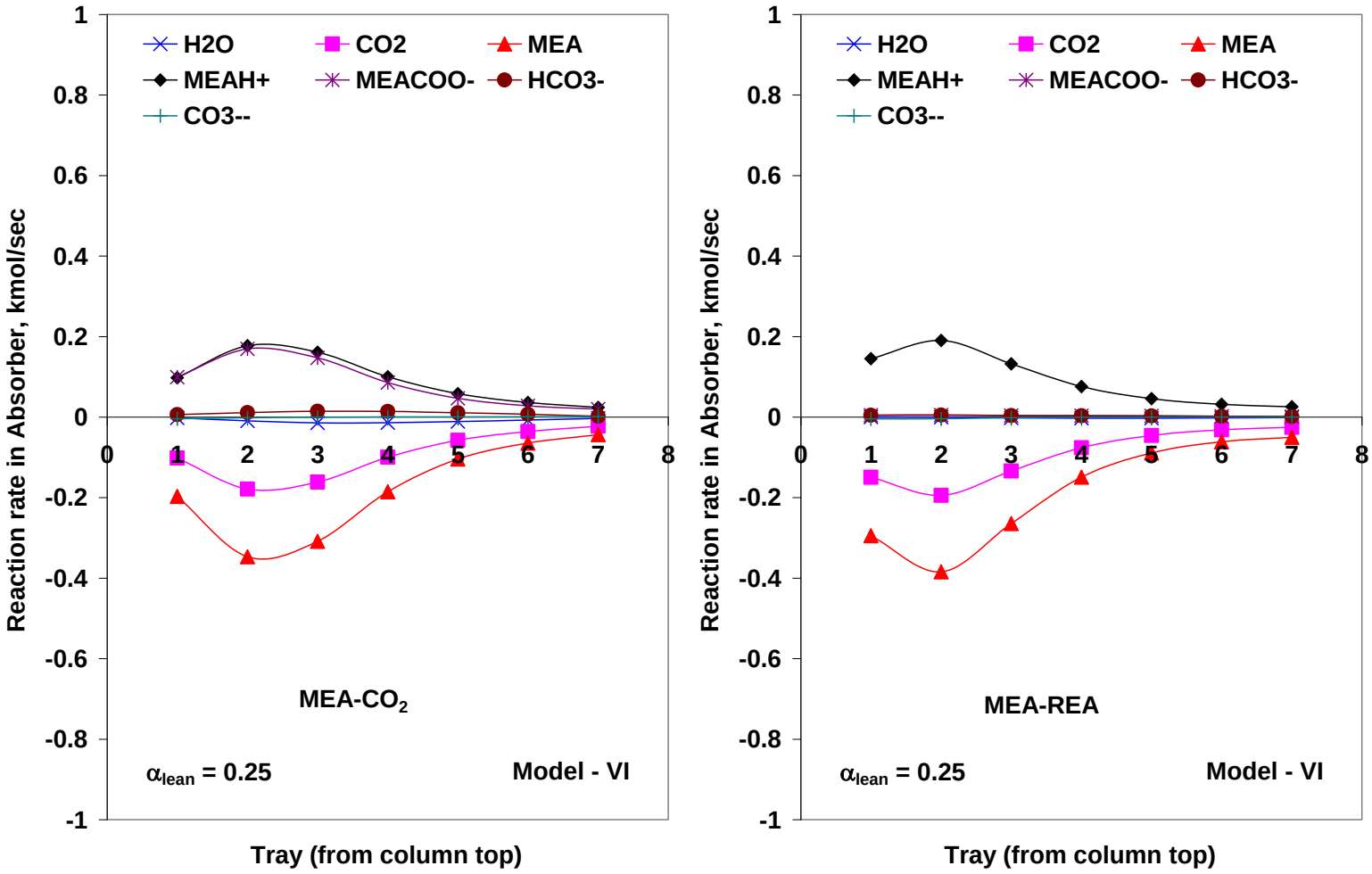

Figure 7.7: Effect of kinetics on Reaction Rate profile of Absorber at lean loading of 0.25 for Model-VI (CO_2 recovery: 85%; Operational flooding approach: 70%)

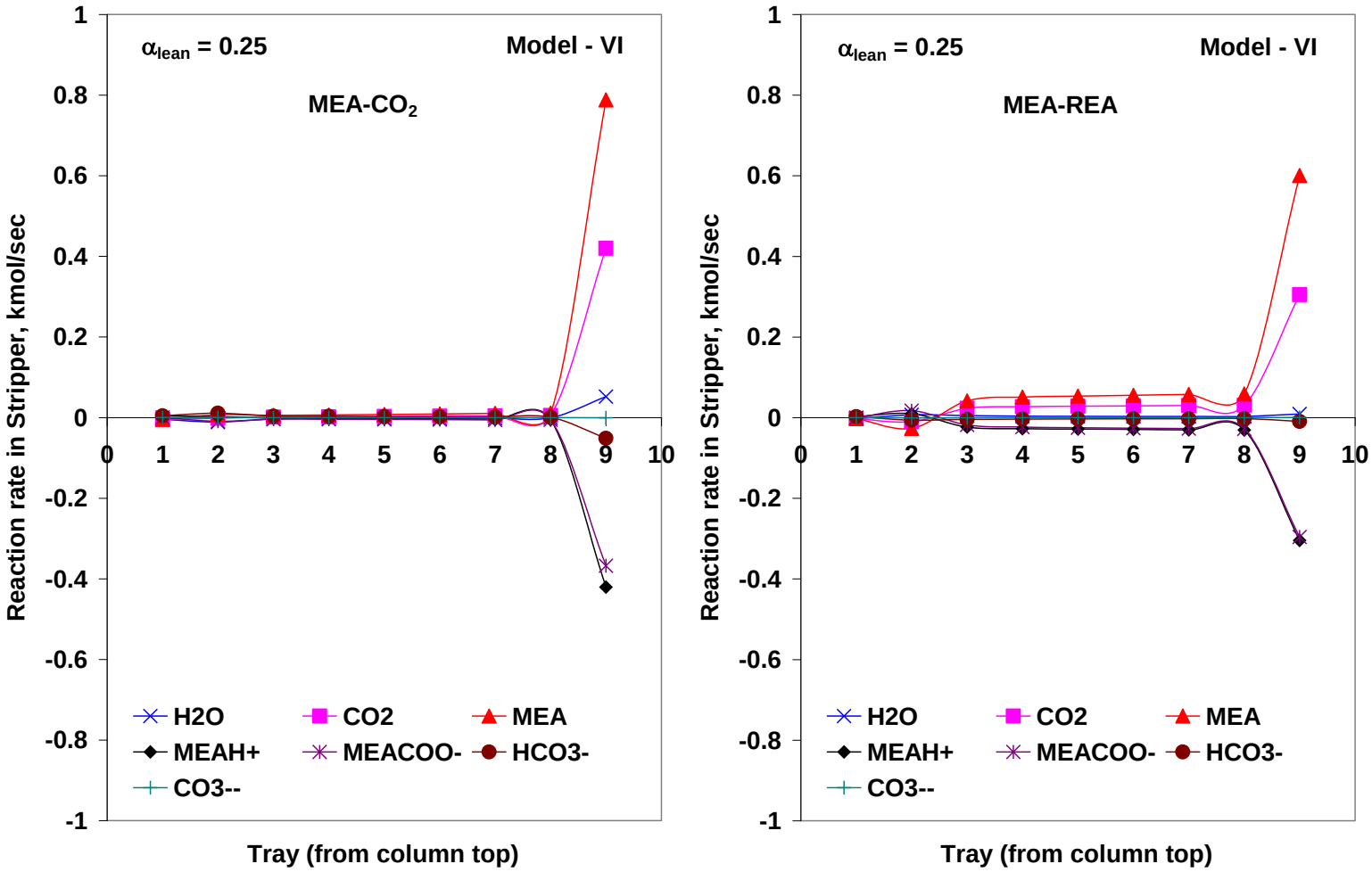

Figure 7.8: Effect of kinetics on Reaction Rate profile of Stripper at lean loading of 0.25 for Model-VI (CO_2 recovery: 85%; Operational flooding approach: 70%)

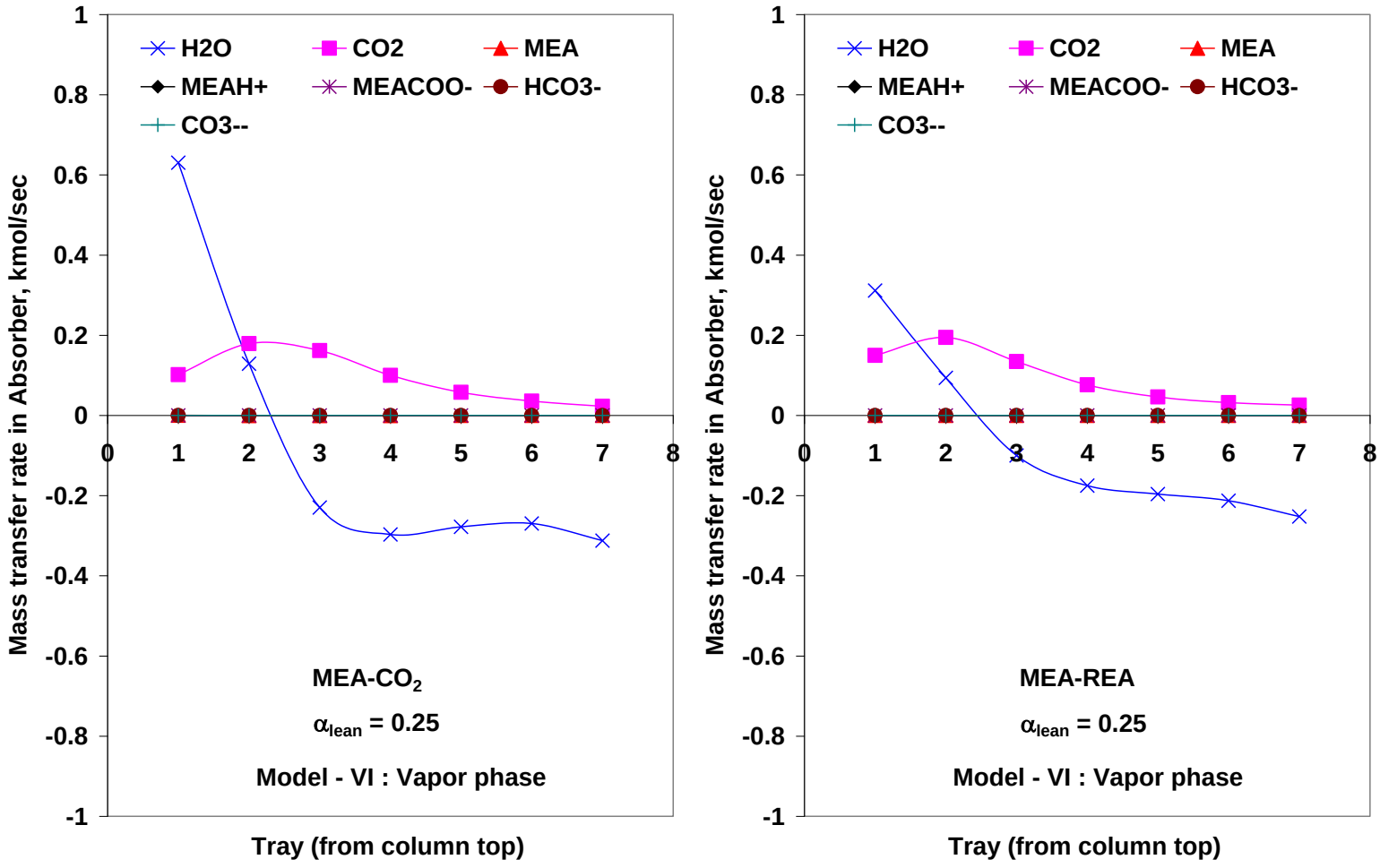

Figure 7.9: Effect of kinetics on Interfacial Mass Transfer Rate profile of Vapor phase in Absorber at lean loading of 0.25 for Model-VI (CO_2 recovery: 85%; Operational flooding approach: 70%)

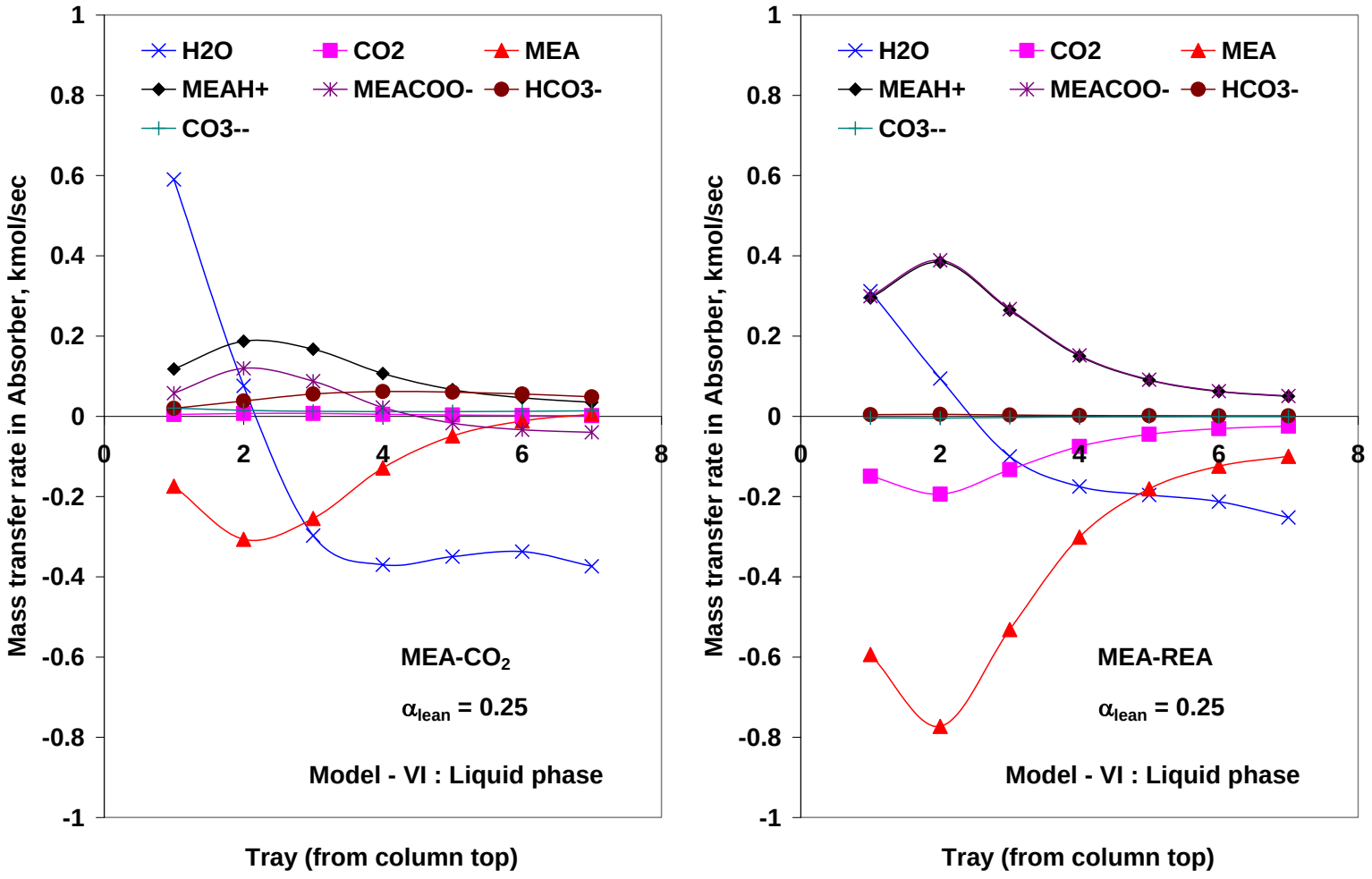

Figure 7.10: Effect of kinetics on Interfacial Mass Transfer Rate profile of Liquid phase in Absorber at lean loading of 0.25 for Model-VI (CO_2 recovery: 85%; Operational flooding approach: 70%)

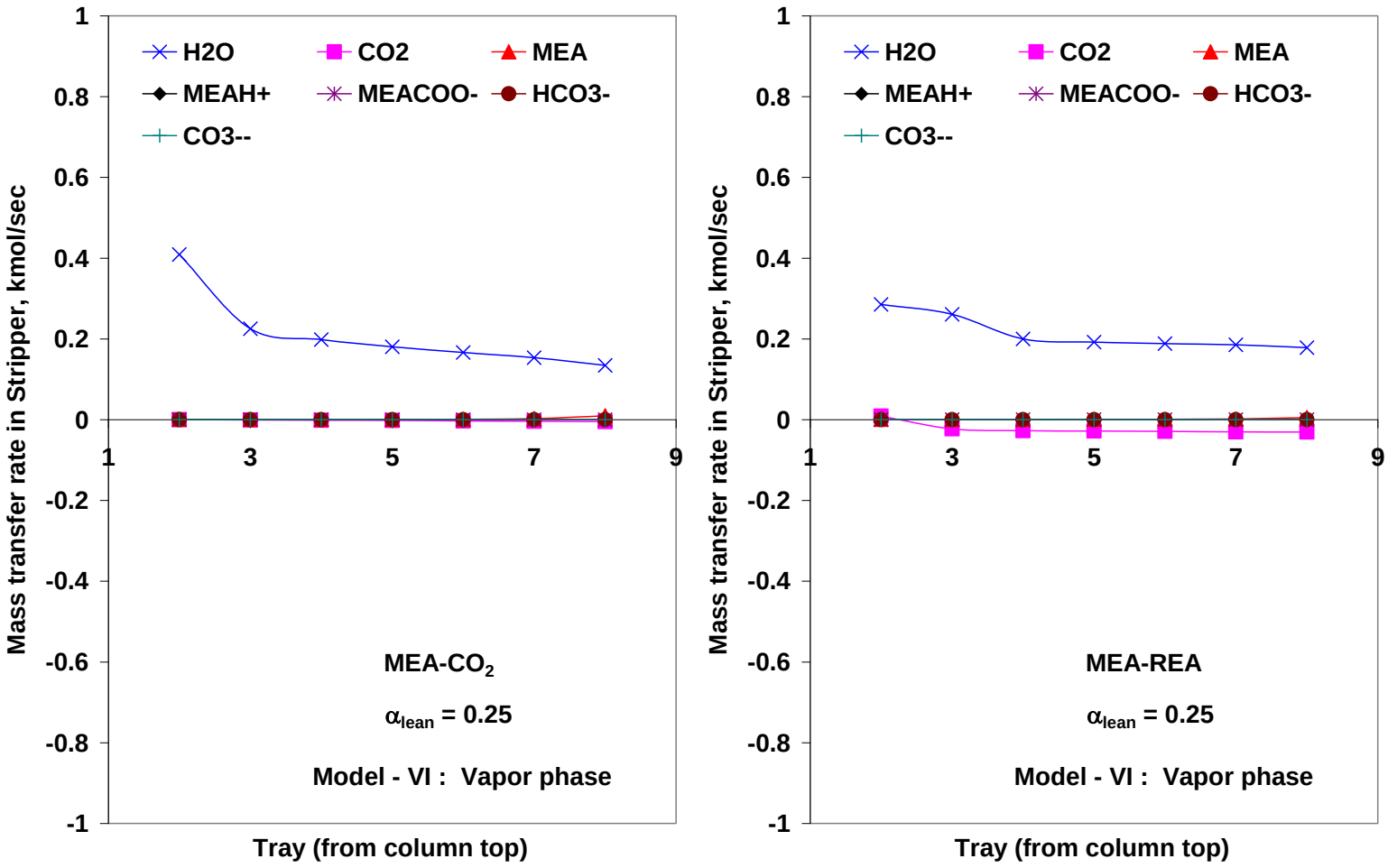

Figure7.11: Effect of kinetics on Interfacial Mass Transfer Rate profile of Vapor phase in Stripper at lean loading of 0.25 for Model-VI (CO_2 recovery: 85%; Operational flooding approach: 70%)

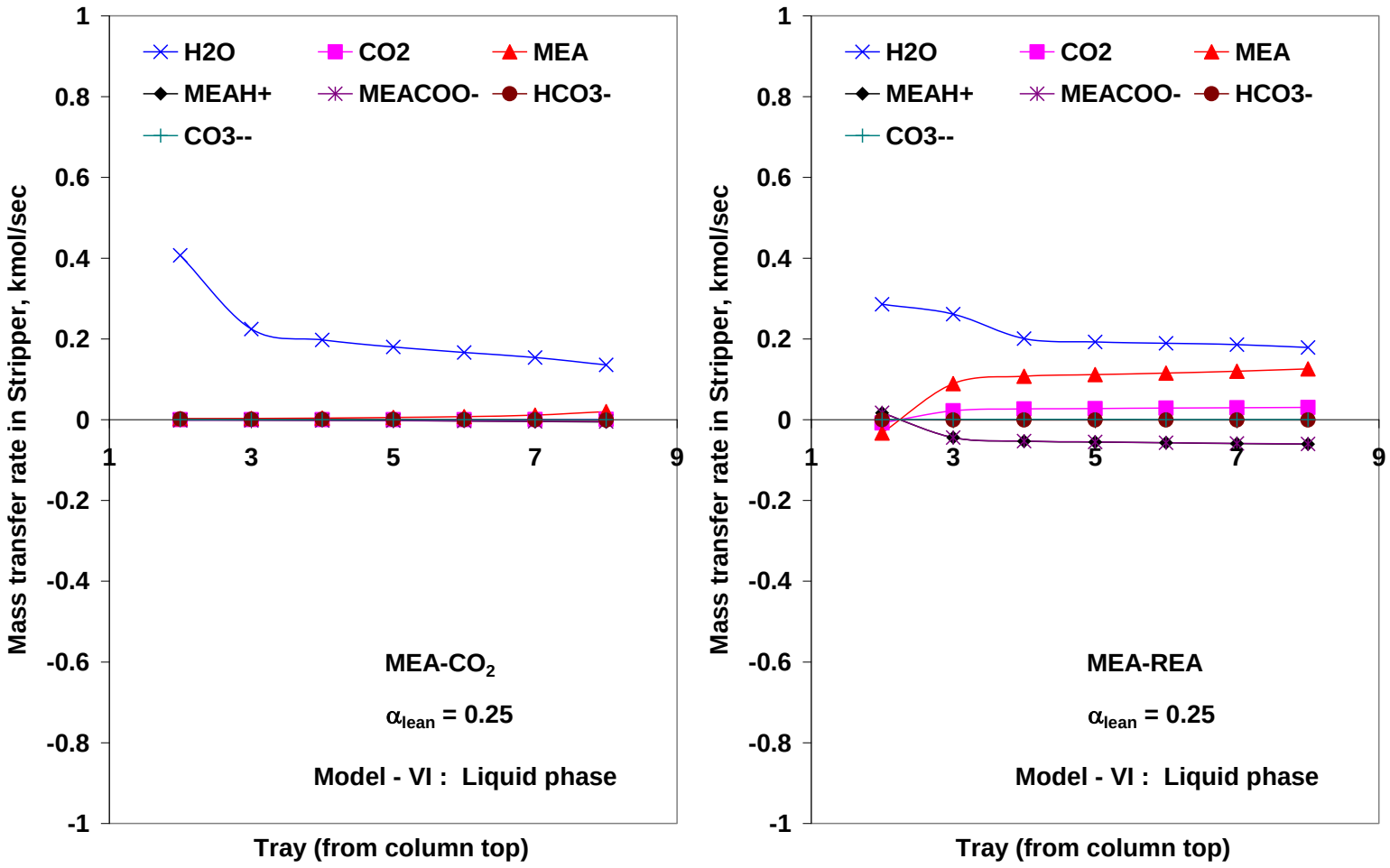

Figure 7.12: Effect of kinetics on Interfacial Mass Transfer Rate profile of Liquid phase in Stripper at lean loading of 0.25 for Model-VI (CO_2 recovery: 85%; Operational flooding approach: 70%)

7.6.2 Approach to Operational (i.e., Jet/Entrainment) Flooding

The maximum allowable capacity of a tray-deck for handling gas and liquid flow is of primary importance because it determines the minimum possible diameter of the column. At high gas flow rate significant quantities of liquid droplets reach the tray deck above and pass through to the upper tray which eventually results in excessive entrainment and flooding. It is difficult to obtain net downward flow of liquid at flood point, and any liquid feed to the column is carried out with overhead gas. The column control system may no longer allow stable operation. Realistic design demands operation at a safe margin below this maximum allowable condition. Prudent designs call for approaches to flooding in the range of 60-85% (Alie, 2004).

While performing the rate based calculations in AspenPlus, it is necessary to provide the diameter and height of the column (i.e., number of stages/trays, and tray spacing). RateSep has an option wherein diameter calculation can be performed based on certain design parameters. It is decided to size the columns on an approach to flooding basis on indicated stage. It is found that 80% flooding approach uses smaller size (dia.) tower compare to that of 70% but maintain higher downcomer flooding level (Table 7.14). Skinny (i.e., smaller diameter) column may lower the plant capital and operating cost but higher downcomer flooding due to higher pressure drop in the both absorber and stripper will negatively affects the stable operation of the columns (Table 7.14). Higher pressure drop means greater loss of irreversible work in the column. As the reboiler duties are not affected much for both models, 70% approach to flooding will be used for next process design studies since this might accommodate some safety factors incase of change in the operating conditions.

Table 7.14: Effect of varying approach to flooding (lean loading: 0.3; CO_2 recovery: 85%)

Operational flooding approach, %	**70**	**80**	**70**	**80**
Model	Model-II		Model-VI	
Absorber				
No of Trays (double pass)	7	7	7	7
Tray spacing, m	1.4	1.4	1.4	1.4
Column diameter, m	7.2	6.7	7.2	6.7
Downcomer flooding, %	**46**	**51**	**46.6**	**51**
Film resistance with/or without reaction				
Liquid Phase	Discxrn	Discrxn	Discxrn	Discxrn
Vapor Phase	Film	Film	Film	Film
Film nonideality correction				
Liquid Phase	Yes	Yes	Yes	Yes
Vapor Phase	Yes	Yes	Yes	Yes
Lean stream flow rate, kmol/sec	31.3	31.5	33.5	32.6
Bottom Stage pressure, N/m^2	121028	124317	120741	124114
Bottom stage temperature (liquid), K	327.3	327.4	326.8	327.1
Column section pressure drop, N/m^2	22877	26651	22561	26427
Stripper				
No of Trays (double pass)	9	9	9	9
Tray spacing, m	1.8	1.8	1.7	1.7
Column diameter, m	4.3	4	4.8	4.4
Downcomer flooding, %	**53**	**59.7**	**52**	**57.5**
Film resistance with/or without reaction				
Liquid Phase	**Nofilm**	**Nofilm**	**Discrxn**	**Discrxn**
Vapor Phase	**Nofilm**	**Nofilm**	**Film**	**Film**
Film nonideality correction				
Liquid Phase	**No**	**No**	**Yes**	**Yes**
Vapor Phase	**No**	**No**	**Yes**	**Yes**
Bottom Stage pressure, N/m^2	133619	138164	130660	134775
Bottom stage temperature (liquid), K	382.4	383.3	381.6	382.5
Column section pressure drop, N/m^2	28982	33527	26022	30138
Reboiler duty, MWth	146.2	145.9	156.6	155.1
Reboiler duty (4 trains), MWth	**584.6**	**583.7**	**626.4**	**620.5**

7.6.3 Tray pass

By "pass," we mean the number of downcomers per tray. Multi-pass trays are often used to increase the weir length for a larger diameter column to maintain proper liquid inventory on the tray (Bennett and Kovak, 2000). To investigate the influence of tray pass on the performance of the capture process, simulation and design study are conducted based on design basis described in the previous section for two absorber-stripper integrated models, and results are summarized in Table 7.15. The simulation results reveal no change in reboiler duty for Model I and a little increase for Model-II. The changes in absorber and stripper diameter are also negligible for both models. Only significant differences are observed for both models in absorber-stripper downcomer flooding levels. It is found that double pass tray are operationally safer due to maintaining of lower flooding level in both models compare to that of single pass tray. Although from a fabrication and economic point of view single pass tray are preferable, double pass tray leads to safer column operation and thus will be used in next simulation and design study.

Table 7.15: Single pass and double pass tray performance (lean loading: 0.25; CO_2 recovery: 85%; Operational flooding approach: 70%)

	Single Pass	**Double** Pass	***Single*** Pass	**Double** Pass
Model	Model-I		Model-II	
Absorber				
No of Trays (sieve)	7	7	7	7
No. of pass (i.e., downcomers)	***1***	**2**	***1***	**2**
Tray spacing, m	1.4	1.4	1.4	1.4
Column diameter, m	***6.9***	**7.0**	***6.9***	**7.0**
Downcomer flooding, %	***60***	**44**	***59.9***	**44**
Stripper				
No of Trays (sieve)	9	9	9	9
No. of pass (i.e., downcomers)	***1***	**2**	***1***	**2**
Tray spacing, m	1.7	1.7	1.8	1.8
Column diameter, m	4.3	4.3	4.4	4.4
Downcomer flooding, %	***74.9***	**46.9**	***79.4***	**54.7**
Thermal energy requirement				
Reboiler duty (total), MWth	***501.7***	**501.2**	***756.9***	**767.9**

7.6.4 Film Resistance

Aspen RateSep considers mass and heat transfer resistances according to the film theory to model reactive multistage separation problems rigorously and accurately. The film model equations are combined with relevant diffusion and reaction kinetics and include the specific features of electrolyte solution chemistry, electrolyte thermodynamics, and electroneutrality where appropriate. Aspen RateSep offers several options for modeling film resistance, the film discretization option "Discrxn" is chosen for liquid film with film non-ideality correction where diffusion resistance with reaction is considered. For vapour phase, 'Film" option is chosen where only diffusion resistance is considered in the film. The consideration of film resistance in the absorber shows that the reboiler duty increases almost 18% and 4% for Model-VII and III, respectively (Table 7.16). From the stripper study it is found that the reboiler duty only increases by 2.5% as shown in Table 7.17. This suggests that liquid film resistance in the Absorber has significant affect on the performance of the absorber/stripping system which can not be realized by equilibrium-based model.

Table 7.16: Effect of film resistance in Absorber on reboiler duty (Lean loading: 0.3; CO_2 recovery: 85%; Operational flooding approach: 70%)

	Absorber **with** film resistance	Absorber **without** film resistance	Absorber **with** film resistance	Absorber **without** film resistance
Model	Model-II	Model-VII	Model-VIII	Model-III
Absorber				
No of Trays (double pass)	9	9	9	9
Tray spacing, m	1.7	1.7	1.7	1.7
Column diameter, m	5.7	5.8	5.7	5.7
Downcomer flooding, %	55	55	55	55
Film resistance with/or without reaction				
Liquid Phase	**Discxrn**	**Nofilm**	**Discxrn**	**Nofilm**
Vapor Phase	**Film**	**Nofilm**	**Film**	**Nofilm**
Film nonideality correction				
Liquid Phase	Yes	No	Yes	No
Vapor Phase	Yes	No	Yes	No
Stripper				
No of Trays (double pass)	9	9	9	9
Tray spacing, m	1.8	1.8	1.7	1.7
Column diameter, m	4.4	4.2	4.1	3.8
Downcomer flooding, %	53.6	51.9	47.8	47
Film resistance with/or without reaction				
Liquid Phase	**Nofilm**	**Nofilm**	**Nofilm**	**Nofilm**
Vapor Phase	**Nofilm**	**Nofilm**	**Nofilm**	**Nofilm**
Film nonideality correction				
Liquid Phase	No	No	No	No
Vapor Phase	No	No	No	No
Reboiler duty, MWth	161.2	136.7	109.7	105.7
Reboiler duty (4 trains), MWth	**644.8**	**546.7**	**438.7**	**422.8**

Table 7.17: Effect of film resistance in Stripper on reboiler duty (lean loading: 0.3; CO_2 recovery: 85%; Operational flooding approach: 70%)

	Stripper **with** film resistance & reaction	Stripper **without** film resistance & reaction
Model	Model-VI	Model-II
Absorber		
No of Trays (double pass)	9	9
Tray spacing, m	1.7	1.7
Column diameter, m	5.7	5.7
Downcomer flooding, %	55	55
Film resistance with/or without reaction		
Liquid Phase	Discxrn	Discrxn
Vapor Phase	Film	Film
Film nonideality correction		
Liquid Phase	Yes	Yes
Vapor Phase	Yes	Yes
Lean stream flow rate, kmol/sec	29.8	28.8
Rich stream flow rate, kmol/sec	29.4	28.4
Bottom stage temperature (liquid), K	327.5	327.5
Stripper		
No of Trays	9	9
Tray spacing, m	1.7	1.8
Column diameter, m	4.7	4.4
Downcomer flooding, %	51	53.6
Film resistance with/or without reaction		
Liquid Phase	**Discrxn**	**Nofilm**
Vapor Phase	**Film**	**Nofilm**
Film nonideality correction		
Liquid Phase	**Yes**	**No**
Vapor Phase	**Yes**	**No**
Reboiler duty, MWth	164.9	161.2
Total Reboiler duty (4 trains), MWth	**659.6**	**644.8**

7.6.5 Film Discretization

RadFrac allows discretizing liquid and vapour film by choosing "Discrxn" under film resistance option of RateSep for precise modeling of the chemical reactions taking place in the films. RadFrac usually calculate the film reaction rates based on average liquid/vapor phase composition when the film is not discretized. For systems in which there are rapid reactions, it is necessary to discretize the film properly in order to accurately account for the amount of reaction in the film. If the reaction is very fast and the film is not discretized, then RateSep will calculate the reaction in the film based on the concentration at the interface. This will be higher than the actual film reaction and hence will not accurately model the system. Also, the number of discretization points should be such that the solution is stable while at the same time not compromising the computation time. The film material and energy balances apply to each film region where the film is discretized. The reaction rates are computed separately in each film region. The effects of liquid film discretization methods on an absorber performance are investigated at a CO_2 lean loading of 0.3 for 85% capture. Diffusion resistance in vapour film and non-ideality correction for both films (liquid and vapour) are also considered in the absorber modeling. The various liquid film discretization schemes (Table 7.18) based on the consideration of additional number of discretization points and film discretization ratio are studied, and their results are presented in Table 7.19 and in Figure 7.13. The discretization S-1 & -2 produce slight different results mainly in terms of CO_2 rich loading, but significant temperature changes are observed in the top half of the column. It is not clear why tighter convergence tolerance does not work for S-2 as it works for the other one under similar conditions. The number of film discretization points has been increased gradually to see the various effects on the absorber performance using S-2, -3 & -4. It is observed that due to the consideration of more film regions with diffusion resistances as a result of increased number of points, CO_2 absorption gradually decreases resulting in lower CO_2 loading in the rich solvent stream. As a result, a bigger column size is required to maintain the same CO_2 capture target, i.e., 85%. The significant changes in the column temperature profiles are visible due to the changes in the number of discretization points from 1(S-2) to 3 (S-3). The temperature profiles for S-3 & -4 are very similar in pattern and the temperature is increased gradually from the column top to

the bottom due to very high solvent flow rate. Another case is investigated for 10 discretization points with same discretization ratio i.e., 2 under S-4′. It is found that both cases (i.e., 5 and 10 points) produce exactly identical results which imply that impact of discretization points diminishes as the number of discretization points becomes large. The film discretization ratio is changed from 2 (S-4) to 10 (S-5) to obtain more thin film regions near to the vapour-liquid interface. This helps to increase CO_2 absorption by allowing higher CO_2 concentration to calculate film reaction rate. As a result higher rich loading and smaller column size are predicted. But for further increase in film discretization ratio, e.g. 20 (S-5′), it is found that the impact of discretization ratio diminishes like discretization points. The reaction condition factor is varied from 0.5 (S-5) to 0.9 (S-6) which means the condition close to bulk liquid phase is chosen to calculate film reaction rate where CO_2 concentration is lower. This effect is reflected in CO_2 loading changes from 0.389 to 0.357 (Table 7.19). There are also observed changes in temperature profiles (Figure 7.13). It is found that the temperature profile of S-6 is almost identical to that of S-4 but there exist some differences in CO_2 loadings. It is also found that the profiles of S-3 and S-5 overlap each other and the calculated rich loadings are almost the same. Due to the identical results of S-4 & S-4′ schemes, and S-5 & S-5′ schemes, only single column is used for data presentation for each pair and as shown as S-4(/4′) and S-5(/5′) in the Table 7.19. The results shown in Table 7.19 and in Figure 7.13, highlights the importance of film discretization. The success of modeling CO_2 capture with MEA depends upon how the film discretization is carried out because it allows the account of concentration gradients and the corresponding reaction rates in the various film segments (Zhang et al., 2009). The default values for discretization ratio and reaction condition factor will be considered in our simulation without additional discretization point to avoid convergence difficulty.

Table 7.18: Film discretization schemes

Scheme Name	Additional discretization points	Film discretization ratio	Reaction condition factor
S-1	0	2	0.5
S-2	1	2	0.5
S-3	3	2	0.5
S-4	5	2	0.5
S-4′	10	2	0.5
S-5	5	10	0.5
S-5′	5	20	0.5
S-6	5	10	0.9

Table 7.19: Absorber study (Model-VI) for liquid film discretization (at lean loading of 0.3 and CO_2 recovery of 85%)

Discretization Scheme*	**S-1**	**S-2**	**S-3**	**S-4(/4′)**	**S-5(/5′)**	**S-6**
	Input specifications for Absorber					
Simulation approach	Rate-based					
Flue gas flow rate, kmol/sec	5.467					
Flue gas temperature, ^{0}C	40					
CO_2 composition, mol %	14.2					
Lean solvent temperature, ^{0}C	40					
Reaction ID	MEA-REA (1-9)					
System foaming factor	0.85					
Flow model	mixed					
Pressure profile update	Yes					
Design mode	Yes					
Approach to flooding, %	70					
Trays/stages (no. of downcomer pass)	9 (2)					
Tray spacing, m	1.5					
Weir height, m	0.15					
Downcomer clearance, m	0.125					
Film resistance option	Discrxn					
Convergence tolerance	10^{-5}	10^{-3}	10^{-3}	10^{-5}	10^{-5}	10^{-5}
	Results					
Base stage	4	5	9	9	9	9
Max^m downcomer flooding (/at tray)	0.5/4	0.5/5	0.6/9	0.6/9	0.6/9	0.7/9
Max^m flooding factor (/at tray)	0.7/4	0.7/5	0.7/9	0.7/9	0.7/9	0.7/9
Column diameter, m	6.7	6.7	7.3	7.5	7.3	8.2
Column section pressure drop, N/m^2	34350	33808	29027	28307	28999	27024
Pressure drop/tray (max.), N/m^2	4218	4112	3543	3471	3542	3349
Bottom stage pressure, N/m^2	132132	131500	127003	126373	126978	125259
Bottom stage temp., K	327.0	328.8	322.6	321.5	322.6	319.1
Tray (max^m) efficiency, %	9.6	9.8	11.8	12.2	11.8	13.1
Lean solvent flow rate, kmol/sec	31.2	32.9	60.9	69.3	61.0	95.9
Rich solvent flow rate, kmol/sec	30.9	32.7	60.8	69.3	60.9	95.8
Rich loading (mol CO_2/mol MEA)	0.473	0.464	0.389	0.378	0.389	0.357

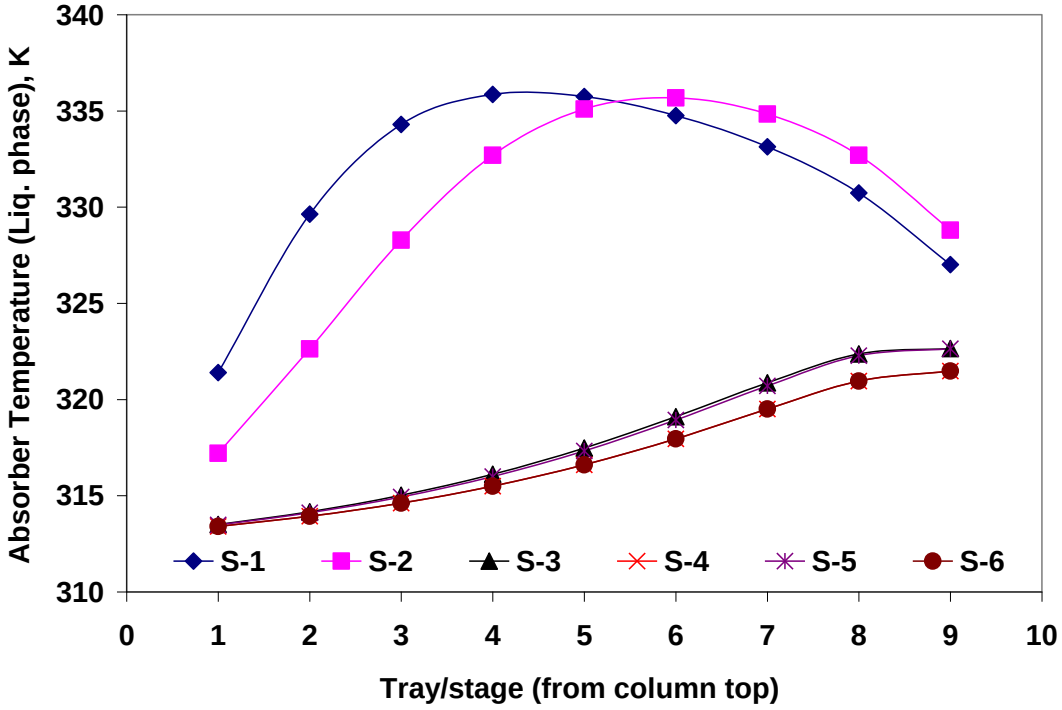

Figure 7.13: Absorber temperature profile for all discretization schemes

7.6.6 Efficiency in Equilibrium-stage Modeling

In equilibrium-stage modeling, RadFrac allows to use Murphree or Vaporization efficiency for stages or components to account for departure from equilibrium. When Murphree or Vaporization efficiency is specified, RadFrac will treat the stages as actual trays. Efficiencies vary from component to component, and from tray to tray, in a multicomponent mixture. Very rarely is this fact taken into account in a simulation model that uses efficiencies. When actual plant data are available and efficiencies are unknown, efficiencies can be manipulated to match the plant data. The effects of variation of Murphree efficiency in tray column for Model-IV are presented in Table 7.20. Same efficiencies are specified for both absorber and stripper stages in a simulation run. It is found that decreases of Murphree efficiencies for column stages increases column size and reboiler energy requirement as expected. To avoid uncertainties in efficiency specification during process simulation, Murphree efficiency of 100% for all stages is used for further equilibrium-stage modeling calculation.

Table 7.20: Effect of Murphree Stage efficiency for Model-IV (lean loading: 0.3; CO_2 recovery: 85%; Operational flooding approach: 70%)

Murphree Stage Efficiency (%)	**100**	**75**	**25**
Absorber			
No of Trays (double pass sieve)	9	9	9
Tray spacing, m	1.7	1.7	1.6
Column diameter, m	**5.8**	**5.8**	**5.9**
Downcomer flooding, %	55	55	51
Lean stream flow rate, kmol/sec	30.3	31.1	32.1
Stripper			
No of Trays (double pass sieve)	9	9	9
Tray spacing, m	1.7	1.7	1.7
Column diameter, m	**4.5**	**4.7**	**4.9**
Downcomer flooding, %	50	50	51
Thermal Energy requirement			
Reboiler duty (total), MWth	**551.9**	**571.9**	**660.9**

7.6.7 Pressure (last stage) update in Absorber

Radfrac can update the column pressure with the pressure drops calculated during tray ratings. Radfrac compute the pressure drop from the correlation for the specific tray type. The pressure drop calculated for stage N is the pressure difference between stage N and stage N+1. Normally, in columns without reboiler where the last stage is included in a pressure update section, the pressure drop for the last stage is not used because there is no stage below to receive the updated pressure. As a workaround, a dummy stage (where no appreciable reaction or separation occurs) at the bottom of the column is added to allow the pressure drop to be applied appropriately. The workaround details are presented in Appendix D The effects of not updating absorber last stage pressure with pressure drop calculation are presented in Table 7.21. Higher pressure and temperature of absorber's rich stream due to the consideration of last stage pressure drop helps to lower the reboiler duty by 9% for Model-VI and also slightly lower the stripper size. For Model-I, the influence of last stage pressure drop update for exit rich stream is not significant.

Table 7.21: Effect of not updating Absorber last stage pressure with pressure drop calculation to obtain rich stream's actual pressure (lean loading: 0.3; CO_2 recovery: 85%; Operational flooding approach: 70%)

Last Stage pressure	**Not updated**	**Updated**	**Not updated**	**Updated**
Model	Model-VI		Model-I	
Absorber				
No of Trays (double pass)	9	9 (+1 dummy)	9	9 (+1 dummy)
Tray spacing, m	1.7	1.7	1.7	1.7
Column diameter, m	5.7	5.7	5.7	5.7
Downcomer flooding, %	55	55	55	55
Film resistance with/or without reaction				
Liquid Phase	Discxrn	Discrxn	Discxrn	Discxrn
Vapour Phase	Film	Film	Film	Film
Film nonideality correction				
Liquid Phase	Yes	Yes	Yes	Yes
Vapour Phase	Yes	Yes	Yes	Yes
Lean stream flow rate, kmol/sec	29.8	29.8	29.8	29.8
Bottom Stage pressure, N/m^2	**146486**	**151726**	**146779**	**151726**
Bottom stage temp. (liquid), K	327.5	327.9	327.9	327.9
Stripper				
No of Trays (double pass)	9	9	9	9
Tray spacing, m	1.7	1.7	1.6	1.6
Column diameter, m	**4.7**	**4.6**	**4.4**	**4.4**
Downcomer flooding, %	51	50	47.6	47.2
Film resistance with/or without reaction				
Liquid Phase	Discrxn	Discrxn	Nofilm	Nofilm
Vapour Phase	Film	Film	No	No
Film nonideality correction				
Liquid Phase	Yes	Yes	No	No
Vapour Phase	Yes	Yes	No	No
Reboiler duty, MWth	164.9	150.1	112.5	112.5
Reboiler duty (4 trains), MWth	**659.6**	**600.4**	**450.2**	**449.8**

7.6.8 Approach temperature

Temperature approach plays an important role as heat exchanger specification in the process design. Hot outlet temperature approach i.e., hot outlet-cold inlet temperature

difference is specified for the Lean/rich heat exchanger in this study. A heat transfer coefficient of 1134 W/m^2-C for hot water-watery solution (liquid-liquid) system is considered (Alie, 2004). Table 7.22 shows that 5°C temperature approach helps to reduce the reboiler energy requirements which in turn will reduce the operating cost. This decreased in reboiler energy is due to a lower temperature drop across the column which results in reduced sensible heat requirements. But as the total amount of heat transferred is increased due to the lower temperature approach, the corresponding capital cost will increase for the heat exchanger. The capital cost for the stripper will also be increased due to the larger size requirement at lower temperature approach.

Table 7.22: Effect of lean/rich heat exchanger's temperature approach (Model-I; lean loading: 0.4; CO_2 recovery: 85%; Operational flooding approach: 70%)

Temperature approach (°C)	**5**	**10**
Absorber		
No of Trays (double pass sieve)	7	7
Tray spacing, m	1.4	1.4
Column diameter, m	7.6	7.6
Downcomer flooding, %	55	52
Stripper		
No of Trays (double pass sieve)	9	9
Tray spacing, m	1.6	1.6
Column diameter, m	**6.8**	**5.6**
Downcomer flooding, %	49	53
Feed temperature, K	358.1	359.4
Reboiler temperature, K	369.8	374.2
Reboiler duty, MWth	**96.8**	**117.6**
Lean/rich exchanger		
Heat duty, MW	**169**	**149**
Area, 10^3 m^2	**18.9**	**10.7**

7.6.9 CO_2 loading (lean) analysis

Based on the process flowsheet in Figure 7.1 and specifications described in Section 7.5, important simulation and design results for a single train are presented in Table 23-28 for 85% CO_2 capture with purity ≥ 98% from a 500 MW power plant flue gas at different lean solvent loading. These tables might be very helpful to compare all

the cases on the same basis for each model. The material balances are given in the Appendix E and F at CO_2 lean loading of 0.3 for the both process alternatives shown in Figure 7.1 and Figure 7.2. Each material balance gives the stream composition, flow rate, temperature, pressure, vapour fraction, density, and average molecular weight. The stream names/numbers at the top of the table correspond to flow diagrams presented in Section 7.3. The "Max^{m} backup/Tray spacing" in Table 23-28 is the term used for downcomer flooding (fractional). The absorber and stripper pressure profiles are updated with the tray pressure drop. In column designing, the downcomer flooding level at both columns and the stripper reboiler temperature are designed to maintain close to or less than 50%, and not to exceed 122ºC, respectively. It is also designed to maintain a reasonable column pressure drop, i.e., less than 40 kPa for both columns. The result analysis based on these tables for different models are described below.

Table 7.23: Process simulation and design results - single train - Model I

Results for Model-I										
Lean loading (mol CO_2/mol MEA)	**0.2**		**0.25**		**0.3**		**0.35**		**0.4**	
Rich loading (mol CO_2/mol MEA)	0.466		0.467		0.467		0.47		0.472	
Water make-up rate, kmol/sec	0.9		0.8		0.7		0.5		0.4	
MEA make-up rate, kmol/sec	5.1e-4		3.7e-4		2.6e-4		2.4e-4		1.7e-4	
Lean solvent flow rate, kmol/sec	20.9		24.9		30.1		33.5		45.9	
Rich solvent flow rate, kmol/sec	20.2		24.4		29.7		33.5		45.8	
	Absorber	**Stripper**	**Absorber**	**Stripper**	**Absorber**	**Stripper**	**Absorber**	**Stripper**	**Absorber**	**Stripper**
Trays/stages (no. of downcomer pass)	7 (2)	9 (2)	7 (2)	9 (2)	7 (2)	9 (2)	7 (2)	9 (2)	7 (2)	9 (2)
Tray spacing, m	1.4	1.7	1.4	1.7	1.4	1.6	1.4	1.6	1.4	1.6
Weir height, m	0.14	0.15	0.14	0.15	0.14	0.15	0.14	0.15	0.14	0.15
Downcomer clearance, m	0.115	0.125	0.115	0.125	0.115	0.125	0.115	0.125	0.115	0.125
Max^m backup/Tray spacing (/at stage)	0.4/3	0.5/8	0.4/3	0.5/8	0.5/4	0.5/8	0.5/4	0.5/8	0.5/6	0.5/8
Max^m flooding factor (/at stage)	0.7/3	0.7/8	0.7/3	0.7/8	0.7/4	0.7/8	0.7/4	0.7/8	0.7/5	0.7/8
Column diameter, m	6.9	4.4	7.0	4.3	7.2	4.4	7.3	4.6	7.6	6.8
Reflux ratio		2.0		1.1		0.7		0.4		0.1
Bottom to feed ratio		0.98		0.98		0.98		0.98		0.98
Column section pressure drop, N/m^2	24830	32244	24002	23001	23074	18581	22644	17025	21513	18221
Pressure drop/tray (max.), N/m^2	3884	5095	3738/3	3938	3597/4	3212	3517	2774	3355	2882
Bottom stage pressure, N/m^2	122875	136882	122098	127638	121207	123218	120760	121662	119700	122858
Stripper's Feed stream temp., K		370		368		367		364		358
Bottom stage (/Reboiler) temp., K	327	385	327	383	328	381	328	378	325	370
Tray (max^m) efficiency, %	5.5		5.9		6.3		6.3		6.6	
Reboiler duty, MW_{th}		163		125		114		103		97

Table 7.24: Process simulation and design results - single train - Model II

Results for Model-II										
Lean loading (mol CO_2/mol MEA)	**0.2**		**0.25**		**0.3**		**0.35**		**0.4**	
Rich loading (mol CO_2/mol MEA)	0.468		0.467		0.468		0.560		0.471	
Water make-up rate, kmol/sec	0.9		0.8		0.6		0.6		0.4	
MEA make-up rate, kmol/sec	4.7e-4		3.7e-4		2.3e-4		1.3e-4		1.7e-4	
Lean solvent flow rate, kmol/sec	21.6		24.9		31.3		36.3		46.9	
Rich solvent flow rate, kmol/sec	21.0		24.4		31.0		35.7		46.8	
	Absorber	**Stripper**	**Absorber**	**Stripper**	**Absorber**	**Stripper**	**Absorber**	**Stripper**	**Absorber**	**Stripper**
Trays/stages (no. of downcomer pass)	7 (2)	9 (2)	7 (2)	9 (2)	7 (2)	9 (2)	7 (2)	9 (2)	7 (2)	9 (2)
Tray spacing, m	1.4	1.9	1.4	1.8	1.4	1.8	1.4	1.8	1.4	1.8
Weir height, m	0.14	0.15	0.14	0.15	0.14	0.15	0.14	0.15	0.14	0.15
Downcomer clearance, m	0.115	0.125	0.115	0.125	0.115	0.125	0.115	0.125	0.115	0.125
Max^m backup/Tray spacing (/at stage)	0.4/3	0.7/2	0.4/3	0.5/2	0.5/4	0.5/8	0.5/4	0.6/8	0.5/6	0.6/8
Max^m flooding factor (/at stage)	0.7/3	0.7/2	0.7/3	0.7/2	0.7/4	0.7/8	0.7/4	0.7/8	0.7/5	0.7/8
Column diameter , m	6.9	4.5	7.0	4.4	7.2	4.3	7.4	4.9	7.7	5.2
Reflux ratio		4.4		2.7		1.6		2.7		0.4
Bottom to feed ratio		0.98		0.98		0.98		0.99		0.99
Column section pressure drop, N/m^2	24626	58568	24009	39749	22876	28981	21255	32681	21451	19191
Pressure drop/tray (max.), N/m^2	3854	9555	3739	6239	3567	4746	3317	5129	3346	3156
Bottom stage pressure, N/m^2	122692	163205	122104	144387	121028	133619	119609	137318	119647	123828
Stripper's Feed stream temp., K		372		370		368		370		358
Bottom stage (/Reboiler) temp., K	327	390	327	386	327	382	325	383	325	370
Tray (max^m) efficiency, %	5.7		6		6.4		7.1		6.7	
Reboiler duty, MW_{th}		260		192		146		196		107

Table 7.25: Process simulation and design results - single train - Model III

Results for Model-III										
Lean loading (mol CO_2/mol MEA)	**0.2**		**0.25**		**0.3**		**0.35**		**0.4**	
Rich loading (mol CO_2/mol MEA)	0.506		0.513		0.498		0.496		0.497	
Water make-up rate, kmol/sec	1.2		1.0		0.9		0.7		0.5	
MEA make-up rate, kmol/sec	5.7e-4		2.5e-4		3.0e-4		1.8e-4		1.0e-4	
Lean solvent flow rate, kmol/sec	18.3		26.3		27.5		36.3		52.1	
Rich solvent flow rate, kmol/sec	17.4		25.6		26.9		35.9		51.9	
	Absorber	**Stripper**	**Absorber**	**Stripper**	**Absorber**	**Stripper**	**Absorber**	**Stripper**	**Absorber**	**Stripper**
Trays/stages (no. of downcomer pass)	9 (2)	9 (2)	9 (2)	9 (2)	9 (2)	9 (2)	9 (2)	9 (2)	9 (2)	9 (2)
Tray spacing, m	1.7	1.7	1.7	1.6	1.7	1.7	1.7	1.7	1.7	1.8
Weir height, m	0.15	0.15	0.15	0.15	0.15	0.15	0.15	0.15	0.15	0.15
Downcomer clearance, m	0.125	0.125	0.125	0.125	0.125	0.125	0.125	0.125	0.125	0.125
Max^m backup/Tray spacing (/at stage)	0.6/2	0.5/8	0.6/2	0.5/8	0.5/2	0.5/8	0.6/3	0.5/2	0.6/3	0.5/8
Max^m flooding factor (/at stage)	0.7/2	0.7/8	0.7/2	0.7/8	0.7/2	0.7/8	0.7/3	0.7/2	0.7/3	0.7/7
Column diameter, m	5.5	4.1	5.6	4.3	5.7	4.0	5.9	4.4	6.3	5.8
Reflux ratio		1.6		0.9		0.6		0.5		0.2
Bottom to feed ratio		0.98		0.98		0.98		0.99		0.99
Column section pressure drop, N/m^2	56465	32169	53652	21855	51371	20376	47987	18060	41949	17873
Pressure drop/tray (max.), N/m^2	7709	5008	7109	3707	6652	3538	6035	3337	5210	2882
Bottom stage pressure, N/m^2	152612	136807	149922	126492	147764	125013	144518	122697	138882	122510
Stripper's Feed stream temp., K		369		368		367		365		358
Bottom stage (/Reboiler) temp., K	321	385	323	381	325	381	325	377	323	372
Tray (max^m) efficiency, %										
Reboiler duty, MW_{th}		142		118		107		106		124

Table 7.26: Process simulation and design results - single train - Model IV

Results for Model-IV										
Lean loading (mol CO_2/mol MEA)	**0.2**		**0.25**		**0.3**		**0.35**		**0.4**	
Rich loading (mol CO_2/mol MEA)	0.483		0.482		0.480		0.481		0.484	
Water make-up rate, kmol/sec	1.2		1.1		0.8		0.6		0.5	
MEA make-up rate, kmol/sec	4.8e-4		4.3e-4		3.0e-4		1.7e-4		9.3e-5	
Lean solvent flow rate, kmol/sec	20.7		24.1		30.3		40.4		62.6	
Rich solvent flow rate, kmol/sec	19.9		23.3		29.8		40.1		62.4	
	Absorber	**Stripper**	**Absorber**	**Stripper**	**Absorber**	**Stripper**	**Absorber**	**Stripper**	**Absorber**	**Stripper**
Trays/stages (no. of downcomer pass)	9 (2)	9 (2)	9 (2)	9 (2)	9 (2)	9 (2)	9 (2)	9 (2)	9 (2)	9 (2)
Tray spacing, m	1.8	1.8	1.7	1.7	1.7	1.7	1.7	1.7	1.7	1.7
Weir height, m	0.15	0.15	0.15	0.15	0.15	0.15	0.15	0.15	0.15	0.15
Downcomer clearence, m	0.125	0.125	0.125	0.125	0.125	0.125	0.125	0.125	0.125	0.125
Max^m backup/Tray spacing (/at stage)	0.6/2	0.6/2	0.6/1	0.5/2	0.5/2	0.5/8	0.6/2	0.5/2	0.6/2	0.6/8
Max^m flooding factor (/at stage)	0.7/2	0.7/2	0.7/1	0.7/2	0.7/2	0.7/8	0.7/2	0.7/2	0.7/2	0.7/5
Column diameter, m	5.1	4.9	5.5	4.6	5.8	4.5	6.0	4.8	6.8	6.0
Reflux ratio		4.0		2.2		1.3		0.9		0.4
Bottom to feed ratio		0.98		0.98		0.98		0.99		0.99
Column section pressure drop, N/m^2	64709	46597	54755	34915	48826	25707	45601	20201	36403	18442
Pressure drop/tray (max.), N/m^2	9344	7895	7538	5638	6339	4251	5796	3664	4513	2979
Bottom stage pressure, N/m^2	160245	151234	151094	139553	145602	130345	142508	124838	133953	123080
Stripper's Feed stream temp., K		371		368		369		368		359
Bottom stage (/Reboiler) temp., K	321	388	322	385	324	382	324.0	378	322	372
Tray (max^m) efficiency, %	100	100	100	100	100	100	100	100	100	100
Reboiler duty, MW_{th}		253		183		138		119		140

Table 7.27: Process simulation and design results - single train - Model V

Results for Model-V										
Lean loading (mol CO_2/mol MEA)	**0.2**		**0.25**		**0.3**		**0.35**		**0.4**	
Rich loading (mol CO_2/mol MEA)	0.509		0.502		0.498		0.496		0.500	
Water make-up rate, kmol/sec	1.2		1.1		0.9		0.7		0.5	
MEA make-up rate, kmol/sec	5.3e-4		4.4e-4		3.0e-4		1.8e-4		9.3e-5	
Lean solvent flow rate, kmol/sec	18.8		22.2		27.6		36.3		52.6	
Rich solvent flow rate, kmol/sec	17.9		21.4		27.0		35.9		52.46	
	Absorber	**Stripper**	**Absorber**	**Stripper**	**Absorber**	**Stripper**	**Absorber**	**Stripper**	**Absorber**	**Stripper**
Trays/stages (no. of downcomer pass)	9 (2)	9 (2)	9 (2)	9 (2)	9 (2)	9 (2)	9 (2)	9 (2)	9 (2)	9 (2)
Tray spacing, m	1.7	1.7	1.7	1.7	1.7	1.7	1.7	1.7	1.8	1.8
Weir height, m	0.15	0.15	0.15	0.15	0.15	0.15	0.15	0.15	0.15	0.15
Downcomer clearance, m	0.125	0.125	0.125	0.125	0.125	0.125	0.125	0.125	0.125	0.125
Max^m backup/Tray spacing (/at stage)	0.6/1	0.5/2	0.5/1	0.5/8	0.5/1	0.5/8	0.5/2	0.5/8	0.6/2	0.5/8
Max^m flooding factor (/at stage)	0.7/1	0.7/2	0.7/1	0.78	0.7/1	0.7/8	0.7/2	0.7/8	0.7/2	0.7/6
Column diameter, m	5.5	4.2	5.6	4.0	5.7	4.1	5.9	4.5	5.9	5.5
Reflux ratio		1.6		0.8		0.6		0.3		0.1
Bottom to feed ratio		0.98		0.98		0.98		0.99		0.99
Column section pressure drop, N/m^2	54060	32237	52075	24155	50569	20539	47057	18068	48145	18072
Pressure drop/tray (max.), N/m^2	7548	5260	7081	4080	6635	3787	5967	3229	6060	2929
Bottom stage pressure, N/m^2	150419	136874	148609	128792	147187	125177	143848	122706	144659	122710
Stripper's Feed stream temp., K		368.68		367.59		366.64		361.80		354.73
Bottom stage (/Reboiler) temp., K	321	385	323	383	325	380	325	377	323	372
Tray (max^m) efficiency, %	100	100	100	100	100	100	100	100	100	100
Reboiler duty, MW_{th}		144		112		106		116		143

Table 7.28: Process simulation and design results - single train - Model-VI

Results for Model-VI										
Lean loading (mol CO_2/mol MEA)	**0.2**		**0.25**		**0.3**		**0.35**		**0.4**	
Rich loading (mol CO_2/mol MEA)	0.467		0.468		0.469		0.471		0.477	
Water make-up rate, kmol/sec	0.9		0.8		0.6		0.5		0.4	
MEA make-up rate, kmol/sec	5.3e-4		3.5e-4		1.9e-4		1.7e-4		7.9e-5	
Lean solvent flow rate, kmol/sec	20.5		25.4		33.5		38.8		66.0	
Rich solvent flow rate, kmol/sec	19.9		24.9		33.1		38.5		65.9	
	Absorber	**Stripper**	**Absorber**	**Stripper**	**Absorber**	**Stripper**	**Absorber**	**Stripper**	**Absorber**	**Stripper**
Trays/stages (no. of downcomer pass)	7 (2)	9 (2)	7 (2)	9 (2)	7 (2)	9 (2)	7 (2)	9 (2)	7 (2)	9 (2)
Base stage	3		4		4		5		5	
Fractional flooding approach (base stage)	0.7		0.7		0.7		0.7		0.7	
Tray spacing, m	1.4	1.9	1.4	1.7	1.4	1.7	1.4	1.7	1.4	1.7
Weir height, m	0.14	0.15	0.14	0.15	0.14	0.15	0.14	0.15	0.14	0.15
Downcomer clearence, m	0.115	0.125	0.115	0.125	0.115	0.125	0.115	0.125	0.115	0.125
Max^m backup/Tray spacing (/at stage)	0.4/3	0.7/2	0.4/4	0.5/2	0.5/4	0.5/8	0.5/5	0.5/8	0.6/6	0.6/8
Max^m flooding factor (/at stage)	0.7/3	0.7/2	0.7/4	0.7/2	0.7/4	0.7/8	0.7/5	0.7/8	0.7/5	0.7/3
Column diameter, m	6.8	4.7	7.0	4.8	7.2	4.8	7.9	4.7	8.1	4.6
Reflux ratio		5.2		3.2		1.8		0.8		0.3
Bottom to feed ratio		0.98		0.98		0.98		0.99		0.99
Column section pressure drop, N/m^2	24936	64688	23889	37078	22561	26022	22093	20452	20412	18465
Pressure drop/tray (max.), N/m^2	3900	10815	3719	5754	3517	4177	3431	3423	3199	2992
Bottom stage pressure, N/m^2	122969	169326	121995	141716	120741	130659	120266	125090	118762	123103
Stripper's Feed stream temp., K		372		370		368		365		359
Bottom stage (/Reboiler) temp., K	327	392	327	385	327	382	326	378	322	372
Tray (max^m) efficiency, %	5.3	6.1	6.1	7.3	6.7		6.8	9.0	7.9	10.9
Reboiler duty, MW_{th}		294		212		157		121		142

The CO_2 loading of the lean solvent which represents the degree of regeneration is an important parameter concerning the energy demand for regeneration. This value is optimized by varying the solvent flow rate to achieve the same CO_2 removal capacity. In this way the reboiler duty is changed to maintain the degree of separation. This thermal energy requirement for the reboiler is expected to be a major contributor to the production cost, and a change in the energy required will give a clear effect on the operating costs. The amount of solvent required affects the size of the absorption/stripping equipments, which in turn influences the capital costs.

At low values of lean solvent loading, the amount of stripping steam required to achieve this low solvent loading is dominant in the thermal energy requirement. At high values of lean solvent loading the heating up of the solvent at high solvent circulation flow rates is dominant in the thermal energy requirement. Therefore a minimum is expected in the thermal energy requirement. From Fig. 7.14 it is observed that the thermal energy requirement decreases with increase of lean solvent loading until a minimum is attained. The point at which the energy requirement is lowest defined as the optimum lean solvent loading. The optimum lean solvent loadings for all the models based on Fig. 7.14 are presented in the Table 7.29 along with the corresponding thermal energy requirement per ton CO_2 captured with a 30 wt% MEA solution. The range of optimum lean loading found varies from 0.29 to 0.36 depending on the model considered in the simulation and design study except for Model-I where the reboiler duty decreases continuously when increasing the lean solvent loading. Model-II exhibits a local minimum near the lean loading of 0.3 and then a local maximum before decreasing downward. This abnormal behaviour is difficult to explain. From Fig. 7.15 it is noted that the solvent circulation rate increases with increase of the lean solvent loading. The result of Alie et al. (2005) is also plotted in the Figure 7.14 for comparison purpose. The authors considered rate-based modeling approach using solution chemistry and RateFrac model (was available in the previous version of AspenPlus). Model-III of the present study is close to Alie's model.

Table 7.29: Optimum lean solvent loading (mol CO_2/mol MEA) for various models

Absorber-Stripper Models	Optimum Lean Loading (mol CO_2/mol MEA)	Reboiler Energy (GJ/ton captured CO_2)
Model-I	0.4	3.3
Model-II	0.30	5.1
Model-III	0.32	3.7
Model-IV	0.35	4.1
Model-V	0.29	3.7
Model-VI	0.36	4.2
Alie et al. (2005)	0.25	4.0

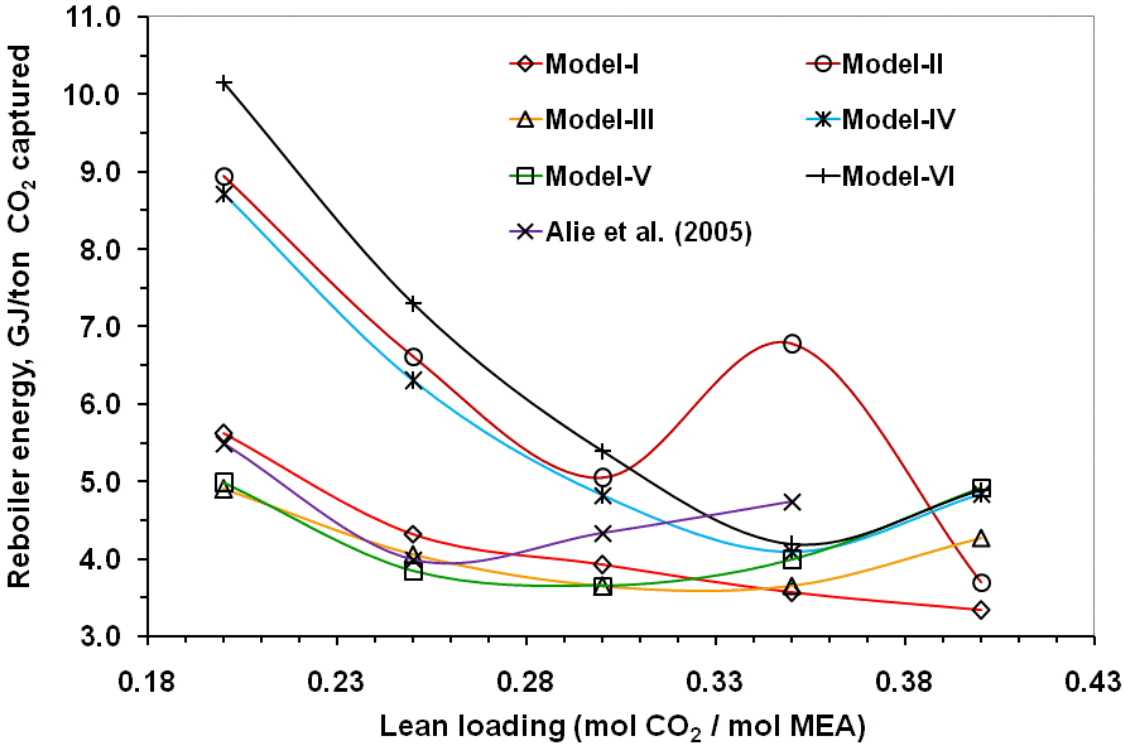

Figure7.14: Regeneration energy requirement for various models at different CO_2 lean solvent loadings (CO_2 recovery: 85%; Operational flooding approach: 70%)

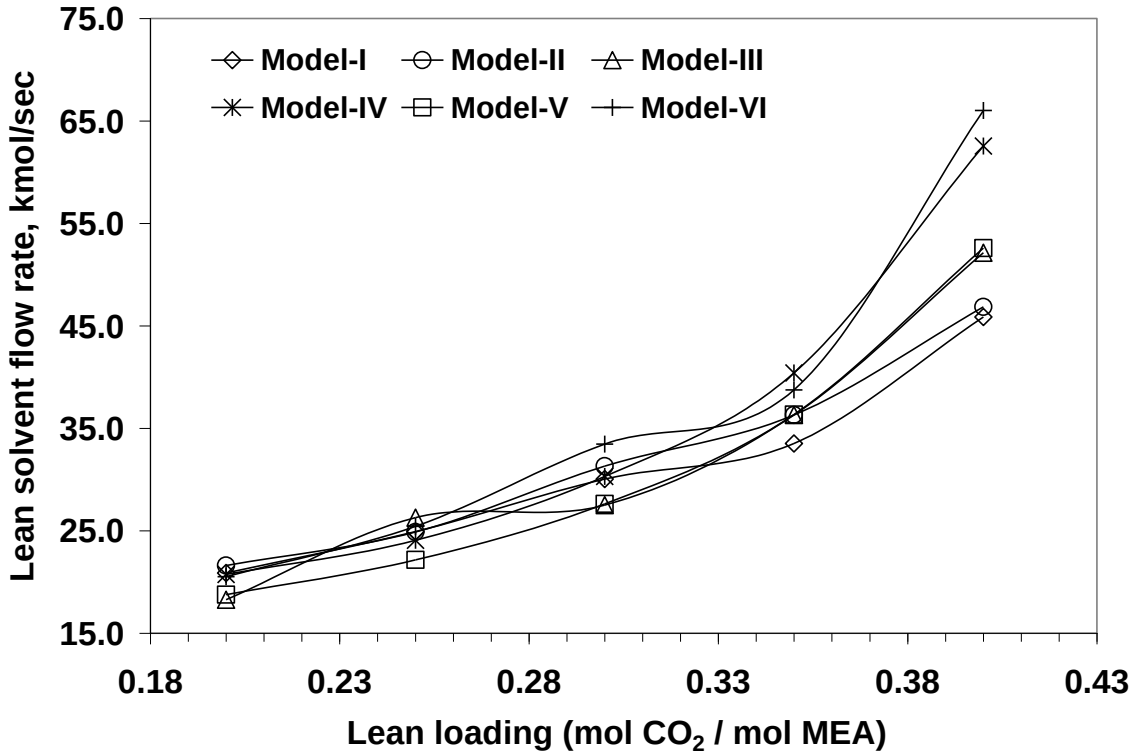

Figure7.15: Solvent flow requirement for various models at different CO_2 lean loadings

In Figure 7.16, the rich loading shows only slight increase for Model-IV, V & VI as the lean loading increases. But for Model-III, there is a local maximum near a lean loading of 0.25 which corresponds to the local minimum of the absorber temperature bulge. This lower absorber temperature bulge allows the rich amine to achieve a higher CO_2 loading. A steep increase of rich loading is observed for Model-II when the lean loading increases from 0.3 and reaches a maximum before decreasing, although maximum temperature gradually decreases as in the other models. The magnitude and location of the maximum temperature in the absorber for each lean loading are plotted in Figure 7.17. It is found that the maximum temperature location in the absorber for each lean loading for rate-based model with equilibrium reaction (Model-III) and equilibrium-stage models (Model-IV & V) ranges between trays 2 and 4. For Model-I, II & VI, the tray range for maximum temperature location for all lean loadings considered is greater i.e., between 3 and 6. Figure 7.18 confirms that the maximum reboiler temperature in stripper attained is 392K (i.e., 119ºC) at lean loading of 0.2 for Model-VI (rate-based model with kinetic consideration for absorber and stripper). This validates the assumption of negligible thermal degradation of MEA solution by obeying highest temperature restriction ($\leq$120-122^{0}C) for MEA degradation. This figure also shows that there is a local minimum for the reboiler temperature for Model-II at around lean solvent loading of 0.3. Corresponding to the reboiler maximum temperature of 119ºC for Model-VI, the maximum bottom stage pressure of the stripper is found around 170 kPa (Figure 7.19a) which is appropriate for utilization of less expensive LP or IP steam from power plant for solvent regeneration instead of more expensive high pressure steam to lower the operating cost. The lowest bottom stage temperature and pressure in stripper reported in Figure 7.18 and Figure 7.19a are 372.0K (99ºC) and 122.5 kPa respectively at lean loading of 0.4 for the majority of the models. From Figure 7.19b, it is observed that rate-base absorber models with kinetic considerations predict lower absorber pressure for all lean loadings studied.

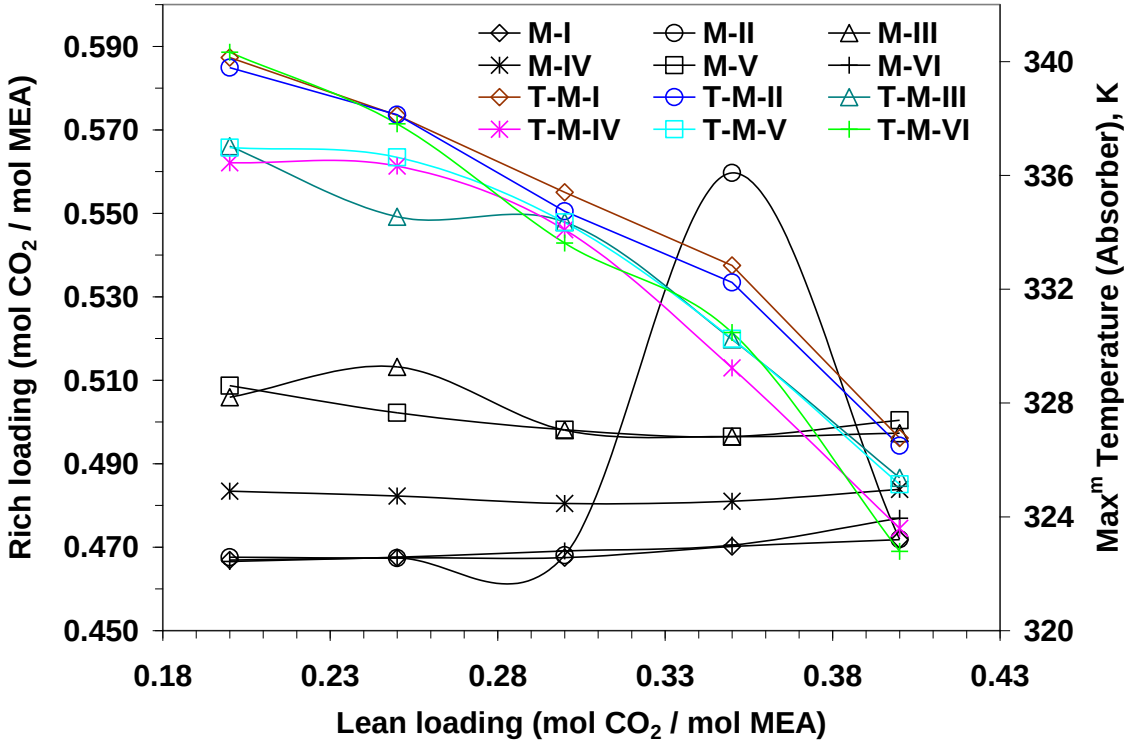

Figure 7.16: Rich loadings and maximum temperature for absorber at various lean loadings (CO_2 recovery: 85%; Operational flooding approach: 70%)

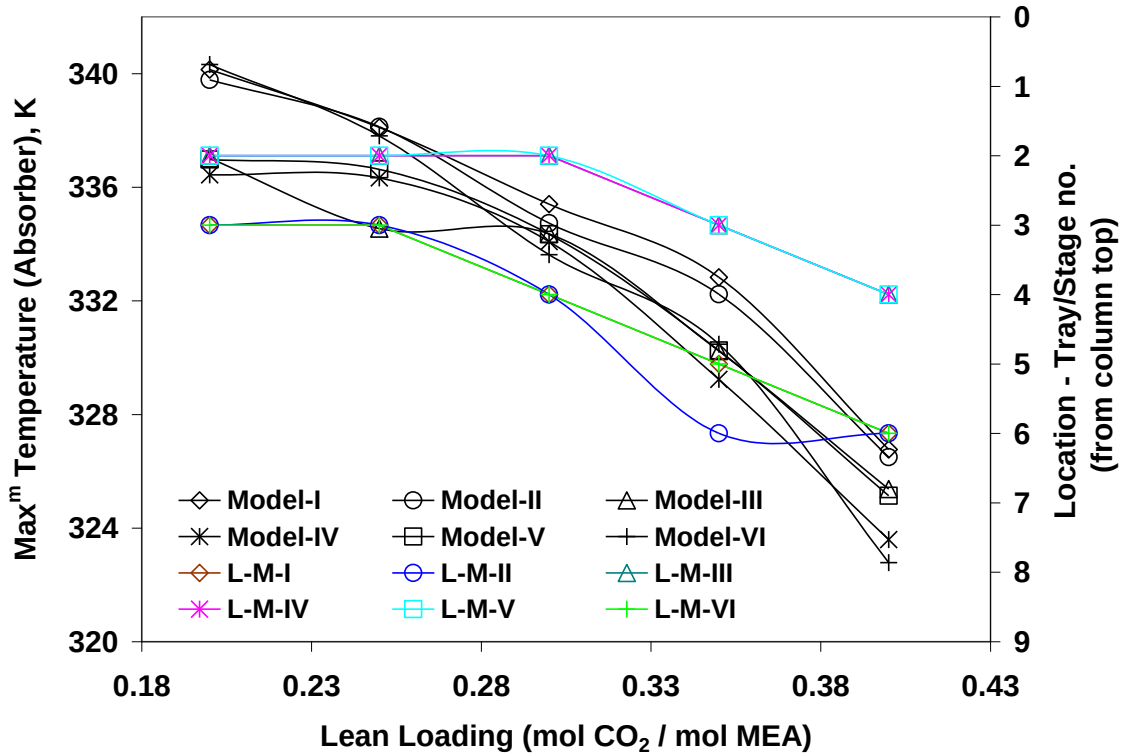

Figure7.17: Magnitude and location of maximum temperature bulge in Absorber at different lean loadings (CO_2 recovery: 85%; Operational flooding approach: 70%)

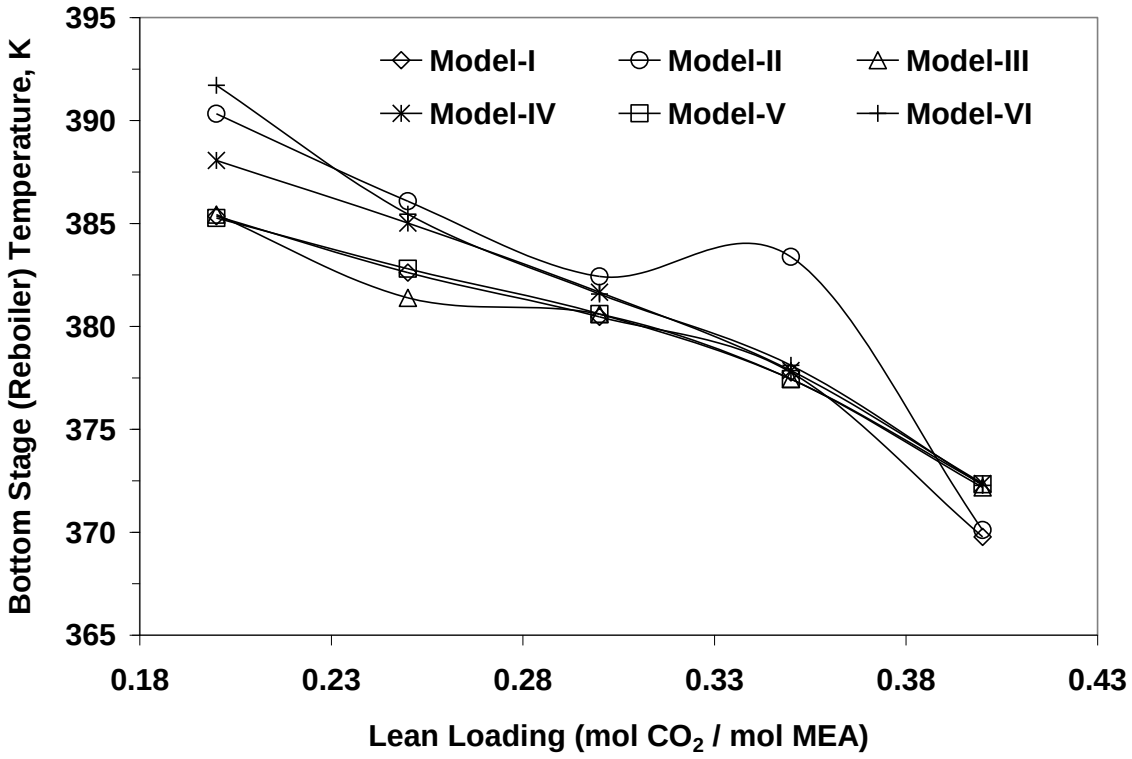

Figure 7.18: Variation in reboiler temperature at different lean loading (CO_2 recovery: 85%; Operational flooding approach: 70%)

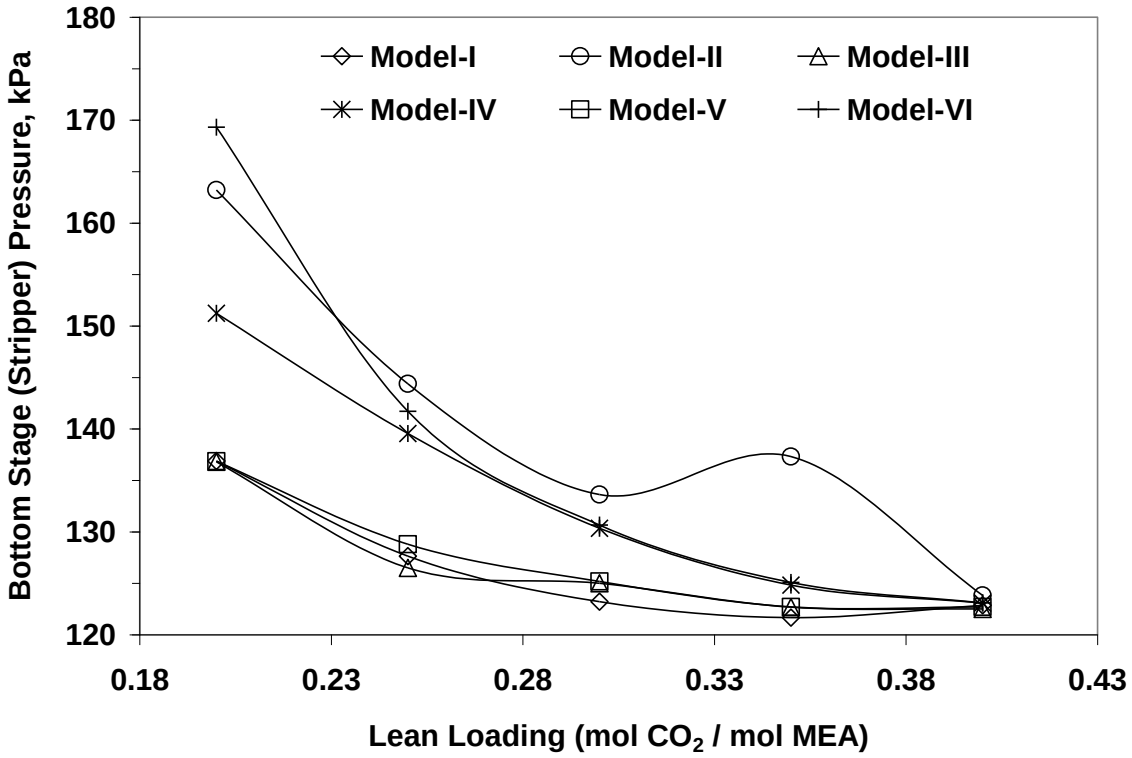

Figure 7.19a: Variation in stripper bottom stage pressure at different lean loading (CO_2 recovery: 85%; Operational flooding approach: 70%)

The highest total column pressure drop, predicted by Model-IV, is 65 kPa for both the absorber and stripper at a low lean solvent loading of 0.2 (Figure 7.20). Rate-based Models e.g., I, II & VI with kinetic consideration in absorber computed total pressure drop in the range of 25 to 20 kPa but other models with equilibrium reactions in absorber e.g., III, IV & V predicted higher pressure drop in absorber i.e., 35 to 65 kPa at all lean loadings studied. In the stripper pressure drop calculation, it is observed that all models predicted very reasonable column pressure drop i.e., less than or close to 40 kPa except at lean loading of 0.2 where Model-II and VI predict higher pressure drop i.e., 58 and 65 kPa, respectively. Overall, the total pressure drop in both tray type columns predicted by all models is realistic for large scale processing of flue gas.

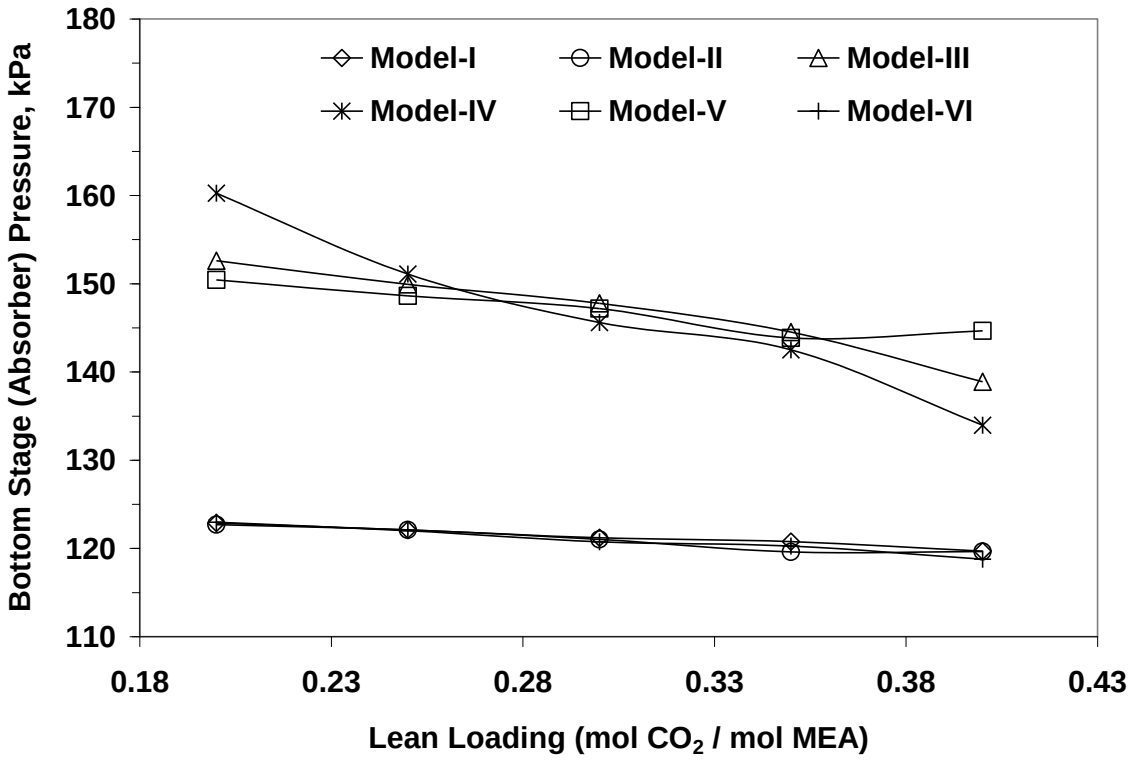

Figure 7.19b: Variation in absorber bottom stage pressure at different lean loading (CO_2 recovery: 85%; Operational flooding approach: 70%)

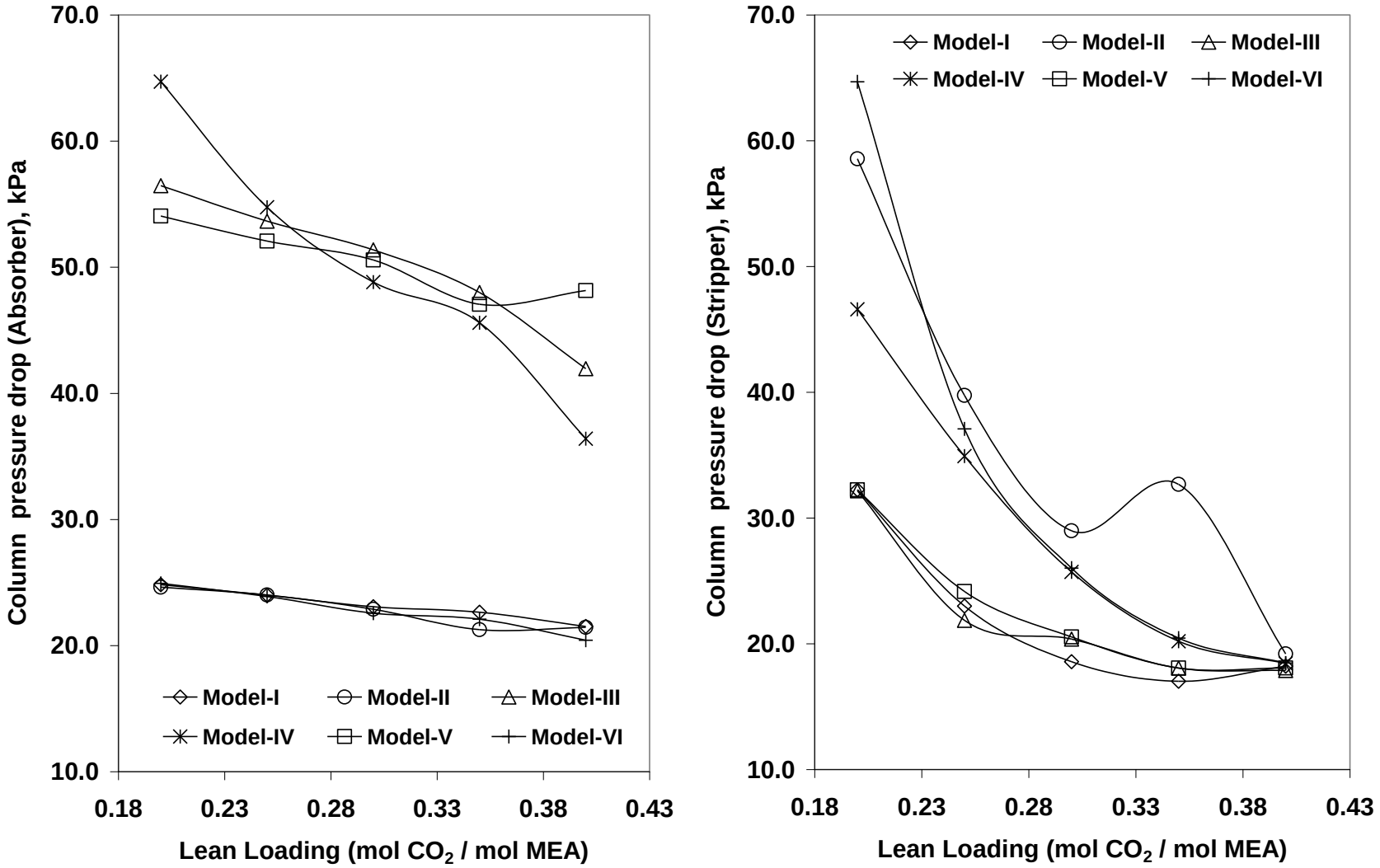

Figure7.20: Total pressure drop in Absorber and Stripper at various lean solvent loadings (CO_2 recovery: 85%; Operational flooding approach: 70%)

7.6.9.1 Absorber profile analysis

RadFrac generates column temperature profile for gas (vapour) and liquid phases and also at interface for the rate-based models. It is always found that the interface temperature is close to the liquid phase temperature. For equilibrium-stage models, usually one temperature profile is generated. For rate-based absorbers with kinetic consideration a lower number of trays is required than that for equilibrium-stage absorbers for meeting same design specifications. Figure 7.21 shows the differences in absorber temperature profiles in gas and liquid phases at CO_2 lean loading of 0.3 for the rate-based models with kinetic reactions consideration in absorber. The slight differences in temperature bulge for Model-I, II & VI be contributed to the reaction schemes and film conditions considered in the stripper model. Model-I has the highest temperature rise in the absorber because of equilibrium reactions in the stripper. Model-II and Model-VI consider kinetic reactions in the stripper without and with film resistance, respectively. The effect of CO_2 lean loading on absorber temperature is presented in Figures 7.22 and 7.23. The temperature profiles are very consistent for rate-based models (I, II & VI) with kinetic considerations and the magnitude of the maximum temperature is in decreasing trend with increasing the lean loading and shifting from column top to middle (Figure 7.22). For equilibrium-stage models (IV, V) and rate-based model (III) with equilibrium reactions, some crossovers are found between the temperature profiles and the highest temperature is observed at the second tray/stage of the column for most lean loadings. Figure 7.23 gives a clearer picture of the absorber temperature profile for all models at each CO_2 lean loading.

The calculated tray pressure drop profile in the absorber for each lean loading reveals that there exists a maximum (Figure 7.24). The maximum tray pressure drop is observed near the top of the absorber for equilibrium–stage based models and in the middle of the column for rate-based models with kinetic consideration at each lean loading. At lower lean loading, it is found that the pressure drop in the tray is higher. It is observed that calculated tray pressure drop in the Absorber varies between 2.5 to 4.0 kPa for rate-based models with kinetics and 4.2 to 9.5 kPa for equilibrium-stage based models.

Figure 7.25 presents mass transfer rate profile of different components across the vapour-liquid film interface in the absorber for rate-based model with kinetic consideration

such as Model-I at different lean loadings. Model-II & VI also have similar profiles (see Appendix G). Positive value indicates mass transfer from vapour to liquid phase. As CO_2 mass transfer rate from vapour to liquid phase is higher near the top of the column, bulk of CO_2 is absorbed near the top portion of the column except for high lean loading (i.e., 0.4) where it occurs in the middle of the column. The interfacial CO_2 mass transfer rate follows the trend of the absorber temperature profile. Therefore, the maximum in the CO_2 mass transfer rate results from a combination of temperature effects on the reaction kinetics, diffusivity and solubility of CO_2.

The reaction rate profiles for CO_2 and MEA in the absorber are presented in Figures 7.26 and 7.27, respectively. One can observe an initial rise in the reaction rates for both components at the top of the column and then a gradual decrease of the reaction rates throughout the rest of the column for the rate-based absorber model with kinetic consideration (Model-I, II, VI). But sharp drop in reaction rates for both components from column top to middle and then very low constant rates for the rest of the absorber are observed in equilibrium-stage absorber models (Model-IV, V) and rate-based absorber model with equilibrium reaction consideration (Model-III). The rate-based absorber models with kinetics calculate reactions in the liquid film and bulk liquid. It is found that all of the CO_2 is reacted in the film for rate-based absorber models with kinetic considerations. The interfacial CO_2 mass transfer rate profiles (Figure 7.25) in absorber are basically the same as the profiles of the CO_2 reaction rate in the film. This suggests that the film reaction dictates the mass transfer rate for CO_2 capture with aqueous MEA which could not be represented with equilibrium-stage models. The reaction rate profiles for other major components are presented in Figures 7.28 to 7.30. Negative value indicates reactant and positive value is for product. Model-II &VI have almost identical profiles as Model-I, and are shown in Appendix H.

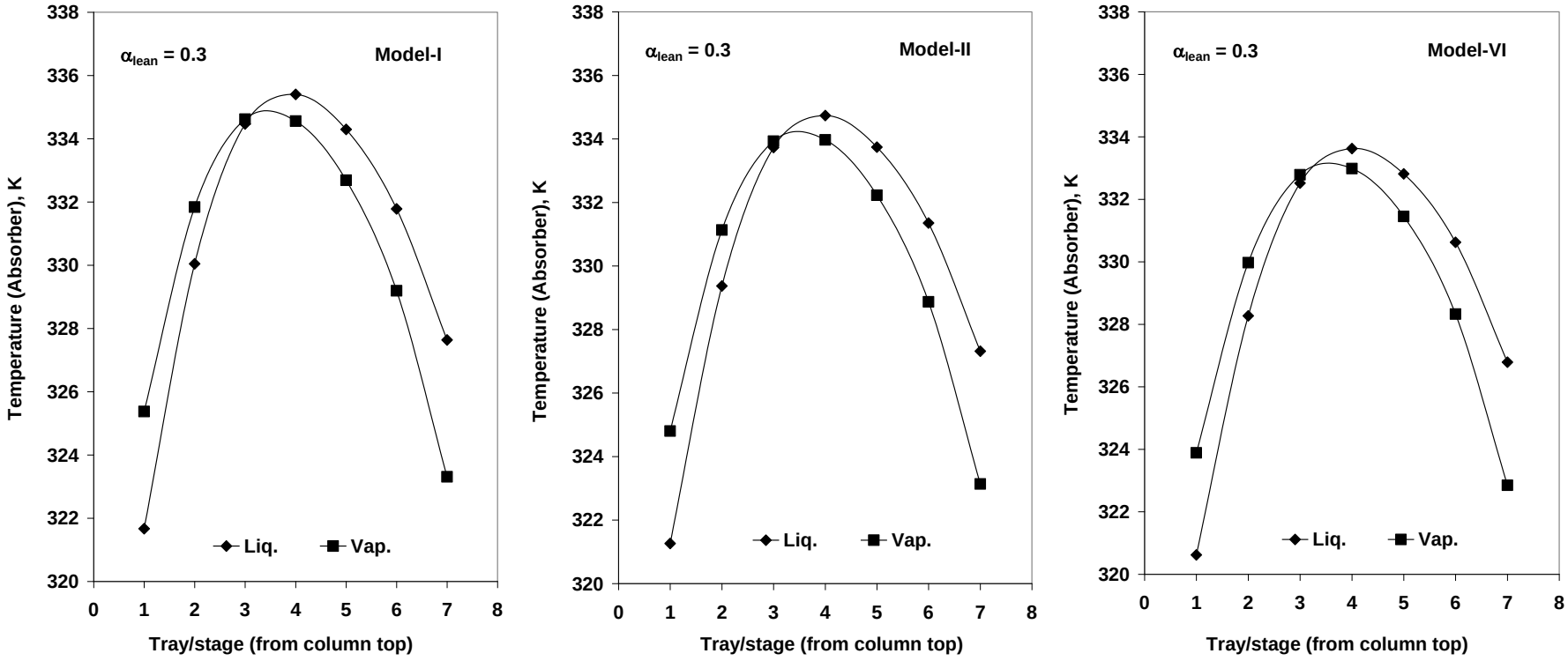

Figure 7.21: Gas and liquid phase temperature profiles in Absorber for Model-I, II and VI (lean loading: 0.3, operational flooding approach: 70% and CO_2 recovery: 85%)

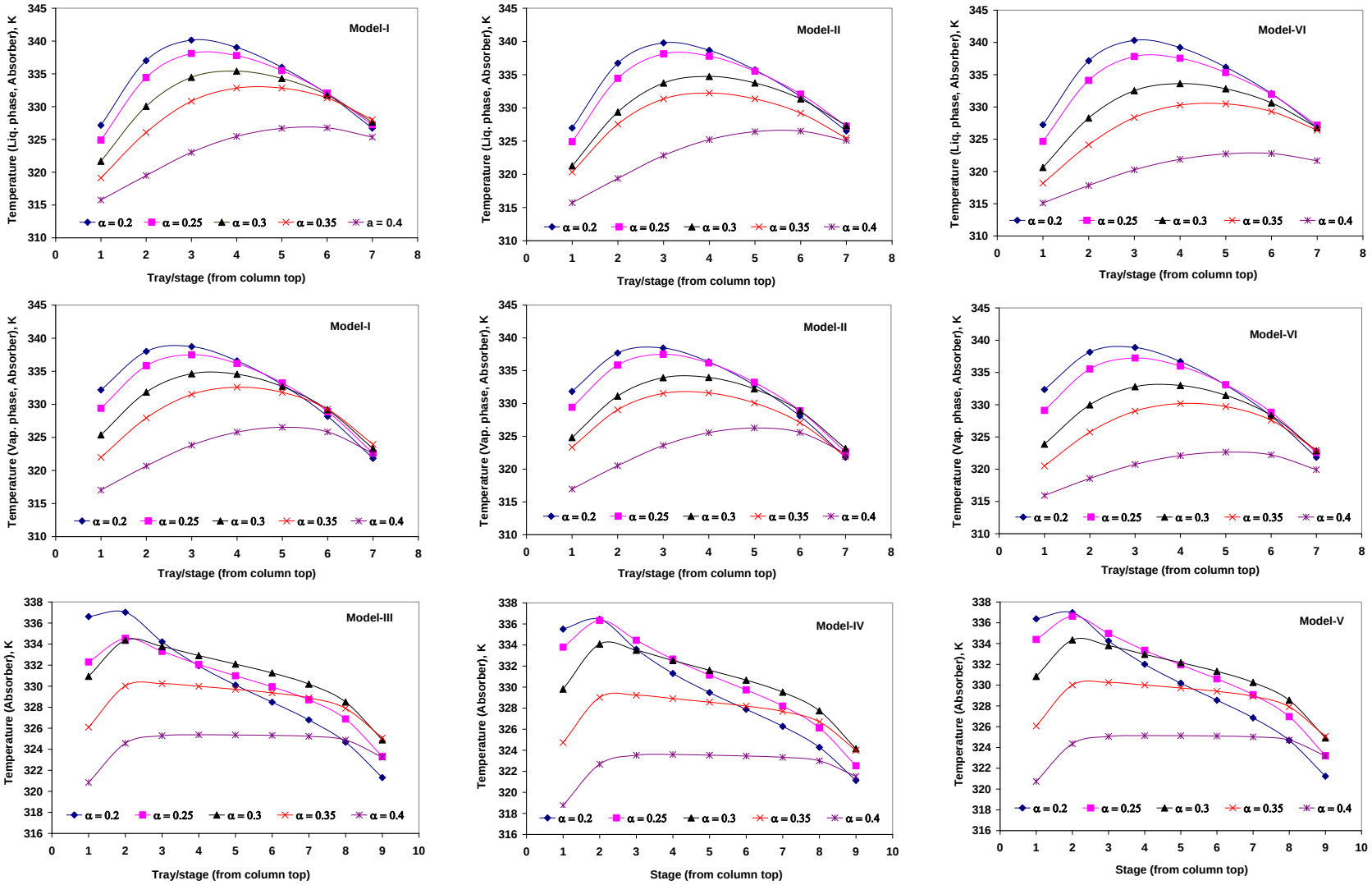

Figure7.22: Effect of lean loading on Absorber temperature for various modeling options (operational flooding approach: 70% and CO_2 recovery: 85%)

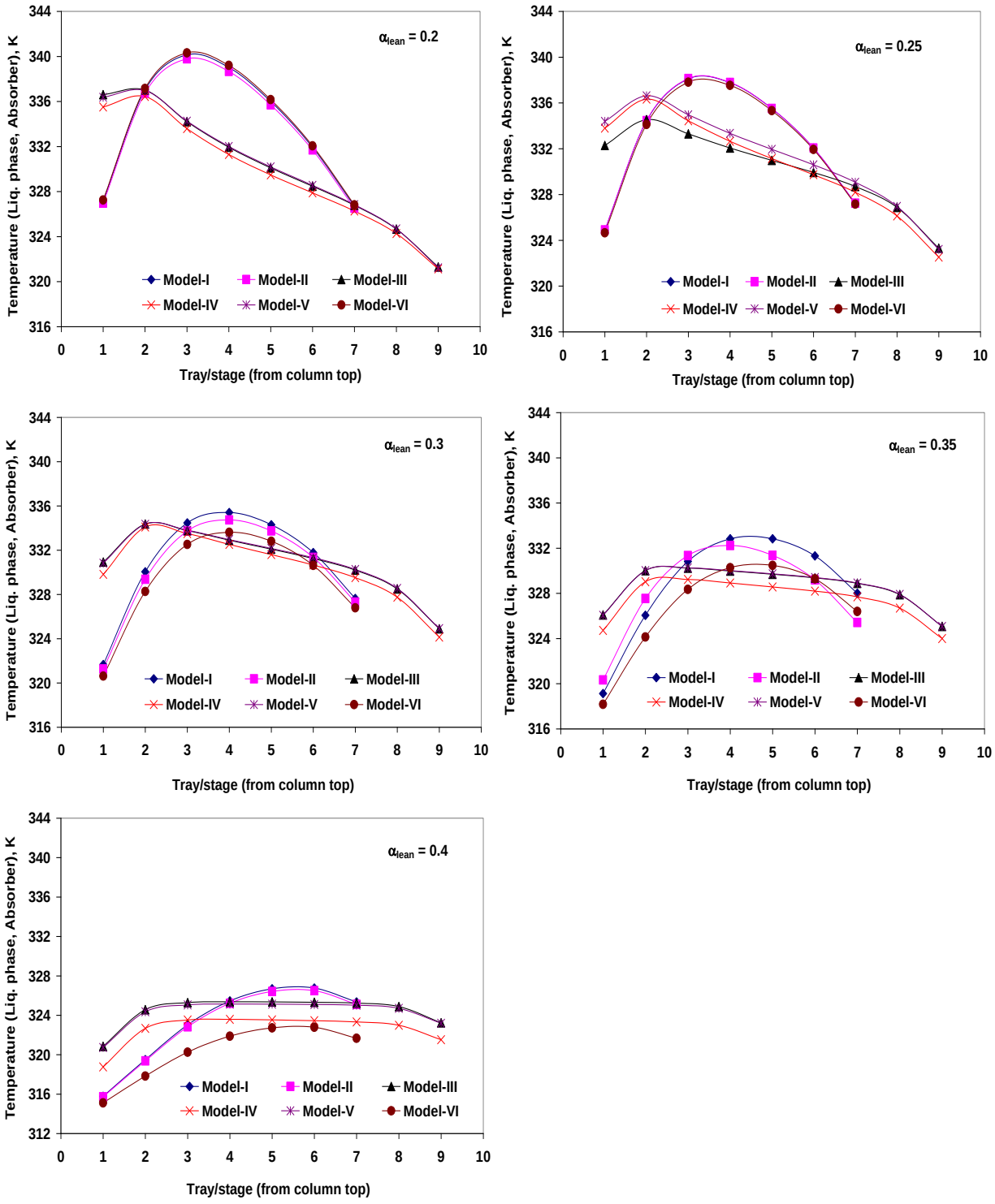

Figure 7.23: Absorber temperature profile for different modeling approaches at a fixed lean solvent (CO_2/MEA) loading (operational flooding approach: 70% and CO_2 recovery: 85%)

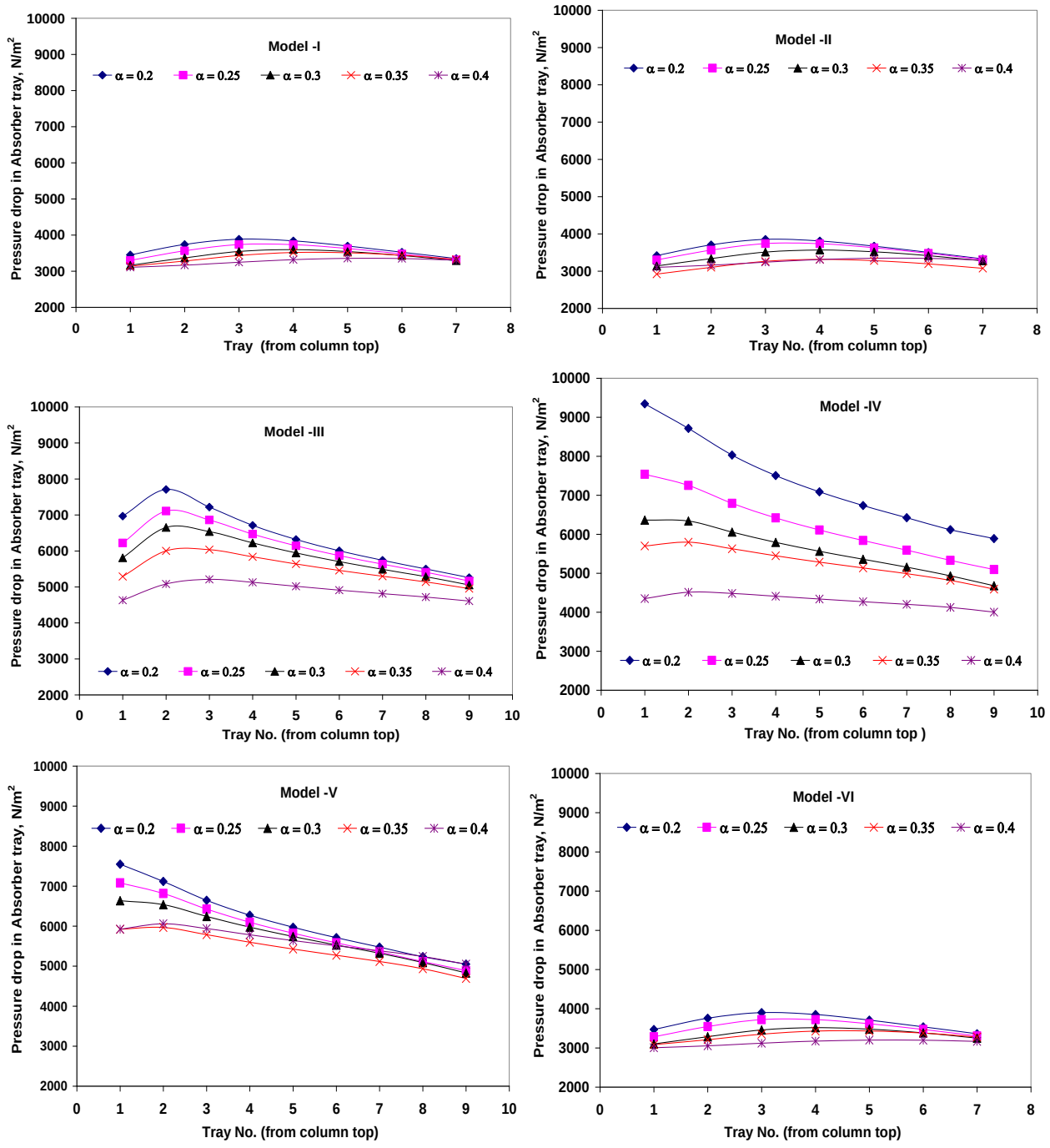

Figure 7.24: Effect of lean solvent loadings on tray/stage pressure drop of Absorber for different modeling options (operational flooding approach: 70% and CO_2 recovery: 85%)

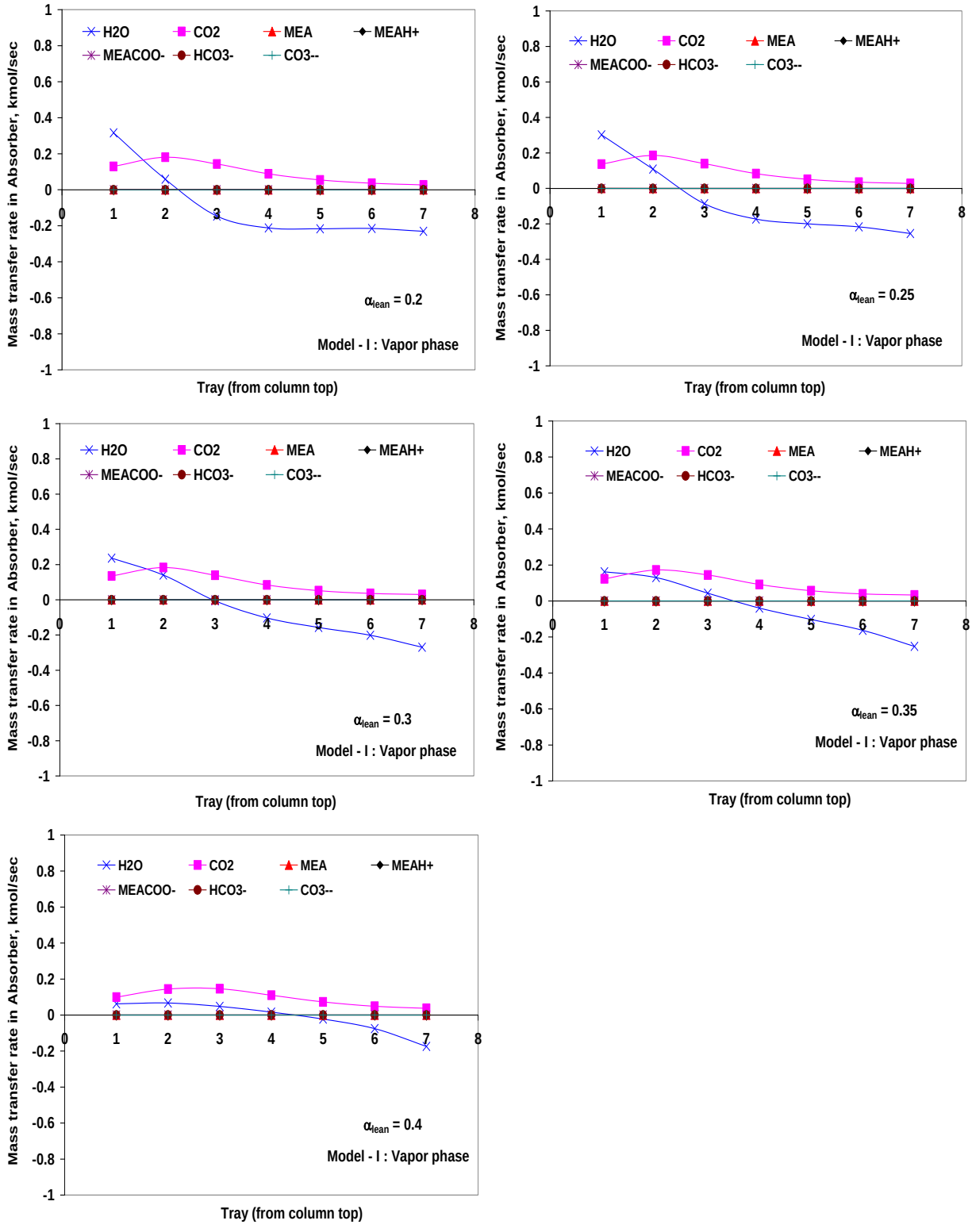

Figure 7.25: Mass transfer rate of different components for vapour phase in Absorber for Model-I at different lean loadings (operational flooding approach: 70% and CO_2 recovery: 85%)

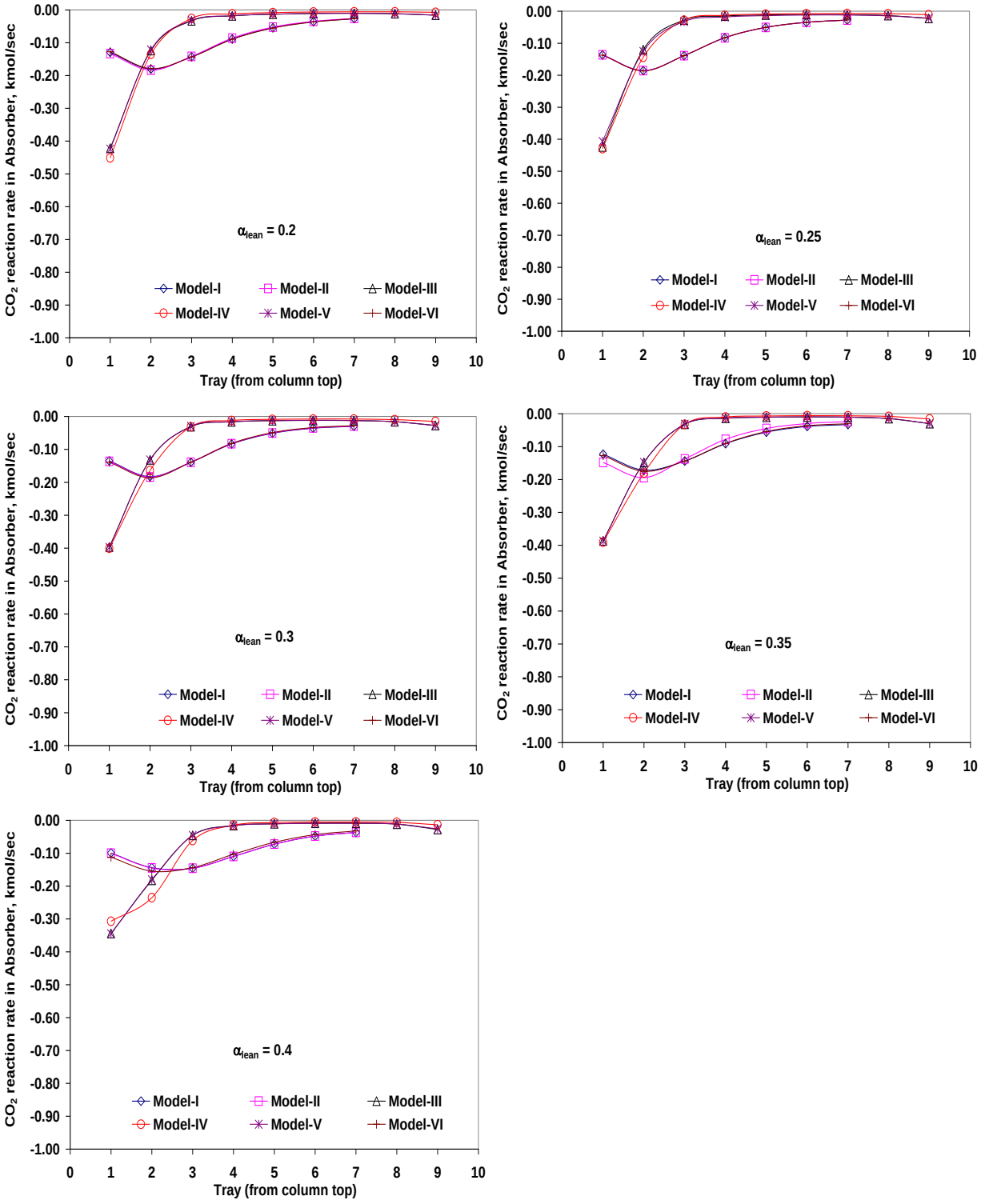

Figure 7.26: CO_2 reaction rate profiles in Absorber at various lean solvent loadings for different modeling options (operational flooding approach: 70% and CO_2 recovery: 85%)

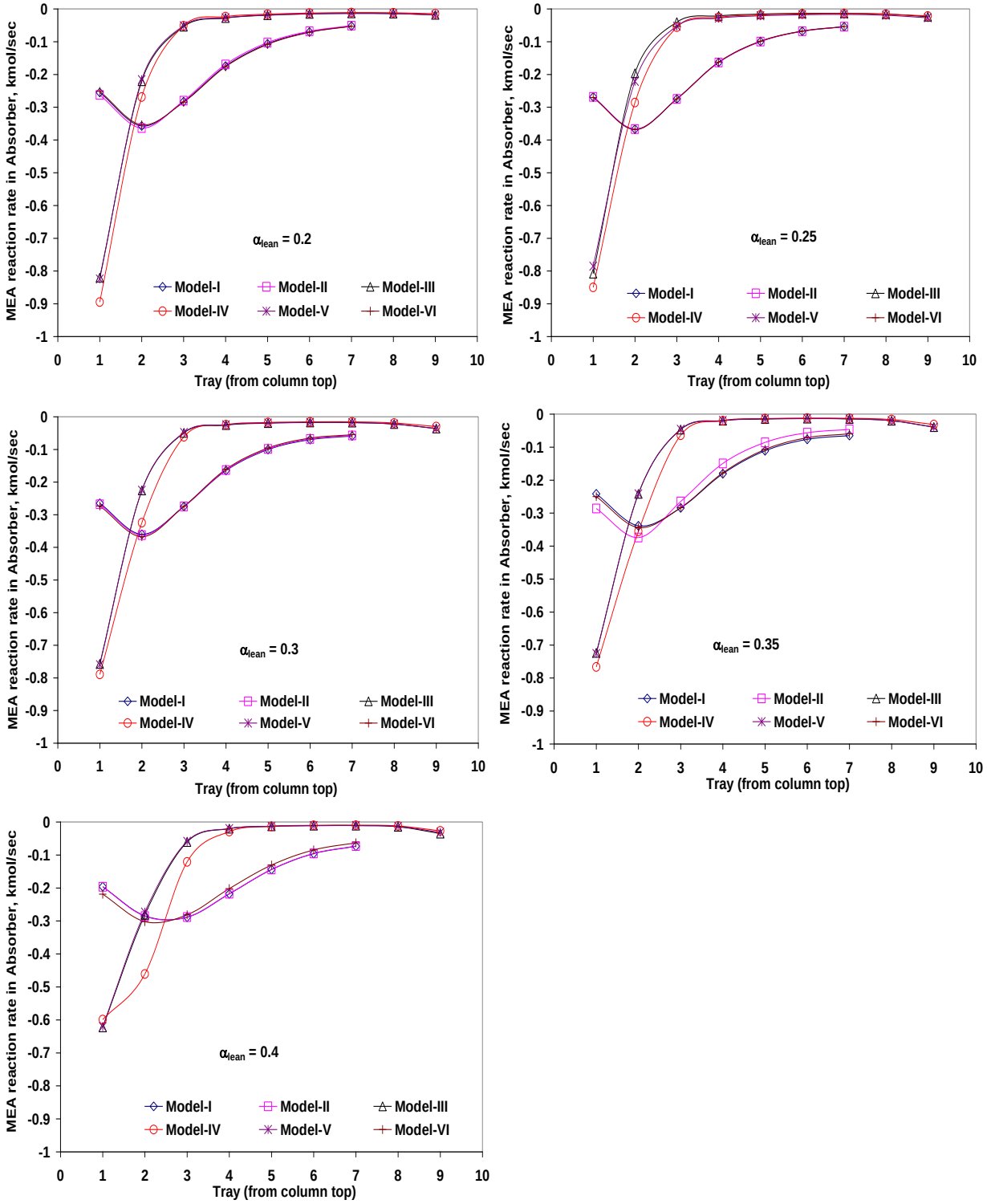

Figure 7.27: MEA reaction rate profiles in Absorber at various lean solvent loadings for different modeling options (operational flooding approach: 70% and CO_2 recovery: 85%)

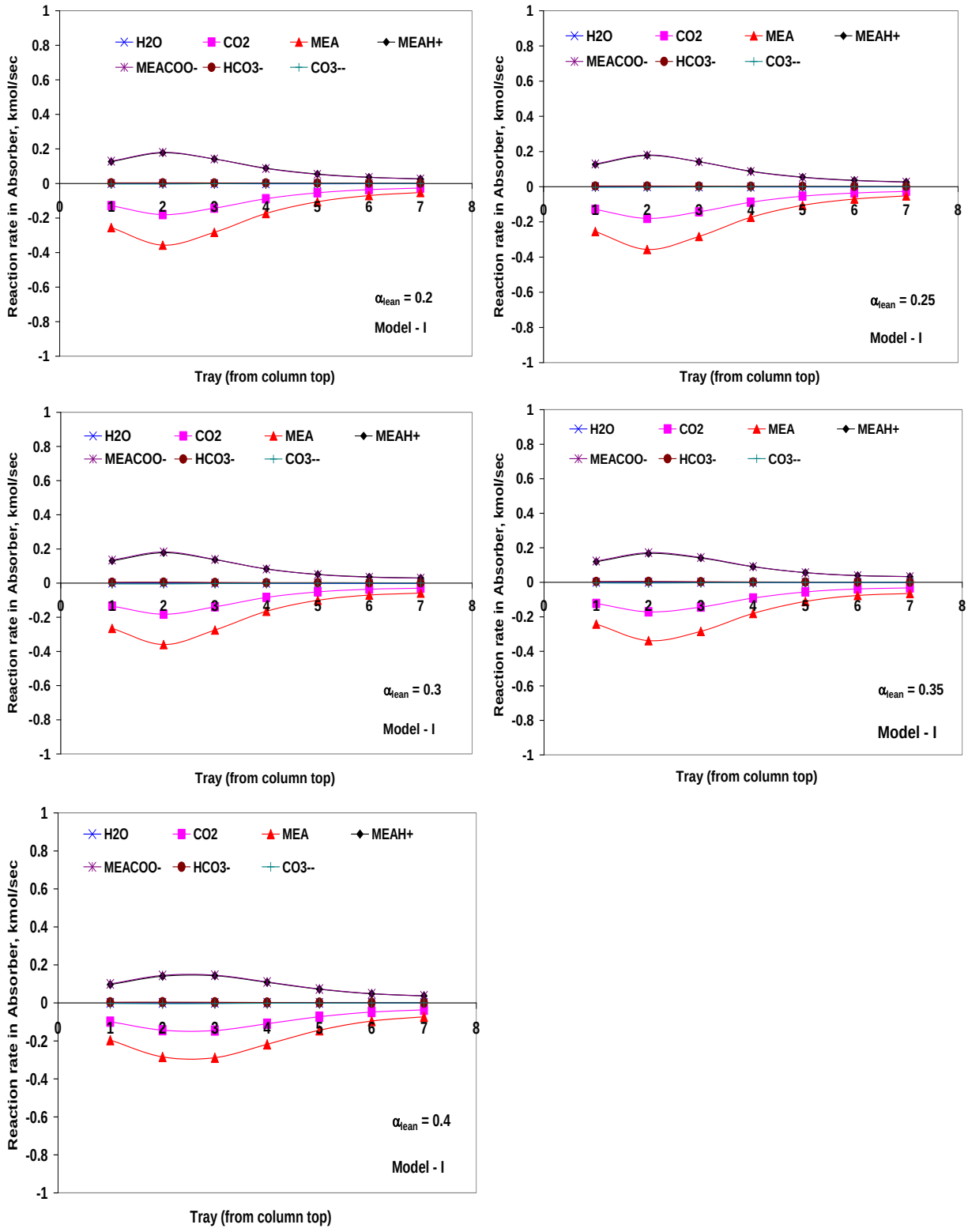

Figure 7.28: Component reaction rate in Absorber for Model-I at different lean loading (operational flooding approach: 70% and CO_2 recovery: 85%)

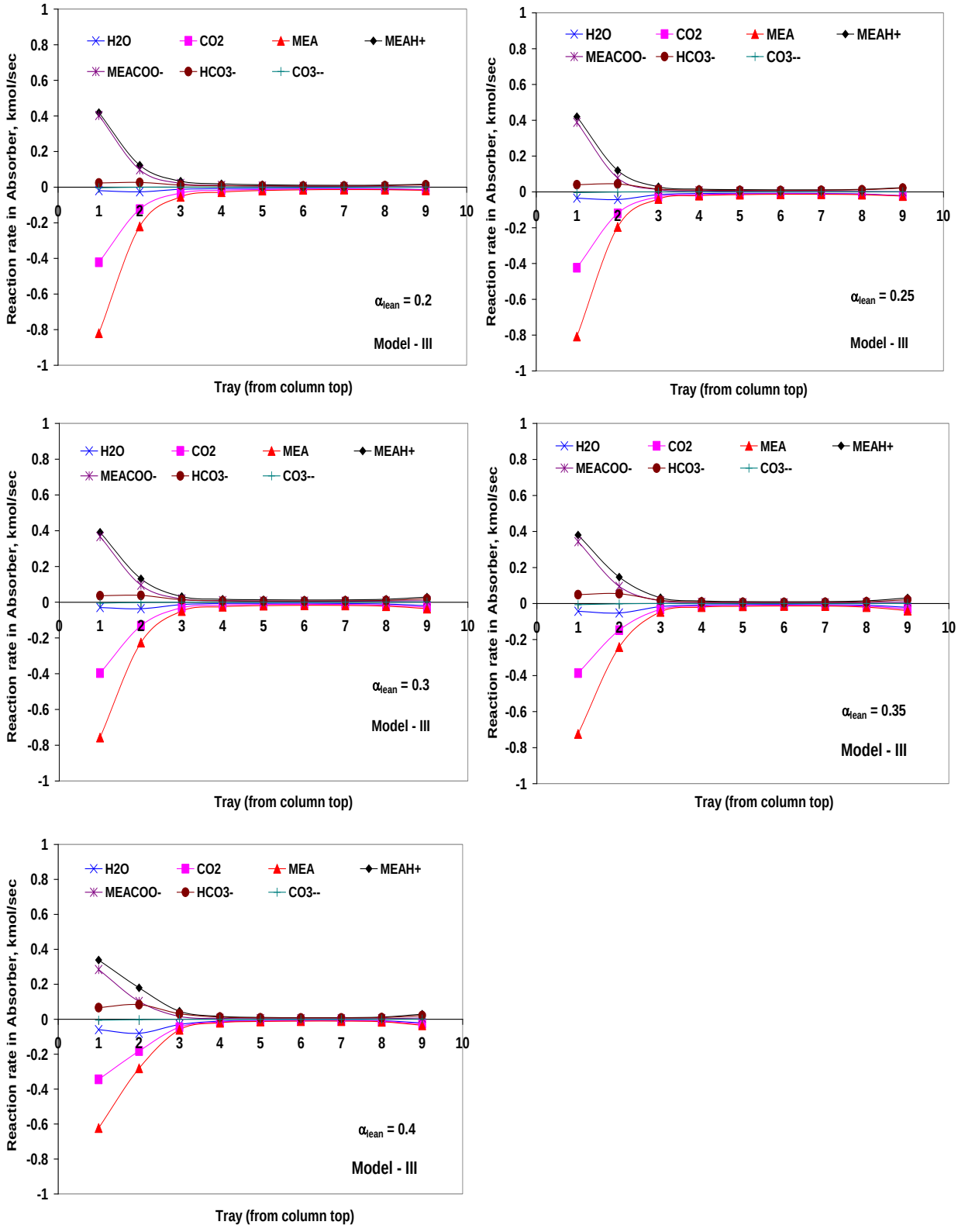

Figure 7.29: Component reaction rate in Absorber for Model-III at different lean solvent loadings (operational flooding approach: 70% and CO_2 recovery: 85%)

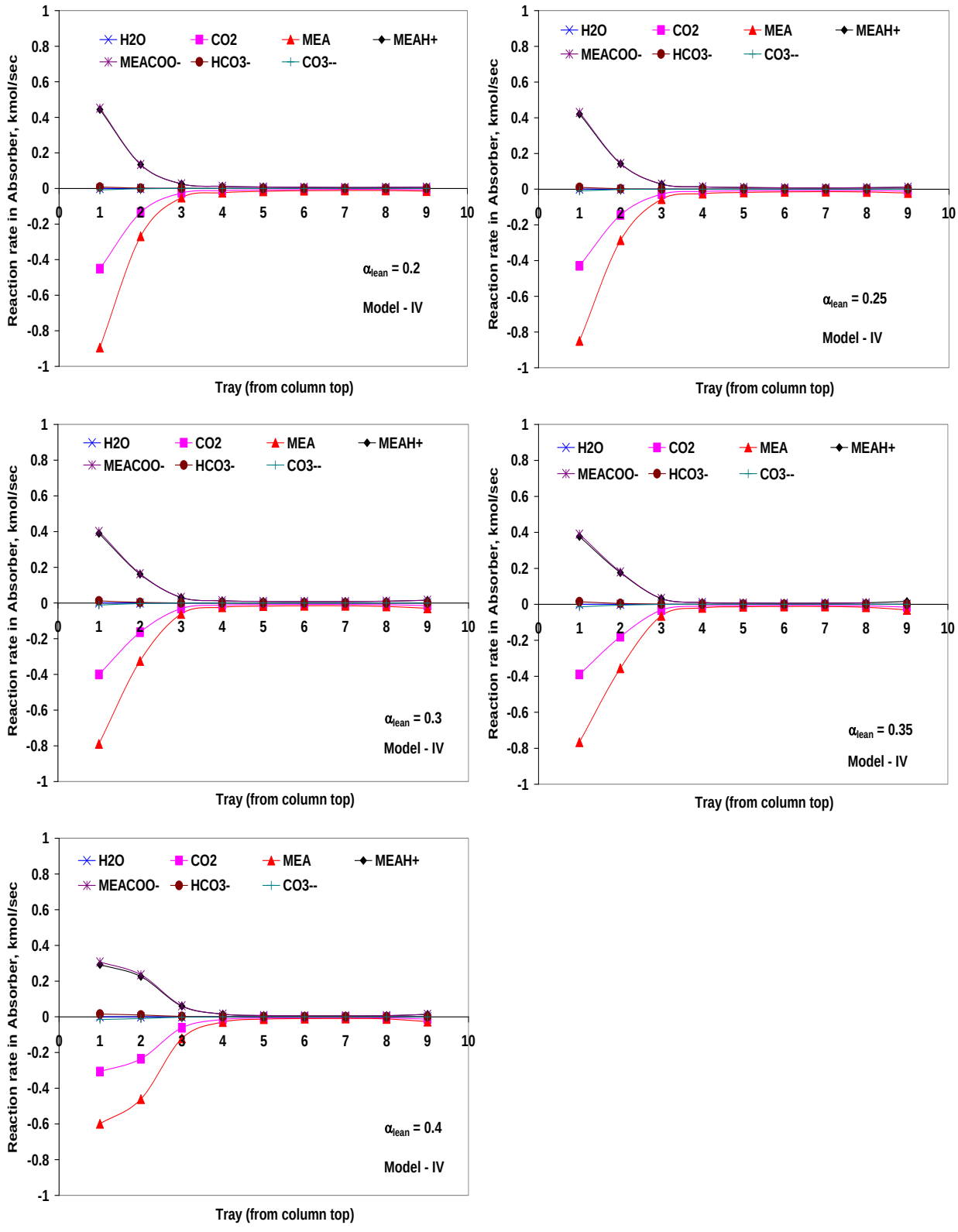

Figure 7.30: Component reaction rate in Absorber for Model-IV at different lean solvent loadings (operational flooding approach: 70% and CO_2 recovery: 85%)

7.6.9.2 Stripper profile analysis

The stripper temperature profiles (Figure 7.31) for all models have similar patterns for all lean loadings studied i.e., monotonously decreasing from bottom to the top of stripper. The lower the lean loading, the higher the temperature profile, with the only exception occurring at a lean loading of 0.35 for Model-II where crossover is detected. Figure 7.32 presents stripper temperature profiles at various lean loadings for both the vapour and the liquid phase for rate-based model (Model-VI) with kinetics and film resistances. The temperature difference between the two phases is quite small which indicate that film resistances are not significant in the stripper. At low lean loading, the tray pressure drop in the stripper is found very significant especially for those models which considered reaction kinetics as shown in Figure 7.33. From the reaction rate profiles of CO_2 and MEA in Figure 7.34 & 7.35, it is observed that both components are acting as reactants instead of products on stripper feed tray for lean loadings greater than 0.3 for the models with kinetics consideration. Figures 7.36 to 7.39 present the reaction rate profiles of all important components for different models at various lean loadings. It is found that the patterns of reaction rate profiles for Model I, III and V are similar due the consideration of only equilibrium reactions. For rate-based stripper models with kinetics and film resistance, mass transfer of major components is investigated and presented in Figure 7.40 for tray section. The mass transfer of CO_2 from liquid phase to vapour phase is almost evenly distributed along the entire stripper column but still with higher rate near the bottom for lean loading ranges from 0.2 to 0.3. For higher lean loading (>0.3) it is found that transfer of CO_2 is also occurring significantly in the opposite direction, i.e., from vapour phase to liquid phase near the top of the column. This phenomenon can be justified from the reaction rate profiles of CO_2 and MEA presented in Figures 7.34 and 7.35 where some reactions involving CO_2 occurred.

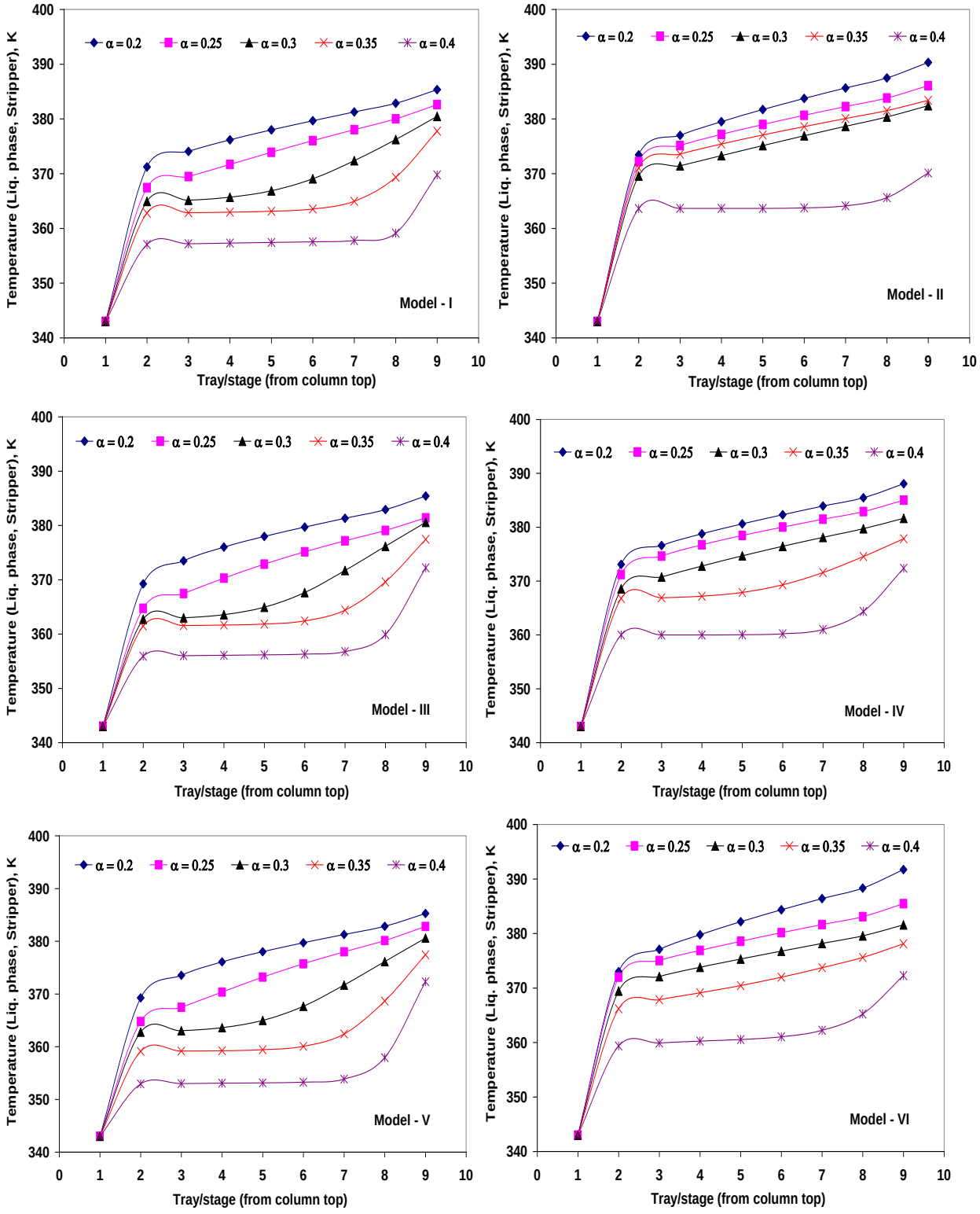

Figure 7.31: Effect of lean loading on Stripper temperature profile for various modeling options (operational flooding approach: 70% and CO_2 recovery: 85%)

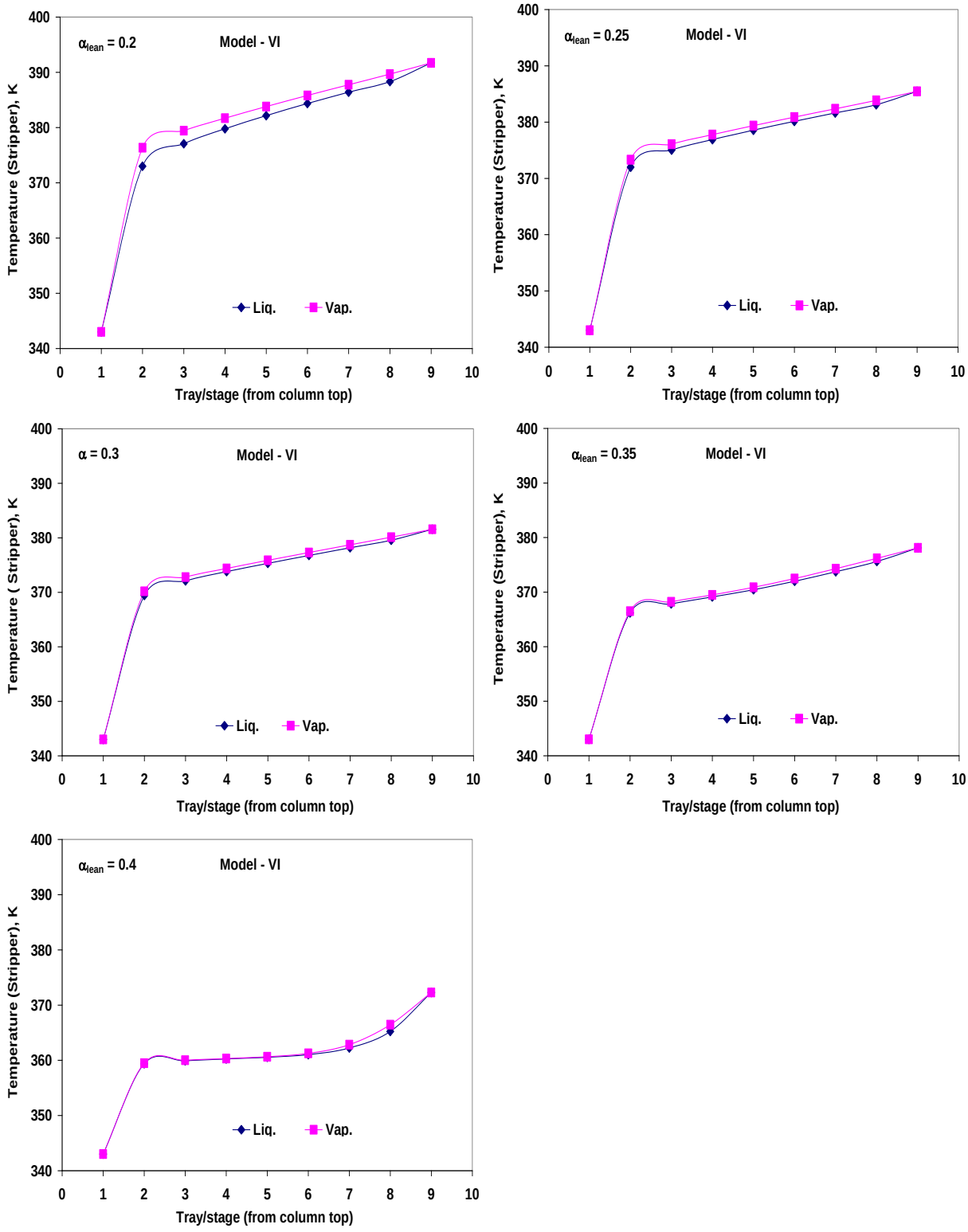

Figure 7.32: Vapour and liquid phase temperature profiles of Absorber for Model-VI at various lean solvent loadings (operational flooding approach: 70% and CO_2 recovery: 85%)

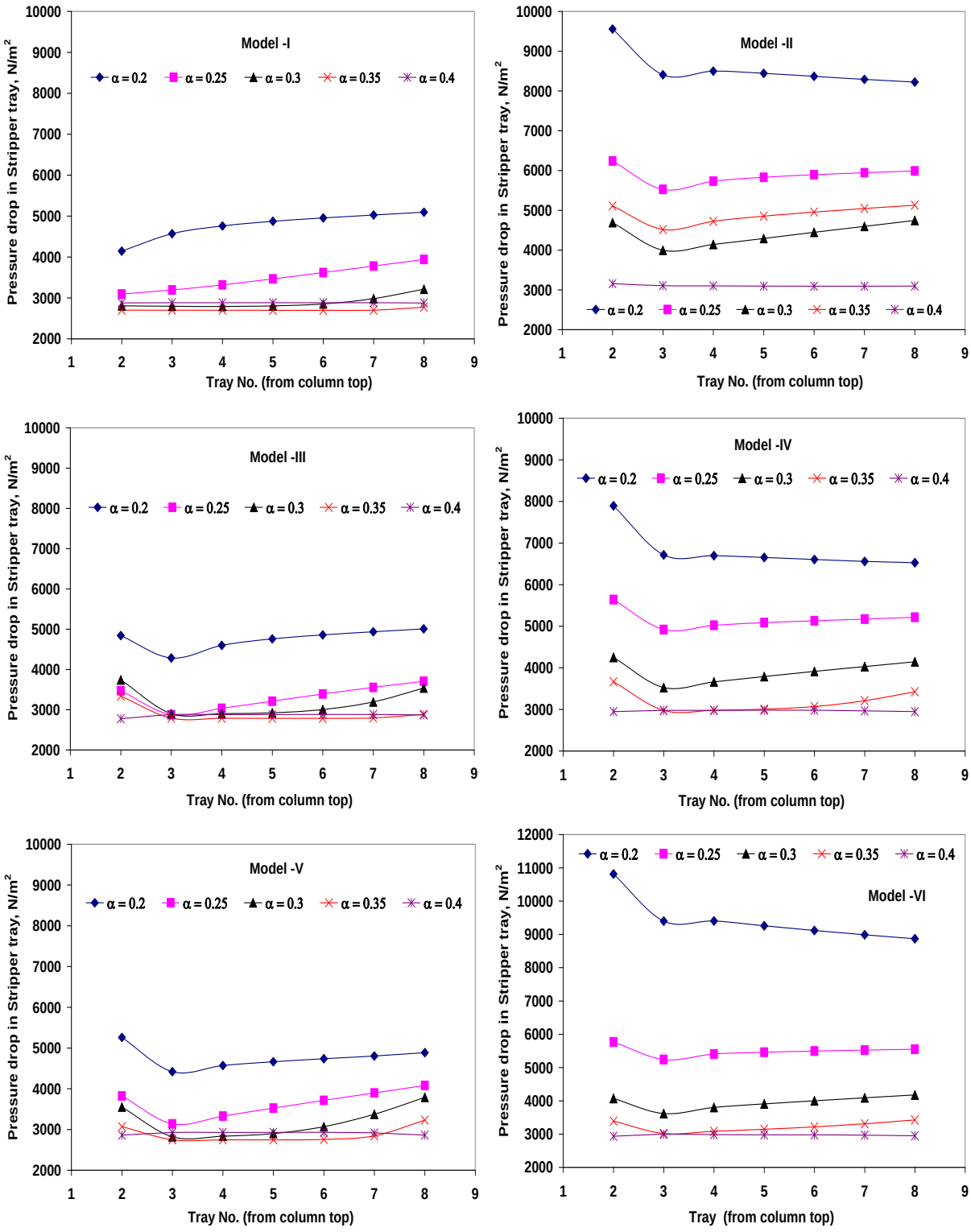

Figure 7.33: Effect of lean solvent loadings on tray/stage pressure drop in Stripper for different modeling options (operational flooding approach: 70% and CO_2 recovery: 85%)

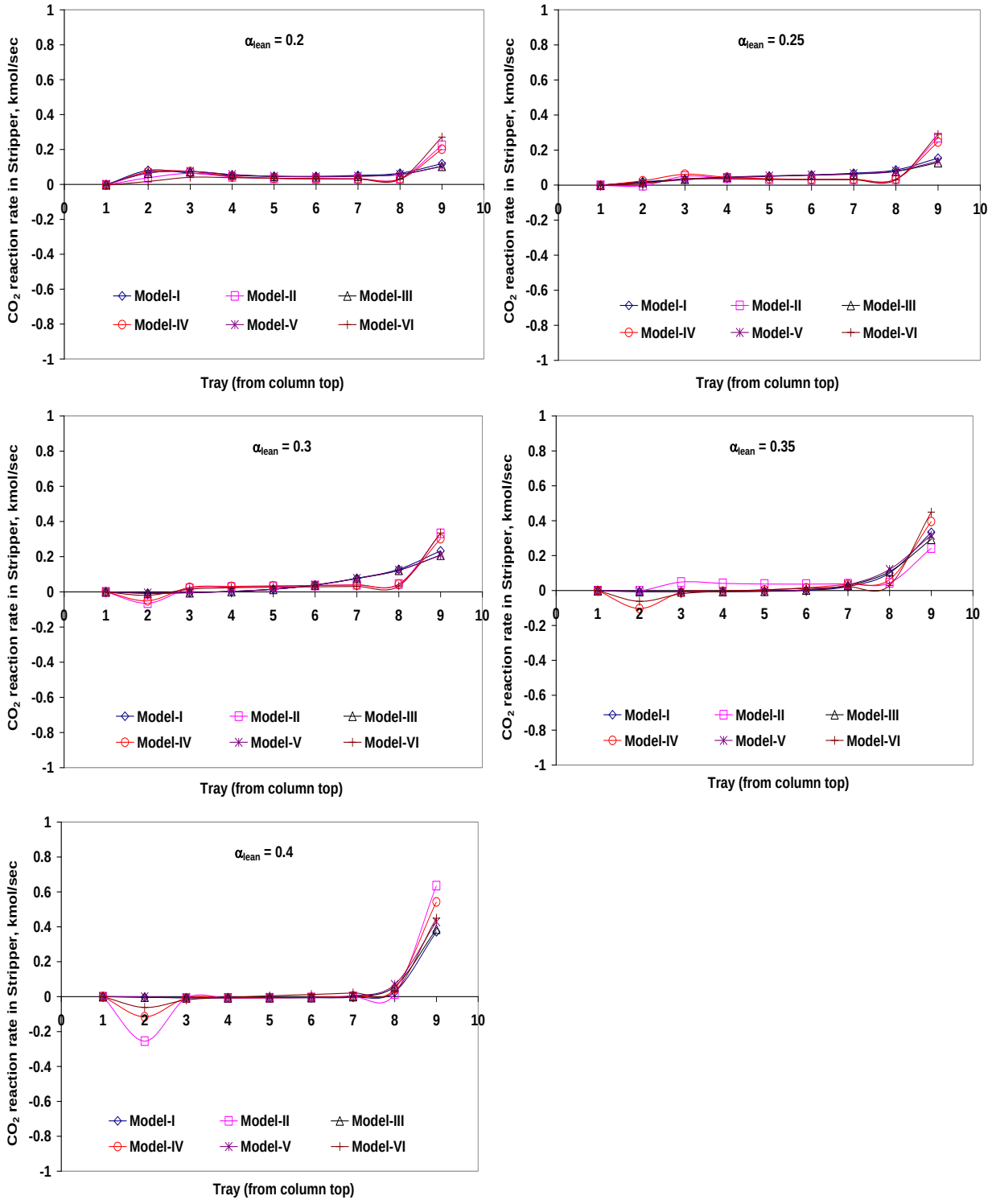

Figure 7.34: CO_2 reaction rate profiles in Stripper at various lean solvent loadings for different modeling options (operational flooding approach: 70% and CO_2 recovery: 85%)

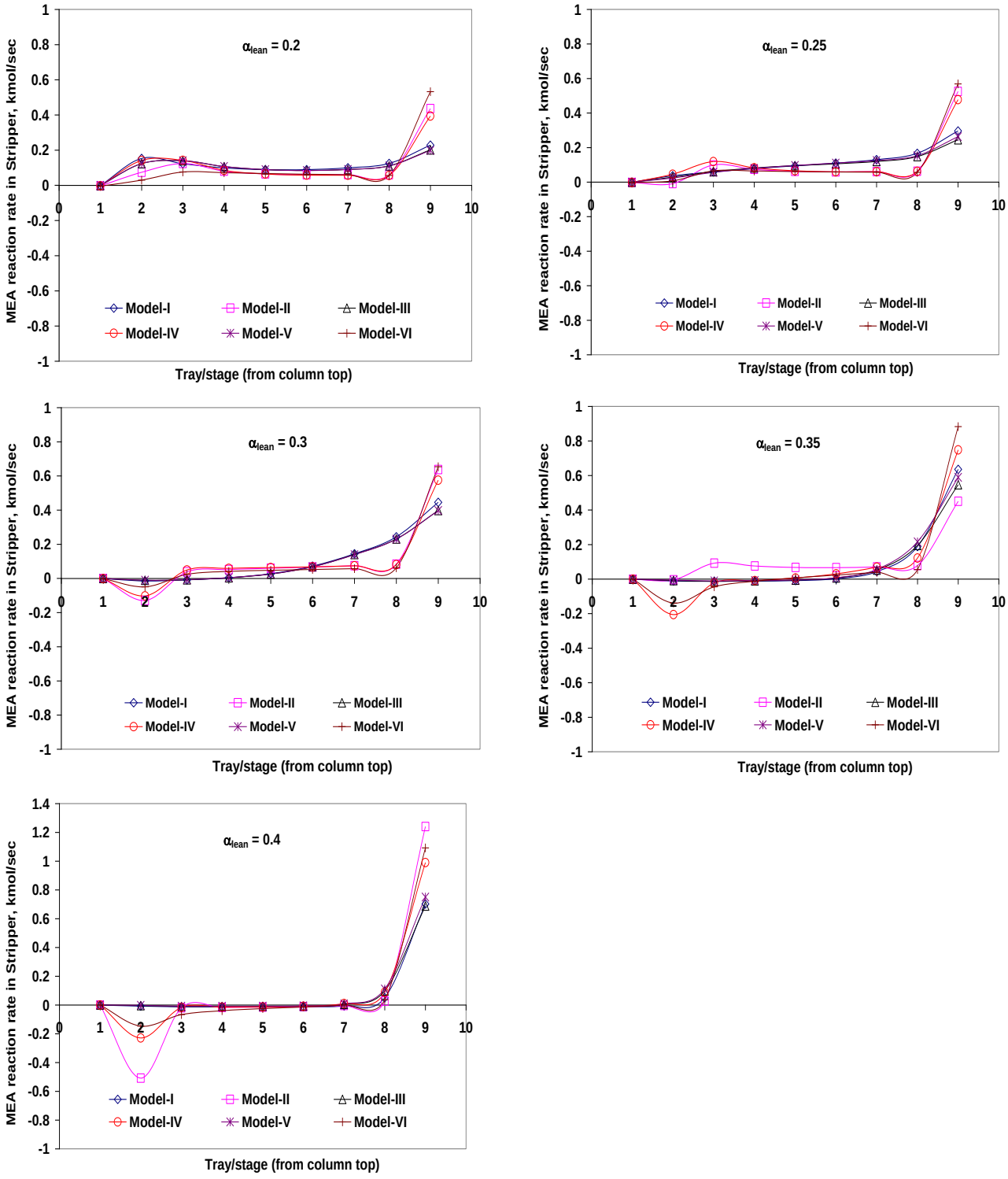

Figure 7.35: MEA reaction rate profiles in Stripper at various lean solvent loadings for different modeling options (operational flooding approach: 70% and CO_2 recovery: 85%)

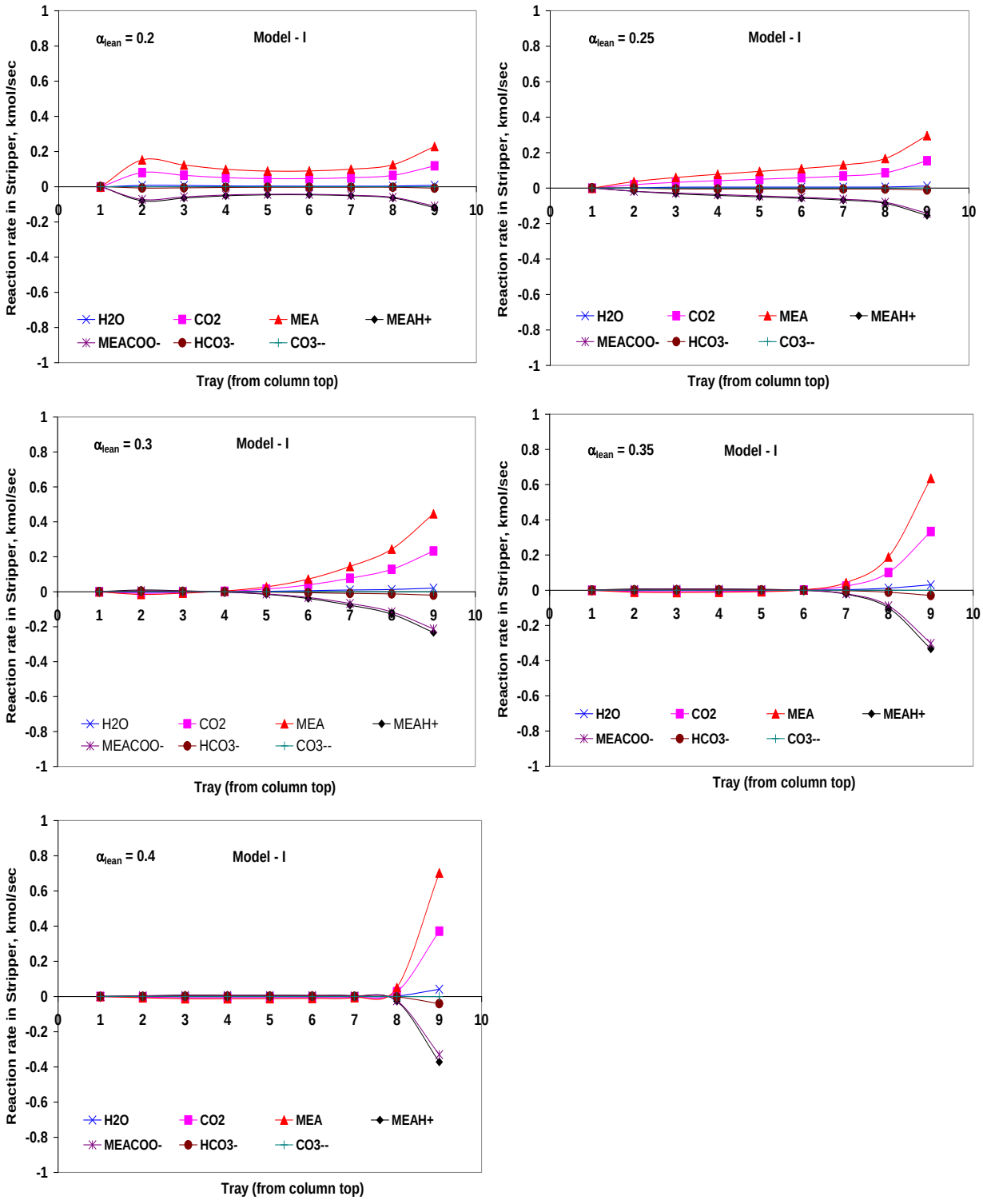

Figure 7.36: Component reaction rate in Stripper for Model-I at different lean solvent loadings (operational flooding approach: 70% and CO_2 recovery: 85%)

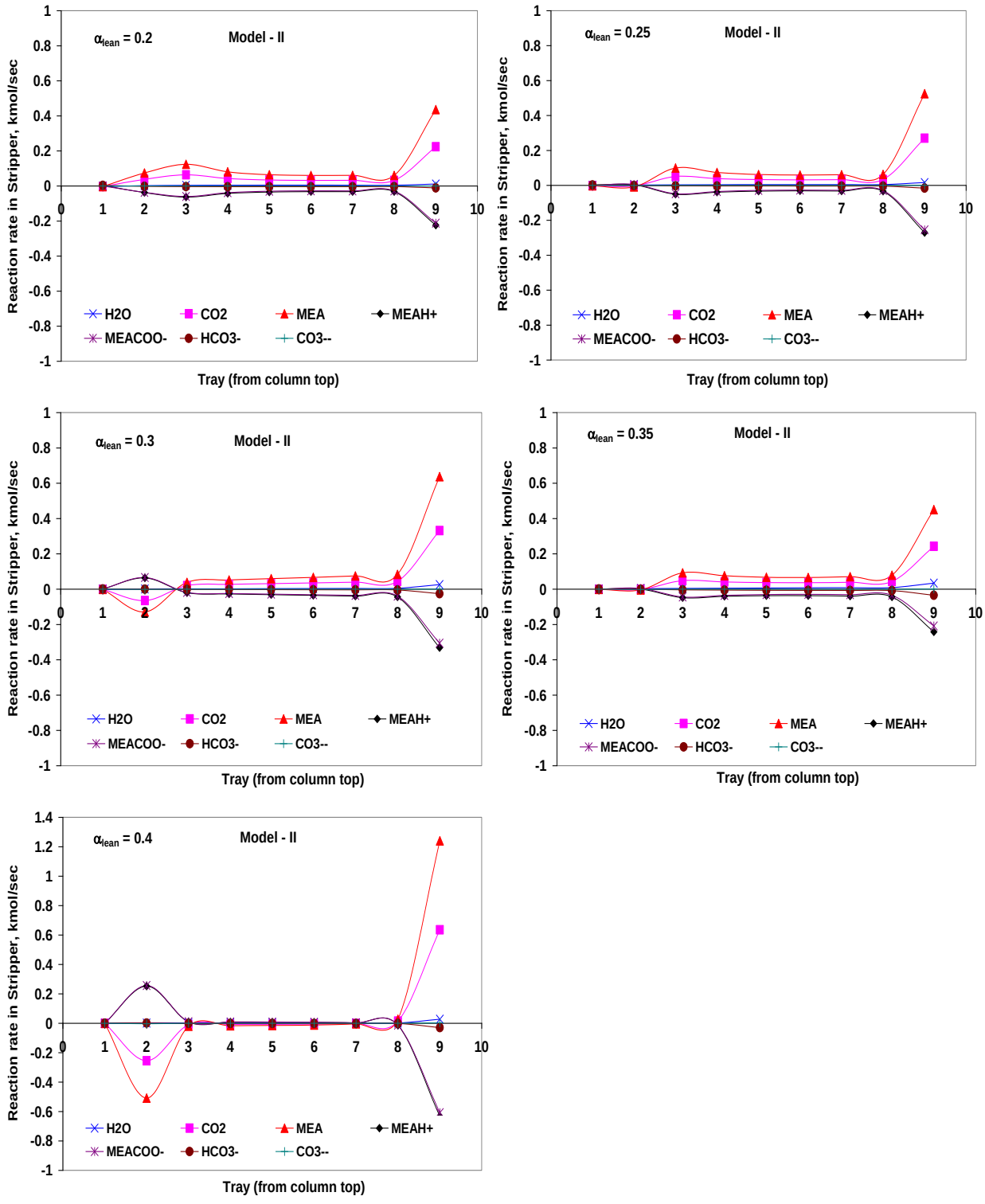

Figure 7.37: Component reaction rate in Stripper for Model-II at different lean solvent loadings (operational flooding approach: 70% and CO_2 recovery: 85%)

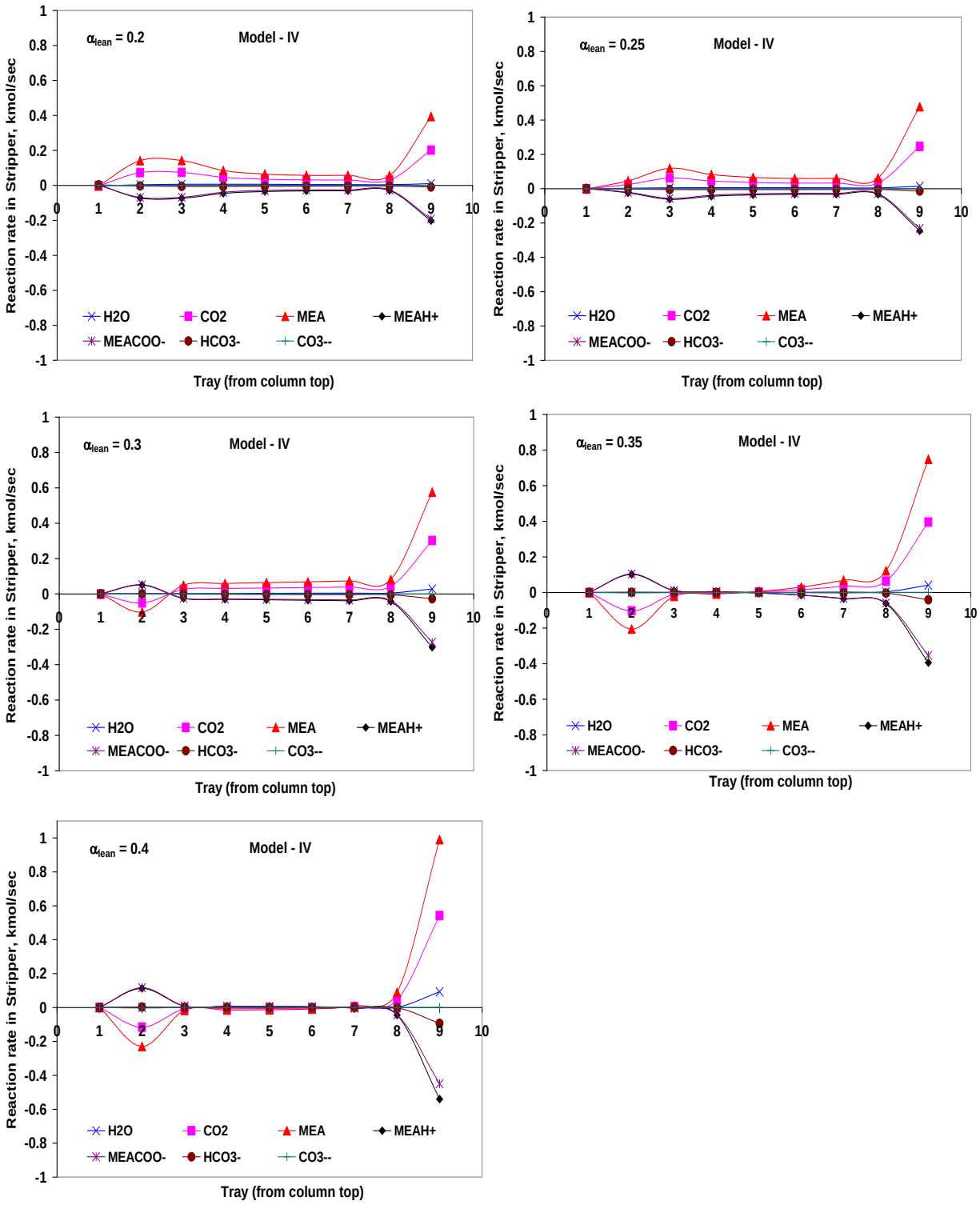

Figure 7.38: Component reaction rate in Stripper for Model-IV at different lean solvent loadings (operational flooding approach: 70% and CO_2 recovery: 85%)

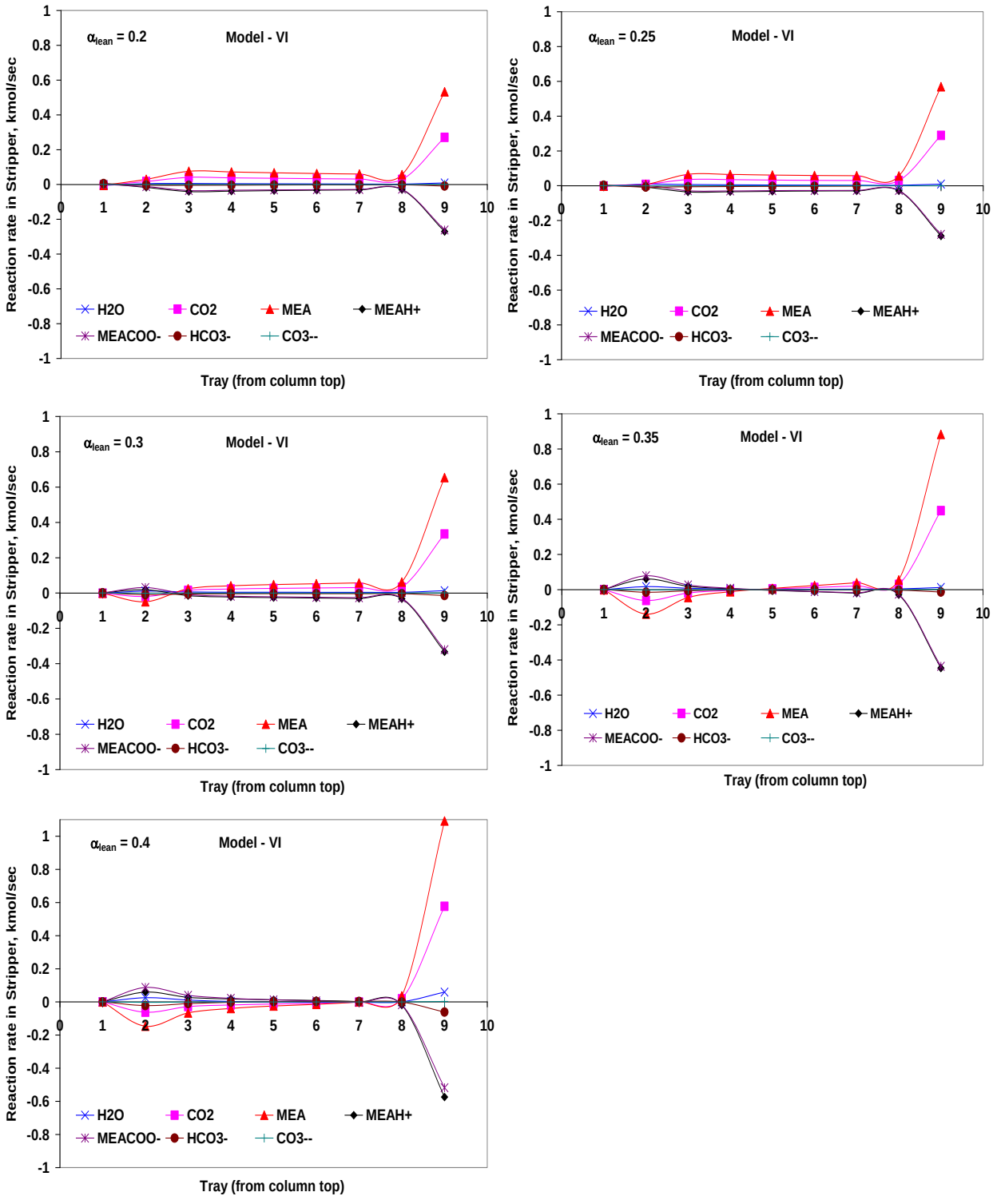

Figure 7.39: Component reaction rate in Stripper for Model-VI at different lean solvent loadings (operational flooding approach: 70% and CO_2 recovery: 85%)

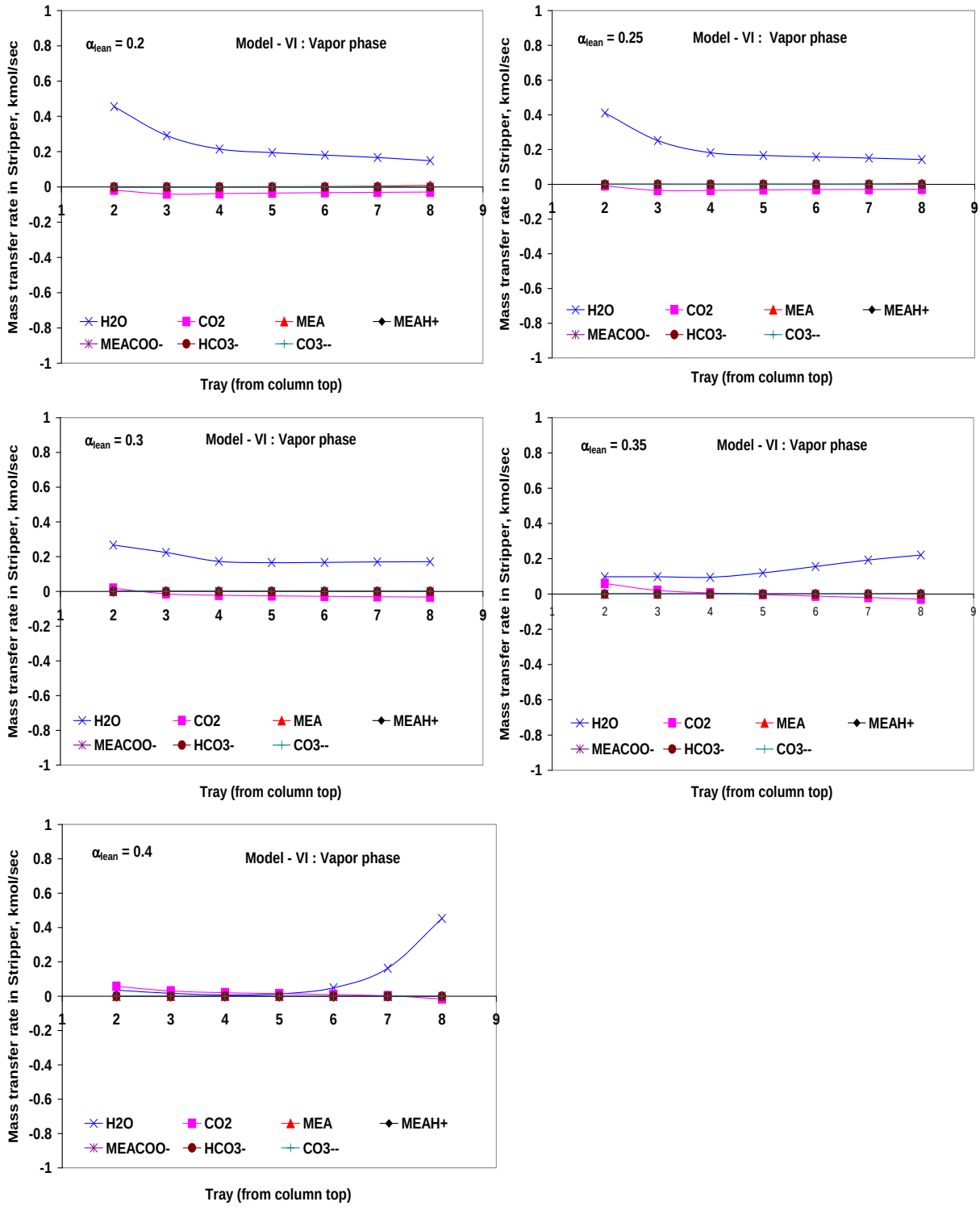

Figure 7.40: Mass transfer rate of different components in Stripper for Model-VI at different lean loading (positive for mass transfer from vapour to liquid)

7.6.10 Processes Comparison

All the results presented above are based on the conventional (base) MEA process flowsheet as illustrated in Figure 7.1. Table 7.30 present a comparison between the conventional process (Figure 7.1) and the Fluor process (Simmonds et al., 2003) shown in Figure 7.2 using Model-VI. This rate-based model considers kinetics for both the absorber and stripper with diffusion resistances and reactions in film for liquid phase, and diffusion resistances in film for gas phase. The base process uses four trains, and each train has one Absorber and one Stripper. The Fluor process has two trains, and each train uses two Absorber and one Stripper, simultaneously. Two design cases were considered for Fluor process. The difference between these two design cases is mainly the consideration of different number of downcomers in the tray of the stripper. Both design cases of Fluor process exhibit lower energy requirement compare to the conventional process. It is found that downcomer flooding level is significantly reduced from 65% to 51% by just increasing the number of downcomers in the tray by one. This increase of downcomer number is accompanied by only a slight increase in column diameter of the stripper. Therefore, from an operational and energy requirement (8.5% less energy) point of view design-II of the Fluor process is the preferred MEA process for CO_2 capture from power plant flue gas. The other advantage of the Fluor process over the base process is the lower number of strippers required which might reduce the plant capital cost significantly.

Table 7.30: Comparison of Base process with Fluor Ltd. process (lean loading: 0.3; CO_2 recovery: 85%; Operational flooding approach: 70%)

Model-VI	**Base** Process	**Fluor** Concept	
		Design-I	Design-II
Absorber			
No of Trays (sieve)	9	9	9
No. of pass (i.e., downcomers)	2	2	2
Tray spacing, m	1.7	1.7	1.7
Column diameter, m	5.7	5.7	5.7
Downcomer flooding, %	55	55	55
Stripper			
No of Trays (sieve)	9	9	9
No. of pass (i.e., downcomers)	**2**	**2**	**3**
Tray spacing, m	1.7	1.7	1.7
Column diameter, m	**4.7**	**6.5**	**6.7**
Downcomer flooding, %	**51**	**65**	**51**
Reboiler duty (total), MWth	**659.6**	**599.9**	**603.8**

7.7 Summary

Two different MEA-based absorption/striping process configurations were examined. One is a conventional and the other is a Fluor concept (Simmonds et al., 2003). The conventional process uses four trains, and each train has one absorber and one stripper. The Fluor process has two trains, and each train uses two absorbers and one stripper, simultaneously. Both configurations were examined to simulate and design industrial scale post combustion CO_2 capture process for flue gas stream of 500MW power plant, using AspenPlus. Aspen RadFrac model which supports both the equilibrium-stage and rate-based approach for modeling the absorption/stripping system was employed in this study. Eight different models were categorized for the absorption/stripping system based on the options to account for mass transfer, and the chemical reactions in the liquid phase. Simulation and design results from those models were investigated and compared in details. The convergence of the MEA process flowsheet was found very challenging and difficult due to the highly nonlinear nature of the process and the involvement of a recycle stream. Trying to meet some other realistic concerns such as maintaining downcomer flooding level on the tray ($\leq$ 50%), total pressure drop in the tray column ($\leq$ 40 kPa) and stripper reboiler temperature ($<$ 120°C) within industrial norm and practice, have added extra convergence challenges to the process simulation. In spite of that, all simulation and design results presented in this chapter are based on closed-loop flowsheets. Without closed loop simulation, the proper estimation of the actual amount of make-up water and MEA needed to maintain the design concentration of MEA solution in the system due to water and MEA vapour losses.

Two kinetic models for modeling reactive absorption/stripping process for CO_2 capture by aqueous MEA solution were investigated, one is consists of two kinetic reactions (Table 7.4) and the other has four kinetic reactions (Table 7.5). It was found that the later kinetic model does not need a large interfacial area factor multiplier for calculating interfacial area as does the previous model.

The effects of approach to flooding and the tray pass on column sizing and column stable operation for reactive absorption/stripping system were investigated. Multi-pass trays were found suitable for maintaining proper liquid inventory on the tray. The effect of temperature approach

specification in lean/rich heat exchanger on stripper design and overall process performance was also investigated.

In the rate-based absorption modeling with reaction kinetics, the effects of film discretization on modeling of mass transfer resistance and the chemical reactions taking place in the liquid film were investigated in details. For systems in which there are rapid reactions, it is necessary to discretize the film properly in order to accurately account for the amount of reaction in the film. If the reaction is very fast and the film is not discretized, then RateSep will calculate the reaction in the film based on the concentration at the interface. This will be higher than the actual film reaction and hence will not accurately model the system. It was realized that the success of modeling CO_2 capture with MEA depends upon how the film discretization is carried out.

In equilibrium-stage modeling, the Murphree efficiency for stages was specified to account for departure from equilibrium. It was found that a decrease of Murphree efficiencies for column stages increased column size and reboiler energy requirement, as expected.

In RadFrac, for the column without reboiler the pressure drop for the last stage is not used normally, because there is no stage below to receive the updated pressure. A workaround was implemented to allow the pressure drop to be applied appropriately.

The CO_2 loading in the lean solvent was optimized in a closed-loop simulation environment using six different models by varying the lean solvent flow rate to achieve the same CO_2 removal capacity (85%) to obtain minimum energy requirement for reboiler in the stripper. It was found that the optimum lean solvent loading ranges from 0.29 to 0.36 for most of the models, and the reboiler energy ranges from 3.3 to 5.1 GJ/ton CO_2 captured depending on the model considered.

Tray spacing ranges from 1.4m to 1.8m for the absorber, and 1.6m to 1.9m for stripper for all the simulation runs. This variation was the result of fine tuning the downcomer flooding level. The calculated column diameter was found to be between 5.0 m to 8.0 m for absorber, and 4.0 m to 6.8 m for stripper. The number of trays/stages considered for the absorber were 7 and 9, and for stripper 9.

Finally, a comparison was presented between the two process alternatives and it was found that Fluor concept process is the preferred one in terms of plant operating (i.e., lower energy requirement) and capital cost (i.e., fewer number of stripper needed).

Chapter 8

Hybrid Process Simulation and Design for Post-combustion CO_2 Capture in AspenPlus®

8.1 Introduction

There are many hybrid systems currently operating around the world for treating natural gas. Several EOR projects in West Texas employ a combination of membrane and amine technologies to recover CO_2 and hydrocarbons in the gas (Echt, 2002). Economic viability of hybrid processes combination of membrane permeation and amine technologies for the removal of acid gases (i.e., CO_2 & H_2S) from crude natural gas have been investigated by some researchers (McKee et al., 1991; Bhide et al., 1998; Echt, 2002). In general, high CO_2 content of a gas is a good indicator for the use of membranes and/or hybrid systems. The CO_2 content in EOR plants is extremely high, 70% or more (Echt, 2002). McKee et al. (1991) reported that hybrid systems can be economical when CO_2 concentrations are lower than those found in EOR applications using a feed stream of moderate flow rate and no H_2S. Bhide et al. (1998) also conducted a process design and economic assessment study for a hybrid process for sweetening crude natural gas. In a two-in-series arrangement, membrane separation was used first for the bulk removal of the acid gases while final purification to pipeline specifications was done by gas absorption/stripping process using diethanolamine. The effects of several factors such as feed conditions and compositions, cost of lost methane, membrane replacement cost, etc. on the cost of acid gas removal were examined. Mixed findings were reported for the hybrid process depending on the feed stream conditions and compositions considered. Echt (2002) reported substantial cost benefits of hybrid systems for processing large volume of natural gas from a techno-economic analysis. Conditioning of a high-pressure gas with a high concentration of CO_2 to the pipeline specification is a very good candidate for using a hybrid system consisting of a membrane unit followed by a solvent unit. Hot potassium carbonate and amine were used as solvents.

The potentialities of a hybrid process combining oxygen enriched air combustion and membrane separation for post-combustion carbon dioxide capture for a natural gas power plant were investigated through a simulation study from an energy requirement point of view (Favre et al., 2009). The cryogenic oxygen production process for the upstream part was employed. It was reported that the hybrid process can lead to a 35% decrease of the energy requirement compared to oxycombustion within certain operating conditions and limitations.

No research article is available in the open literature for a hybrid system for post-combustion CO_2 separation from a coal-fired power plant flue gas. The performance of a hybrid separation process which combines membrane permeation and conventional gas absorption/stripping using MEA is examined in this study to capture CO_2 from a 500 MW coal-fired power plant exhaust gas stream. This is a conventional power plant that uses atmospheric air for the combustion.

8.2 Hybrid process configuration and scenarios

Usually a high-pressure gas with a high concentration of CO_2 is a very good candidate for membrane gas separation. That is why the membrane is placed first for the bulk removal of CO_2 in natural gas sweetening in a hybrid arrangement. The pressure of the exhaust flue gas stream coming out of a 500 MW coal-fired power plant is slightly above the atmospheric pressure, and the concentration of CO_2 in the stream ranges between 12 and 14 mol%. Two-in-series hybrid arrangement by putting membrane unit first and two-in-parallel hybrid arrangement by flow splitting will be investigated in details in this study in terms of total capture and compression energy requirements. Different stand-alone membrane configurations were investigated in Chapter 5 and 6 to minimize the energy requirement for post-combustion CO_2 capture. The configuration presented in Figure 5.7 in Chapter 5 will be considered for the membrane process in two-in-series hybrid arrangement for further concentrating the flue gas stream which uses feed pressurisation and permeate vacuuming simultaneously. For two-in-parallel hybrid arrangement, the configuration presented in Figure 6.3 in Chapter 6 will be considered for the membrane process. The conventional amine process presented in Figure 7.1 in

chapter 7 will be considered here for investigating the hybrid process with membrane unit.

The hybrid process flowsheets, and flow-split scenarios for two-in-parallel arrangement are presented in Figure 8.1 and in Table 8.1, respectively.

Table 8.1: Flow-schemes for hybrid process simulation for post-combustion CO_2 capture

Scenarios	**Flow split fraction**	
	MEA	Membrane
Membrane (alone)		1.0
Hybrid-Case-1	0.25	0.75
Hybrid-Case-2	0.5	0.5
Hybrid-Case-3	0.75	0.25
MEA (alone)	1.0	
Two-in-series hybrid	→ Membrane → MEA	

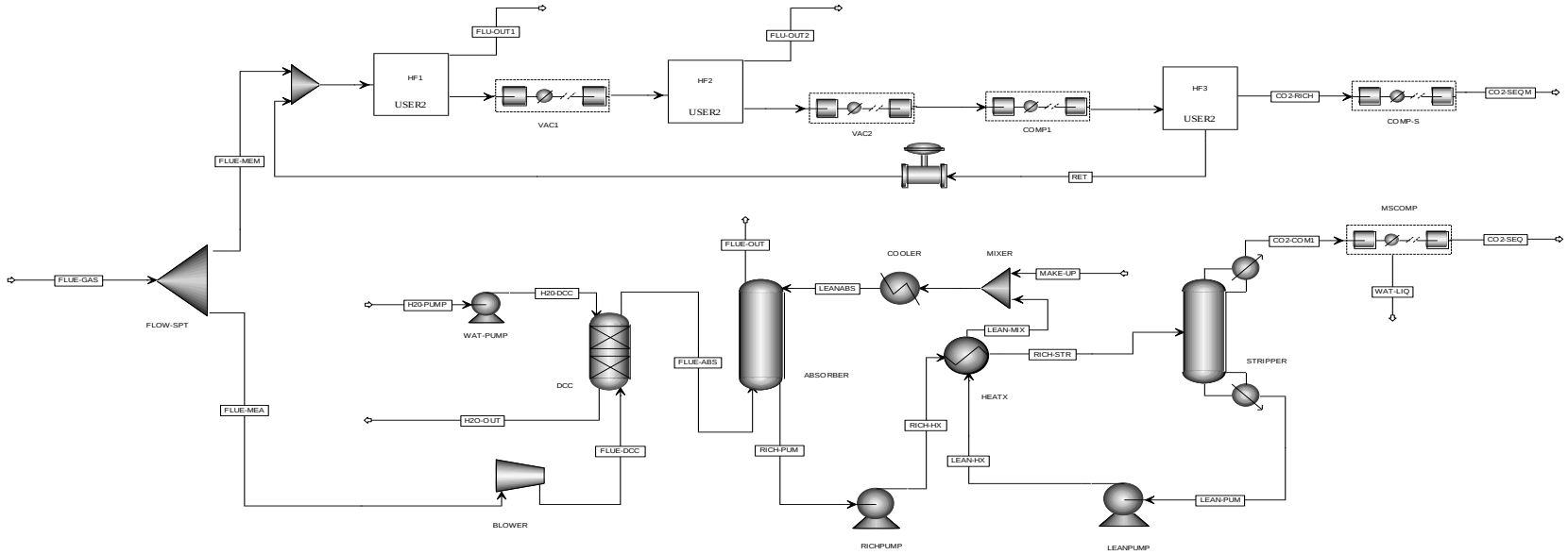

(a) Two-in-parallel

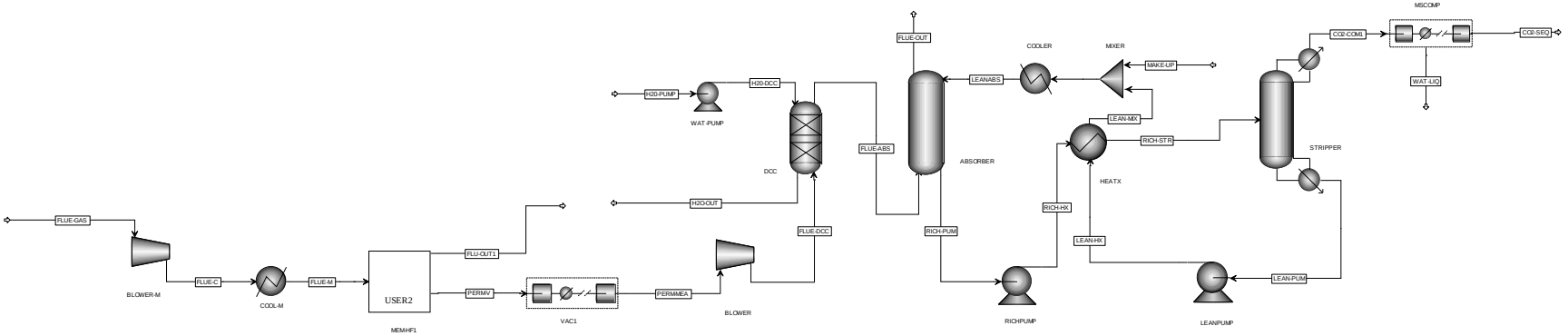

(b) Two-in-series

Figure 8.1: Hybrid process flowsheets in AspenPlus for the post-combustion CO_2 capture with combination of membrane gas separation process and amine (MEA) process

8.3 Process simulation

Same design basis, feed condition, module/unit input specifications, and properties are considered in simulating the hybrid process as in the simulation of the stand-alone membrane processes in Chapter 5 and Chapter 6, and MEA process in Chapter 7. The 85% CO_2 recovery from the flue gas stream with 98% purity is desired for EOR application. To meet overall 85% CO_2 recovery in two-in series arrangement, upstream membrane unit is designed to capture 90% CO_2 from the flue gas stream, and downstream MEA process requires 94.5% CO_2 capture from the permeate stream of membrane process. The injection pressure for the captured CO_2 is specified here at 110 bar. The flue gas which is entering the membrane unit in two-in-parallel hybrid arrangement is always dehydrated beforehand, but for the two-in-series arrangement, hydrated flue gas was considered for the membrane unit. For the stand-alone membrane process ten trains are considered to process the large flue gas stream. Each train consists of three membrane stages, two vacuum pumps, one permeate compressor and one injection/sequestration compressor. Four trains are considered for stand-alone MEA process to process the complete flue gas stream. Each train consists of one blower, one direct-contact cooler, one absorber, one lean/rich heat exchanger, one stripper and one injection/sequestration compressor. In two-in-series arrangement, membrane train consists of one feed blower/compressor, one membrane stage and one vacuum pump, and MEA train uses two strippers per train for Model-I and one stripper per train for model-II. Table 8.2 presents the number of trains required for each process scenarios. Model-I and Model-II, as described in Chapter 7, are used for MEA process simulation at a lean loading of 0.4 and 0.3, respectively. The main difference between the two rate-based models is one (Model-I) considers equilibrium reactions only in the stripper modeling, and the other (Model-II) considers kinetics. Both models consider kinetics in the absorber modeling. These two optimum lean loadings for these models are chosen because they showed the lowest and highest minimum reboiler duties requirement in the previous chapter among the models studied.

Table 8.2: Total number of trains requirement for each process scenario

Scenarios	**Number of Trains**	
	Membrane	MEA
Membrane (stand-alone)	10	n/a
Hybrid-Parallel-Case-1	8	1
Hybrid-Parallel-Case-2	5	2
Hybrid-Parallel-Case-3	3	3
MEA (stand-alone)	n/a	4
Two-in-series	11*	2

* With different membrane process configuration

8.4 Results and discussion

The results for the membrane process simulation and design are presented in Table 8.3 for both arrangements for single train. The results for the MEA process are presented in Table 8.4 for the Model-I and in Table 8.5 for the Model-II for single train. The thermal efficiency of the plant is assumed to be 33% based on low heating value (Herzog, 1999). The total energy requirements for capture and compression for the stand-alone membrane process, stand-alone MEA process with two models and hybrid processes are tabulated in Table 8.6. The total energy demand for each type of capture processes is graphically visualised in Figures 8.2 and 8.3. It is found that the stand-alone membrane gas separation process exhibits the lowest energy demand and the two-in-series hybrid process requires the highest energy, although plant size for the hybrid process is much smaller. The difference in total energy demand between the stand-alone membrane and two-in-series hybrid process is almost 44%. It is also found that membrane capture process can save up to 15.5 ~ 35% energy compared to the stand-alone MEA capture process depending on the absorption/stripping model used in the simulation. The energy requirement prediction of the kinetic-based stripper model (Model-II) is almost 20% more than the equilibrium reactions based prediction (Model-I). The position of the hybrid process for all scenarios is in between the Membrane and the MEA process, and the Hybrid-Case-1 (75% membrane and 25% MEA) is closer to the Membrane process in terms of energy requirement. This primarily indicates that hybrid process (combination of membrane and MEA) might not be a good choice for the post-combustion CO_2 capture from a 500 MW coal-fired power plant as it is in natural gas sweetening by acid gas removal. A detailed economic study based on this realistic design study might help to identify the best process for the post-combustion CO_2 capture by determining the overall plant cost. The main obstacle found to perform a realistic techno-economic study for this large plant size is the acquisition of equipments' price data from the concerned parties i.e., vendors.

Table 8.3: Results for the membrane process-single train

Membrane Process mode	Parallel	Series
Flue gas flow rate, kmol/sec	2.1	2.1
CO_2 capture rate, %	85	90
Purity of captured CO_2, %	98	29.7
Permeate side Vacuum condition, [10^5 Pa]	0.1	0.2
Permeate Compressor pressure, [10^5 Pa]	9.3	
Blower pressure, [10^5 Pa]		1.2
Membrane requirement		
Number of fibres, Stage-I [10^6]	685.2	858.3
Number of fibres, Stage-II [10^6]	166.3	
Number of fibres, Stage-III [10^6]	2.1	
Total Membrane **Area** requirement, [10^6 m^2]	0.67	0.674
Power requirement		
Permeate Vacuum pump-stage I power, MWe	5.8	5.3
Permeate Vacuum pump-stage II power, MWe	3.4	
Permeate Compressor power, MWe	3.2	
Blower power, MWe		1.8
Capture Power, MWe	12.4	7.1
Compression power, MWe	5.0	
Total (Capture + Compression**)** power, MWe	17.3	

Table 8.4: MEA process simulation and design results, single train - Model I

MEA process (Model-I) mode	Parallel		Series	
Lean loading (mol CO_2/mol MEA)	**0.4**		**0.4**	
Flue gas flow rate, kmol/sec	5.7		4.7	
CO_2 flue gas conc.(Absorber inlet), mol%	13.5		29.7	
Lean solvent flow rate, kmol/sec	45.9		116.7	
	Absorber	**Stripper**	**Absorber**	**Stripper (2)**
Trays/stages (no. of downcomer pass)	7 (2)	9 (2)	9 (3)	9 (2)
Tray spacing, m	1.4	1.6	1.5	1.5
Weir height, m	0.14	0.15	0.15	0.15
Downcomer clearance, m	0.115	0.125	0.125	0.125
Max^m backup/Tray spacing (/at stage)	0.5/6	0.5/8	0.6/9	0.6/8
Max^m flooding factor (/at stage)	0.7/5	0.7/8	0.7/9	0.7/6
Column diameter, m	7.6	6.8	8.9	6.8
Reflux ratio		0.11		0.24
Bottom to feed ratio		0.98		0.99
Column section pressure drop, N/m^2	21513	18220	22298	17556
Pressure drop/tray (max.), N/m^2	3355	2882	2561	2816
Bottom stage pressure, N/m^2	119700	122858	121042	122193
Stripper's Feed stream temp., K		358		358
Bottom stage temp., K	325	370	324	373
Tray (max^m) efficiency, %	6.6		14	16
Reboiler duty, MW_{th}		97		135.1×2
Blower power, MWe	7.2		4.8	
Compression power, MWe	14.3		14.3	

Table 8.5: MEA process simulation and design results, single train - Model II

MEA process (Model-II) mode	Parallel		Series	
Lean loading (mol CO_2/mol MEA)	**0.3**		**0.3**	
Flue gas flow rate, kmol/sec	5.7		4.7	
CO_2 flue gas conc.(Absorber inlet), mol%	13.5		29.7	
Lean solvent flow rate, kmol/sec	31.3		61.9	
	Absorber	**Stripper**	**Absorber**	**Stripper**
Trays/stages (no. of downcomer pass)	7 (2)	9 (2)	7 (2)	9 (3)
Tray spacing, m	1.4	1.8	1.5	1.7
Weir height, m	0.14	0.15	0.15	0.15
Downcomer clearance, m	0.115	0.125	0.125	0.125
Max^m backup/Tray spacing (/at stage)	0.5/4	0.5/8	0.6/5	0.5/8
Max^m flooding factor (/at stage)	0.7/4	0.7/8	0.7/5	0.7/8
Column diameter , m	7.2	4.3	7.1	6.8
Reflux ratio		1.5		1.7
Bottom to feed ratio		0.98		0.98
Column section pressure drop, N/m^2	22877	28981	20640	26272
Pressure drop/tray (max.), N/m^2	3567	4746	3445	4040
Bottom stage pressure, N/m^2	121028	133619	118794	130910
Stripper's Feed stream temp., K		368		368
Bottom stage temp., K	327	382	333	382
Tray (max^m) efficiency, %	6.4		12.7	11.4
Reboiler duty, MW_{th}		146		299
Blower power, MWe	7.2		4.8	
Compression power, MWe	14.3		14.3	

Table 8.6: Total energy requirements for all processes

Scenarios	**Energy** (Capture + Compression) requirements, **MWe**				
	Membrane	**MEA**		**Mem+MEA$_{M-I}$**	**Mem+MEA$_{M-II}$**
		Model-I	Model-II		
Membrane (alone)	181.7			181.7	181.7
Hybrid-Parallel-Case-1	136.3	53.8	70.2	190.1	206.5
Hybrid-Parallel-Case-2	90.9	107.6	140.5	198.4	231.3
Hybrid-Parallel-Case-3	45.4	161.3	210.7	206.8	256.1
MEA (alone)		215.1	281	215.1	281
Hybrid-series	76.9 + 57.21 (for compression)	190.0	208.9	323.8	343.0

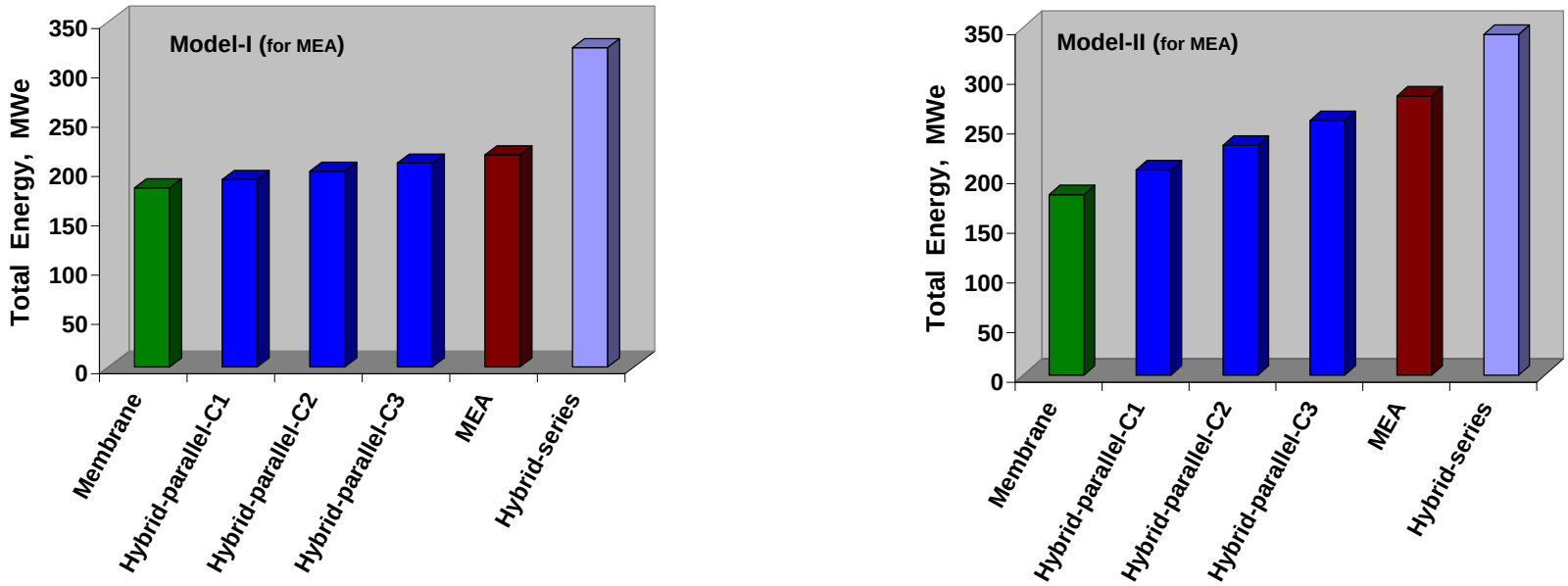

Figure 8.2: Total energy demand by each process for post-combustion CO_2 capture with compression for transportation

8.5 Summary

Three hybrid process (combination of membrane permeation and MEA process) scenarios in two-in-parallel arrangement and one in two-in-series arrangement were simulated and designed in AspenPlus® platform for post-combustion CO_2 capture from a 500MW coal-fired power plant exhaust gas stream, and compared with the stand-alone MEA and membrane gas separation processes in terms of total energy requirement for CO_2 capture and compression. It is found that the stand-alone membrane gas separation process utilizes the lowest energy and no hybrid processes were competitive, the worse being the two-in series hybrid arrangement.

Chapter 9

Economic Evaluation

9.1 Introduction

Economics is one of the most important parameters to be investigated during the development of any new technology or process or modification of an existing process configuration besides the technical evaluation. The economic assessment of a process depends on the method of analysis used and on the values assigned to the economic parameters. Therefore, economic assessments made by different evaluators may differ considerably from each other. Economic analysis of a new process or process modifications requires knowledge of capital and operating costs. The capital costs are based on equipment sizes and capacities and their associated costs. Several studies have been reported in the area of techno-economic analysis of post-combustion processes mainly based on absorption and stripping using monoethanolamine (MEA) as a solvent for capturing carbon dioxide from flue gases of different types and sizes of power plants (Mariz, 1998; Tontiwachwuthikul et. al., 1998; Chapel et al., 1999; Rao and Rubin, 2002; Singh et al., 2003; Abu-Zahra et al., 2007; Fisher et al., 2005, 2007; Romeo et al., 2008; Ho et al., 2009, 2011; Bin et al., 2010; Schach et al., 2010; Gerbelová et al., 2011). Although economics of membrane gas separation processes are widely studied for upgrading low quality natural gas, only few studies are available for post-combustion CO_2 capture from low pressure exhaust gas stream of coal fired power plant (Ho et al., 2008; Merkel et al., 2010). The economic assumptions and other parameters considered in the above studies vary significantly from each other for both technologies, as described below.

Mariz (1998) reported on the main cost factors, potential savings, and capital and operating costs for a 1000 tonne/d MEA solvent based CO_2 recovery plant over a range of flue gas CO_2 contents, from 3 vol% for natural-gas-fired turbines to 13 vol% for coal-fired boilers. Chapel et al. (1999) concluded that it is possible to lower the costs in comparison to an MEA reference plant significantly by using Fluor Econamine FG process for large scale CO_2 capture (4000 tonne/d) of power plant flue gases.

Tontiwachwuthikul et al. (1998) re-examined CO_2 recovery from coal-fired flue gas in large scale plants for the purpose of EOR. They also investigated the integration of the utility requirements for both the amine process and the downstream steam turbine driven CO_2 compressor with steam from the power generation unit to reduce the operating and capital costs.

Rao and Rubin (2002) developed performance and cost models of a MEA-based CO_2 absorption/stripping process for post-combustion flue gas applications. The models were integrated with an existing power plant modeling framework. The integrated model was used to study the feasibility and cost of carbon capture and sequestration for both new and existing coal-burning power plants. The limitation of this integrated model is that only parameter studies for the implemented standard absorption/stripping process could be performed because of fixed process configurations. Singh et al. (2003) presented a techno-economic comparison of CO_2 capture from a 400 MW coal-fired power plant for two processes, MEA scrubbing and O_2/CO_2 recycle combustion. The results showed that both processes are expensive, however O_2/CO_2 recycle combustion appears to be a more attractive retrofit option than MEA scrubbing.

Fisher et al. (2005) investigated the economic and technical feasibility of MEA-based absorption/stripping processes with different stripper configurations for capturing CO_2 from a 500 MW coal-fired power plants with respect to technical performance and costs under a US DOE funded project. The cost of CO_2 capture (cost per tonne avoided) was compared among the base case and the alternative process configurations. Cost savings per tonne of CO_2 avoided reported range from 4.3 to 9.8 percent. Fisher et al. (2007) further extended their work under another US DOE funded project by considering different solvents (such as MEA/Piperazine (PZ) and Methyldiethanolamine (MDEA)/PZ) and another stripper configuration called double matrix. When compared to the base case, systems employing advanced solvent formulations and process configurations were estimated to reduce the cost of CO_2 avoided by 10 to 18%.

Abu-Zahra et al. (2007) performed a study about the influences of the design and economic parameters of the simple MEA based absorption/stripping process on MEA on capture and compression costs. A 600 MW gross coal-fired power plant was chosen as the reference power plant. An improved process in terms of the cost of CO_2-avoided

(10% less than base case) was proposed. Romeo et al. (2008) compared the power plant performance with special attention to the power output and efficiency penalty, and investment cost and specific price of CO_2 when MEA scrubbing is integrated with the steam cycle. They evaluated different alternatives to provide heat and power in order to minimize the cost of CO_2 avoided and the cost of electricity after adding the MEA capture process to the power plant. The alternatives included integration using a natural gas auxiliary boiler, internal energy flows and natural gas auxiliary gas turbine. They concluded that using a gas turbine to supply compression electrical energy requirements and extracting steam from the steam cycle is the optimum option with regard to the efficiency penalty on the power plant performance but the cost-effective option is the installation of new steam generator for the striper energy requirements.

Ho et al. (2009) investigated the cost of retrofitting CO_2 capture to a 500 MW lignite coal-fired power plant in Australia. It was found that CO_2 capture and compression cost was over $70 per tonne CO_2 avoided using MEA solvent and less than $30 per tonne CO_2 avoided using enhanced potassium carbonate solution. Ho et al. (2011) also compared the estimated capture cost of three Australian industrial emission sources from iron and steel production, oil refineries and cement manufacturing with those of post-combustion capture from a pulverised black coal power plant using MEA solvent. The costs of capture for the iron and steel and cement industries were found comparable to or less than that for post-combustion capture from a pulverised black coal power plant. They also concluded that estimated costs are highly dependent on the characteristics of the industrial emission source, the assumptions related to the type and price of energy used by the capture facilities, and the economic parameters of the project such as the discount rate and capital costs.

Bin et al. (2010) analyzed the equipment investment and consumptive costs of a MEA-based CO_2 capture plant with 12 tonne/day capture capacity in Huaneng Beijing coal-fired power (845 MW) station in China. The amount of flue gas extracted for the capture plant was only 2500-3000 N m^3/h. The results showed that the cost of the absorber and the stripper accounted for about 50% of main equipment; the consumptive cost was about US$ 25.3/tons of CO_2, of which the steam requirement accounted for

about 55%. The cost of electricity increased by 0.02 US$/kWh and the electricity purchase price increased by 29%.

Schach et al. (2010) evaluated and compared three alternative configurations economically and technically to a baseline process represented by a standard absorption/stripping process using monoethanolamine (MEA) as a solvent for capturing CO_2 from power plant flue gas. Savings in cost of CO_2-avoided of 2-5% were attained. Regarding the total power required, savings of 4-7% were obtained. The results showed that not the process with the highest energy savings had the lowest cost of CO_2-avoided, but that the influence of rising investment costs of more complex configurations could not be ignored.

Gerbelová et al. (2011) investigated the possibilities of CO_2 reductions in the electricity sector in Portugal. The study considered CO_2 post-combustion capture for the fossil fuel based thermoelectric power plants. A techno-economical analysis was performed using the Integrated Environmental Control Model (IECM) software developed by Carnegie Mellon University to study the feasibility of retrofitting existing power plants with MEA-based CO_2 capture technology. It was found that the addition of capture unit increased the energy requirement by 15% and the cost of electricity by twice, compared to a plant without CO_2 capture.

An IEA working paper (2011) analysed the techno-economic data for MEA-based CO_2 capture from power generation, including CO_2 conditioning and compression. Cost and performance trend were presented based on estimates published over the last five years in major engineering studies from seven organisations for about fourteen CO_2 capture cases for coal power plants. Capital cost and levelised cost of electricity were re-evaluated and updated to 2010 cost levels. Presented data accounted for CO_2 capture but not transportation and storage. The data did not reflect project-specific cost or cost for first large-scale demonstration plants, which are likely higher. Average costs of CO_2 avoided were reported at US$ 55 per tonne of CO_2 from the pulverised coal power plants sizes from 500 MW to 758 MW for OECD region. The highest and lowest costs of CO_2 avoided reported in that report were 74 and 42 US$ per tonne of CO_2 avoided based on the data of GCCSI (2009) for 550 MW supercritical pulverized coal (bituminous) plant and the data of GHG IA (2005) for 758 MW ultra-supercritical pulverized coal

(bituminous) plant. The cost and performance data of IEA paper (2011) for post combustion CO_2 capture from coal-fired power generation are reproduced here in Table 9.1 due to the importance of the data.

Table 9.1: Post-combustion capture from coal-fired power generation by amines (IEA, 2011)

Regional focus	**OECD**													**China**	**Average (OECD)**
Year of cost data	2005	2005	2005	2005	2007	2007	2007	2007	2007	2007	2009	2009	2009	2009	
Year of publication	2007	2007	2007	2007	2009	2009	2009	2009	2010	2010	2009	2009	2009	2009	
Organisation	CMU	MIT	GHG IA	GHG IA	EPRI	EPRI	EPRI	MIT	NETL	NETL	GCCSI	GCCSI	GHG IA	NZEC	
ORIGINAL DATA AS PUBLISHED (converted to USD)															
Region	US	US	EU	EU	US	US	US	US	US	US	US	US	EU	CHN	
Specific fuel type	Bit coal	Lignite	Bit coal	Bit coal	Sub-bit coal	Sub-bit coal	Bit coal	Bit coal	Bit coal	Bit coal	Bit coal	Bit coal	Bit+10% Biomass	Bit coal	
Power plant type	SCPC	CFB	USCPC	USCPC	SCPC	USCPC	SCPC	SCPC	SCPC	Sub-PC	SCPC	USCPC	SCPC	USCPC	
Net power output w/o capture (MW)	528	500	758	758	600	600	600	500	550	550	550	550	519	824	582
Net power output w/ capture (MW)	493	500	666	676	550	550	550	500	550	550	550	550	399	622	545
NET efficiency w/o capture, LHV (%)	41.3	36.5	44.0	44.0	39.2	39.8	40.0	40.4	41.2	38.6	41.4	46.8	44.8	43.9	41.4
Net efficiency w/ capture, LHV (%)	31.4	26.7	34.8	35.3	28.2	28.8	29.1	30.7	29.9	27.5	29.7	34.9	34.5	33.1	30.9
CO_2 emissions w/o capture (kg/MWh)	811	1030	743	743	879	865	836	830	802	856	804	707	754	797	820
CO_2 emissions w/ capture (kg/MWh)	107	141	117	92	124	121	126	109	111	121	112	95	73	106	111
Capital cost w/o capture (USD /kW)	1442	1330	1408	1408	2061	2089	2007	1910	2024	1996	2587	2716	1710	856	1899
Capital cost w/ capture (USD /kW)	2345	2270	1979	2043	3439	3485	3354	3080	3570	3610	4511	4279	2790	1572	3135
Relative decrease in net efficiency	24%	27%	21%	20%	28%	28%	27%	24%	28%	29%	28%	26%	23%	25%	25%
RE-EVALUATED DATA (2010 USD)															
LCOE w/o capture (USD/MWh)	50	49	69	69	62	63	73	70	65	66	70	70	78	51	66
LCOE w/ capture (USD/MWh)	80	84	95	97	107	109	121	112	113	117	121	112	118	80	107
Cost of CO_2 avoided (USD/tCO_2)	**43**	**40**	**42**	**42**	**60**	**61**	**68**	**58**	**69**	**69**	**74**	**68**	**59**	**42**	**58**

For membrane gas separation process, Ho et al. (2008) investigated the reduction of CO_2 capture cost by operating under vacuum condition. The flue gas from a 500 MW coal-fired power plant was pressurised to 1.5 bar, whereas the permeate stream was kept at 0.08 bar. The membrane CO_2/N_2 selectivity of 20 and CO_2 permeabilty of 70 barrer were used with a membrane thickness of 125 μm which resulted in membrane CO_2 permeance of 0.56 gpu. The estimated capture cost was U.S. $54/tonne CO_2 avoided at 2005 dollar value. They assumed a baseline cost of electricity of 34 $/MWh. The CO_2 concentration in the final permeate stream was reported to be 45% which would not be used in EOR applications.

Merkel et al. (2010) conducted a techno-economic comparison of two membrane process designs (classified as two-step/two-stage and two-step counter-current sweep) for 90% CO_2 capture from a 600 MW coal-fired power plant. The feed and permeate pressures were considered 2.0 and 0.2 bar respectively, and the membrane properties used for CO_2 permeance and selectivity with respect to N_2 were 1000 gpu and 50 respectively. The percentage of CO_2 concentration in the permeate stream was reported 95^+. The two-step counter-current sweep design used less power and membrane area compared to the two-step/two-stage design. The CO_2 capture cost estimated for two-step/two-stage design and two-step counter-current sweep were $39 and $23 per ton CO_2, respectively which might make membrane gas separation technology in the area of post-combustion CO_2 capture competitive in the near future. The equipment cost for compressor, vacuum pump and expander were calculated using 500 $/kW basis. The cost of power was taken as 0.04 $/kWh. Membrane skid cost used was 50 $/m^2. No information regarding membrane life and replacement cost were reported. The counter-flow module design used all the incoming combustion air as a sweep to generate maximum driving force for CO_2 separation which helped to avoid the energy penalty for compression or vacuum treatment. The air stream going to the boiler contained 8.7% CO_2 and 18% O_2. The impact of increased CO_2 content in the air sent to a conventional pulverized coal boiler was not clear at this stage. Without some changes to boiler operating conditions, this recycle stream might have the potential to lower the performance of the boiler.

It was found that the majority of these studies did not give much details about equipment sizing needed for proper costing of the equipments. In the present study,

mainly AspenPlus simulation software and other sizing sources will be used to design and size the majority of the process equipments. The general approach used to size and selects the equipment and to estimate the capital and operating costs for the CO_2 capture processes will be described in the following sections first. The total capture cost (including CO_2 compression) of each process (operating + capital) will be translated into a value of $/tonne of CO_2 avoided.

9.2 MEA Process Economics

For the MEA process, it is assumed that the power plant output reduction owes to steam and electricity de-rate. In order to supply this energy, two possible options are considered:

- The first option (classified as Case-1) uses a natural gas auxiliary boiler to produce steam for the absorption/stripping process avoiding any impact on the original plant steam cycle efficiency. But for the compression energy requirement, the plant's electricity is used which ultimately derates the plant. The CO_2 generated by the combustion of natural gas is not captured because of the lower CO_2 concentrations in the flue gas. But the additional CO_2 generated is reflected in the calculation of the net plant emissions.
- The second option is integrating the absorption process into the original power plant to satisfy both the electrical and thermal energy for capture process. This is classified as Case-2 (33%, Herzog, 1999) or Case-3 (22.5%, Alie, 2004) depending on the plant net thermal efficiency considered for converting the thermal energy to electrical energy. The power plant output and efficiency is reduced due to the direct supply of electricity and steam to the capture process. Alie (2004) studied the stream extraction location from a 500 MW coal power plant unit of OPG's Nanticoke Generating Station, Ontario for supplying steam to the stripper reboiler. The author concluded that the IP/LP (Intermediate Pressure/. Low Pressure) crossover pipe is the preferred extraction location for LP steam (459 kPa and 251^{o}C) as it is easily accessible and supplies steam at required conditions. The power plant efficiency reported without CO_2 capture at 36% (HHV). The plant thermal efficiency reported after stream extraction for the rebolier ranged between 22.1 and 22.5% for different lean loadings studied which de-rated the plant up to 38.6%. In the Fisher et al. (2007) study, the de-rating factor used was 145 W de-rating for every 1 kg/h of steam diverted from the LP turbine of the main facility which translated to the thermal efficiency of 24.3%. The present study has adopted the study of Alie (2004) for plant de-rating due to steam extraction for stripper reboiler duty.

9.2.1 Equipment Sizing and Selection for MEA

Equipment sizing is a prerequisite to costing. Sizing of equipment includes the calculation of all physical attributes (capacity, height, cross sectional area, power rating, etc.) that allow a unique costing of this unit based on flowrates, temperatures, pressures, and heat duties from the flowsheet mass and energy balance. This section describes the general approach used to size and select the equipment for CO2 capture and compression system. Equipments are sized for a 500 MW coal-fired unit. The details of design basis, streams and unit operations data were provided in Chapter 7. A wet flue gas desulfurization unit was assumed to be located upstream of the capture unit. A combination of spreadsheet calculations and simulation tools (AspenPlus 2006.5, Aspen Icarus Process Evaluator 2006.5; Biegler et al., 1997; Peters et al., 2003) were used to size the equipment in the process. The whole capture and compression unit is divided into three blocks: a single inlet gas train (gas blower, direct contact cooler); four parallel CO2 capture trains (amine trains); and a single CO2 compression train. The key assumptions used to size the equipments are discussed below. Table 9.2 presents the major equipments used in this study along with the key sizing parameters for 85% CO_2 capture by MEA (30 wt%) process at lean loading of 0.4 using absorption/stripping Model-I and final CO_2 product delivery at 40^{o}C and 110 bar.

9.2.1.1 Gas Blower

The blower will increase the pressure of the flue gas to overcome the pressure drop through the direct contact cooler and absorber. The maximum pressure increase is 30 kPa and the design flow rate is 615.6 m^3/s at a nominal suction pressure of 101 kPa. This is a very unusual application because of the large volume. Turbo type blower with stainless steel construction is selected. A polytropic efficiency of 80% and mechanical efficiency of 90% is assumed for this compressor, which yielded a power requirement of 23,264 kW/unit.

9.2.1.2 Direct Contact Cooler and Water Pump

The direct contact cooler (DCC) sprays water counter currently into the blower outlet flue gas stream. The DCC water cools the flue gas not by evaporation, but by direct

contact. The required water circulation rate is 0.35 m^3/s. A dedicated cooling tower provides evaporative cooling for the recirculating DCC water. The water pump is considered centrifugal, constructed from stainless steel, and has an efficiency of 65%.

9.2.1.3 Absorber

The absorber is a vertical tray column. The amine-based sorbent contacts the flue gas and absorbs CO_2 inside the absorber tower. Double-pass sieve trays are considered. The absorber was sized using RateSep with kinetic consideration at a 70% approach to flooding. The maximum pressure drop calculated is 28 kPa. The diameter and height (including feed space, top and bottom disengagement space, skirt height) of the column are 7.7 and 13.8 m, respectively, with tray spacing of 1.4 m. Carbon steel is considered for the tower and stainless steel for trays.

9.2.1.4 Rich Amine Pump

It pumps rich amine solution from the bottom of the absorber to an elevated pressure to account for pressure drop through the lines and rich/lean exchanger, and to overcome the operating pressure and height requirements in the stripper. A pump efficiency of 65% is considered in the study. Stainless steel metal components were selected for this centrifugal pump. The pressure increase provided by this rich amine pump is 202 kPa.

9.2.1.5 Rich/Lean Exchanger

The rich amine is preheated prior to regeneration by heat exchange with the hot lean amine flowing from the regenerator in the rich/lean exchanger. A 5^oC hot outlet and cold inlet temperature difference approach was considered. A heat transfer coefficient of 1134 W/m^2-K was used for the floating-head shell and tube heat exchanger of stainless steel material.

9.2.1.6 Stripper

The removal of CO2 from the rich amine solution takes place in a stripper by steam stripping. The absorption reactions are reversed through heat supplied via a reboiler. The rich solution flows down through the stripper and steam rising up through

the column strips the CO2 from the amine solution. The stripper is also considered as a vertical tray tower like absorber, and same tray type is considered for internal. The stripper was sized using RateSep with equilibrium reactions at a 70% approach to flooding. The maximum pressure drop calculated is 18 kPa. The diameter and height (including feed space, top and bottom disengagement space, skirt height) of the column are 6.8 and 15.13 m respectively with tray spacing of 1.6 m. Carbon steel is selected for the tower and stainless steel for trays. The reboiler pressure is 123 kPa.

9.2.1.7 Reboiler

Kettle-type shell and tube reboiler is considered. The solution flows by gravity from the base of the stripper into the reboiler. The lean amine flows on the shell side of the reboiler, and utility steam flows on the tube side. Heat supplied in the reboiler vaporizes part of the lean amine solution and generates steam for stripping. The vapour is piped back to the regenerator column to provide stripping vapour, while bottom product is drawn from the reboiler. LP steam is extracted at 459 kPa and 251^{o}C from the IP/LP crossover pipe and the condensate is re-injected into the cycle at the fourth feed water pre-heater (Alie, 2004). The saturation temperature of the steam is 149^{o}C. A heat transfer coefficient of 852 W/m^{2}-K was used to size the reboiler tubes. The log mean temperature difference (LMTD) considered is 21^{o}C. The reboiler tube bundle is stainless steel, and the shell is carbon steel (Fisher et al., 2007).

9.2.1.8 Stripper Condenser and Accumulator

The stripper condenser cools the hot overhead vapours exiting from the top of the stripper. This cooling reduces amine and water losses. Condensed liquids are separated from the CO_2 and water vapour in the stripper condenser accumulator, a horizontal vessel located downstream of the condenser. Vapour exiting the condenser accumulator flows to the first stage of compression. The condensed liquid is sent back to the stripper as a reflux via a reflux pump. The condenser is a shell and tube type exchanger. Process material flows on the tube side, and cooling water flows on the shell side. The tubes are constructed of stainless steel, and the shell is constructed of carbon steel. Cooling water supply temperature is 12°C and the temperature rise is 10°C. The process outlet

temperature is 70°C for the stripper condenser. A heat transfer coefficient of 454 W/m^2-K was used for the condenser (Fisher et al., 2007). A horizontal vessel is considered for the condenser accumulator and sized using the method described in the "User Guide" of Aspen Icarus Process Evaluator 2006.5 (aspenOne Engineering suite, AspenTech Inc. 2007). Liquid entrainment method is used to calculate vapour velocity. A minimum liquid residence time of five seconds is assumed. Stainless steel is selected as the material of construction for the stripper condenser accumulator.

9.2.1.9 Stripper Reflux Pump

The condensed liquid from the stripper condenser accumulator is sent back to the stripper as a reflux via a reflux pump. The reflux pump is a centrifugal type, constructed from stainless steel, and has an efficiency of 65%.

9.2.1.10 Lean Amine Pump

Using this pump lean amine solution from the bottom of the stripper is pumped to an elevated pressure to overcome line losses, pressure drops in the rich/lean amine exchanger and lean amine cooler, and the elevation at the top of the absorber. A pump efficiency of 65% and stainless steel is selected for this centrifugal type pump. The pressure increase provided by this lean amine pump is 202 kPa.

9.2.1.11 Lean Amine Cooler

The lean amine needs further cooling in a trim cooler to avoid excessive amine evaporative loss and to improve absorption effectiveness in the absorber by lowering the lean amine temperature to 40^{o}C before it is pumped back into the absorber column. The cooler uses cooling water in a counter-current, shell and tube exchanger. The exchanger shell is made of carbon steel, and the tubes are stainless steel. A heat transfer coefficient of 795 W/m^2-K was used to size the exchanger.

9.2.1.12 Lean Surge Tank

The surge tank for the lean amine solution is sized based on a 15-minute residence time. Carbon steel material is selected for the surge tank.

9.2.1.13 Makeup Systems

Amine and water losses occur due to vaporisation. It is usually necessary to add make-up amine and water to maintain the desired solution strength. In addition to vaporization, losses of the amine solution may also occur from degradation due to formation of heat stable salts. The nominal loss of amine was estimated at 1.5 kg amine/tonne CO_2 (Rao and Rubin, 2002). The amine makeup tank was sized to hold one month's worth of chemical and the makeup water tank about one day. A makeup amine pump along with a water pump also included. The costing for both pumps was conducted in a similar manner.

9.2.1.14 Cooling Water Systems

Two separate cooling towers were included for the unit. One for the direct contact cooler (DCC) system that provides water to the direct contact cooler. The second for the utility system that provides cooling water to all other water-cooled exchangers this water never directly contacts process material. The DCC system will have different needs with regard to the material of construction, cooling tower chemical addition, etc. However, the design and costing for both systems were conducted in a similar manner. Mechanical draft cooling towers are used with cooling water return and supply temperatures of 22^{o}C to 12^{o}C. The DCC cooling water flow rate is 0.35 m^3/s. The utility cooling water flow rates is 11.3 m^3/s

9.2.1.15 Filtration System

A filtration step is needed to minimize the operating problems caused by solids and other contaminants in the amine solution. It was assumed that a slipstream of the circulating amine (typically 15%) is filtered to remove suspended solids then sent to an activated carbon bed filter that adsorbs impurities (degradation products of MEA) and other contaminants from the sorbent stream. The mechanical filters remove particulate matter. Activated carbon beds can remove high-molecular weight degradation products but cannot remove heat stable salts and chlorides. Carbon filters generally need at least 15 minutes of contact time (Fisher et al., 2007).

9.2.1.16 Reclaimer

For this study, the cost for a thermal reclaimer system is included. In a conventional reclamation system, a small slipstream of the amine solution in circulation (0.5 to 3%) would be routed from the reboiler to a batch distillation reclaimer. MEA solvent may be reclaimed by low pressure steam (Fisher et al., 2007).

9.2.1.17 CO_2 Compression system

The CO2 captured by the MEA unit is compressed to a pipeline pressure of 110 bar for transport and injection at an off-site location. A four-stage large centrifugal compressor with inter-stage cooling and separators is used for CO_2 compression. Electric type driver is chosen for this purpose. A maximum temperature limit of 200^{o}C is used to choose the number of compression stages. A 80% polytropic efficiency is chosen for this type of compressor. The material of construction considered is stainless steel. Water-cooled exchangers are used for inter-stage compression cooling. The target outlet CO_2 temperature is 40^{o}C on the tube side of the exchanger based on a cooling water at 12^{o}C. The exchanger shell is constructed from carbon steel, and the tubes are constructed from stainless steel. A heat transfer coefficient of 454 W/m^2-K was used for the exchanger. A horizontal vessel is considered for the separator. A minimum liquid residence time of five minute is assumed. Stainless steel is selected as the material of construction for the separator.

9.2.1.18 Equipments not included

CO_2 dehydration system and flue gas pre-treatment units are not included in this study.

Table 9.2: Equipment sizing information for MEA process

Description	Units	Values
Number of inlet gas trains		1
Number of CO_2 capture trains		4
Number of CO_2 compression trains		1
Inlet Gas Blower		
Quantity per unit		1
Flow rate per unit	m^3/s	615.6
Pressure increase	kPa	30
Brake power	kW	23264.0
Direct Contact Cooler (DCC) system		
DCC-Tower		
Quantity per unit		1
Cooling water flow rate at 12^OC	m^3/s	0.354
Gas flow rate	m^3/s	512.9
Outlet gas temperature	K	313
DCC-Water Pump		
Quantity per unit		1
Flow rate	m^3/s	0.354
Pressure increase	kPa	84
Brake Power	kW	34.4
Absorber Column		
Quantity per unit		4
Diameter	m	7.7
Height (calculated separation height)	m	9.8
Extra feed space	m	1.0
Disengagement space (top & bottom)	m	2
Skirt height	m	1.0
Total Column Height	m	13.8
Bottom pressure	kPa	123
Column internal		
Tray type		Sieve
Downcomer pass		2
Downcomer clearance	m	0.115
Weir height	m	0.14
Tray spacing	m	1.4
No of Trays		7
Rich Amine Pump		
Quantity per unit		4
Flow rate per train	m^3/s	1.242
Flow rate per unit	m^3/s	4.97
Pressure increase	kPa	202
Brake power per train	kW	288.9
Brake power per unit	kW	1155.7

Table 9.2: Equipment sizing information for MEA process (continued)

Description	Units	Values
Rich/Lean Amine Exchanger		
Quantity per unit		4
Duty per train	kW	167797.4
Duty per unit	kW	671189.6
Heat transfer coefficient	W/m^2-K	1134
LMTD	K	7.83
Area per train	m^2	18898.9
Area per unit	m^2	75595.6
Stripper Column		
Quantity per unit		4
Diameter	m	6.84
Height (calculated separation height)	m	11.1
Extra feed space	m	1.0
Disengagement space (top & bottom)	m	2.0
Skirt height	m	1.0
Total Column Height	m	15.1
Bottom pressure	kPa	123
Column internal		
Tray type		Sieve
Downcomer pass		2
Downcomer clearance	m	0.125
Weir height	m	0.15
Tray spacing	m	1.6
No of Trays		7
Stripper Reboiler		
Quantity per unit		4
Duty per train	kW	96945
Duty per unit	kW	387780
Heat transfer coefficient	W/m^2-K	852
Steam pressure	kPa	239
LMTD	K	21
Area per train	m^2	5418.3
Area per unit	m^2	21673.4
LP steam required per train (@ 459 kPa & 251^{o}C)	kg/sec	41.5
Stripper Condenser		
Quantity per unit		4
Duty per train	kW	5210.6
Duty per unit	kW	20842.4
Heat transfer coefficient	W/m^2-K	454
LMTD	K	28
Area per train	m^2	409.9
Area per unit	m^2	1639.6
Cooling water required at 12^{o}C with 10^{o}C rise	kg/s	124.7

Table 9.2: Equipment sizing information for MEA process (continued)

Description	Units	Values
Stripper Condenser Accumulator		
Quantity per unit		4
Vapor flow rate	m^3/s	26.6
Liquid flow arte	m^3/s	0.002
Residence time	s	5.0
Diameter	m	3.3
Length	m	15.3
Stripper Reflux Pump		
Quantity per unit		4
Flow rate per train	m^3/s	0.002
Flow rate per unit	m^3/s	0.008
Brake power per train	kW	1.1
Brake power per unit	kW	4.4
Lean Amine Pump		
Quantity per unit		4
Flow rate per train	m^3/s	1.2
Flow rate per unit	m^3/s	4.92
Pressure increase	kPa	202
Brake power per train	kW	289.1
Brake power per unit	kW	1156.4
Lean Cooler		
Quantity per unit		4
Duty per train	kW	78560
Duty per unit	kW	314240
Heat transfer coefficient	W/m^2-K	795
LMTD	K	12
Area per train	m^2	8234.8
Area per unit	m^2	32939.2
Cooling Water required at 12 C with 10 C rise	kg/s	1879.7
Makeup Amine Pump		
Quantity per unit		1
Flow rate per train	m^3/s	3.65E-05
Flow rate per unit	m^3/s	1.46E-04
Pressure increase	kPa	202
Brake power per train	kW	0.025
Brake power per unit	kW	0.1
Makeup Amine Tank		
Quantity per unit		1
Flow rate per unit	m^3/s	1.46E-04
Residence time	days	30
Capacity	m^3	378.0

Table 9.2: Equipment sizing information for MEA process (continued)

Description	Units	Values
Makeup Water Pump		
Quantity per unit		1
Flow rate per train	m^3/s	5.02E-03
Flow rate per unit	m^3/s	0.02
Pressure increase	kPa	202
Brake power per train	kW	2.01
Brake power per unit	kW	8.03
Water Tank		
Quantity per unit		1
Flow rate per unit	m^3/s	0.02
Residence time	day	1
Capacity	m^3	1744.3
Lean Surge Tank		
Quantity per unit		4
Flow rate per train	m^3/s	1.2
Residence time	min	15
Capacity per train	m^3	1107
CO_2 Compression		
Compressors		
Quantity per unit		1
Number of stages		4
Compressor discharge pressure	kPa	11143
Total brake power required (total unit)	kW	57214.5
Inlet gas flow rate - Stage 1	m^3/s	106.4
Inlet gas pressure - Stage 1	kPa	101
Compressor Inter-stage Coolers		
Quantity per unit	kW	1
Cooler duty (total)	kg/s	119466
Cooling water required (total) at 12^oC with 10^oC rise		2858.5
Compressor Inter-stage Separators		
Quantity per unit		1
Liquid flow rate (total)	m^3/s	0.058
Residence time	min	5.0
Total capacity	m^3	17.4
Cooling Water System-utility		
Water rate per unit		
DCC	m^3/s	0.354
Lean amine cooler	m^3/s	7.6
Stripper condenser	m^3/s	0.5
Compressor Inter-stage Coolers	m^3/s	2.9
Total water rate	m^3/s	11.3

9.2.2 Cost Analysis for MEA

The information on both equipment and operating cost was obtained from a number of sources (Fisher et al., 2007; Peters et al., 2003; Turton et al., 2003; www.matche.com; Singh et al. 2003). The main source of evaluating the carbon dioxide capture equipment cost is the US DOE report of Fisher et al. (2007). They used combination of vendor quotes and PDQ$ (Preliminary Design and Quoting Service) software to obtain purchased equipment costs. The software estimated costs for fabricated equipment and catalogue items based on vendor information. Their reported costs were in September 2004 dollars. Peter et al. (2003) provided online equipment cost estimator tool elsewhere (www.mhhe.com). The calculated equipment cost basis was Jan. 2002 with CEPCI (Chemical Engineering Plant Cost Index) of 390.4. The CAPCOST© xls program available with Turton et al. (2003) calculates equipment cost on 2001 basis with CEPCI of 397). All equipment cost data were adjusted for inflation by adopting current CEPCI value for 2010 i.e., 550.8. The six-tenths-rule was applied to scale up/down to a new capacity or power or area for new equipment. The assumptions and specifications used in this economic evaluation for MEA-based capture process are presented in Table 9.3.

Table 9.3: Assumptions and cost parameters for economic evaluation-MEA process

All values in 2010 US dollars	
Project life	25 years
Equipment salvage value	0.0
Construction periods	3 years
Plant operation	7500 h/year
Interest rate	7%
Process water price	\$ 1.24 /m^3
Cooling water price	\$ 0.02 /m^3
MEA price	\$ 1.6 /Kg
Natural gas price	\$ 4.4 /GJ
MEA degradation rate	1.5 kg /ton CO_2 captured (Rao and Rubin, 2002)
Labour cost	\$ 45 /h/operator

9.2.2.1 Capital Cost of MEA Process

The unit capital cost consists of a single inlet gas train, four capture trains and one compression train. Equipment not simulated, such as reclaimer, cooling tower and rich amine filters, are costed by considering scaling factors based on the flow rate of the stream related to those units and similar size of amine plant cost study (Fisher et al., 2007). Flue gas pre-treatment system (bag house, flue gas desulphurisation unit, etc.), CO_2 dehydration system and CO_2 pipeline for transportation and sequestration were not included in the cost analysis. A natural gas auxiliary boiler unit is considered for generating steam for the stripper reboiler in one of the case studies. The cost of this unit is calculated based on the data of Singh et al. (2003). Table 9.4 presents a list of the major equipments and their purchased costs for MEA capture plant with compression unit for 85% recovery of CO_2 from a 500 MW coal-fired power plant flue gas stream. The sum of the component costs represents the total purchased equipment cost (PEC). It is observed from Table 9.4 that the major contributors to the purchased equipment costs are the absorbers, CO_2 compressor and strippers besides the auxiliary unit. They contribute respectively to 24%, 21% and 15% of the total purchased equipment cost for both steam and electricity de-rating. The total purchased equipment cost for the amine plant including compression is $ 199 million which is higher than the $ 157 million figure reported in Fisher et al. (2007) for the same size of the power plant (i.e., 500 MW) for both steam and electricity de-rating. The difference in total purchased cost can be attributed to the purchased cost of the stripper and absorber tower mainly. Due to the addition of feed space, top and bottom disengagement space, and skirt height with calculated separation height in the present study, the volume of the columns had been increased, and so thus the cost. In Fisher et al. (2007) study, the estimated cost of stripper (packed) was $ 2.4 million which is very low compared to the figure of $ 31.0 million reported in this study for tray type stripper. In the Fisher et al. study (2007), the absorber (packed) cost is 8.8 times greater than that of stripper (packed) cost. But in this study, the estimated absorber (tray) cost is 1.6 times higher than that of stripper (tray) cost. In other studies, the absorber-stripper cost ratio reported was 2.7 with the stripper cost of $ 11 million (Singh et al., 2003) and 3.2 (Abu-Zahra et al., 2007) with the stripper cost of $ 13

million for a 400 MW and 600 MW coal-fired plant with 90% CO_2 capture, respectively. The contribution of the auxiliary natural gas boiler unit's cost to the total equipment purchased cost is 22%.

Capital investment can be divided into two major categories namely direct and indirect cost. The major direct cost includes purchased equipment cost, purchased equipment installation, instrumentation and control, piping, electrical, building and services. The indirect cost includes mainly engineering, construction expenses, contingency and interest. Direct and indirect costs were estimated as a factor of the total purchased equipment cost (PEC) mainly using the methodology reported in Peters et al. (2003) and other different sources (Abu-Zahra et al., 2007; Fisher et al., 2007; Schach et al., 2010) and then added to come up with the fixed capital investment. Working capital and start-up cost along with MEA cost were then estimated and added to the fixed capital cost to arrive at the total capital investment (TCI). Table 9.5 presents the factors used and the compositions of the total capital investment (TCI). The total capital investment for the amine plant including compression is $ 1559/kW for Case-2 & 3 which is higher than the $ 1098/kW figure reported in Fisher et al. (2007).

Table 9.4: Purchased equipment cost for MEA process

Description	Type	Material of Construction	Costing source	Scaling factor	Quantity	Cost (US$)	
						Case-1 (Aux.)	Case-2 & -3
Inlet Gas Blower	Turbo, 10 psi	SS	www.matche.com	Flow rate and pressure	1	4,718,352	4,718,352
Direct Contact Cooler (DCC)	Tower	CS	Fisher et al., 2007	Volume (m^3)	1	484,987	484,987
Water pump-DCC	Centrifugal	SS	Fisher et al., 2007	Power (kW)	1	65,074	65,074
Absorber Column	Sieve tray tower	Tower-CS, Sieve-SS	www.mhhe.com, Turton et al., 2003	Volume (m^3)	4	49,007,252	49,007,252
Rich Amine Pump	Centrifugal	SS	Fisher et al., 2007	Power (kW)	4	878,759	878,759
Filtration (Rich Amine) System	Particulate &Carbon filter	CS, Teflon gasket	Fisher et al., 2007		8	1,324,698	1,324,698
Rich/Lean Amine Exchanger	Floating-head shell & tube	SS shell &tubes	www.mhhe.com	Area, m^2	4	8,626,438	8,626,438
Regeneration System							
Stripper Column	Sieve tray tower	Tower-CS, Sieve-SS	www.mhhe.com, Turton et al., 2003	Volume (m^3)	4	31,027,992	31,027,992
Reboiler	kettle-type shell & tube	SS tubes & CS shell	Fisher et al., 2007	Area, m^2	4	14,803,430	14,803,430
Condenser	Shell & tube	SS tubes & CS shell	Fisher et al., 2007	Area, m^2	4	1,262,736	1,262,736
Condenser Accumulator	Horizontal vessel	SS	Fisher et al., 2007	Volume (m^3)	4	754,482	754,482
Reflux Pump	Centrifugal	SS	Fisher et al., 2007	Power (kW)	4	19,670	19,670
Lean Amine Pump	Centrifugal	SS	Fisher et al., 2007	Power (kW)	4	709,817	709,817
Lean Cooler	Shell & tube, water cooled	SS tubes & CS shell	Fisher et al., 2007	Area, m^2	4	10,785,201	10,785,201
Makeup Amine Pump	Centrifugal	CS	Fisher et al., 2007	Power (kW)	1	1,642	1,642
Makeup Amine Tank	Fixed roof tank	CS	Fisher et al., 2007	Volume (m^3)	1	89,668	89,668
Makeup Water Pump	Centrifugal	CS	Fisher et al., 2007	Power (kW)	1	11,851	11,851
Water Tank	Fixed roof tank	CS	Fisher et al., 2007	Volume (m^3)	1	247,467	247,467
Lean Surge Tank	Fixed roof tank	CS	Fisher et al., 2007	Volume (m^3)	4	1,438,176	1,438,176
Reclaimer			Fisher et al., 2007		4	12,237,180	12,237,180
Cooling Water System-Utility	Includes cooling tower, basin, fans and pumps		Fisher et al., 2007	Water Flow rate (m^3/h)	1	13,836,149	13,836,149
CO_2 Compression train							
Compressor	Centrifugal compressor including drive, gear, plate	SS	www.mhhe.com	Power (kW)	1	43,941,098	43,941,098
Compressor Inter-stage Coolers	Shell & tube, water cooled	SS tubes & CS shell	Fisher et al., 2007	Area, m^2	1	3,132,646	3,132,646
Compressor Inter-stage Separators	Horizontal vessel	SS	Fisher et al., 2007	Volume (m^3)	1	128,695	128,695
Natural Gas Auxiliary Boiler			Singh et al. (2003)		1	56,197,768	
Total **P**urchased **E**quipment **C**ost (**PEC**)						255,731,228	199,533,460

Table 9.5: Total capital requirement for MEA process with CO_2 compression

Description		Cost (US$)		
		Case-1 (Aux.)	Case-2 (33.0%)	Case-3 (22.5%)
Direct	% of PEC			
Purchased equipment cost (PEC)	100	255,731,228	199,533,460	199,533,460
Purchased equipment installation	55	140,652,176	109,743,403	109,743,403
Instrumentation and control	20	51,146,246	39,906,692	39,906,692
Piping	25	63,932,807	49,883,365	49,883,365
Electrical	11	28,130,435	21,948,681	21,948,681
Building and building services	15	38,359,684	29,930,019	29,930,019
Yard improvements	10	25,573,123	19,953,346	19,953,346
Service facilities	20	51,146,246	39,906,692	39,906,692
Land	5	12,786,561	9,976,673	9,976,673
Spare parts (Schach et al., 2010)	4	10,229,249	7,981,338	7,981,338
Total direct cost		677,687,755	528,763,669	528,763,669
Indirect cost				
Engineering (Abu-Zahra et al., 2007)	10	25,573,123	19,953,346	19,953,346
Construction expenses (Abu-Zahra et al., 2007)	10	25,573,123	19,953,346	19,953,346
Contactor's fee (Abu-Zahra et al., 2007)	0.5	1,278,656	997,667	997,667
Contingency (Abu-Zahra et al., 2007)	17	43,474,309	33,920,688	33,920,688
Interest and inflation (Fisher et al., 2007)	10	25,573,123	19,953,346	19,953,346
Total indirect cost		121,472,333	94,778,394	94,778,394
Fixed capital investment (FCI)	Dir. + Ind. cost	799,160,088	623,542,063	623,542,063
	% of FCI			
Working investment	15	119,874,013	93,531,309	93,531,309
Start-up+ MEA cost	10	79,916,009	62,354,206	62,354,206
Total Capital Investment (TCI)		998,950,111	779,427,578	779,427,578

9.2.2.2 Operating Cost of MEA Process

The total operating cost can be divided into two main categories: manufacturing cost and general expenses. Manufacturing cost includes all expenses directly connected with the manufacturing operation or the physical equipment of a process plant. These expenses are grouped under three classifications: direct production costs, fixed charges and plant-overhead costs. General expenses which include administrative and R&D cost are added with manufacturing cost to calculate total operating cost. Raw material cost is considered here zero because the initial MEA cost is already included with start-up cost during total capital investment calculation. Makeup MEA includes both the evaporation and degradation losses. Solvent loss due to degradation is estimated assuming a factor of 1.5 kg MEA/tonne CO_2 (Rao and Rubin, 2002). The solvent loss due to evaporation from the absorber and stripper is obtained from simulation. The CO2 capture and compression unit requires electricity to drive inlet gas blower, all pumps and CO_2 compressor, and steam to operate the stripper reboiler. These utilities are taken into account with the derating of the power plant; therefore, no explicit cost is associated with them. Table 9.6 summarizes the energy requirements for the MEA process which contribute to the plant derating. The base plant has auxiliary power requirements of ~29 MW as reported in Fisher et al. 2007. Therefore, the net capacity without capture is considered here at 471 MW. The total electricity consumed by the blower, pumps and compressor is 82.8 MW which is responsible for the de-rating a 500 MW power plant by 16.5% and steam requirement for stripper reboiler could de-rate the plant by 27% and 18.5% for consideration of 33% and 22.5% net plant thermal efficiency respectively.

The major components and associated factors/parameters for calculating the total operating cost for CO_2 capture by MEA process and compression are presented in Table 9.7. The total operating cost was found to be $113 and $49 million per year respectively for the CO_2 capture plant with auxiliary NG boiler for steam supply for reboiler and for the CO_2 capture plant with use of power plant's own electricity for compression requirement and steam for reboiler. The contribution of the auxiliary natural gas boiler unit's fuel cost to the total operating cost is 44%.

Table 9.6: Plant de-rating results with MEA capture process

Description			Plant Derated for		
			Electricity	Steam & Electricity	
			Case-1 (Aux.)	Case-2 (33%)	Case-3 (22.5%)
		Units			
Inlet Gas Blower	Electricity	MWe	23.3	23.3	23.3
Rich Amine Pump	Electricity	MWe	1.2	1.2	1.2
Stripper Reflux Pump	Electricity	MWe	0.004	0.004	0.004
Lean Amine Pump	Electricity	MWe	1.2	1.2	1.2
Make-up Pump	Electricity	MWe	0.008	0.008	0.008
CO_2 Compressor	Electricity	MWe	57.2	57.2	57.2
Reboiler*	Steam	MWe	0	128.0	87.3
Base Plant derating before capture		MWe	29.0	29.0	29.0
Total De-rating		MWe	111.8	239.8	199.1
Plant Gross generating capacity before capture		MWe	500.0	500.0	500.0
Plant Net generating capacity with capture		MWe	388.2	260.2	301

*Thermal energy converted to electric energy

Table 9.7: Total operating cost for MEA capture process with CO_2 compression

Description		Cost (US$)		
		Case-1 (Aux.)	Case-2 (33.0%)	Case-3 (22.5%)
Direct production cost				
Raw material (initial start-up MEA)	Included in TCI	0	0	0
Cooling water	\$ 0.02 /m^3	10,847	10,847	10,847
Makeup water (process)	\$ 1.24 /m^3	4,883	4,883	4,883
Makeup MEA (evap. + degradation)	\$ 1.6 /Kg	8,877,420	8,877,420	8,877,420
Natural gas for Auxiliary boiler	\$ 4.4 /GJ	49,947,553		
Maintenance and repair (M) (Fisher et al., 2007)	2.2 % of FCI	17,581,522	13,717,925	13,717,925
Operating labor (OL) (Rao and Rubin, 2002)	Two jobs per shift @ \$ 45 /h	675,000	675,000	675,000
Supervision and supports (S) (Rao and Rubin, 2002)	30% of OL	202,500	202,500	202,500
Operating supplies	15% of M	2,637,228	2,057,689	2,057,689
Laboratory charges	10% of OL	67,500	67,500	67,500
Fixed Charge				
Local taxes	1% of FCI	7,991,601	6,235,421	6,235,421
Insurance	1% of FCI	7,991,601	6,235,421	6,235,421
Plant overhead cost	60% of (M + OL + S)	11,075,413	8,757,255	8,757,255
General Expenses				
Administrative	15% of OL	101,250	101,250	101,250
R & D	5% of TOPC	5,640,227	2,470,690	2,470,690
Total Operating Cost (OPC)		112,804,545	49,413,801	49,413,801

9.2.2.3 Annual Capital Requirement for MEA

The total annual cost is comprised of amortized capital cost and the plant operating cost. The amortized capital cost is calculated over 25 years with 7% interest rate and $0.0 salvage value. Table 9.8 summarizes the total annual cost for MEA case. The annual payment for the total capital cost is $ 86 million and $ 67 million for Case-1 (aux.) and Case-2/3 respectively. The operating cost represents 57% and 42% of the total annual cost of CO_2 capture and compression. The total annual cost for CO_2 capture and compression for MEA case (at 0.4 lean loading and 85% capture) is calculated to be $397/kW and 232/kW respectively. In an exactly same size coal power plant (i.e., 500 MW), the study by Fisher et al. (2007) reported a total annual cost for CO_2 capture and compression of $195/kW.

Table 9.8: Annual CO_2 Capture and Compression Cost for MEA

Description	Cost (US$)		
	Case-1 (Aux.)	Case-2 (33.0%)	Case-3 (22.5%)
Total Capital Investment	998,950,111	779,427,578	779,427,578
Amortized Capital Cost ($/year)	85,720,426	66,883,084	66,883,084
Total Operating Cost ($/year)	112,894,545	49,413,801	49,413,801
Total Annual Cost	198,524,971	116,296,884	116,296,884

9.2.2.4 Cost of CO_2 Avoided for MEA process

The base plant cost of electricity (COE) was assumed at 5.5 cents/kWh. This is the updated value of the 5.0 cents/kWh (2006 dollar basis) for 2010 year (Fisher et al. 2007). The cost of CO_2 avoided is calculated as follows.

$$\text{Cost of } CO_2 \text{ avoided} = \frac{\left(\text{COE}_{\text{with capture}} - \text{COE}_{\text{without caputre}}\right)}{\left(CO_2 \text{ emissions without capture} - CO_2 \text{ emissions with capture}\right)}$$

$$\frac{\$}{\text{tonne } CO_2} = \frac{\frac{\text{cents}}{\text{kWh}} \; \frac{1000 \text{ kWh}}{1 \text{MWh}} \; \frac{1\$}{100 \text{ cents}}}{\frac{\text{tonne } CO_2}{\text{MWh}}}$$

Table 9.9 shows the overall results of the before and after CO_2 capture and compression from a coal fired power plant. An increase in the cost of electricity of around 8, 10 and 8 cents/kWh can be seen as a result of adding a MEA capture and compression plant in a power plant with an auxiliary NG boiler and with internal steam extraction for stripper reboiler respectively. The estimated cost of CO_2 avoided for the above cases are found 126, 137 and 103 \$/tonne CO_2 respectively. Comparing these results with the results reported in the IEA paper (2011) and in Fisher et al. (2007), we observe that the values estimated here are higher than those of IEA and Fisher et al. (2007). These higher values can be foreseen by the differences in different factors and utility prices used in capital and operating cost estimation with inclusion of almost all of the equipments. These will be explained in the following section in details.

Table 9.9: Cost of CO_2 avoided for MEA process

Description		Plant derated for		
		Electricity	Steam and electricity	
		Case-1 (Aux.)	Case-2 (33%)	Case-3 (22.5%)
	Units			
Gross generating capacity	MWe	500	500	500
Net generating capacity without CO_2 capture	MWe	471	471	471
CO_2 emitted - without capture	tonne/h	491	491	491
	tonne/MWh	1.04	1.04	1.04
Base plant cost of electricity (COEb)	cent/kWh	5.5	5.5	5.5
Base plant annual cost	$/year	194,287,500	194,287,500	194,287,500
Net generating capacity with CO_2 capture	MWe	388	260	301
Annual CO_2 capture and compression cost	$/year	198,524,971	116,296,884	116,296,884
Base plant annual cost with CO_2 capture and compression	$/year	392,812,471	310,584,384	310,584,384
CO_2 emission with capture plant				
Auxiliary natural gas boiler (directly emitted)	tonne/h	85	0	0
CO_2 emitted after capture	tonne/h	74	74	74
CO_2 emitted (total) - with capture	tonne/h	158.37	73.69	73.69
	tonne/MWh	0.41	0.28	0.24
Cost of Electricity (COE) with capture and compression	cent/kWh	13.5	15.9	13.8
Increase in COE	%	145	189	150
Cost of CO_2 avoided	$/tonne	126	137	103

9.3 Membrane Process Economics

For the membrane process it is assumed that the power plant output reduction is due the electricity requirements by the membrane CO_2 capture plant. Two membrane process configurations are considered for economic analysis. One considers feed compression and permeate vacuum for first membrane stage (Conf. 14) and the other considers permeate vacuum for first membrane stage (Conf. 15).

9.3.1 Equipment Sizing and Selection for Membrane

Based on the same design basis described in Chapter 6 and in the previous subsection, the membrane process related equipments have been sized. The vacuum pumps used here are two stage liquid seal blower with made of stainless steel (www.matche.com). For the expander, a radial type has been used (www.mhhe.com). The membrane skids consist of hollow fibre modules with Polaris^{TM} membrane (Merkel et al., 2010) which has CO_2/N_2 selectivity of 50 and permeance of 1000 gpu. Another membrane with same selectivity but higher permeance i.e, 1850 gpu is also considered although the reported selectivity for this membrane was 60 (Yave et al. 2010). The membrane capture and compression unit is divided into two blocks: five parallel capture trains and a single CO_2 compression train. One cooling water utility system is considered for providing cooling water. Table 9.10 presents the major equipments used in this study along with the key sizing parameters for 85% CO_2 capture with CO_2 purity $\geq$ 98% and final CO_2 product delivery at 40^{o}C and 110 bar.

Table 9.10: Equipment sizing information for Membrane process

Description	Units	CO_2 Permeance, gpu			
		1000 (original)		1850 (new)	
Process Configurations (in Chapter 5)		Conf. 15	Conf. 14	Conf. 15	Conf. 14
Number of CO_2 capture trains		5	5	5	5
Number of CO_2 compression trains		1	1	1	1
Flue gas Cooler					
Quantity per unit		5	5	5	5
Cooler duty per train	kW	1914	1914	1914	1914
Vacuum Pump 1					
Quantity per unit		5	5	5	5
Flow rate per train	m^3/s	353	38	375	51
Vacuum condition (suction pressure)	kPa	10	10	10	10
Outlet pressure	kPa	101	101	101	101
Brake power per train	kW	12180	1300	12948	1743
Vacuum Pump 2					
Quantity per unit		5	5	5	5
Flow rate per train	m^3/s	205	360	214	271
Vacuum condition (suction pressure)	kPa	10	10	10	10
Outlet pressure	kPa	101	101	101	101
Brake power per train	kW	7029	12234	7360	9191
Feed Compressor					
Quantity per unit			5		5
Number of stages			5		5
Compressor discharge pressure	kPa		214		300
Total brake power required per train	kW		12099		17920
Inlet gas flow rate - Stage 1	m^3/s		112		113
Inlet gas pressure - Stage 1	kPa		101		101
Compressor Inter-stage Coolers					
Quantity per unit			5		5
cooler duty per train	kW		10888		16128
Permeate Compressor					
Quantity per unit		5	5	5	5
Number of stages		5	5	5	5
Compressor discharge pressure	kPa	926	576	759	800
Total brake power required per train	kW	6715	9090	6365	8179
Inlet gas flow rate - Stage 1	m^3/s	20	36	21	27
Inlet gas pressure - Stage 1	kPa	101	101	101	101
Compressor Inter-stage Coolers					
Quantity per unit		5	5	5	5
cooler duty per train	kW	8221	8181	5729	7361

Table 9.10: Equipment sizing information for Membrane process (continued)

Description	Units	CO_2 Permeance, gpu			
		1000 (Merkel et al. 2010)		1850 (Yave et al., 2010)	
Process Configurations (in Chapter 5)		Conf. 15	Conf. 14	Conf. 15	Conf. 14
Membrane Module					
Length (Hollow fibre)	m	0.5	0.5	0.5	0.5
Outer Diameter	m	0.0005	0.0005	0.0005	0.0005
Membrane CO_2/N_2 selectivity		50	50	50	50
Stage –I					
Quantity per unit		5	5	5	5
Area per train	m^2	1.13E+06	2.96E+05	7.18E+05	8.97E+04
Stage –II					
Quantity per unit		5	5	5	5
Area per train	m^2	2.74E+05	6.58E+04	1.94E+05	3.29E+04
Stage –III					
Quantity per unit		5	5	5	5
Area per train	m^2	3.48E+03	6.28E+03	2.70E+03	2.55E+03
Total membrane area per train	m^2	1.41E+06	3.68E+05	9.15E+05	1.25E+05
Expander					
Quantity per unit		5	5	5	5
Flow rate per train	m^3/s	0.7	3.8	1	1.6
power recoverable per train	kW	494.5	1040	732.6	889.8
Inlet pressure	kPa	926	576	759	800
Outlet pressure	kPa	303	303	303	303
CO_2 Compression train					
Compressors					
Quantity per unit		1	1	1	1
Number of stages		5	5	5	5
Compressor discharge pressure	kPa	110000	110000	110000	110000
Brake power required per train	kW	52074.8	52075.8	52042.9	52060.8
Inlet gas flow rate - Stage 1	m^3/s	69.8	69.8	69.9	69.8
Inlet gas pressure - Stage 1	kPa	101	101	101	101
Compressor Inter-stage Coolers					
Quantity per unit		1	1	1	1
Cooler duty per train	kW	4489	4489	4489.5	4489
Cooling Water System-Utility					
Cooling water requirement (total)	m^3/s	4.1	4.6	4.0	5.0

9.3.2 Cost Analysis for Membrane

The information on both equipment and operating cost was obtained from the same sources as for the MEA case (Fisher et al., 2007; Peters et al., 2003; www.matche.com; www.mhhe.com) except for the membrane skid (Merkel et al., 2010). All equipment cost data were adjusted for inflation by adopting current CEPCI value for 2010 i.e., 550.8. The same six-tenths-rule is applied to scale up/down to a new capacity or power or area for new equipment as used for MEA. The assumptions and specifications used in this economic evaluation for membrane gas separation based capture process are presented in Table 9.11.

Table 9.11: Assumptions and parameters for membrane processes evaluation

All values in 2010 US dollars	
Project life	25 years
Equipment salvage value	0.0
Construction periods	2 years
Plant operation	7500 h/year
Interest rate	7%
Membrane cost (Skid)	\$50 /m^2
Membrane life	4 years
Membrane replacement cost	25% total membrane cost (per year operating cost)
Cooling water price	\$0.02 /m^3
Membrane CO_2 permeance, gpu	1000 (Merkel et al., 2010) and 1850 (Yave et al., 2010)
Membrane CO_2/N_2 selectivity	50 (Merkel et al., 2010)

9.3.2.1 Capital Cost for Membrane Process

The Membrane capture and compression unit capital cost consists of five capture trains and one compression train. Equipment not simulated, such as cooling tower is costed by considering a scaling factor based on the flow rate of the stream related to those units. Flue gas pre-treatment system, CO_2 dehydration system and CO_2 pipeline for transportation and sequestration are not included in the cost analysis. Table 9.12 presents the list of equipments and their purchased costs for 85% recovery of CO_2 from a 500 MW coal-fired power plant flue gas stream. The sum of the component costs represents the total purchased equipment cost (PEC). It is observed from Table 9.12 that the major contributors to the purchased equipment cost are the membrane skids, feed compressor (for Configuration 14) and permeate compressor (for both configurations). Membrane cost is the major cost for the process Conf. 15 which uses permeate vacuum for 1^{st} stage. The cost comprises of 67% (1850 gpu) to 75% (1000 gpu) of the total purchased cost, and the next is permeate compressor. For Conf. 14, the feed and permeate compressors are found the main cost contributors. Conf. 14 with 1850 gpu shows the lowest membrane cost. The highest total purchased equipment cost is $466 million for Conf. 15 with 1000 gpu permenace and the lowest cost is $200 million for Conf. 14 with 1850 gpu.

Table 9.13 presents the factors used and the compositions of the total capital investment (TCI). The highest and the lowest capital investment for the membrane processes including compression are found to be $2681 /kW and $1149 /kW, respectively. The lowest capital cost estimated for MEA is $ 1559/kW.

Table 9.12: Purchased Equipment Cost for Membrane process

Description	Type	Material Construct.	Costing source	Scaling factor	Cost (US$)			
					CO_2 Permeance, gpu			
Process Configurations					1000 (Merkel et al. 2010)		1850 (Yave et al., 2010)	
					Conf. 15	Conf. 14	Conf. 15	Conf. 14
Membrane Skids	Hollow fibre module	Polymers	Merkel et al., 2010	Area, m^2	351,255,103	92,000,000	228,518,879	31,304,070
Flue gas Cooler	SS shell & tubes	SS tubes & CS shell	Fisher et al., 2007	Area (m^2)	688,881	688,881	688,881	688,881
Vacuum pump 1	Blower type (two stage liquid seal); incl. electric motor	SS	www.matche.com	Flow rate (m^3/min)	17,518,564	4,571,129	18,045,419	5,453,461
Vacuum pump 2	Blower type (two stage liquid seal); incl. electric motor	SS	www.matche.com	Flow rate (m^3/min)	12,621,540	17,594,973	12,896,084	13,171,236
Feed Compressor	Centrifugal compressor including drive, gear mounting, base plate and cooler	SS	www.mhhe.com	Power (kW)	n/a	47,390,190	n/a	59,985,439
Permeate Compressor	Centrifugal compressor including drive, gear mounting, base plate and cooler	SS	www.mhhe.com	Power (kW)	33,565,307	39,920,011	32,235,733	37,467,636
Expander	Radial	SS	www.mhhe.com	Power (kW)	766,818	1,198,023	970,706	1,090,831
CO_2 compression	Centrifugal compressor including drive, gear mounting, base plate and cooler	SS	Fisher et al., 2007 & www.mhhe.com	Power (kW)	41,966,118	41,966,118	41,966,118	41,966,118
Cooling Water System-Utility	Includes cooling tower, basin, fans and pumps		Fisher et al., 2007	Flow rate (m^3/h)	7,472,395	8,073,894	7,448,230	8,520,596
Total **P**urchased **E**quipment **C**ost (**PEC**)					**465,854,726**	**253,403,219**	**342,770,051**	**199,648,267**

Table 9.13: Total capital requirement for Membrane process with CO_2 compression

Process configurations		Cost (US$)			
		CO_2 Permeance, gpu			
		1000 (Merkel et al. 2010)		1850 (Yave et al., 2010)	
		Conf. 15	Conf. 14	Conf. 15	Conf. 14
	% of PEC				
Direct					
Purchased equipment cost (PEC)	100	465,854,726	253,403,219	342,770,051	199,648,267
Purchased equipment installation	50	232,927,363	126,701,610	171,385,025	99,824,134
Instrumentation and control	10	46,585,473	25,340,322	34,277,005	19,964,827
Piping	10	46,585,473	25,340,322	34,277,005	19,964,827
Electrical	5	23,292,736	12,670,161	17,138,503	9,982,413
Building and building services	15	69,878,209	38,010,483	51,415,508	29,947,240
Yard improvements	10	46,585,473	25,340,322	34,277,005	19,964,827
Service facilities	10	46,585,473	25,340,322	34,277,005	19,964,827
Land	5	23,292,736	12,670,161	17,138,503	9,982,413
Spare parts (Schach et al., 2010)	4	18,634,189	10,136,129	13,710,802	7,985,931
Total direct cost		1,020,221,850	554,953,050	750,666,412	437,229,705
Indirect cost					
Engineering (Abu-Zahra et al., 2007)	10	46,585,473	25,340,322	34,277,005	19,964,827
Construction expenses (Abu-Zahra et al., 2007)	10	46,585,473	25,340,322	34,277,005	19,964,827
Contactor's fee (Abu-Zahra et al., 2007)	0.5	23,292,736	12,670,161	17,138,503	9,982,413
Contingency (Abu-Zahra et al., 2007)	10	46,585,473	25,340,322	34,277,005	19,964,827
Interest and inflation (Fisher et al., 2007)	10	46,585,473	25,340,322	34,277,005	19,964,827
Total indirect cost		209,634,627	114,031,449	154,246,523	89,841,720
Fixed capital investment (FCI)	Dir.+Ind.	1,229,856,476	668,984,891	904,912,934	527,071,426
	% of FCI				
Working investment	8	98,388,518	53,518,760	72,393,035	42,165,714
Start-up cost	1	12,298,565	6,689,845	9,049,129	5,270,714
Total Capital Investment (TCI)		**1,340,543,559**	**729,193,103**	**986,355,099**	**574,507,854**

9.3.2.2 Operating Cost of Membrane Process

The same methodology has been adopted for estimating operating cost of the membrane processes. Membrane life is considered four years and replacement cost per year is considered 25% of the total membrane cost. One job per shift is considered for calculating operating labour for the membrane plant. It is assumed that membrane processes use base plant's electricity for driving vacuum pumps and compressors. Table 9.14 summarizes the energy requirements for MEA process which contribute to the plant de-rating. The base plant has auxiliary power requirements of ~29 MW as reported in Fisher et al. 2007. Therefore, the net capacity without capture is considered 471 MW. The percentage of base plant de-rating ranges from 42% to 52% due to electricity consumption by the capture and compression plant.

The major components and associated factors/parameters for calculating the total operating cost for CO_2 capture by membrane gas separation processes are presented in Table 9.15. The total operating cost estimated ranges from $ 42 and $ 167 million per year. For the MEA case it ranges from $ 49 to $ 112 million per year.

Table 9.14: Plant de-rating results with Membrane capture process

Process Configurations	Units	Derating contribution			
		CO_2 Permeance, gpu			
		1000 (Merkel et al. 2010)		1850 (Yave et al., 2010)	
		Conf. 15	Conf. 14	Conf. 15	Conf. 14
Vacuum Pump 1	MWe	60.90	6.50	64.74	8.71
Vacuum Pump 2	MWe	35.14	61.17	36.80	45.96
Feed Compressor	MWe	0	60.49	0	89.60
Permeate Compressor	MWe	33.6	45.5	31.8	40.9
Expander	MWe	-2.5	-5.2	-3.7	-4.5
CO_2 Compressor	MWe	52.1	52.1	52.0	52.1
Base Plant derating	MWe	29	29	29	29
Total De-rating	MWe	208.2	249.5	210.6	261.8
Gross generating capacity before capture	MWe	500	500	500	500
Net generating capacity with capture	MWe	291.8	250.5	289.3	238.2

Table 9.15: Total operating cost for membrane capture process with CO_2 compression

Process Configurations	Unit or basis	Cost (US$/year)			
		CO_2 Permeance, gpu			
		1000 (Merkel et al. 2010)		1850 (Yave et al., 2010)	
		Conf. 15	Conf. 14	Conf. 15	Conf. 14
Direct production cost					
Cooling water	\$ 0.02 /m^3	2,182,740	2,700,000	2,182,740	2,700,000
Membrane replacement	25% of membrane cost	87,813,776	23,000,000	57,129,720	7,826,018
Maintenance and repair (M)	2% of FCI	24,597,130	13,379,690	18,098,259	10,541,429
Operating labor (OL) (Rao and Rubin, 2002)	One job per shift @ \$ 45 /h	337,500	337,500	337,500	337,500
Supervision and supports (S) (Rao and Rubin, 2002)	30% of OL	101,250	101,250	101,250	101,250
Operating supplies	15% of M	3,689,569	2,006,953	2,714,739	1,581,214
Laboratory charges	10% of OL	33,750	33,750	33,750	33,750
Fixed Charge					
Local taxes	1% of FCI	12,298,565	6,689,845	9,049,129	5,270,714
Insurance	1% of FCI	12,298,565	6,689,845	9,049,129	5,270,714
Plant overhead cost	60% of (M + OL + S)	15,021,528	8,291,064	11,122,205	6,588,107
General Expenses					
Administrative	15% of OL	50,625	50,625	50,625	50,625
R & D	5% of TOPC	8,338,158	3,330,554	5,782,581	2,121,122
Total Operating Cost (OPC)		166,763,154	66,611,076	115,651,627	42,422,443

9.3.2.3 Annual Capital Requirement for Membrane Process

Table 9.16 summarizes the total annual cost for the membrane processes. The total annual capture cost for CO_2 capture by membrane gas separation processes ranges from $ 92 million to $ 282 million whereas for MEA process it ranges from $ 116 to $ 199 million. The operating cost constitutes 46% to 59% of the total annual cost.

Table 9.16: Annual CO_2 Capture and Compression Cost for Membrane

Description	Cost (US$)			
	CO_2 Permeance, gpu			
	1000 (Merkel et al. 2010)		1850 (Yave et al., 2010)	
Process Configurations	Conf. 15	Conf. 14	Conf. 15	Conf. 14
Total Capital Investment	$ 1,340,543,559	$ 729,193,103	$ 986,355,099	$ 574,507,854
Amortized Capital Cost ($/year)	$ 115,032,736	$ 62,572,437	$ 84,639,641	$ 49,298,816
Total Operating Cost ($/year)	$ 166,763,154	$ 66,611,076	$ 115,651,627	$ 42,422,443
Total Annual Cost	$ 281,795,891	$ 129,183,514	$ 200,291,268	$ 91,721,259

9.3.2.4 Cost of CO_2 Avoided for Membrane Process

The cost of CO_2 avoided for the membrane processes is calculated the same way as the MEA process. Table 9.17 shows the cost of CO_2 avoided and increase of electricity price for the base power plant. An increase in the cost of electricity ranges from 10.5 cents/kWh to 16 cents/kWh which is much higher than that of the MEA process, ranges from 8 to 10 cents/kWh. The estimated cost of CO_2 avoided for membrane processes ranges from 143 to 206 $/tonne which are also higher than those of the MEA process.

Table 9.17: Cost of CO_2 avoided for membrane process

	Unit	CO_2 Permeance, gpu			
		1000 (Merkel et al. 2010)		1850 (Yave et al., 2010)	
Process Configurations		Conf. 15	Conf. 14	Conf. 15	Conf. 14
Gross generating capacity	MWe	500	500	500	500
Net generating capacity without CO_2 capture	MWe	471	471	471	471
CO_2 emitted - without capture	tonne/h	491	491	491	491
	tonne/MWh	1.04	1.04	1.04	1.04
Base plant cost of electricity	cent/kWh	5.5	5.5	5.5	5.5
Base plant annual cost	$/year	194,287,500	194,287,500	194,287,500	194,287,500
Net generating capacity with CO_2 capture	MWe	291.8	250.5	289.3	238.2
Annual CO_2 capture and compression cost	$/year	281,795,891	129,183,514	200,291,268	91,721,259
Base plant annual cost with CO_2 capture and compression	$/year	476,083,391	323,471,014	394,578,768	286,008,759
CO_2 emitted (total) - with capture	tonne/h	74.0	74.0	74.0	74.0
	tonne/MWh	0.25	0.30	0.26	0.31
Cost of Electricity (COE) with capture and compression	cent/kWh	21.8	17.2	18.2	16.0
Increase in COE	%	296	213	231	191
Cost of CO_2 avoided	$/tonne	206	157	161	143

9.4 Comparison with other studies

9.4.1 MEA process

As mentioned at the beginning of this chapter, there are several published studies reported in the area of techno-economic analysis of MEA based post-combustion CO_2 capture process for coal-fired power plant. Only the work of Fisher et al. (2007), a DOE/NETL report will be compared with this study. Their overall works were very transparent and comprehensive, especially in terms of equipment sizing. The authors considered a similar size of power plant, i.e. 500 MW, as considered here. They de-rated the plant for both the steam and the electricity, i.e. the energy requirements to operate the main facility and the CO_2 capture unit were withdrawn from the main power facility output either through electricity or steam. To make comparison easier, the dollar basis for Fisher's (2007) study is updated to 2010 year from 2006 year. Table 9.18 summarizes the different costs for the present study with 22.5% net thermal efficiency of the power plant (after de-rating for steam and electricity requirements) and the study of Fisher et al. (2007). It is clear from Table 9.18 that the present study estimates higher capture cost ($103/tonne CO_2 avoided) than that of Fisher's study ($74/tonne CO_2 avoided). This is due to the several reasons. For example, $ 42.8 million extra purchased equipment cost is mainly coming from the increased cost of the absorber and stripper towers due to the consideration of feed space, top and bottom disengagement space and skirt height (total four meters) with the calculated separation height in the present study. Without this extra height for absorber and stripper, the estimated capture cost is $91/tonne CO_2 avoided as shown in Table 9.18 (last column).

The costs estimated in the present study for some capital investment components such as working capital and start-up cost are higher than that of the Fisher's study due to different methods of estimation and also consideration of different weights for the factors. These contribute to the increase of capital cost in the present study. The capital cost also increased due to the consideration of components, such as service facilities, building and building services, yard improvement, electric services, etc., which were not considered in the Fisher's study. In the present study the amortized capital cost is calculated over 25 years with 7% interest rate and $0.0 salvage value. As Fisher et al. (2007) used a capital

recovery factor of 0.14 to calculate the annual capital investment, it resulted ultimately in higher annual capital cost in the Fisher's study.

The operating cost estimated by Fisher et al. (2007) is much lower than that of the present study. The difference is coming from different ways of estimating maintenance costs in the two studies, and also for not considering some cost components in the Fisher's study, such as plant overhead cost, local taxes, insurance, administrative and R&D expenses.

The difference in plant de-rating between the two studies for steam and electricity usage by the capture plant from the base plant is 38 MW. The lower usage of electricity by the blower considered in the Fisher's study was due to the lower pressurisation of flue gas (10 kPa, to overcome the pressure drop in the direct contact cooler and in the absorber) compared to the higher pressurisation (30 kPa) in the present study. This 20 kPa pressure rise by the blower consumed 15 MW of extra power in the present study which contributed 39% of the total de-rating difference. Another reason for lower de-rating in the Fisher's study was the use of steam turbine for driving the CO_2 compressor instead of electric driver. They used the same superheated steam (at intermediate pressure) for the turbine and also to supply the necessary heat to the stripper reboiler. Using this approach they had been able to supply 10 MW excess power to the grid by satisfying the electricity demand for CO_2 compressor and at the same time met the energy demand of the reboiler. This approach looks very attractive for fulfilling demands for both the electricity (for compressor) and energy (reboiler) at the same time with same amount of steam, but implementation of this approach may be technically challenging. To assess the capital intensity of this approach, all the necessary equipment cost in the economic analysis should be included.

This is true that the values of the factors considered for calculating components of the capital and operating cost have a great influence on overall economic analysis of the plant. The present study tried to consider the factors' values for most of the components between the ranges mentioned elsewhere (Peters et al., 2003). The use of the six-tenths-factor rule in the present study for estimating equipments costs (by scaling) from different sources might also have contributed to some differences in purchased equipment cost.

Table 9.18: Comparison of MEA based capture processes

Description	**Unit**	**Fisher et al. (2007)**	**This study** (with extra height for Ab. And St.)	**This study** (without extra height)
Costing year		2010	2010	2010
Dollar basis		US	US	US
Gross power output	MW	500	500	500
Fuel type		Sub bituminous coal	Mixture of PRB and USLS coal	Mixture of PRB and USLS coal
Net power output without capture	MW	471	471	471
Base plant cost of electricity (COE)	cent/kWh	5.5	5.5	5.5
CO_2 capture efficiency	%	90	85	85
CO_2 compression	bar	150	110	110
Total de-rating	MW	161	199	199
Net power output with capture and compression	MW	339	301	301
Purchased equipment cost	$	157,685,955	199,533,460	156,667,491
Capital investment	$	548,494,710	779,427,578	611,982,387
Amortized Capital cost	$/year	76,842,994	66,883,084	52,514,525
Operating cost	$/year	20,854,549	49,413,801	41,164,922
Total annual cost	$/year	97,697,543	116,296,884	93,679,447
Cost of Electricity (COE) with capture and compression	cent/kWh	11.8	15	12.8
Increase in COE	%	113	150	132
Cost of CO_2 avoided	$/tonne	74.1	103	91

9.4.2 Membrane Process

Among the reported economic evaluation studies of membrane gas separation processes in Section 9.1 (Ho et al., 2008 and Merkel et al., 2010), neither of them was comprehensive in terms of equipment sizing and the equipment cost. Ho et al. (2008) investigated the reduction of CO_2 capture cost by operating under vacuum condition. The flue gas from a 500 MW coal-fired power plant was used and the target for CO_2 recovery ranged from 85% to 90%. The reported CO_2 purity ranged from 43% to 77% which was very low compared to 98%. The base line cost of electricity assumed was 3.7 cents/kWh (updated for 2010) which is much lower than the value of 5.5 cents/kWh considered in the present study. The equipment costs and the material of construction information for vacuum pump and compressor were not provided, even the value of the total purchased equipment cost. Some of the plant's outside battery limits (OSBL) parameters such as building and building services, yard improvements, land and service facilities were not considered by Ho et al. (2008) in the capital cost estimation as considered in the present study. Ho et al. (2008) did not consider many parameters in similar fashion for estimating operating cost such as plant overhead cost, supervision and support labour, administrative cost, operating supplies, R&D cost etc. The estimated lowest capture cost reported was US$ 59.5/tonne CO_2 avoided for vacuum operation compared to US$ 90.4/tonne CO_2 avoided using a pressurized feed (values updated at 2010 dollar value). The lowest capture cost estimated in the present study ($143/tonne CO_2 avoided), as shown in Table 9.17, is found much higher than the lowest cost reported by Ho et al. (2007) due to the above mentioned reasons. Another difference is the consideration of 29 MW power de-rating of base plant before capture in the present study.

Merkel et al. (2010) reported $39 and $23 per ton CO_2 capture cost for two membrane process designs i.e., two-step/two-stage design and two-step counter-current sweep, respectively. The later uses incoming boiler air as sweep stream which helps to reduce the energy usage. The impact of increased CO_2 content in the air sent to the boiler is not clear yet. The costs were calculated in a different way than the method used in the present study to calculate the cost of CO_2 avoided. They considered the flue gas from a 600 MW coal-fired power plant along with a 90% CO_2 capture. The percentage of CO_2

concentration in the permeate stream was reported 95^{+}%. They used compression and condensation method to produce high pressure supercritical CO_2 for sequestration. The equipment cost for compressor, vacuum pump and expander were calculated using 500.0 $/kW basis. No cost for liquefaction unit was considered. Membrane skid cost was calculated at 50 $/m^2, same as in the present study. The total capital cost was calculated by multiplying the total equipment cost by an installation factor of 1.6. The cost of electricity was considered at 4.0 cents/kWh to calculate the operating cost. The annual capital cost was calculated based on 20% of the total membrane plant cost. No information regarding membrane life and replacement cost was reported. Many parameters related to plant operating cost, such as plant overhead cost, operating supplies, administrative cost, R&D cost, etc. that not included in their study. The plant indirect cost components such as engineering, construction expenses, contractor's fee, contingency and other direct cost parameters related with building and building services, land, etc., were also not considered in the estimation of the total capital cost. No start-up cost was considered. Their study did not consider base-plant de-rating as mentioned earlier for the present study. These contributed to lower capture cost estimation in their study. They concluded that if high permeance membranes could be developed with 4000 gpu or more or membrane skid costs could be reduced below $50/m^2, no feed compression will be the preferred approach from an energy and cost standpoint. They also concluded that increasing membrane CO_2/N_2 selectivity above 30 has little benefit (Merkel et al., 2010).

9.5 MEA and Membrane Process Comparison: Present study

After comparing the present economic studies for each process with the published works of similar process, this section compares the economics of the MEA process and membrane gas separation process simulated in the present study. Figure 9.1 compares the two processes in terms of increase in cost of electricity (%) and cost of CO_2 avoided ($/tonne). In all case studies, membrane gas separation processes are found more expensive than the MEA process either in terms of the cost of CO_2 avoided or the increase in cost of electricity (COE). The CO_2 capture cost for the membrane process ranges from $143 to $206/tonne of CO_2 avoided, whereas for the amine (MEA) case it ranges from $103 to $137/tonne of CO_2 avoided. The percent increase in COE ranges from 191 to 296 for membrane and from 145 to 189 for MEA. This section explains why the capture cost by membrane is higher than that of MEA in the present study. Two membrane configurations, one with feed compression (Conf. 14) and the other with permeate vacuum (Conf. 15) were considered, and compared to the MEA process with lowest capture cost. Details of the comparison are presented in Table 9.19 (third, fourth and fifth columns). It is found that the membrane process with feed compression along with permeate vacuum i.e., Conf. 14 (with recently developed and reported membrane properties, CO_2 Permeance: 1850 gpu, CO_2/N_2 Selectivity: 50) performs marginally better in terms of both the cost of CO_2 avoided and the percent increase in the cost of electricity compared to the vacuum operation, i.e. Conf. 15, but still can not compete with the MEA process economically. It is found that membrane process with Conf.14 can be a potential game changer due to process simplicity if membrane with CO_2/N_2 selectivity $\geq$ 80 can be materialised in a near future (selectivity of 60 has already been reported in Yave et al. 2010) which can be seen from the last column of Table 9.19. This is completely in contrast with the finding of Merkel et al. (2010) based on their two-step counter-current sweep design as mentioned earlier.

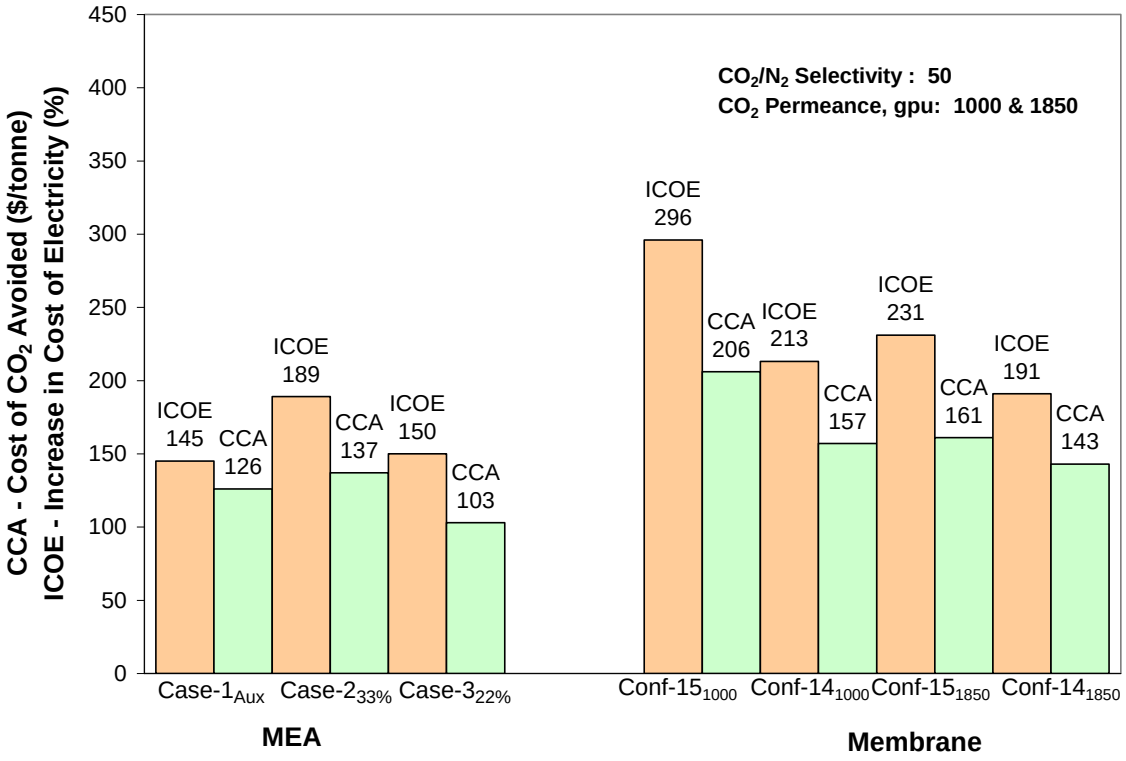

Figure 9.1: Cost of CO_2 Avoided and percent increase in the Cost of Electricity for MEA and Membrane processes

Table 9.19: Comparison of MEA and Membrane Processes

Description	**Unit**	**MEA**	**Membrane**		
		Case-3 (22.5%)	Conf.-14 (Permeance 1850 gpu, Selectivity 50)	Conf.-15 (Permeance 1850 gpu, Selectivity 50)	Conf.-14 (Permeance 1850 gpu, Selectivity 80)
Gross power output	MW	500	500	500	500
Net power output without capture	MW	471	471	471	471
Net power output with capture and compression	MW	301	238	289	276
Purchased equipment cost	$	199,533,460	199,648, 262	342,770,051	208,049,104
Capital investment	$	779,427,578	574,507,854	986,355,099	598,682,100
Amortized Capital cost	$/year	66,883,084	49,298,816	84,639,641	51,373,221
Operating cost	$/year	49,413,801	42,422,443	115,651,627	43,706,445
Total annual cost	$/year	116,296,884	91,721,259	200,291,268	95,079,665
Increase in cost of electricity (COE)	%	150	191	231	154
Cost of CO_2 avoided	$/tonne	103	143	161	110

9.6 Summary

A detailed techno-economic analysis for CO_2 capture from coal fired power plant flue gas has been investigated for both the MEA and membrane gas separation technologies. For MEA case, two options for stripper reboiler energy demand fulfilment have been adopted, one considering auxiliary NG boiler unit and another using steam from the power plant itself, i.e. de-rating the plant. For membrane, the de-rating option for electricity demand was adopted. It was found that MEA process results in a lower cost of CO_2 avoided and lower increase in cost of electricity compared to the membrane process. But still, the MEA process estimated a higher cost of CO_2 avoided, and higher increase of COE compared to figures reported in the IEA paper (2011) and Fisher et al. (2007) study, as shown in Table 9.1. This discrepancy is attributed mainly to extra height (feed space, top and bottom disengagement space and skirt height) consideration for absorbers and strippers in the present study and no consideration of different cost components by other authors in their studies. The variation in values of the different factors and assumptions considered and the methodology adopted also contribute to differences in economic analysis. The membrane process with lower energy requirement, i.e. vacuum operation, is found very capital intensive due to higher membrane area requirements. To be competitive with MEA process, improvement in membrane properties in terms of selectivity is required for feed compression with permeate vacuum type process. As current membrane exhibits CO_2 permeance of 1850 gpu and CO_2/N_2 selectivity of 60 (Yave et al., 2010), the prospect for developing desired membrane selectivity of 80 or above is bright.

Chapter 10

Conclusions and Recommendations

The importance of greenhouse gas mitigation technologies is gaining considerable attention in light of increasing concerns about climate change due to global warming through greenhouse effects. Carbon capture and sequestration (CCS) is one of the options that can enable the utilization of fossil fuels with lower CO_2 emissions. Post-combustion capture technologies represent one of the most promising methods of CO_2 capture. This class of technology can easily be retrofitted onto the existing fleet of power plants. The systematic design methodology developed in this thesis were employed to investigate the performance of two different technologies, i.e. membrane gas permeation and Monoethanolamine (MEA) based chemical absorption for post-combustion CO_2 capture from a 500MW power plant flue gas streams in the same simulation platform along with a techno-economic study. This chapter summarizes the conclusions from this research work and presents recommendations for future work.

10.1 General Conclusions and Contributions

From the work completed in this study, a number of important conclusions can be drawn with respect to the design viability and performance of membrane gas separation and MEA absorption/stripping to recover CO_2 from a coal-fired power plant in a retrofit case.

10.1.1 Membrane Gas Separation

AspenPlus software has applications in wide range of areas such as investigating alternative process flow sheets in R&D, optimizing plant and process schemes in design work, improving yield and throughput of existing plants, and training operators. As a detailed membrane model for multicomponent gas separation processes is not available in AspenPlus as a built-in model, a custom-built membrane unit was interfaced with the development of a FORTRAN subroutine based on a new solution algorithm (Chowdhury et al., 2005) for a widely accepted model, i.e. Pan (1986) for hollow fibre membrane to utilize the full capability of AspenPlus for simulating overall membrane and hybrid

processes in convenient and time saving means. The new solution algorithm overcame the complexities of the original approach to handle both rating and design type of problems without need of initial estimate of pressure profile, and then flow and concentration profiles. The portability of the developed model to any PCs for using by other end users to design other membrane gas separation systems (Tarun et al., 2007) or hybrid systems in AspenPlus® is a contribution from this research work.

Fifteen various single and multi-stage membrane process configurations with or without recycle streams and permeate sweep were examined through simulation and design study in AspenPlus® for post-combustion CO_2 capture from a 500 MW coal-fired power plant flue gas stream. The performance of all process configurations was compared on the basis of membrane area and power consumption requirements. It was found that only two process configurations, both having three membrane-stages as represented in Figure 5.14 and 5.15, were able to satisfy the design specifications i.e., 85% CO_2 recovery and 98% CO_2 purity using Polaris™ membrane (Lin et al., 2007) with a selectivity of 50 (CO_2/N_2) and CO_2 permeane of 1000 GPU. The net lowest energy requirement found for capture and compression was 40% of the total plant's generation output.

Optimization-based design methodology had been employed for selecting optimal process configuration from the two membrane process alternatives as represented in Figure 5.14 and 5.15, and the associated optimum operating and design conditions. It was found that power consumption and membrane area requirement can be saved up to 13% and 8% respectively by the optimization based design compare to the base case design for the final optimal process configuration. It was revealed from a post-optimal sensitivity analysis that any changes in any of these factors such as feed flow rate, feed concentration (CO_2), permeate vacuum and compression condition had great impact on plant performance especially on power consumption and product recovery.

10.1.2 MEA Process

Two different MEA solvent (30% wt) based absorption/stripping process configurations, the conventional and the Fluor concept, were examined realistically by considering all levels of modeling complexities to simulate and design industrial scale post combustion CO_2 capture process for flue gas stream of same capacity coal-fired power plant. AspenPlus® RadFrac model and both rate-based and equilibrium-stage based modeling approaches were employed. Eight different absorber/stripper models were

categorized based on the options to account for mass transfer, and the chemical reactions in the liquid film/phase. Initially, the following important points were investigated and resolved before detailed design studies, i.e. selection of kinetic models, approach to flooding and the tray pass, heat exchanger temperature approach, and film discretization methods. It was realized that the success of modeling CO_2 capture with MEA depends upon how the film discretization was carried out. It was found that most of the CO_2 was reacted in the film not in the bulk liquid. This insight could not be recognized with the traditional equilibrium-stage modeling.

Detailed simulation and design studies were conducted based on six different absorber/stripper models with a view towards minimizing the plant operating cost by reducing the reboiler energy requirements. It was found that the optimum/or minimum lean solvent loading ranges from 0.29 to 0.4 for most of the models and the reboiler energy ranges from 3.3 to 5.1 (GJ/ton captured CO_2) depending on the model considered. The calculated column diameter was found in the range 5.0-8.0 m for the absorber, and 4.0-6.8 m for stripper for all simulation runs. The column height ranges from 9.8-16.2 m for the absorber, and 14.4-17.1 m for stripper.

A performance study was conducted between the two process alternatives based on the same design condition, and it was found that Fluor concept process performed well in terms of plant operating (i.e., 8.5% less energy) and capital cost (i.e., 50% less number of strippers).

Finally, the closed-loop simulation of MEA capture process was found very challenging and difficult to convergence due to the highly nonlinear nature of the process, and the involvement of recycle stream. Trying to satisfy some realistic concerns other than process design specifications within industrial norm and practice, such as maintaining downcomer flooding level $\leq$ 50% for column stable operation, total pressure drop in the column $\leq$ 40 kPa to minimize upstream units' power requirement, and stripper reboiler temperature $\leq$ 120ºC to reduce thermal degradation of the solvent had added extra convergence challenges to the process simulation and design.

10.1.3 Hybrid Process

The potentialities of hybrid process which combines membrane permeation and conventional gas absorption/stripping using MEA in a two-in-parallel and two in-series arrangement was examined for post-combustion CO_2 capture. It was revealed that the

hybrid process was not a good choice for post-combustion CO_2 capture in terms of total energy requirement for capture and compression. By comparing the hybrid process with the stand-alone MEA and stand-alone membrane process, it was found that the stand-alone membrane gas separation process utilized the lowest energy.

10.1.4 Economic Evaluation

A detailed techno-economic analysis for CO_2 capture from coal fired power plant flue gas has been investigated for both the MEA and membrane gas separation processes. It was found that the MEA process results in a lower cost of CO_2 avoided and lower increase in cost of electricity compared to the membrane process. But the estimated cost of CO_2 avoided for the MEA process in this study (103 $/tonne) is higher than the figures reported in the IEA paper (2011) and in the DOE report (Fisher et al., 2007), i.e. 42 $/tonne (lowest) and 74 $/tonne, respectively. This discrepancy is attributed mainly to extra height (feed space, top and bottom disengagement space and skirt height) consideration for absorbers and strippers in the present study. The cost of CO_2 avoided estimated without consideration of extra height for absorber and stripper is 91 $/tonne, which is closer to DOE (Fisher et al., 2007) reported value. The membrane process with lower energy requirement as found in Chapter 6, i.e. vacuum operation, is found capital intensive due to higher membrane area requirements compared to feed compression and permeate vacuum process. To be competitive with MEA process, improvement in membrane properties in terms of selectivity (greater than 80) is required for feed compression with permeate vacuum type process. When the membrane selectivity is changed from 50 (presently available) to 80, the cost of CO_2 avoided decreases from 143 $/tonne to 110 $/tonne.

Both technologies studied for post-combustion CO_2 capture, i.e. membrane gas separation and solvent (MEA) based chemical absorption/stripping, have advantages and disadvantages. Research works are continuing to overcome those disadvantages in respective areas. In the near future, either improvement in present membrane and solvent properties, or development of new kind of membrane and solvent may be materialised. To investigate the impact of those findings or inventions in both technologies, the framework developed in this study for both technologies using the same process software platform, i.e. AspenPlus®, could be an excellent basis for design, simulation, optimization and economic study.

10.2 Recommendations

10.2.1 Membrane Gas Separation

- MTR has developed a membrane process to capture CO_2 from coal-fired power plant flue gas with a proprietary membrane (Lin et al., 2007; Merkel et al., 2009 and 2010). They utilized atmospheric air going to the coal combustion unit as a permeate sweep stream for a membrane unit to provide free driving force before sending it to the coal combustion chamber. To simulate MTR membrane type process with the proposed new process capable of handling sweep stream in this study, inclusion of a coal combustion model is recommended.
- The pressure and concentration dependent permeability correlation is recommended for a more realistic design instead of constant pure gas permeability.
- The membrane model interfaced with AspenPlus® simulation environment can be extended to process development of other systems such as natural gas treatment for CO_2/H_2S removal, air separation (oxygen enrichment), hydrogen recovery from ammonia purge stream, low temperature CO_2 separation in coal IGCC process, CO_2 capture from natural gas based H_2 plant, and also CO_2 capture from post-combustion where oxygen enriched air combustion is considered.

10.2.2 MEA Process

- The present MEA process simulation and design study evaluated the performance of sieve tray columns for absorber and stripper. It is recommended to extend the present technical know-how to design other types of tray columns (valve tray, bubble cape) and also packed columns (either random or structured packing) for post-combustion CO_2 capture from power plant exhaust gas to see how the column internals affects the process performance in terms of energy requirement.

- The design framework developed in this study can be extended to use for evaluating the process performance with the new activity and concentration based kinetic model reported elsewhere (Plaza et al., 2010; Aboudheir, 2003) using user kinetic subroutine.
- A comparative study is recommended to evaluate the performances of other amines or blend of amines with respect to MEA in terms of energy requirement for CO_2 capture from flue gas using the design framework developed in this study.
- The developed design methodology can be extended to CO_2 capture from other sources or areas such as natural gas treatment, from exhaust stream of natural gas fired power plant, and cement industry.
- Different absorber (with intercooling) and stripper (split flow, vacuum, vapour compression and multipressure) configurations can be evaluated for energy performance by using developed design setup (Oyenekan and Rochelle, 2006).
- A power plant steam cycle model and the CO_2 capture model would be integrated to a coal-fired power plant model for whole plant analyses and energy integration.
- To understand the impact of the varying loads of power plant on the CO_2 capture unit and to implement an off/on operation for capture, dynamic models can be developed from the present steady-state capture models exporting the models in Aspen Dynamics environment. Dynamic model can be utilized to develop operator training simulator (OTS) later on.

10.2.3 Economic Evaluation

To make economic analysis more credible, apple-to-apple comparisons are required between different capture technologies during the evaluation process. Utilization of equipment and material pricing from firm/vendor delivered quotations is recommended for more realistic and detailed cost estimation.

References

Aboudheir, A., P. Tontiwachwuthikul, A. Chakma, and R. Idem, Kinetics of the reactive absorption of carbon dioxide in high CO_2-loaded, concentrated aqueous monoethanolamine solutions, Chem. Eng. Sci., 58 (2003) 5195.

Abu-Zahra, M.R.M., J.P.M. Neiderer, P.H.M. Feron and G.F. Versteeg, CO_2 capture from power plants, Part II. A parametric study of the economical performance based on mono-ethanolamine, International Journal of Greenhouse Gas Control, 1 (2007) 135.

Ahmad, F., K.K. Lau and A.M. Shariff, Removal of CO_2 from natural gas using membrane separation system: modeling and process design, Journal of Applied Sciences, 10 (2010) 1134.

Agrawal, R., A simplified method for synthesis of gas separation membrane cascades with limited numbers of compressors, Chem. Eng. Sci., 52 (1997) 1029.

Agrawal, R., and J. Xu, Gas separation membrane cascades utilizing limited number of compressor cascades, AIChE J., 42 (1996b) 2141.

Agrawal, R., and J. Xu, Gas separation membrane cascades. II. Two compressor cascades, J. Memb. Sci., 112 (1996a) 129.

Alatiqi, I., M.F. Sabri, W. Bouhamra and E. Alper, Steady-state rate-based modelling for CO_2/amine absorption–desorption systems, Gas Sep. Purif., 8 (1994) 3.

Al-Baghli N. A., S.A. Pruess, V.F. Yesavage, and M.S. Selim, A rate-based model for the design of gas absorbers for the removal of CO_2 and H_2S using aqueous solutions of MEA and DEA, Fluid Phase Equilib., 185 (2001) 31.

Alie, C., L. Backham, E. Croiset, P.L. Douglas, Simulation of CO_2 capture using MEA scrubbing: a flowsheet decomposition method, Energy Conversion & Management, 46 (2005) 475.

Alie, C. F., CO_2 capture with MEA: integrating the absorption process and steam cycle of an existing coal-fired power plant, MSc Thesis, University of Waterloo. 2004.

Austgen, D.M., A Model of Vapor–Liquid Equilibria for Acid Gas– Alkanolamine–Water System, Ph. D. Dissertation: The University of Texas at Austin. 1989.

Aron, D., and C. Tsouris, Separation of CO_2 from flue gas: A review, Sep. Purif. Tech., 40 (2005) 321.

AspenPlus® 2006.5, Help, aspenOne Engineering Suite, Aspen Technology, Inc. Cambridge, MA USA (2007).

AspenPlus™ User Manual & Guide, Aspen Engineering Suite, Aspen Technology, Inc. Cambridge, MA USA (2001).

Aspen Icarus Process Evaluator 2006.5, User Guide, aspenOne Engineering Suite, Aspen Technology, Inc. Cambridge, MA, USA (2007).

Babcock, R.E., R.W. Spillman, C.S. Goddin and T.E. Cooley, Natural gas cleanup: a comparison of membrane and amine treatment processes, Energy Progress, 8 (1988) 135.

Baker, R. W., Future directions of membrane gas separation technology, Ind. Eng. Chem. Res., 41 (2002) 1393.

Baker, R. W., Membrane Technology and Applications, McGraw-Hill, NY, (2000).

Barchas, R. and R. Davis, The Kerr-McGee/ABB Lummus Crest technology for the recovery of CO_2 from stack gases, Energy Conversion and Management, 33 (1992) 333.

Barrer, R. M., Diffusion in and through solids, Cambridge University Press, London, (1951).

Bennett, D.L. and K.W. Kovak, Optimize distillation columns, Chem. Eng. Prog., May 2000, p. 19.

Biegler, L.T., I.E. Grossmann and A.W. Westerberg, Systematic methods of chemical process design, Prentice-Hall, Inc., New Jersey (1997).

Bhide, B.D., A. Voskericyan and S.A. Stern, Hybrid processes for the removal of acid gases from natural gas, J. Memb. Sci., 140 (1998) 27.

Bhide, B.D., A. Voskericyan and S.A. Stern, Hybrid processes for the removal of acid gases from natural gas, J. Memb. Sci., 140 (1998) 27.

Bhide, B.D., and S.A. Stern, A new evaluation of membrane process for the oxygen-enrichment of air. I. Identification of optimum operating conditions and process configuration, J. Memb. Sci., 62 (1991a) 13.

Bhide, B.D., and S.A. Stern, A new evaluation of membrane process for the oxygen-enrichment of air. I. Effect of economic parameters and membrane properties, J. Memb. Sci., 62 (1991b) 37.

Bhide, B.D., and S.A. Stern, Membrane processes for the removal of acid gases from natural gas. I. Process configuration and optimisation of operating conditions, J. Memb. Sci., 81 (1993a) 209.

Bhide, B.D., and S.A. Stern, Membrane processes for the removal of acid gases from natural gas. II. Effect of operating conditions, economic parameters, and membrane properties, J. Memb. Sci., 81 (1993b) 239.

Bin, H., X. Shisen, G. Shiwang, L. Lianbo, T. Jiye, N. Hongwei, C. Ming and C. Jian, Industrial test and techno-economic analysis of CO_2 capture in Huaneng Beijing coal-fired power station, Applied Energy, 87 (2010) 3347.

Bouclf, N., A. Sengupta and K.K. Sirkar, Hollow fiber gas permeator with countercurrent or cocurrent flow: series solutions, Ind. Eng. Chem. Fundam., 25 (1986) 217.

Bounaceur, R., N. Lape, D. Roizard, C. Valli`eres, and E. Favre, Membrane processes for post-combustion carbon dioxide capture: a parametric study, Energy, 31 (2006) 2220.

Bouton, G. R., and W. L. Luyben, Optimum economic design and control of a gas permeation membrane coupled with the hydrodealkylation (HAD) process, Ind. Eng. Chem. Res., 47 (2008) 1221.

Chang, H. and W. Hou, Optimization of membrane gas separation systems using genetic algorithm, Chem. Eng. Sci., 61 (2006) 5355.

Chang, H. and C.M. Shih, Simulation and optimization for power plant flue gas CO_2 absorption-stripping systems, Sep. Sci. Tech., 40 (2005) 877.

Chapel, D.; J. Ernst and C. L. Mariz, Recovery of CO_2 from Flue Gases: Commercial Trends. Presented at the Canadian Society of Chemical Engineers annual meeting, Saskatoon, Saskatchewan, Canada, Oct 4-6, 1999.

Chen, E., Carbon dioxide absorption into piperazine promoted potassium carbonate using structured packing, Ph. D. Dissertation: The University of Texas at Austin. 2007.

Chen, C. C., D. Tremblay, and C. Bhat, A rate-based process modeling study of CO_2 capture with aqueous amine solutions using aspenONE Process Engineering™, presented at the Clearwater Coal Conference, Clearwater Florida, June 04, 2008.

Chern, R.T., W.J. Koros and P.S. Fedkiw, Simulation of a hollow-fiber gas separator: the effects of process and design variables, Ind. Eng. Chem. Process Des. Dev., 24 (1985) 1015.

Chowdhury, M.H.M, X. Feng, P. Douglas, and E. Croiset, A new numerical approach for a detailed multicomponent gas separation membrane model and Aspen Plus simulation, Chem. Eng. Technol., 28 (2005) 773.

Coker, D.T., B.D. Freeman and G.K. Fleming, Modeling multicomponent gas separation using hollow-fiber membrane contactors, AIChE J., 44 (1998) 1289.

Coker, D.T., G.K. Fleming and B.D. Freeman, Tools for teaching gas separation using polymers, Membranes in Chemical Engineering Education (2003). http://membrane.ces.utexas.edu.

Compaq Visual Fortran Professional Edition 6.1, Digital Equipment Corporation**,** USA, 1997-1999.

Corriou, J., C. Fonteix, and E. Favre, Optimization of a pulsed operation of gas separation by membrane, AIChE J., 54 (2008) 1224.

Croiset, E. and K.V. Thambimuthu, A novel strategy for greenhouse gas abatement in coal fired power plants; enriched oxygen combustion, Proceedings of Combustion Canada, Calgary, Canada (1999).

Datta, A.K., Sen, P.K., Optimization of membrane unit for removing carbon dioxide from natural gas, J. Memb. Sci., 283 (2006) 291.

Davis, R.A., Simple gas permeation and pervaporation membrane unit operation models for process simulators, Chem. Eng. Technol., 25 (2002) 7.

Davidson, O., and B. Metz, Special report on carbon dioxide capture and storage, International Panel on Climate Change, Geneva, Switzerland, 2005. www.ipcc.ch.

Davison, J., K. Thambimuthu, Technologies for capture of carbon dioxide. Proceedings of the 7th Greenhouse Gas Technology Conference, Vancouver, Canada. International Energy Association (IEA), Greenhouse Gas R&D Programme, 2004 (www.ghght7.ca).

deMontigny, D., A. Aboudheir, P. Tontiwachwuthikul, A. Chakma, Using a packed-column model to simulate the performance of a membrane absorber, Ind. Eng. Chem. Res., 45 (2006a) 2580.

deMontigny D., P. Tontiwachwuthikul, and A. Chakma, Using polypropylene and polytetrafluoroethylene membranes in a membrane contactor for CO_2 absorption, J. Memb. Sci., 277 (2006b) 99.

deMontigny, D., A. Aboudheir, P. Tontiwachwuthikul, A. Chakma, Modelling the performance of a CO_2 absorber containing structured packing, Ind. Eng. Chem. Res., 45 (2006c) 2594.

Desideri, U., and A. Paolucci, Performance modeling of a carbon dioxide removal system for power plants, Energy Conv. Manag., 40 (1999) 1899.

DOE, Fossil Energy: DOE's Oil Recovery R&D programm, http://www.energy.ca.gov/process/pubs/electrotech_opps_tr113836.pdf, February 8. 2008.

Donohue, M.D., B.S. Minhas and S.Y. Lee, Permeation behavior of carbon dioxide methane mixture in cellulose acetate membranes, J. Memb. Sci., 42 (1989) 197.

Douglas, P.L., Process Optimisation, Class lecture handouts, University of Waterloo, Ontario, Canada, Spring (2002).

Drioli, E and M. Romano, Progress and new perspectives on integrated membrane operations for sustainable industrial growth, Ind. Eng. Chem. Res., 40 (2001) 1277.

Du, R., X. Feng, and A. Chakma, Poly(N,N-dimethylaminoethyl methacrylate)/polysulfone composite membranes for gas separations, J. Memb. Sci., 279 (2006) 76.

Echt, W., Hybrid systems: combining technologies leads to more efficient gas conditioning, 52nd Laurance Reid Gas Conditioning Conference, Oklahoma, 2002.

Edgar, T.F., D.M. Himmelblau and L. S. Lasdon, Optimization of chemical processes, 2nd Ed., McGraw Hill, NY, (2001).

EPA, Climate Change, Greenhouse Gas Emissions, Global Greenhouse Gas data, http://epa.gov/climatechange/emissions/globalghg.html, February 07, 2009.

Ettouney, H.M., G. Al-Enezi, S.E.M. Hamam and R. Huges, Characterization of the permeation properties of CO_2-N_2 gas mixtures in silicone rubber membranes, Gas Sep. Purif., 8 (1994) 31.

Favre, E., R. Bounaceur, and D. Roizard, A hybrid process combining oxygen enriched air combustion and membrane separation for post-combustion carbon dioxide capture, Sep. Purif. Tech., 68 (2009) 30.

Farve, E., Carbon dioxide recovery from post-combustion processes: can gas permeation membranes compete with absorption? J. Memb. Sci., 294 (2007) 50.

Feng, X., and J. Ivory, Development of hollow fiber membrane systems for nitrogen generation from combustion exhaust gas. Part I. Effects of module configurations, J. Memb. Sci., 176 (2000) 197.

Feng, X., J. Ivory and V.S.V. Rajan, Air separation by integrally asymmetric hollow-fiber membranes, AIChE J., 45 (1999) 2142.

Feng, X., Membrane Separation, Class Lectures, University of Waterloo, On, Canada, Fall (2002).

Feron, P.H.M., A.E. Jansen and R. Klaassen, Membrane technology in carbon dioxide removal, Energy Convers. Mgmt., 33 (1992) 421.

Feron, P.H.M., and A.E. Jansen, Capture of carbon dioxide using membrane gas absorption and reuse in the horticultural industry, Energy Convers. Mgmt., 36 (1995) 411.

Fisher, K., C. Beitler, C. Rueter, K. Searcy, G. Rochelle, and M. Jassim. Integrating MEA regeneration with CO_2 compression and peaking to reduce CO_2 capture costs." Final Report under DOE Grant DE-FG02-04ER84111, June 9, 2005.

Fisher, K.S. , K. Searcy, G.T. Rochelle, S. Ziaii and C. Schubert, Advanced amine solvent formulations and process integration for near-term CO_2 capture success, Department of Energy (DOE)/National Energy Technology Laboratory (NETL), Final Report under DOE Grant DE-FG02-06ER84625, June 28, 2007.

Floudas, C.A., Non-linear and mixed-integer optimization, Scientific Press, Oxford, UK, (1995).

Franco, J., D. deMontigny, S. Kentish, J. Perera, G. Stevens, A study of the mass transfer of CO2 through different membrane materials in the membrane gas absorption process, Separation Science and Technology, 43 (2008) 225.

Freeman, B., Basis of permeability/selectivity trade-off relations in polymeric gas-separation membranes, Macromolecules, 32 (1999) 375.

Freguia, S. and G.T. Rochelle, Modeling of CO_2 capture by aqueous Monoethanolamine, AIChE, 49 (2003) 1676.

Freund, P., and K. Thambimuthu, Options for decarbonising fossil energy supplies, Paper presented at Combustion Canada '99, Telus Convention Centre, Calgary, Alberta, Canada (May, 1999).

Gerbelová, H., C. Ioakimidis and P. Ferrão, A techno-economical study of the CO_2 capture in the energy sector in Portugal, Energy Procedia 4 (2011) 1965.

Giglia, S., B. Bikson and J.E. Perrin, Mathematical and experimental analysis of gas separation by hollow fiber membranes, Ind. Eng. Chem. Res., 30 (1991) 1239.

Gottlicher, G., The energetics of carbon dioxide capture in power plants, in: DOE, U.S., available in full at www.netl.doe.gov/publications/carbon_seq/refshelf.html, National Energy Technology Laboratory (NETL), 2004.

Grossmann, I.E., and M.M. Daichendt, New trends in optimization-based approaches to process synthesis, Computers Chem. Eng., 20 (1996) 665.

Hao, J., P.A. Rice and S.A Stern, Upgrading of low quality natural gas with H_2S- and CO_2-selective polymer membranes. Part I. Process design and economics of membrane stages without recycle streams, J. Memb. Sci., 209 (2002) 177.

Hao, J., P.A. Rice, and S.A. Stern, Upgrading low-quality natural gas with H_2S- and CO_2-selective polymer membranes Part II. Process design, economics, and sensitivity study of membrane stages with recycle streams, J. Memb. Sci., 320 (2008) 108.

Haraya, K., K. Obata, T. Hakuta and H. Yoshitome, Performance of gas separator with high-flux polyimide hollow fiber membrane, Sep. Sci. Tech., 23 (1988) 305.

He, X., J.A. Lie, E. Sheridan, and May-Britt Hägg, CO_2 capture by hollow fibre carbon membranes: experiments and process simulations, Energy Procedia, 1 (2009) 261.

Henis, J.M.S., and M.K. Tripodi, A novel approach to gas separations using composite hollow fiber membranes, Sep. Sci. & Tech., 15 (1980) 1059.

Hennis, J.M.S., and M.K. Tripodi, Multicomponent membranes for gas separations, U.S. Patent 4,230,463, 1980.

Herzog, H., An introduction to CO_2 Separation and capture technologies, A white report, MIT Energy Laboratory, August (1999).

Herzog, H., and D. Golomb, Massachusetts Institute of Technology, Laboratory for Energy and the Environment, contribution to Encyclopedia of Energy, (2003).

Hinchlife, A.B., and K.E. Porter, Gas separation using membranes. I. Optimization of the separation process using new cost parameters, Ind. Eng. Chem. Res., 36 (1997) 821.

Ho, M.T., G.W. Allinson, and D.E. Wiley, Reducing the Cost of CO_2 Capture from Flue Gases Using Membrane Technology, Ind. Eng. Chem. Res. 2008, 47, 1562.

Ho, M.T., G.W. Allinson and D.E. Wiley, Factors affecting the cost of capture for Australian lignite coal fired power plants, Energy Procedia, 1 (2009) 763.

Ho, M.T., G.W. Allinson and D.E. Wiley, Comparison of MEA capture cost for low CO_2 emissions sources in Australia, International Journal of Greenhouse Gas Control, 5 (2011) 49.

Hwang, S.T., and S. Ghalchi, Methane separation by a continuous membrane column, J. Memb. Sci., 11 (1982) 187.

IMSL subroutine DIVPAG and DNEQNF, IMSL Math/Library volume 1 and 2, IMSL Computational Technology Toolkits, Visual Numerics, Inc. Texas, (1997).

Kai, T., T. Kouketsu, S. Duan, S. Kazama, and K. Yamada, Development of commercial-sized dendrimer composite membrane modules for CO_2 removal from flue gas, Sep. Purif. Tech., 63 (2008) 524.

Kaldis, S.P., G.C. Kapantaidakis and G.P. Sakellaropoulos, Simulation of multicomponent gas separation in hollow fiber membranes by orthogonal collocation – hydrogen recovery from refinery gases, J. Memb. Sci., 173 (2000) 61.

Kaldis, S.P., G.C. Kapantaidakis, T.I. Papadopoulos and G.P. Sakellaropoulos, Simulation of binary gas separation in hollow fiber asymmetric membranes by orthogonal collocation, J. Memb. Sci., 142 (1998) 43.

Kaldis, S. P., G. Skodras and G. P. Sakellaropoulos, Energy and capital cost analysis of CO_2 capture in coal IGCC processes via gas separation membranes, Fuel Process, Tech., 85 (2004) 337.

Katoh, T., M. Tokumura, H. Yoshikawa, and Y. Kawase, Dynamic simulation of multicomponent gas separation by hollow-fiber membrane module: Nonideal mixing flows in permeate and residue sides using the tanks-in-series model, Sep. Purif. Tech., 76 (2011) 362.

Kenig, E.Y., R. Schneider, and A. Gorak, Reactive Absorption: Optimal Process Design via Optimal Modeling. Chem. Eng. Sci., 56 (2001) 343.

Kazama, S., S. Morimoto, S. Tanaka, H. Mano, T. Yashima, K. Yamada, and K. Haraya, Cardo polyimide membranes for CO_2 capture from flue gases, in: E.S. Rubin, D.W. Keith, C.F. Gilboy (Eds.), Greenhouse Gas Control Technologies, vol. I. Peer Reviewed Papers, Elsevier, Amsterdam, 2005, p. 75.

Kesting, R.E. and A.K. Fritzsche, Polymeric gas separation membranes, John Wiley & Sons, Inc. New York, (1993).

Khaisri, S., D. deMontigny, P. Tontiwachwuthikul and R. Jiraratananon, A mathematical model for gas absorption membrane contactors that studies the effect of partially wetted membranes, J. Memb. Sci., 347 (2010) 228.

Khaisri, S., D. deMontigny, Tontiwachwuthikul, P.and R. Jiraratananon, Membrane contacting process for CO_2 desorption, Energy Procedia, 4 (2011) 688.

Kohl, A. L.; and R. B. Neilsen, Gas Purification. 5th ed.; Gulf Publishing Co., Houston, 1997.

Kookos, I.K., Optimal design of membrane/distillation column hybrid processes, Ind. Eng. Chem. Res., 42 (2003) 1731.

Kookos, I.K., A targeting approach to the synthesis of membrane networks for gas separations, J. Memb. Sci., 208 (2002) 193.

Koros, W.J., and R. T. Chern, Separation of gaseous mixtures using polymer membranes, in Handbook of Separation Process Technology, in R. W. Rousseau (Ed.), John Wiley and Sons, Inc. (1987).

Koros, W.J., and G.K. Fleming, Membrane based gas separations, J. Memb. Sci., 83 (1993) 1.

Kovvali, A.S., S. Vemury and W. Admassu, Modeling of multicomponent countercurrent gas permeators, Ind. Eng. Chem. Res., 33 (1994) 896.

Krishna, R. and G. L. Standard, A multicomponent film model incorporating an exact matrix method of solution to the Maxwell-Stefan equations, AIChE J., 22 (1976) 383.

Lababidi, H., G.A. Al-Enezi and H.M. Ettouney, Optimization of module configuration in membrane gas separation, J. Memb. Sci., 112 (1996) 185.

Lababidi, H.M.S., Air separation by polysulfone hollow fibre membrane permeators in series – experimental and simulation results, Trans IChemE, 78 (2000) 1066.

Lawal, A., M. Wang, P. Stephenson and H. Yeung, Dynamic modeling of CO_2 absorption for post combustion capture in coal-fired power plants, Fuel, 88 (2009) 2455.

Lee, K.R., and S.T. Hwang, Separation of propylene and propane by polyimide hollow-fiber membrane module, J. Memb. Sci., 73 (1992) 37.

Lee, S.Y., B.S. Minhas, and M.D. Donohue, Effect of gas composition and pressure on permeation through Cellulose Acetate membranes, in *New Membrane Materials and*

Processes for Separation, K. K. Sirker and D. R. Lioyd, eds., AIChE Symposium Series no. 261, vol. 84, p. 93 (1988).

Li, K., and W.K. Teo, Use of permeation and absorption methods for CO_2 removal in hollow fibre membrane modules, Sep. Purif. Tech., 13 (1998) 79.

Li, K., D.R. Acharya and R. Hughes, Mathematical modeling of multicomponent membrane permeators, J. Memb. Sci., 52 (1990) 205.

Li, K., Y. Chen and W.K. Teo, Removal of CO_2 from a breathing gas mixture using a hollow-fibre permeator with permeate purge and absorption, Gas Sep. Purif., 9 (1995) 93.

Lie, J.A., T. Vassbotn, M. Ha¨gg, D. Grainger, T. Kim, and T. Mejdell, Optimization of a membrane process for CO_2 capture in the steelmaking industry, International journal of greenhouse gas control, I (2007) 309.

Lim, S.P., X. Tan and K. Li, Gas/vapor separation using membranes: Effect of pressure drop in lumen of hollow fibers, Chem. Eng. Sci., 55 (2000) 2641.

Lin, H, T. Merkel and R. Baker, The Membrane Solution to Global Warming, 6th Annual Conference on Carbon Capture & Sequestration, Pittsburgh, Pennsylvania, May 2007, http://www.netl.doe.gov/publications/proceedings/07/carbon-seq/data/papers/tue_189.pdf

Liu, L., Gas Separation by Poly(Ether Block Amide) Membranes, PhD Thesis, University of Waterloo (2008).

Luque, O., J.M. Benito and J. Coca, The importance of specification sheets for pressure-driven membrane processes, Filtration+Separation, January/February (2004), 24. www.filtsep.com.

Maclean, D. L., W.A. Bollinger, D.E. King, and R.S. Narayan, Gas separation design with membranes, in Recent Developments in Separation Science, N. N. Li and J. M. Calo, eds., CRC Press, Boca Raton, FL, (1986).

Mariz, C.L., Carbon dioxide recovery: large-scale design trends, J. Can. Pet. Technol., 37 (1998) 42–47.

Marriott, J.I., E. Sørensen and I.D.L. Bogle, Detailed mathematical modeling of membrane modules, Computers Chem. Engng., 25 (2001) 693.

Marriott, J.I. and E. Sørensen, A general approach to modelling membrane modules, Chem. Eng. Sci., 58 (2003a) 4975.

Marriott, J. and E. Sørensen, The optimal design of membrane systems, Chem. Eng. Sci., 58 (2003b) 4991.

Matsuura, T., Synthetic Membranes and membrane separation process, CRC Press Inc., (1994).

McKee, R.L., M.K. Changela, and G.J. Reading, CO_2 removal: membrane plus amine, Hydrocarbon process., 70 (1991) 63.

Mears, P., Diffusion of gases through Polyvinyl Acetate, J. Am. Chem. Soc., 76 (1954) 3415.

Meisen, A., and X. Shuai, Research and development issues in CO_2 capture, Energy Convers. Mgmt., 38, Suppl. (1997) S37.

Merkel, T., H. Lin, X. Wei, J. He, B. Firat, K. Amo, R. Daniels, and R. Baker, A Membrane Process to Capture CO_2 from Coal-Fired Power Plant Flue Gas, DOE NETL Projects NT43085 and NT05312, (www.mtrinc.com), 2009.

Merkel, T.C., H. Lin, X. Wei, and R. Baker, Power plant post-combustion carbon dioxide capture: An opportunity for membranes, J. Memb. Sci., 359 (2010) 126.

Metz, B., O. Davidson, H. de Coninck, M. Loos, and L. Meyer, IPCC Special Report on Carbon Dioxide Capture and Storage, Cambridge University Press, United Kingdom & New York, USA, available in full at www.ipcc.ch, 2005.

Mulder, M., Basic Principles of Membrane Technology, 2nd ed., Kluwer Academic Publishers, Netherlands, (1996).

Nishikawa, N., M. Ishibashi, H. Ohta, N. Akutsu, H. Matsumoto, T. Kamata and H. Kitamura, CO_2 removal by hollow-fiber gas-liquid contactor, Energy Convers. Mgmt., 36 (1995) 415.

O'Brian, K.C., W.J. Koros and T.A. Barabari, A new technique for the measurement of multicomponent gas transport through polymeric films, J. Memb. Sci., 29 (1986) 299.

O'Keefe L.F., R.C. Weissman, R.A. De Puy, J. Griffiths, and J.M. Wainwright. An IGCC design for CO2 capture. In: Paper presented at the 18th annual international Pittsburgh coal conference. Newcastle, Australia, December 2001.

Oexmann, J., C. Hensel, and A. Kather, Post-combustion CO_2-capture from coal-fired power plants: Preliminary evaluation of an integrated chemical absorption process with piperazine-promoted potassium carbonate, international journal of greenhouse gas control, 2 (2008) 539.

Oyenekan, B. A., and G. T. Rochelle, Energy Performance of Stripper Configurations for CO_2 Capture by Aqueous Amines, Ind. Eng. Chem. Res., 45 (2006) 2457.

Pacheco, M.A. and G.T Rochelle, Rate-based modeling of reactive absorption of CO_2 and H_2S into aqueous methyldiethanolamine. Ind. Eng. Chem. Res., 37 (1998) 4107.

Pan, C. Y., and H. W. Habgood, An analysis of the single-stage gaseous permeation process, Ind. Eng. Chem. Fundam., 13 (1974) 323.

Pan, C.Y., and H.W. Habgood, Gas separation by permeation: Part I. calculation methods and parametric, Can. J. Chem. Eng., 56 (1978a) 197.

Pan, C.Y., and H.W. Habgood, Gas separation by permeation: Part II. effect of permeate pressure drop and choice of permeate pressure, Can. J. Chem. Eng., 56 (1978b) 210.

Pan, C.Y., Gas separation by permeators with high flux asymmetric membranes, AIChE J., 29 (1983) 546.

Pan, C.Y., Gas separation by high-flux, asymmetric hollow-fiber membrane, AIChE J., 32 (1986) 2020.

Paul, D.R., and Yu.P. Yampol'skii, Polymeric gas separation membranes, CRC Press, Inc., Florida, USA (1994).

Pellegrini, G., R. Strube and G. Manfrida, Comparative study of chemical absorbents in postcombustion CO_2 capture, Energy, 35 (2010) 851

Perry, R.H. and D.W. Green, Perry's chemical engineers' handbook, seventh (international) edition, McGraw-Hill (1997), USA.

Perry's Chemical Engineers' Handbook, 5th ed., Chap. 18, McGraw-Hill, New York, 1973.

Peterson, T., and K.M. Lien, Design studies of membrane permeator processes for gas separation, Gas Sep. Purif., 9 (1995) 151.

Peters, M., K. Timmerhaus, and W. Ronald, Plant design and economics for chemical engineers, 5th ed., (2003) McGraw-Hill.

Piccolo, M., and P.L. Douglas, Data reconciliation using AspenPlus^{TM}, Develop. Chem. Eng. Miner. Proc., 4 (1996) 157.

Pintola, T., P. Tontiwachukwuthikul and A. .Meisen, Simulation of pilot plant and industrial CO_2 MEA absorbers, Gas Sep Purif, 7 (1993) 47.

Plasynski, S. I., and Z-Y. Chen, Review of CO_2 capture technologies and some improvement opportunities, presented at the American Chemical Society, Washington National Meeting, Washington, DC, Aug. 22 (2000).644.

Plaza, J.M., D.V. Wagener, and G.T. Rochelle, Modeling CO_2 capture with aqueous Monoethanolamine, International Journal of Greenhouse Gas Control, 4 (2010) 161.

Powell, C.E., and G.G. Qiao, Polymeric CO_2/N_2 gas separation membranes for the capture of carbon dioxide from power plant flue gases, J. Membr. Sci., 279 (2006) 1.

Purnomo, I.S.K. and E. Alpay, Membrane column optimization for the bulk of air, Chem. Eng. Sci., 55 (2000) 3559.

Oexmann, J., C. Hensel, and A. Kather, Post-combustion CO_2-capture from coal-fired power plants: Preliminary evaluation of an integrated chemical absorption process with piperazine-promoted potassium carbonate, International journal of greenhouse gas control, 2 (2008) 539.

Qi, R., and M.A. Henson, Membrane system design for multicomponent gas mixtures via mixed-integer nonlinear programming, Computers Chem. Engng., 24 (2000) 2719.

Qi, R., and M.A. Henson, Optimal design of spiral-wound membrane networks for gas separations, J. Memb. Sci., 148 (1998a) 71.

Qi, R., and M.A. Henson, Optimization-based design of spiral-wound membrane systems for CO_2/CH_4 separation, Sep. Purif. Tech., 13 (1998b) 209.

Qui, M., S. Hwang and Y. Kao, Economic Evaluation of gas membrane separator designs, Ind. Eng. Chem. Res., 28 (1989) 1670.

Oyenekan, B. A. and G.T. Rochelle, Energy performance of stripper configurations for CO_2 capture by aqueous amines, Ind. Eng. Chem. Res., 45 (2006) 2457.

Rao, A.B., and E.S. Rubin, A technical, economic, and environmental assessment of amine-based CO2 capture technology for power plant greenhouse gas control, Environ, Sci. Technol., 36 (2002) 4467.

Rautenbach, R., R. Knauf, A. Struck, and J. Vier, Simulation and design of membrane plants with AspenPlus, Chem. Eng. Technol., 19 (1996) 391.

Reid, R.C., J.M. Prausnitz and T.K. Sherwood, The properties of Gases and liquids, Fourth edition, McGraw-Hill, New York (1987).

Riemer, P., The capture of carbon dioxide from fossil fuel fired power stations, IEA Greenhouse Gas R&D Programme, Cheltenham, IEAGHG/SR2, December (1993).

Robenson, L.M., Correlation of separation factor versus permeability for polymeric membranes, J. Memb. Sci., 62 (1991) 165.

Romeo, L.M., I. Bolea and J.M. Escosa, Integration of power plant and amine scrubbing to reduce CO_2 capture costs, Applied Thermal Engineering, 28 (2008) 1039.

Rubin, E.S. and A.B. Rao, Uncertainties in CO_2 capture and sequestration costs, Greenhouse gas control technologies: Proceedings of the 6th International Conference on Greenhouse Gas Control Technologies, Elsevier Science Ltd., 2 (2002) 1119.

Sada, E., H. Kumazawa, J.S. Wang and M. Koizumi, Separation of carbon dioxide by asymmetric hollow fiber membrane of cellulose triacetate, J. Appl. Polym. Sci., 45 (1992) 2181.

Safari, M., A. Ghanizadeh, and M. M. Montazer-Rahmati, Optimization of membrane-based CO_2-removal from natural gas using simple models considering both pressure and temperature effects, Int. J. Green house gas control, 13 (2009) 3.

Sander, M.T., and C.L. Mariz, The Fluor Daniel '"Econamine FG" process: past experience and present day focus, Energy Conversion and Management, 33 (1992) 341.

Sanpasertparnich, T., R. Idem, I. Bolea, D. deMontigny and P. Tontiwachwuthikul, Integration of post-combustion capture and storage into a pulverized coal-fired power plant, International Journal of Greenhouse Gas Control, 4 (2010) 499.

Scholes, C.A., S.E. Kentish, and G.W. Stevens, Effects of Minor Components in Carbon Dioxide Capture Using Polymeric Gas Separation Membranes, Sep. & Purif. Reviews, 38 (2009) 1.

Schach, M.O., R.D. Schneider, H. Schramm, and J.U. Repke, Techno-economic analysis of postcombustion processes for the capture of carbon dioxide from power plant flue gas, Ind. Eng. Chem. Res., 49 (2010), 2363.

Sengupta, A., and K.K. Sirkar, Ternary gas mixture separation in two-membrane permeators, AIChE J., 33 (1987) 529.

Shindo, Y., T. Hakuta, H. Yoshitome & H. Inoue, Calculation methods for multicomponent gas separation by permeation, Sep. Sci. Technol., 20 (1985) 445.

Shekhawat, D., D.R. Luebke and H.W. Pennline, A review of carbon dioxide selective membranes, DOE/NETL-2003/1200.

Sidhoum, M., A. Sengupta and K.K. Sirkar, Asymmetric cellulose acetate hollow fibers: studies in gas permeation, AIChE J., 34 (1988) 417.

Simmonds, M., P. Hurst, M.B. Wilkinson, C. Watt and C.A. Roberts,. A study of very large scale post combustion CO_2 capture at a refining & petrochemical complex. (www.co2captureproject.org) 2003.

Singh, D.J., Simulation of CO_2 capture strategies for an existing coal fired power plant: MEA scrubbing versus O_2/CO_2 recycle combustion, M. A. Sc Thesis, University of Waterloo, Ontario, Canada, 2001.

Singh, D., E. Croiset, P.L. Douglas and M.A. Douglas, Techno-economic study of CO_2 capture from an existing coal-fired power plant: MEA scrubbing vs. O_2/CO_2 recycle combustion, Energy Conversion and Management, 44 (2003) 3073.

Smith, B.D., Design of Equilibrium Stage Processes, Chap. 14, McGraw-Hill, New York, 1963.

Smith, R. and P. Varbanov, what's the price of Steam? July 2005, p-29, www.cepmagazine.org.

Song, I., H. Ahn, H. Jeon, H. Jeong, Y. Lee, S. Choi, J. Kim, and S. Lee, Optimal design of multiple stage membrane process for carbon dioxide separation, Desalination, 234 (2008) 307.

Spillman, R.W., Economics of gas separation membranes, Chem. Eng. Prog., 85 (1989) 41.

Stern, S.A., Industrial applications of membrane processes: the separation of gas mixtures, in Membrane Processes for Industry, Proceedings of the Symposium, Southern Research Institute, Birmingham, Al, May 1966.

Stern, S.A., Polymers for gas separation: the next decade, J. Memb. Sci., 94 (1994) 1.

Stevens, S., V. Kuuskarra and J'Odonnell, Enhanced oil recovery scoping study, EPRI, CA:. TR-113836, www.energy.ca.gov/process/pubs/electrotech_opps_tr113836.pdf, (1999).

Tarun, C.B., E. Croiset, P.L. Douglas, M. Gupta, and M.H.M. Chowdhury, Techno-economic study of CO_2 capture from natural gas based hydrogen plants, International Journal of Greenhouse Gas Control, 1 (2007) 55.

Takaba, H., and S. Nakao, Computational fluid dynamics study on concentration polarization in H_2/CO separation membranes, J. Memb. Sci., 249 (2005) 83.

Taylor, R., R. Krishna and H. Kooijman, Real-world modeling of distillation, Chem. Eng. Prog., 99 (2003) 28.

Tessendorf, S., R. Gani and M.L. Michelsen, Aspects of modeling, design and operation of membrane-based gas separation processes for gaseous mixtures, Computers Chem. Eng., 20 (1996) S 653.

Tessendorf, S., R. Gani and M.L. Michelsen, Modeling, simulation and optimization of membrane-based gas separation systems, Chem. Eng. Sci., 54 (1999) 943.

Thundyil, M.J., Y.H. Jois and W.J. Koros, Effect of permeate pressure on the mixed gas permeation of carbon dioxide and methane in a glassy polyimide, J. Memb. Sci., 152 (1999) 29.

Thundyil, M.J., and W.J. Koros, Mathematical modeling of gas separation permeators – for radial crossflow, countercurrent, and cocurrent hollow fiber membrane modules, J. Memb. Sci., 125 (1997) 275.

Tobiesen, F.A., H.F. Svendsen, and O. Juliussen, Experimental validation of a rigorous absorber model for CO_2 postcombustion capture, AIChE J., 53 (2007) 846.

Tontiwachwuthikul, P, C.W. Chan, W. Kritpiphat, D. deMontigny, D. Skoropad, D. Gelowitz and A. Aroonwilas, Large scale carbon dioxide production from coal-fired power stations for enhanced oil recovery: A new economic feasibility study, Journal of Canadian Petroleum Technology, 37 (1998) 48.

Tranchino, L., R. Santarossa and F. Carta, Gas separation in a membrane unit: experimental results and theoretical predictions, Sep. Sci. Tech., 24 (1989) 1207.

Turton, R., R.C. Bailie, W.B. Whiting and J.A. Shaeiwitz, Analysis, synthesis, and design of chemical processes, 2nd Edition, Prentice Hall, New Jersey, (2003).

Vallieres, C., and E. Favre, Vacuum versus sweeping gas operation for binary mixtures separation by dense membrane processes, J. Memb. Sci., 244 (2004) 17.

Van Amerongen, G. J., Influence of structure of elastomers on their permeability to gases, J. Appl. Poly. Sci., 5 (1950) 307.

Van der Sluijs, J.P., C.A. Hendriks, and K. Blok, Feasability of polymer membranes for carbon dioxide recovery from flue gases, Energy Conversion & Management, 33 (1992) 429.

Versteeg, G.F. and W.P.M.V. Swaaij, On the kinetics between CO_2 and alkanolamines both in aqueous and non-aqueous solutions—I. Primary and secondary amines, Chem. Eng. Sci., 43 (1988) 573.

Versteeg, G.F., J.A.M. Kuipers., F.P.H.V. Beckum, and W.P.M.V. Swaaij, Mass transfer with complex reversible chemical reactions—II. Parallel reversible chemical reaction, Chem. Eng. Sci., 45 (1990) 183.

Wang, R., S.L. Liu, T.T. Lin and T.S. Chung, Characterization of hollow fiber membranes in a permeator using binary gas mixtures, Chem. Eng. Sci., 57 (2002) 967.

Weller, S., and W. A. Steiner, Engineering aspects of separation of gases, Chem. Eng. Prog., 46 (1950) 585.

Xu, J., and R. Agrawal, Gas separation membrane cascades. I. One compressor cascades with minimal energy losses due to mixing, J. Memb. Sci., 112 (1996) 115.

Xu, J., Low pressure feed membrane separation process, US Patent: 5,306,427 (1994).

Yave, W., A. Car, J. Wind, and Klaus-Viktor Peinemann, Nanometric thin film membranes manufactured on square meter scale: ultra-thin films for CO_2 capture, Nanotechnology 21 (2010) 395301 (7pp).

Zhang, Y., H. Chen, C. Chen, J. M. Plaza, R. Dugas and G. T. Rochell, Rate-based process modeling study of CO_2 capture with aqueous Monoethanolamine solution, Ind. Eng. Chem. Res., 48 (2009) 9233.

Zhao, L., E. Riensche, R. Menzer, L. Blum, and D. Stolten, A parametric study of CO_2/N_2 gas separation membrane processes for post-combustion capture, J. Memb. Sci., 325 (2008) 284.

www.worldcoal.org/pages/content/index.asp?PageID=188

www.eia.doe.gov/cneaf/electricity/epa/figes1.html. Retrieved 2010-11-07

www.mhhe.com/engcs/chemical/peters/data

Appendix A: User and User2 Fortran Subroutine Arguments Description

The unit operation models User and User2 allow user to interface their own unit operation model with Aspen Plus by supplying a subroutine and entering its name in the Model or Report field on the User or User2 Input Specifications sheet.

The only differences in the argument lists for User and U ser2 are:

- User can have up to four inlet and four outlet material streams, one information inlet stream, and one information outlet stream.
- User2 has no limit on the number of inlet or outlet streams.

Calling Sequence for User2

```
SUBROUTINE subrname† (NMATI,  SIN,    NINFI,  SINFI,  NMATO,
                      SOUT,   NINFO,  SINFO,  IDSMI,  IDSII,
                      IDSMO,  IDSIO,  NTOT,   NSUBS,  IDXSUB,
                      ITYPE,  NINT,   INT,    NREAL,  REAL,
                      IDS,    NPO,    NBOPST, NIWORK, IWORK,
                      NWORK,  WORK,   NSIZE,  SIZE,   INTSIZ,
                      LD)
```

†*Subroutine name you entered on the User2 Input Specifications sheet.*

Argument List Descriptions for User2

Variable	I/O†	Type	Dimension	Description
NMATI	I	INTEGER	—	Number of inlet material streams
SIN	I/O	REAL*8	NTOT, NMATI	Array of inlet material streams (see Stream Structure and Calculation Sequence)
NINFI	I	INTEGER	—	Number of inlet information streams
SINFI	I/O	REAL*8	NINFI	Vector of inlet information streams (see Stream Structure and Calculation Sequence)
NMATO	I	INTEGER	—	Number of outlet material streams
SOUT	O	REAL*8	NTOT, NMATO	Array of outlet material streams
NINFO	I	INTEGER	—	Number of outlet information streams
SINFO	O	REAL*8	NINFO	Vector of outlet information streams (see Stream Structure and Calculation Sequence)
IDSMI	I	INTEGER	2, NMATI	IDs of inlet material streams
IDSII	I	INTEGER	2, NINFI	IDs of inlet information streams

† *I = Input to subroutine*
O = Output from subroutine
W = Workspace

Argument List Descriptions for User2 (continued)

Variable	I/O†	Type	Dimension	Description
IDSMO	I	INTEGER	2, NMATO	IDs of outlet material streams
IDSIO	I	INTEGER	2, NINFO	IDs of outlet information streams
NTOT	I	INTEGER	—	Length of material streams
NSUBS	I	INTEGER	—	Number of substreams in material streams
IDXSUB	I	INTEGER	NSUBS	Location of substreams in stream vector
ITYPE	I	INTEGER	NSUBS	Substream type vector (1-MIXED, 2-CISOLID, 3-NC)
NINT	I	INTEGER	—	Number of integer parameters (see Integer and Real Parameters)
INT	I/O	INTEGER	NINT	Vector of integer parameters (see Integer and Real Parameters)
NREAL	I	INTEGER	—	Number of real parameters (see Integer and Real Parameters)
REAL	I/O	REAL*8	NREAL	Vector of real parameters (see Integer and Real Parameters)
IDS	I	INTEGER	2, 3	Block IDs: (*,1) - Block ID (*, 2) - User model subroutine name (*, 3) - User report subroutine name
NPO	I	INTEGER	—	Number of property option sets (always 2)
NBOPST	I	INTEGER	6, NPO	Property option set array (see NBOPST)
NIWORK	I	INTEGER	—	Length of integer work vector (see Local Work Arrays)
IWORK	W	INTEGER	NIWORK	Integer work vector (see Local Work Arrays)
NWORK	I	INTEGER	—	Length of real work vector (see Local Work Arrays)
WORK	W	REAL*8	NWORK	Real work vector (see Local Work Arrays)
NSIZE	I	INTEGER	—	Length of size results vector
SIZE	O	REAL*8	NSIZE	Real sizing results (see Size)
INTSIZ	O	INTEGER	NSIZE	Integer size parameters (see Size)
LD	I	INTEGER	—	Plex location of the stream class descriptor bead

† *I = Input to subroutine*
O = Output from subroutine
W = Workspace

Appendix B: FORTRAN Code for Hollow Fiber Membrane Module

```
C            ======================================================================
C
C             STEADY STATE calculation -Countercurrent mode
c            Shell side Feed
C            Rating problem (given membrane area and calculate product purity and flow)
C            Without sweep gas
C            ======================================================================
C
C
C    User Unit Operation Model (or Report) Subroutine for USER2
C
     SUBROUTINE SFCRGE (NMATI,  SINv,    NINFI,   SINFI,  NMATO,
    2                SOUT,   NINFO,  SINFO,   IDSMI,  IDSII,
    3                IDSMO,  IDSIO,  NTOT,    NSUBS,  IDXSUB,
    4                ITYPE,  NINT,   INTv,     NREAL,  realv,
    5                IDS,    NPO,    NBOPST,  NIWORK, IWORK,
    6                NWORK,  WORK,   NSIZE,   SIZEv,   INTSIZ,
    7                LD)
C
     IMPLICIT NONE
C
#include "ppexec_user.cmn"
c            INTEGER USER_NHSTRY
C
#include "dms_plex.cmn"
C
     Real*8 B(1)
c            integer IB(1)
             EQUIVALENCE (B(1), IB(1))
C
#include "dms_ncomp.cmn"
c            INTEGER NCOMP_NCC
C
C    DECLARE ARGUMENTS

C
             INTEGER MXPARM
             integer nmaxco
             integer NEQ

             parameter (mxparm=50, nmaxco=10, neq=nmaxco+2)

c

     INTEGER NMATI, NINFI, NMATO, NINFO, NTOT,
    +       NSUBS, NINT, NPO, NIWORK,NWORK,
    +       NSIZE, NREAL
```

```
C
C
      INTEGER IDSMI(2,NMATI), IDSII(2,NINFI),
     +        IDSMO(2,NMATO), IDSIO(2,NINFO),
     +        IDXSUB(NSUBS), ITYPE(NSUBS), INTv(NINT),
     +        IDS(2,3), NBOPST(6,NPO),
     +        IWORK(NIWORK),INTSIZ(NSIZE), LD

      REAL*8 SINv(NTOT,NMATI), SINFI(NINFI),
     +       SOUT(NTOT,NMATO),  SINFO(NINFO),
     +       WORK(NWORK),  SIZEv(NSIZE), REALv(NREAL)
C
C     DECLARE LOCAL VARIABLES
C
      INTEGER OFFSET, IERR, LDATA, KDIAG, IDX(4), NCP, I, J,
     +        LMW, LTC,LPC,LVC,LOMEGA,LMUP, NTUBES, IPERM, IRET, IFAIL

              integer index(1)
              Double precision perm(nmaxco)

      REAL*8 DIAM, LEN, DIFF, CG, REJ_COEF, C1, C2, C3, C4, P_PERM,
     +       DELTA_P, RHO, MU, FIN, CIN, PIN, UAVE, RE, SC, X(nmaxco),
     +       CP, CR, KM, JM, FP, PRET, XMW, FLOW
c
C             Declare Functions
c
              INTEGER USRUTL_GET_REAL_PARAM,
     +        USRUTL_GET_INT_PARAM,
     +        USRUTL_SET_REAL_PARAM

              INTEGER DMS_IFCMNC

              REAL*8  DLOG
              double precision ABS
c
c             Declaration for main HOLLOW FIBER CALCULATION program start here

              INTEGER NCOMPS
c             REAL(8), ALLOCATABLE :: SQR(:)
C
C
              INTEGER MABSE,MBDF,MSOLVE
              PARAMETER (MABSE=3, MBDF=2, MSOLVE=2)
C
              INTEGER IDO
              INTEGER NF
              INTEGER NV
              INTEGER SOLVER
              INTEGER M
              integer istep
```

```
            integer iter
            integer nsegm
C
     CHARACTER*4 CTAG(nmaxco)
     CHARACTER*15 CNAME(nmaxco)
            integer iprnt
C
            DOUBLE PRECISION A(1,1),PARAM(MXPARM)
            DOUBLE PRECISION Z,ZEND,TOL,W(neq),DW(neq)
c           DOUBLE PRECISION DWW(nmaxco)
            DOUBLE PRECISION PI
CSUBROUTINE MAT(N)
c  REAL(4), ALLOCATABLE :: SQR(:)      ! Declares SQR as a one-dimensional
                              !        allocatable array
c  ALLOCATE (SQR(N))                  ! Allocates array SQR

c  DO J=1,N
c    SQR(J) = SQRT(FLOATJ(J))         ! FLOATJ converts integer to REAL
c  ENDDO

c  WRITE (6,*) SQR                    ! Displays calculated values
c  DEALLOCATE (SQR)                   ! Deallocates array SQR
c  END SUBROUTINE MAT

c           real*8 X(4)
c           real*8 XF(4)
            double precision XXX(nmaxco)
            double precision XF(nmaxco)
            DOUBLE PRECISION XR(nmaxco)
            DOUBLE PRECISION Y(nmaxco)
            DOUBLE PRECISION YGUESS(nmaxco)
            DOUBLE PRECISION YYY(nmaxco)
            DOUBLE PRECISION YB(nmaxco)
            DOUBLE PRECISION YBB(nmaxco)
            DOUBLE PRECISION QD(nmaxco)
            DOUBLE PRECISION ODIA, IDIA
            DOUBLE PRECISION P
            DOUBLE PRECISION PP
            double precision ppzo
            DOUBLE PRECISION T, R
            DOUBLE PRECISION U
            DOUBLE PRECISION V
            DOUBLE PRECISION UF
            DOUBLE PRECISION DELZ
            DOUBLE PRECISION LENGTH
c
     DOUBLE PRECISION TCT(nmaxco),VFAC(nmaxco),PCP(nmaxco)
            DOUBLE PRECISION MWW(nmaxco)
            DOUBLE PRECISION MWV(nmaxco)
            DOUBLE PRECISION VCC(nmaxco),DPM(nmaxco),KAPA(nmaxco),
```

```
     &       OMEGAC(nmaxco), DPMR(nmaxco)
      DOUBLE PRECISION TC(nmaxco),PC(nmaxco),VC(nmaxco)
            DOUBLE PRECISION MW(nmaxco)
            DOUBLE PRECISION OMEGA(nmaxco),MUP(nmaxco)
            DOUBLE PRECISION TOT1,TOL1, TOT2, TOL2
            DOUBLE PRECISION SUM1,SUM2
            DOUBLE PRECISION RECOV, SCUT
            double precision qd1, qd2, qd3, qd4, qd5, qd6, qd7, qd8, qd9, qd10
C
            EXTERNAL DIVPAG, DIVPRK, DSET
            EXTERNAL fcnsg,fcnjsg
C
            COMMON /CMAIN1/ NV
            COMMON /CMAIN2/ ODIA, IDIA
            COMMON /CMAIN3/ QD
            COMMON /CMAIN4/ P
            COMMON /CMAIN5/ UF
            COMMON /CMAIN6/ T, R
            COMMON /CMAIN8/ PI
            COMMON /CMAIN9/ NF
            COMMON /CMAIN10/ Y
            COMMON /CMAIN11/ YBB
            COMMON /CMAIN12/ nsegm
            COMMON /CMAIN13/ istep
c           COMMON /CMAIN14/ NCOMP_NCC
C
      COMMON /CINIT/ TCT,VFAC,PCP
            COMMON /CINIT1/ MWV
C
c           Declaration for main program end here
C
C     BEGIN EXECUTABLE CODE
C
C           Get configured REAL variables from Aspen Plus
c
            IFAIL=0
            INDEX(1)=0
c
            IERR=USRUTL_GET_INT_PARAM('NF', INDEX, NF)
c
            IF(IERR.NE.0) THEN
                  WRITE(USER_NHSTRY,*)'ERROR FETCHING NUMBER OF FIBERS'
                  IFAIL=1
      END IF

            IERR=USRUTL_GET_REAL_PARAM('IDIA', INDEX, IDIA)
C
            IF(IERR.NE.0) THEN
                  WRITE(USER_NHSTRY,*)'ERROR FETCHING INNER FIBER DIAMETER'
                  IFAIL=1
```

```
      END IF
C
            IERR=USRUTL_GET_REAL_PARAM('ODIA', INDEX, ODIA)
C
            IF(IERR.NE.0) THEN
                  WRITE(USER_NHSTRY,*)'ERROR FETCHING OUTER FIBER DIAMETER'
                  IFAIL=1
      END IF

C
            IERR=USRUTL_GET_REAL_PARAM('LENGTH', INDEX, LENGTH)
            IF(IERR.NE.0) THEN
                  WRITE(USER_NHSTRY,*)'ERROR FETCHING LENGTH'
                  IFAIL=1
      END IF
C
            IERR=USRUTL_GET_REAL_PARAM('PPZO', INDEX, PPZO)
            IF(IERR.NE.0) THEN
                  WRITE(USER_NHSTRY,*)'ERROR FETCHING PERMEATE PRESSURE AT Z=0'
                  IFAIL=1
      END IF
c

C           read permeance ===
            go to 1514
            do i=1,NCOMP_NCC
                  index(1)=i
            IERR=USRUTL_GET_REAL_PARAM('PERMN',INDEX,qd(i))
c           QD(i)=C(i)
c
            end do
            IF(IERR.NE.0) THEN
                  WRITE(USER_NHSTRY,*)'ERROR FETCHING PERMN'
                  IFAIL=1
            END IF
 1514 continue
c           qd=perm
C           ===
            IERR=USRUTL_GET_REAL_PARAM('PERMN1', INDEX, QD1)
            IF(IERR.NE.0) THEN
                  WRITE(USER_NHSTRY,*)'ERROR FETCHING permn1',qd1
                  IFAIL=1
      END IF
C
            IERR=USRUTL_GET_REAL_PARAM('PERMN2', INDEX, QD2)
            IF(IERR.NE.0) THEN
                  WRITE(USER_NHSTRY,*)'ERROR FETCHING permn2', qd2
                  IFAIL=1
      END IF
C
```

```
      IERR=USRUTL_GET_REAL_PARAM('PERMN3', INDEX, QD3)
      IF(IERR.NE.0) THEN
            WRITE(USER_NHSTRY,*)'ERROR FETCHING permn3',qd3
            IFAIL=1
   END IF
C
      IERR=USRUTL_GET_REAL_PARAM('PERMN4', INDEX, QD4)
      IF(IERR.NE.0) THEN
            WRITE(USER_NHSTRY,*)'ERROR FETCHING permn4',qd4
            IFAIL=1
   END IF
c
C
      IERR=USRUTL_GET_REAL_PARAM('PERMN5', INDEX, QD5)
      IF(IERR.NE.0) THEN
            WRITE(USER_NHSTRY,*)'ERROR FETCHING permn5',qd5
            IFAIL=1
   END IF
c
C
      IERR=USRUTL_GET_REAL_PARAM('PERMN6', INDEX, QD6)
      IF(IERR.NE.0) THEN
            WRITE(USER_NHSTRY,*)'ERROR FETCHING permn6',qd6
            IFAIL=1
   END IF
c
C
      IERR=USRUTL_GET_REAL_PARAM('PERMN7', INDEX, QD7)
      IF(IERR.NE.0) THEN
            WRITE(USER_NHSTRY,*)'ERROR FETCHING permn7',qd7
            IFAIL=1
   END IF
c
C
      IERR=USRUTL_GET_REAL_PARAM('PERMN8', INDEX, QD8)
      IF(IERR.NE.0) THEN
            WRITE(USER_NHSTRY,*)'ERROR FETCHING permn8',qd8
            IFAIL=1
   END IF
c
C
      IERR=USRUTL_GET_REAL_PARAM('PERMN9', INDEX, QD9)
      IF(IERR.NE.0) THEN
            WRITE(USER_NHSTRY,*)'ERROR FETCHING permn9',qd9
            IFAIL=1
   END IF
c
C
      IERR=USRUTL_GET_REAL_PARAM('PERMN10', INDEX, QD10)
      IF(IERR.NE.0) THEN
```

```
                WRITE(USER_NHSTRY,*)'ERROR FETCHING permn10',qd10
                IFAIL=1
    END IF
c

        QD(1)=QD1
        QD(2)=QD2
        QD(3)=QD3
        QD(4)=QD4
        QD(5)=QD5
        QD(6)=QD6
        QD(7)=QD7
        QD(8)=QD8
        QD(9)=QD9
        QD(10)=QD10
C
C       GET location of molecular weight data
C MOLECULAR WEIGHTS OF THE COMPONENTS

        LMW=DMS_IFCMNC('MW')
C
        do i=1, NCOMP_NCC
        MWW(i)=B(LMW+I)
        END DO
C
        mwv=mww

cC CRITICAL TEMPERATURES OF THE COMPONENTS IN DEG. K

        LTC=DMS_IFCMNC('TC')
C
        do i=1, NCOMP_NCC
        TCT(i)=B(LTC+I)
        END DO
C CRITICAL PRESSURES OF THE COMPONENTS IN Pa (N/M2)
C
        LPC=DMS_IFCMNC('PC')
C
        do i=1, NCOMP_NCC
        PCP(i)=B(LPC+I)
        END DO
C
C CRITICAL VOLUMES OF THE COMPONENTS IN CM3/MOL
C
        LVC=DMS_IFCMNC('VC')
C
        do i=1, NCOMP_NCC
        VCC(i)=B(LVC+I)
C       CONVERT IT TO CM3/MOL FROM M3/KMOL
        VCC(I)=VCC(I)*1.0D+03
```

```
            END DO
C
C ACENTRIC FACTORS OF THE COMPONENT (DIMENSIONLESS)
C
            LOMEGA=DMS_IFCMNC('OMEGA')
C
            do i=1, NCOMP_NCC
            OMEGAC(i)=B(LOMEGA+I)
            END DO

C
C           KAPA FACTORS OF THE COMPONENT (DIMENSIONLESS)
            do i=1, NCOMP_NCC
     KAPA(I) = 0.0D0
            END DO
C
C DIPOLE MOMENTS OF THE COMPONENTS IN DEBYES
C
            LMUP=DMS_IFCMNC('MUP')
C
            do i=1, NCOMP_NCC
            DPM(i)=B(LMUP+I)
            END DO
c
c     DPM(1) = 0.0D0
c     DPM(2) = 0.0D0
c     DPM(3) = 0.0D0
c     DPM(4) = 0.0D0
C
C COMPRESSIBILITY FACTORS FOR VISCOCITY CALCULATION
     DO 7 I=1,NCOMP_NCC
     DPMR(I)=131.3D0*DPM(I)/(VCC(I)*TCT(I))**0.5D0
     VFAC(I)=0.0040785D0*MWW(I)**(0.5D0)*(1D0-0.2756D0*OMEGAC(I)
    &+KAPA(I)+0.059035D0*DPMR(I)**4)/VCC(I)**(2.0D0/3.0D0)
  7  CONTINUE

C
C           ===
c           QD(1)=1.91d-07                  !co2
c           QD(2)=9.57d-09                  !N2
c           QD(3)=4.78d-08                  !o2
c           QD(4)=1.91d-08                  !Ar

C           Get feed temp., pressure, flow rates and composition
c           Total feed flow rate, mol/sec (in aspen it is kmol/sec)
            UF=SINv(NCOMP_NCC+1,1)*1000.0D0
c           feed temp. (K)
            T=SINv(NCOMP_NCC+2,1)
c           feed pressure, Pa(N/m2)
            P=SINv(NCOMP_NCC+3,1)
```

```
c           feed composition
            DO I=1, ncomp_ncc
            XF(I)=SINv(I,1)/SINv(NCOMP_NCC+1,1)
            END DO
            PP=PPZO
C
C           Calculate FEED viscosity
c
            CALL SHS_CPACK(SINv(1,1), NCP, IDX, X, FLOW)
            KDIAG=4
            CALL PPMON_VISCL(SINv(NCOMP_NCC+2,1), SINv(NCOMP_NCC+3,1), X, NCP,
     +          IDX, NBOPST, KDIAG, MU, IERR)
C
            IF(IERR.NE.0) THEN
                  WRITE(USER_NHSTRY,*)'ERROR EVALUATING VISCOSITY FOR FEED'
                  IFAIL=1
     END IF

            IF(IFAIL.EQ.1) RETURN
C
C
C
c           Z start from close end of fibre
c
C           Set SOLVER option (Gear's BDF / Adams-Moulton (1) OR RK (2))
C
            SOLVER=1
C
c           MXPARM = 50
c           NCOMP_NCC=nmaxco

c           NEQ=NCOMP_NCC+2

c
C           Number of components
C
            NCOMPS=NCOMP_NCC
C--
C           Number of dependent variable ===
C
            NV=ncomp_ncc+2
C
c
            PI=3.1415936536D0
C
C           Universal gas constant, Pa.m3/mol.K
C
            R=8.314D0
C
C
```

```
      XXX=XF

c
c     Call data initialization routine
c
C     CALL SINIT1 (CTAG,IPRNT,NCOMPS,MWW,TCT,PCP,VCC,DPM,KAPA,OMEGAC)
C
C
C     SET PARAM TO DEFAULT, I.E., SET ALL PARAM EQUAL TO ZERO
C
      CALL DSET (MXPARM, 0.0D0, PARAM, 1)
C
C     SET ERROR TOLERANCE FOR ODE SOLVER
C
      TOL = 1.0D-5
C
C     PARAM FOR DIVPAG
C      1=INIT. SS; 2=MIN. SS; 3=MAX. SS; 4=MAX. NO. OF STEPS
C      5=MAX. NO. OF FUNCTIONS
C
      PARAM(1)=0.000001D0
      PARAM(4)=2000000
      PARAM(10)=MABSE
      PARAM(12)=MBDF
      PARAM(13)=MSOLVE
      PARAM(19)=0

C
C     assume PERMEATE PRESSURE (PP), Pa at z=0 AND
C
C
C     PP=1123.046D+03
C
C    Calc. LOCAL PERMEATE CONCENTRATION Y(I) i.e., mole fraction AT FIBRE CLOSEd END (I.E.,Z=0)
c     by providing initial values
c
      M=1
      YGUESS=XXX
 45  CONTINUE
            CALL dneqnsg (ncomps,M,XXX,QD,P,PP,YGUESS,YYY)
                  SUM1=0.0D0
            DO 40 I=1,NV-2
 40                 SUM1=SUM1+YYY(I)
            TOT1=SUM1
            TOL1=TOT1-1.0D0
            IF (ABS(TOL1) .LE. 0.0001) THEN
                  Y=YYY
            ELSE
            YGUESS=YYY
                  GO TO 45
```

```
                ENDIF
C
                Y=YYY

C
C       INTEGRATION STEP SISE
C
        DELZ=0.0001  !Z IN METRE
c
c       Z start from close end of fibre
C
        Z=0.0D0
C
        U=UF
C
        W(1)=U
C

        W(2)=PP
C
        DO 21 I=3,NV
 21     W(I)=XXX(I-2)
c
        ISTEP=0
c
c
c       call FCNS to get value of DW at z=0
c
         CALL  fcnsg (NEQ, Z, W, DW)
C
C               DWW=DW
c
C       write(*,*)DW(1)

                IF (U.EQ.UF) THEN
                        DO 29 I=1,NV-2
                        YB(I)=U*(DW(I+2)/DW(1))+XXX(I)
C                       write(*,*)yb(i)
C       PAUSE
 29             continue
                ENDIF
        ybb=yb
C
C       CALL THE ODE SOLVER
C
        NSEGM=LENGTH/DELZ
        IDO=1
        ZEND=0.0D0
c       WRITE(10, *)'     STAGE CUT', '          PERMEATE PRES.',
c    &     '         FEED CONC. (H2)'
```

```
C       JJ11=0
C
 99     CONTINUE
C
        ISTEP=ISTEP+1
        ZEND=ZEND+DELZ
C
C
        IF(SOLVER.EQ.1) THEN
         CALL DIVPAG (IDO, NEQ, fcnsg, fcnjsg, A, Z, ZEND, TOL, PARAM, W)
        ELSEIF(SOLVER.EQ.2) THEN
                CALL DIVPRK (IDO, NEQ, fcnsg, Z, ZEND, TOL, PARAM, W)
        ENDIF
C       WRITE (*,*)Y
C       PAUSE
C
C       write(*,*)istep,nsegm
        IF (ISTEP.LE.NSEGM) THEN
C
                U=W(1)
C
                PP=W(2)
C
                DO 26 I=3,NV
 26                     XXX(I-2)=W(I)
C
                DO 27 I=1,NV-2
 27                     YGUESS(I)=Y(I)
C
C       WRITE(*,*)YGUESS
C       PAUSE
                M=2
 46  CONTINUE
                CALL dneqnsg (ncomps,M,XXX,QD,P,PP,YGUESS,YYY)
C
                        SUM2=0.0D0
                DO 41 I=1,NV-2
 41                     SUM2=SUM2+YYY(I)
                TOT2=SUM2
C               WRITE(*,*)TOT2
C       PAUSE
                TOL2=TOT2-1.0D0
                IF (ABS(TOL2) .LE. 0.0001) THEN
                        Y=YYY
                ELSE
                YGUESS=YYY
                        GO TO 46
                ENDIF


C
```

```
                Y=YYY
C
C       WRITE(*,*) PP/1000
C
                IF      (U.NE.UF) THEN
                        DO 28 I=1,NV-2
 28                     YB(I)=(UF*XF(I)-U*XXX(I))/(UF-U)
                ELSEIF (U.EQ.UF) THEN
                        DO 299 I=1,NV-2
 299                    YB(I)=U*(DW(I+2)/DW(1))+XXX(I)
                ENDIF
C
                YBB=YB
C
                V=(UF-U)
C
        IF (ISTEP.GE.NSEGM) IDO=3
                GO TO 99
        ENDIF
C
C CALCULATE STAGE CUT AND RECOVERY IN PERCTANTAGE FOR FIRST PERMEATING COMPONENT
C
        SCUT=V/UF
C
        RECOV=((SCUT*YBB(1))/XF(1))*100.0D0
C
C       Assume(incorrectly) PERMEATE STREAM IS FIRST, SWITCH IF NOT.

    IPERM=1
        IRET=2
        IF(IDSMO(1,1).EQ.'RETE') THEN
                IPERM=2
                IRET=1
        END IF
C
        do i =1, ncomp_ncc
        SOUT(i,IPERM)=V/1000.0d0*ybb(i)
        end do
        SOUT(ncomp_ncc+1,IPERM)=V/1000.0d0
        SOUT(NCOMP_NCC+2,IPERM)=SINv(NCOMP_NCC+2,1)
        SOUT(NCOMP_NCC+3,IPERM)=ppzo
C
C       Fill SOUT array for RETENTAT stream using values from PERMEATE stream
c
        do i =1, ncomp_ncc
        SOUT(i,IRET)=u/1000.0d0*XXX(i)
        end do
        SOUT(ncomp_ncc+1,IRET)=u/1000.0d0
        SOUT(NCOMP_NCC+2,IRET)=SINv(NCOMP_NCC+2,1)
        SOUT(NCOMP_NCC+3,IRET)=SINv(NCOMP_NCC+3,1)
```

```
C
C-----Now set values of the two variables designated as output parameters.----
            IERR=USRUTL_SET_REAL_PARAM('STAGE_CUT', INDEX, SCUT)
            IF(IERR.NE.0) THEN
                        WRITE(USER_NHSTRY,*)'ERROR STORING STAGE CUT'
                        IFAIL=1
      END IF
C
            IERR=USRUTL_SET_REAL_PARAM('RECOVERY', INDEX, RECOV)
            IF(IERR.NE.0) THEN
              WRITE(USER_NHSTRY,*)'ERROR STORING RECOVERY OF FIRST COMPONENT'
                        IFAIL=1
      END IF
C
            RETURN
            END
C-----------------------------END MAIN PROGRAM---------------------------------
C
C=======================================================================
C
C           SUBROUTINE FCNJS : NEED FOR CALLING DIVPAG FOR STEADY STATE
C
C=======================================================================
C
            SUBROUTINE fcnjsg (NEQ, Z, W, DYPDY)
C
            INTEGER NEQ
            DOUBLE PRECISION Z,W(NEQ),DYPDY(NEQ,*)
C                 THIS SUBROUTINE IS NEVER CALLED
            RETURN
            END
C-----------------------------END OF SUB. FCNJS--------------------------------
C
CC=====================================================================================
C
C           SUBROUTINE FCNS : ROUTINE TO CALCULATE DERIVATIVES FOR STEADY STATE
C
C=====================================================================================
C
            SUBROUTINE fcnsg (NEQ, Z, W, DW)
C
            INTEGER NEQ
            INTEGER NV
c           integer nvv
            integer istep
            integer nsegm
            integer i
C
            DOUBLE PRECISION Z,W(NEQ),DW(NEQ)
c           DOUBLE PRECISION DWW(6)
```

```
C
      DOUBLE PRECISION PI
C
      DOUBLE PRECISION Y(10)
      DOUBLE PRECISION ODIA, IDIA
      DOUBLE PRECISION QD(10)
      DOUBLE PRECISION P
      DOUBLE PRECISION T, R
c     DOUBLE PRECISION UR
      DOUBLE PRECISION UF
C     DOUBLE PRECISION VISMIX
      DOUBLE PRECISION FLSUM
      DOUBLE PRECISION SUM1
      DOUBLE PRECISION VAV
      DOUBLE PRECISION YBB(10)
C
      COMMON /CMAIN1/ NV
      COMMON /CMAIN2/ ODIA, IDIA
      COMMON /CMAIN3/ QD
      COMMON /CMAIN4/ P
c     COMMON /CMAIN5/ UR
      COMMON /CMAIN5/ UF
      COMMON /CMAIN6/ T, R
C     COMMON /CMAIN7/ VISMIX
      COMMON /CMAIN8/ PI
      COMMON /CMAIN9/ NF
      COMMON /CMAIN10/ Y
      COMMON /CMAIN11/ YBB
      COMMON /CMAIN12/ nsegm
      COMMON /CMAIN13/ istep

C
c     COMMON /fcnsg/ DWW
C
C
C      PERMEATION EQUATION (du/dz)
C
C
      SUM1=0.0D0
            DO 101 I=1,NV-2
101                  SUM1=SUM1+QD(I)*(P*W(I+2)-W(2)*Y(I))
   FLSUM=SUM1
C
C     if(nsegm-2.EQ.istep)then
C     dw(1)=0.0d0
C     else
            DW(1)=-(PI*ODIA*NF)*FLSUM
C     endif
C
```

```
C           PERMEATE SIDE PRESSURE DROP (dp/dz)
C           CALCULATE GAS MIXTURE VISCOSITY, VAV IN C.P.
C
C
c     nvv=nv
            CALL vistcong (nv,T,YBB,VAV)
C
C           Convert VAV from c.p. TO Pa.s (1 C.P. = 10^(-3) PA.S)
            VAV=VAV*1.0D-03
C
C           if(nsegm-2.EQ.istep)then
C           dw(2)=0.0d0
C           else
                        DW(2)=((128.0*R*T*VAV)/(NF*PI*IDIA**4.0*W(2)))*(UF-W(1))
C           endif
C
C           PERMEATION EQUATION (COMPOSITION) (dxi/dz)
C
C           if(nsegm-2.EQ.istep)then
C                       DO 137 I=3,NV
C 137       dw(i)=0.0d0
C           else
                        DO 127 I=3,NV
 127                    DW(I)=((-W(I)*DW(1)-PI*ODIA*NF*QD(I-2)*(P*W(I)-W(2)*Y(I-2)))
    &/W(1))
C           endif
C
c                       DO 128 I=1,NV
c 128                   DWW(I)=DW(I)
C
c           pause

c           WRITE(*,*)DW(2)
c           PAUSE
            RETURN
            END
C-----------------------------END OF SUB.FCNS---------------------------------
C
C-------------------------------------------------------------------------
c           Subroutine DNEQNS contains Nonlinear equation solver DNEQNF
c-------------------------------------------------------------------------------
C
            SUBROUTINE dneqnsg (ncomps,M,XXX,QD,P,PP,YGUESS,YYY)
C                       Declare variables

    INTEGER    ITMAX, N
            INTEGER MM
            integer ncomps
    DOUBLE PRECISION      ERRREL
c     PARAMETER  (ncomps)
```

```
C
      DOUBLE PRECISION FNORM, YY(ncomps), YGUESS(ncomps)
            DOUBLE PRECISION YYY(ncomps)
            DOUBLE PRECISION XXX(ncomps)
            DOUBLE PRECISION XX(10)
            DOUBLE PRECISION QD(ncomps)
            DOUBLE PRECISION QDD(10)
            DOUBLE PRECISION P
            DOUBLE PRECISION PF
            DOUBLE PRECISION PP
            DOUBLE PRECISION PPP

C
      EXTERNAL fcnng,DNEQNF
C

            COMMON /FCNN1/ XX
            COMMON /CMAIN33/ QDD
            COMMON /CMAIN44/ PF
            COMMON /FCNN2/ PPP
            COMMON /FCNN3/ MM

C                       Set values of initial guess
C                       YGUESS = (  )
C
C     DATA YGUESS/68.0, 0.0, 0.0, 0.0/
C
            XX=XXX
            QDD=QD
            PF=P
            PPP=PP
            MM=M
            N=NCOMPS
C
      ERRREL = 0.0001D0
      ITMAX  = 100000
C           WRITE(*,*)YGUESS

C                       Find the solution
      CALL DNEQNF (fcnng, ERRREL, N, ITMAX, YGUESS, YY, FNORM)
C                       Output
c     WRITE (*,*) x(1)
C
            YYY=YY
C
      RETURN
            END
C                       User-defined subroutine
      SUBROUTINE fcnng (YY, F, N)
```

```
      INTEGER N
      INTEGER i
            INTEGER MM
      DOUBLE PRECISION YY(N), F(N)
            DOUBLE PRECISION SUM1, SUM2, YNMIN1, YNMIN2
            DOUBLE PRECISION XX(10)
            DOUBLE PRECISION QDD(10)
            DOUBLE PRECISION PF
            DOUBLE PRECISION PPP
C
            COMMON /FCNN1/ XX
            COMMON /CMAIN33/ QDD
            COMMON /CMAIN44/ PF
            COMMON /FCNN2/ PPP
            COMMON /FCNN3/ MM
C
C
C           WRITE(*,*)YY
C           PAUSE
C           IF (MM.EQ.1) THEN
                  SUM1=0.0D0
                  DO 40 I=1,N
 40                     SUM1=SUM1+YY(I)/QDD(I)
c 40                    SUM1=SUM1+YY(I)/(QDD(I)/QDD(1))
                  YNMIN1=SUM1
                  DO 60 I=1, N
 60                     F(I) =YY(I)-(QDD(I)*XX(I)*YNMIN1)/
     &(1.0D0-PPP/PF+PPP/PF*QDD(I)*YNMIN1)
c 60                    F(I) =YY(I)-((QDD(I)/QDD(1))*XX(I)*YNMIN1)/
c    &(1.0D0-PPP/PF+PPP/PF*(QDD(I)/QDD(1))*YNMIN1)
C
c           GO TO 11
C           ENDIF
C
C
      RETURN
      END
C-----------------------------END OF SUB.DNEQNS---------------------------------
C
C=======================================================================
C
C   SUBROUTINE INIT : INITIALIZATION OF VARIOUS DATA
C
C=======================================================================
C
C     SUBROUTINE SINIT1 (CTAG,IPRNT,NCOMPS,MWW,TCT,PCP,VCC,DPM,KAPA,
C    &      OMEGAC)

C
C     CHARACTER*4 CTAG(4)
```

```
C     CHARACTER*15 CNAME(4)
C           integer iprnt
C           INTEGER NCOMPS
c
C     INTEGER NV
C           integer i
C           DOUBLE PRECISION VCC(NCOMPS),DPM(NCOMPS),DPMR(NCOMPS),
C    &      KAPA(NCOMPS),OMEGAC(NCOMPS)
C     DOUBLE PRECISION TCT(NCOMPS),VFAC(NCOMPS),PCP(NCOMPS)
C           DOUBLE PRECISION MWW(NCOMPS)
c
C     COMMON /CINIT/ TCT,VFAC,PCP
c           COMMON /CINIT1/ MWW
C           COMMON /CMAIN1/ NV
C
C           data taken from Perry's Chemical Engineers Handbook (seventh edition)
C           page 2-136
C
C
C COMPONENTS TAGS
C
CC
C
C     CTAG(1)='CO2 '
C     CTAG(2)='N2 '
C     CTAG(3)='O2'
C     CTAG(4)='Ar '
C
C COMPONENTS NAMES
C
C     CNAME(1)='CARBON DI OXIDE      '
C     CNAME(2)='NITROGEN      '
C     CNAME(3)='OXYGEN       '
C     CNAME(4)='ARGON         '
C


C MOLECULAR WEIGHTS OF THE COMPONENTS


C     MWW(1) = 44.01D0
C     MWW(2) = 28.014D0
C     MWW(3) = 32.0D0
C     MWW(4) = 39.948D0


C
C CRITICAL TEMPERATURES OF THE COMPONENTS IN DEG. K
C
C     TCT(1) =304.1D0
C     TCT(2) =126.2D0
C     TCT(3) =154.6D0
C     TCT(4) =150.86D0
```

```
C
C CRITICAL PRESSURES OF THE COMPONENTS IN Pa
C
C     PCP(1) =7.38D+06
C     PCP(2) =3.39D+06
C     PCP(3) =5.04D+06
C     PCP(4) =4.90D+06
C
C
C DIPOLE MOMENTS OF THE COMPONENTS IN DEBYES
C
C     DPM(1) = 0.0D0
C     DPM(2) = 0.0D0
C     DPM(3) = 0.0D0
C     DPM(4) = 0.0D0
C
C KAPA FACTORS OF THE COMPONENT (DIMENSIONLESS)
C
C     KAPA(1) = 0.0D0
C     KAPA(2) = 0.0D0
C     KAPA(3) = 0.0D0
C     KAPA(4) = 0.0D0
C
C ACENTRIC FACTORS OF THE COMPONENT (DIMENSIONLESS)
C
C     OMEGAC(1) = 0.239D0
C     OMEGAC(2) = 0.037D0
C     OMEGAC(3) = 0.025D0
C     OMEGAC(4) = 0.00D0
C
C CRITICAL VOLUMES OF THE COMPONENTS IN CM3/MOL
C
C     VCC(1) = 0.0939D+03
C     VCC(2) = 0.089D+03
C     VCC(3) = 0.0734D+03
C     VCC(4) = 0.075D+03
C
C COMPRESSIBILITY FACTORS
C
C
C     RETURN
C     END
C-----------------------------END OF SUB.SINIT-----------------------------------
C
C===============================================================================
C
C   SUBROUTINE VISTCON : CALULATES VISCOSITIES & THERMAL CONDUCTIVITIES
C
C===============================================================================
C
```

```
      SUBROUTINE vistcong (nv,TT1,YYY,VAV)
C
      INTEGER NP,NV
            integer i, j
            double precision DEXP

            DOUBLE PRECISION TT1,TT,OV,BB,BI(nv-2,nv-2),YYY(nv-2),VS(nv-2),
     & VAV
      DOUBLE PRECISION TCT(10),VFAC(10),PCP(10)
            DOUBLE PRECISION MWW(nv-2)
            DOUBLE PRECISION MWV(10)
      COMMON /CINIT/ TCT,VFAC,PCP
            COMMON /CINIT1/ MWV
c           COMMON /CMAIN1/NV

c
            mww=mwv
C
C     VISCOCITY IN CP
C
      DO 5 I=1,NV-2
      TT=1.2593D0*TT1/TCT(I)
      OV=1.16145D0*TT**(-0.14874D0)+0.52487D0*DEXP(-0.7732D0*TT)
     &+2.16178D0*DEXP(-2.43787D0*TT)
      VS(I)=VFAC(I)*TT1**0.5/OV
 5    CONTINUE
C
      DO 7 I=1,NV-2
      DO 7 J=1,NV-2
      BI(I,J)=(1.D0+((VS(I)/VS(J))**(1.0D0/2.0D0))*((MWW(J)/MWW(I))**
     &(1.0D0/4.0D0)))**2.0/(8.D0*(1.D0+(MWW(I)/MWW(J))))**(1.0D0/2.0D0)
 7    CONTINUE
      VAV=0.D0
C
      DO 9 I=1,NV-2
      BB=0.D0
C
      DO 11 J=1,NV-2
      BB=BB+BI(I,J)*YYY(J)
 11   CONTINUE
C
      VAV=VAV+VS(I)*YYY(I)/BB
 9    CONTINUE
C
C
      RETURN
      END
C-----------------------------END OF SUB. VISTCON-----------------------------
```

Appendix C: Coal characteristics (Alie 2004)

	Units	PRB	USLS
Proximate analysis (dry):			
Moisture	%	28.1	7.5
Volatiles	%	42.92	33.69
Ash	%	7.13	10.36
Fixed carbon	%	49.95	55.95
Ultimate analysis (dry):			
Carbon	%	69.4	77.2
Hydrogen	%	4.9	4.9
Nitrogen	%	1.0	1.5
Sulphur	%	0.4	1.0
Oxygen	%	17.2	5.0
Ash	%	7.1	10.4
High heating value:			
Dry	KJ/kg	27637	31768
As fired	KJ/kg	19912	29385

Appendix D: Procedure for Updated Last Stage Pressure Drop in Absorber

No appreciable reaction or separation occurs in the dummy stage, but its presence allows the pressure drop to be applied appropriately (AspenPlus help documentation).

1. Increase the number of stages by 1.
2. Adjust feed locations for feeds to the bottom of the column. Adjust any other inputs as necessary. Note that the new bottom stage should not be part of any reaction section.
3. Set the **Calculation type** to **Rate-Based** on the **Setup | Configuration** sheet.
4. Create a Pack-Rating section that contains only the last stage. Select a packing that doesn't require any additional input parameters. Use a small pack height. Mark this section as rate-based. Use a small number such as 1E-5 for **Interfacial Area Factor** and **Heat Transfer Factor**.

Appendix E: Material Balance for the Conventional Flowsheet at the Lean Loading of 0.3 for Model-VI

Stream name	FLUE-BLO	FLUE-DCC	H20-PUMP	H20-DCC	H2O-OUT	FLUE-ABS	FLUEABS1
Substream: MIXED							
Mole Flow kmol/sec							
H2O	1.866989	1.866989	44.79951	44.79951	45.74675	0.9196734	0.2299184
CO2	3.099475	3.099475	0	0	3.07E-03	3.096371	0.7740926
MEA	0	0	0	0	4.58E-29	4.68E-33	0
N2	17.04711	17.04711	0	0	5.07E-04	17.04661	4.261652
O2	0.8079634	0.8079634	0	0	4.33E-05	0.8079201	0.20198
MEAH+	0	0	0	0	4.58E-29	0	0
MEACOO-	0	0	0	0	4.58E-29	0	0
HCO3-	0	0	0	0	3.67E-05	0	0
CO3--	0	0	0	0	6.17E-11	0	0
H3O+	0	0	4.78E-08	4.78E-08	3.67E-05	0	0
OH-	0	0	4.78E-08	4.78E-08	1.81E-09	0	0
H2S	0	0	0	0	1.29E-23	9.36E-27	0
HS-	0	0	0	0	1.32E-20	0	0
S-2	0	0	0	0	4.58E-29	0	0
AR	0	0	0	0	0	0	0
NO	0	0	0	0	0	0	0
CO	0	0	0	0	0	0	0
SO2	0	0	0	0	0	0	0
H2	0	0	0	0	0	0	0
Mole Frac							
H2O	0.0818081	0.0818081	1	1	0.9999193	0.0420507	0.0420507
CO2	0.1358136	0.1358136	0	0	6.71E-05	0.141577	0.141577
MEA	0	0	0	0	1.00E-30	2.14E-34	0
N2	0.7469747	0.7469747	0	0	1.11E-05	0.7794313	0.7794313
O2	0.0354035	0.0354035	0	0	9.46E-07	0.0369409	0.0369409
MEAH+	0	0	0	0	1.00E-30	0	0
MEACOO-	0	0	0	0	1.00E-30	0	0
HCO3-	0	0	0	0	8.01E-07	0	0
CO3--	0	0	0	0	1.35E-12	0	0
H3O+	0	0	1.07E-09	1.07E-09	8.01E-07	0	0
OH-	0	0	1.07E-09	1.07E-09	3.95E-11	0	0
H2S	0	0	0	0	2.82E-25	4.28E-28	0
HS-	0	0	0	0	2.88E-22	0	0
S-2	0	0	0	0	1.00E-30	0	0
AR	0	0	0	0	0	0	0
NO	0	0	0	0	0	0	0
CO	0	0	0	0	0	0	0
SO2	0	0	0	0	0	0	0
H2	0	0	0	0	0	0	0
Total Flow kmol/sec	22.82154	22.82154	44.79951	44.79951	45.75044	21.87057	5.467643
Total Flow cum/sec	764.3347	497.9251	0.8073911	0.80736	0.8386666	321.0193	80.25481
Temperature K	407	484.4987	285.15	285.1539	333.4304	313.0004	313.0004
Pressure N/sqm	1.01E+05	1.85E+05	1.01E+05	1.85E+05	1.77E+05	1.77E+05	1.77E+05
Vapor Frac	1	1	0	0	0	1	1
Liquid Frac	0	0	1	1	1	0	0
Density kmol/cum	0.029858	0.0458332	55.48675	55.4889	54.55141	0.0681285	0.0681285
Average MW	29.50916	29.50916	18.01528	18.01528	18.01718	30.00498	30.00498

Appendix E continued…

Stream name	STACK1	LEANABS1	LEAN-ABS	RICHPUM1	RICH-HX	RICH-HX1	RICH-STR
Substream: MIXED							
Mole Flow kmol/sec							
H2O	0.608505	26.21666	26.21666	25.82779	25.7449	25.74489	25.76617
CO2	0.115422	2.61E-06	2.61E-06	1.00E-03	6.49E-04	6.50E-04	0.1468595
MEA	1.82E-04	1.510309	1.510309	0.2218794	0.295169	0.2951742	0.5741655
N2	4.261542	5.39E-15	5.39E-15	1.10E-04	1.10E-04	1.10E-04	1.10E-04
O2	0.201971	2.87E-15	2.82E-15	9.45E-06	9.45E-06	9.45E-06	9.45E-06
MEAH+	2.56E-05	0.978265	0.9782649	1.619182	1.628431	1.62843	1.474358
MEACOO-	2.43E-05	1.018892	1.018892	1.666174	1.583634	1.583631	1.458711
HCO3-	9.47E-07	0.0134884	0.0134886	0.0404975	0.1144958	0.1145005	0.1010826
CO3--	1.86E-07	0.0198563	0.0198562	3.21E-03	0.0121051	0.0121039	4.23E-03
H3O+	3.11E-14	2.26E-10	2.26E-10	4.98E-09	3.82E-09	3.82E-09	1.64E-08
OH-	2.69E-10	9.08E-05	9.08E-05	7.31E-06	9.85E-06	9.85E-06	2.04E-05
H2S	3.69E-14	3.20E-17	3.15E-17	2.53E-17	1.90E-17	1.90E-17	5.07E-16
HS-	4.23E-19	3.86E-14	3.86E-14	1.94E-15	1.92E-15	1.92E-15	1.40E-15
S-2	1.50E-23	4.29E-18	4.33E-18	3.13E-20	4.23E-20	4.23E-20	1.93E-19
AR	0	0	0	0	0	0	0
NO	0	0	0	0	0	0	0
CO	0	0	0	0	0	0	0
SO2	0	0	0	0	0	0	0
H2	0	0	0	0	0	0	0
Mole Frac							
H2O	0.117298	0.8810083	0.8810082	0.8790984	0.8762875	0.8762873	0.8726687
CO2	0.022249	8.78E-08	8.78E-08	3.41E-05	2.21E-05	2.21E-05	4.97E-03
MEA	3.50E-05	0.0507537	0.0507537	7.55E-03	0.0100467	0.0100469	0.0194462
N2	0.821475	1.81E-16	1.81E-16	3.73E-06	3.73E-06	3.73E-06	3.71E-06
O2	0.038933	9.64E-17	9.46E-17	3.22E-07	3.22E-07	3.22E-07	3.20E-07
MEAH+	4.94E-06	0.0328745	0.0328745	0.0551119	0.0554274	0.0554273	0.0499347
MEACOO-	4.69E-06	0.0342397	0.0342397	0.0567114	0.0539026	0.0539025	0.0494047
HCO3-	1.83E-07	4.53E-04	4.53E-04	1.38E-03	3.90E-03	3.90E-03	3.42E-03
CO3--	3.59E-08	6.67E-04	6.67E-04	1.09E-04	4.12E-04	4.12E-04	1.43E-04
H3O+	6.00E-15	7.58E-12	7.58E-12	1.69E-10	1.30E-10	1.30E-10	5.56E-10
OH-	5.18E-11	3.05E-06	3.05E-06	2.49E-07	3.35E-07	3.35E-07	6.89E-07
H2S	7.10E-15	1.08E-18	1.06E-18	8.62E-19	6.46E-19	6.46E-19	1.72E-17
HS-	8.16E-20	1.30E-15	1.30E-15	6.61E-17	6.54E-17	6.54E-17	4.73E-17
S-2	2.89E-24	1.44E-19	1.46E-19	1.07E-21	1.44E-21	1.44E-21	6.54E-21
AR	0	0	0	0	0	0	0
NO	0	0	0	0	0	0	0
CO	0	0	0	0	0	0	0
SO2	0	0	0	0	0	0	0
H2	0	0	0	0	0	0	0
Total Flow kmol/sec	5.187672	29.75756	29.75756	29.37986	29.37951	29.37951	29.52572
Total Flow cum/sec	138.5335	0.6613352	0.6613333	0.6877292	0.6786101	0.6786095	6.847881
Temperature K	325.6912	313.0006	313	327.5444	327.8689	327.8691	370.1032
Pressure N/sqm	1.01E+05	1.01E+05	1.01E+05	1.46E+05	1.46E+05	1.46E+05	1.46E+05
Vapor Frac	0.99991	0	0	0	0	0	0.0100009
Liquid Frac	8.96E-05	1	1	1	1	1	0.9899991
Density kmol/cum	0.037447	44.99618	44.99632	42.7201	43.29365	43.29369	4.311658
Average MW	27.35347	24.64457	24.64457	25.71542	25.71573	25.71573	25.5884

Appendix E continued…

Stream name	LEAN-HX	LEAN-MIX	LEAN-COO	MAKE-UP	CO2-COMP	CO2-COM	WAT	CO2-SEQ
Substream: MIXED								
Mole Flow, kmol/sec								
H2O	25.53837	25.54818	26.21875	0.671297	0.2927102	1.170841	1.162968	7.87E-03
CO2	1.41E-03	1.80E-05	1.77E-05	0	0.6586385	2.634554	1.83E-03	2.632717
MEA	1.536446	1.515101	1.515706	2.32E-04	6.60E-08	2.64E-07	2.15E-12	0
N2	5.51E-15	1.16E-14	5.51E-15	0	1.10E-04	4.38E-04	7.31E-09	4.38E-04
O2	1.15E-15	8.79E-15	2.84E-15	0	9.45E-06	3.78E-05	1.19E-09	3.78E-05
MEAH+	0.960311	0.970454	0.970825	1.01E-05	0	0	2.64E-07	0
MEACOO-	1.010487	1.021689	1.020952	0	0	0	5.72E-15	0
HCO3-	0.037046	0.018486	0.0188533	0	0	0	2.39E-06	0
CO3--	3.29E-03	0.012039	0.0124106	0	0	0	1.47E-12	3.39E-16
H3O+	8.01E-09	7.22E-10	7.27E-10	4.42E-13	0	0	2.12E-06	7.76E-09
OH-	8.70E-05	9.38E-05	9.67E-05	1.01E-05	0	0	5.96E-12	2.99E-16
H2S	2.09E-17	5.53E-14	4.31E-18	0	3.94E-15	1.58E-14	7.75E-09	0
HS-	3.16E-15	3.99E-11	3.14E-15	0	0	0	6.18E-12	5.14E-20
S-2	2.15E-17	7.59E-15	5.88E-19	0	0	0	2.50E-22	2.47E-31
AR	0	0	0	0	0	0	0	0
NO	0	0	0	0	0	0	0	0
CO	0	0	0	0	0	0	0	0
SO2	0	0	0	0	0	0	0	0
H2	0	0	0	0	0	0	0	0
Mole Frac								
H2O	0.877985	0.878365	0.881077	0.99962	0.3076407	0.307640	0.998421	2.98E-03
CO2	4.84E-05	6.20E-07	5.96E-07	0	0.6922341	0.692234	1.57E-03	0.99684
MEA	0.052821	0.052090	0.050935	3.45E-04	6.93E-08	6.93E-08	1.85E-12	0
N2	1.89E-16	3.99E-16	1.85E-16	0	1.15E-04	1.15E-04	6.28E-09	1.66E-04
O2	3.94E-17	3.02E-16	9.53E-17	0	9.94E-06	9.94E-06	1.02E-09	1.43E-05
MEAH+	0.033014	0.033364	0.0326245	1.51E-05	0	0	2.27E-07	0
MEACOO-	0.034739	0.035126	0.0343089	0	0	0	4.91E-15	0
HCO3-	1.27E-03	6.36E-04	6.34E-04	0	0	0	2.05E-06	0
CO3--	1.13E-04	4.14E-04	4.17E-04	0	0	0	1.26E-12	1.29E-16
H3O+	2.75E-10	2.48E-11	2.44E-11	6.59E-13	0	0	1.82E-06	2.94E-09
OH-	2.99E-06	3.23E-06	3.25E-06	1.51E-05	0	0	5.12E-12	1.13E-16
H2S	7.20E-19	1.90E-15	1.45E-19	0	4.14E-15	4.14E-15	6.65E-09	0
HS-	1.09E-16	1.37E-12	1.05E-16	0	0	0	5.31E-12	1.95E-20
S-2	7.38E-19	2.61E-16	1.98E-20	0	0	0	2.15E-22	9.36E-32
AR	0	0	0	0	0	0	0	0
NO	0	0	0	0	0	0	0	0
CO	0	0	0	0	0	0	0	0
SO2	0	0	0	0	0	0	0	0
H2	0	0	0	0	0	0	0	0
Total Flow kmol/sec	29.08745	29.08606	29.75761	0.6715495	0.9514678	3.805871	1.164807	2.641062
Total Flow cum/sec	0.676220	0.654992	0.6671112	0.0121953	26.65741	106.6296	0.058693	0.352317
Temperature K	382.5076	332.8672	332.5086	313	343	343	312.7191	313
Pressure N/sqm	1.32E+05	1.32E+05	1.01E+05	1.01E+05	1.01E+05	1.01E+05	1.01E+05	1.10E+07
Vapor Frac	0	0	0	0	1	1	1.26E-03	1
Liquid Frac	1	1	1	1	0	0	0.998738	0
Density kmol/cum	43.01472	44.4067	44.60668	55.06604	0.0356924	0.035692	19.8456	7.49626
Average MW	24.79609	24.79727	24.64457	18.03079	36.01087	36.01087	18.05631	43.92953

Appendix F: Material Balance for Flour Concept Flowsheet at the Lean Loading of 0.3 for Model-VI

Stream name	FLUE-BLO	FLUE-DCC	H20-PUMP	H20-DCC	H2O-OUT	FLUE-ABS	FLUEABS1
Mole Flow kmol/sec							
H2O	1.866989	1.866989	44.79951	44.79951	45.74675	0.9196734	0.2299184
CO2	3.099475	3.099475	0	0	3.07E-03	3.096371	0.7740926
MEA	0	0	0	0	4.58E-29	4.68E-33	0
N2	17.04711	17.04711	0	0	5.07E-04	17.04661	4.261652
O2	0.8079634	0.8079634	0	0	4.33E-05	0.8079201	0.20198
MEAH+	0	0	0	0	4.58E-29	0	0
MEACOO-	0	0	0	0	4.58E-29	0	0
HCO3-	0	0	0	0	3.67E-05	0	0
CO3--	0	0	0	0	6.17E-11	0	0
H3O+	0	0	4.78E-08	4.78E-08	3.67E-05	0	0
OH-	0	0	4.78E-08	4.78E-08	1.81E-09	0	0
H2S	0	0	0	0	1.29E-23	9.36E-27	0
HS-	0	0	0	0	1.32E-20	0	0
S-2	0	0	0	0	4.58E-29	0	0
AR	0	0	0	0	0	0	0
NO	0	0	0	0	0	0	0
CO	0	0	0	0	0	0	0
SO2	0	0	0	0	0	0	0
H2	0	0	0	0	0	0	0
Mole Frac							
H2O	0.0818081	0.0818081	1	1	0.9999193	0.0420507	0.0420507
CO2	0.1358136	0.1358136	0	0	6.71E-05	0.141577	0.141577
MEA	0	0	0	0	1.00E-30	2.14E-34	0
N2	0.7469747	0.7469747	0	0	1.11E-05	0.7794313	0.7794313
O2	0.0354035	0.0354035	0	0	9.46E-07	0.0369409	0.0369409
MEAH+	0	0	0	0	1.00E-30	0	0
MEACOO-	0	0	0	0	1.00E-30	0	0
HCO3-	0	0	0	0	8.01E-07	0	0
CO3--	0	0	0	0	1.35E-12	0	0
H3O+	0	0	1.07E-09	1.07E-09	8.01E-07	0	0
OH-	0	0	1.07E-09	1.07E-09	3.95E-11	0	0
H2S	0	0	0	0	2.82E-25	4.28E-28	0
HS-	0	0	0	0	2.88E-22	0	0
S-2	0	0	0	0	1.00E-30	0	0
AR	0	0	0	0	0	0	0
NO	0	0	0	0	0	0	0
CO	0	0	0	0	0	0	0
SO2	0	0	0	0	0	0	0
H2	0	0	0	0	0	0	0
Total Flow kmol/sec	22.82154	22.82154	44.79951	44.79951	45.75044	21.87057	5.467643
Total Flow cum/sec	764.3347	497.9251	0.8073911	0.8073599	0.8386666	321.0193	80.25481
Temperature K	407	484.4987	285.15	285.1539	333.4304	313.0004	313.0004
Pressure N/sqm	1.01E+05	1.85E+05	1.01E+05	1.85E+05	1.77E+05	1.77E+05	1.77E+05
Vapor Frac	1	1	0	0	0	1	1
Liquid Frac	0	0	1	1	1	0	0
Density kmol/cum	0.029858	0.0458332	55.48675	55.4889	54.55141	0.0681285	0.0681285
Average MW	29.50916	29.50916	18.01528	18.01528	18.01718	30.00498	30.00498

Appendix F continued…..

Stream name	STACK1	LEANABS1	LEAN-ABS	RICHPUM1	RICH-HX1	RICH-HX	RICH-STR
Mole Flow kmol/sec							
H2O	0.574927	26.66598	53.33196	26.31163	26.22863	52.45725	52.50101
CO2	0.11543	3.22E-06	6.43E-06	1.05E-03	7.25E-04	1.45E-03	0.3118657
MEA	1.78E-04	1.530974	3.061948	0.2398232	0.3140537	0.62811	1.219193
N2	4.261543	7.77E-15	1.55E-14	1.09E-04	1.09E-04	2.17E-04	2.17E-04
O2	0.201971	3.05E-15	6.10E-15	9.37E-06	9.37E-06	1.87E-05	1.87E-05
MEAH+	2.51E-05	1.155328	2.310656	1.79807	1.806512	3.613024	3.288584
MEACOO-	2.39E-05	1.10593	2.21186	1.754112	1.671439	3.342877	3.076234
HCO3-	8.86E-07	0.0141509	0.0283021	0.0383325	0.1132232	0.226449	0.1967192
CO3--	1.73E-07	0.0175858	0.0351709	2.81E-03	0.0109205	0.02184	7.80E-03
H3O+	2.80E-14	2.70E-10	5.40E-10	5.34E-09	4.15E-09	8.31E-09	3.48E-08
OH-	2.34E-10	7.58E-05	1.52E-04	6.80E-06	9.03E-06	1.81E-05	3.73E-05
H2S	8.69E-14	1.09E-17	2.22E-17	5.70E-17	4.33E-17	8.65E-17	2.24E-15
HS-	9.21E-19	1.11E-14	2.22E-14	4.06E-15	4.01E-15	8.03E-15	5.70E-15
S-2	3.08E-23	1.04E-18	2.10E-18	5.56E-20	8.17E-20	1.63E-19	7.17E-19
AR	0	0	0	0	0	0	0
NO	0	0	0	0	0	0	0
CO	0	0	0	0	0	0	0
SO2	0	0	0	0	0	0	0
H2	0	0	0	0	0	0	0
Mole Frac							
H2O	0.111548	0.8745804	0.8745804	0.872808	0.870064	0.870064	0.8663293
CO2	0.022396	1.05E-07	1.05E-07	3.50E-05	2.40E-05	2.40E-05	5.15E-03
MEA	3.45E-05	0.0502122	0.0502122	7.96E-03	0.0104178	0.010418	0.0201181
N2	0.826826	2.55E-16	2.55E-16	3.60E-06	3.60E-06	3.60E-06	3.58E-06
O2	0.039186	9.99E-17	1.00E-16	3.11E-07	3.11E-07	3.11E-07	3.09E-07
MEAH+	4.87E-06	0.037892	0.037892	0.0596454	0.0599261	0.059926	0.0542655
MEACOO-	4.63E-06	0.0362718	0.0362718	0.0581873	0.0554454	0.055445	0.0507615
HCO3-	1.72E-07	4.64E-04	4.64E-04	1.27E-03	3.76E-03	3.76E-03	3.25E-03
CO3--	3.36E-08	5.77E-04	5.77E-04	9.32E-05	3.62E-04	3.62E-04	1.29E-04
H3O+	5.44E-15	8.85E-12	8.85E-12	1.77E-10	1.38E-10	1.38E-10	5.75E-10
OH-	4.55E-11	2.49E-06	2.49E-06	2.25E-07	3.00E-07	3.00E-07	6.16E-07
H2S	1.69E-14	3.58E-19	3.64E-19	1.89E-18	1.44E-18	1.44E-18	3.70E-17
HS-	1.79E-19	3.63E-16	3.64E-16	1.35E-16	1.33E-16	1.33E-16	9.41E-17
S-2	5.98E-24	3.42E-20	3.45E-20	1.84E-21	2.71E-21	2.71E-21	1.18E-20
AR	0	0	0	0	0	0	0
NO	0	0	0	0	0	0	0
CO	0	0	0	0	0	0	0
SO2	0	0	0	0	0	0	0
H2	0	0	0	0	0	0	0
Total Flow kmol/sec	5.154098	30.49003	60.98005	30.14596	30.14563	60.29126	60.60167
Total Flow cum/sec	137.3055	0.6788974	1.357794	0.7070339	0.6977502	1.3955	14.01913
Temperature K	324.8965	313.0005	313	327.7597	328.0707	328.0708	369.558
Pressure N/sqm	1.01E+05	1.01E+05	1.01E+05	1.46E+05	1.46E+05	1.46E+05	1.46E+05
Vapor Frac	0.999916	0	0	0	0	0	9.98E-03
Liquid Frac	8.42E-05	1	1	1	1	1	0.9900171
Density kmol/cum	0.037537	44.91109	44.91111	42.63722	43.20404	43.20405	4.322786
Average MW	27.41429	25.01396	25.01396	26.05439	26.05467	26.05467	25.92122

Appendix F continued…..

Stream name	LEAN-HX	LEAN-MIX	LEAN-COO	MAKE-UP	CO2-COMP	CO2-COM	WAT	CO2-SEQ
Mole Flow, kmol/sec								
H2O	52.03819	52.06007	53.33408	1.275399	0.585379	1.170759	1.162886	7.87E-03
CO2	3.66E-03	4.69E-05	4.60E-05	0	1.317277	2.634554	1.83E-03	2.632717
MEA	3.116323	3.071929	3.073131	4.54E-04	1.40E-07	2.79E-07	2.29E-12	0
N2	1.55E-14	1.76E-14	1.55E-14	0	2.17E-04	4.34E-04	7.25E-09	4.34E-04
O2	3.26E-15	8.15E-15	6.10E-15	0	1.87E-05	3.75E-05	1.18E-09	3.75E-05
MEAH+	2.277811	2.296701	2.29737	1.95E-05	0	0	2.79E-07	0
MEACOO-	2.189871	2.215376	2.213978	0	0	0	6.09E-15	0
HCO3-	0.0758599	0.0386987	0.0394341	0	0	0	2.40E-06	0
CO3--	5.97E-03	0.0212351	0.0218987	0	0	0	1.48E-12	3.39E-16
H3O+	1.89E-08	1.76E-09	1.77E-09	8.28E-13	0	0	2.11E-06	7.76E-09
OH-	1.45E-04	1.56E-04	1.61E-04	1.95E-05	0	0	5.98E-12	2.99E-16
H2S	0	5.60E-14	4.08E-17	0	7.89E-15	1.58E-14	7.75E-09	0
HS-	1.69E-14	3.39E-11	2.50E-14	0	0	0	6.20E-12	5.14E-20
S-2	0	5.51E-15	4.01E-18	0	0	0	2.52E-22	2.47E-31
AR	0	0	0	0	0	0	0	0
NO	0	0	0	0	0	0	0	0
CO	0	0	0	0	0	0	0	0
SO2	0	0	0	0	0	0	0	0
H2	0	0	0	0	0	0	0	0
Mole Frac								
H2O	0.8715472	0.8719664	0.8746145	0.999614	0.307626	0.3076261	0.998421	2.98E-03
CO2	6.13E-05	7.86E-07	7.55E-07	0	0.692249	0.6922498	1.57E-03	0.996842
MEA	0.0521928	0.0514524	0.0503956	3.55E-04	7.34E-08	7.34E-08	1.96E-12	0
N2	2.60E-16	2.94E-16	2.55E-16	0	1.14E-04	1.14E-04	6.22E-09	1.65E-04
O2	5.45E-17	1.37E-16	1.00E-16	0	9.84E-06	9.84E-06	1.01E-09	1.42E-05
MEAH+	0.0381493	0.0384679	0.0376741	1.53E-05	0	0	2.40E-07	0
MEACOO-	0.0366764	0.0371058	0.0363065	0	0	0	5.23E-15	0
HCO3-	1.27E-03	6.48E-04	6.47E-04	0	0	0	2.06E-06	0
CO3--	9.99E-05	3.56E-04	3.59E-04	0	0	0	1.27E-12	1.29E-16
H3O+	3.17E-10	2.94E-11	2.90E-11	6.49E-13	0	0	1.81E-06	2.94E-09
OH-	2.43E-06	2.62E-06	2.64E-06	1.53E-05	0	0	5.13E-12	1.13E-16
H2S	0	9.38E-16	6.69E-19	0	4.15E-15	4.15E-15	6.66E-09	0
HS-	2.83E-16	5.68E-13	4.09E-16	0	0	0	5.33E-12	1.95E-20
S-2	0	9.23E-17	6.57E-20	0	0	0	2.16E-22	9.36E-32
AR	0	0	0	0	0	0	0	0
NO	0	0	0	0	0	0	0	0
CO	0	0	0	0	0	0	0	0
SO2	0	0	0	0	0	0	0	0
H2	0	0	0	0	0	0	0	0
Total Flow, kmol/sec	59.70782	59.70421	60.9801	1.275891	1.902893	3.805785	1.164725	2.641058
Total Flow, cum/sec	1.390097	1.346915	1.369918	0.0231704	53.31361	106.6272	0.058689	0.3523185
Temperature, K	382.009	333.0692	332.7365	313	343	343	312.7191	313
Pressure, N/sqm	1.32E+05	1.32E+05	1.01E+05	1.01E+05	1.01E+05	1.01E+05	1.01E+05	1.10E+07
Vapor Frac	0	0	0	0	1	1	1.26E-03	1
Liquid Frac	1	1	1	1	0	0	0.998738	0
Density, kmol/cum	42.95227	44.32662	44.51369	55.06544	0.035692	0.0356924	19.8454	7.496222
Average MW	25.16167	25.16319	25.01397	18.03125	36.01126	36.01126	18.05632	43.92955

Appendix G: Mass transfer rate profile for different components in absorber for Model-II and Model-VI

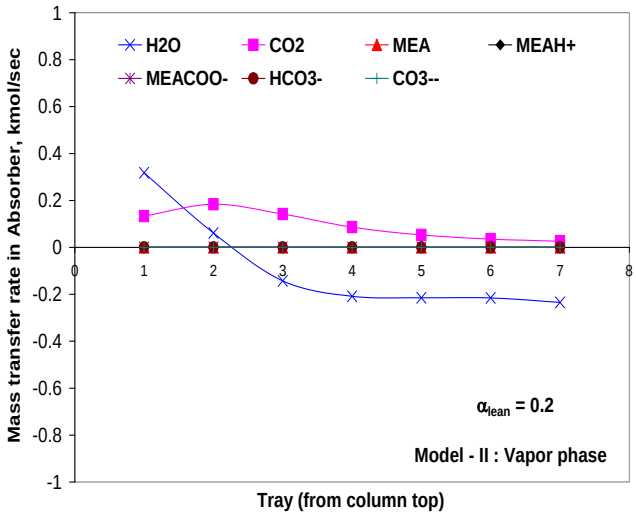

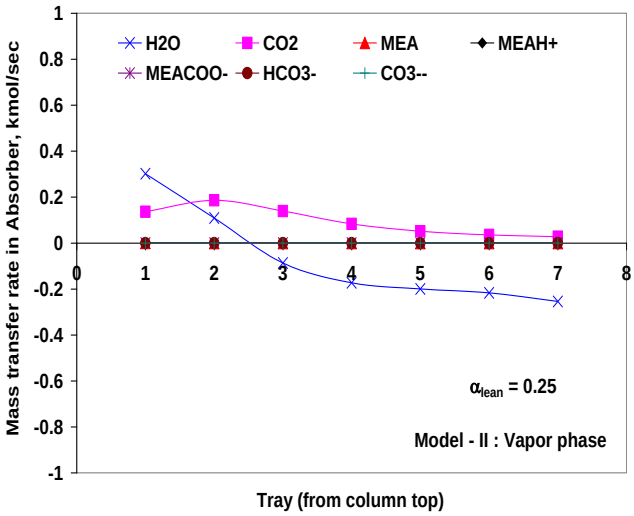

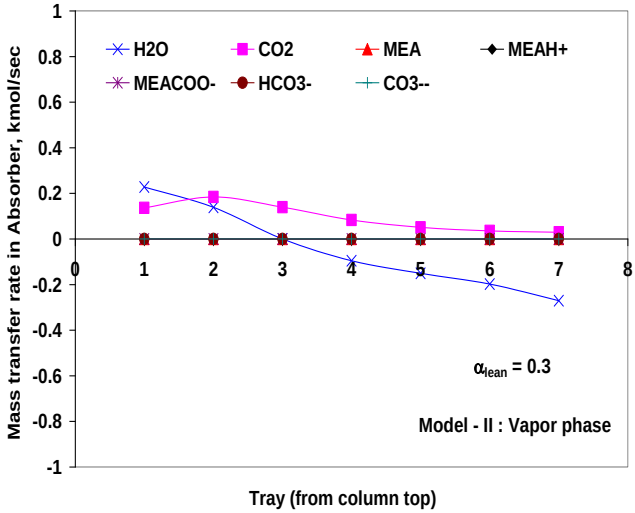

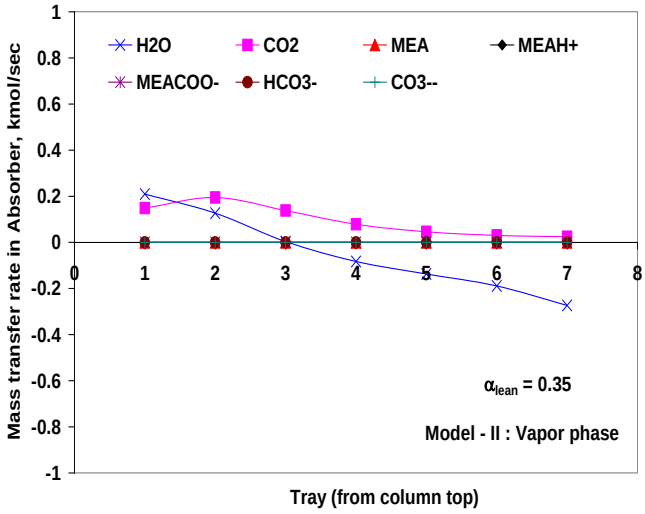
H2O
CO2
MEA
MEAH+
MEACOO-
HCO3-
CO3--
Mass transfer rate in Absorber, kmol/sec
Tray (from column top)
α_{lean} = 0.35
Model - II : Vapor phase

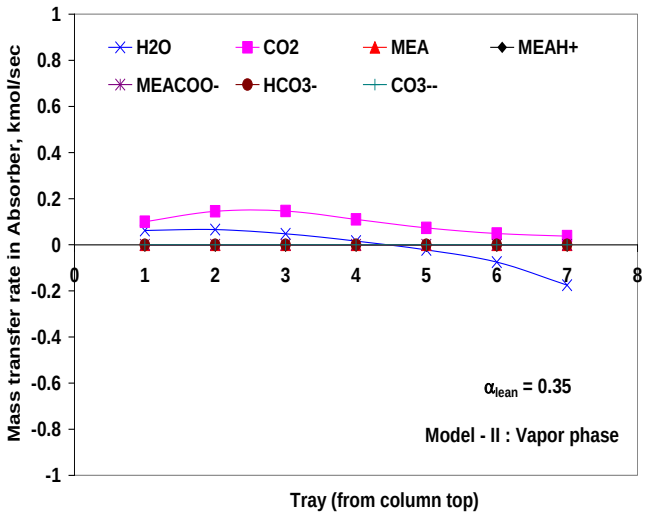
H2O
CO2
MEA
MEAH+
MEACOO-
HCO3-
CO3--
Mass transfer rate in Absorber, kmol/sec
Tray (from column top)
α_{lean} = 0.35
Model - II : Vapor phase

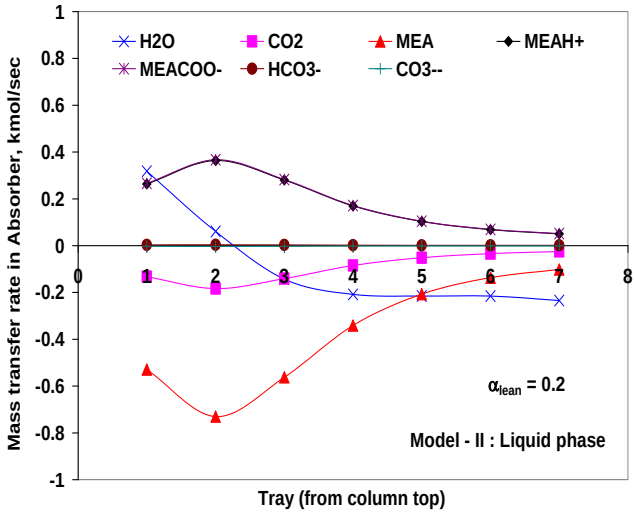
H2O
CO2
MEA
MEAH+
MEACOO-
HCO3-
CO3--
Mass transfer rate in Absorber, kmol/sec
Tray (from column top)
α_{lean} = 0.2
Model - II : Liquid phase

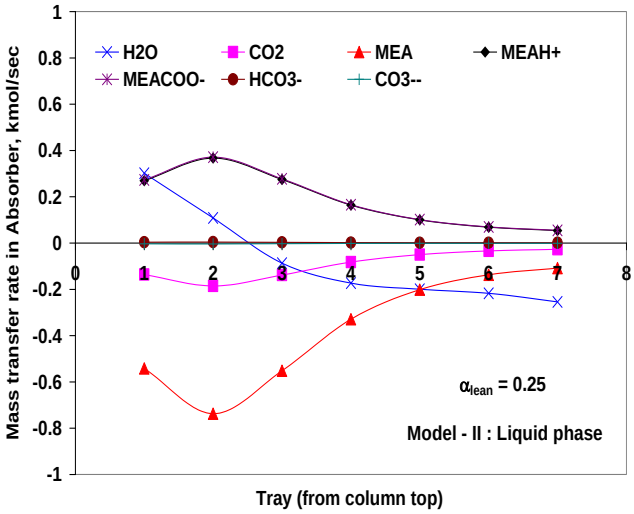
H2O
CO2
MEA
MEAH+
MEACOO-
HCO3-
CO3--
Mass transfer rate in Absorber, kmol/sec
Tray (from column top)
α_{lean} = 0.25
Model - II : Liquid phase

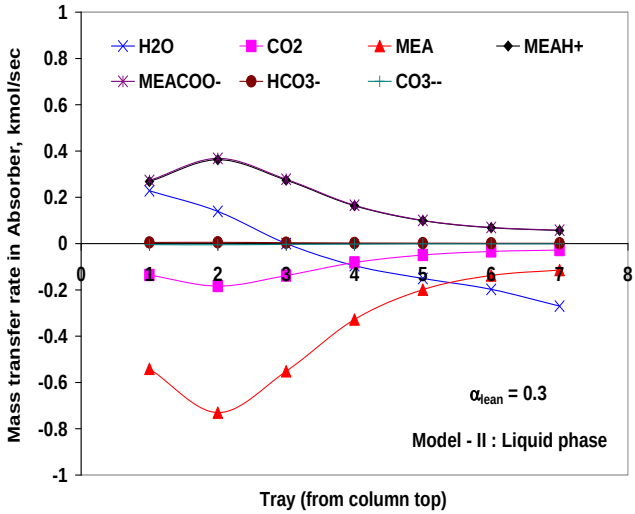
H2O
CO2
MEA
MEAH+
MEACOO-
HCO3-
CO3--
Mass transfer rate in Absorber, kmol/sec
Tray (from column top)
α_{lean} = 0.3
Model - II : Liquid phase

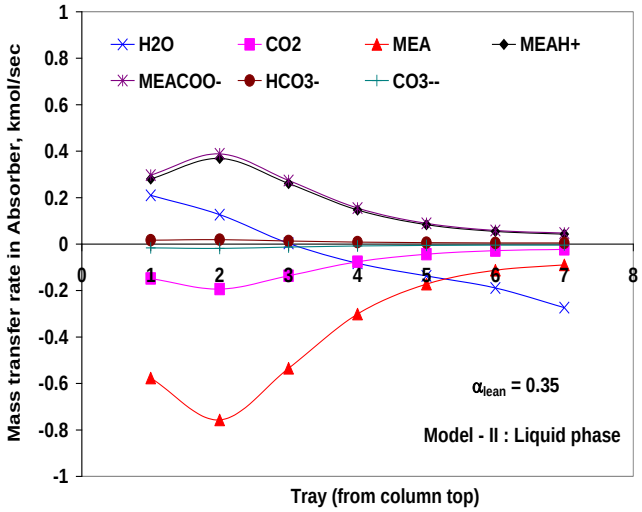
H2O
CO2
MEA
MEAH+
MEACOO-
HCO3-
CO3--
Mass transfer rate in Absorber, kmol/sec
Tray (from column top)
αlean = 0.35
Model - II : Liquid phase

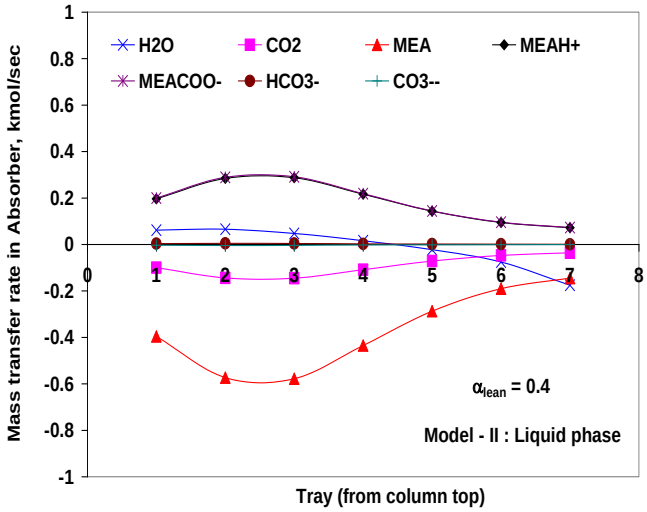
H2O
CO2
MEA
MEAH+
MEACOO-
HCO3-
CO3--
Mass transfer rate in Absorber, kmol/sec
Tray (from column top)
αlean = 0.4
Model - II : Liquid phase

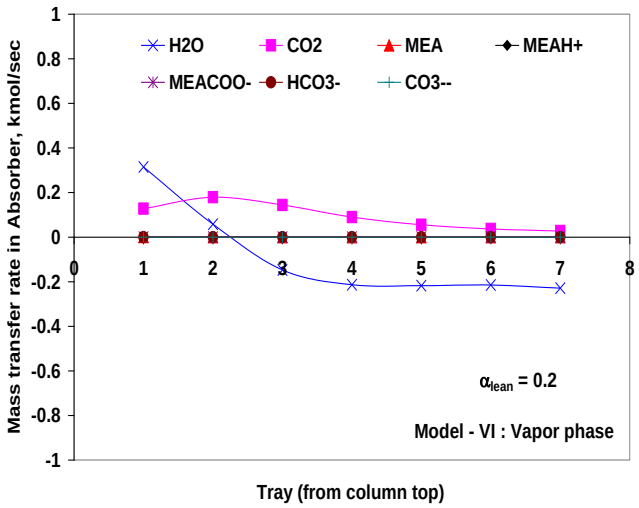
H2O
CO2
MEA
MEAH+
MEACOO-
HCO3-
CO3--
Mass transfer rate in Absorber, kmol/sec
Tray (from column top)
α_{lean} = 0.2
Model - VI : Vapor phase

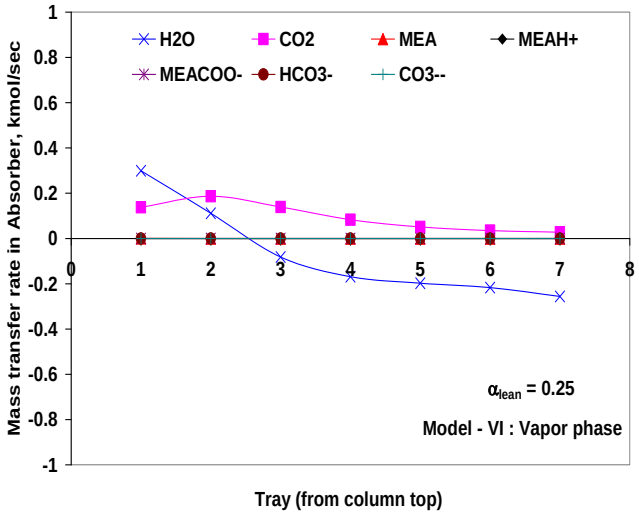
H2O
CO2
MEA
MEAH+
MEACOO-
HCO3-
CO3--
Mass transfer rate in Absorber, kmol/sec
Tray (from column top)
α_{lean} = 0.25
Model - VI : Vapor phase

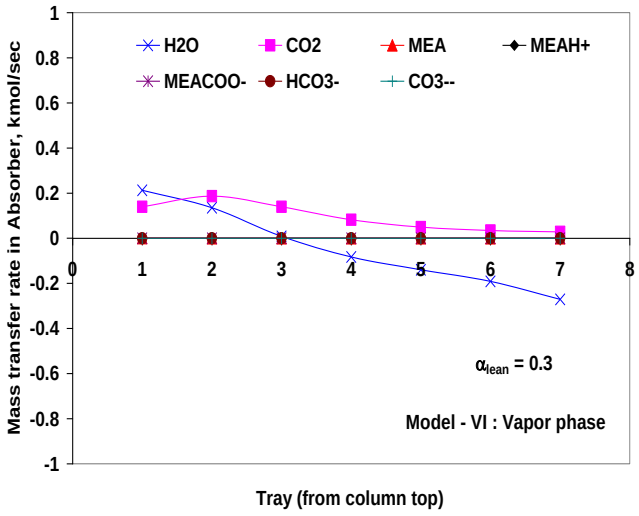
H2O
CO2
MEA
MEAH+
MEACOO-
HCO3-
CO3--
Mass transfer rate in Absorber, kmol/sec
Tray (from column top)
α_{lean} = 0.3
Model - VI : Vapor phase

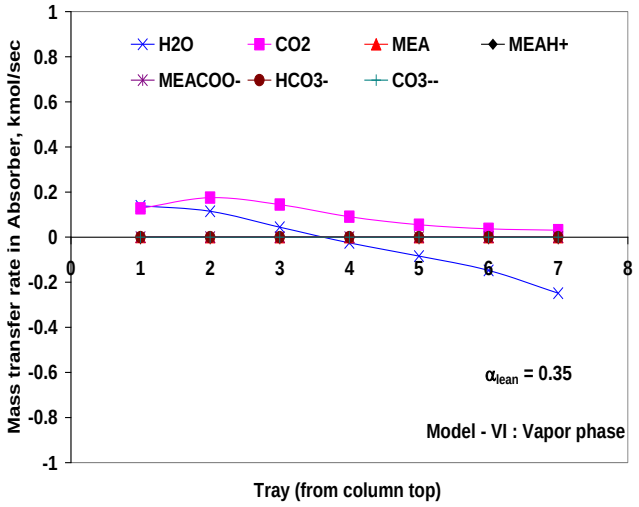
H2O
CO2
MEA
MEAH+
MEACOO-
HCO3-
CO3--
Mass transfer rate in Absorber, kmol/sec
Tray (from column top)
α_{lean} = 0.35
Model - VI : Vapor phase

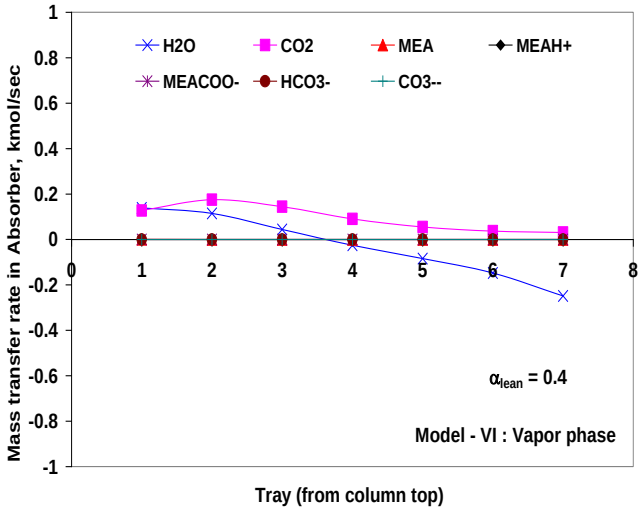
H2O
CO2
MEA
MEAH+
MEACOO-
HCO3-
CO3--
Mass transfer rate in Absorber, kmol/sec
Tray (from column top)
α_{lean} = 0.4
Model - VI : Vapor phase

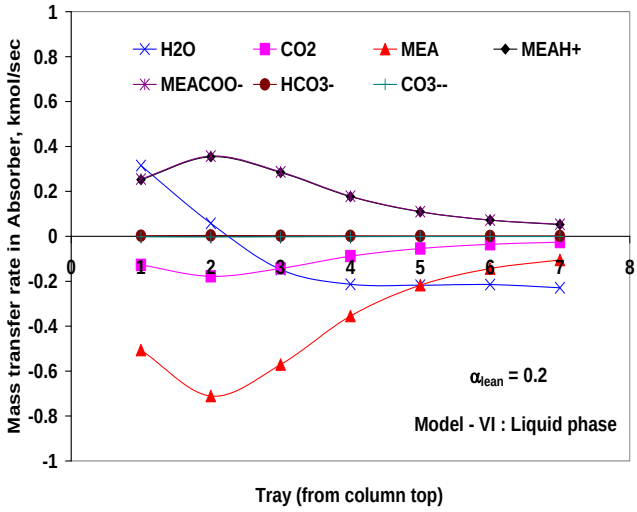
H2O
CO2
MEA
MEAH+
MEACOO-
HCO3-
CO3--
Mass transfer rate in Absorber, kmol/sec
Tray (from column top)
α_{lean} = 0.2
Model - VI : Liquid phase

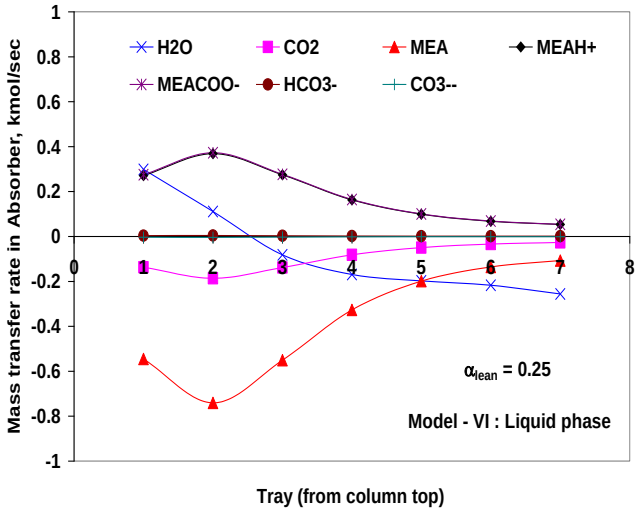
H2O
CO2
MEA
MEAH+
MEACOO-
HCO3-
CO3--
Mass transfer rate in Absorber, kmol/sec
Tray (from column top)
α_{lean} = 0.25
Model - VI : Liquid phase

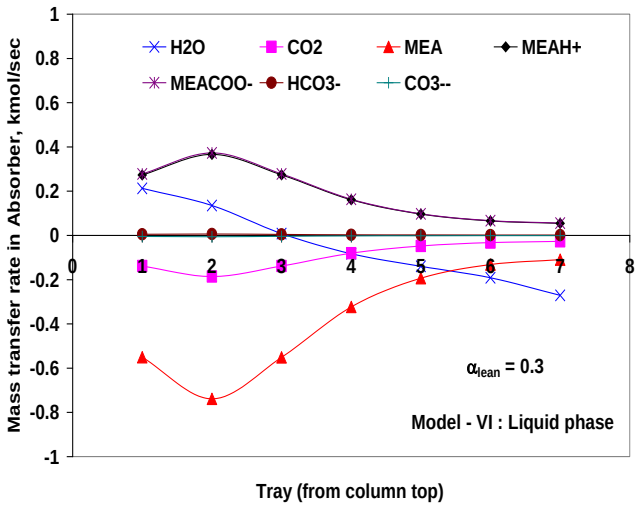
H2O
CO2
MEA
MEAH+
MEACOO-
HCO3-
CO3--
Mass transfer rate in Absorber, kmol/sec
Tray (from column top)
α_{lean} = 0.3
Model - VI : Liquid phase

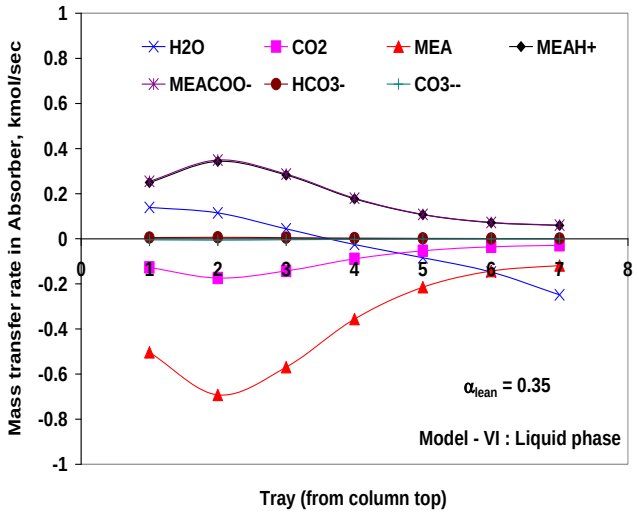
H2O
CO2
MEA
MEAH+
MEACOO-
HCO3-
CO3--
Mass transfer rate in Absorber, kmol/sec
Tray (from column top)
α_{lean} = 0.35
Model - VI : Liquid phase

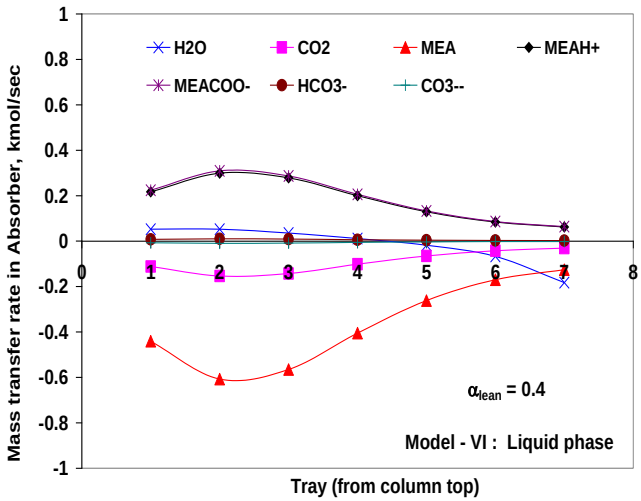
H2O
CO2
MEA
MEAH+
MEACOO-
HCO3-
CO3--
Mass transfer rate in Absorber, kmol/sec
Tray (from column top)
α_{lean} = 0.4
Model - VI : Liquid phase

Appendix H: Reaction rate profile for different components in absorber for Model-II and Model-VI

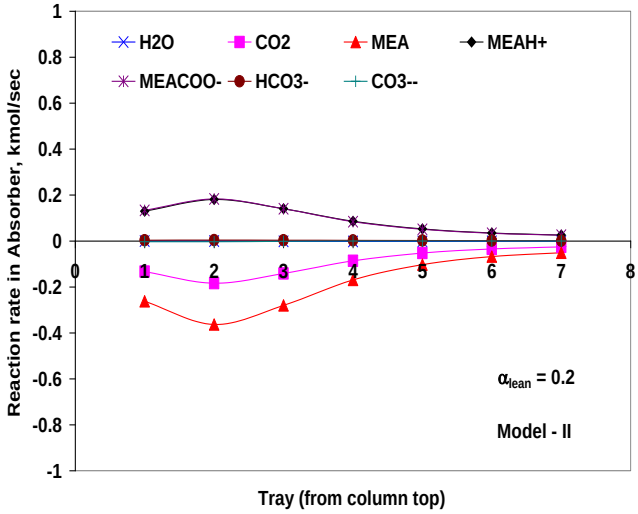

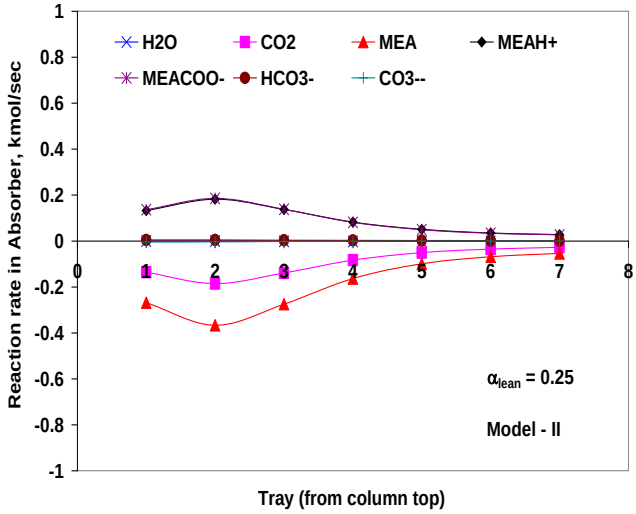

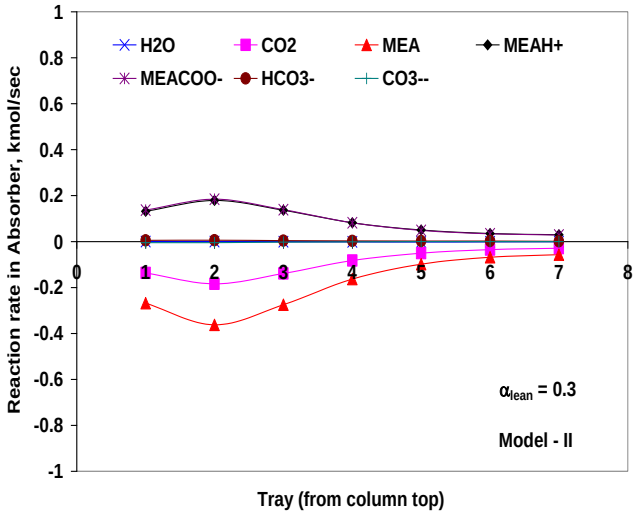

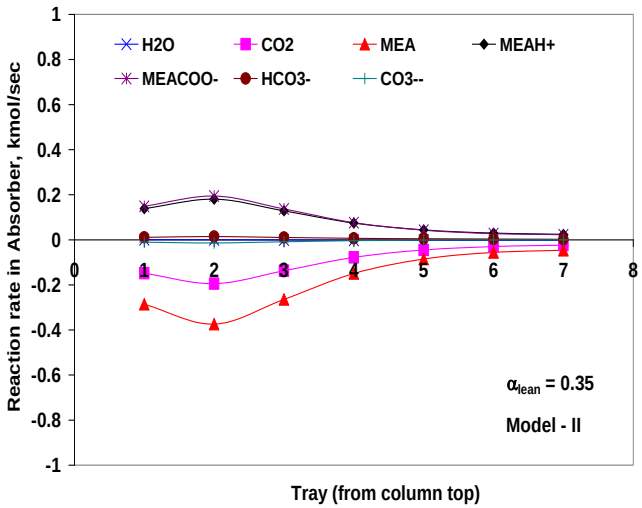
H2O
CO2
MEA
MEAH+
MEACOO-
HCO3-
CO3--
Reaction rate in Absorber, kmol/sec
Tray (from column top)
α_{lean} = 0.35
Model - II

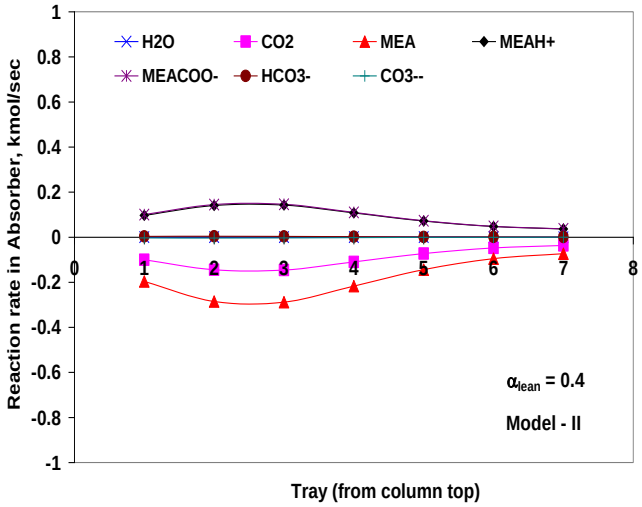
H2O
CO2
MEA
MEAH+
MEACOO-
HCO3-
CO3--
Reaction rate in Absorber, kmol/sec
Tray (from column top)
α_{lean} = 0.4
Model - II

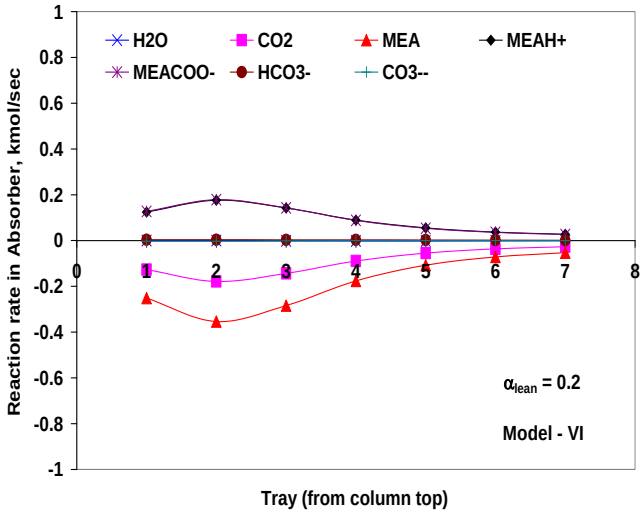
H2O
CO2
MEA
MEAH+
MEACOO-
HCO3-
CO3--
Reaction rate in Absorber, kmol/sec
Tray (from column top)
αlean = 0.2
Model - VI

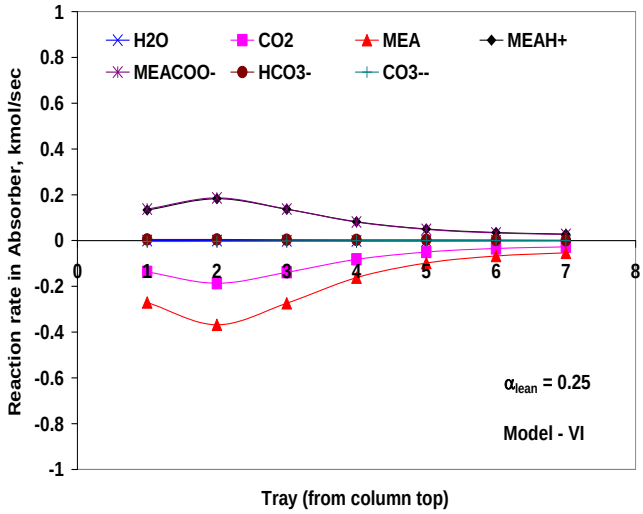
H2O
CO2
MEA
MEAH+
MEACOO-
HCO3-
CO3--
Reaction rate in Absorber, kmol/sec
Tray (from column top)
αlean = 0.25
Model - VI

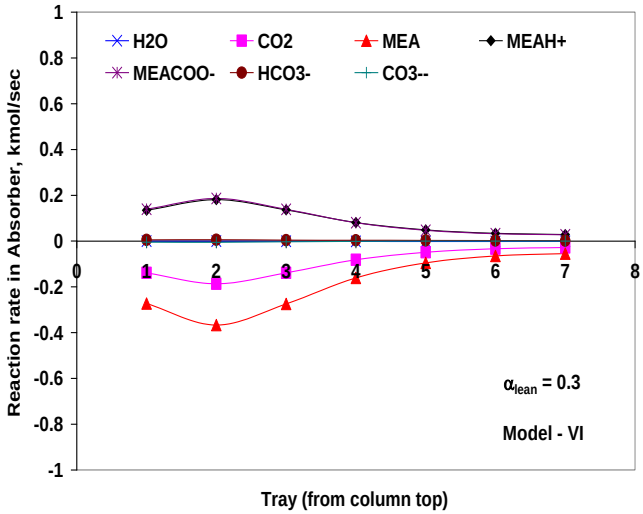
H2O
CO2
MEA
MEAH+
MEACOO-
HCO3-
CO3--
Reaction rate in Absorber, kmol/sec
Tray (from column top)
αlean = 0.3
Model - VI

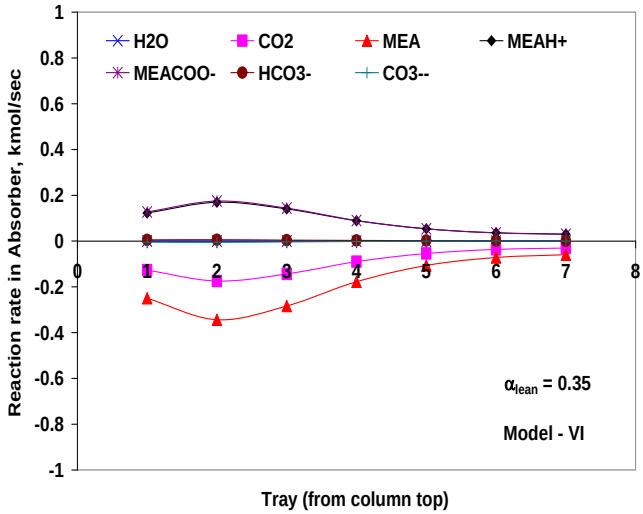
H2O
CO2
MEA
MEAH+
MEACOO-
HCO3-
CO3--
Reaction rate in Absorber, kmol/sec
Tray (from column top)
αlean = 0.35
Model - VI

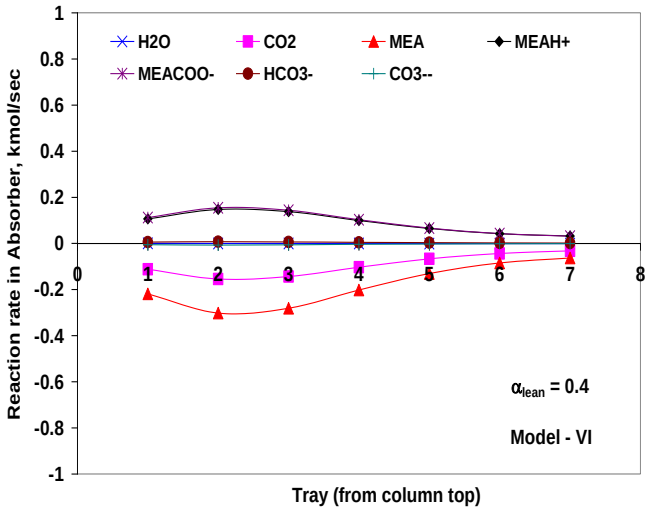
H2O
CO2
MEA
MEAH+
MEACOO-
HCO3-
CO3--
Reaction rate in Absorber, kmol/sec
Tray (from column top)
αlean = 0.4
Model - VI

Appendix I: AspenPlus® Input file for Flour MEA Process

```
;Input Summary created by Aspen Plus Rel. 21.0 at 18:46:30 Fri Jan 28, 2011
;Directory C:\sim-mu\thesis MEA Same simulation with different result  Runid THEIS-ASPEN TEXUS
KINETICS-RATE_BASED_MEA_MODEL-INSERT-FLOUR TWO TRAINS-RATESEP 2006.5- JULY 12, 2010-KINETIC-EQUILI-
STRIPPER-ALPA 0.3 WITH FILM RESISTANE ST 3 PASS  AND AB 9 STAG

DYNAMICS
    DYNAMICS RESULTS=ON

TITLE 'UT_Austin_Case47'

IN-UNITS SI

DEF-STREAMS CONVEN ALL

DIAGNOSTICS
    HISTORY STREAM-LEVEL=4
    TERMINAL STREAM-LEVEL=4

SIM-OPTIONS
    IN-UNITS ENG
    SIM-OPTIONS FLASH-TOL=0.0001 NPHASE=2 ATM-PRES=1. <atm>  &
        GAMUS-BASIS=AQUEOUS

RUN-CONTROL MAX-TIME=84600. MAX-FORT-ERR=1000

DESCRIPTION "
    H2O-MEA-H2S-CO2
    Property method: ELECNRTL with kinetic consideration
    Temperature: up to 120 C
    MEA Concentration up to 50wt.%
    "

DATABANKS PURE20  / AQUEOUS  / SOLIDS  / INORGANIC  /  &
        ASPENPCD  / PURE856

PROP-SOURCES PURE20  / AQUEOUS  / SOLIDS  / INORGANIC  /  &
        ASPENPCD  / PURE856

COMPONENTS
    H2O H2O /
    CO2 CO2 /
    MEA C2H7NO /
    N2 N2 /
    O2 O2 /
    MEAH+ C2H8NO+ /
    MEACOO- C3H6NO3- /
    HCO3- HCO3- /
    CO3-- CO3-2 /
    H3O+ H3O+ /
    OH- OH- /
    H2S H2S /
    HS- HS- /
    S-2 S-2 /
    AR AR /
    NO NO /
    CO CO /
    SO2 O2S /
    H2 H2

ADA-SETUP
    ADA-SETUP PROCEDURE=REL9

HENRY-COMPS KEMEA CO2 H2S N2 O2

HENRY-COMPS MEA CO2 N2 O2 H2S

CHEMISTRY KEMEA
    PARAM KBASIS=MOLEFRAC
    STOIC 1 MEA+ -1.0 / H2O -1.0 / MEA 1.0 / H3O+ 1.0
    STOIC 2 CO2 -1.0 / H2O -2.0 / H3O+ 1.0 / HCO3- 1.0
```

```
    STOIC 3 HCO3- -1.0 / H2O -1.0 / H3O+ 1.0 / CO3-2 1.0
    STOIC 4 MEACOO- -1.0 / H2O -1.0 / MEA 1.0 / HCO3- 1.0
    STOIC 5 H2O -2.0 / H3O+ 1.0 / OH- 1.0
    STOIC 6 H2O -1.0 / H2S -1.0 / HS- 1.0 / H3O+ 1.0
    STOIC 7 H2O -1.0 / HS- -1.0 / S-2 1.0 / H3O+ 1.0
    K-STOIC 1 A=-3.0383250 B=-7008.3570 C=0.0 D=-.00313489
    K-STOIC 2 A=231.4650 B=-12092.10 C=-36.78160 D=0.0
    K-STOIC 3 A=216.0490 B=-12431.70 C=-35.48190 D=0.0
    K-STOIC 4 A=-.521350 B=-2545.530 C=0.0 D=0.0
    K-STOIC 5 A=132.8990 B=-13445.90 C=-22.47730 D=0.0
    K-STOIC 6 A=214.5820 B=-12995.40 C=-33.54710 D=0.0
    K-STOIC 7 A=-9.7420 B=-8585.470 C=0.0 D=0.0

CHEMISTRY MEA
    STOIC 1 H2O -2. / H3O+ 1. / OH- 1.
    STOIC 2 CO2 -1. / H2O -2. / HCO3- 1. / H3O+ 1.
    STOIC 3 HCO3- -1. / H2O -1. / CO3-- 1. / H3O+ 1.
    STOIC 4 MEAH+ -1. / H2O -1. / MEA 1. / H3O+ 1.
    STOIC 5 MEACOO- -1. / H2O -1. / MEA 1. / HCO3- 1.
    STOIC 6 H2O -1. / H2S -1. / HS- 1. / H3O+ 1.
    STOIC 7 H2O -1. / HS- -1. / S-2 1. / H3O+ 1.
    K-STOIC 1 A=132.89888 B=-13445.9 C=-22.4773
    K-STOIC 2 A=231.465439 B=-12092.1 C=-36.7816
    K-STOIC 3 A=216.05043 B=-12431.7 C=-35.4819
    K-STOIC 4 A=-3.038325 B=-7008.357 D=-0.0031348
    K-STOIC 5 A=-0.52135 B=-2545.53
    K-STOIC 6 A=214.582 B=-12995.4 C=-33.5471
    K-STOIC 7 A=-9.742 B=-8585.47

FLOWSHEET
    BLOCK BLOWER IN=FLUE-BLO OUT=FLUE-DCC
    BLOCK WAT-PUMP IN=H20-PUMP OUT=H20-DCC
    BLOCK DCC IN=H20-DCC FLUE-DCC OUT=FLUE-ABS H2O-OUT
    BLOCK RICHPMP1 IN=RICHPUM1 OUT=RICH-HX1
    BLOCK HEATX IN=LEAN-HX RICH-HX OUT=LEAN-MIX RICH-STR
    BLOCK MIX-LNMK IN=MAKE-UP LEAN-MIX OUT=LEAN-COO
    BLOCK COOLER IN=LEAN-COO OUT=LEAN-ABS
    BLOCK B1 IN=RICH-HX1 OUT=RICH-HX
    BLOCK B2 IN=LEAN-ABS OUT=LEANABS1
    BLOCK B3 IN=FLUE-ABS OUT=FLUEABS1
    BLOCK ABSORBR1 IN=LEANABS1 FLUEABS1 OUT=STACK1 RICHPUM1
    BLOCK STRIPPER IN=RICH-STR OUT=CO2-COMP LEAN-HX
    BLOCK MCOMP IN=1 OUT=CO2-SEQ WAT
    BLOCK B5 IN=CO2-COMP OUT=1

PROPERTIES ELECNRTL HENRY-COMPS=MEA CHEMISTRY=MEA TRUE-COMPS=YES

PROP-REPLACE ELECNRTL ELECNRTL
    MODEL VAQCLK 1 1
    MODEL MUL2JONS 1 1 1 2
    MODEL DL1NST 1 1
    MODEL SIG2ONSG 1 -9 1
    MODEL DL0NST 1 1

ESTIMATE ALL
    IN-UNITS SI FLOW='kg/hr' MASS-FLOW='kg/hr'  &
        MOLE-FLOW='kmol/hr' VOLUME-FLOW='cum/hr' PRESSURE=psi  &
        TEMPERATURE=F DELTA-T=F FLUX='l/sqm-hr'  &
        MASS-FLUX='kg/sqm-hr' PDROP='N/sqm'

PROP-DATA DATA4
    IN-UNITS SI
    PROP-LIST RKTZRA / DHFORM
    PVAL MEA .19852040 / -2.101930E+08
    PROP-LIST CHARGE / IONTYP / MW / DHAQFM
    PVAL MEACOO- -1.0 / 3.0 / 104.08240 / -6.8750E+08
    PVAL MEA+ 1.0 / 1.0 / 62.0880 / -3.3750E+08

PROP-DATA DHAQFM
    IN-UNITS SI FLOW='kg/hr' MASS-FLOW='kg/hr'  &
        MOLE-FLOW='kmol/hr' VOLUME-FLOW='cum/hr' PRESSURE=psi  &
        TEMPERATURE=F DELTA-T=F FLUX='l/sqm-hr'  &
        MASS-FLUX='kg/sqm-hr' PDROP='N/sqm'
    PROP-LIST DHAQFM
    PVAL MEAH+ -3.5E+8
    PVAL MEACOO- -6.83E+8
```

```
PROP-DATA CPAQ0-1
    IN-UNITS SI MOLE-HEAT-CA='kJ/kmol-K'
    PROP-LIST CPAQ0
    PVAL MEAH+ 171.1
    PVAL HCO3- 115
    PVAL CO3-- 115

PROP-DATA CPAQ0-1
    IN-UNITS SI
    PROP-LIST CPAQ0
    PVAL MEACOO- 0.0 298.50 0.0 0.0 0.0 0.0
    PVAL MEA+ 0.0 295.120 0.0 0.0 0.0 0.0

PROP-DATA CPDIEC-1
    IN-UNITS SI
    PROP-LIST CPDIEC
    PVAL MEA 35.760 14836.0 273.150

PROP-DATA CPIG-1
    IN-UNITS SI
    PROP-LIST CPIG
    PVAL MEACOO- 20800.0 0.0 0.0 0.0 0.0 0.0 0.0 2000.0
    PVAL MEA+ 20800.0 0.0 0.0 0.0 0.0 0.0 0.0 2000.0

PROP-DATA IONMUB-1
    IN-UNITS SI
    PROP-LIST IONMUB
    PVAL CO3-- 0.5641176540
    PVAL HCO3- .0946944018
    PVAL MEAH+ .1319464670
    PVAL MEACOO- .3558342510

PROP-DATA PLXANT-1
    IN-UNITS SI
    PROP-LIST PLXANT
    PVAL MEA 172.780 -13492.0 0.0 0.0 -21.9140 .0000137790  &
        2.0 283.0 638.0
    PVAL H2O 72.550 -7206.70 0.0 0.0 -7.13850 .0000040460  &
        2.0 273.0 650.0
    PVAL MEACOO- -1.0E+20 0.0 0.0 0.0 0.0 0.0 0.0 0.0  &
        2000.0
    PVAL MEA+ -1.0E+20 0.0 0.0 0.0 0.0 0.0 0.0 0.0 2000.0

PROP-DATA VLBROC-1
    IN-UNITS SI
    PROP-LIST VLBROC
    PVAL H2O .04640
    PVAL CO2 .09390
    PVAL H2S .09390

PROP-DATA VLQKIJ-1
    IN-UNITS ENG
    PROP-LIST VLQKIJ
    BPVAL MEA H2O -0.0711319026
    BPVAL H2O MEA -0.0711319026

PROP-DATA HENRY-1
    IN-UNITS SI
    PROP-LIST HENRY
    BPVAL CO2 H2O 170.71260 -8477.7110 -21.957430 .0057807480  &
        273.0 500.0 0.0
    BPVAL N2 H2O 176.5070000 -8432.770000 -21.55800000  &
        -8.4362400E-3 273.0000000 346.0000000 0.0
    BPVAL O2 H2O 155.9210000 -7775.060000 -18.39740000  &
        -9.4435400E-3 274.0000000 348.0000000 0.0
    BPVAL H2S H2O 358.1380 -13236.80 -55.05510 .0595650 273.0  &
        423.0 0.0

PROP-DATA MUKIJ-1
    IN-UNITS ENG TEMPERATURE=K
    PROP-LIST MUKIJ
    BPVAL H2O MEA .816154241 0.0 0.0 0.0 0.0 298.1500
    BPVAL MEA H2O .816154241 0.0 0.0 0.0 0.0 298.1500

PROP-DATA MULIJ-1
```

```
    IN-UNITS ENG TEMPERATURE=K
    PROP-LIST MULIJ
    BPVAL H2O MEA -1.717793050 0.0 0.0 0.0 0.0 298.1500
    BPVAL MEA H2O 1.717793050 0.0 0.0 0.0 0.0 298.1500

PROP-DATA NRTL-1
    IN-UNITS SI
    PROP-LIST NRTL
    BPVAL H2O CO2 10.06400000 -3268.135000 .2000000000 0.0 0.0  &
        0.0 273.1500000 473.1500000
    BPVAL CO2 H2O 10.06400000 -3268.135000 .2000000000 0.0 0.0  &
        0.0 273.1500000 473.1500000
    BPVAL H2O MEA 1.438498000 99.02104000 .2000000000 0.0 0.0  &
        0.0 298.1500000 423.1500000
    BPVAL MEA H2O -1.046602000 -337.5456000 .2000000000 0.0  &
        0.0 0.0 298.1500000 423.1500000
    BPVAL H2O H2S -3.674000000 1155.900000 .2000000000 0.0 0.0  &
        0.0 273.1500000 423.1500000
    BPVAL H2S H2O -3.674000000 1155.900000 .2000000000 0.0 0.0  &
        0.0 273.1500000 423.1500000

PROP-DATA VLCLK-1
    IN-UNITS SI
    PROP-LIST VLCLK
    BPVAL MEAH+ OH- 0 0.0
    BPVAL H3O+ OH- 0 0.0
    BPVAL H3O+ HCO3- 0 0.0
    BPVAL H3O+ CO3-- 0 0.0
    BPVAL H3O+ MEACOO- 0 0.0

PROP-DATA VLCLK-1
    IN-UNITS SI MOLE-VOLUME='cc/mol'
    PROP-LIST VLCLK
    BPVAL MEAH+ HCO3- 6.13365949 0.0
    BPVAL MEAH+ CO3-- 239.0830670 0.0
    BPVAL MEAH+ MEACOO- 154.48458 0.0

PROP-DATA GMELCC-1
    IN-UNITS SI
    PROP-LIST GMELCC
    PPVAL H2O ( MEAH+ MEACOO- ) 9.887700000
    PPVAL ( MEAH+ MEACOO- ) H2O -4.951100000
    PPVAL H2O ( MEAH+ HCO3- ) 5.354100000
    PPVAL ( MEAH+ HCO3- ) H2O -4.070500000
    PPVAL H2O ( MEAH+ CO3-- ) 8
    PPVAL ( MEAH+ CO3-- ) H2O -4
    PPVAL H2O ( MEAH+ OH- ) 8
    PPVAL ( MEAH+ OH- ) H2O -4
    PPVAL H2O ( H3O+ MEACOO- ) 8.0
    PPVAL ( H3O+ MEACOO- ) H2O -4.0
    PPVAL H2O ( H3O+ HCO3- ) 8.0
    PPVAL ( H3O+ HCO3- ) H2O -4.0
    PPVAL H2O ( H3O+ CO3-- ) 8.0
    PPVAL ( H3O+ CO3-- ) H2O -4.0
    PPVAL H2O ( H3O+ OH- ) 8.0
    PPVAL ( H3O+ OH- ) H2O -4.0
    PPVAL CO2 ( MEAH+ MEACOO- ) 15.00000000
    PPVAL ( MEAH+ MEACOO- ) CO2 -8.000000000
    PPVAL CO2 ( MEAH+ HCO3- ) 15.00000000
    PPVAL ( MEAH+ HCO3- ) CO2 -8.000000000
    PPVAL CO2 ( H3O+ MEACOO- ) 15.0
    PPVAL ( H3O+ MEACOO- ) CO2 -8.0
    PPVAL CO2 ( H3O+ HCO3- ) 15.0
    PPVAL ( H3O+ HCO3- ) CO2 -8.0
    PPVAL MEA ( MEAH+ MEACOO- ) 15.00000000
    PPVAL ( MEAH+ MEACOO- ) MEA -8.000000000
    PPVAL MEA ( MEAH+ HCO3- ) 15.00000000
    PPVAL ( MEAH+ HCO3- ) MEA -8.000000000
    PPVAL MEA ( MEAH+ CO3-- ) 15.00000000
    PPVAL ( MEAH+ CO3-- ) MEA -8.000000000
    PPVAL MEA ( MEAH+ OH- ) 15.00000000
    PPVAL ( MEAH+ OH- ) MEA -8.000000000
    PPVAL MEA ( H3O+ MEACOO- ) 15.0
    PPVAL ( H3O+ MEACOO- ) MEA -8.0
    PPVAL MEA ( H3O+ HCO3- ) 15.0
    PPVAL ( H3O+ HCO3- ) MEA -8.0
```

```
PPVAL MEA ( H3O+ CO3-- ) 15.00000000
PPVAL ( H3O+ CO3-- ) MEA -8.000000000
PPVAL MEA ( H3O+ OH- ) 15.0
PPVAL ( H3O+ OH- ) MEA -8.0
PPVAL H2S ( MEAH+ MEACOO- ) 15.00000000
PPVAL ( MEAH+ MEACOO- ) H2S -8.000000000
PPVAL H2S ( MEAH+ HCO3- ) 15.00000000
PPVAL ( MEAH+ HCO3- ) H2S -8.000000000
PPVAL H2S ( MEAH+ OH- ) 15.00000000
PPVAL ( MEAH+ OH- ) H2S -8.000000000
PPVAL H2S ( H3O+ HCO3- ) 15.0
PPVAL ( H3O+ HCO3- ) H2S -8.0
PPVAL H2S ( H3O+ CO3-- ) 15.00000000
PPVAL ( H3O+ CO3-- ) H2S -8.000000000
PPVAL H2S ( H3O+ OH- ) 15.0
PPVAL ( H3O+ OH- ) H2S -8.0
PPVAL H2O ( MEAH+ HS- ) 4.8865
PPVAL ( MEAH+ HS- ) H2O -2.7592
PPVAL H2O ( H3O+ HS- ) 8.0
PPVAL ( H3O+ HS- ) H2O -4.0
PPVAL CO2 ( MEAH+ HS- ) 15.00000000
PPVAL ( MEAH+ HS- ) CO2 -8.000000000
PPVAL MEA ( MEAH+ HS- ) 15.00000000
PPVAL ( MEAH+ HS- ) MEA -8.000000000
PPVAL MEA ( H3O+ HS- ) 15.0
PPVAL ( H3O+ HS- ) MEA -8.0
PPVAL H2S ( MEAH+ HS- ) 15.00000000
PPVAL ( MEAH+ HS- ) H2S -8.000000000
PPVAL H2S ( H3O+ HS- ) 15.0
PPVAL ( H3O+ HS- ) H2S -8.0
PPVAL H2O ( MEAH+ S-2 ) 8
PPVAL ( MEAH+ S-2 ) H2O -4
PPVAL H2O ( H3O+ S-2 ) 8.0
PPVAL ( H3O+ S-2 ) H2O -4.0
PPVAL MEA ( MEAH+ S-2 ) 15.00000000
PPVAL ( MEAH+ S-2 ) MEA -8.000000000
PPVAL MEA ( H3O+ S-2 ) 15.0
PPVAL ( H3O+ S-2 ) MEA -8.0
PPVAL H2S ( MEAH+ S-2 ) 15.00000000
PPVAL ( MEAH+ S-2 ) H2S -8.000000000
PPVAL H2S ( H3O+ S-2 ) 15.0
PPVAL ( H3O+ S-2 ) H2S -8.0
PPVAL H2O ( MEA+ HCO3- ) 5.35410
PPVAL ( MEA+ HCO3- ) H2O -4.07050
PPVAL H2O ( MEA+ MEACOO- ) 9.88770
PPVAL ( MEA+ MEACOO- ) H2O -4.95110
PPVAL H2O ( MEA+ CO3-2 ) 8.0
PPVAL ( MEA+ CO3-2 ) H2O -4.0
PPVAL H2O ( MEA+ OH- ) 8.0
PPVAL ( MEA+ OH- ) H2O -4.0
PPVAL H2O ( H3O+ CO3-2 ) 8.0
PPVAL ( H3O+ CO3-2 ) H2O -4.0
PPVAL MEA ( MEA+ MEACOO- ) 15.0
PPVAL ( MEA+ MEACOO- ) MEA -8.0
PPVAL MEA ( MEA+ HCO3- ) 15.0
PPVAL ( MEA+ HCO3- ) MEA -8.0
PPVAL MEA ( MEA+ CO3-2 ) 15.0
PPVAL ( MEA+ CO3-2 ) MEA -8.0
PPVAL MEA ( MEA+ OH- ) 15.0
PPVAL ( MEA+ OH- ) MEA -8.0
PPVAL MEA ( H3O+ CO3-2 ) 15.0
PPVAL ( H3O+ CO3-2 ) MEA -8.0
PPVAL CO2 ( MEA+ HCO3- ) 15.0
PPVAL ( MEA+ HCO3- ) CO2 -8.0
PPVAL CO2 ( MEA+ CO3-2 ) 15.0
PPVAL ( MEA+ CO3-2 ) CO2 -8.0
PPVAL CO2 ( MEA+ MEACOO- ) 15.0
PPVAL ( MEA+ MEACOO- ) CO2 -8.0
PPVAL H2O ( MEA+ HS- ) 4.8492720
PPVAL ( MEA+ HS- ) H2O -2.7402230
PPVAL H2O ( MEA+ S-2 ) 8.0
PPVAL ( MEA+ S-2 ) H2O -4.0
PPVAL MEA ( MEA+ HS- ) 15.0
PPVAL ( MEA+ HS- ) MEA -8.0
PPVAL MEA ( MEA+ S-2 ) 15.0
PPVAL ( MEA+ S-2 ) MEA -8.0
```

```
    PPVAL H2S ( MEA+ HS- ) 15.0
    PPVAL ( MEA+ HS- ) H2S -8.0
    PPVAL H2S ( MEA+ S-2 ) 15.0
    PPVAL ( MEA+ S-2 ) H2S -8.0
    PPVAL H2S ( MEA+ OH- ) 15.0
    PPVAL ( MEA+ OH- ) H2S -8.0
    PPVAL H2S ( MEA+ MEACOO- ) 15.0
    PPVAL ( MEA+ MEACOO- ) H2S -8.0
    PPVAL H2S ( MEA+ HCO3- ) 15.0
    PPVAL ( MEA+ HCO3- ) H2S -8.0
    PPVAL H2S ( H3O+ MEACOO- ) 15.0
    PPVAL ( H3O+ MEACOO- ) H2S -8.0
    PPVAL CO2 ( MEA+ HS- ) 15.0
    PPVAL ( MEA+ HS- ) CO2 -8.0
    PPVAL CO2 ( MEA+ S-2 ) 15.0
    PPVAL ( MEA+ S-2 ) CO2 -8.0
    PPVAL CO2 ( MEA+ OH- ) 15.0
    PPVAL ( MEA+ OH- ) CO2 -8.0
    PPVAL CO2 ( H3O+ HS- ) 15.0
    PPVAL ( H3O+ HS- ) CO2 -8.0
    PPVAL CO2 ( H3O+ S-2 ) 15.0
    PPVAL ( H3O+ S-2 ) CO2 -8.0
    PPVAL CO2 ( H3O+ OH- ) 15.0
    PPVAL ( H3O+ OH- ) CO2 -8.0
    PPVAL CO2 ( H3O+ CO3-2 ) 15.0
    PPVAL ( H3O+ CO3-2 ) CO2 -8.0

PROP-DATA GMELCD-1
    IN-UNITS SI
    PROP-LIST GMELCD
    PPVAL H2O ( MEAH+ MEACOO- ) 10.81300000
    PPVAL ( MEAH+ MEACOO- ) H2O 0.0
    PPVAL H2O ( MEAH+ HCO3- ) 965.2400000
    PPVAL ( MEAH+ HCO3- ) H2O -11.06700000
    PPVAL H2O ( MEAH+ CO3-- ) 0
    PPVAL ( MEAH+ CO3-- ) H2O 0
    PPVAL H2O ( MEAH+ OH- ) 0
    PPVAL ( MEAH+ OH- ) H2O 0
    PPVAL H2O ( H3O+ MEACOO- ) 0.0
    PPVAL ( H3O+ MEACOO- ) H2O 0.0
    PPVAL H2O ( H3O+ HCO3- ) 0.0
    PPVAL ( H3O+ HCO3- ) H2O 0.0
    PPVAL H2O ( H3O+ CO3-- ) 0
    PPVAL ( H3O+ CO3-- ) H2O 0
    PPVAL H2O ( H3O+ OH- ) 0.0
    PPVAL ( H3O+ OH- ) H2O 0.0
    PPVAL CO2 ( MEAH+ MEACOO- ) 0.0
    PPVAL ( MEAH+ MEACOO- ) CO2 0.0
    PPVAL CO2 ( MEAH+ HCO3- ) 0.0
    PPVAL ( MEAH+ HCO3- ) CO2 0.0
    PPVAL CO2 ( H3O+ MEACOO- ) 0.0
    PPVAL ( H3O+ MEACOO- ) CO2 0.0
    PPVAL CO2 ( H3O+ HCO3- ) 0.0
    PPVAL ( H3O+ HCO3- ) CO2 0.0
    PPVAL MEA ( MEAH+ MEACOO- ) 0.0
    PPVAL ( MEAH+ MEACOO- ) MEA 0.0
    PPVAL MEA ( MEAH+ HCO3- ) 0.0
    PPVAL ( MEAH+ HCO3- ) MEA 0.0
    PPVAL MEA ( MEAH+ CO3-- ) 0.0
    PPVAL ( MEAH+ CO3-- ) MEA 0.0
    PPVAL MEA ( MEAH+ OH- ) 0.0
    PPVAL ( MEAH+ OH- ) MEA 0.0
    PPVAL MEA ( H3O+ MEACOO- ) 0.0
    PPVAL ( H3O+ MEACOO- ) MEA 0.0
    PPVAL MEA ( H3O+ HCO3- ) 0.0
    PPVAL ( H3O+ HCO3- ) MEA 0.0
    PPVAL MEA ( H3O+ CO3-- ) 0.0
    PPVAL ( H3O+ CO3-- ) MEA 0.0
    PPVAL MEA ( H3O+ OH- ) 0.0
    PPVAL ( H3O+ OH- ) MEA 0.0
    PPVAL H2S ( MEAH+ MEACOO- ) 0.0
    PPVAL ( MEAH+ MEACOO- ) H2S 0.0
    PPVAL H2S ( MEAH+ HCO3- ) 0.0
    PPVAL ( MEAH+ HCO3- ) H2S 0.0
    PPVAL H2S ( MEAH+ OH- ) 0.0
    PPVAL ( MEAH+ OH- ) H2S 0.0
```

```
PPVAL H2S ( H3O+ HCO3- ) 0.0
PPVAL ( H3O+ HCO3- ) H2S 0.0
PPVAL H2S ( H3O+ MEACOO- ) 0.0
PPVAL ( H3O+ MEACOO- ) H2S 0.0
PPVAL H2S ( H3O+ OH- ) 0.0
PPVAL ( H3O+ OH- ) H2S 0.0
PPVAL H2O ( MEAH+ HS- ) 1148.108
PPVAL ( MEAH+ HS- ) H2O -462.521
PPVAL H2O ( H3O+ HS- ) 0.0
PPVAL ( H3O+ HS- ) H2O 0.0
PPVAL CO2 ( MEAH+ HS- ) 0.0
PPVAL ( MEAH+ HS- ) CO2 0.0
PPVAL MEA ( MEAH+ HS- ) 0.0
PPVAL ( MEAH+ HS- ) MEA 0.0
PPVAL MEA ( H3O+ HS- ) 0.0
PPVAL ( H3O+ HS- ) MEA 0.0
PPVAL H2S ( MEAH+ HS- ) 0.0
PPVAL ( MEAH+ HS- ) H2S 0.0
PPVAL H2S ( H3O+ HS- ) 0.0
PPVAL ( H3O+ HS- ) H2S 0.0
PPVAL H2O ( MEAH+ S-2 ) 0
PPVAL ( MEAH+ S-2 ) H2O 0
PPVAL H2O ( H3O+ S-2 ) 0.0
PPVAL ( H3O+ S-2 ) H2O 0.0
PPVAL MEA ( MEAH+ S-2 ) 0.0
PPVAL ( MEAH+ S-2 ) MEA 0.0
PPVAL MEA ( H3O+ S-2 ) 0.0
PPVAL ( H3O+ S-2 ) MEA 0.0
PPVAL H2S ( MEAH+ S-2 ) 0.0
PPVAL ( MEAH+ S-2 ) H2S 0.0
PPVAL H2S ( H3O+ S-2 ) 0.0
PPVAL ( H3O+ S-2 ) H2S 0.0
PPVAL H2O ( MEA+ HCO3- ) 965.240
PPVAL ( MEA+ HCO3- ) H2O -11.0670
PPVAL H2O ( MEA+ MEACOO- ) 10.8130
PPVAL ( MEA+ MEACOO- ) H2O 0.0
PPVAL H2O ( MEA+ CO3-2 ) 0.0
PPVAL ( MEA+ CO3-2 ) H2O 0.0
PPVAL H2O ( MEA+ OH- ) 0.0
PPVAL ( MEA+ OH- ) H2O 0.0
PPVAL H2O ( H3O+ CO3-2 ) 0.0
PPVAL ( H3O+ CO3-2 ) H2O 0.0
PPVAL MEA ( MEA+ MEACOO- ) 0.0
PPVAL ( MEA+ MEACOO- ) MEA 0.0
PPVAL MEA ( MEA+ HCO3- ) 0.0
PPVAL ( MEA+ HCO3- ) MEA 0.0
PPVAL MEA ( MEA+ CO3-2 ) 0.0
PPVAL ( MEA+ CO3-2 ) MEA 0.0
PPVAL MEA ( MEA+ OH- ) 0.0
PPVAL ( MEA+ OH- ) MEA 0.0
PPVAL MEA ( H3O+ CO3-2 ) 0.0
PPVAL ( H3O+ CO3-2 ) MEA 0.0
PPVAL CO2 ( MEA+ HCO3- ) 0.0
PPVAL ( MEA+ HCO3- ) CO2 0.0
PPVAL CO2 ( MEA+ CO3-2 ) 0.0
PPVAL ( MEA+ CO3-2 ) CO2 0.0
PPVAL CO2 ( MEA+ MEACOO- ) 0.0
PPVAL ( MEA+ MEACOO- ) CO2 0.0
PPVAL H2O ( MEA+ HS- ) 1215.540
PPVAL ( MEA+ HS- ) H2O -483.70070
PPVAL H2O ( MEA+ S-2 ) 0.0
PPVAL ( MEA+ S-2 ) H2O 0.0
PPVAL MEA ( MEA+ HS- ) 0.0
PPVAL ( MEA+ HS- ) MEA 0.0
PPVAL MEA ( MEA+ S-2 ) 0.0
PPVAL ( MEA+ S-2 ) MEA 0.0
PPVAL H2S ( MEA+ HS- ) 0.0
PPVAL ( MEA+ HS- ) H2S 0.0
PPVAL H2S ( MEA+ S-2 ) 0.0
PPVAL ( MEA+ S-2 ) H2S 0.0
PPVAL H2S ( MEA+ OH- ) 0.0
PPVAL ( MEA+ OH- ) H2S 0.0
PPVAL H2S ( MEA+ MEACOO- ) 0.0
PPVAL ( MEA+ MEACOO- ) H2S 0.0
PPVAL H2S ( MEA+ HCO3- ) 0.0
PPVAL ( MEA+ HCO3- ) H2S 0.0
```

```
    PPVAL CO2 ( MEA+ HS- ) 0.0
    PPVAL ( MEA+ HS- ) CO2 0.0
    PPVAL CO2 ( MEA+ S-2 ) 0.0
    PPVAL ( MEA+ S-2 ) CO2 0.0
    PPVAL CO2 ( MEA+ OH- ) 0.0
    PPVAL ( MEA+ OH- ) CO2 0.0
    PPVAL CO2 ( H3O+ HS- ) 0.0
    PPVAL ( H3O+ HS- ) CO2 0.0
    PPVAL CO2 ( H3O+ S-2 ) 0.0
    PPVAL ( H3O+ S-2 ) CO2 0.0
    PPVAL CO2 ( H3O+ OH- ) 0.0

    PPVAL ( H3O+ OH- ) CO2 0.0
    PPVAL CO2 ( H3O+ CO3-2 ) 0.0
    PPVAL ( H3O+ CO3-2 ) CO2 0.0

PROP-DATA GMELCE-1
    IN-UNITS SI
    PROP-LIST GMELCE
    PPVAL CO2 ( MEAH+ MEACOO- ) 0.0
    PPVAL ( MEAH+ MEACOO- ) CO2 0.0
    PPVAL CO2 ( MEAH+ HCO3- ) 0.0
    PPVAL ( MEAH+ HCO3- ) CO2 0.0
    PPVAL CO2 ( MEAH+ CO3-- ) 0.0
    PPVAL ( MEAH+ CO3-- ) CO2 0.0
    PPVAL CO2 ( MEAH+ OH- ) 0.0
    PPVAL ( MEAH+ OH- ) CO2 0.0
    PPVAL CO2 ( H3O+ MEACOO- ) 0.0
    PPVAL ( H3O+ MEACOO- ) CO2 0.0
    PPVAL CO2 ( H3O+ HCO3- ) 0.0
    PPVAL ( H3O+ HCO3- ) CO2 0.0
    PPVAL CO2 ( H3O+ CO3-- ) 0.0
    PPVAL ( H3O+ CO3-- ) CO2 0.0
    PPVAL CO2 ( H3O+ OH- ) 0.0
    PPVAL ( H3O+ OH- ) CO2 0.0
    PPVAL MEA ( MEAH+ MEACOO- ) 0.0
    PPVAL ( MEAH+ MEACOO- ) MEA 0.0
    PPVAL MEA ( MEAH+ HCO3- ) 0.0
    PPVAL ( MEAH+ HCO3- ) MEA 0.0
    PPVAL MEA ( MEAH+ CO3-- ) 0.0
    PPVAL ( MEAH+ CO3-- ) MEA 0.0
    PPVAL MEA ( MEAH+ OH- ) 0.0
    PPVAL ( MEAH+ OH- ) MEA 0.0
    PPVAL MEA ( H3O+ MEACOO- ) 0.0
    PPVAL ( H3O+ MEACOO- ) MEA 0.0
    PPVAL MEA ( H3O+ HCO3- ) 0.0
    PPVAL ( H3O+ HCO3- ) MEA 0.0
    PPVAL MEA ( H3O+ CO3-- ) 0.0
    PPVAL ( H3O+ CO3-- ) MEA 0.0
    PPVAL MEA ( H3O+ OH- ) 0.0
    PPVAL ( H3O+ OH- ) MEA 0.0
    PPVAL H2S ( MEAH+ MEACOO- ) 0.0
    PPVAL ( MEAH+ MEACOO- ) H2S 0.0
    PPVAL H2S ( MEAH+ HCO3- ) 0.0
    PPVAL ( MEAH+ HCO3- ) H2S 0.0
    PPVAL H2S ( MEAH+ CO3-- ) 0.0
    PPVAL ( MEAH+ CO3-- ) H2S 0.0
    PPVAL H2S ( MEAH+ OH- ) 0.0
    PPVAL ( MEAH+ OH- ) H2S 0.0
    PPVAL H2S ( H3O+ HCO3- ) 0.0
    PPVAL ( H3O+ HCO3- ) H2S 0.0
    PPVAL H2S ( H3O+ CO3-- ) 0.0
    PPVAL ( H3O+ CO3-- ) H2S 0.0
    PPVAL H2S ( H3O+ OH- ) 0.0
    PPVAL ( H3O+ OH- ) H2S 0.0
    PPVAL CO2 ( MEAH+ HS- ) 0.0
    PPVAL ( MEAH+ HS- ) CO2 0.0
    PPVAL CO2 ( H3O+ HS- ) 0.0
    PPVAL ( H3O+ HS- ) CO2 0.0
    PPVAL MEA ( MEAH+ HS- ) 0.0
    PPVAL ( MEAH+ HS- ) MEA 0.0
    PPVAL MEA ( H3O+ HS- ) 0.0
    PPVAL ( H3O+ HS- ) MEA 0.0
    PPVAL H2S ( MEAH+ HS- ) 0.0
    PPVAL ( MEAH+ HS- ) H2S 0.0
    PPVAL H2S ( H3O+ HS- ) 0.0
```

```
    PPVAL ( H3O+ HS- ) H2S 0.0
    PPVAL CO2 ( MEAH+ S-2 ) 0.0
    PPVAL ( MEAH+ S-2 ) CO2 0.0
    PPVAL CO2 ( H3O+ S-2 ) 0.0
    PPVAL ( H3O+ S-2 ) CO2 0.0
    PPVAL MEA ( MEAH+ S-2 ) 0.0
    PPVAL ( MEAH+ S-2 ) MEA 0.0
    PPVAL MEA ( H3O+ S-2 ) 0.0
    PPVAL ( H3O+ S-2 ) MEA 0.0
    PPVAL H2S ( MEAH+ S-2 ) 0.0
    PPVAL ( MEAH+ S-2 ) H2S 0.0
    PPVAL H2S ( H3O+ S-2 ) 0.0
    PPVAL ( H3O+ S-2 ) H2S 0.0
    PPVAL H2O ( MEA+ HS- ) 0.0
    PPVAL ( MEA+ HS- ) H2O 0.0
    PPVAL H2O ( MEA+ S-2 ) 0.0
    PPVAL ( MEA+ S-2 ) H2O 0.0
    PPVAL H2O ( H3O+ HS- ) 0.0
    PPVAL ( H3O+ HS- ) H2O 0.0
    PPVAL H2O ( H3O+ S-2 ) 0.0
    PPVAL ( H3O+ S-2 ) H2O 0.0
    PPVAL MEA ( MEA+ HS- ) 0.0
    PPVAL ( MEA+ HS- ) MEA 0.0
    PPVAL MEA ( MEA+ S-2 ) 0.0
    PPVAL ( MEA+ S-2 ) MEA 0.0
    PPVAL H2S ( MEA+ HS- ) 0.0
    PPVAL ( MEA+ HS- ) H2S 0.0
    PPVAL H2S ( MEA+ S-2 ) 0.0
    PPVAL ( MEA+ S-2 ) H2S 0.0
    PPVAL H2S ( MEA+ OH- ) 0.0
    PPVAL ( MEA+ OH- ) H2S 0.0
    PPVAL H2S ( MEA+ MEACOO- ) 0.0
    PPVAL ( MEA+ MEACOO- ) H2S 0.0
    PPVAL H2S ( MEA+ HCO3- ) 0.0
    PPVAL ( MEA+ HCO3- ) H2S 0.0
    PPVAL H2S ( H3O+ MEACOO- ) 0.0
    PPVAL ( H3O+ MEACOO- ) H2S 0.0
    PPVAL CO2 ( MEA+ HS- ) 0.0
    PPVAL ( MEA+ HS- ) CO2 0.0
    PPVAL CO2 ( MEA+ S-2 ) 0.0
    PPVAL ( MEA+ S-2 ) CO2 0.0
    PPVAL CO2 ( MEA+ OH- ) 0.0
    PPVAL ( MEA+ OH- ) CO2 0.0
    PPVAL CO2 ( H3O+ CO3-2 ) 0.0
    PPVAL ( H3O+ CO3-2 ) CO2 0.0

PROP-DATA GMELCN-1
    IN-UNITS SI
    PROP-LIST GMELCN
    PPVAL CO2 ( MEAH+ MEACOO- ) .1000000000
    PPVAL ( MEAH+ MEACOO- ) CO2 .1000000000
    PPVAL CO2 ( MEAH+ HCO3- ) .1000000000
    PPVAL ( MEAH+ HCO3- ) CO2 .1000000000
    PPVAL CO2 ( MEAH+ CO3-- ) .1000000000
    PPVAL ( MEAH+ CO3-- ) CO2 .1000000000
    PPVAL CO2 ( MEAH+ OH- ) .1000000000
    PPVAL ( MEAH+ OH- ) CO2 .1000000000
    PPVAL CO2 ( H3O+ MEACOO- ) .10
    PPVAL ( H3O+ MEACOO- ) CO2 .10
    PPVAL CO2 ( H3O+ HCO3- ) .10
    PPVAL ( H3O+ HCO3- ) CO2 .10
    PPVAL CO2 ( H3O+ CO3-- ) .1000000000
    PPVAL ( H3O+ CO3-- ) CO2 .1000000000
    PPVAL CO2 ( H3O+ OH- ) .10
    PPVAL ( H3O+ OH- ) CO2 .10
    PPVAL MEA ( MEAH+ MEACOO- ) .1000000000
    PPVAL ( MEAH+ MEACOO- ) MEA .1000000000
    PPVAL MEA ( MEAH+ HCO3- ) .1000000000
    PPVAL ( MEAH+ HCO3- ) MEA .1000000000
    PPVAL MEA ( MEAH+ CO3-- ) .1000000000
    PPVAL ( MEAH+ CO3-- ) MEA .1000000000
    PPVAL MEA ( MEAH+ OH- ) .1000000000
    PPVAL ( MEAH+ OH- ) MEA .1000000000
    PPVAL MEA ( H3O+ MEACOO- ) .10
    PPVAL ( H3O+ MEACOO- ) MEA .10
    PPVAL MEA ( H3O+ HCO3- ) .10
```

```
PPVAL ( H3O+ HCO3- ) MEA .10
PPVAL MEA ( H3O+ CO3-- ) .1000000000
PPVAL ( H3O+ CO3-- ) MEA .1000000000
PPVAL MEA ( H3O+ OH- ) .10
PPVAL ( H3O+ OH- ) MEA .10
PPVAL H2S ( MEAH+ MEACOO- ) .1000000000
PPVAL ( MEAH+ MEACOO- ) H2S .1000000000
PPVAL H2S ( MEAH+ HCO3- ) .1000000000
PPVAL ( MEAH+ HCO3- ) H2S .1000000000
PPVAL H2S ( MEAH+ CO3-- ) .1000000000
PPVAL ( MEAH+ CO3-- ) H2S .1000000000
PPVAL H2S ( MEAH+ OH- ) .1000000000
PPVAL ( MEAH+ OH- ) H2S .1000000000
PPVAL H2S ( H3O+ HCO3- ) .10
PPVAL ( H3O+ HCO3- ) H2S .10
PPVAL H2S ( H3O+ CO3-- ) .1000000000
PPVAL ( H3O+ CO3-- ) H2S .1000000000
PPVAL H2S ( H3O+ OH- ) .10
PPVAL ( H3O+ OH- ) H2S .10
PPVAL CO2 ( MEAH+ HS- ) .1000000000
PPVAL ( MEAH+ HS- ) CO2 .1000000000
PPVAL CO2 ( H3O+ HS- ) .10
PPVAL ( H3O+ HS- ) CO2 .10
PPVAL MEA ( MEAH+ HS- ) .1000000000
PPVAL ( MEAH+ HS- ) MEA .1000000000
PPVAL MEA ( H3O+ HS- ) .10
PPVAL ( H3O+ HS- ) MEA .10
PPVAL H2S ( MEAH+ HS- ) .1000000000
PPVAL ( MEAH+ HS- ) H2S .1000000000
PPVAL H2S ( H3O+ HS- ) .10
PPVAL ( H3O+ HS- ) H2S .10
PPVAL CO2 ( MEAH+ S-2 ) .1000000000
PPVAL ( MEAH+ S-2 ) CO2 .1000000000
PPVAL CO2 ( H3O+ S-2 ) .10
PPVAL ( H3O+ S-2 ) CO2 .10
PPVAL MEA ( MEAH+ S-2 ) .1000000000
PPVAL ( MEAH+ S-2 ) MEA .1000000000
PPVAL MEA ( H3O+ S-2 ) .10
PPVAL ( H3O+ S-2 ) MEA .10
PPVAL H2S ( MEAH+ S-2 ) .1000000000
PPVAL H2S ( H3O+ S-2 ) .10
PPVAL ( H3O+ S-2 ) H2S .10
PPVAL H2O ( MEAH+ HCO3- ) 0.2
PPVAL ( MEAH+ HCO3- ) H2O 0.2
PPVAL H2O ( MEAH+ MEACOO- ) 0.2
PPVAL ( MEAH+ MEACOO- ) H2O 0.2
PPVAL H2O ( MEAH+ CO3-- ) 0.2
PPVAL ( MEAH+ CO3-- ) H2O 0.2
PPVAL H2O ( MEAH+ OH- ) 0.2
PPVAL ( MEAH+ OH- ) H2O 0.2
PPVAL H2O ( H3O+ HCO3- ) .20
PPVAL ( H3O+ HCO3- ) H2O .20
PPVAL H2O ( H3O+ MEACOO- ) .20
PPVAL ( H3O+ MEACOO- ) H2O .20
PPVAL H2O ( H3O+ CO3-- ) 0.2
PPVAL ( H3O+ CO3-- ) H2O 0.2
PPVAL H2O ( H3O+ OH- ) .20
PPVAL ( H3O+ OH- ) H2O .20
PPVAL H2O ( MEAH+ HS- ) 0.2
PPVAL ( MEAH+ HS- ) H2O 0.2
PPVAL H2O ( H3O+ HS- ) .20
PPVAL ( H3O+ HS- ) H2O .20
PPVAL H2O ( MEAH+ S-2 ) 0.2
PPVAL ( MEAH+ S-2 ) H2O 0.2
PPVAL H2O ( H3O+ S-2 ) .20
PPVAL ( H3O+ S-2 ) H2O .20
PPVAL H2O ( MEA+ HCO3- ) .20
PPVAL ( MEA+ HCO3- ) H2O .20
PPVAL H2O ( MEA+ MEACOO- ) .20
PPVAL ( MEA+ MEACOO- ) H2O .20
PPVAL H2O ( MEA+ CO3-2 ) .20
PPVAL ( MEA+ CO3-2 ) H2O .20
PPVAL H2O ( MEA+ OH- ) .20
PPVAL ( MEA+ OH- ) H2O .20
PPVAL H2O ( H3O+ CO3-2 ) .20
PPVAL ( H3O+ CO3-2 ) H2O .20
```

```
    PPVAL MEA ( MEA+ MEACOO- ) .10
    PPVAL ( MEA+ MEACOO- ) MEA .10
    PPVAL MEA ( MEA+ HCO3- ) .10
    PPVAL ( MEA+ HCO3- ) MEA .10
    PPVAL MEA ( MEA+ CO3-2 ) .10
    PPVAL ( MEA+ CO3-2 ) MEA .10
    PPVAL MEA ( MEA+ OH- ) .10
    PPVAL ( MEA+ OH- ) MEA .10
    PPVAL MEA ( H3O+ CO3-2 ) .10
    PPVAL ( H3O+ CO3-2 ) MEA .10
    PPVAL CO2 ( MEA+ HCO3- ) .10
    PPVAL ( MEA+ HCO3- ) CO2 .10
    PPVAL CO2 ( MEA+ CO3-2 ) .10
    PPVAL ( MEA+ CO3-2 ) CO2 .10
    PPVAL CO2 ( MEA+ MEACOO- ) .10
    PPVAL ( MEA+ MEACOO- ) CO2 .10
    PPVAL H2O ( MEA+ HS- ) .20
    PPVAL ( MEA+ HS- ) H2O .20
    PPVAL H2O ( MEA+ S-2 ) .20
    PPVAL ( MEA+ S-2 ) H2O .20
    PPVAL MEA ( MEA+ HS- ) .10
    PPVAL ( MEA+ HS- ) MEA .10
    PPVAL MEA ( MEA+ S-2 ) .10
    PPVAL ( MEA+ S-2 ) MEA .10
    PPVAL H2S ( MEA+ HS- ) .10
    PPVAL ( MEA+ HS- ) H2S .10
    PPVAL H2S ( MEA+ S-2 ) .10
    PPVAL ( MEA+ S-2 ) H2S .10
    PPVAL H2S ( MEA+ OH- ) .10
    PPVAL ( MEA+ OH- ) H2S .10
    PPVAL H2S ( MEA+ MEACOO- ) .10
    PPVAL ( MEA+ MEACOO- ) H2S .10
    PPVAL H2S ( MEA+ HCO3- ) .10
    PPVAL ( MEA+ HCO3- ) H2S .10
    PPVAL H2S ( H3O+ MEACOO- ) .10
    PPVAL ( H3O+ MEACOO- ) H2S .10
    PPVAL CO2 ( MEA+ HS- ) .10
    PPVAL ( MEA+ HS- ) CO2 .10
    PPVAL CO2 ( MEA+ S-2 ) .10
    PPVAL ( MEA+ S-2 ) CO2 .10
    PPVAL CO2 ( MEA+ OH- ) .10
    PPVAL ( MEA+ OH- ) CO2 .10
    PPVAL CO2 ( H3O+ CO3-2 ) .10
    PPVAL ( H3O+ CO3-2 ) CO2 .10

STREAM FLUE-BLO
    SUBSTREAM MIXED TEMP=407. PRES=101000.  &
        MASS-FLOW=2424400. <kg/hr>
    MOLE-FRAC H2O 0.0818 / CO2 0.1358 / MEA 0. / N2  &
        0.7469 / O2 0.0354 / MEACOO- 0. / HCO3- 0. / H3O+  &
        0. / OH- 0. / H2S 0. / HS- 0. / S-2 0. / MEA+  &
        0. / CO3-2 0. / AR 0. / NO 0. / CO 0. / SO2  &
        0. / H2 0.

STREAM H20-PUMP
    SUBSTREAM MIXED TEMP=12. <C> PRES=101.3 <kPa> MOLE-FLOW=70.
    MOLE-FLOW H2O 70.

STREAM LEAN-ABS
    SUBSTREAM MIXED TEMP=313. PRES=101300. MOLE-FLOW=62.
    MASS-FRAC H2O 0.635 / CO2 0.065 / MEA 0.3

STREAM LEAN-HX
    SUBSTREAM MIXED PRES=128000. VFRAC=0. MOLE-FLOW=62.
    MASS-FRAC H2O 0.635 / CO2 0.065 / MEA 0.3

STREAM MAKE-UP
    SUBSTREAM MIXED TEMP=313. PRES=101300.
    MOLE-FLOW H2O 0.5 / MEA 0.5

BLOCK MIX-LNMK MIXER

BLOCK COOLER HEATER
    PARAM TEMP=313. PRES=101300.

BLOCK HEATX HEATX
```

```
    PARAM DELT-HOT=5. <C> PRES-HOT=0. <kPa> PRES-COLD=0. <kPa>  &
        U-OPTION=CONSTANT F-OPTION=CONSTANT CALC-METHOD=SHORTCUT
    FEEDS HOT=LEAN-HX COLD=RICH-HX
    PRODUCTS HOT=LEAN-MIX COLD=RICH-STR
    HEAT-TR-COEF U=1.134 <kJ/sec-sqm-C>

;=====================================================
;      RateFrac To RateSep (RadFrac) Conversion
;                   (Version 2004.1)

;
;  Conversion time: Thu Aug 31 00:05:29 2006
;
;=====================================================

BLOCK ABSORBR1 RADFRAC
    PARAM NSTAGE=9 ALGORITHM=STANDARD EFF=MURPHREE  &
        INIT-OPTION=STANDARD P-UPDATE=YES
    COL-CONFIG CONDENSER=NONE REBOILER=NONE
    RATESEP-ENAB CALC-MODE=RIG-RATE
    RATESEP-PARA INIT-EQUIL=YES RS-MAXIT=50  &
        RS-STABLE-ME=LINE-SEARCH
    FEEDS LEANABS1 1 ON-STAGE-LIQ / FLUEABS1 10 ABOVE-STAGE
    PRODUCTS STACK1 1 V / RICHPUM1 9 L
    P-SPEC 1 101300. / 9 177000.
    COL-SPECS
    REAC-STAGES 1 9 MEA-REA
    HOLD-UP 1 9 VOL-LHLDP=0.07
    TRAY-REPORT2 COMP-EFF=YES STAGE-EFF=YES MURPH-COMPS=H2O MEA  &
        H2S CO2 HCO3- MEACOO- MEA+ CO3-2 HS- S-2 H3O+ OH-  &
        N2 O2 AR NO CO SO2 H2 NTU-COMPS=H2O MEA H2S CO2  &
        HCO3- MEACOO- MEA+ CO3-2 HS- S-2 H3O+ OH- N2 O2 AR  &
        NO CO SO2 H2
    TRAY-RATE 1 1 9 SIEVE NPASS=2 TRAY-SPACE=1.7 DIAM=7.  &
        SYSFAC=0.85 FLOOD-METH=FAIR P-UPDATE=YES  &
        DECK-THICK=0.074 <IN> WEIR-HT-A=0.15 WEIR-HT-B=0.15  &
        DC-CLEAR-SID=0.125 DC-CLEAR-CTR=0.125
    TRAY-RATE2 1 RATE-BASED=YES LIQ-FILM=DISCRXN VAP-FILM=FILM  &
        LIQ-CORRF=YES VAP-CORRF=YES MTRFC-CORR=ZUIDERWEG-82  &
        INTFA-CORR=ZUIDERWEG-82 FLOW-MODEL=MIXED  &
        HOLDUP-CORR=ZUIDERWEG-82 BASE-STAGE=4 BASE-FLOOD=0.7

BLOCK DCC RADFRAC
    PARAM NSTAGE=2
    COL-CONFIG CONDENSER=NONE REBOILER=NONE
    FEEDS H2O-DCC 1 ON-STAGE-LIQ / FLUE-DCC 2 ON-STAGE-VAP
    PRODUCTS H2O-OUT 2 L / FLUE-ABS 1 V
    P-SPEC 1 177. <kPa>
    COL-SPECS

;=====================================================
;      RateFrac To RateSep (RadFrac) Conversion
;                   (Version 2004.1)
;
;  Conversion time: Thu Aug 31 00:09:53 2006
;
;
;           *** Pre-Conversion Messages ***
;
;
;=====================================================

BLOCK STRIPPER RADFRAC
    PARAM NSTAGE=9 EFF=MURPHREE ABSORBER=NO P-UPDATE=YES
    COL-CONFIG CONDENSER=PARTIAL-V REBOILER=KETTLE
    RATESEP-ENAB CALC-MODE=RIG-RATE
    RATESEP-PARA INIT-EQUIL=YES RS-TOL=0.001 RS-STABLE-ME=DOGLEG
    FEEDS RICH-STR 2 ON-STAGE
    PRODUCTS CO2-COMP 1 V / LEAN-HX 9 L
    P-SPEC 1 101300. / 9 128000.
    COL-SPECS B:F=0.95 MOLE-RR=1.
    REAC-STAGES 2 8 MEA-REA / 1 1 MEA / 9 9 MEA
    HOLD-UP 2 8 VOL-LHLDP=0.2
    SPEC 1 MOLE-FLOW 1.3162 COMPS=CO2 STREAMS=CO2-COMP
    SPEC 2 TEMP 343. STAGE=1
    VARY 1 B:F 0.9 1.
```

```
    VARY 2 MOLE-RR 0.1 10.
    TRAY-REPORT TRAY-OPTION=BRIEF
    TRAY-REPORT2 COMP-EFF=YES STAGE-EFF=YES MURPH-COMPS=H2O MEA  &
        H2S CO2 HCO3- MEACOO- MEA+ CO3-2 HS- S-2 H3O+ OH-  &
        N2 O2 AR NO CO SO2 H2 NTU-COMPS=H2O MEA CO2 N2 O2  &
        H2S HCO3- MEACOO- MEA+ CO3-2 HS- S-2 H3O+ OH- AR NO  &
        CO SO2 H2
    TRAY-RATE 2 2 8 SIEVE NPASS=3 TRAY-SPACE=1.7 DIAM=6.67  &
        SYSFAC=0.85 FLOOD-METH=FAIR P-UPDATE=YES  &
        DECK-THICK=0.074 <IN> WEIR-HT-A=0.15 WEIR-HT-B=0.15  &
        WEIR-HT-C=0.15 DC-CLEAR-SID=0.125 DC-CLEAR-OFC=0.125
    TRAY-RATE2 2 RATE-BASED=YES LIQ-FILM=DISCRXN VAP-FILM=FILM  &
        LIQ-CORRF=YES VAP-CORRF=YES MTRFC-CORR=ZUIDERWEG-82  &
        INTFA-CORR=ZUIDERWEG-82 FLOW-MODEL=MIXED  &
        HOLDUP-CORR=ZUIDERWEG-82 AREA-FACTOR=1.
    PROPERTIES ELECNRTL HENRY-COMPS=MEA CHEMISTRY=MEA  &
        TRUE-COMPS=YES
    BLOCK-OPTION SIM-LEVEL=4 PROP-LEVEL=4 STREAM-LEVEL=4  &
        TERM-LEVEL=4

BLOCK RICHPMP1 PUMP
    PARAM DELP=0. <kPa>

BLOCK WAT-PUMP PUMP
    PARAM DELP=83.6 <kPa>

BLOCK BLOWER COMPR
    PARAM TYPE=ISENTROPIC DELP=83600. SEFF=0.9  &
        MODEL-TYPE=COMPRESSOR

BLOCK MCOMP MCOMPR
    PARAM NSTAGE=4 TYPE=ASME-POLYTROPIC COMPR-NPHASE=1
    FEEDS 1 1
    PRODUCTS CO2-SEQ 4 / WAT GLOBAL L
    COMPR-SPECS 1 PRATIO=3.23 PEFF=0.8 MEFF=0.9 TEMP=473. / 2  &
        PRATIO=3.23 PEFF=0.8 MEFF=0.9 TEMP=473. / 3  &
        PRATIO=3.23 PEFF=0.8 MEFF=0.9 TEMP=473. / 4  &
        PRATIO=3.23 PEFF=0.8 MEFF=0.9 TEMP=473.
    COOLER-SPECS 1 TEMP=313. / 2 TEMP=313. / 3 TEMP=313. /  &
        4 TEMP=313.
    PROPERTIES ELECNRTL HENRY-COMPS=MEA CHEMISTRY=MEA  &
        FREE-WATER=STEAM-TA SOLU-WATER=3 TRUE-COMPS=YES
    BLOCK-OPTION FREE-WATER=NO

BLOCK B1 MULT
    PARAM FACTOR=2.

BLOCK B2 MULT
    PARAM FACTOR=0.5

BLOCK B3 MULT
    PARAM FACTOR=0.25

BLOCK B5 MULT
    PARAM FACTOR=2.

DESIGN-SPEC ALPHA
F     Real*8 MEA
    DEFINE CO2 MOLE-FLOW STREAM=LEAN-ABS SUBSTREAM=MIXED  &
        COMPONENT=CO2
    DEFINE MEA MOLE-FLOW STREAM=LEAN-ABS SUBSTREAM=MIXED  &
        COMPONENT=MEA
F     ALPHA=CO2/MEA
    SPEC "ALPHA" TO "0.25"
    TOL-SPEC "0.005"
    VARY STREAM-VAR STREAM=LEAN-ABS SUBSTREAM=MIXED  &
        VARIABLE=MOLE-FLOW DESCRIPTION="0"
    LIMITS "50" "150"

DESIGN-SPEC ALPHAELC
F     Real*8 MEA, MEAPL, MEACOO
    DEFINE CO2 MOLE-FLOW STREAM=LEAN-ABS SUBSTREAM=MIXED  &
        COMPONENT=CO2
    DEFINE MEA MOLE-FLOW STREAM=LEAN-ABS SUBSTREAM=MIXED  &
        COMPONENT=MEA
    DEFINE MEAPL MOLE-FLOW STREAM=LEAN-ABS SUBSTREAM=MIXED  &
```

```
        COMPONENT=MEAH+
    DEFINE MEACOO MOLE-FLOW STREAM=LEAN-ABS SUBSTREAM=MIXED  &
        COMPONENT=MEACOO-
    DEFINE HCO3M MOLE-FLOW STREAM=LEAN-ABS SUBSTREAM=MIXED  &
        COMPONENT=HCO3-
    DEFINE CO3M2 MOLE-FLOW STREAM=LEAN-ABS SUBSTREAM=MIXED  &
        COMPONENT=CO3--
F     ALPHAE=(CO2+HCO3M+CO3M2+MEACOO)/(MEA+MEAPL+MEACOO)
    SPEC "ALPHAE" TO "0.3"
    TOL-SPEC "0.001"
    VARY STREAM-VAR STREAM=LEANABS1 SUBSTREAM=MIXED  &
        VARIABLE=MOLE-FLOW DESCRIPTION="0"
    LIMITS "15" "150"

DESIGN-SPEC DCC
    DEFINE QDCC STREAM-VAR STREAM=FLUE-ABS SUBSTREAM=MIXED  &
        VARIABLE=TEMP
    SPEC "QDCC" TO "313"
    TOL-SPEC "0.01"
    VARY STREAM-VAR STREAM=H20-PUMP SUBSTREAM=MIXED  &
        VARIABLE=MOLE-FLOW
    LIMITS "10" "150"

DESIGN-SPEC STRIPPER
    DEFINE TN STREAM-VAR STREAM=LEAN-HX SUBSTREAM=MIXED  &
        VARIABLE=TEMP
    SPEC "TN" TO "384"
    TOL-SPEC "1"
    VARY BLOCK-VAR BLOCK=STRIPPER VARIABLE=PRES SENTENCE=P-SPEC  &
        ID1=9
    LIMITS "101300" "221000"

EO-CONV-OPTI

CALCULATOR BLOWPRUP
    DEFINE BLOWPD BLOCK-VAR BLOCK=BLOWER VARIABLE=DELP  &
        SENTENCE=PARAM
    VECTOR-DEF PDABS PROFILE BLOCK=ABSORBR1 VARIABLE=DP-STG  &
        SENTENCE=PROF-RATE2
c       PDABS(LPDABS)=0.0
F       SUM1=0.0
F       Do 10 I=1, 8
F       SUM1=SUM1 + PDABS(I)
F 10    CONTINUE
F       SPDS=SUM1
F       BLOWPD=SPDS
c       Write(nterm,*)SPDS
    READ-VARS PDABS


CALCULATOR C-MAKEUP
F       REAL*8 MEAMU, MEAAB, MEAST, OHMMU, OHMAB, MEAPMU, MEAPAB
    DEFINE H2OFL MOLE-FLOW STREAM=FLUEABS1 SUBSTREAM=MIXED  &
        COMPONENT=H2O
    DEFINE H2OAB MOLE-FLOW STREAM=STACK1 SUBSTREAM=MIXED  &
        COMPONENT=H2O
    DEFINE H2OST MOLE-FLOW STREAM=CO2-COMP SUBSTREAM=MIXED  &
        COMPONENT=H2O
    DEFINE MEAAB MOLE-FLOW STREAM=STACK1 SUBSTREAM=MIXED  &
        COMPONENT=MEA
    DEFINE MEAST MOLE-FLOW STREAM=CO2-COMP SUBSTREAM=MIXED  &
        COMPONENT=MEA
    DEFINE H3OPAB MOLE-FLOW STREAM=STACK1 SUBSTREAM=MIXED  &
        COMPONENT=H3O+
    DEFINE OHMAB MOLE-FLOW STREAM=STACK1 SUBSTREAM=MIXED  &
        COMPONENT=OH-
    DEFINE MEAPAB MOLE-FLOW STREAM=STACK1 SUBSTREAM=MIXED  &
        COMPONENT=MEAH+
    DEFINE MEAMU MOLE-FLOW STREAM=MAKE-UP SUBSTREAM=MIXED  &
        COMPONENT=MEA
    DEFINE H2OMU MOLE-FLOW STREAM=MAKE-UP SUBSTREAM=MIXED  &
        COMPONENT=H2O
    DEFINE H3OPMU MOLE-FLOW STREAM=MAKE-UP SUBSTREAM=MIXED  &
        COMPONENT=H3O+
    DEFINE OHMMU MOLE-FLOW STREAM=MAKE-UP SUBSTREAM=MIXED  &
        COMPONENT=OH-
```

```
    DEFINE MEAPMU MOLE-FLOW STREAM=MAKE-UP SUBSTREAM=MIXED  &
        COMPONENT=MEAH+
F     MEAMU=2.0*MEAAB+MEAST+2.0*MEAPAB
c     MEAMU=MEAAB+MEAST
F     H2OMU=(2.0*H2OAB+H2OST+2.0*H3OPAB+2.0*OHMAB)- 2.0*H2OFL
c     H2OMU=(H2OAB+H2OST)- H2OFL
c     H3OPMU=H3OPAB
c     OHMMU=OHMAB
c     MEAPMU=MEAPAB
C       IF (H2OMU .LT. 0.0) THEN
C          H2OMU=ABS(M2OMU)
C       ENDIF
c     MEAMU=2.0*MEAAB+MEAST
c     H2OMU=(2.0*H2OAB+H2OST-H2OFL*2.0)
    EXECUTE BEFORE BLOCK MIX-LNMK

CALCULATOR C-RECOV
    DEFINE CO2IN MOLE-FLOW STREAM=FLUE-BLO SUBSTREAM=MIXED  &
        COMPONENT=CO2
    DEFINE FCO2 BLOCK-VAR BLOCK=STRIPPER VARIABLE=VALUE  &
        SENTENCE=SPEC ID1=1
F     FCO2=(CO2IN/2.0)*0.85
    EXECUTE BEFORE BLOCK ABSORBR1

CONV-OPTIONS
    PARAM TEAR-METHOD=BROYDEN TRACEOPT=CUTOFF SPEC-METHOD=SECANT  &
        CHECKSEQ=NO
    SECANT STOP=NO
    BROYDEN WAIT=4

TEAR
    TEAR LEAN-HX

CONVERGENCE ABS-LOOP BROYDEN
    TEAR LEAN-ABS / LEAN-HX
    SPEC ALPHAELC
    PARAM MAXIT=100 OPT-TTOL=NO

SEQUENCE S-1 BLOWER WAT-PUMP DCC B3 C-RECOV ABS-LOOP B2  &
        ABSORBR1 RICHPMP1 B1 HEATX STRIPPER C-MAKEUP MIX-LNMK  &
        COOLER (RETURN ABS-LOOP)

STREAM-REPOR MOLEFLOW MASSFLOW MOLEFRAC MASSFRAC

PROPERTY-REP NOPARAM-PLUS

REACTIONS MEA-ACID REAC-DIST
    IN-UNITS SI MOLE-ENTHALP='cal/mol' VFLOW-RPM='cuft/hr/rpm'  &
        F-FACTOR='(lb-cuft)**.5/hr'
    DESCRIPTION "LIQUID PHASE REACTION"
    REAC-DATA 1 EQUIL PHASE=L KBASIS=MOLE-GAMMA
    REAC-DATA 2 EQUIL PHASE=L KBASIS=MOLE-GAMMA
    REAC-DATA 3 EQUIL PHASE=L KBASIS=MOLE-GAMMA
    REAC-DATA 4 EQUIL PHASE=L KBASIS=MOLE-GAMMA
    REAC-DATA 5 KINETIC PHASE=L CBASIS=MOLAR
    REAC-DATA 6 KINETIC PHASE=L CBASIS=MOLAR
    REAC-DATA 7 EQUIL PHASE=L KBASIS=MOLE-GAMMA
    REAC-DATA 8 EQUIL PHASE=L KBASIS=MOLE-GAMMA
    K-STOIC 1 A=-3.0383250 B=-7008.3570 C=0.0 D=-.00313489
    K-STOIC 2 A=132.8990 B=-13445.90 C=-22.47730 D=0.0
    K-STOIC 3 A=216.0490 B=-12431.70 C=-35.48190 D=0.0
    K-STOIC 4 A=-.521350 B=-2545.530 C=0.0 D=0.0
    K-STOIC 7 A=214.5820 B=-12995.40 C=-33.54710 D=0.0
    K-STOIC 8 A=-9.7420 B=-8585.470 C=0.0 D=0.0
    RATE-CON 5 PRE-EXP=4.31520E+13 ACT-ENERGY=13249.0
    RATE-CON 6 PRE-EXP=3.74860E+14 ACT-ENERGY=25271.560
    STOIC 1 MEA+ -1.0 / H2O -1.0 / MEA 1.0 / H3O+ 1.0
    STOIC 2 H2O -2.0 / H3O+ 1.0 / OH- 1.0
    STOIC 3 HCO3- -1.0 / H2O -1.0 / H3O+ 1.0 / CO3-2 1.0
    STOIC 4 MEACOO- -1.0 / H2O -1.0 / MEA 1.0 / HCO3- 1.0
    STOIC 5 CO2 -1.0 / OH- -1.0 / HCO3- 1.0
    STOIC 6 HCO3- -1.0 / CO2 1.0 / OH- 1.0
    STOIC 7 H2O -1.0 / H2S -1.0 / HS- 1.0 / H3O+ 1.0
    STOIC 8 H2O -1.0 / HS- -1.0 / S-2 1.0 / H3O+ 1.0
    POWLAW-EXP 5 CO2 1.0 / OH- 1.0
    POWLAW-EXP 6 HCO3- 1.0
```

```
REACTIONS MEA-CO2 REAC-DIST
    IN-UNITS SI MOLE-ENTHALP='cal/mol' VFLOW-RPM='cuft/hr/rpm'  &
        F-FACTOR='(lb-cuft)**.5/hr'
    DESCRIPTION "LIQUID PHASE REACTION"
    REAC-DATA 1 EQUIL PHASE=L KBASIS=MOLE-GAMMA
    REAC-DATA 2 EQUIL PHASE=L KBASIS=MOLE-GAMMA
    REAC-DATA 3 EQUIL PHASE=L KBASIS=MOLE-GAMMA
    REAC-DATA 4 EQUIL PHASE=L KBASIS=MOLE-GAMMA
    REAC-DATA 5 KINETIC PHASE=L CBASIS=MOLAR
    REAC-DATA 6 KINETIC PHASE=L CBASIS=MOLAR
    K-STOIC 1 A=-3.0383250 B=-7008.3570 C=0.0 D=-.00313489
    K-STOIC 2 A=132.8990 B=-13445.90 C=-22.47730 D=0.0
    K-STOIC 3 A=216.0490 B=-12431.70 C=-35.48190 D=0.0
    K-STOIC 4 A=-.521350 B=-2545.530 C=0.0 D=0.0
    RATE-CON 5 PRE-EXP=4.31520E+13 ACT-ENERGY=13249.0
    RATE-CON 6 PRE-EXP=3.74860E+14 ACT-ENERGY=25271.560
    STOIC 1 MEA+ -1.0 / H2O -1.0 / MEA 1.0 / H3O+ 1.0
    STOIC 2 H2O -2.0 / H3O+ 1.0 / OH- 1.0
    STOIC 3 HCO3- -1.0 / H2O -1.0 / H3O+ 1.0 / CO3-2 1.0
    STOIC 4 MEACOO- -1.0 / H2O -1.0 / MEA 1.0 / HCO3- 1.0
    STOIC 5 CO2 -1.0 / OH- -1.0 / HCO3- 1.0
    STOIC 6 HCO3- -1.0 / CO2 1.0 / OH- 1.0
    POWLAW-EXP 5 CO2 1.0 / OH- 1.0
    POWLAW-EXP 6 HCO3- 1.0

REACTIONS MEA-REA REAC-DIST
    REAC-DATA 1 DELT=0. <F>
    REAC-DATA 2 DELT=0. <F>
    REAC-DATA 3 DELT=0. <F>
    REAC-DATA 4 KINETIC
    REAC-DATA 5 KINETIC
    REAC-DATA 6 KINETIC
    REAC-DATA 7 KINETIC
    REAC-DATA 8
    REAC-DATA 9
    K-STOIC 1 A=-3.038325 B=-7008.357 D=-0.0031348
    K-STOIC 2 A=132.89888 B=-13445.9 C=-22.4773
    K-STOIC 3 A=216.05043 B=-12431.7 C=-35.4819
    K-STOIC 8 A=214.582 B=-12995.4 C=-33.5471
    K-STOIC 9 A=-9.742 B=-8585.47
    RATE-CON 4 PRE-EXP=4.32E+013 ACT-ENERGY=13249. <cal/mol>
    RATE-CON 5 PRE-EXP=2.38E+017 ACT-ENERGY=29451. <cal/mol>
    RATE-CON 6 PRE-EXP=1170000. ACT-ENERGY=1797.1 <cal/mol>
    RATE-CON 7 PRE-EXP=1.93E+014 ACT-ENERGY=7471.7 <cal/mol>
    STOIC 1 H2O -1. / MEAH+ -1. / MEA 1. / H3O+ 1.
    STOIC 2 H2O -2. / H3O+ 1. / OH- 1.
    STOIC 3 HCO3- -1. / H2O -1. / CO3-- 1. / H3O+ 1.
    STOIC 4 CO2 -1. / OH- -1. / HCO3- 1.
    STOIC 5 HCO3- -1. / CO2 1. / OH- 1.
    STOIC 6 MEA -1. / CO2 -1. / H2O -1. / MEACOO- 1. /  &
        H3O+ 1.
    STOIC 7 MEACOO- -1. / H3O+ -1. / MEA 1. / H2O 1. /  &
        CO2 1.
    STOIC 8 H2O -1. / H2S -1. / HS- 1. / H3O+ 1.
    STOIC 9 H2O -1. / HS- -1. / S-2 1. / H3O+ 1.
    POWLAW-EXP 4 CO2 1. / OH- 1.
    POWLAW-EXP 5 HCO3- 1.
    POWLAW-EXP 6 MEA 1. / CO2 1. / H2O 0.
    POWLAW-EXP 7 MEACOO- 1. / H3O+ 1.

DISABLE
    CALCULATOR BLOWPRUP
    DESIGN-SPEC ALPHA STRIPPER
```

Appendix J: AspenPlus® Input file for Membrane Process Optimization

```
;
;Input Summary created by Aspen Plus Rel. 21.0 at 18:35:17 Sun Feb 6, 2011
;Directory N:\Documents\aspen  Runid OTIMIZATION-CASE6-COPY OF THESIS VAC-RUN
STAGE-RECOVERY 85% BASED ON 2 KMOL-S  OCT 08, 2009;


DYNAMICS
    DYNAMICS RESULTS=ON

IN-UNITS SI

DEF-STREAMS CONVEN ALL

DATABANKS PURE12  / AQUEOUS  / SOLIDS  / INORGANIC  /  &
        NOASPENPCD

PROP-SOURCES PURE12  / AQUEOUS  / SOLIDS  / INORGANIC

COMPONENTS
    CO2 CO2 /
    N2 N2 /
    O2 O2 /
    AR AR /
    H2O H2O /
    H2 H2 /
    NO NO /
    CO CO /
    SO2 O2S /
    N2O N2O

FLOWSHEET
    BLOCK HF1 IN=10 OUT=RETENT 3
    BLOCK VAC1 IN=3 OUT=16
    BLOCK HF2 IN=2 OUT=13 RET2
    BLOCK VAC2 IN=13 OUT=5
    BLOCK HF3 IN=14 OUT=8 RET3
    BLOCK COMP110B IN=7 OUT=CO2-SEQ
    BLOCK B2 IN=1 OUT=11
    BLOCK COMP1 IN=5 OUT=14
    BLOCK B1 IN=8 OUT=7 9
    BLOCK B3 IN=11 15 OUT=10
    BLOCK B5 IN=RET3 OUT=15
    BLOCK B6 IN=16 9 OUT=2

PROPERTIES IDEAL

STREAM 1
    SUBSTREAM MIXED TEMP=313. PRES=101000. MOLE-FLOW=1.
    MOLE-FRAC CO2 0.14947716 / N2 0.80198129 / O2 0.03896532 / &
        AR 0.00957622 / H2O 1E-010 / H2 1E-010 / NO 1E-010 / &
        CO 1E-010 / SO2 1E-010 / N2O 1E-010

STREAM 14
    SUBSTREAM MIXED TEMP=313. PRES=2000000. MOLE-FLOW=0.38586661
    MOLE-FLOW CO2 0.29519198 / N2 0.07372631 / O2 0.01360477 / &
        AR 0.00334354 / H2O 1.1861E-022 / H2 1.1861E-022 /  &
```

```
        NO 1.1861E-022 / CO 1.1861E-022 / SO2 1.1861E-022 /  &
        N2O 1.1861E-022

BLOCK B3 MIXER

BLOCK B6 MIXER

BLOCK B1 FSPLIT
    FRAC 9 0.1

BLOCK COMP1 MCOMPR
    PARAM NSTAGE=5 TYPE=ASME-POLYTROPIC PRES=25. <bar>
    FEEDS 5 1
    PRODUCTS 14 5
    COMPR-SPECS 1 PEFF=0.8 MEFF=0.9 / 2 PEFF=0.8 MEFF=0.9 /  &
        3 PEFF=0.8 MEFF=0.9 / 4 PEFF=0.8 MEFF=0.9 / 5  &
        PEFF=0.8 MEFF=0.9
    COOLER-SPECS 1 TEMP=313. / 2 TEMP=313. / 3 TEMP=313. /  &
        4 TEMP=313. / 5 TEMP=313.

BLOCK COMP110B MCOMPR
    PARAM NSTAGE=5 TYPE=ASME-POLYTROPIC PRES=110. <bar>
    FEEDS 7 1
    PRODUCTS CO2-SEQ 5
    COMPR-SPECS 1 PEFF=0.8 MEFF=0.9 / 2 PEFF=0.8 MEFF=0.9 /  &
        3 PEFF=0.8 MEFF=0.9 / 4 PEFF=0.8 MEFF=0.9 / 5  &
        PEFF=0.8 MEFF=0.9
    COOLER-SPECS 1 TEMP=313. / 2 TEMP=313. / 3 TEMP=313. /  &
        4 TEMP=313. / 5 TEMP=313.

BLOCK VAC1 MCOMPR
    PARAM NSTAGE=5 TYPE=ASME-POLYTROPIC PRES=101000.
    FEEDS 3 1
    PRODUCTS 16 5
    COMPR-SPECS 1 PEFF=0.8 MEFF=0.9 / 2 PEFF=0.8 MEFF=0.9 /  &
        3 PEFF=0.8 MEFF=0.9 / 4 PEFF=0.8 MEFF=0.9 / 5  &
        PEFF=0.8 MEFF=0.9
    COOLER-SPECS 1 TEMP=313. / 2 TEMP=313. / 3 TEMP=313. /  &
        4 TEMP=313. / 5 TEMP=313.

BLOCK VAC2 MCOMPR
    PARAM NSTAGE=5 TYPE=ASME-POLYTROPIC PRES=101000.
    FEEDS 13 1
    PRODUCTS 5 5
    COMPR-SPECS 1 PEFF=0.8 MEFF=0.9 / 2 PEFF=0.8 MEFF=0.9 /  &
        3 PEFF=0.8 MEFF=0.9 / 4 PEFF=0.8 MEFF=0.9 / 5  &
        PEFF=0.8 MEFF=0.9
    COOLER-SPECS 1 TEMP=313. / 2 TEMP=313. / 3 TEMP=313. /  &
        4 TEMP=313. / 5 TEMP=313.

BLOCK B2 MULT
    PARAM FACTOR=2.

BLOCK HF1 USER2
    IN-UNITS ENG
    SUBROUTINE SFCRGE
    PARAM NREAL=16
    INT VALUE-LIST= &
        685203290 ;NF
    REAL VALUE-LIST= &
```

```
        0.0003 & ;IDIA
        0.0005 & ;ODIA
        0.5 & ;LENGTH
        10000 & ;PPZO
        3.35E-007 & ;PERMN1
        6.7E-009 & ;PERMN2
        1.68E-008 & ;PERMN3
        1.68E-008 & ;PERMN4
        1.91E-015 & ;PERMN5
        1.91E-015 & ;PERMN6
        1.91E-015 & ;PERMN7
        1.91E-015 & ;PERMN8
        1.91E-015 & ;PERMN9
        1.91E-015 & ;PERMN10
        0.3055699 &
        90.0637884
    CHAR CHAR-LIST="NUM FIBERS AND INNER DIAMETER, METER"
    FLASH-SPECS RETENT TP
    FLASH-SPECS 3 TP
    USER-MODELS CONFIG=SFCRGEVR

BLOCK HF2 USER2
    IN-UNITS ENG
    SUBROUTINE SFCRGE
    PARAM NREAL=16
    INT VALUE-LIST= &
        166272310 ;NF
    REAL VALUE-LIST= &
        0.0003 & ;IDIA
        0.0005 & ;ODIA
        0.5 & ;LENGTH
        10000 & ;PPZO
        3.35E-007 & ;PERMN1
        6.7E-009 & ;PERMN2
        1.68E-008 & ;PERMN3
        1.68E-008 & ;PERMN4
        1.91E-015 & ;PERMN5
        1.91E-015 & ;PERMN6
        1.91E-015 & ;PERMN7
        1.91E-015 & ;PERMN8
        1.91E-015 & ;PERMN9
        1.91E-015 & ;PERMN10
        0.580512997 &
        96.2154479
    CHAR CHAR-LIST="NUM FIBERS AND INNER DIAMETER, METER"
    FLASH-SPECS RET2 TP
    FLASH-SPECS 13 TP
    USER-MODELS CONFIG=SFCRGEVR

BLOCK HF3 USER2
    IN-UNITS ENG
    SUBROUTINE SFCRGE
    PARAM NREAL=16
    INT VALUE-LIST= &
        2113340 ;NF
    REAL VALUE-LIST= &
        0.0003 & ;IDIA
        0.0005 & ;ODIA
        0.5 & ;LENGTH
        101000 & ;PPZO
```

```
        3.35E-007 & ;PERMN1
        6.7E-009 & ;PERMN2
        1.68E-008 & ;PERMN3
        1.68E-008 & ;PERMN4
        1.91E-015 & ;PERMN5
        1.91E-015 & ;PERMN6
        1.91E-015 & ;PERMN7
        1.91E-015 & ;PERMN8
        1.91E-015 & ;PERMN9
        1.91E-015 & ;PERMN10
        0.687659551 &
        85.3216618
    CHAR CHAR-LIST="NUM FIBERS AND INNER DIAMETER, METER"
    FLASH-SPECS 8 TP
    FLASH-SPECS RET3 TP
    USER-MODELS CONFIG=SFCRGEVR

BLOCK B5 VALVE
    PARAM P-OUT=101000.

DESIGN-SPEC DS-1
    DEFINE RECOV MOLE-FLOW STREAM=3 SUBSTREAM=MIXED  &
        COMPONENT=CO2
    DEFINE FLUEIN MOLE-FLOW STREAM=10 SUBSTREAM=MIXED  &
        COMPONENT=CO2
    SPEC "RECOV" TO "FLUEIN*0.92"
    TOL-SPEC "0.001"
    VARY BLOCK-VAR BLOCK=HF1 VARIABLE=VALUE-LIST SENTENCE=INT  &
        ELEMENT=1
    LIMITS "200000" "10000000000"

DESIGN-SPEC DS-2
    DEFINE RECOV2 MOLE-FLOW STREAM=13 SUBSTREAM=MIXED  &
        COMPONENT=CO2
    DEFINE FLUIN2 MOLE-FLOW STREAM=2 SUBSTREAM=MIXED  &
        COMPONENT=CO2
    SPEC "RECOV2" TO "FLUIN2*0.94"
    TOL-SPEC "0.001"
    VARY BLOCK-VAR BLOCK=HF2 VARIABLE=VALUE-LIST SENTENCE=INT  &
        ELEMENT=1
    LIMITS "80000" "2000000000"

DESIGN-SPEC DS-3
    DEFINE RECOV3 MOLE-FLOW STREAM=8 SUBSTREAM=MIXED  &
        COMPONENT=CO2
    DEFINE FLUIN3 MOLE-FLOW STREAM=14 SUBSTREAM=MIXED  &
        COMPONENT=CO2
    SPEC "RECOV3" TO "FLUIN3*0.935"
    TOL-SPEC "0.001"
    VARY BLOCK-VAR BLOCK=HF3 VARIABLE=VALUE-LIST SENTENCE=INT  &
        ELEMENT=1
    LIMITS "10000" "1000000000"

EO-CONV-OPTI

CONSTRAINT C-1

    DEFINE RECOV MOLE-FLOW STREAM=7 SUBSTREAM=MIXED  &
        COMPONENT=CO2
    DEFINE FEEDCO MOLE-FLOW STREAM=11 SUBSTREAM=MIXED  &
```

```
        COMPONENT=CO2
    SPEC "RECOV" GE "FEEDCO*0.85"
    TOL-SPEC "0.001"

CONSTRAINT C-2
    DEFINE PURITY MOLE-FRAC STREAM=7 SUBSTREAM=MIXED  &
        COMPONENT=CO2
    SPEC "PURITY" GE "0.98"
    TOL-SPEC "0.001"

OPTIMIZATION O-1
F     REAL*8 TOTDU
    DEFINE VPM1DU BLOCK-VAR BLOCK=VAC1 VARIABLE=NET-WORK  &
        SENTENCE=RESULTS
    DEFINE VPM2DU BLOCK-VAR BLOCK=VAC2 VARIABLE=NET-WORK  &
        SENTENCE=RESULTS
    DEFINE COM1DU BLOCK-VAR BLOCK=COMP1 VARIABLE=NET-WORK  &
        SENTENCE=RESULTS
F     TOTDU=VPM1DU+VPM2DU+COM1DU
F     WRITE(NHSTRY,*)TOTDU
    MINIMIZE "TOTDU"
    CONSTRAINTS C-1 / C-2
    VARY BLOCK-VAR BLOCK=HF1 VARIABLE=VALUE-LIST SENTENCE=INT  &
        ELEMENT=1
    LIMITS "100000" "1000000000"
    VARY BLOCK-VAR BLOCK=HF2 VARIABLE=VALUE-LIST SENTENCE=INT  &
        ELEMENT=1
    LIMITS "100000" "1000000000"
    VARY BLOCK-VAR BLOCK=HF3 VARIABLE=VALUE-LIST SENTENCE=INT  &
        ELEMENT=1
    LIMITS "100000" "3000000"
    VARY BLOCK-VAR BLOCK=B1 SENTENCE=FRAC VARIABLE=FRAC ID1=9
    LIMITS "0.0" "0.25" STEP-SIZE=0.01
    VARY BLOCK-VAR BLOCK=COMP1 VARIABLE=PRES SENTENCE=PARAM
    LIMITS "700000" "5000000"

CONV-OPTIONS
    PARAM TOL=0.0001
    WEGSTEIN MAXIT=100

STREAM-REPOR MOLEFLOW MOLEFRAC

DISABLE
    DESIGN-SPEC DS-1 DS-2 DS-3
;
;
;
;
;
```